(2)

AD-A174 859

AFWAL-TR-86-3098

1986 INTERNATIONAL AEROSPACE AND GROUND CONFERENCE
ON LIGHTNING AND STATIC ELECTRICITY

Proceedings of a Technical Symposium held at
Stouffer Dayton Plaza Hotel, Dayton, Ohio
24 - 26 June 1986

October 1986

DTIC
ELECTE
DEC 1 0 1986
S D
D

Approved for Public Release; Distribution Unlimited

DTIC FILE COPY

FLIGHT DYNAMICS LABORATORY
AIR FORCE WRIGHT AERONAUTICAL LABORATORIES
AIR FORCE SYSTEMS COMMAND
WRIGHT-PATTERSON AIR FORCE BASE, OHIO 45433-6553

86 12 09 031

UNCLASSIFIED
SECURITY CLASSIFICATION OF THIS PAGE

REPORT DOCUMENTATION PAGE

1a. REPORT SECURITY CLASSIFICATION UNCLASSIFIED	1b. RESTRICTIVE MARKINGS N/A A174839
2a SECURITY CLASSIFICATION AUTHORITY	3. DISTRIBUTION / AVAILABILITY OF REPORT Approved for Public Release; Distribution Unlimited.
2b. DECLASSIFICATION / DOWNGRADING SCHEDULE	
4. PERFORMING ORGANIZATION REPORT NUMBER(S)	5. MONITORING ORGANIZATION REPORT NUMBER(S) AFWAL-TR-86-3098
6a. NAME OF PERFORMING ORGANIZATION Air Force Wright Aeronautical Laboratories 6b. OFFICE SYMBOL (If applicable) AFWAL/FIESL	7a. NAME OF MONITORING ORGANIZATION
6c. ADDRESS (City, State, and ZIP Code) Wright-Patterson AFB, OH 45433-6553	7b. ADDRESS (City, State, and ZIP Code)
8a NAME OF FUNDING / SPONSORING ORGANIZATION National Interagency Coordination Group(NICG) 8b OFFICE SYMBOL (If applicable)	9. PROCUREMENT INSTRUMENT IDENTIFICATION NUMBER
8c. ADDRESS (City, State, and ZIP Code)	10. SOURCE OF FUNDING NUMBERS PROGRAM ELEMENT NO. 62201F; PROJECT NO. 2402; TASK NO. 02; WORK UNIT ACCESSION NO. 23

11 TITLE (Include Security Classification)

1986 International Aerospace and Ground Conference on Lightning and Static Electricity

12 PERSONAL AUTHOR(S)

13a TYPE OF REPORT	13b. TIME COVERED	14. DATE OF REPORT (Year, Month, Day)	15. PAGE COUNT
Conference Publication	FROM 24Jun86 TO 26Jun86	October 1986	429

16. SUPPLEMENTARY NOTATION The NICG consists of members from the U.S. Air Force, U.S. Army, U.S. Navy, NASA, NOAA, and the FAA.

17 COSATI CODES			18 SUBJECT TERMS (Continue on reverse if necessary and identify by block number)
FIELD	GROUP	SUB-GROUP	

19 ABSTRACT (Continue on reverse if necessary and identify by block number)

This report is a compilation of papers presented at the 1986 International Aerospace and Ground Conference on Lightning and Static Electricity, held at the Stouffer Dayton Plaza Hotel, Dayton, Ohio, June 24-26 1986. It includes papers concerning lightning phenomenology, lightning characterization, modeling and simulation, test criteria and techniques, and protection of both Airborne and Ground Systems.

This conference was sponsored by the National Interagency Coordination Group (NICG) of the National Atmospheric Electricity Hazards Protection Program in concert with the Florida Institute of Technology and in association with the SAE-AE4 Committee on Lightning, the United Kingdom Civil Aviation Authority, the Royal Aircraft Establishment, Farnborough, U.K., and Culham Laboratories, U.K.

20 DISTRIBUTION / AVAILABILITY OF ABSTRACT	21 ABSTRACT SECURITY CLASSIFICATION
☒ UNCLASSIFIED/UNLIMITED ☐ SAME AS RPT ☐ DTIC USERS	UNCLASSIFIED
22a NAME OF RESPONSIBLE INDIVIDUAL LAWRENCE C. WALKO	22b TELEPHONE (Include Area Code) (513) 257-7718 22c OFFICE SYMBOL AFWAL/FIESL

DD FORM 1473, 84 MAR 83 APR edition may be used until exhausted
All other editions are obsolete.

SECURITY CLASSIFICATION OF THIS PAGE
UNCLASSIFIED

1986 NATIONAL INTERAGENCY COORDINATION GROUP

INTERNATIONAL AEROSPACE and GROUND CONFERENCE on LIGHTNING and STATIC ELECTRICITY

DTIC COPY INSPECTED

June 24-26, 1986

Dayton, Ohio, U.S.A.

Accesion For
NTIS CRA&I ☑
DTIC TAB ☐
Unannounced ☐
Justification
By
Distribution/
Availability Codes
Dist | Avail and/or Special
A-1

INTERNATIONAL AEROSPACE and GROUND CONFERENCE on LIGHTNING and STATIC ELECTRICITY

1986

TECHNICAL PAPERS

THE WRIGHT PLACE TO BE

June 24-26, 1986

Dayton, Ohio, U.S.A.

CHAIRMAN'S MESSAGE

Welcome to the 1986 International Aerospace and Ground Conference on Lightning and Static Electricity.

The theme of this year's conference symbolizes the City of Dayton, "The Wright Place to Be". How fitting a location for this conference; the birthplace of the pioneers of aviation, Wilbur and Orville Wright. From the beginning of manned flight to our leap for the stars today, Dayton and the U.S. Air Force at Wright-Patterson Air Force Base have played an important part in this progress. Many papers that will be presented during this conference reflect this progress; not only in further understanding the phenomena of lightning and static electricity, but also in protecting existing and future systems from the effects of the atmospheric electricity threat.

The technical program consists of fifty-two papers to be presented during parallel sessions. This year's papers offer the most recent information obtained on lightning characteristics, essential for determining protection methods for both ground and airborne systems. In addition, the means for developing these protection schemes through analysis and test are addressed. A good percentage of the papers are on work that is going on outside the United States to truly make this an international forum.

I feel confident that all attendees will leave this conference with an increased knowledge of lightning and static electricity and, hopefully, with information useful for them to practically apply it to their professional endeavors. I would like to express my appreciation to many talented people who have worked so hard to make this a successful conference. This includes the conference speakers, session chairpersons and organizers, advisors, and last but certainly not least, the Conference Steering Committee and all their staff.

Lawrence C. Walko
Conference Chairman

NICG
COMMITTEE CHAIRPERSONS

Chairman	L.C. Walko U.S. Air Force Wright Aeronautical Laboratories
Vice Chairman	D. MacGorman NOAA National Severe Storms Laboratory
NICG Secretary	M. Glynn FAA Technical Center
Conference Coordinator	Dr. A. Revay Florida Institute of Technology
Aircraft/Aerospace	F.L. Pitts NASA Langley Research Center
Simulation	W.T. Walker U.S. Naval Air Development Center
Ground & Ship Systems	J. Foster U.S. Naval Air Engineering Center
Helicopters	D.L. Albright U.S. Army Aviation Systems Command
European Coordinator	G.A.M. Odam Royal Aircraft Establishment United Kingdom

CONTENTS

Session 1: Opening Session

Welcome: Dr. Joseph Taillet, Conference Chairman 1985
Office National d'Etudes et de Recherches Aerospatiales, France

Introduction: Lawrence C. Walko, Conference Chairman 1986
Air Force Wright Aeronautical Laboratories

Key Note Speaker: Brigadier General Philippe O. Bouchard
Vice Commander, Aeronautical Systems Division
U. S. Air Force Systems Command

1988 Lightning Conference Chairman
Dr. Donald MacGorman
National Severe Storms Laboratory

Session 2: Plenary

The Wright Place To Be

Dr. Pedro L. Rustan, U.S. Air Force Air Command and Staff College 1-1
A Review of Aerospace and Ground Lightning Threat Characteristics and Application

Session 3A: Composite Materials Testing
Chairman: Mr. E. H. Schulte, McDonnell Aircraft Company

Predicting Temperature Rises in Conductors Carrying Lightning Impulse Currents 2-1
R. E. Baldwin and G. W. Reid (Culham Lightning Studies Unit) and C.C.R. Jones (British Aerospace)

CW Testing of Composite and Hybrid Structures - Practical Difficulties and Interpretation of Results 3-1
C.C.R. Jones, I. P. MacDiarmid and D. Kershaw (British Aerospace) and B. Olson (SAAB-Scania)

Session 3B: Lightning/Aircraft Interaction I
Chairman: Dr. C. D. Skouby, McDonnell Aircraft Company

Summary of NASA Storm Hazards Lightning Research, 1980-1985 4-1
B. D. Fisher and P. W. Brown (NASA Lar ey Research Center) and J. A. Plumer (Lightning Technologies, Inc.)

F-106 Data Summary and Model Results Relative to Threat Criteria and Protection Design Analysis 5-1
F. L. Pitts and G. B. Finelli (NASA Langley Research Center) and R. A. Perala and T. H. Rudolph (Electro Magnetic Applications, Inc.)

Interpretation of a Class of In-Flight Lightning Signatures 6-1
Dr. T. F. Trost (United States Military Academy)

Session 4A: Lightning Simulation
Chairman: Mr. K. E. Crouch, Lightning Technologies, Inc.

A Threat-Level Lightning Simulator 7-1
J. L. Harrison, Y. G. Chen, E. Galicki, and W. Richardson (Maxwell Laboratories)

State-of-the-Art Techniques for Lightning Susceptibility/Vulnerability Assessments 8-1
J. G. Schneider, M. D. Risley, J. S. Reazer and A. V. Serrano (Technology/-Scientific Services, Inc.) and 1 Lt. J. L. Hebert (AF Wright Aeronautical Laboratories)

Comparison of Low Level Frequency Domain Lightning Simulation Tests to Pulse Measurements 9-1
D. B. Walen (Boeing Military Airplane Company)

Session 4B: Lightning/Aircraft Interaction II
Chairman: Mr. J. A. Plumer, Lightning Technologies, Inc.

Lightning Strikes to Aircraft of the German Federal Armed Forces 10-1
W. Ziegler (Federal Republic of Germany, Office for Military Technology and Procurement)

Zoning of Aircraft for Lightning Attachment and Current Transfer 11-1
C.C.R. Jones (British Aerospace) and G.A.M. Odam (Royal Aircraft Establishment) and A. W. Hanson (Consultant)

Session 5A: Helicopters I
Chairman: Mr. G. Heiderscheidt, Boeing Vertol

Airworthiness Considerations of Lightning Strike Protection for Helicopter Digital Engine Controls 12-1
R. L. Vaughn (Federal Aviation Administration Rotorcraft Standards Staff)

Simulated Lightning Current Tests on a Lynx Helicopter 13-1
C. J. Hardwick and V. P. Dunkley (Culham Laboratories), R. H. Evans (Consultant), and J.S.P. Hardy and R. A. Hobbs (Royal Aircraft Establishment)

Prediction of Skin Currents Flowing on a Helicopter Due to a Simulated Lightning Strike 14-1
Dr. A. Mallik (Kimberley Communications Consultants) and Dr. C. Christopoulos (University of Nottingham)

Session 5B: Lightning/Aircraft Interaction III
Chairman: Mr. N. Rasch, Federal Aviation Administration

Spatial and Temporal Description of Strikes to the FAA CV-580 15-1
J. S. Reazer and A. V. Serrano (Technology/Scientific Services, Inc.)

Simultaneous Airborne and Ground Measurement of Low Altitude Cloud-to-Ground Lightning Strike on CV-580 Aircraft 16-1
J. S. Reazer (Technology/Scientific Services, Inc.) and R. D. Richmond (AF Wright Aeronautical Laboratories)

Comparison of Electromagnetic Measurements on an Aircraft from Direct Lightning Attachment and Simulated Nuclear Electromagnetic Pulse 17-1
1 Lt. H. D. Burket (AF Wright Aeronautical Laboratories)

Session 6B: Lightning/Aircraft Interaction IV
Chairman: Dr. J. Corbin, Consultant

Analysis of the First Milliseconds of Aircraft Lightning Attachment 18-1
J. P. Moreau and J. C. Alliot (Office National d'Etudes et de Recherches Aerospatiales de France)

Current Levels and Distributions on an Aircraft During Ground Lightning Simulator Tests and In-Flight Lightning Attachments 19-1
1 Lt. J. L. Hebert (AF Wright Aeronautical Laboratories) and J. G. Schneider (Technology/Scientific Services, Inc.)

Joint Thunderstorm Operation Using the NASA F-106B and FAATC/AFWAL Convair 580 Airplanes 20-1
B. D. Fisher and P. W. Brown (NASA Langley Research Center), Major A. J. Wunschel, Jr. and 1 Lt. H. D. Burket (AF Wright Aeronautical Laboratories) and J. S. Terry (Federal Aviation Administration Technical Center)

Session 7A: Triggered Lightning I
Chairman: Dr. J. Taillet, Office National d'Etudes et de Recherches Aerospatiales

Current and Current-Derivatives in Triggered Lightning Flashes - Florida 1985 21-1
J. Hamelin, C. Leteinturier and C. Weidman (Centre National d'Etudes des Telecommunications) and A. Eybert-Berard and L. Barrett (Centre d'Etudes Nucleaires de Grenoble)

Electrical Onset Conditions of Upward Flashes Triggered by the Rocket and Wire Technic 22-1
P. LaRoche (Office National d'Etudes et de Recherches Aerospatiales) and A. Eybert-Berard and L. Barret (Centre d'Etudes Nucleaires de Grenoble)

1985 Rocket-Triggered Lightning Program Lightning Strike Object Results 23-1
R. D. Richmond (AF Wright Aeronautical Laboratories)

Session 7B: Indirect Effects Protection
Chairman: Mr. R. Beavin, AF Wright Aeronautical Laboratories

Atmospheric Electricity Hazards Protection (AEHP) Demonstration 24-1
R. Beavin and Capt. M. P. Hebert (AF Wright Aeronautical Laboratories)

Aircraft Lightning-Induced Transient Test and Predictions Comparison 25-1
M. M. Simpson (Boeing Military Airplane Company)

Session 8A: Triggered Lightning II
Chairman: Mr. W. Jafferis, NASA Kennedy Space Center

Submicrosecond Structure of the Radiation Fields Produced by Lightning Correlated Current-Derivative (dI/dt) and Electric Field Derivative (dE/dt) Emitted by Triggered Flashes 26-1
J. Hamelin, C. Leteinturier, L. Nicot and C. Weidman (Centre National d'Etudes des Telecommunications)

Experimental Study of the Interaction Between and Arc and an Electrically Floating Structure 27-1
G. Labaune, J. P. Moreau, J. C. Alliot and V. Gobin (Office National d'Etudes et de Recherches Aerospatiales) and B. Hutzler, G. Ricquel and R. Garabedian (Electricite de France)

Corona from Simulated Aircraft Surfaces and Their Contribution to the Triggered Discharge 28-1
J. A. Bicknell and R. Shelton (University of Manchester)

Session 8B: Lightning Protection
Chairman: 1 Lt. J. Hebert, AF Wright Aeronautical Laboratories

Lightning Protection of Adcock Antenna Systems 29-1
J. L. ter Haseborg (Technical University, Hamburg) and F. Wolf (C. Plath GMBH Company for Nautical Electronics)

EMI/EMP - The Connector Solution 30-1
L. A. Krantz (Allied Amphenol Products)

Session 9A: Electric Field Measurements I
Chairman: Dr. H. Kasemir, Colorado Scientific Research Corporation

Effect of E-Field Mill Location on Accuracy of Electric Field Measurements With Instrumented Airplane 31-1
Dr. V. Mazur (National Severe Storms Laboratory), Dr. L. Ruhnke (Naval Research Laboratory) and Dr. T. Rudolph and R. A. Perala (Electro Magnetic Applications, Inc.)

A Wide Bandwidth Electrostatic Field Sensor for Lightning Research 32-1
K. P. Zaepfel (NASA Langley Research Center)

Experimental Calibration of an Aircraft Vector Electric Field Meter System 33-1
Dr. R. V. Anderson and J. C. Bailey (Naval Research Laboratory)

Session 9B: Lightning Characterization I
Chairman: Dr. L. Ruhnke, Naval Research Laboratory

Lightning Return Stroke Current Computation 34-1
P.R.P. Hoole and J. E. Allen (Oxford University)
Lightning Return-Stroke Transmission Line Model 35-1
Dr. L. Baker and Dr. R. L. Gardner (Mission Research Corp.) and Dr. C. E. Baum (Air Force Weapons Laboratory)
A Simple Return Stroke Current Model for Predicting Lightning-Generated Electromagnetic Fields 36-1
Dr. T. A. Seliga (Pennsylvania State University) and W. J. White and K. A. Ostrander (3M Aviation Safety Systems)

Session 10A: Electric Field Measurements II
Chairman: Mr. R. Richmond, AF Wright Aeronautical Laboratories

A Fiber Optic Electric Field Sensor for Lightning Research 37-1
B. Nelson, C. Menzel and Dr. T. G. Digiuseppe (Geo-Centers, Inc.)
A Lightning Data Acquisition System 38-1
B. M. Stevens, Jr. (3M Aviation Safety Systems) and Dr. T. A. Seliga (Pennsylvania State University)

Session 10B: Lightning Characterization II
Chairman: Dr. D. LeVine, NASA Goddard Spaceflight Center

Model of Lightning Flashes Triggered From the Ground 39-1
Dr. H. W. Kasemir (Colorado Scientific Research Corp.)
Electron Fluid Model Simulations of Lightning Return Strokes 40-1
Dr. Z. Kawasaki and Dr. S. Israelsson (Uppsala University)
Calculation of Electromagnetic Fields From the Lightning Return Stroke Using the Charge Simulation Method 41-1
P.R.P. Hoole (Wolfson College, Oxford University) and Dr. S.R.H. Hoole (Drexel University)

Session 11A: Analysis Techniques
Chairman: Dr. T. H. Rudolph, Electro Magnetic Applications, Inc.

Implementation of GEMACS for Lightning Interactions Analysis 42-1
Dr. E. L. Coffey (Advanced Electromagnetics) and 1 Lt. J. L. Hebert (AF Wright Aeronautical Laboratories)

Lightning Current Redistribution 43-1
Dr. P. Geren (Science and Engineering Associates)

Comparison of Absorption and Radiation Boundary Conditions in 3DFD Code 44-1
Capt. C. Williford and 1 Lt. R. Jost (Air Force Institute of Technology) and 1 Lt. J. L. Hebert (AF Wright Aeronautical Laboratories)

Session 11B: Lightning Characterization III
Chairman: Dr. V. Mazur, NOAA National Severe Storms Laboratory

A Comparison of Calculated and Measured Values of the Optical Power Radiated by a Lightning Channel 45-1
Dr. A. H. Paxton and Dr. R. L. Gardner (Mission Research Corp.), W. Rison (New Mexico Institute of Mining and Technology) and Dr. C. E. Baum (AF Weapons Laboratory)

Spectrum Analysis of Positive Ground Strokes During Winters in Japan 46-1
Dr. Z. Kawasaki and Dr. S. Israelsson (Uppsala University) and T. Takeuti and M. Nakano (Nagoya University)

Session 12A: Electrostatics/Fuels
Chairman: Dr. J. Nanevicz, Stanford Research Institute

Electrostatic Field Measurements in a Foam Filled C-130 Fuel Tank During Fuel Sloshing 47-1
1 Lt. A. R. Bigelow, Capt. M. P. Hebert and 1 Lt. H. Jibilian (AF Wright Aeronautical Laboratories) and J. S. Reazer (Technology/Scientific Services, Inc.)

Minimum Ignition Levels of Aircraft Fuel Constituents to Lightning-Related Ignition Sources 48-1
K. E. Crouch (Lightning Technologies, Inc.)

Improved Electrostatic Discharge Wicks for Aircraft 49-1
Dr. R. V. Anderson and J. C. Bailey (Naval Research Laboratory)

Session 12B: Lightning Characterization IV
Chairman: Dr. V. Mazur, NOAA National Severe Storms Laboratory

Spatial and Temporal Characterization of the VHF-UHF Lightning Radiation 50-1
A. Bondiou, I. Taudiere and P. Richard (Office National d'Etudes et de Recherches Aerospatiales)

Some Remarks on Lightning Characteristics Near the Ground 51-1
Y. Nagai (Sagami Institute of Technology) and Y. Edano and S. Kawamata (Utsunomiya University)

Intracloud Discharges Studied from the Simultaneous Measurements of Electrostatic Field Changes, Thunder and Radiation Fields from Overhead Tropical Thunderstorms 52-1
Dr. P. Kumar and Dr. J. Rai (University of Roorkee)

A REVIEW OF AEROSPACE AND GROUND LIGHTNING THREAT CHARACTERISTICS AND APPLICATIONS

Pedro L. Rustan Jr.
Air Force Wright Aeronautical Laboratory (AFWAL/FIESL)
Wright-Patterson AFB, OH 45433

ABSTRACT

During the last ten yeers a vast amount of information hes been obteined ebout the lightning and static electricity threet to aerospece vehicles. Experimental reseerch aircreft flying inside thunderstorms have obteined consistent stetistics on the currents, stetic fields, end electromagnetic fields during lightning ettechment. The enelysis of these experimentei results hes affected the design of lightning simuletors, lightning locetors, aircreft lightning protections, and the development of standerds. Additionally, the anelysis of ground meesurements of the cherecteristics of the lightning discharge has affected the design of ground system protections and lightning locetors. Finally, new work hes been performed to compare lightning meesurements with simulated nucleer electromagnetic pulse (NEMP). This peper summarizes briefly some of the work in these erees and provides suggestions for additional reseerch.

I. INTRODUCTION

THE GOAL OF THIS conference is to share new information in the following three areas: 1) the effect of lightning and static electricity on aerospace vehicles, (2) the effect of lightning on ground systems, and (3) the relationship between lightning and other events that can cause interference in aerospace and ground systems. Nearly all the research articles presented here and in the last ten conferences belong to one of these categories. The goal of this introductory paper is to subdivide the research being performed in the above three areas, to outline some of the key accomplishments and to make suggestions for future research.

II. AEROSPACE VEHICLES

Fig. 1 shows the key research areas required to define the aerospace ligthning and atatic electricity threat characteristics and the use of these characteristics in the study of lightning simulators and test techniques, aircraft effects, lightning locators, aircraft protection, and the development of military and commercial standards. The characteristica of the lightning threat to the aircraft have a vital influence on the other research areas. However, external factors such as the incorporation of composite materials and faster digital electronics in new generation aircraft influence the aircraft effects, protection, and testing techniques. Next, the research on each of these areas will be summarized and some suggestions for future research will be considered.

AEROSPACE LIGHTNING AND STATIC ELECTRICITY THREAT CHARACTERISTICS.

In the last ten years at least five aircraft have been instrumented and flown inside or near a thunderstorm to measure various electromagnetic characteristics of the lightning discharge [1-5]. This work has been necessary to identify the expected lightning threat to a flying aircraft.

From these programs the NASA F-106 aircraft collected the largest amount of information, being struck by lightning about 680 times in the 1979-1985 time period. The data collected in the F-106 included the currents, fields, induced voltages, radar characteristics, and photography during lightning discharges to the aircraft. Most of these data were collected at altitudes between 20,000 and 40,000 ft where very little amount of data was available prior to this program.

In addition to the NASA F-106 aircraft, the Air Force Wright-Aeronautical Laboratory in conjunction with the FAA, the Navy, NASA, and ONERA instrumented and flew an FAA CV-580 aircraft at altitutes between 1500 and 18,000 ft inside thunderstorms to obtain direct strike lightning data during 1984 and 1985. The primary interest was in obtaining data to quantify the lightning threat to the aircraft at low altitudes. The maximum measured parameters were: peak current, 12 kA; rate-of-rise of the current 3.8×10^{10} A/s, surface current density, 3950 Teslas/sec, displacement current density, 33 Amps/m^2; charge transfer, 103 coulombs; and pulse repetition rate, 10^4 pulses/sec. Also the static field was measured continuously during the flight by using nine field mill

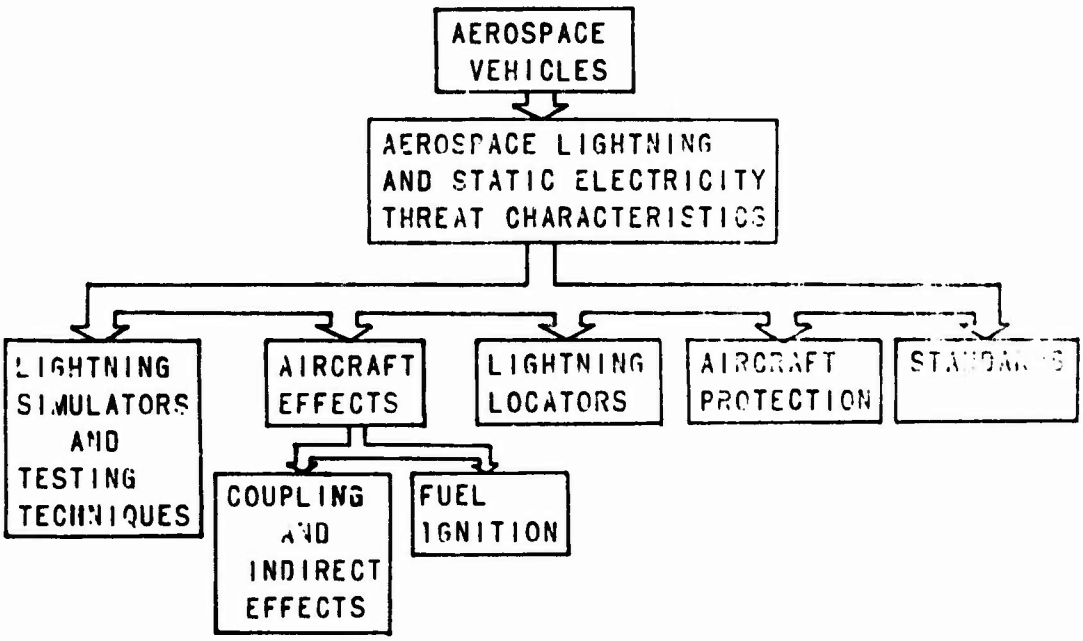

Fig. 1. Aerospace Llghtning and Static Electriclty Research Areas.

sensors mounted throughout the aircraft. Pictures of the discharge were obtained by using four Silicon Intensified Cameras mounted inside the aircraft and pointed toward the wingtips and the top and the bottom of the fuselage. Fifty direct lightning strikes were collected in this program and the results were fairly comparable to those obtained in the F-106 aircraft.

Results from the French C-160 aircraft also appear to be comparable to those in the the F-106 and the CV-580 aircraft. The C-160 aircraft was struck by lightning 12 times during the summer of 1984 in South France. The electric and magnetic field transients recorded during the discharge were comparable to the respective measurements in the CV-580 aircraft. However, the C-160 showed a consistent pulse repetition rate of about 10^4 pulses/sec which was near the peak value observed in the CV-580 aircraft. Similar high pulse repetition rates during aircraft lightning attachments have been measured in the WC-130 [4], and in the Learjet aircraft [5].

Now after concluding these five major experimental research programs, there is a need to summarize the results and to interpret the data using mathematical and physical models of the process. The validity of this analysis will depend on how well we prove that our assumptions are correct. Since many simultaneous measurements were performed during these research programs, the number of assumptions can be reduced. For example, 1) the ground and aircraft lightning location systems used during these experimental research programs provide additional information on the location and intensity of the discharge; 2) the simultaneous measurements of the electric and magnetic fields on the ground at the time of the aircraft lightning discharge for a few of these events provides a key relationship to interpret the differences between lightning measured airborne and on the ground; 3) ground and aircraft radar echoes at the time of the discharge can provide significant information on the precipitation regions surrounding the aircraft; 4) simultaneous measurements of the static electric fields on several aircraft locations can be interpreted to determine the aircraft charge and the vertical and horizontal static fields; and 5) simultaneous measurements of the induced voltages for various aircraft wiring configurations can be analyzed to estimate coupling mechanisms and aircraft transfer functions. The analyses of these results should drive the research in all the other areas shown in Fig. 1. It should be possible, using all the available data, to develop some theories about the physics of the aircraft lightning discharge which are consistent with the actual data. Some of the researchers in these programs have taken part of the data to provide an explanation of certain aspects of the physical discharge such as the initiation of the discharge [6], length and size of the discharge [7], analogy between the aircraft discharge and long air-gap breakdowns [8], correlation of radar signatures with lightning electromagnetic fields during aircraft strikes [9], analysis of the natural aircraft resonant frequencies excited by lightning discharges [10], LRC computer code analysis and nonlinear parameter study of the CV-580 and F-106 data [11], and the analysis of the energy requirements of an aircraft triggered discharge [12]. Additional work on these types of analyses based on the available data is highly encouraged to increase our understanding not only of the threat level but also of the physical aspects of the lightning strike to the aircraft which can be used for lightning protection.

While some aircraft lightning research experiments were designed to measure the currents and the fields associated with a lightning discharge [1-4], the instrumented Aerocommander aircraft operated by the Desert Research Institute (DRI) was utilized to measure the electric field, aircraft charge, ice particle type and concentration, particle precipitation charge and meteorological parameters [13]. So far, the DRI research suggests that charging is a result of aircraft-ice impacts rather than a stripping of the charge already carried by the ice particles [13].

Combining the results of the DRI aircraft and the field mill data collected in the F-106 and CV-580 with the electrostatic laborstory experiments conducted by SRI International [14] should clearly identify the aircraft charging and discharging processes. Before deciding to acquire additional airborne research data to determine the lightning and electrostatic threat charscteristics, the available data must be throughly analyzed and the goals of any new research program clearly defined.

LIGHTNING SIMULATORS AND TESTING TECHNIQUES. Many lightning simulator configurations have been developed in the last ten years to assess the vulnerability of aerospace vehicles to direct lightning attachment. Basically, three test techniques were available ten years ago to perform lightning tests. First, the full scale indirect effect test was developed by using a Marx bank through a long arc into the aircraft. Second, the lightning transient analysis (LTA) technique was introduced by using a small impulse generator to inject low currents to the vehicles and then using linear extrapolation for higher currents. Third, the CW test technique was designed to sweep a relatively low level source over a wide frequency range and using s network analyzer to determine the aircraft transfer function. This latter technique has been primarily used by the Boeing Company.

The first two techniques were later modified to include various configurations. The full scale induced effect testing was

expanded when McDonnell Aircraft Co. developed a shock excitation test by electrically isolating the test vehicle and producing a Megavolt discharge to the vehicle which then arcs over a ground plane. Similarly, the LTA technique was expanded for higher currents and rates-of-rise using ground return configurations to produce E and H field distributions comparable to the aircraft during flight [15],[16].

In 1979 testing confirmed and demonstrated the feasibility of using a gas-dielectric, triggered-spark gap as a 1 MV crowbar switch for lightning simulators [17]. The use of the crowbarred Marx surge generators was a significant step to achieve lightning simulators with current waveforms comparable to those measured in the F-106 and CV-580 aircraft. Additionally, the UV laser triggering of crowbars used in the Sandia Lightning Simulator can produce four current pulses in a short interval by using four crowbars [18]. Peaking capacitors similar to those used for NEMP simulators were being used for lightning simulators to obtain a peak current of about 40 kA and a risetime near 100 ns [19],[20].

This brief summary illustrates some of the changes that were incorporated in the design of lightning simulators to account for the increased knowledge in the lightning threat characteristics. One area where research might be required is trying to reproduce the high pulse repetition rate measured in aircraft lightning strikes. However, the design of such a simulator is extremely complex and impractical. We recommend that theoretical analysis be performed to determine the effect of the pulse repetition rate, both, internal and external to the aircraft, but no additional simulators be designed to account for this effect.

AIRCRAFT EFFECTS. The aircraft effects during lightning attachments are usually classified as directs and indirects. We will briefly discuss both of these effects.

Direct effects cause external physical damage to the aircraft and are primarily produced by the charge and energy transfer during the strike. The electrical sparkings that can be produced inside a fuel tank during a lightning strike are also considered direct effects. In metallic structures the typical direct effect damages are melting and burnthrough, pitting at structural interfaces, resistive heating, magnetic force effects, and arcing across bonds, hinges and joints [21]. In nonmetallic structures the direct effects can puncture or produce large holes on fiberglass or kevlar structures and delamination or burning of graphite composite structures. In the fuel tanks, lightning can cause fuel-vapor ignition produced by electrical or thermal ignition sources [21]. The fuel tank ignition problem is a major area of concern in aircraft lightning protection due to the possibility of a fuel tank explosion.

To determine the indirect effects, one must calculate the relationship between the lightning entry current and the external surface currents and charge densities throughout the aircraft surface and the induced transients on aircraft avionic systems. To determine the level of electromagnetic interference inside the aircraft, a lightning interaction model must be used to define the surface current and charge densities across the entire aircraft surface. The stick model and the three dimensional finite difference models such as THREDE and T3DFD are some of the most common models to determine the skin current distribution throughout the aircraft. To determine the internal-interaction problems, the effect of apertures, seams and joints; slots and cracks; diffusion, radomes, antennas, and wing wiring must be considered [22]. Once the electromagnetic energy penetrates to the aircraft interior it might excite internal cables and produce transients. These transients may upset or damage essential aircraft avionic systems.

The Atmospheric Electricity Hazard Protection (AEHP) program performed by the Boeing Company under the direction of the Air Force Wright-Aeronautical Laboratory has investigated the lightning produced direct and indirect effects in a modern aircraft [23]. The lightning simulated measurements performed in the AEHP program coupled with the airborne induced voltage measurements performed in the NASA F-106 and in the FAA CV-580 aircraft should provide meaningful results to prove the validity of some of the theoretical analysis on direct and indirect effects. Future research in this area should include taking the data collected in the CV-580 and F-106 aircraft and applying it to the existent models and analysis techniques. In both of these airborne programs, the currents and electromagnetic fields were measured simultaneously on various locations on the aircraft surface and some internal wirings. Additionally, for some of these strikes the entry and exit points have been determined, thereby reducing the uncertainty of the application of any electromagnetic models.

LIGHTNING LOCATORS. At this time the Stormscope appears to be the only commercially available lightning locator system than can be installed in an aircraft to locate a lightning discharge [24]. The Stormscope uses a single crossed loop to determine the bearing of the lightning discharge. The distance to the discharge is estimated by the relative magnitude of the fields. The Stormscope displays in real-time the relative location of the discharge in a CRT display.

Other systems could be developed to be mounted in an aircraft for real-time location of a lightning discharge. These systems could use crossed magnetic loops, time-of-arrival techniques, optical sensors, or newly developed techniques. Additionally, an interferometer system could be easily developed to be incorporated in an aircraft.

The incorporation of a Stormscope or any other aircraft lightning locators must be related to the airborne weather radar. It eppears that an overlay of the weather radar and the Stormscope displays would give the operator the choice of having either or both displays. Present cockpit configurations are so crowded that any possibility of adding a lightning locator in a civilian or military aircraft is not likely unless is superimposed with an existent display. Research in this area should be directed to develop new lightning locators for aircraft applications, to improve the accuracy of the Stormscope system, and to incorporate the lightning locators with other available weather displays in the aircraft.

AIRCRAFT PROTECTION. Once the direct and indirect effects produced by lightning in the aircraft have been determined using an acceptable threat level, aircraft protection may be required. Protection might include increasing the aircraft thickness around the fuel tanks, correcting electromagnetic cracks or joints on the aircreft surface, changing the shielding of some wiring and connectors, placing a grounded aluminum floor in the cockpit area or many other techniques. Two questions should be considered: 1) What is an acceptable threat level? and 2) Should the same protection level be applied to all aircraft?

The lightning threat charecteristics collected in the NASA F-106 and the CV-580 aircraft suggest e peak lightning current much lower than the 200 kA standard peak current level. However, the rate-of-rise of the current and other standard perameters appear to be consistent with the lightning threet data. Therefore, based on the recent airborne data, a peek current level of 50 kA can be recommended.

The second question may also be subjected to great debate. The present lightning protection requirements for fighter aircreft ere epplied without considerations of missions, probability of strike occurrence, or penalties associated with protective designs [25]. The cost end additionel weight associeted with the perfect protection of e fighter aircraft to the worst possible lightning strike appears to be unreesonable. Any lightning protection technique which has an edverse impect on the performance of a fighter aircreft must be studied carefully end trede-off curves established. However, e civilan or milltary cargo aircraft might be designed for continuous operetion for 99.9% of ell lightning strikes.

Much work hes to be done before large composite eircreft can be considered to have no fundamentel lightning protection deficiencies. Some of the reseerch areas being considered ere the electrical bonding and grounding of composite materials, the design of lightning-sefe composite fuel tanks, testing of kevlar and composite fibers to a lightning threat level pulse, and software routines requlred after system upset during a lightning strike.

STANDARDS. It appears that the best available document for eerospace lightning protection entitled "Lightning Test Waveforms and Techniques for Aerospace Vehicles and Hardware,' was published by the SAE Committee AE4L in June 1978 [26]. This report includes all the tests used by the government and industry during the 1970s. MIL-STD-1757 published in 1980 contained the noncontroversial tests in the SAE AE4L report. This standard was updated in March 1983, MIL-STD-1757A, to provide guidance in the application of the standard and to establish the various test techniques.

Two other general standards used by government and industry are MIL-STD-461 and MIL-STD-462 which describe electromegnetic interference characteristics, meesurements, and equipment requirements. However, MIL-B-5087 has remained to be the principal document to perform electrical bonding and protection to aircraft and aerospace systems. These military standards and specification documents must be carefully reviewed after analyzing the CV-580 and F-106 lightning data. It does not appear that any changes are required to MIL-STD-1757A. However, the lightning threat waveform of 200 kA in MIL-B-5087B might have to be changed to reflect an upper limit based on the actual lightning measurements. This upper limit might not exceed 50 kA.

III. GROUND SYSTEMS

Prior to the birth of aviation and lightning protection of aerospace vehicles, critical ground systems had failed after been struck by lightning. Lightning protection had been used primarily to protect electronic, radio, communicetion, and power systems. As the complexity of ground systems increased over the years, new anelytical and modelling techniques were being developed for lightning protection. However, one cannot protect against lightning without knowing the charecteristics of the discharge. Therefore, during the lest sixty years investigators have performed lightning meesurements to identify the most critical parameters in a lightning discharge. Figure 2 shows the practical research areas to define and epply ground lightning protection related to this conference. These areas will be briefly discussed.

GROUND LIGHTNING THREAT CHARACTERISTICS. The most important perameters to characterize a cloud-to-ground flash ere the currents and the fields produced by the discharge. Umen [27] summarized the published work in lightning characterization in the article "Revlew of Natural Lightning," published in a special lightning issue of the IEEE EMC Trans. in May 1982. Additionel research is definitely needed in the modelling of return strokes to estimete the current in the return stroke channel. Since the current waveform is probably the key paremeter in ground lightning protection, any lightning research work to

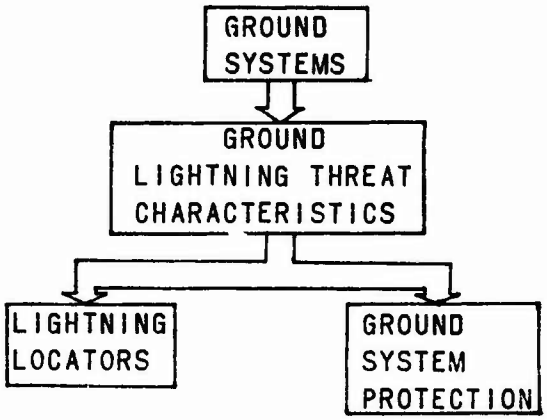

Fig. 2. Ground Lightning Research Areas.

measure the return stroke current or to estimate the current based on electromagnetic field measurements will have many practical applications.

LIGHTNING LOCATORS. The best known lightning locator systems commercially available use either crossed magnetic fields or time-of-arrival (TOA) techniques. It appears that either technique can be used to develop a fairly accurate system.

The crossed magnetic field system detects the induced voltages produced by two orthogonal loops by using the Faraday's principle. The Lightning Location and Protection (LLP) System is a commercially available lightning detector system which uses several distant stations with crossed magnetic field systems [28]. The system is used to determine cloud-to-ground flashes and is used extensively throughout parts of the U.S., Canada, and other foreign countries. A single station Stormscope system has also been developed for ground use by using crossed magnetic loops.

By using the difference of the TOA of the electromagnetic fields produced by a lightning discharge in different locations, one can calculate the actual location of the discharge. The Lightning Position and Tracking System (LPATS) is a commercially available lightning locator system that uses the TOA principle [29]. Similar to the LLP system, the LPATS system is also widely used. Other experimental systems designed using the basic TOA principle include the Lightning Detection and Ranging System (LDAR), and the interferometer system.

In addition to the two previously described techniques, much work has been done to determine the source of lightning discharge using optical and acoustical detectors. However, the crossed loop direction finders and the TOA techniques appear to be the most promising. Additional research work should continue in the area of lightning detectors to improve their accuracy and reduce their cost. It is highly likely that some type of lightning locator systems will be incorporated in every major airport to assist traffic controllers in locating the most active part of thunderstorms.

GROUND SYSTEM PROTECTION. Most ground systems are protected against natural lightning by lightning rods. In transmission lines the lightning rod is the overhead earth wire. Transmission lines are designed so that lightning is not likely to hit the phase conductor. Towers are usually designed to provide an excellent conductive path deep into the earth surface. Communication systems which are vulnerable to the electromagnetic interference produced by the electromagnetic fields in a lightning discharge should be shielded by the use of metallic enclosures and lightning protection devices to divert the lightning current. Additional information provided by researchers studying the parameters of a lightning discharge can be used by ground protection engineers to determine the expected threat level to their systems or equipment.

IV. LIGHTNING/NEMP/EMI

The NASA F-106 and the CV-580 aircraft were recently exposed to NEMP simulators and to small scale model testing to determine the relationship between actual lightning strike data and simulated and scale model NEMP data in the same aircraft. Preliminary CV-580 comparisons indicate that the magnitude of the NEMP spectrum exceeds that of lightning at frequencies above 4 Mhz. Even though this specific work was not performed for frequencies below 1 MHz, the lightning spectrum is clearly much larger than NEMP below few Megaherts [30]. The CV-580 work is now being published [31], [32]. At the VHF and UHF frequencies where most of the EMI interference sources exist, these EMI radiation sources will be much larger than the NEMP or lightning spectrum at those frequencies.

The combined NEMP and lightning work performed in the NASA F-106 and the CV-580 aircraft suggests the development of a common lightning/NEMP specification to be used for bomber aircraft which must be protected against both phenomena. At this time, the Air Force Weapons Laboratory is analyzing these data with the purpose of deciding how to approach the development of a common specification.

V. CONCLUSIONS AND RECOMMENDATIONS

We have briefly reviewed some of the most important research in the aerospace and ground lightning protection areas and the lightning threat specifications. We have limited our discussions to the typical scope of the conference. The aerospace lightning threat has been treated in more detail because of the recent completion of two fairly extensive research programs in the NASA F-106 and in the FAA CV-580 aircraft. The influence of the data collected in these programs on other areas of research will depend primarily on how thoroughly that data is analyzed. Some of

the research being performed with the data collected in these programs represent the beginning of our effort to interpret the results. We encourage researchers to analyze the aircraft lightning data to assist in the understanding of the physics of the discharge, the waveforms measured during the program, and most importantly, the interpretation of the overall results.

The state-of-the-art in lightning simulators and aircraft lightning protection techniques were briefly summarized. The use of crowbarred switching, peaking capacitors and UV lasers to achieve moderate peak currents with high rates-of-rise have permitted the simulation of recent aircraft lightning data. Electromagnetic models must be applied to the lightning simulation data to increase our understanding of the aircraft lightning interaction.

Since only very limited funding is available in this research area, researchers must know their objectives clearly and closely coordinate their results. We must be alert of the possible applications of our results and be ready to inform the appropriate governments and civilian offices.

REFERENCES

[1] F. L. Pitts, "Electromagnetic Measurements of Lightning Strikes to Aircraft," AIAA 19th Aeros. Science Meeting, Paper No. 81-0083, Jan 1981.

[2] P. L. Rustan, B. P. Kuhlman, H. Burket, M. Reazer, and A. Serrano, "Low Altitude Lightning Attachment to an Aircraft," Air Force Wright Aeronautical Lab, Tech Report, AFWL-TR-86-3009, 1986.

[3] P. LaRoche, M. Dill, J. Guyet, and M. Friedlander, "In-flight Thunderstorm Environment Measurements During the Landes 84 Campaign," 10th Procedings of this Conference, Paris, France, June 1985.

[4] P. L. Rustan, B. P. Kuhlman, A. Serrano, J. Reazer, and M. Risley, "Airborne Lightning Characterization," Air Force Wright Aeronautical Lab, Tech Report, AFWAL-TR-83-3013, 1983.

[5] J. Nanevicz, R. Adamo, and R. Bly, "Airborne Measurements of Electromagnetic Environment near Thunderstorm Cells," TRIP 76, Stanford Res. Institute, March 1977.

[6] P. L. Rustan and J. P. Moreau, "Aircraft Lightning Attachment at Low Altitudes," 10th Proceedings of this Conference, Paris, France, June 1985.

[7] P. L. Rustan, B. P. Kuhlman, and J. M. Reazer, "Airborne and Ground Electromagnetic Field Measurements of Lightning," 10th Proc. of this Conf., Paris, France, June 1985.

[8] G. LaBaune, J. P. Moreau, et al., "Experimental Study of the Interaction Between an Arc and an Electrically Floating Structure," these proceedings.

[9] V. Mazur, B. D. Fisher, and J. C. Gerlsch, "Lightning Strikes to an Airplane Penetrating Thunderstorms at Low Altitudes," 10th Proc. of this Conf., Paris, France, June 1985.

[10] T. F. Trost, C. D. Turner, and C. T. Wen, "Some Results and Limitations of Prony Analysis of In-Flight Lightning Data," 8th Proc. of this Conf., Fort Worth, Texas, June 1985.

[11] F. L. Pitts, L. D. Lee, R. A. Perala, and J. H. Rudolph, "An Evaluation and Appraisal of the Direct Strike Lightning Threat to Aircraft," these proceedings.

[12] J. A. Bicknell and R. W. Shelton, "The Energy Requirements of an Aircraft Triggered Discharge," 10th Proc. of this Conf., Paris, France, June 1985.

[13] B. Gardiner, J. Hallet, and C. Saunders, "Field Observations of Aircraft Charging in Convective Fields," 10th Proc. of this Conf., Paris, France, June 1985.

[14] J. E. Nanevicz and E. F. Vance, "Corona Threshold Determination by Three-State Physical Modelling of Aircraft," 10th Proc. of this Conf., Paris, France, June 1985.

[15] P. F. Little, A. W. Hanson, and B. J. Burrows, "Tests Techniques for Simulation Lightning Strikes to Carbon (Graphite) Fibre Composite Structures," FAA-FIT Workshop on Lightning Technology, Florida Institute of Technology, Melbourne, FL, 1979.

[16] L. C. Walko and J. L. Hebert, "Lightning Simulation on FAA CV-580 Lightning Research Aircraft," 10th Proc. of this Conf., Paris, France, June 1985.

[17] R. L. Parker, "Feasibility Studies for Crowbarring one Megavolt on the LILI Facility," Sandia Lab, SAND78-1700, Ap 1978.

[18] M. J. Landry and W. P. Brigham, "UV Laser Triggering of Crowbars Used in the Sandia Lightning Simulator," 9th Proc. of this Conf., Orlando, Fl, June 1985.

[19] R. A. Perala, T. H. Rudolph, and P. M. McKenna, "The Use of a Distributed Peaking Capacitor and a Marx Generator for Increasing Current Rise Rates and the Electric Field for Lightning Simulators," 9th Proc. of this Conf., Orlando, Fl, 1985.

[20] J. L. Hebert, J. G. Schneider, and J. S. Reazer, "Current Levels and Diatributions on an Aircraft During Ground Lighning Simulation Tests and In-Flight Lightning Attachments," these proceedings.

[21] J. A. Plumer and J. D. Robb, "The Direct Effects of Lightning on Aircraft," IEEE Trans. on Electromagnetic Comp., Vol EMC-24, No. 2, May 1982.

[22] R. A. Perala, T. Rudolph and F. Erikssen, "Electromagnetic Intersction of Lightning with Aircraft," IEEE Trans. on Electromagnetic Comp., Vol EMC 24, May 1982.

[23] R. C. Beavin and M. P. Hebert, "Atmospheric Electricity Hazards Protection (AEHP) Demonstration," theae proceedings.

[24] L. C. Walko and J. M. Reazer, "Data Acquisition for Evaluation of a Lighning Detector System," Air Force Wright Aeronautical Lab, Tech Report, AFWAL-TR-3083, Sept 1983.

[25] G. L. Weinstock, "Probabillstic Approach to Aircraft Lightning Protection," 7th Proc. of this Conf., Oxford, England, March 1982.

[26] Lightning Test Waveforms and Techniques for Aerospace Vehicles and Hardware. Report of SAE Committee AE4L, June 1978.

[27] M. A. Uman and E. P. Krider, "A Review of Natural Lightning: Experimental Data and Modelling," IEEE Trans. on Electromagnetic Comp., Volume EMC-24, No. 2, May 1982.

[28] W. L. Hiscox, E. P. Krider, A. E. Pifer, and M. A. Uman, "A Systematic Method for Identifying and Correcting Site Errors in a Network of Magnetic Direction Finders," 9th Proc. of this Conf., Orlando, Fl., 1984.
[29] R. B. Bent and W. Highlands, "Theoretical and Operational Evaluation of Time-of-Arrival (TOA) Lightning Position and Tracking System (LPATS), 9th Proc. of this Conf., Orlando, Fl., 1984.
[30] M. A. Uman, M. J. Master, and E. P. Krider, "A Comparison of Lightning Electromagnetic Fields with the Nuclear Elactromagnetic Pulse in the Frequency Range 10^4-10^7 Hz," IEEE Trans. on Electromagnetic Comp., Vol EMC-24, pp. 410-416, Nov. 1982.
[31] P. L. Rustan, "Description of an Aircraft Lightning and Simulated Nuclear Electromagnetic Pulse (NEMP) Threat Based on Experimental Data," Submitted to the IEEE Trans. on EMC, March 1986.
[32] H. D. Burket, "Comparison of Electromagnetic Measurements of an Aircraft from Direct Lightning Attachment and Simulated Nuclear Electromagnetic Pulse," these proceedings.

PREDICTING TEMPERATURE RISES IN CONDUCTORS CARRYING LIGHTNING IMPULSE CURRENTS

R. E. Baldwin, G. W. Reid, and C. C. R. Jones
Culham Lightning Studies Unit, UKAEA, United Kingdom

ABSTRACT

Conductors of small cross-section can be heated to quite high temperatures by lightning type impulse currents and this can cause significant problems on certain aircraft components by softening glue bonds or by different thermal expansion coefficients producing high stresses. If temperatures get high enough, some of the mechanical properties of the material can be affected. In some cases the possibility of a conductor fusing must be considered. Simple temperature calculations can give guidance on cross-sections that would be acceptable, but lower weight and drag requirements mean that better prediction is needed. This is especially so when fusing of a conductor is possible, and here the simple calculation techniques become even less accurate.

In this paper, a technique is presented for predicting temperature rises allowing for temperature dependent parameters and also inductive current distribution, diffusion and redistribution into the conductor material concerned. Results are included demonstrating the accuracy of the method for both aluminium and carbon fibre composite materials.

CW TESTING OF COMPOSITE AND HYBRID STRUCTURES - PRACTICAL DIFFICULTIES AND INTERPRETATION OF RESULTS

C. C. R. Jones, UKAEA, Culham Laboratory
I. P. Macdiarmid, British Aerospace (Warton)
D. Kershaw, British Aerospace (Warton)
B. Olsson, SAAB-SCANIA

ABSTRACT

CW testing of composite and hybrid structures appears to be done more frequently than in the past and is being proposed in more development programmes. Aluminium structures are quite amenable to such tests and, with an important proviso, can yield useful results. However, composite and hybrid constructions present a new set of problems. There are practical problems of driving sufficient power into such structures for diagnostic measurements to provide signals well above noise levels. There is also the difficulty of taking measurements of currents in resistive materials and understanding what they mean. However, it is probable that the most significant problem is interpreting the results in terms of the structure carrying real lightning currents. This problem arises because very few non-linearities will be evident at the low current levels typical of the CW tests. Lightning current, on the other hand, can produce voltages both directly and indirectly that will bring such non-linearities into play.

This paper identifies the difficulties and problems associated with CW testing and proposes minimum requirements for adequately carrying out such tests. The interpretation of results and scaling to full threat lightning parameters is also considered. The usefulness of these tests is discussed and guidance on the limitations given.

SUMMARY OF NASA STORM HAZARDS LIGHTNING RESEARCH, 1980-1985

Bruce D. Fisher and Philip W. Brown
NASA Langley Research Center
Hampton, Virginia 23665
USA

J. Anderson Plumer
Lightning Technologies, Inc.
Pittsfield, Massachusetts 01201
USA

ABSTRACT

Lightning swept-flash attachment patterns and the associated flight conditions were recorded from 1980-1985 during 1378 thunderstorm penetrations and 690 direct strikes with a NASA F-106B research airplane. The individual lightning attachment spots, along with crew comments and onboard photographic data have been used to identify lightning swept-flash attachment patterns and the orientations of the lightning channels with respect to the airplane. The altitudes, ambient temperatures, and the relative turbulence and precipitation levels at which the strikes occurred also are summarized and discussed, with an emphasis on the differences between high and low altitude strikes.

INTRODUCTION

THE NASA LANGLEY RESEARCH CENTER Storm Hazards Program (1-9)* was conducted to improve the state of the art of severe storm hazards detection and avoidance, as well as protection of aircraft against those hazards which cannot reasonably he avoided. The primary emphasis of the program was placed on lightning hazard research, although research into such areas as wind shear and turbulence (10) was also conducted. From 1980 to 1985, 1378 thunderstorm penetrations were made with an instrumented and lightning-hardened NASA F-106B airplane in Oklahoma and Virginia in conjunction with ground-based weather radar measurements by NOAA National Severe Storms Laboratory (NSSL) and the NASA Wallops Flight Facility, respectively. During these penetrations, 690 direct lightning strikes were experienced; in addition, lightning transient data were recorded from 188 nearby lightning flashes. Starting in 1982, the UHF-band radar at NASA Wallops was used to guide the airplane through the upper electrically-active regions of thunderstorms (11). In 1984 and 1985, the UHF-band radar also was used to provide guidance to electrically-active regions in thunderstorms at altitudes below 6 km (20 000 ft) (12 and 13).

The three principal purposes of the Storm Hazards Program were to gather detailed measurements of the electromagnetic characteristics of airplane lightning strikes (14-17) (not discussed in this paper), to quantify those conditions which are conducive to lightning strikes to aircraft, and to clarify some of the more questionable aspects of establishing lightning strike zones on aircraft. Since some new aircraft designs are incorporating large areas of skin and structure of composite materials, improved knowledge of the susceptibility of various parts of the aircraft surface to lightning strikes is essential. The present definitions of probable lightning strike zones (18 and 19) are based on prior experience and tests in which scale models are subjected to simulated lightning strikes. Data from this program verified the need for further clarification of probable lightning strike zones. To facilitate the determination of the lightning swept-flash patterns on the F-106B airplane, an extensive onboard photographic system was used (5, 8 and 20). The purposes of this paper are to update the lightning strike condition data presented to this forum in 1985 (9) by summarizing the data from 1980-1985, to discuss the lightning attachment zones on this airplane based on the Storm Hazards data, and to provide an example of the capabilities of the onboard photographic systems.

TEST EQUIPMENT AND TEST PROCEDURES

TEST EQUIPMENT -

F-106B research airplane - A thoroughly instrumented and lightning-hardened F-106B "Delta Dart" airplane (Fig. 1) is used to make thunderstorm penetrations (2 and 3). Based on the lightning experiences of this program, the lightning hardening procedures (2) now include removing paint from most exterior surfaces of the airplane to reduce swept-stroke lightning dwell time, hence minimizing the chance of a lightning melt-through anywhere on the airplane. Prior to each thunderstorm season, the lightning hardening integrity is verified during ground tests in which simulated lightning currents and voltages of greater than average intensity are conducted through the airplane with the airplane manned and all systems operating (2).

Airborne cameras and optics- The lightning attachments to the airplane have been filmed by combinations of eight onboard cameras (5, 7, 8, 9, and 20). The locations of the airborne camera systems are shown in Fig. 2(a). In 1985 only six cameras were used (20); the fields of view of these cameras are shown in Fig. 2(b), and their characteristics are summarized in Table 1. These cameras were:

- one 16-mm movie camera mounted under a fairing on the left side of the fuselage, looking aft with a field of view including the left wing tip and vertical tail
- one black and white video camera installed in the cockpit between the pilot's ejection seat and the flight test engineer's forward instrument panel, facing aft with a field of view encompassing both wing tips
- one black and white video camera installed in the air conditioner access compartment aft of the cockpit, facing upward with a 60° field of view, coincident with that of the University of Washington lightning X-ray sensor (Fig. 1(h) and (21)).
- three 70-mm still cameras installed on the same platform as the cockpit video camera, with two cameras facing forward to provide a stereo pair, and one camera facing aft with the same field of view as the cockpit-mounted video camera.

The two black and white video cameras, which used a Charge Induction Device (CID) sensor (8) were operated continuously throughout the flight, recording 30 frames/sec. Each frame was composed of alternating, interleaved rastor lines from the last 1/60 sec of the previous frame and the first 1/60 sec of the current frame. The two cameras were synchronized, and the time from the battery-operated time-code generator in the Aircraft Instrumentation System was recorded in each frame on each video cassette recorder via a character generator.

The 16-mm movie camera and the three 70-mm still cameras triggered automatically via inputs from two light-sensitive diodes mounted behind the pilot's rear view mirror (see Fig. 2(a) and (8)). The movie camera ran at a nominal frame rate of 200 frames/sec for 1 sec for each actuation. At this nominal frame rate, there were approximately 120 exposed frames per actuation, primarily due to the lag associated with camera motor start and motor acceleration/deceleration characteristics. The 70-mm still cameras could be programmed as to number of exposures per frame, time duration of each exposure, time duration between each exposure, and time interval for automatically advancing the film after an unexposed frame had been fogged by light leakage through the closed shutter. Film capacity was 15 ft, allowing about 70 exposures without reloading, a procedure which could only be performed on the ground. The operation and design of the system of the three 70-mm still cameras is discussed in detail in (20).

*Numbers in parentheses designate References at end of paper.

Other airborne data systems - The direct-strike lightning instrumentation system (DLite) (14-16) recorded electromagnetic waveforms from direct lightning strikes and nearby lightning flashes in flight by using electromagnetic sensors (Fig. 1(a)) and a shielded recording system with 5 nanosecond time resolution located in the weapons bay. Outputs from several of the DLite sensors also were recorded on a Boeing Data Logger System (22) which was mounted in the weapons bay through the 1983 season. The airplane altitude, Mach number, attitudes, ambient temperature, and other flight conditions were measured by the Aircraft Instrumentation System (AIS) and the Inertial Navigation System (INS) (6 and 10).

Ground-based systems at NASA Wallops Flight Facility - For the research flights in Oklahoma in 1980 and 1981, the NSSL Doppler radar at Norman was used to measure the precipitation reflectivity data (23) and wind velocity data (10). Additionally, an incoherent 10-cm-wavelength surveillance radar (23) was used to provide air traffic control guidance to the airplane.

Instrumentation from the Atmospheric Sciences Research Facility at NASA Wallops (7 and 24) was used to provide guidance to the F-106B flight crew during storm penetrations in Virginia. The facility included a UHF-band and an S-band (SPANDAR) radar, each with the capability of airplane tracking via inputs from a third radar which tracked a C-band transponder mounted on the airplane. In 1981 and 1982, the SPANDAR was modified by personnel from the Air Force Geophysics Laboratory (AFGL) to provide Doppler radar measurements showing mean radial wind velocity and spectrum width (a measure of turbulence) as well as precipitation reflectivity (25). In 1985, SPANDAR was modified by NASA Wallops personnel to again enable Doppler radar measurements to be made.

Since 1982, the NASA Wallops UHF-band radar has been used to obtain the range, azimuth, and elevation angle of echoes from lightning channels in real time (11-13). The lightning flash rate was estimated by use of an echo transient counter which counted the number of lightning echoes in a selectable range interval along the radar beam of the UHF-band radar.

NASA Langley Flight Service Station - The primary responsibility to launch and recall the airplane, select the storms and altitudes of interest, and provide real-time flight support and guidance to the aircrew was assigned to the Storm Hazards project personnel located in a dedicated area of the NASA Langley Flight Service Station. The NASA Langley personnel worked in concert with their counterparts at NASA Wallops, with real-time discussions of radar data and flight strategy taking place over a dedicated telephone line between the two sites. Personnel at both sites could communicate with the flight crew via radio. A map of the Storm Hazards test area used during the missions based at NASA Langley is shown in Fig. 3. Generally, the airplane was flown within 150 n.mi. of NASA Langley to maintain line of sight communications with NASA Langley and NASA Wallops.

The equipment installed at NASA Langley to support the mission (8 and 26) included communications systems, lightning detection systems, time displays, and an integrated video display which tied much of these data together. The specifics on the integrated video display are given in (8 and 26).

By using the integrated video display system, it was possible for the NASA Langley personnel to better utilize the NASA Wallops data in recommending safe headings to targets of interest. In fact, the display allowed the NASA Langley staff to independently support flights when NASA Wallops support was not available.

TEST PROCEDURES -

Flight Procedures - In the Storm Hazards program, it has been assumed that storm regions containing the greatest natural lightning activity were the most likely regions in which to experience a direct strike. The lightning echo location data from the UHF-band radar and the storm's precipitation reflectivity data from SPANDAR were used to select the storm of interest and the desired altitude for each penetration, with the pilots operating the airplane according to the flight safety procedures established at the beginning of the program (6). In 1985, most penetrations were made at altitudes below 6 km (20 000 ft).

Data Reduction - Static temperature and pressure altitude were determined from parameters measured and recorded by the AIS. The pressure altitude was determined from static pressure values which were corrected for position error. The ambient temperature was determined from the total temperature measurement. The relative intensities of turbulence and precipitation at the times of the lightning events were based on flight crew observations as extracted from the cockpit voice transcripts.

The lightning events experienced by the F-106B airplane are categorized as direct strikes or as nearby flashes (8). Following each flight in which there were direct lightning strikes, the lightning attachment points were located by careful inspection of the airplane surface. Using the procedure given in (6), an attempt was made to postulate, based on the various data types, the initial orientation of the lightning channel with respect to the airplane, the initial and final attachment points, swept-flash path(s), and direction(s) from which the flash exited the airplane (see (5) for definitions of swept-flash attachment terms).

The motion picture sequences of lightning from the 16-mm movie camera and the still photographs from the three 70-mm still cameras (Table 1) were time-correlated with the other data via the AIS using the techniques given in (5, 8 and 20). The time code from the AIS was recorded with the video data using the technique given in (20).

DISCUSSION OF RESULTS

FLIGHT CONDITIONS CONDUCIVE TO LIGHTNING STRIKES - The number of missions, thunderstorm penetrations, direct strikes and nearby flashes for the Storm Hazards '80-'85 Programs are summarized by year in Table 2. The data show that the 175 thunderstorm research missions resulted in 690 direct lightning strikes and 188 nearby flashes during 1378 penetrations. The geographical location of the F-106B airplane at the time of each direct strike and nearby flash is shown in Figs. 3(a) and 3(b), respectively.

Histograms showing the number of penetrations, duration of each penetration and the number of strikes and nearby flashes experienced from 1980-1985 are shown for altitude intervals of

2000 ft in Fig. 4, and for ambient temperature intervals of 5°C in Fig. 5. Penetrations were made at pressure altitudes ranging from 20 000 ft to 40 000 ft with a mean penetration altitude of 23 400 ft (Fig. 4). Temperature data (mean value during the penetration) were available for 1250 penetrations, with values ranging from 20°C to -60°C, with an overall mean value of -20°C (Fig. 5). The distributions of penetration time with altitude and temperature are very similar to the corresponding penetration distributions.

A plot of lightning strike incidents as a function of altitude for commercial aircraft in routine operations is shown in Fig. 6 (from (27) with updated information from (28)). Based on data such as that shown in Fig. 6, most penetrations in 1980 and 1981 were made at altitudes corresponding to ambient temperatures between ±10°C in expectation of receiving a large number of strikes. However, few strikes were experienced (see Table 2 and (3 and 4)). Starting in 1982, the NASA Wallops UHF-band radar was used to guide the F-106B airplane through the upper electrically-active regions of thunderstorms (11 and 29), resulting in hundreds of high-altitude direct lightning strikes (Table 2 and (5, 6, 7 and 11)). In 1984 and 1985, the UHF-band radar was used to provide guidance to electrically-active regions in thunderstorms at altitudes below 20 000 ft (12 and 13), the same area studied previously in 1980 and 1981. The low altitude research efforts of 1980-81 and 1984-85 are shown in the low altitude/warm temperature peaks in the penetration and duration data in Figs. 4 and 5.

The Storm Hazards Program strike statistics shown in Figs. 4 and 5 differ significantly from the published strike data for commercial aircraft ((27 and 28) - see Fig. 6) and for U.S. Air Force aircraft (30), in which most lightning strikes were found to occur between ambient temperatures of ±10°C. In the Storm Hazards Program, direct strikes were experienced at pressure altitudes ranging from 14 000 ft to 40 000 ft with a mean value of 30 000 ft (Fig. 4). The corresponding ambient temperature ranged from 5°C to -65°C, with a mean value of -30°C (Fig. 5). The nearby flash data are very similar to the direct strike data. Despite spending approximately 1250 mins of penetration time at altitudes below 20 000 ft (32 percent), only 75 direct strikes were experienced (11 percent) (see Table 2). In fact, the peak strike rates in Fig. 4 of 7 strikes/penetration and 1.4 strikes/min occurred at pressure altitudes between 38 000 ft and 40 000 ft corresponding to ambient temperatures colder than -40°C. (During one research flight through a thunderstorm anvil at 38 000 ft altitude in 1984, the F-106B experienced 72 direct strikes in 45 mins of penetration time, with the instantaneous strike rate twice reaching a value of 9 strikes/min.) On the other hand, the peak strike rate near the freezing level (0°C) was only 0.1 strike/min (in the altitude interval between 18 000 ft and 20 000 ft, corresponding to ambient temperatures of -5°C to -10°C).

The NASA Storm Hazards data differ from the commercial and U.S Air Force data for two reasons. First, the NASA data came solely from intentional thunderstorm penetrations, while the commercial and military data were derived from a variety of meteorological conditions, mostly in nonstormy clouds. (The NASA Storm Hazards Program has not studied the non-thunderstorm lightning strike phenomenon.) Second, commercial and military aircraft will normally deviate from course to avoid thunderstorms which reach cruise altitudes, and only penetrate when required to do so in the terminal area, where typical assigned altitudes are near the freezing level. Therefore, the NASA distributions of lightning strikes with respect to pressure altitude and ambient temperature differ from the commercial/military data because of the higher percentage of time spent by the NASA F-106B research airplane in the upper flash density center of thunderstorms, compared with the low percentage of time spent in thunderstorms at those altitudes by aircraft in routine operations. However, lightning strikes have been encountered at nearly all temperatures and altitudes in the Storm Hazards Program, indicating that there is no altitude at which aircraft are immune from the possibility of a lightning strike in a thunderstorm.

Although the Storm Hazards data differ from the commercial/military data, there is strong agreement with the results of two other thunderstorm flight test programs. The high altitude strike data are in good agreement with the results of the U.S. Air Force Rough Rider Program (31), in which the peak lightning activity was found to occur at an ambient temperature of -40°C. In addition, the low altitude strike data are nearly identical to the data from the USAF/FAA Convair 580 Measurement Program (32), in which the peak lightning activity in thunderstorms at altitudes below 20 000 ft was found to occur in the range between 18 000 ft and 20 000 ft.

The most successful piloting technique used in searching for lightning was to fly through the thunderstorm cells which were the best defined visually and on the airborne weather radar. Frequently, heavy turbulence and precipitation were encountered during these penetrations. However, the lightning strikes rarely occurred in the heaviest turbulence and precipitation, and occassionally, there was no lightning activity whatsoever. These findings are shown in Fig. 7, in which the percentage of direct strikes to the F-106B airplane are plotted as a function of the flight crew's opinion of relative turbulence and precipitation intensity at the time of the strikes. The data are plotted for those strikes which occurred above and below 20 000 ft altitude. In both altitude regimes, most lightning strikes occurred in thunderstorm regions in which the crews characterized the turbulence and precipitation as negligible to light. However, for those strikes which occurred below 20 000 ft altitude, the crews called a higher percentage of the strikes in light turbulence and precipitation and a lower percentage in the negligible category than for those strikes which occurred at altitudes above 20 000 ft. In general, though, the data in this paper have shown that the number of direct strikes in thunderstorms do not show a positive correlation to turbulence and precipitation intensities. This finding is in agreement with commercial/military aircraft data (27, 28 and 30) and with the low altitude thunderstorm data collected in the USAF/FAA Convair 580 program (32).

Precipitation and turbulence also are not necessarily related. Although the Doppler radar data recorded in 1981 by the NASA Wallops SPANDAR (25) showed heavy turbulence within the high precipitation reflectivity cores of thunderstorms,

heavy turbulence also was found between cells, near storm boundaries, and in innocuous-appearing low reflectivity factor regions. This finding is in agreement with the results of the Rough Rider Program turbulence studies (33). In addition, it has heen found (11) that the average probability for the airplane to he struck was greater in storm regions with a flash rate of 0 to 10 flashes/min than in regions with flash rates greater than 10 flashes/min. Therefore, it appears that an airborne device which detects a single thunderstorm hazard (precipitation, turbulence, or lightning) will not necessarily provide information as to the location or intensity of the other two hazards.

In order to minimize the chances of encountering hail, the F-106B airplane was not flown into thunderstorm regions where the precipitation reflectivity values exceeded 50 dBZ, although the UHF-band radar studies found that the lower altitude lightning flash density center was closely associated with high reflectivity cores (29). Therefore, no comments can he made from the Storm Hazards data concerning the probability of encountering direct lightning strikes in such areas of thunderstorms. The data in this paper show that the greatest probability of experiencing a direct lightning strike in a thunderstorm occurred in regions where ambient temperature was colder than -40°C, where the relative turbulence and precipitation intensities were characterized as negligible to light, and where the lightning flash rate was less than 10 flashes/min. The most likely region to encounter lightning strikes at low altitudes in thunderstorms was found in the altitude hand between 18 000 ft and 20 000 ft, in negligible to light turbulence and precipitation and where the lightning flash rate was less than 10 flashes/min. (However, the strike rate per minute was an order of magnitude less at low altitudes than at high altitudes). Finally, it has been shown that the presence and location of lightning do not necessarily coincide with the presence and location of hazardous precipitation and turbulence.

LIGHTNING ATTACHMENT PATTERNS - Lightning strike zones on aircraft have been defined as follows (18 and 19):

- o Zone 1:
  - o Zone 1A - Initial attachment point with low possibility of lightning arc channel hang-on
  - o Zone 1B - Initial attachment point with high possibility of lightning arc channel hang-on
- o Zone 2:
  - o Zone 2A - A swept-stroke zone with low possibility of lightning arc channel hang-on
  - o Zone 2B - A swept stroke zone with high possibility of lightning arc channel hang-on
- o Zone 3: All of the vehicle areas other than those covered by zone 1 and 2 regions. In zone 3, there is a low possibility of any attachment of the lightning channel. Zone 3 areas may carry substantial amounts of electrical current, but only by conduction between some pair of attachment points.

Although the defining documents (18 and 19) contain guidelines for determining the location of each zone on airplanes, such was not done for the F-106 airplane since it was designed prior to the creation of the specifications. Application of the zones to an existing aircraft can be controversial, due to differing interpretations of the guidelines. However, in the case of the Storm Hazards Program's F-106B airplane, it is possible to locate the zones on the airplane's exterior from direct observation of the lightning attachment points left from the 690 direct lightning strikes which have heen experienced. Specifically four general strike scenarios were found in the swept-flash attachment patterns (5, 6, 8, and 9):

1. Flashes which initially attach to the nose of the aircraft and subsequently "sweep" alongside it, reattaching at a succession of spots along the fuselage. In these cases, the initial and final exit point is usually the trailing edge of an extremity such as a wing or vertical fin tip. The final entry point is a trailing edge of the fuselage, because the flash is usually still alive by the time the aircraft has flown completely through it.
2. Similar to (1) except that the entry channel sweeps aft across the top or bottom wing surface instead of the fuselage.
3. Strikes in which the initial entry and exit points occur at the nose. In this case, the lightning flash appears to "touch" the aircraft nose but continues on from this point to another destination. The aircraft then flies through the flash, resulting in successive entry points along one side of the fuselage or wing and exit points along the other. Again, because the flash usually exists for a longer time than it takes the aircraft to fly its length, the final entry and exit points are located along trailing edges.
4. Strikes in which the initial and final entry and exit points are confined to the aft extremities.

With most of these general scenarios, swept-flash channels frequently have been found which rejoin behind the airplane after the airplane has flown through the channel (6, 8, and 9).

Applying the zone definitions (18 and 19) to these four attachment patterns results in the F-106 lightning attachment zones shown in Fig. 8. The nose boom, wing and vertical fin tips, speed brake, afterburner and fuselage trailing edges are known to have received initial lightning leader attachments, and thus are located in zone 1. In some cases, these locations have been struck by lightning leaders approaching the airplane; during these strikes the intense electric field associated with the approaching leaders induces junction leaders from one or more of the above extremities. In other cases, the leaders appear to have initiated from the airplane itself, propagating outward from opposite extremities such as the nose and tail, or the wing tips. In these situations, the airplane is believed to have "triggered" a lightning flash that would not otherwise have occurred (12 and 13). Though not specifically stated in the definitions (18 and 19), zone 1A locations are intended to include surfaces which may be reached by the first return stroke. A finite time period may elapse between initial leader attachment and return stroke arrival, so that the distance the aircraft travels during this period must also be included within

zone 1A. This distance depends on the time required for the leader to reach the earth or other region of opposite polarity charge. A leader propagating at 1.5×10^5 m/s from 20 000 ft will require approximately 40 msec to reach the earth, during which time an aircraft travelling at 450 ft/sec would move 180 in. and the leader channel would be positioned over a spot this distance aft of its initial attachment location. For the F-106B airplane, this implies that surfaces up to 180 in. aft of the forward tip of the nose boom may fall within zone 1A. The outboard edges of wing tips are also within zone 1A for the same reason (see Fig. 8). (The arrival times of return strokes associated with the NASA F-106B airplane have not been determined, since most of the flashes encountered to date have been intra-cloud discharges at high altitudes which have not had well-defined return strokes such as occur in flashes between clouds and earth.) Finally, the upper portion of the canopy also is considered in zone 1A because it represents a significant projection above the fuselage. However, it is not known whether leaders have initially struck or originated from the canopy of the NASA F-106B airplane.

Since the airplane is moving forward when leader attachment occurs, the leaders do not remain attached to forward extremities but "sweep" aft and reattach successively to additional spots along surfaces aft of the initial strike locations. When the airplane has travelled completely through the flash channel, the channels hang onto the aircraft trailing edges, usually (but not always) for the remaining lifetime of the flash. In accordance with the zone definitions, initial attachment spots where the flash does remain attached are within zone 1B. For the F-106B airplane then, zone 1B includes the trailing edges of the wing tips, vertical fin tip, speed brake and fuselage. The zone 1B region also included the afterburner, including the area up to 14 in. inside the afterburner (Fig. 8).

In accordance with (18), surfaces which lie directly aft of zone 1A are in zone 2A, with trailing edges aft of zone 2A, falling in zone 2B. These surfaces include the elevon and rudder trailing edges. The entire top and bottom surfaces of the wings are in zone 2A, as lightning channels were observed to sweep across each of these after attaching initially to the nose boom. However, no leaders are known to have initially struck the leading edges of the wings or vertical fin; therefore, these surfaces are located in zone 2A instead of zone 1A. Swept flashes which reach the wing leading edge usually originate at the nose boom, sweep aft along either side of the fuselage, and then sweep outboard along the wing leading edge a random distance before continuing directly aft across the top or bottom surface of the wing. The tendency for swept flashes to sweep aft across the wing surfaces may be influenced by the wing leading edge sweep angle, since lightning flashes are not known to sweep outboard along straight (unswept) wings. Operational data have suggested that the critical wing sweep angle for this phenomenon may be 45 deg. The wing leading edge is swept 60 deg on the F-106B airplane.

Finally, the NASA data illustrate that much, if not all, of an aircraft surface may be exposed to "direct" or "swept" lightning strikes. In fact, there was no zone 3 on the F-106B airplane (Fig. 8). Therefore, new delta-wing aircraft designs will probably require surface protection from lightning attachment over the complete exterior, an especially significant design feature should that design incorporate surfaces of composite materials.

The digital peak counters used in the DLite system have recorded a peak current amplitude of 54 kA. Wing-tip erosion damage and the depth and size of several burn marks on the aluminum skin are physically similar to the damage created by simulated lightning discharges in the laboratory with peak current amplitudes of 100 kA. Even with lightning strikes of this magnitude, the adverse physical effects of the lightning on the F-106B airplane have been relatively minor, both structurally and electrically (8). These benign results can be attributed to the use of a metal-skinned aircraft with an hydraulic control system, and to the close attention paid to maintaining the additional lightning hardening provisions installed in this airplane. Although the technologies already exist to produce equally benign results on composite-structure airplanes using digital control systems, the results will be more difficult to achieve. Specifically, close attention will be required in the detailed design of the lightning hardening features on such aircraft, as well as to their installation on the production line and to their maintenance in the field.

AIRBORNE PHOTOGRAPHY - Removal of most paint from the exterior metal surfaces of the airplane in order to minimize the lightning dwell times made it very difficult to track the swept-stroke attachment paths because of the small size of the points. The onboard camera systems provided an alternate means of documenting these patterns. One example of the photographic coverage possible with the systems used in 1985 (20) is provided by the photographs from strike 48 of 1985. Photographs from the three cockpit-mounted still cameras, the cockpit-mounted aft-facing video camera and the upward-facing video camera are shown in Figs. 9-11, respectively. Although the fuselage-mounted, aft-facing movie camera also was triggered by the photoelectric diodes, the lightning channel was not in the field of the camera; therefore, no photographs are shown from this camera.

The lightning strike scenario for this strike is shown in Fig. 12. At the instant of strike initiation, the lightning channel orientation was inferred to be as shown in Fig. 12(a), with the entry portion of the channel descending downward from the left of the airplane centerline to the nose boom, and the exit channel continuing on to the right and downward from the exit point on the right wingtip. The initial entry channel to the nose boom can be seen in the photograph from the left forward-facing still camera (Fig. 9(a)). Most of the entry channel is blocked from view by the overhead canopy rail in the view from the right-side still camera, Fig. 9(b). The exit channel at the right wingtip can be seen in the photograph from the aft-facing still camera (Fig. 9(c)) as well as in the first two video frames from the cockpit-mounted video camera (cockpit video frame 1 at 19:30:32.795 GMT is shown in Fig. 10(a)). As the F-106B airplane flew forward through the lightning channel, the entry portion of the channel swept back over the radome along a segmented diverter strip and momentarily attached to a fastener on the right-side canopy frame. This attachment appears as the "tongue" of flame

on the right side of the still photographs in Figs. 9(a and b). The entry portion of the channel then continued to sweep back along the right side of the fuselage below the canopy rail, while the exit portion of the channel streamered aft from the right wingtip, as shown schematically in Fig. 12 (b). The aft-sweeping entry channel can be seen as the bright blur of light outside the right-side canopy glass panels in the three still photographs (Fig. 9) and in frame 3 from the cockpit-mounted video camera at 19:30:32.863 GMT (Fig. 10(b)). A portion of the entry channel above the fuselage can be seen sweeping aft in frame 1 from the upward-facing video camera (Fig. 11(a)) at 19:30:32.863 GMT. The wingtip exit channel also can be seen in Figs. 9(c) and 10(b).

There is a 66 msec lag between the appearance of the first lightning image at the right wingtip in the cockpit-mounted video camera field of view (Fig. 10(a)) and the appearance of the swept entry channel in the fields of view of both video cameras (Figs. 10(b) and 11(a)). This lag time compares favorably with the value of 57 msec computed for the F-1068 airplane to travel forward 405 in. (10.28 m), the approximate distance from the tip of the nose boom to the location of the upward-facing video camera, at a true airspeed of 349 knots (180 m/sec).

The final entry attachment point was located on the vertical tail, while the final exit point was located at the right wingtip (Fig. 12(c)). Both the entry and exit channels can be seen in frames 4-17 from the cockpit-mounted video camera (frame 4 is shown in Fig. 10(c)). The view from the upward-facing video camera, Fig. 11(b) (frame 2), for example, shows that the entry channel is located above the airplane, with the channel oriented parallel to the airplane centerline, as shown schematically in Fig. 12(c). No further lightning attachments can be seen on the F-106B airplane after frame 17 from the cockpit-mounted video camera at 19:30:33.337 GMT. However, the lightning channel is still visible in the field of view of the upward-facing video camera until its frame 21 at 19:30:33.542 GMT. Video frame 16, 19:30:33.372 GMT, from the upward-facing video camera is shown in Fig. 11(c). These video images indicate that the F-1068 airplane flew out of the lightning channel, with the channel persisting for approximately 0.2 sec afterward (see Fig. 12(d)). In summary, the on-board photographic systems were able to document that strike 4B of 1985 was a nose-to-tail swept strike fitting the definition of general strike scenario 1 described earlier in this paper, with a rejoined flash channel which persisted after airplane passage through the channel.

In addition to documenting the swept-stroke attachment patterns on the exterior of the airplane, the forward-facing still cameras are also being used in an attempt to determine the three-dimensional locations of the lightning channel with respect to the airplane (20). Three sets of simultaneous views from the two forward-facing 70-mm still cameras (20), (Figs. 9(a and b), for example) have verified the necessary fundamental assumption for photogrammetric analysis; i.e., by inspection, the same point along the lightning channel can be identified in both views. However, it has not yet been possible to accomplish photogrammetric analyses of these figures because of the inability to reconcile the views of a ground target array from the two cameras (20).

SUMMARY OF RESULTS

During the NASA Langley Research Center Storm Hazards Program, 690 direct lightning strikes were experienced between 1980 and 1985 by an F-1068 research airplane during penetrations through regions of thunderstorms where the peak values of precipitation reflectivity were less than 50 dBZ. This study produced the following results:

1. The peak strike rates of 1.4 strikes/min and 7 strikes/penetration occurred at pressure altitudes between 38 000 ft and 40 000 ft, corresponding to ambient temperatures colder than -40°C. The peak strike rate near the freezing level, where most previously reported strikes have occurred, was only 0.1 strike/min, in the altitude interval between 18 000 ft and 20 000 ft (-5°C to -10°C).
2. The thunderstorm regions with highest risk for an aircraft to experience a direct lightning strike were those areas where the ambient temperature was colder than -40°C, where the relative turbulence and precipitation intensities were characterized as negligible to light, and where the lightning flash rate was less than 10 flashes/min. However, direct lightning strikes were encountered at nearly all temperatures and altitudes.
3. The presence and location of lightning do not necessarily coincide with the presence or location of hazardous precipitation and turbulence. In addition, hazardous precipitation and turbulence are not necessarily related to one another.
4. The entire exterior surface of this airplane may be susceptible to direct lightning attachment; i.e., there is no lightning attachment zone 3 on the F-1068 airplane or on aircraft with geometries similar to that of the F-106.

REFERENCES

1. Fisher, Bruce O.; and Crabill, Norman L.: Summary of Flight Tests of an Airborne Lightning Locator System and Comparison With Ground-Based Measurements of Precipitation and Turbulence. 1980 Aircraft Safety and Operating Problems, Joseph W. Stickle, compiler. NASA CP-2170, Part 1, 1981, pp. 251-277.
2. Fisher, Bruce D.; Keyser, Gerald L., Jr.; Deal, Perry L.; Thomas, Mitchel E.; and Pitts, Felix L.: Storm Hazards '79 - F-106B Operations Summary. NASA TM-81779, Mar. 1980.
3. Fisher, Bruce O.; Keyser, Gerald L., Jr.; and Deal, Perry L.: Lightning Attachment Patterns and Flight Conditions for Storm Hazards '80. NASA TP-2087, Dec. 1982.
4. Fisher, Bruce D.: Lightning Swept-Stroke Attachment Patterns and Flight Conditions for Storm Hazards '81. NASA TM-86279, Aug. 1984.
5. Zaepfel, Klaus P.; Fisher, Bruce O.; and Ott, Merle S.: Direct Strike Lightning Photographs, Swept-Flash Attachment Patterns and Flight Conditions for Storm Hazards '82. NASA TM-87647, Feb. 1985.
6. Fisher, Bruce, D.; and Plumer, J. Anderson: Lightning Attachment Patterns and Flight Conditions Experienced by the NASA F-106B Airplane. Procs. Addendum, Eighth Inter. Aero. and Ground Conf. on Lightning and Static Elec., Ft. Worth, TX, June 1983. DOT/FAA/CT-83/15(A), pp. 26-1 - 26-14.

7. Fisher, Bruce D.; and Plumer, J. Anderson: Lightning Attachment Patterns and Flight Conditions Experienced by the NASA F-106B Airplane from 1980 to 1983. AIAA-84-0466, Jan. 1984.

8. Fisher, Bruce D.; Brown, Philip W.; and Plumer, J. Anderson: NASA Storm Hazards Lightning Research. Procs., Flight Safety Foundation 30th Corporate Aviation Safety Seminar, Dallas/Fort Worth Airport, TX, Apr. 1985, pp. 117-155.

9. Fisher, Bruce D.; Brown, Philip W.; and Plumer, J. Anderson: Research in Lightning Swept Stroke Attachment Patterns and Flight Conditions with the NASA F-106B Airplane. Procs., Tenth Inter. Aero. and Gnd. Conf. on Lightning and Static Elec., Paris, France, June 1985, pp. 152-160.

10. Usry, Jimmy W.; Dunham, R. Earl, Jr.; and Lee, Jean T.: Comparison of Wind Velocity in Thunderstorms Determined From Measurements by a Ground-Based Doppler Radar and a F-1068 Airplane. NASA TM-86348, Apr. 1985.

11. Mazur, Vladislav; Fisher, Bruce D.; and Gerlach, John C.: Lightning Strikes to an Airplane in a Thunderstorm. J. Aircraft, vol. 21, no. 8, Aug. 1984, pp. 607-611. (Supercedes AIAA-84-0468.)

12. Mazur, Vladislav; Fisher, Bruce D.; and Gerlach, John C.: Lightning Strikes to a NASA Airplane Penetrating Thunderstorms at Low Altitudes. Presented at Tenth Inter. Aero. and Gnd. Conf. on Lightning and Static Elec., Paris, France, June 1985.

13. Mazur, Vladislav; Fisher, Bruce D.; and Gerlach, John C.: Lightning Strikes to a NASA Airplane Penetrating Thunderstorms at Low Altitudes. AIAA-86-0021, Jan. 1986.

14. Pitts, Felix L.: Electromagnetic Measurement of Lightning Strikes to Aircraft. J. Aircraft, vol. 19, no. 3, March 1982, pp. 246-250. (Supercedes AIAA-81-0083.)

15. Thomas, Mitchel E.: Direct Strike Lightning Measurement System. AIAA-81-2513, Nov. 1981.

16. Lee, Larry D.; Finelli, George B.; Thomas, Mitchel E.; and Pitts, Felix L.: Statistical Analysis of Direct-Strike Lightning Data (1980 to 1982). NASA TP-2252, Jan. 1984.

17. Pitts, Felix L.; Lee, Larry D.; Perala, Rodney A.; and Rudolph, Terence H.: F-106 Data Summary and Model Results Relative to Threat Criteria and Protection Design Analysis. Presented at Inter. Conf. on Lightning and Static Elec.; Dayton, OH, June 1986.

18. Protection of Aircraft Fuel Systems Against Lightning. AC no. 20-53A, FAA, Apr. 1985.

19. SAE Committee AE4L: Lightning Test Waveforms and Techniques for Aerospace Vehicles and Hardware. Soc. Automot. Eng., Inc., June 20, 1978.

20. Brown, Philip W.: Development of and Results from Camera Systems for Recording Daytime Lightning Strikes to an Airplane in Flight. AIAA-86-0020, Jan. 1986.

21. McCarthy, Michael; and Parks, George K.: Further Observations of X-Rays Inside Thunderstorms. Geophys. Res. Letters, vol. 12, June 1985, pp. 393-396

22. von Bokern, Greg J.: In-Flight Lightning Data Measurement System for Fleet Application-Flight Test Results. Proc., National Aero. and Elec. Conf., Dayton, OH, vol. 1, May 1982, pp. 25-31.

23. Doviak, R. J., ed.: 1980 Spring Program Summary. NOAA Tech. Mem. ERL NSSL-91, Apr. 1981. (Available from NTIS as PB81-234940.)

24. Gerlach, John C.; and Carr, Robert E.: Wallops Severe Storms Measurement Capability. Preprint Vol. - Fifth Symp. on Met. Obs. and Instr., Toronto, Canada, Apr. 1983. Amer. Met. Soc. and Canadian Met. and Oceanographic Soc, pp. 449-453.

25. Bohne, Alan R.: Joint Agency Turbulence Experiment Interim Report. AFGL-TR-83-0180, July 1983.

26. Fisher, Bruce D.: Brown, Philip W.; Wunschel, Maj. Alfred J., Jr.; Burket, 1Lt. Harold O.; and Terry, Jesse L.: Joint Thunderstorm Operations Using the NASA F-106B and FAATC/AFWAL Convair 580 Airplanes. Presented at Inter. Conf. on Lightning and Static Elec., Dayton, OH, June 1986.

27. Fisher, Franklin A.; and Plumer, J. Anderson: Lightning Protection of Aircraft. NASA RP-1008, 1977.

28. Plumer, J. Anderson; Rasch, Nickolus O.; and Glynn, Michael S.: Recent Data From the Airlines Lightning Strike Reporting Project. J. Aircraft, vol. 22, May 1985, pp. 429-433. (Supercedes AIAA 84-2406).

29. Mazur, Vladislav; Gerlach, John C.; and Rust, W. David: Lightning Flash Density Versus Altitude and Storm Structure From Observations with UHF-and S-Band Radars. Geophys. Res. Letters, vol. 11, no. 1, Jan. 1984, pp. 61-64.

30. Corbin, John C.: Lightning Interaction with USAF Aircraft. Procs., Eighth Inter. Aero. and Gnd. Conf. on Lightning and Static Elec., Fort Worth, TX, June 1983. DOT/FAA/CT-83/15, pp. 66-1 through 66-6.

31. Fitzgerald, Donald R.: USAF Flight Lightning Research. Lightning and Static Elec. Conf., Dec. 1968-Part II. Conf. Papers, AFAL-TR-68-290, May 1969, pp. 123-134. (Available from OTIC as AD 693 135.)

32. Rustan, Pedro L., Jr.; and Hebert, J. L.: Lightning Measurements on an Aircraft Flying at Low Altitude. Preprints, Second Inter. Conf. on the Avia. Wea. Sys. , Montreal, Que., Canada, June 1985, pp. 220-225.

33. Lee, Jean T.; and Carpenter, O. M.: 1973-1977 Rough Rider Turbulence-Radar Intensity Study. FAA-RD-78-115, Mar. 1979.

Table 1 - Characteristics of Airborne Photographic Systems Used in 1985

Location	Camera				Lens	
	Type	Orientation	Type	Film or Imager Size	Make/Type	Description
Aft of Cockpit	Movie	Aft-facing	Milliken DBM-54	16mm	Century	F1.8, 5.7mm
Cockpit	Video	Aft-facing	GE4TN2505	0.67 in.	Century	F1.8, 5.7mm
Cockpit	Still	Aft-facing	Hassel-blad 500 EL/M	70mm	Zeiss	Distagon, F4, 40mm
Cockpit	Still (Stereo pair)	Forward-facing	↓	70mm	Zeiss	Distagon, F4, 50mm
Top of fuselage	Video	Upward-facing	GE4TN2505	0.67 in.	Century	F1.8, 5.7mm

Camera Location	Film/Sensor		Mode of Operation	Aperture	Neutral density filter	Frame rate, frame/sec (c)
	Type	Sensitivity				
Aft of Cockpit (Movie)	Kodak Ekta-chrome, MS or Video News	ASA64	Automatic (b)	F11	1.5	200
Cockpit (Video)	CID(a)	Full out-put at face plate. Il-lumination of 0.8 f.c.	Manual	F16	1.5	30
Cockpit (Still)	Vericolor II or III	ASA125 or 160	Automatic (b)	F11	None	(f)
Cockpit (Still pair)	↓		Automatic (b)	F11	None	(f)
Top of fuselage (Video)	CID(a)	Full out-put at face plate. Il-lumination of 0.8 f.c.	Manual	F16	1.5	30

TABLE 1 - Concluded

Camera Location	Type	Shutter: Rotary shutter ang., deg.	Shutter: Speed, msec
Aft of Cockpit (Movie)	Rotary	160	2.2
Cockpit (Video)	(d)	Unshuttered. See note (d)	(d)
Cockpit (Still)	Electro-optic (e)	(e) & (f)	(f)
Cockpit (Still pair)	Electro-optic (e)	(e) & (f)	(f)
Top of fuselage (Video)	(d)	Unshuttered. See note (d)	(d)

Notes:
(a) General Electric Charge Induction Device (CID). Silicon 248 x 388 pixel array.
(b) Automatic mode uses 2 photographic diodes for lightning-tripped camera actuation. Sensor response is 4.5 usec.
(c) Movie camera frame rates are for steady-state operation. Acceleration/deceleration characteristics results in 126 frames in 2 sec at 200 frames/sec.
(d) 1:1 field interlace for video frame; frame integration time of 33 msec.
(e) Electrooptical between-the-lens shutter with 50 usec response time.
(f) Camera control circuitry provided the following four functions: control of shutter speed; selection and control of single and multiple-exposures-per-frame modes; and limiting of the fogging of the film frame which was in place behind the shutter, resulting from ambient light leakage through the shutter.
The single-exposure-per-frame mode allowed selecting shutter open times from 4 sec to 1/8192 sec in $(1/2)^m$ (m=-2,-1,0,..11, 12, 13) steps. In the multiple-exposure-per-frame mode, the number of exposures could be selected in 2^n (n=1,2,3..6,7,8) steps. There was a selectable shutter-closed time over the same range of times as the shutter-opened time control. The film was advanced as soon as a shutter actuation cycle (up to a maximum of 256 shutter openings) was complete.
The time delay imposed by the camera control circuitry was in the nanosecond range and therefore not significant compared to other system delays.

Table 2 - Storm Hazards Mission Summary

CY / CATEGORIES		1980	1981	1982	1983	1984	1985	TOTAL
MISSIONS		19	24	35	40	38	19	175
PENE- TRATIONS	HIGH	23	29	191	298	273	25	839
	LOW	46	82	50	26	136	199	539
	TOTAL	69	111	241	324	409	224	1378
STRIKES:	HIGH	6	7	153	214	223	12	615
	LOW	4	3	3	0	24	41	75
	TOTAL	10	10	156	214	247	53	690
NEARBYS:	HIGH	1	9	26	110	11	11	168
	LOW	5	13	0	2	0	0	20
	TOTAL	6	22	26	112	11	11	188

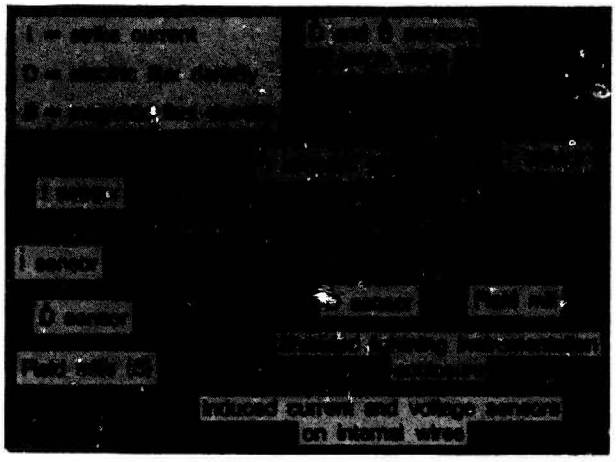

(a) Location of electromagnetic sensors on the F-106B airplane

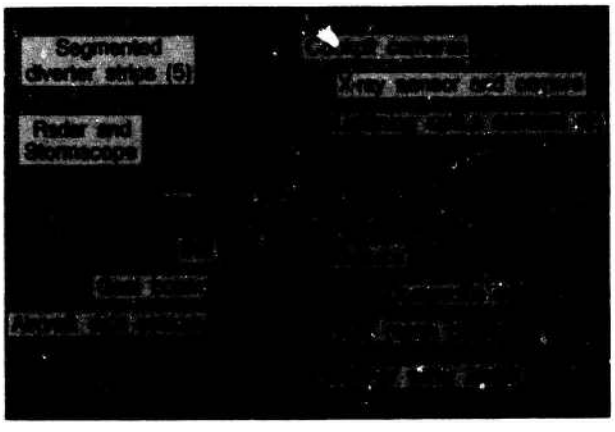

(b) Location of additional research sensors on the F-106B airplane

Fig. 1 - NASA Langley Research Center Storm Hazards '85 research vehicle

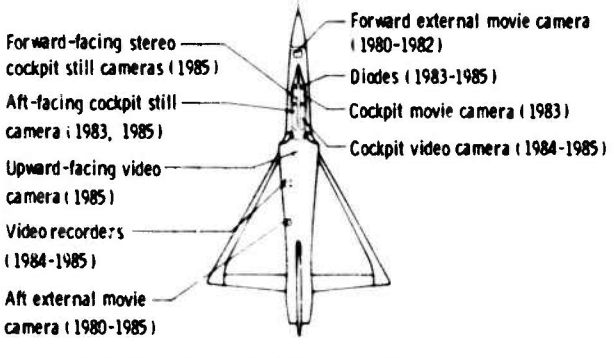

(a) Location of airborne camera systems

Fig. 2 - Airborne camera systems used on the F-106B airplane from 1980-1985

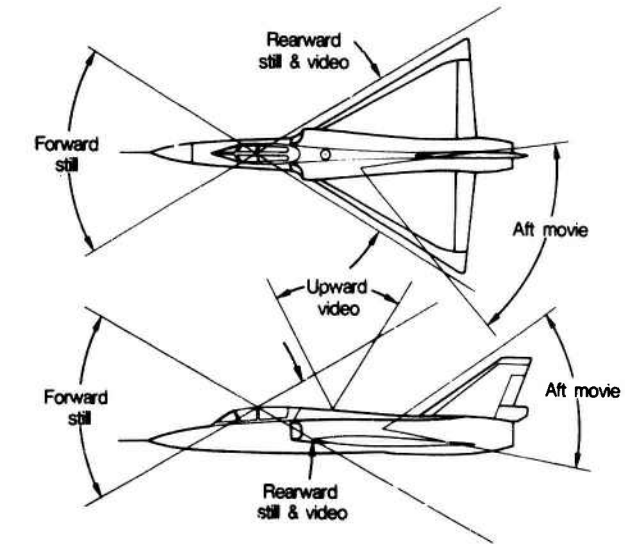

(b) Photographic and video coverage during Storm Hazards '85

Fig. 2 - Concluded

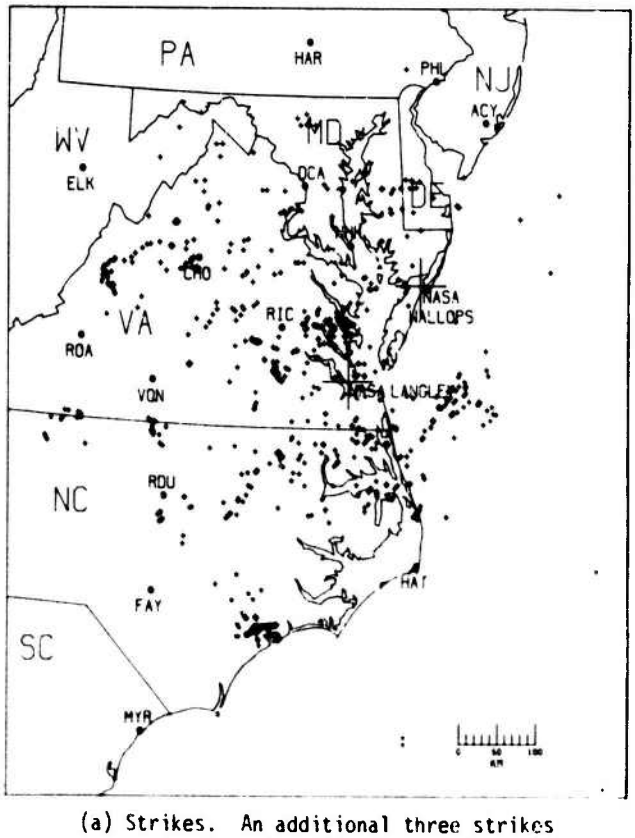

(a) Strikes. An additional three strikes occurred during flights in Oklahoma

Fig. 3 - Geographical locations of the F-106B airplane at times of direct strikes and nearby flashes, 1980-1985

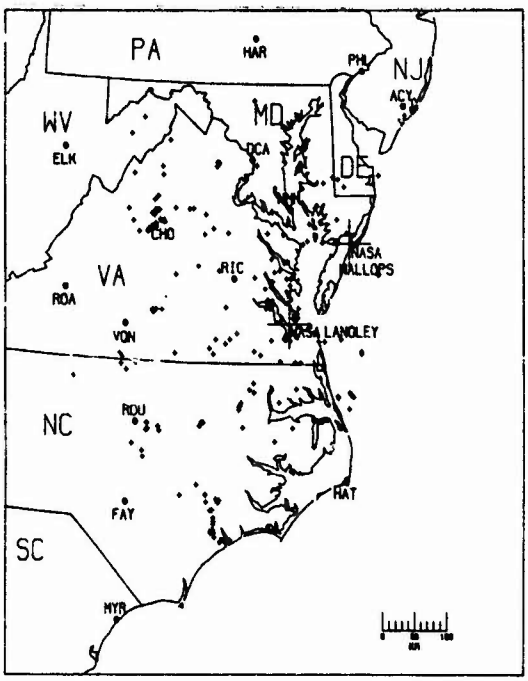

(b) Nearby flashes

Fig. 3 - Concluded

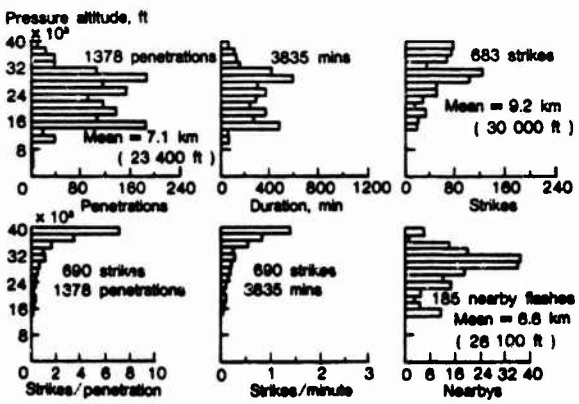

Fig. 4 - Thunderstorm penetrations and lightning statistics as a function of pressure altitude for Storm Hazards '80-'85

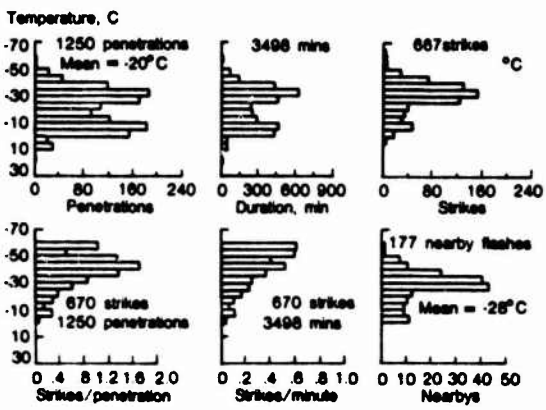

Fig. 5 - Thunderstorm penetrations and lightning statistics as a function of ambient temperature for Storm Hazards '80-'85

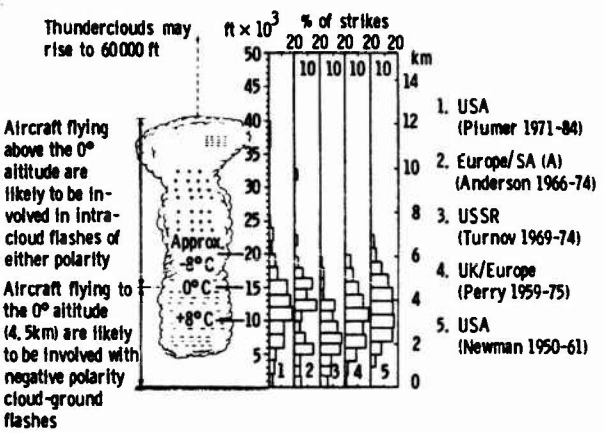

Fig. 6 - Aircraft lightning strike incidents as a function of altitude. From (27) with updated data from (28)

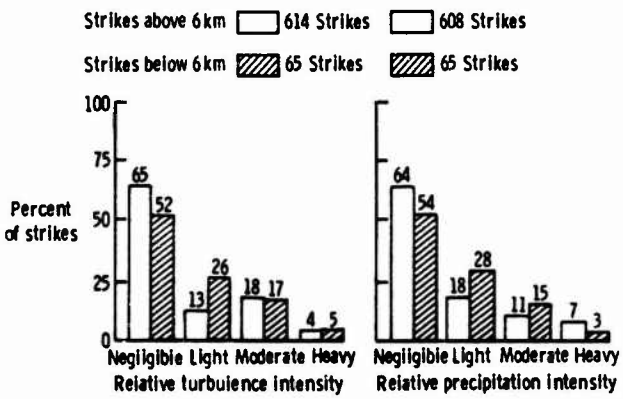

Fig. 7 - Relationship of lightning strikes to relative turbulence and precipitation intensities for Storm Hazards '80-'85

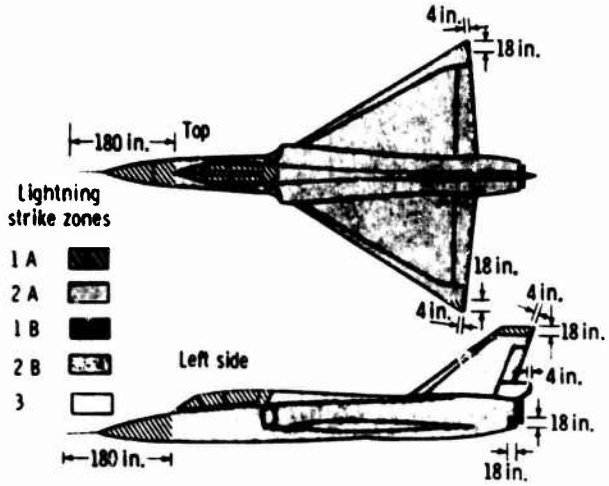

Fig. 8 - Locations of lightning attachment zones on the F-106B airplane based on Storm Hazards strike data

(a) Photograph from stereo camera on left side of cockpit showing channel attaching to nose boom with swept attachment to fastener on right-side canopy frame

(c) Photograph from aft-facing camera showing entry channel sweeping down the right side of the fuselage and the exit channel streaming aft from the right wing tip

Fig. 9 - Concluded

(b) Photograph from stereo camera on right side of cockpit

Fig. 9 - Hasselblad still photographs of strike 48 of 1985; flight 85-037; Aug. 17, 1985; altitude of 14 800 ft over Elizabeth City, NC; 19:30:32.8 GMT

(a) Frame 1 of 17. 19:30:32.795 GMT

Fig. 10 - Photographs from cockpit-mounted video camera of strike 48 of 1985

(b) Frame 3 of 17. 19:30:32.863 GMT

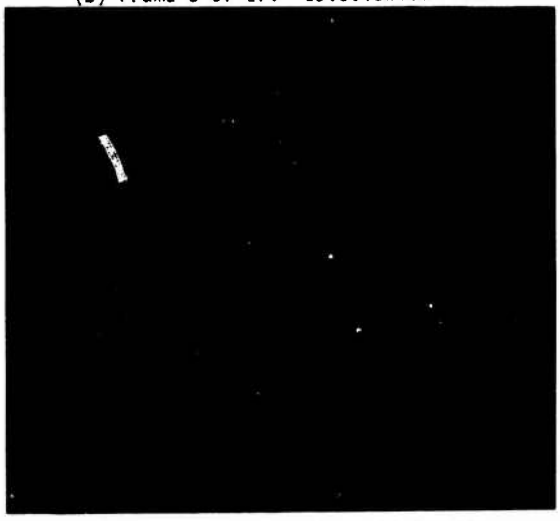

(c) Frame 4 of 17. 19:30:32.897 GMT

Fig. 10 - Concluded

(a) Frame 1 of 21. 19:30:32.861 GMT

Fig. 11 - Photographs from the upward-facing video camera of strike 48 of 1985. Nose towards top of screen; left wing towards right side of screen. The lightning channel is oriented parallel to the airplane centerline

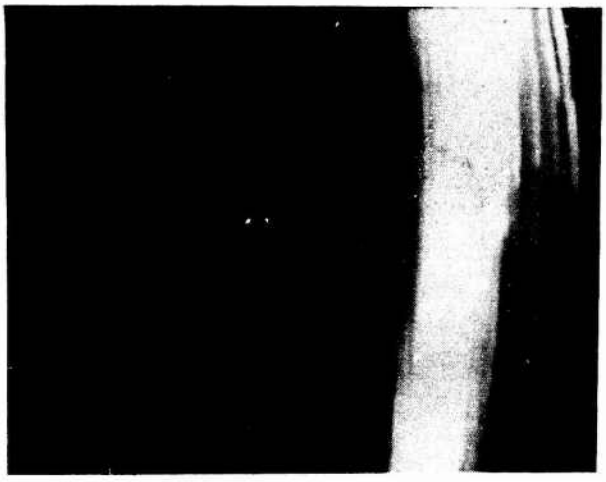

(b) Frame 2 of 21. 19:30:32.897 GMT

(c) Frame 16 of 21. 19:30:33.372 GMT

Fig. 11 - Concluded

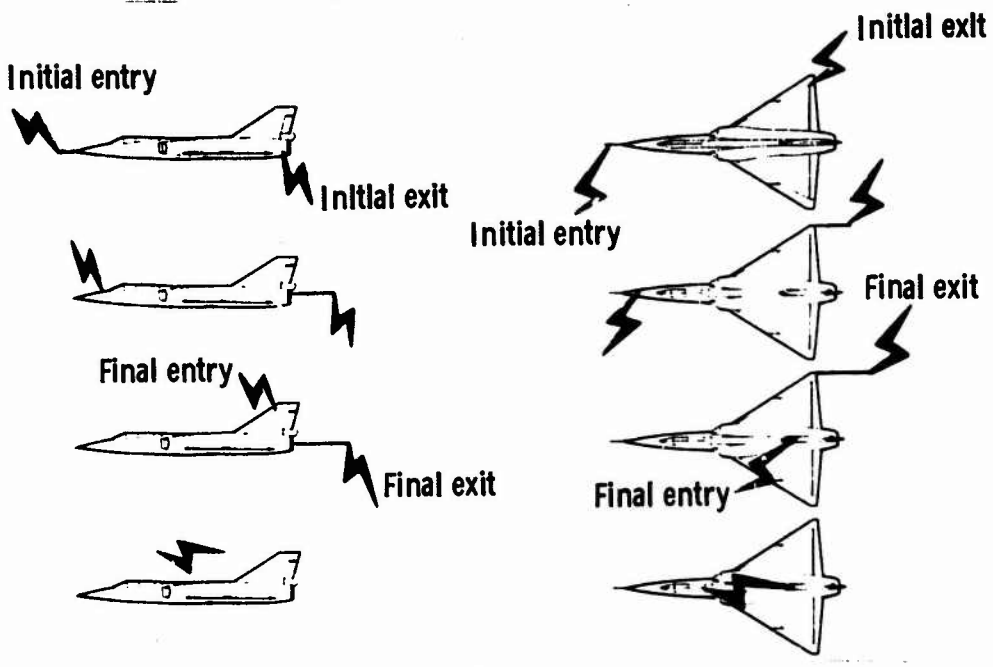

A. Initial entry at nose boom; initial exit at right wingtip.

Video frames: Cockpit 1 (Figure 10(a)) and 2/upward-none

Hasselblad photos (Figure 9)

B. Entry swept back along right side of canopy and fuselage; exit hanging onto wingtip.

Video frames: Cockpit 3 (Figure 10(b))/upward 1 (Figure 11(a))

Hasselblad photos (Figure 9)

C. Entry attached to vertical tail; exit hanging onto right wingtip.

Video frames: Cockpit 4 (Figure 10(c))-17/upward 2 (Figure 11(b))-15

D. Channel detached from airplane.

Video frames: Cockpit-none/upward 16 (Figure 11(c))-21

Fig. 12 - Lightning strike scenario for strike 48 of 1985; flight 85-037; Aug. 17, 1985

F-106 DATA SUMMARY AND MODEL RESULTS RELATIVE TO THREAT CRITERIA AND PROTECTION DESIGN ANALYSIS

Felix L. Pitts and George B. Finelli
NASA Langley Research Center, Hampton, VA 23665
Rodney A. Perala and Terence H. Rudolph
Electro Magnetic Applications, Lakewood, CO 80228

ABSTRACT

The NASA F-106 has acquired considerable data on the rates-of-change of electromagnetic parameters on the aircraft surface during 690 direct lightning strikes while penetrating thunderstorms at altitudes ranging from 15,000 to 40,000 feet. These in-situ measurements have provided the basis for the first statistical quantification of the lightning electromagnetic threat to aircraft appropriate for determining lightning indirect effects on aircraft. The data are presently being used in updating previous lightning criteria and standards developed over the years from ground-based measurements. The new lightning standards will, therefore, be the first which reflect actual aircraft responses measured at flight altitudes. The modeling technique developed to interpret and understand the direct strike electromagnetic data acquired on the F-106 provides a means to model the interaction of the lightning channel with the F-106. The reasonable results obtained with the model, compared to measured responses, yield confidence that the model may be credibly applied to other aircraft types and used in the prediction of internal coupling effects in the design of lightning protection for new aircraft.

INTRODUCTION

THE PROJECTED APPLICATION of composite structure in advanced aircraft, along with flight critical digital electronics, compounds lightning problems and motivates the need to quantify and model the lightning generated electromagnetic environment affecting aircraft. A statistical characterization of the lightning/aircraft electromagnetic interaction process is necessary to provide a theoretical basis for determining the lightning susceptibility of electronic systems aboard advanced aircraft, and to guide in devising protection measures for these systems.

The NASA Langley Research Center has conducted direct strike lightning characterization research using a specially instrumented F-106 since 1980. During these tests, the F-106 has acquired direct strike lightning data on 690 strikes at altitudes between 15,000 and 40,000 feet. Most of the strikes occurred above 30,000 feet with 43 strikes occurring between 15,000 and 20,000 feet. The goal of this research is to contribute to characterization of the lightning electromagnetic threat by establishing a credible lightning/aircraft interaction data base, obtained in-situ during direct strike flight tests, and to develop modeling techniques for use in interpreting and generalizing the data to other aircraft designs. Emphasis in the research, largely motivated by the technical community's interest in indirect effects, has been on the rates-of-change associated with the lightning external interaction with the aircraft. The acquired electromagnetic data includes the rate-of-change of current to the pitot boom, the rates-of-change of electric and magnetic flux density at a number of locations on the aircraft, and currents to the pitot boom and vertical fin.

This paper includes a summary of the direct strike data and acquisition, results of statistical analysis of the data, and a description of the lightning/aircraft interaction mathematical modeling used in data interpretation and analysis. The lightning modeling effort was performed to aid in interpretation of the data and is motivated by the need to generalize the data for other aircraft geometries and structural materials. This modeling effort has resulted in a numerical approach to modeling the interaction of lightning with the F-106 which yields results consistent with the acquired inflight strike data. Impact of the F-106 data on lightning test criteria is discussed in the final section.

DIRECT STRIKE DATA SUMMARY

The measurements made on the F-106 are electromagnetic parameters at the aircraft surface and induced voltages on a few internal wires. The electromagnetic parameters include current and rate-of-change of current on the pitot boom; current in the vertical fincap; rate-of-change of electric flux density under the forward fuselage, at the base of the vertical fin, and under the outboard section of each wing; and rate-of-change of magnetic flux density on opposing sides of the aft fuselage and under each wing at about midspan. The lightning measurements and design of the F-106 experiment are described in detail in Reference [1]* and [2], and the instrumentation is described in Reference [3]. The sensors, which are generally based on designs developed for nuclear electromagnetic pulse measurements, are described in Reference [4].

*Numbers in brackets designate References at end of paper.

The data are recorded in a shielded, self-contained instrumentation package which is mounted in the aircraft missile bay. Power for the instrumentation is obtained using a motor-generator set which decouples any lightning-induced transients in the aircraft power system to guard against spurious instrumentation system response. The electromagnetic sensors are electrically connected to the instrumentation package using foam-filled heliax cable. Control and diagnostics for the instrumentation are accomplished using fiber optic data links.

The direct strike lightning process may last up to a second or so and consists of a complex interaction of extremely fast electromagnetic pulses with the aircraft structure as discussed in References [5-7]. Three basic recording techniques which have evolved during the NASA direct strike lightning research as appropriate and complementary for investigating inflight direct strike lightning are continuous analog recorders, digital transient recorders, and peak recording instruments. The continuous analog recorders yield temporal information on the overall lightning process; they do not, however, have sufficient bandwidth to record the fast pulses with suitable fidelity. The digital transient recorders have sufficiently wide bandwidth but can record only during a small interval of the lightning event and thus yield information only on typical pulses which exceed their trigger threshold. The peak recorders supplement both the analog and digital transient recorders by obtaining information on the maximum parameter value attained during a strike.

Central to the data acquisition system in obtaining time domain information appropriate for development of lightning interaction models are the digital transient recorders which have a Nyquist bandwidth of dc to 100 Mhz operating at the maximum selectable sample rate of 5 ns per data sample. These recorders have 12 channels with 65,536 8-bit words each, yielding a data window of 327 microseconds at the maximum sample rate and have replaced the 2 channel, 131,072 6-bit word units used during the first several years of the research. The analog instrumentation tape recorders have a nominal bandwidth of 400 Hz to 100 kHz, and, for current sensors with dc response, have been frequency division multiplexed using subcarrier oscillators to obtain dc response to record the continuing current during strikes. The peak reading instruments store the maximum voltage attained by the sensor connected to its input during a flight and are specified for operation over a bandwidth equivalent to half sine pulses with base line widths between 5 ns and 10 μs.

Table 1 is a tabulation of the number of the individual time domain waveforms obtained from the various sensors during 671 strikes and the number of peak recorder readings from somewhat fewer strikes (as shown in parentheses). The column headings correspond to the various sensors and locations as described in [11]; 2574 time domain waveforms and 128 peak values have been recorded as noted in the table. The maximum value recorded to date on the peak recorder monitoring the noseboom current rate-of-change (I_B) is 380 kA/μs; the largest rate-of-change of electric flux density under the forward fuselage (D_F) exceeded the full-scale range of 97 A/m^2; and the largest peak vertical fin current (I_F)

recorded is 54 kA.

Figs. 1 through 4 show examples of the types of time domain waveforms recorded. These waveforms illustrate the overall lightning process, the triggering time of the transient recorder, and some of the wide bandwidth transient recorder data. Fig. 1 shows the current for three different strikes flowing in the tip of the vertical fin which were recorded from a current sensor with dc response on a frequency division multiplexed analog recording system also with dc response. Note the unipolar dc continuing current on the order of 80 amperes lasting 0.3 seconds, or so, with a number of pulses superimposed on it. As mentioned previously, the recording channel upper frequency response limit of 400 Hz does not allow sufficient fidelity to determine the peak values of the individual pulses and thus the channel provides information useful only in studying the overall character and temporal nature of the lightning currents. Of interest in late time lightning channel model studies, for example, is the abrupt reversal of polarity during the last 0.05 seconds of the upper trace. Also in Fig. 1, the transient recorder trigger times are shown by the arrows. Fig. 2 shows a vertical fin current recorded with a much greater time resolution of 40 ns per data sample using the transient digital recorder. This waveform has a high repetition rate with only about 50 μs spacing between the 12 kA current pulses. Figs. 3 and 4 are typical transient recorder waveforms of simultaneously recorded rate-of-change of electric and magnetic flux density from sensors located under the forward fuselage and on the side of the aft fuselage. A multitude of time domain waveforms have been published in References [8-12] which include all of the transients recorded through the 1984 tests for 627 strikes. Photographs of lightning attachments taken from on-board motion picture cameras during 156 strikes in 1982 have been published in Reference [13]. Reference [14] summarizes the strike conditions and attachment patterns studied through the 1984 tests as gleaned from the attachment photographs and lightning patterns on the aircraft structure.

ESTIMATION OF DISTRIBUTION OF PEAK RATES BASED ON PEAK RECORDER DATA

Many flights experienced multiple strikes with the number of strikes per flight ranging from 1 to 72. The peak recording instrument "saves" the largest peak of all strikes received on a given flight. Since the acquired largest peak readings are the maxima for variable numbers of strikes per flight, the logic of the peak recording technique does not allow construction of frequency-of-occurrence diagrams directly on a per-strike basis. Previous analysis, reported in Reference [15], based estimation of the statistical distribution of the peak rates-of-change on time domain records provided by the transient recorders; this data was gathered on a per-strike basis. The present statistical analysis estimates the distribution of the individual, per-strike peak values based on the largest, per-flight readings.

A nonparametric maximum likelihood estimation technique was developed and used in this analysis. (Details concerning the development of the technique are not included here but will be published at a later date.) The estimates are based wholly on the data samples and on the assumption that the peak values are the result of statistically independent processes and that the variables have a common distribution.

Boom current rate-of-change and electric flux density rate-of-change were measured by the peak recorders. Estimates of the cumulative distributions of these measurements given in Table 2 and Table 3 were derived from a likelihood function and from the previously stated assumptions. These estimates are calculated by grouping the maxima in a series of intervals having equal length, except for the last interval. The estimates are nonparametric maximum likelihood estimates because they can be calculated without assuming a particular form for the underlying distribution.

To aid in interpretation of the tables, consider the first grouping interval of the I-dot data. Here, [0,50) refers to a left closed and right open interval in the usual mathematical sense, i.e. all values greater than or equal to 0 but less than 50 kiloamperes per microsecond are included. For this interval there were 27 flights during which 125 strikes were sustained wherein the largest peak boom current rate-of-change was less than 50 kiloamperes per microsecord. The maximum likelihood estimate of the proportion of strikes giving peak rates-of-change of current less than 50 kiloamperes per microsecond is 0.8762, meaning that on average, 87.62 percent of the strikes gave peak values less than 50 kiloamperes per microsecond. Similarly, there were 13 flights covering 120 strikes wherein the largest peak boom current rate-of-change was between 50 and 100 kiloamperes per microsecond with the maximum likelihood estimate of the proportion of strikes with peak rates-of-change in this interval being 0.0749. Adding the two proportions yields 95.11 as the estimated percentage of strikes with peak rates-of-change less than 100 kiloamperes per microsecond, and so forth for the rest of the table.

The data were obtained with sensors designed to measure rates-of-change in the differential sense, and thus represent the peak instantaneous rate-of-change as opposed to an average change over a long time interval. As mentioned earlier, the data were recorded over an altitude range from 15,000 to 40,000 feet.

LINEAR LIGHTNING/AIRCRAFT INTERACTION MODELING

In order to understand and interpret the lightning data collected, it is necessary to model the lightning/aircraft interaction. The model developed for this investigation is based on the finite difference methodology first developed by Yee in Reference [16]. The methodology of the finite difference modeling will be discussed briefly, followed by specific descriptions of the linear modeling technique, selected results from the model, and comparisons with measured flight data.

The main analytical tool used in the analysis of the lightning/aircraft interaction is the computer code T3DFD, which stands for Time domain 3 Dimensional Finite Difference code. The code solves Maxwell's equations in three dimensions, and is capable of modeling complex geometries, and space and time varying permittivity, permeability, and conductivity. The particular problem space is a cartesian mesh enclosing a space approximately twice the size of the aircraft itself. The spatial resolution is one meter in the direction along the fuselage and one-half meter in the wing-wing and vertical directions. The temporal resolution of the model is one nanosecond. The nominal frequency resolution of the mesh, assuming a minimum of five cells per wavelength, is therefore 60 MHz. The F-106 is placed within the problem space by insuring that all electric fields tangential to the surface

are zero at all times. Hence, the aircraft is assumed to be perfectly conducting, with no significant apertures to alter the external response. This is a good approximation except for the immediate vicinity of the cockpit.

The F-106 as it appears in the finite difference code is shown in Fig. 5. The coordinate system is also indicated in Fig. 5, as are the locations of the external sensors which were modeled. The large scale structure of the aircraft is well resolved, but it is clear from the nature of the block model that details (such as the nose boom) are not well resolved. In most cases, however, the model as shown is adequate to predict the response of the sensor system to a given lightning event. This is because the sensors have been placed away from those portions of the aircraft that are not well resolved by the finite difference code.

Linear modeling of the lightning/aircraft interaction can be very useful in many situations. If one assumes that the current flowing onto the aircraft is given as a function of position and time, the calculation of the aircraft sensor responses from that current can be accomplished linearly. A technique employing the use of transfer functions has been developed to determine the lightning current which caused a given set of measured electromagnetic responses on the aircraft. The transfer function is a functional relationship in the frequency domain between a source function and a response function. The use of a transfer function requires that the system under consideration be linear. This requirement is satisfied by a linear finite difference code, but is, of course, not satisfied by a real lightning/aircraft system. The justification for using the transfer function technique is that the nonlinearity in the real system is confined mostly to the lightning channel itself. The electromagnetic responses on the aircraft are quite often approximately linear functions of the lightning current which flows onto the aircraft at the lightning attachment point. That is, although the formation of the lightning channel, its evolution, and the lightning current are complicated nonlinear functions of geometry and initial conditions, the aircraft responses usually depend in a linear fashion only on the current at the attachment point.

There are four assumptions which must be made using the transfer function technique. These are discussed individually below.

(1) Lighting Attachment Locations Must be Known. These locations are necessary to define the problem for analysis using the T3DFD computer code. In addition, the attachment locations cannot change with time. Also, if there are multiple channel attachments, only one of these can act as a source, while the others just drain charge from the aircraft. Although having more than one source does not violate linear constraints, the problem no longer has a unique solution if more than one source is involved.

(2) Relative Formation Times of Multiple Channels Must be Known. Because it is likely that exit channels for lightning current form later than entry channels, it is necessary to have knowledge of their formation times. In a sense, these channels which appear during the course of a problem constitute boundary conditions which change with time. This does not violate the linearity requirement as long as the formation times are fixed and do not vary with the time evolution of the problem.

(3) Lightning Channel Geometry Should be Known. Although less important than the first two requirements, it is desirable to know the orientation of the lightning channel with respect to the aircraft. This also constitutes boundary conditions which can affect aircraft responses to some extent. The responses are affected because electromagnetic radiation from current in the channel also produces some response on the aircraft, in addition to the current which flows onto the aircraft. The contribution of the current is much larger, however, so the channel radiation can be considered as a perturbation.

(4) Lightning Channel Impedance Should be Known. This is of lesser importance than the first two requirements, but can affect the linear relationship between source and response somewhat. The reason for this is that the back effect of the aircraft on the lightning current is different depending on the channel impedance. For example, a channel with infinite impedance is completely unaffected by the presence of the aircraft. In this case, whatever current is flowing in the channel is the current which is injected onto the aircraft, and reflections and responses on the aircraft behave as if the channel were nonexistent. For any other impedance, the response of the aircraft can affect the current in the channel. This then alters the responses on the aircraft slightly. Hence, it is desirable to know the channel impedance as a boundary condition on the problem. It is possible to handle a time-varying impedance, as long as the variation is specified in advance, and does not depend on the evolution of the problem.

The transfer function technique can be used either for triggered or natural lightning. The distinction between the two is that triggered lightning begins at the aircraft and moves away, while natural lightning begins away from the aircraft and moves toward it. Typical geometries for each of these cases are shown in Fig. 6. The case for natural lightning is shown in Fig. 6a. A current channel having a specified impedance and velocity of propagation is attached to the nose of the F-106. The impedance and velocity of propagation are determined from the per unit length inductance and capacitance of the channel, which are in turn determined from the physical diameter of the channel. Therefore, in the linear model, the size of the lightning channel determines all of its electrical properties. The attachment to the nose depicted in Fig. 6 is simply a concession to the point at which many lightning strikes attach to the F-106. The model allows attachment at any point on the aircraft and, in fact, allows multiple channels as long as there is only one current source in the problem. The sole difference between Figs. 6a and 6b is in the location of the current source. For natural lightning, it is located at the edge of the problem space, as far from the aircraft as possible. This is done in an effort to model the fact that the initiating and driving forces for a natural lightning strike occur away from the aircraft, and the lightning current propagates toward the plane. The current source in Fig. 6b is located near the point where the channel attaches to the F-106. This models the phenomenon of initiation at the surface of the aircraft with propagation outward.

The mathematics of the model is handled identically in the two cases. A transfer function

is determined from the Fourier transforms of the current source and the response waveforms.

$$T(\omega) = R(\omega)/I(\omega) \qquad (2)$$

Here $T(\omega)$ is the transfer function in the frequency domain, $R(\omega)$ is the Fourier transform of the calculated response waveform, and $I(\omega)$ is the Fourier transform of the current source waveform. Because the model is linear, $T(\omega)$ is source independent; that is, changing I will change R in such a way as to keep T the same. Note that there can be as many transfer functions as there are separate responses on the aircraft. If there are N sensors on the aircraft, there will be N different transfer functions for a single current source.

To determine the current source necessary to produce a given measured response, $R_m(\omega)$, the measured response waveform must be Fourier transformed. Then the transfer function for the particular sensor is used to calculate the Fourier transform of the current source necessary to produce the measured response.

$$I(\omega) = R_m(\omega)/T(\omega) \qquad (3)$$

The current is then transformed into the time domain. It can then be used in the linear model as a check, to make sure the measured response is reproduced. It should be noted that the current source, $I(\omega)$, in equation (3) is not necessarily the same as the current injected on the aircraft in the lightning strike. The current source is a mathematical artifice used to drive the lightning channel. The aircraft attached to the lightning channel establishes the actual injected lightning current for a given current source. The current source can be thought of as a normalized current, because it would represent the lightning current if the aircraft were replaced by a continuation of the lightning channel.

The transfer function technique is useful in modeling interactions where multiple simultaneous sensor responses have been recorded; several current sources can be derived, one for each of the multiple responses. In principle, if the model geometry chosen is correct, all of the current sources should be the same. This is virtually never the case, however, for the following reasons. The channel geometry may be incorrect. Attachment points are usually determined by direct observation of the strike, or examination of pit marks after a flight. If this information is unavailable, ratios of sensor response amplitudes can be used to give a crude idea of attachment locations. In addition to the uncertainty of attachment locations, the presence of multiple channels and the timing of their appearance is often unknown. Also, the orientations of the attached channels are uncertain. Even if the channel orientation were known precisely, it would probably be difficult to model accurately if a significant amount of bending or tortuosity were present. The electrical properties of the channel are generally unknown, too, so an estimate must be made. Another source for error in the model is the gridding of the F-106 itself. Because of the .5m x 1m x .5m cell size, the aircraft cannot be represented in the problem space to arbitrary precision. This results in slight differences between the responses of the real aircraft and the model aircraft even if channel properties and attachment locations are known exactly. The differences are largest in places where the grid resolution is most inadequate, such as wing tips, nose, tail tip, and sharp leading and trailing surfaces. In most cases, the F-106 sensors are located away from these regions, but some inaccuracy is expected.

The modeling procedure, in view of these difficulties, is to calculate all of the current sources for a given geometry, and then to analyze the differences found. If all of the sources are similar, it may be that the geometry chosen is close to the physical situation of the actual lightning strike. If large differences are present, the model geometry must be changed significantly.

In practice, the derived sources are heavily dependent on attachment point and much less dependent on all other factors. Hence, if the attachment point is accurately chosen, it is very likely that the derived current sources will all be similar. This is evidence that the aircraft responses are strong functions of the injected lightning current.

The transfer function technique has been applied to measured responses from Flight 84-017. An example of the calculated responses overlaid on the measured responses is shown in Fig. 7. For this case, the transfer function to calculate nose current was based on the B-dot longitudinal sensor, so the matching for that sensor is exact to within numerical limitations as shown on Fig. 7(a). The comparison for some of the other sensor points (particularly D-dot on the left wing), are quite good, lending credence to the choice of the nose of the aircraft as the lightning channel location.

This example shows that the transfer function technique can be used to model the interaction of a lightning channel with the F-106 aircraft. All of the sensor responses can be modeled simultaneously, and the entering current can be determined assuming that the channel location is known or can be inferred from available data.

The transfer function technique has been used to analyze the response of the F-106 to a moderate intensity, high peak rate-of-change current pulse. The current was injected at the nose of the aircraft and allowed to leave from a preformed exit channel on the vertical stabilizer. The current waveform was a sine squared leading edge of one microsecond rise time to a constant amplitude of 50 kA with a peak rate-of-change of about 75 kA/μS. Although the interaction between the aircraft and the lightning strike is expected to be nonlinear for such a high current, it is of interest to investigate the linear responses as upper limits of the expected responses. The calculated responses are shown in Figure 8. The response amplitudes are typical of amplitudes which have been measured on the F-106. However, the duration of the F-106 measurements is typically shorter than the calculation indicating that most of the measurements were associated with lower intensity currents which had a relatively high peak rate-of-change. The technique has been used to investigate the response of four additional aircraft of varying shapes and sizes including a double- and half-size F-106, a "straight winged" F-106, and a C-130. As expected, the responses were largest for the smaller aircraft. The D-dot responses scaled roughly with the surface area of the aircraft, and the B-dot responses scaled with the linear size.

The transfer function technique has also been used to investigate the effect of varying the characteristics of the lightning channel which supplies current to the aircraft. Two different channel radii (1 cm and 10 cm) and three different resistances per unit length (1 ohm/m, 10 ohm/m, 50

ohm/m) were examined. The intent of varying these parameters was to determine if any change occurred in the injected lightning current. If there was a change, then the channel impedance had a significant effect on the aircraft response; if there was no change, then the channel impedance did not matter. The results are shown in Figs. 9 and 10, which overlay the measured nose current from Flight 84-017 with the calculated currents. Notice that there is virtually no difference between the currents for the various channels. This indicates that the channel impedance is unimportant for the determination of aircraft responses over this range of channel radii and resistance per unit length.

IMPACT ON FORMULATION OF CRITERIA

Lightning hazards to aircraft are generally thought of as being divided into two types. The first type, direct effects, refers to the physical damage that can occur on an aircraft, such as pitting, burning, magnetic deformation, and destruction of dielectric materials such as radomes. The second type, indirect effects, refers to the hazards caused by electromagnetic coupling. These hazards take the form of transient voltages and currents induced on antennas and cables connecting various electronic boxes. These transients can cause damage or upset of flight or mission critical electronic systems. Because the F-106 data is primarily useful for indirect effects, the scope of the remainder of this discussion will be limited to this topic.

INTERNAL COUPLING OF LIGHTNING INDUCED ELECTROMAGNETIC FIELDS - In order to understand the impact of the lightning research program on the formulation of criteria, it is first necessary to discuss how energy couples into electronic systems. The overall coupling problem is usually considered as being separated into two parts. The first part, external coupling, refers to the generation of surface currents and charges (or tangential magnetic fields, H, and normal electric fields, E) by a lightning event. The second part, internal coupling, refers to the generation of electromagnetic fields, currents, and voltages on elements of the aircraft interior.

Conceptually, it is usually thought that the two parts can be treated separately, and that the external coupling problem defines the sources which then drive the internal response. This is a good approximation if the internal coupling events do not significantly "feed back" and alter the external coupling results. Usually this is the case except for perhaps large apertures such as an open bomb bay or wheel wells.

There are three basic mechanisms for penetration of electromagnetic energy into an aircraft interior: apertures, exposed conductors, and diffusion. Apertures refer to openings in the aircraft skin, and include such items as the cockpit, wheel wells, engine exhaust, seams on doors and panels, and areas covered by dielectrics such as kevlar or fiberglass. Exposed conductors include antennas of various kinds, pitot tubes, and perhaps electrical or control cables in some cases. These may be excited either by lightning directly attaching to them, or by the induced fields from lightning attached elsewhere on the aircraft. Diffusion is usually important only for carbon fiber composite (CFC) materials. A surface current $J_s(\omega)$ induces an internal tangential electric field $E_s(\omega)$ by means of the surface transfer impedance $Z_t(\omega)$ according to

$$E_s(\omega) = Z_t(\omega)J_s(\omega) \qquad (4)$$

where

$$Z_t(\omega) = \frac{\eta(\omega)}{\sinh k(\omega)d} \qquad (5)$$

and where ω is the angular frequency, d is the material thickness, and $\eta(\omega)$ and $k(\omega)$ are the intrinsic impedance and the propagation constant, respectively, of the surface material (e.g., CFC). At late times (or, alternatively, low frequencies), equation (4) reduces to the resistive voltage drop along the surface.

It is useful to summarize the parameters which are important to lightning coupling through these penetrations. In order to do so, a simple model of an internal or exposed cable is employed and is shown in Fig. 11. The cable is approximated by a transmission line of characteristic impedance Z_0 and having termination loads on each end of impedances Z_1 and Z_2 as shown. The electromagnetic coupling sources are approximated in this illustration as point sources which include a series voltage source V_s and a shunt current source I_s as shown. In the figure, the transmission line is indicated schematically by its equivalent circuit model.

Included in Fig. 11 is a table of the penetrations of interest and the lightning coupling variable upon which the source V_s or I_s linearly depends. That is to say, for example, that the source V_s for an open hole aperture is a constant times $\dot{B}$. In parenthesis is shown how the source variable relates to the lightning current, which in this example is $\dot{I}$.

It should also be pointed out that the table does not by itself give the entire picture with respect to what is important for coupling. For example, if Z_1 and Z_2 are small or zero, and the cable is short with respect to wavelengths in the lightning pulse (which is often the case), then for aperture coupling dominated by the B field, the current I_1 is proportional to B(I), because I_1 for this situation is simply proportional to the time integral of V_s. Therefore, even though V_s is proportional to $\dot{I}$, I_1 is proportional to I. On the other hand, if Z_1 and Z_2 are large, then V_1 relates to $\dot{I}$, and not I.

In addition, because in some cases the transient responses of the cable are related to $\dot{I}$, the total waveshape of I is important. This also requires that the energy delivered to a load be quantified, which places a requirement on the action integral, $\int_0^\infty I^2 dt$. This would be particularly important for damage of electronics as well as upset. Therefore, even for aperture coupling $\dot{I}$, I, $\dot{B}$, and $\int_0^\infty I^2 dt$ are all important. For diffusion, only I and $\int_0^\infty I^2 dt$ appear to be important.

There are other requirements placed on the knowledge of lightning environments by system considerations. For example, upset of a digital system is determined by the amplitude of a pulse, the pulse width, and the repetition rate of pulses. Therefore, specifications on these parameters are also of interest.

An example of a comparison of a calculation and a measurement on an internal wire based on the model of Fig. 11 is shown in Fig. 12. The wire is inside the F-106 fuselage and is 9m long, shorted to structure on one end, and terminated in 50 Ω on the other end. The wire routes past some closed wheel well doors whose seams in the analysis were modeled as inductive seams because of their large gaps. The lightning nose current I is given in Figure 7. By inspection, it is clear that the large oscillations dominating the current response are related to the derivative of nose current. This is plausible when one considers that the wire inductance is found to be 1.5 μH, and the L/R time constant with the 50 Ω load is only 30 ns, much shorter than the period of oscillation (~ 250 ns) of the cable current. In this frequency regime, the current response is limited by the 50 Ω load impedance, which is a large impedance compared to the cable inductance. Therefore, the induced current (or voltage) would be proportional to $\dot{I}$, which is clearly the case.

It should also be pointed out that this is an example of an internal wire response caused by a lightning event of low peak current, but high $\dot{I}$ ($\approx 2 \times 10^{10}$ A/s peak). It produces an internal current pulse having frequencies related to aircraft and cable resonances. It is conceivable that the resonant frequencies could be close to that of clock frequencies for computer systems. Therefore, the possibility exists for a pulse of this low amplitude, by virtue of its high frequency spectral content, to affect computer operations.

RELATIONSHIP OF F-106 DATA TO EXISTING CRITERIA - Previous estimates of the inflight lightning hazard to aircraft were inferred from ground-based measurements. The electromagnetic measurements made on the F-106 aircraft during these strikes have established the statistical basis for determination of quantities and "worst case" amplitudes of electromagnetic parameters such as current rate-of-change, and the rates-of-change of electric and magnetic flux density. The research results have contributed to basic scientific knowledge by quantifying with these parameters the electromagnetic interaction of lightning with aircraft. These data are currently being used by the Federal Aviation Administration and the Department of Defense in updating or replacing previous lightning criteria and standards developed over the years from ground-based measurements of lightning strikes to instrumented towers. The new lightning criteria and standards will, therefore, be the first which reflect actual aircraft responses to lightning measured at flight altitudes.

It should be pointed out that at the present time there are no specifications on $\dot{D}$ or on the temporal durations of $\dot{I}$ or $\dot{D}$ exceeding a prescribed value. The F-106 data are being used for determining criteria for these environments which are presently a subject of interest in the lightning community.

IMPACT ON TESTING - The testing of aircraft to lightning indirect effects is a subject of much current interest in the lightning community. The main issues of interest include $\dot{I}$, $\dot{D}$, the temporal durations of $\dot{I}$ and $\dot{D}$, and the late time currents which are important for diffusion through CFC structures. Approaches which have been used to increase both $\dot{I}$ and $\dot{D}$ include the use of discrete peaking capacitors [17-20], distributed peaking capacitors [21], high voltage oil-filled, low inductance Marx generators [22-23], and the so-called shock excitation techniques [24]. In order to increase late time currents, a crowbar switch is used to provide for an exponential decay of a Marx generator as opposed to the normal damped sinusoid [25]. It is clear that there is no consensus on the best way to accomplish these types of tests.

The impact on testing of the new criteria for $\dot{I}$, $\dot{D}$, and their temporal durations is not fully known, but some general observations can be made. In order to increase $\dot{I}$ or $\dot{D}$, and to lengthen their duration, either the use of peaking capacitors with high inductance Marx generators, or low inductance oil-filled Marx generators are needed. A low voltage capacitor bank can possibly also be used but the transmission line return conductor system must be carefully designed and be very close to the aircraft under test [26]. The relative expense of providing large values of these parameters increases greatly as the size of the test object increases. For example, testing a vehicle the size of a large transport aircraft at $\dot{I} = 2 \times 10^{11}$ A/s is not within the state of the art, but this type of test can be done on fighter size aircraft.

CONCLUDING REMARKS

The NASA F-106 has acquired considerable data on the rates-of-change of electromagnetic parameters on the aircraft surface during 690 direct lightning strikes while penetrating thunderstorms at altitudes ranging from 15,000 to 40,000 feet. These in-situ measurements have provided the basis for the first statistical quantification of the lightning electromagnetic threat to aircraft appropriate for determining lightning indirect effects on aircraft. The data are presently being used in updating previous lightning criteria and standards developed over the years from ground-based measurements. The new lightning standards will, therefore, be the first which reflect actual aircraft responses measured at flight altitudes. The modeling technique developed to interpret and understand the direct strike electromagnetic data acquired on the F-106 provides a means to model the interaction of the lightning channel with the F-106. The reasonable results obtained with the model, compared to measured responses, yield confidence that the model may be credibly applied to other aircraft types and used in the prediction of internal coupling effects in the design of lightning protection for new aircraft.

REFERENCES

1. F.L. Pitts; M.E. Thomas; R.E. Campbell; R.M. Thomas; and K.P. Zaepfel: "In-Flight Lightning Characteristics Measurement System." Federal Aviation Administration - Florida Institute of Technology Workshop on Grounding and Lightning Technology, FAA-RD-79-6, March 1979, pp. 105-111.

2. Felix L. Pitts: "Electromagnetic Measurement of Lightning Strikes to Aircraft." AIAA Journal of Aircraft, Vol.19, No.3, March 1982, pp.246-250.

3. Mitchel E. Thomas: "Direct Strike Lightning Measurement System." AIAA/SETP/SFTE/SAE, 1st Flight Testing Conference, Las Vegas, Nevada, Nov. 1981, AIAA 81-2513.

4. Thomas F. Trost and Klaus P. Zaepfel: "Broadband Electromagnetic Sensors for Lightning Research." NASA CP-2128, FAA-RD-6-30, Lightning Technology, NASA Langley Research Center, April 22-24, 1980, pp. 131-152.

5. Thomas F. Trost and Felix L. Pitts: "Analysis of Electromagnetic Fields on an F-106B Aircraft During Lightning Strikes." International

Aerospace Conference on Lightning and Static Electricity, St. Catherines College, United Kingdom, Vol. I, March, 1982, p. B3-3.

6. P.L. Rustan, Jr.; and J.P. Moreau: "Aircraft Lightning Attachment at Low Altitudes." 10th International Aerospace and Ground Conference on Lightning and Static Electricity, Paris, France, June 1985, p. 262.

7. J.P. Moreau, and J.C. Alliot: "E and H Field Measurements on the Transall C160 Aircraft During Lightning Flashes." 10th International Aerospace and Ground Conference on Lightning and Static Electricity. Paris, France, June 1985, p.282.

8. Felix L. Pitts and Mitchel E. Thomas: "1980 Direct Strike Lightning Data." NASA TM-81946, Feb. 1981.

9. Felix L. Pitts and Mitchel E. Thomas: "1981 Direct Strike Lightning Data." NASA TM-83273, March 1982.

10. Mitchel E. Thoms and Felix L. Pitts: "1982 Direct Strike Lightning Data." NASA TM-84626, March 1985.

11. Mitchel E. Thomas: "1983 Direct Strike Lightning Data." NASA TM-86426, Aug. 1985.

12. Mitchel E. Thomas: "1984 Direct Strike Lightning Data." NASA TM-87690, March 1986.

13. Klaus P. Zaepfel, Bruce D. Fisher, and Merle S. Ott: "Direct Strike Lightning Photographs, Swept-Flash Attachment Patterns, and Flight Conditions for Storm Hazards '82." NASA TM-86347, Feb. 1985.

14. B.D. Fisher, P.W. Brown, and J.A. Plumer: "Research in Lightning Swept Stroke Attachment Patterns and Flight Conditions with the NASA F-106B Airplane." 10th International Aerospace and Ground Conference on Lightning and Static Electricity, Paris, France, June 1985, pp. 267-280.

15. L.D. Lee, G.B. Fin elli, M.E. Thomas, and F.L. Pitts: "Statistical Analysis of Direct-Strike Lightning Data (1980 to 1982)." NASA TP-2252, Jan. 1984.

16. K.S. Yee: "Numerical Solution of Initial Boundary Value Problems Involving Maxwell's Equations in Isotropic Media." IEEE Transactions Ant. & Prop., AP-14, May 1966, pp. 302-307.

17. J.D. Robb and R.A. Perala: "Evaluation of a Fast Risetime, High Current Lightning Indirect Effects Simulator." Presented at and published in the Proc. of the Int. Aerospace Conf. on Lightning and Static Electricity, Oxford, England, March 1982.

18. R.A. Perala and J.D. Robb: "Measurements with Theoretical Analysis of a Full Scale NEMP Type Lightning Simulator for Aerospace Vehicles." DOT/FAA/CT-83/25, Proceedings of the 8th International Aerospace and Ground Conference on Lightning and Static Electricity, Ft. Worth, Texas, June 1983.

19. R.A. Perala and S.L. Parker: "Numerical Modeling of the Response of an Aircraft in a Fast Risetime Threat Level Lightning Simulator." EMA-83-R-18, March 1983.

20. J.L. Herbert, L.C. Waiko, and J.G. Schneider: "Design of a Fast Risetime Lightning Generator." Proceedings of the 10th Int. Aerospace and Ground Conference on Lightning and Static Electricity, Paris, France, June 1985.

21. R.A. Perala, T.H. Rudolph, and P.M. McKenna,: "The Use of a Distributed Peaking Capacitor and Marx Generator for Increasing Current Rise Rates and the Electric Field for Lightning Simulation." NADC-84104-20, Proceedings of the International Aerospace and Ground Conference on Lightning and Static Electricity, Orlando, Florida, June 1984.

22. J.L. Harrison, Y.G. Chen, F. Galicki, and W. Richardson: "A Threat Level Lightning Simulator." To be presented at the 11th Annual Int. Aerospace and Ground Conf. on Lightning and Static Electricity, Dayton, Ohio, 1986.

23. R.A. White: "Lightning Simulator Circuit Parameters and Performance for Severe-Threat High Action Integral Testing." NADC-84104-20 Proceedings of the International Aerospace and Ground Conference on Lightning and Static Electricity, Orlando, Florida, June 1984.

24. W.G. Butters, D.W. Clifford, K.P. Murphy, K.S. Zeisel, and B.P. Kuhlman: "Assessment of Lightning Simulation Test Techniques." Proceedings of the International Conference on Lightning and Static Electricity, Oxford, U.K., March 1982.

25. R.A. Perala, P.M. McKenna, T.H. Rudolph, and J.D. Robb: "Implementation of a Crowbar Switch in a Marx Generator/Peaking Capacitor Lightning Simulator System." Proceedings of the 1985 Int. Conf. on Lightning and Static Electricity, Paris, France, 10 June 1985.

26. B.J.C. Burrows, et al. "Induced Voltages in Full Size Aircraft at 10^{11} A/s." Proceedings of the 1977 IEEE Int. Symposium on Electromagnetic Compatibility, Seattle, Washington, 1977.

TABLE 1 - TOTAL DATA BASE THROUGH 1985

	$\dot{B}_L$	D_F	$\dot{D}_F$	I_B	$\dot{I}_B$	$\dot{B}_T$	$\dot{D}_T$	$\dot{D}_{WL}$	D_{WR}	$\dot{D}_{WR}$	B_{WL}	$\dot{B}_{WL}$	$\dot{B}_{WR}$	I_{VF}	INT. RESP.
o 1982 and prior	46		93	27	8										
o 1983	166		216	17	56	23	56	24	15		16	34	48	39	29
o 1984	119	117	105	120	126		125	105		91		43	37	120	150
o 1985	27		41	3	38		40			44		41	40	14	115
o 2574 total wave-forms	358	117	455	167	228	23	221	129	15	135	16	118	125	173	294
o 128 peak values (strikes)			62 (399)	2 (13)	60 (418)									6 (49)	

TABLE 2 - DISTRIBUTION OF PEAK BOOM CURRENT RATE-OF-CHANGE

INTERVAL KILOAMPERE PER MICROSECOND	#FLIGHTS	#STRIKES	MAXIMUM LIKELIHOOD ESTIMATE	CUMULATIVE PERCENTAGE %
[0,50)	27	125	0.8762	87.62
[50,100)	13	120	0.0749	95.11
[100,150)	5	21	0.0188	96.99
[150,200)	4	47	0.0135	98.34
[200,250)	3	50	0.0088	99.22
[250,300)	1	20	0.0027	99.49
[300,350)	1	3	0.0026	99.75
[350,400)	1	9	0.0025	100.0

TABLE 3 - DISTRIBUTION OF PEAK RATE-OF-CHANGE OF ELECTRIC FLUX DENSITY

(D-DOT SENSOR UNDER FUSELAGE 6 FEET FORWARD OF NOSE GEAR STRUT)

INTERVAL AMPERE PER SQUARE METER	#FLIGHTS	#STRIKES	MAXIMUM LIKELIHOOD ESTIMATE	CUMULATIVE PERCENTAGE
[0,6)	1	1	.098	9.8
[6,12)	3	5	.197	29.5
[12,18)	10	27	.314	60.9
[18,24)	4	8	.070	67.9
[24,30)	13	47	.162	84.1
[30,36)	6	43	.048	88.9
[36,42)	9	66	.051	94.0
[42,48)	5	25	.023	96.3
[>48	11*	177	.037	100.0

*NOTE: SIX FLIGHTS WITH 81 STRIKES HAD STRIKES EXCEEDING THE INITIAL FULL SCALE RANGE OF A/M^2; AFTER SCALE CHANGE TO 97 A/M^2 THERE WAS A FLIGHT WITH A READING OF 75 A/M^2 COVERING 5 STRIKES AND A FLIGHT WITH A READING OF 78 A/M^2 COVERING 6 STRIKES AND THERE WERE 3 FLIGHTS WITH READINGS EXCEEDING 97 A/M^2 COVERING 85 STRIKES.

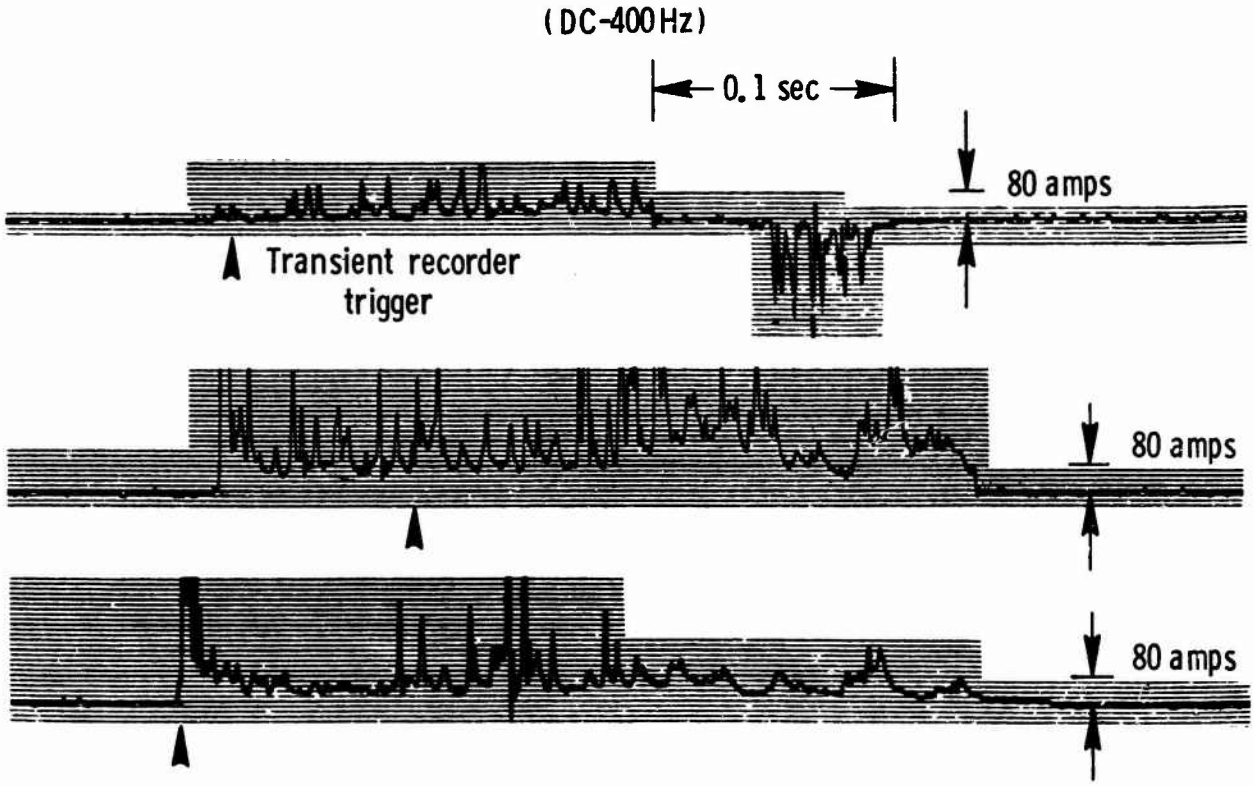

Fig. 1 - Vertical fin current (dc to 400 Hz recording bandwidth)

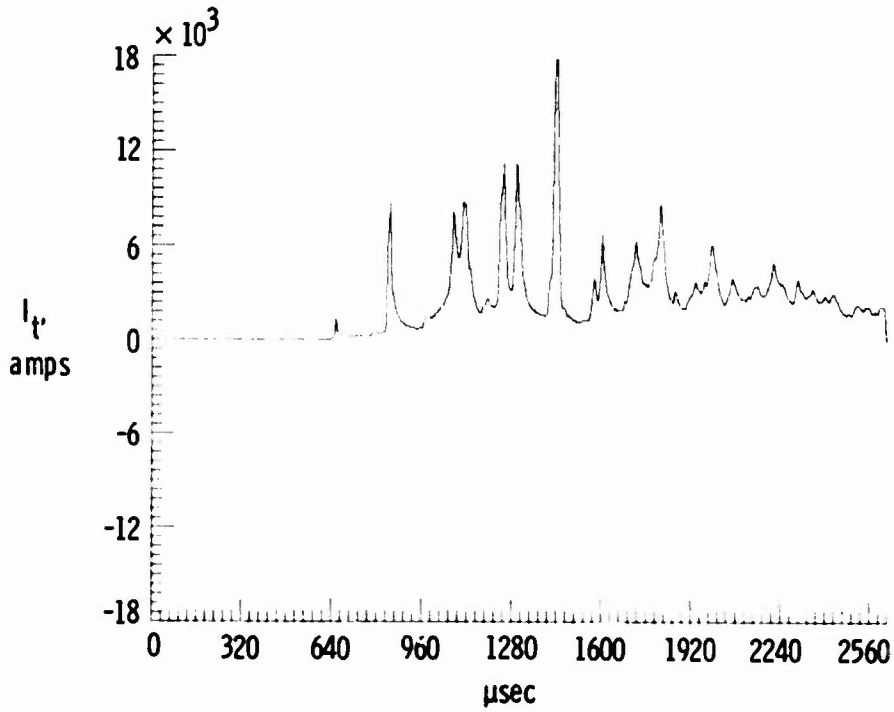

Fig. 2 - Vertical fin current (40 ns sample interval)

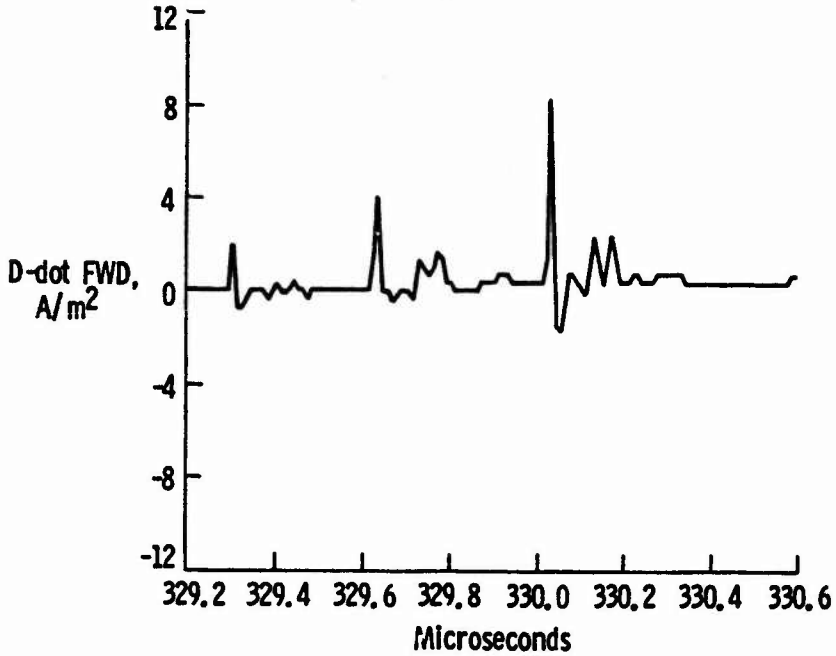

Fig. 3 - Electric flux density rate-of-change (10 ns sample interval)

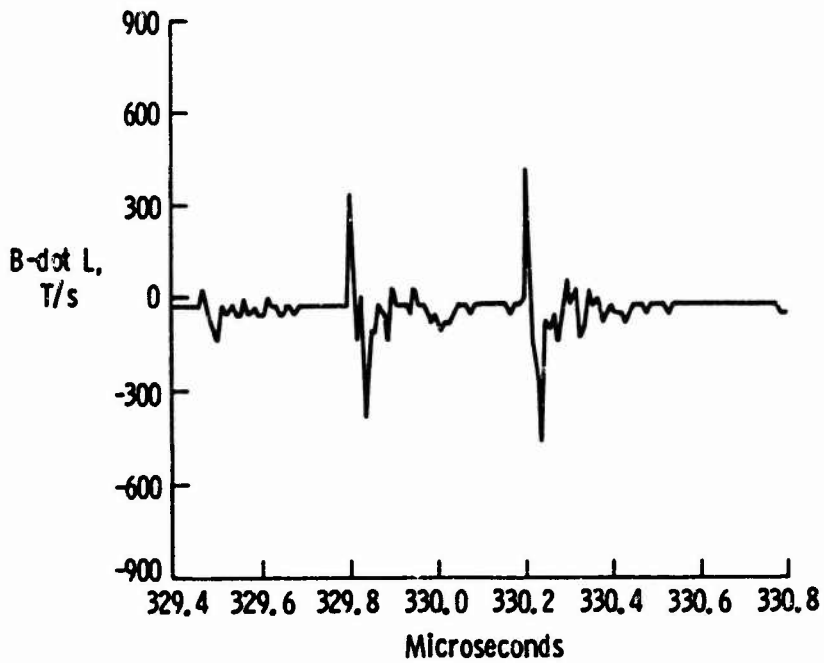

Fig. 4 - Magnetic flux density rate-of-change (10 ns sample interval)

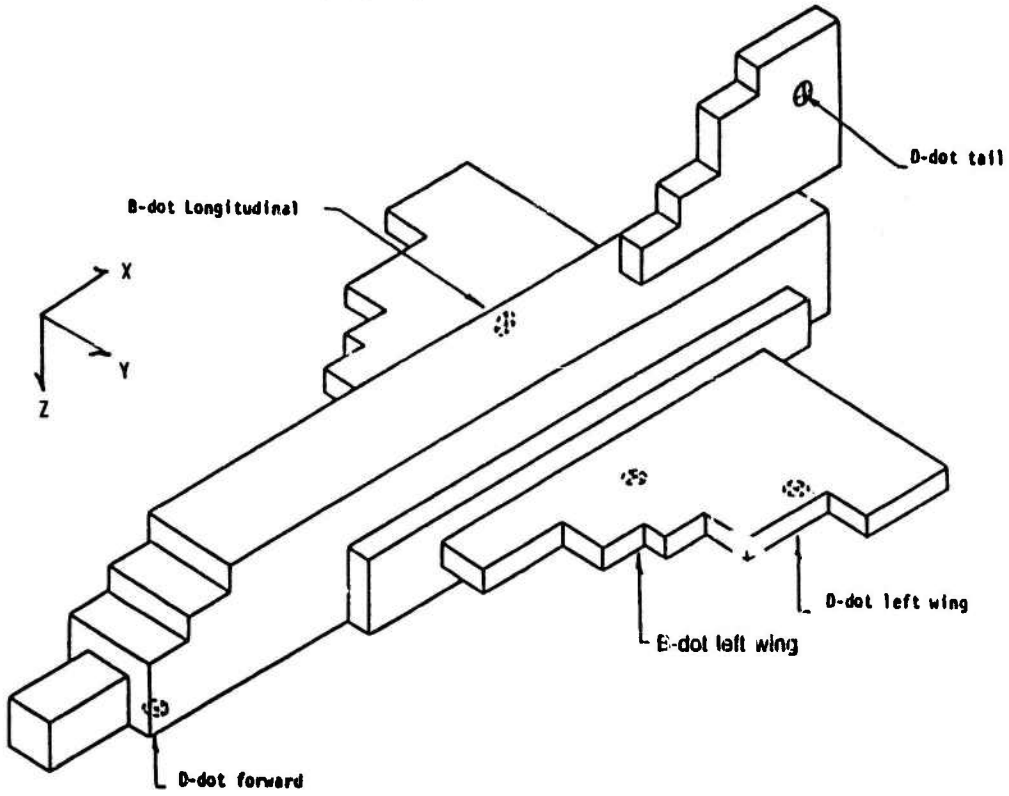

Fig. 5 - Model of F-106 and sensor locations used in finite difference code

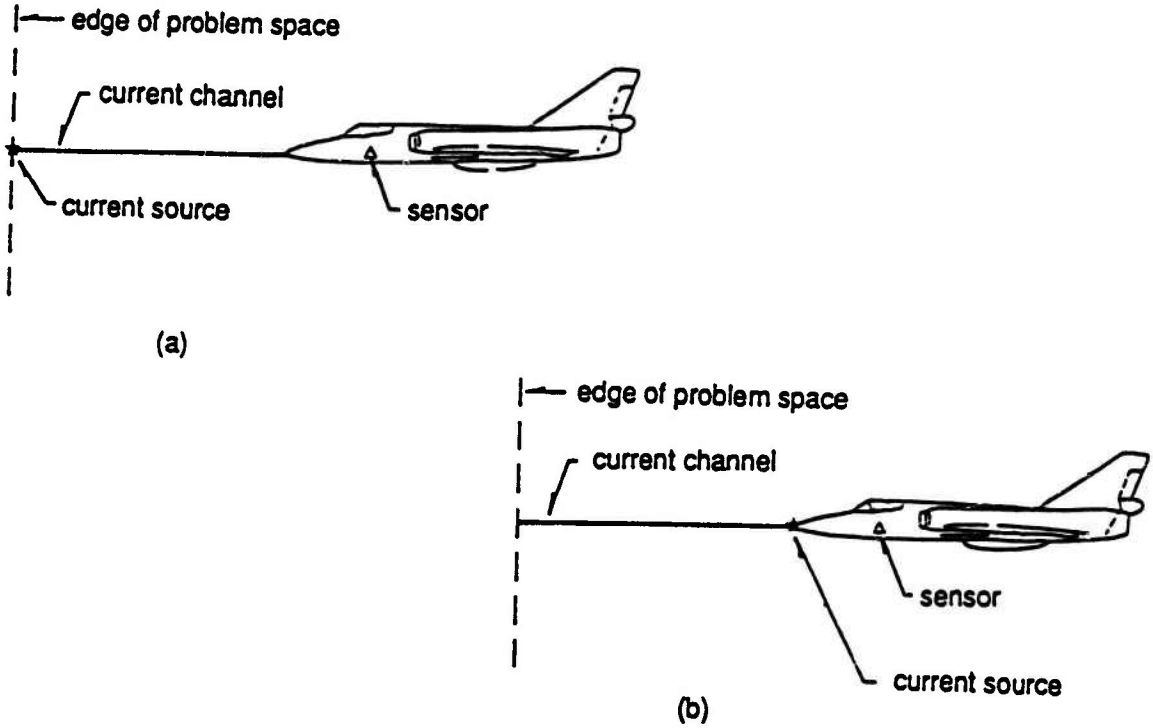

Fig. 6 - Model geometry for (a) natural lightning, and (b) triggered lightning

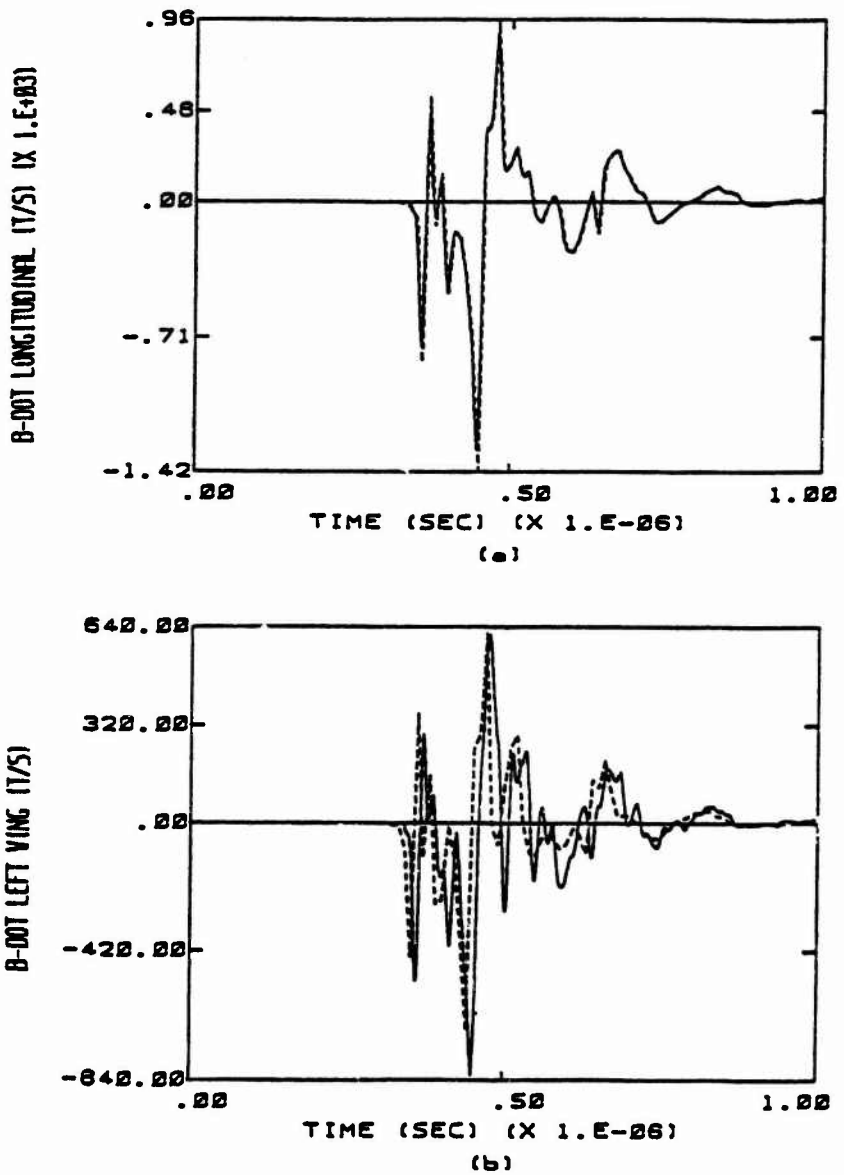

Fig. 7 - Overlay of calculated responses (solid line) and measured responses (dashed line)

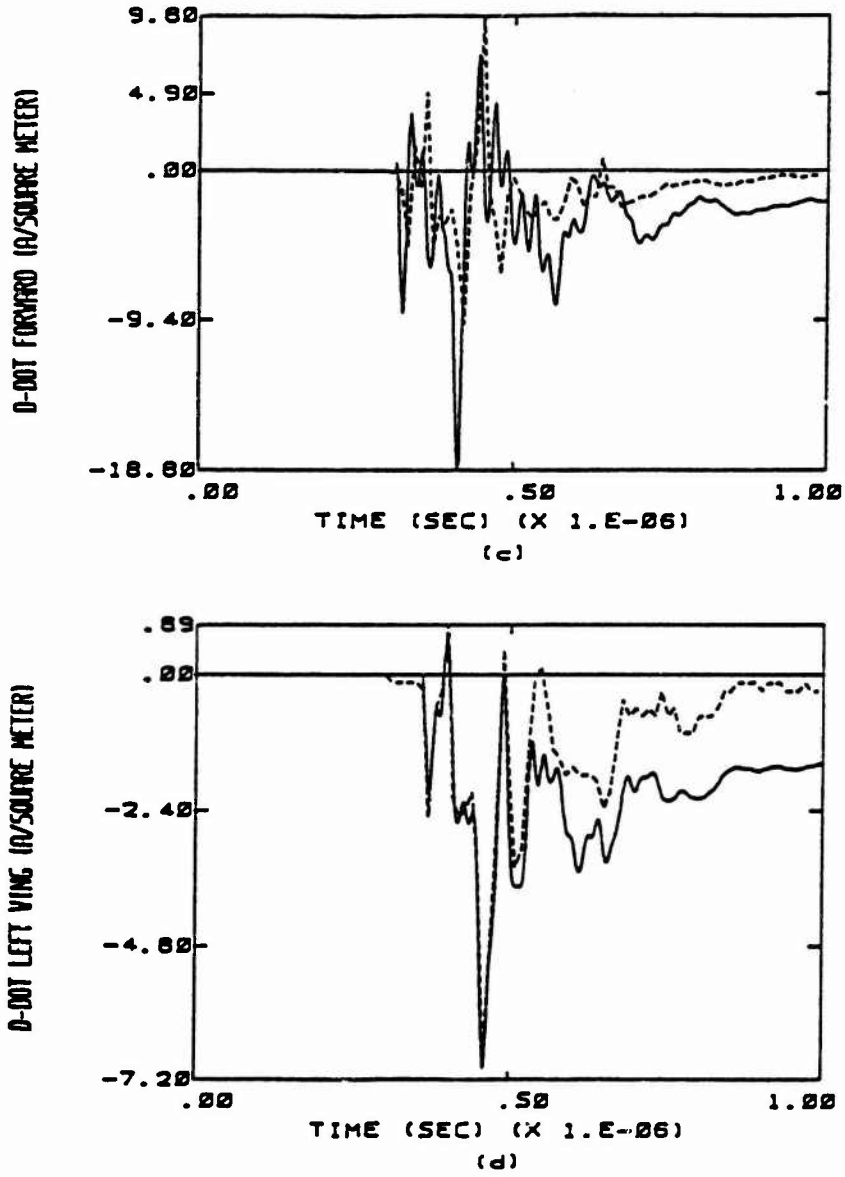

Fig. 7 - Overlay of calculated responses (solid line) and measured responses (dashed line) - continued

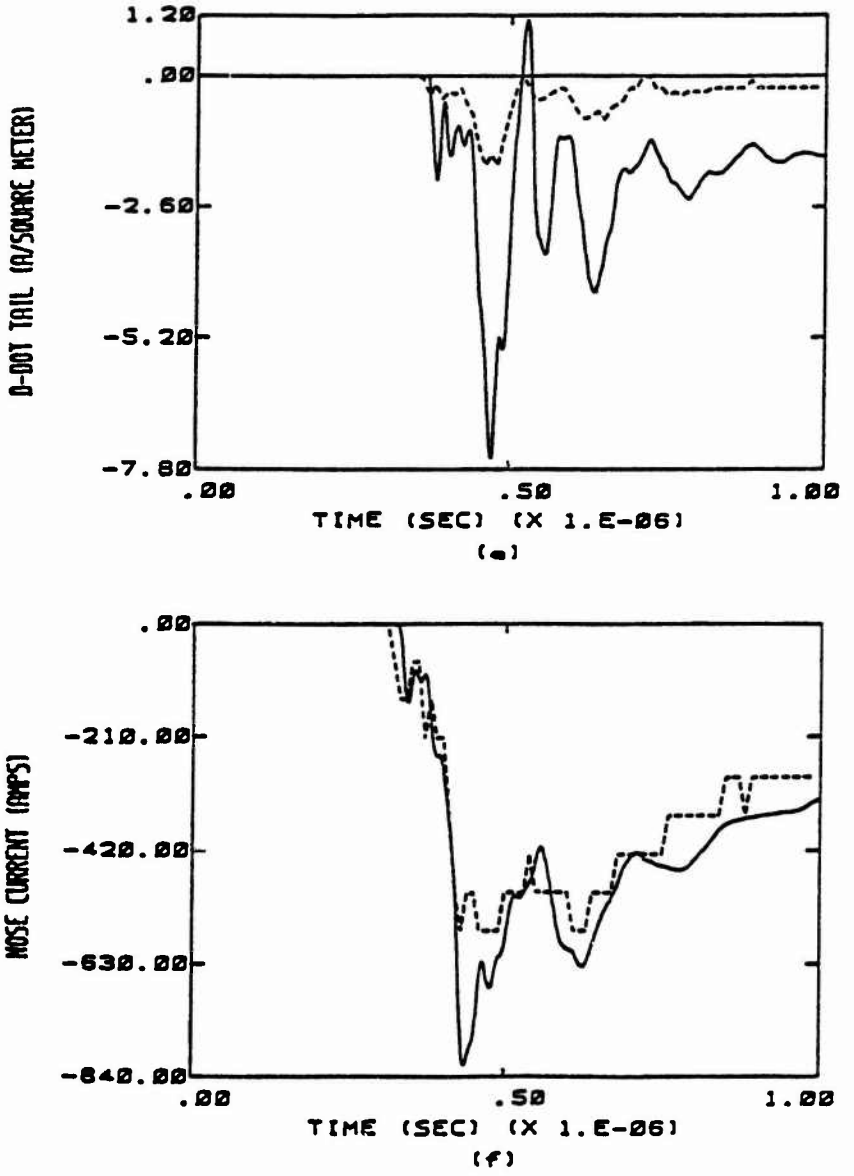

Fig. 7 - Overlay of calculated responses (solid line) and measured responses (dashed line) - continued

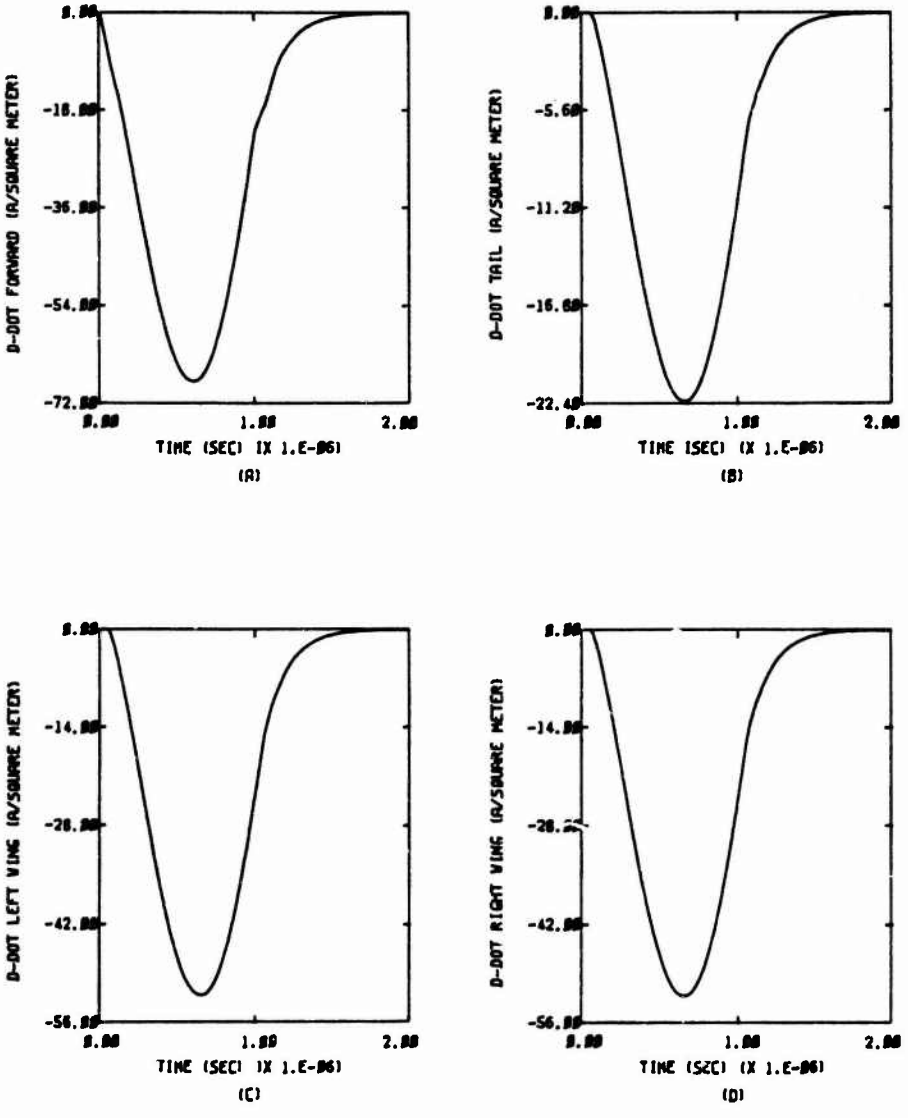

Fig. 8 - F-106 calculated response to 50 KA current pulse

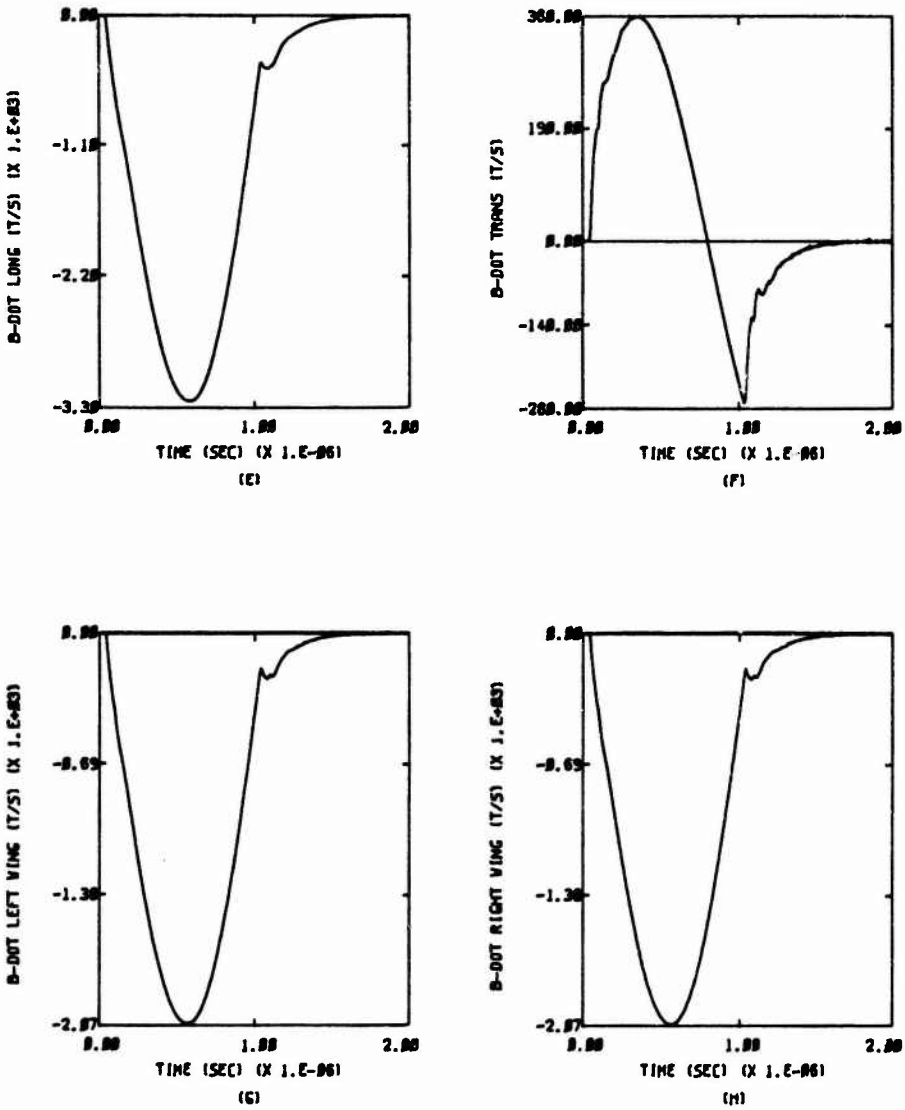

Fig. 8 - F-106 calculated response to 50 KA current pulse - continued

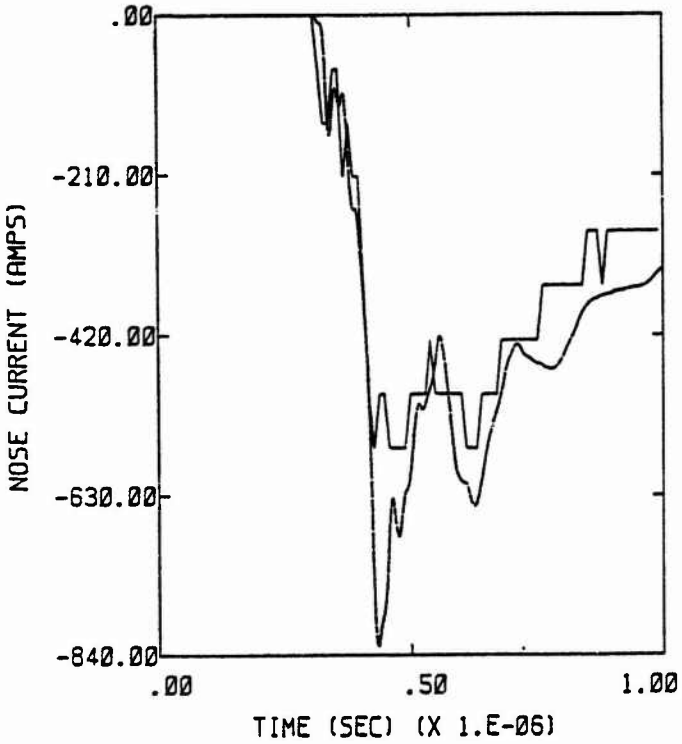

Fig. 9 - Overlay of measured (solid line) and calculated (dashed line) nose currents for the case of a 1 cm radius channel and resistance per unit length of 1 ohm/m, 10 ohm/m, and 50 ohm/m

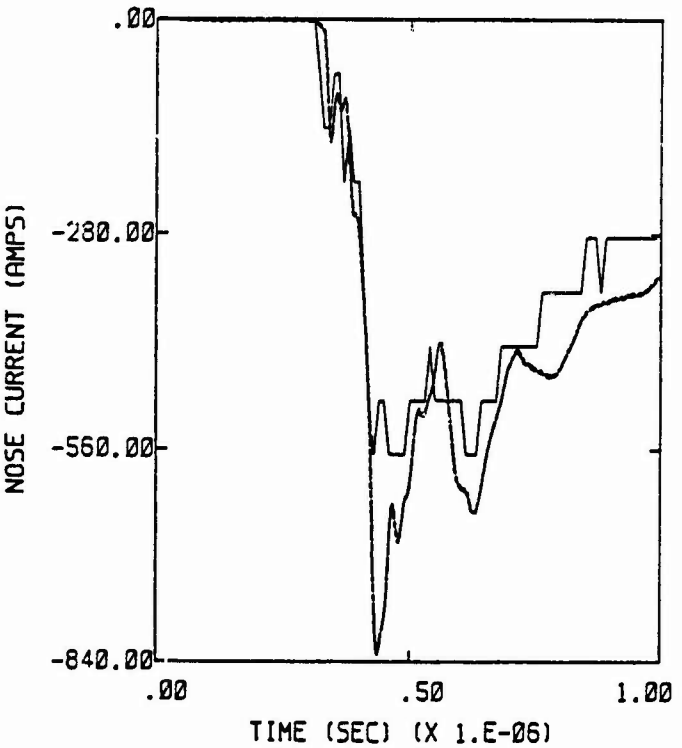

Fig. 10 - Overlay of measured (solid line) and calculated (dashed line) nose currents for the case of a 10 cm radius channel and resistance per unit length of 1 ohm/m, 10 ohm/m, and 50 ohm/m

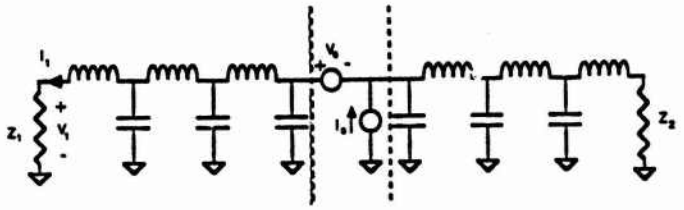

Transmission Line of Characteristic Impedance Z_0

Simple Model of Lightning Coupling to a Cable

Penetration	V_s	I_s
Open hole aperture	$\dot{B}$ (I)	$\dot{D}$ (I)
Resistive seam aperture	B (I)	negligible
Inductive seam aperture	$\dot{B}$ (I)	negligible
Diffusion through CFC	Z_tB(I)	negligible
Exposed Conductor - direct attachment	negligible	I
Exposed Conductor - lightning strikes aircraft nearby	$\dot{B}$(I)	$\dot{D}$(I)

Fig. 11 - Internal coupling model and parameters

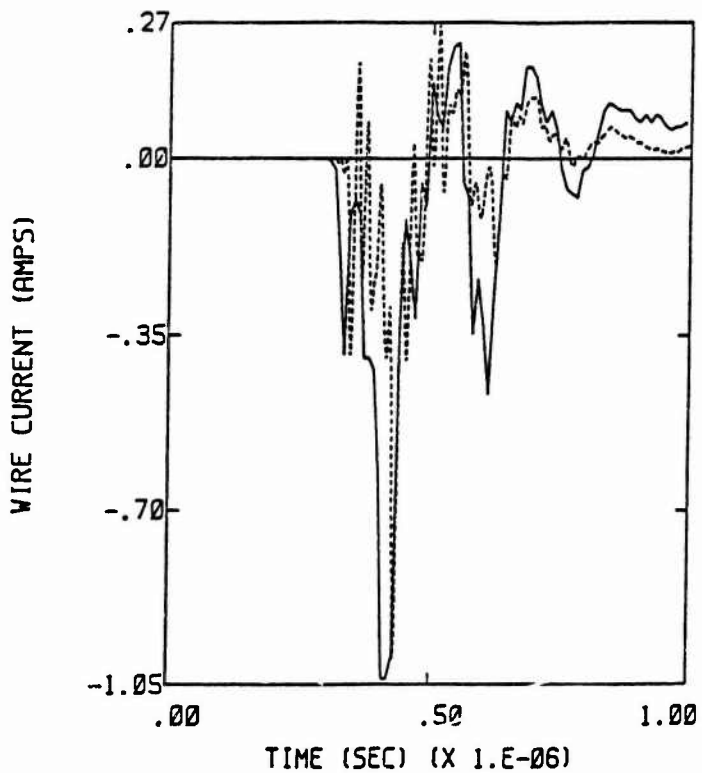

Fig. 12 - Overlay of measured (solid Line) and calculated (dashed line) currents for an internal wire

INTERPRETATION OF A CLASS OF IN-FLIGHT LIGHTNING SIGNATURES

Thomaa F. Trost
Department of Electrical Engineering
United Statea Military Academy
West Point, New York

ABSTRACT

Data recorded on the NASA F-106B reaearch aircraft during lightning strikea often reveals electric-field waveforma which begin with a seriea of abrupt changes and end in an exponential variation. A poasible interpretation of such eventa ia that an ionized channel is completed to the aircraft during the time of the abrupt changea, and the charge on the aircraft dumpa into this channel during the time of the exponential. An analysis of measured waveforms assuming a simple RC-circuit model haa been carried out for one event, and the results include I = 1000 A, V = - 650 kV, R = 1000 Ω, and W = 100 J.

INTRODUCTION

DURING THE PAST few years, lightning strikes to the NASA F-106B aircraft have yielded much new electromagnetic data on aircraft-lightning interactions [1]*. In this paper we discuss one type of lightning signature which has often been observed on the F-106B, with a time scale of a few microseconds. We interpret this signature as representing a component of a lightning event in which negative charge stored on the aircraft is rapidly discharged into a lightning channel attached to the noseboom. Although this interpretation is not unique, it is consistent with the available data and is quite reasonable. By invoking a simple RC-circuit model for the discharge, estimates of the values of various basic parameters are obtained. These include channel resistance, aircraft charge and voltage, and expended power and energy. Most of the lightning strikes under discussion are from 1982, with just a single, although important, strike from 1984.

In 1982 two digital transient recorders were carried on board and were switched among the four sensors shown in Fig. 1. The sensors measured I and I-dot, the current and the time derivative of the current on the noseboom, D-dot, the time derivative of electric displacement on the forward fuselage, and B-dot, the time derivative of magnetic flux density on the aft fuselage. The orientation of the B-dot sensor is such that the sensor responds to circumferential magnetic fields, which correspond to fore-to-aft currents.

For the strike from 1984, the availability of new transient recorders meant that simultaneous data was recorded from all of the sensors shown in Fig. 1 and from some additional sensors as well. The quality of the 1984 data was further improved because the new recorders employ 8 bits rather than 6.

RESULTS FROM 1982 DATA

Fast Pulses in the Time-Derivative Waveform-- A common feature of the lightning time-derivative waveforms is the appearance of very fast pulses. The pulses occur either singly or in groups, and the average number of pulses per group for 1982 was 2.4. An example of a group of 3 pulses in a D-dot waveform is shown in Fig. 2 (82-38-02). The 10 ns sample interval of the transient recorders is not short enough to provide detailed pulse shapes. In fact, the pulses are only two or three samples in width, and their true peak values are probably often missed in the sampling process. In 1982, surprisingly, all of the D-dot and B-dot pulses were of positive polarity. This corresponds to increasing positive charge (or decreasing negative charge) at the front of the aircraft, where the D-dot sensor is located, and increasing current fore-to-aft along the aft fuselage, where the B-dot sensor is located. The fact that all the pulses had the same polarity implies a charging mechanism attached to the airplane. That is, an explanation for charge motion based solely on polarization of the airplane by an ambient electric field is not satisfactory since the ambient field would not always be oriented so as to put the same polarity of charge on the nose.

For the pulses that occurred in groups of two or more we have measured the time intervals between adjacent pulses. Fig. 3 shows the distribution of these time intervals; the average value is 300 ns. Unfortunately, there is probably some inaccuracy in the distribution at short times because of the ringing of the aircraft. The pulses excite the electromagnetic resonances of the aircraft, which take about 300 ns to ring down [2]. (The period of the lowest-frequency resonance is about 160 ns.) Thus a weak pulse following within 300 ns of a strong one may be obscured by the ringing.

F-106B Signature-- A typical example of aircraft ringing is seen in Fig. 2 following the second, and largest, pulse. An expanded plot of this portion of the waveform is shown in Fig. 4, labelled "F-106." Notice that the ringing consists in part of a prominent double hump shape. This shape has also been observed in laboratory scale-model tests [3], and one of the waveforms from the laboratory model is shown in Fig. 4 for comparison with the F-106 data. From the laboratory tests it has been found that the double hump results from the reflection from the rear of the aircraft of a fast current change. That is, the shape is produced by a current step which is injected at the front of the aircraft, travels to the rear, and then partially reflects from the trailing edge of the wings (first hump) and then from the end of the fuselage and tail (second hump). This shape is a characteristic signature of the F-106 in response to current injection at the nose. It is clearly observed 58 times in the 1982 D-dot data.

The positive polarity of the pulse preceding the humps means a positive change in the charge on the nose, so that electrons must have exited there. See Fig. 5. This is an interesting result because it means that the nose of the aircraft was acting as a negative tip, and it is known from laboratory studies [4] that in a rod-plane gap, if the rod is negative, a higher voltage must be applied to cause sparkover than if the rod is positive.

Aircraft Discharging-- The variation of electric field, E, corresponding to the D-dot waveform in Fig. 2 has been obtained by integrating and dividing by ε_0. The result is shown in Fig. 6. The fast pulses in D-dot appear as small, abrupt increases in electric field, while the main feature of E is an approximately exponential rise to 360 kV/m. This indicates that the aircraft experienced an increase in positive charge or a decrease in negative charge, with a time constant of 680 ns. The location of the zero electric-field level is not known and has been arbitrarily located at the bottom of the plot.

Values of maximum E and time constant, τ, for several lightning strikes which showed approximately exponential discharging, or charging, like that in Fig. 6 are given in Table 1. All of these waveforms were similar to Fig. 6 in that they contained, first, a brief slowly rising portion, then a few rapid increases, and finally

*Numbers in brackets designate References at end of paper.

a longer, quasi-exponential rise. The τ values were measured as the time required for the curves to reach $(1 - e^{-1})$ of their final value, not including the slow rise at the beginning. The accuracy of the Max. E values, based on ± 1/2 LSB error in D-dot, is about ± 15%.

The strikes listed in Table 1 occurred at rather high altitudes, 8.2 to 9.5 km, with air temperatures ranging from -40 °C to -33 °C.

B-dot data recorded simultaneously with the D-dot data discussed here suggests current in the form of a pulse, although no actual current data, I-dot or I, was recorded. However, a look at the results of strike No. 84-17-01 from 1984 shows a D-dot waveform similar to that here, and in addition, thanks to the increase in the number of data channels, it also shows I; and the I waveform is a pulse. Assuming the same type of I waveform here, we see that the current looks like the derivative of the electric field, and the picture that emerges is that of a capacitive circuit. We assume that the airplane is the capacitor, that is, the airplane itself forms one plate and a distant charged sphere forms the other plate. Taking the airplane capacitance to be approximately 500 pF (Appendix I) and using τ = RC, the 680 ns time constant from Table 1 gives a resistance of 1.4 kΩ for the circuit. The 370 ns time constant gives 740 Ω.

RESULTS FROM STRIKE 84-17-01

Introduction-- The waveforms from the 1984 strike 84-17-01 (May 28) are similar to the 1982 aircraft-discharging waveforms already discussed, but they represent a more complete set, originating from eight rather than two external sensors, plus one internal sensor. Basically the event consisted of a one kiloampere pulse at the noseboom, with a peak I-dot of 26.6 E+9 A/s (or 26.6 kA/μs). This is not a large current for lightning, but it produced a significant transient on the internal sensor, a wire running along the fuselage, which went off-scale at 52 V. The signature of the current is a common one for strikes to the F-106B, consisting of a fast rise with some structure and a slow fall. The altitude was 7.6 km, and the temperature was -28 °C.

Comparison of I and Integrated I-dot-- In order to test the consistency of the results obtained from the I and I-dot sensors, we have compared the waveforms of I and integrated I-dot. (The I-dot wsveform itself is shown in Fig. 11.) In contrast to previous results [5], the agreement is not very good. The waveforms are shown in Figs. 7 and 8, and several differences between them may be noted. The trailing edge of the pulse is almost completely missing in Fig. 8. This is due to insufficient dynamic range in the I-dot record. More specifically, the slope on the trailing edge in Fig. 7 varies from -8.7 E+8 A/s toward zero and thus is always less than the first digitized level (below zero) in the I-dot record, -19 E+8 A/s. Other differences between the waveforms are that the peak vslue in Fig. 8 is much greater, and the curve descends more quickly following the peak than in Fig. 7. We expected that the amplitude of integrated I-dot would be greater than I, because the arrangement of sensors on the aircraft was such that some of the current bypassed the I sensor but all of it went through the I-dot sensor; but the two waveforms were expected to have the same shape. Further studies should be done to determine the reason for this difference in shape and thus eliminate a point of uncertainty.

Comparison of I snd E-- Integration of the forward-fuselage D-dot signal in Fig. 9 (and division by ε_0) leads to the E waveform of Fig. 10. This reveals aircraft discharging like that discussed above for the 1982 data. However, for 84-17-01 more complete data is available. In addition to the four sensors already described (Fig. 1), other sensors were used as follows: I on the tail, D-dot on the tail, D-dot under the port wing, and B-dot under the port wing for transverse currents. The tail I record consists of fluctuations between 0 and 71 A during the entire length of the transient recorder memory, 650 μs. 71 A is the first digitized level above zero, and so the average current was very roughly, 35 A. The polarity was such that electrons were flowing onto the airplane. We interpret this as a weak, continuing lightning-channel current which was charging the airplane. A large amount of corona would be expected on the airplane extremities during this charging phase. When the required conditions were met, a new channel formed from the noseboom, and the sirplane was discharged. Of course, other, more complicated interpretstions are possible. These would involve such things as additional simultaneous channel attachments and charging rather than discharging through the noseboom.

The final development of the noseboom channel probably took place in step-wise fashion. This is suggested by the structure on the leading edge of the current pulse in Fig. 7. Two consecutive sharp rises in current are seen; they are labeled P_1 and P_2 in the figure. (There is also a small rise between P_1 and P_2.) These sharp increases correspond to pulses in the I-dot waveform, and the pulses hsve been labeled with the same notation in Fig. 11, which shows I-dot. In fact, the two events are also revesled in forward D-dot and E. See Figs. 9 and 10. The situation here is an example of a group of fast pulses like those analyzed in Fig. 3. We thus come to interpret these pulses as corresponding to the connection of a discharge channel.

Once the peak current is reached in Fig. 7, there is a brief oscillation, which is probably due to aircraft ringing, and then an exponential decay begins as the charge stored on the aircraft pours into the new channel. The exponential discharge is also seen in the E waveform of Fig. 10. Remember that, with this interpretation, the true zero of E would be at the top of the curve, not at the bottom.

Time-integration of D-dot records from the tail and wing sensors produces E wsveforms very similsr to Fig. 10. Integration of the B-dot records from the fuselsge and wing sensors gives results similar to Fig. 8.

RC-Circuit Model-- A simplified equivalent circuit for the overall scenario is shown in Fig. 12. The airplane is represented by the capacitor, C. Chsrging current at the tail is supplied by

the source I_c, and the channel at the noseboom is represented by the variable resistor. One imagines that the resistance of the resistor drops from a high value in step-wise fashion, producing the pulses P_1 and P_2, and reaches a value, R, for the discharge phase.

We have taken the beginning of the diacharge phase to be at point X in Fig. 7. The time constant, τ, for the discharge (the time to fall to e^{-1}) is found from Fig. 7 to be 520 ns. With reference to the circuit in Fig. 12, a number of electrical parameters can now be computed. Using $\tau = RC$, the resistance, R, is found to be 1040 Ω. The voltage across the capacitor, C, and thus the airplane, after the channel has connected and the discharge begins is given simply by $V = - IR$. Taking I as the current at point X in Fig. 8, 665 A, gives V = - 692 kV. Here it is better to use Fig. 8 than Fig. 7 because, as mentioned above, some fraction of the total current bypassed the sensor which was used to obtain Fig. 7. Next, the total energy, W, stored in the capacitor is given by $W = 1/2\ CV^2 = 120$ J. The peak power delivered to the channel can also be found: P = - IV = 4.60 E+8 W, or 460 MW. This is the power at point X. At slightly earlier times the power may have been higher, but we cannot calculate it because we do not know the channel resistance.

An alternative method for calculating the voltage and energy uses the charge, q, transferred from the capacitor. From Fig. 12 one sees that the capacitor current is the difference between the tail current (I_c) and the noseboom current (current through R). We have computed the time integral of this difference to find q = -298 E-6 C. To determine the charge, Q, on the capacitor at time X, q must be added to the charge remaining at the end of the pulse, which is given by $-CI_cR$ = - 18.2 E-6 C. Thus Q = - 316 E-6 C, and V = Q/C = - 632 kV. Then $W = 1/2\ CV^2$ = 99.9 J.

The two methods in the preceding paragrsphs for calculating the energy give nearly the same results, and we conclude that W = 100 J. Note that our calculations apply to the discharge phase of the event; a quantitative analysis for the channel development phase, when the resistor in Fig. 12 is varying, has not yet been carried out.

A small but interesting effect, which we neglected, is the very slight drop in E after 1.3 μs in Fig. 10. This may be due to a late-time increase in the channel resistance, R. Another result from Fig. 10 is that the time constant for discharge of E is less than that for I in Fig. 7. This indicates the approximate nature of our understanding of this type of lightning event; future data should help to provide a better understsnding.

To put the values calculated sbove into perspective, we have compared the electrical discharge from the airplane to the discharge of a typical power-supply capacitor in an electronics package. The results are shown in Table 2. The peak power, P, was calculated in both cases assuming a resistance of 1040 Ω. One can see from the values that C and Q are smsll for the airplane, but V is lsrge. Thus the energy stored and the peak power delivered are large for the airplane.

CONCLUSIONS

Characteristics of the Lightning-- Fast pulses, like those marked with arrows in Fig. 2, are very prominent in the time-derivative data. They come in bunches of two or three and are among the fastest components ever observed in lightning fields. They are associated with the development of ionized channels on the noseboom, as illustrated in Fig. 5, where negative charge is carried off of the airplane. The time required for three pulses is typically in the range 100 to 700 ns. By integrating D-dot waveforms like the one in Fig. 2, one discovers that there is an approximately exponential variation in D, and E, following the occurrence of the fast pulses. This is aimilar to the decay of the voltage of a capacitor as it discharges into a resistor. The time constant is about 500 ns. A possible interpretation of the overall event is that a channel is completed during the time of the pulses, with some charge abruptly leaving the aircraft, and then the bulk of the charge flows into this channel during the time of the exponential variation. Values of various basic electrical quantities have been calculated for the exponential discharge phase (Tables 1 and 2), and all values seem reasonable. In the particular strike 84-17-01 it appears that the aircraft was subjected to a 100 J event, which is fairly potent.

During the capacitive discharge phase of 84-17-01 the current (and thus the magnetic field) varied roughly as the derivative of the electric field, as seen from Figs. 7 and 10. This relationship can slso be written $I = C\ dV/dt$. However st early times, short disturbances propagated over the aircraft, and in this propagating-wave situation one would expect I-dot proportional to D-dot and thus I proportional to D. This is just what happened, and the close similarity between I-dot and D-dot waveforms can be seen during the pulsea P_1 and P_2 in figs. 9 and 11. In fact, a simple charge-conservation argument can be used to find the proportionality constant between I-dot and D-dot. See Appendix II.

Laboratory Simulation-- If the RC-discharge idea for strike 84-17-01 is correct, the necessary apparatus for an approximate simulation of this event on the ground is suggested by Fig. 12: A high-voltage power supply is connected to the tail of the aircraft through a large resistor to simulate the aource, I_c. The aircraft is charged to - 650 kV and then allowed to apark over at the noseboom to a 1000 Ω resistor connected to ground.

Characteristics of the F-106B-- The double-hump signature shown in Fig. 4 is a characteristic of a nose-mounted D-dot sensor on the F-106B or other similar delta-wing aircraft subjected to a fast transient input at the nose. It is an example of the influence of aircraft shape on lightning waveforms.

As a final comment, it is interesting that the time-derivstive data reveals important short-time-scale information-- fast lightning pulses

and aircraft resonances and reflections (double hump)— while by merely integrating, one gets data which emphaaize a longer-time-scale picture, giving the overall discharge time and energy and suggesting the RC circuit interpretation.

APPENDIX I: CAPACITANCE OF THE F-106B

The capacitance between a circular disk of radius r and a sphere at infinity is given by $C_d = 8\varepsilon_0 r$. For a sphere rather than a disk, $C_s = 4\pi\varepsilon_0 r$. We approximate the capacitance of the F-106B to lie between that of a disk of radius 5.8 m and that of a sphere of the same radius. We obtain C_d = 410 pF and C_s = 645 pF, and thus for the airplane we take C = 500 pF.

APPENDIX II: RELATION BETWEEN D-DOT AND I-DOT

The aimplest case for the propagation of an electromagnetic disturbance is one where the disturbance maintains the same shape as it travels and thus is given by f(z-vt). This would be the situation for a wave inside a uniform, lossless coaxial transmission line, for example. We will assume this is approximately correct for propagstion of lightning disturbances along the noseboom and forward fuselage of the F-106B. For the propagation speed, v, we use c = 3.00 E+8 m/s.

We will let the z axis run through the noseboom and forward fuselage and take the fore-to-aft lightning current and surface charge to be approximately symmetrically distributed about this axis. The equation of conservation of charge can now be written in the form

$$\partial i/\partial z + \partial q/\partial t = 0 \quad ,$$

where i is current and q is surface charge per unit length in the axial direction. If i is a function of z-ct, then

$$\partial i/\partial z = - 1/c \; \partial i/\partial t \quad .$$

Charge conservation now becomes

$$\partial q/\partial t = 1/c \; \partial i/\partial t \quad .$$

If the fuselage is approximately circular with radius r, then the charge per unit area is $q/(2\pi r)$, and this is the ssme as the electric displacement, D. Thus, dividing the equation above by $2\pi r$, we find

$$\text{D-dot} = \text{I-dot}/ (2\pi rc) \quad ,$$

using the "-dot" notation employed in the body of this paper.

In order to see how closely the actual results follow the simple theory, we have taken the values 5.07 A/m^2 and 1.14 E+10 A/s from the first peaks (P_1) in D-dot and I-dot for substitution into this equation. The waveforma are shown in Figs. 9 and 11, respectively. Using r = 0.8 m, the result is 5.07 = 7.56, which is not too bad.

REFERENCES

1. Thomas, M. E. and F. L. Pitts, 1982 Direct Strike Lightning Data, NASA Technical Memo. 84626, March 1983.

2. Trost, T. F. et al. "Some Results and Limitations of Prony Analysis of In-Flight Lightning Data, "Proc. Intl. Conf. on Lightning, Ft. Worth, Texas, 1983.

3. Turner, C. D. and T. F. Trost, "Laboratory Modeling and Analysis of Aircraft-Lightning Interactions," NASA Contractor Rpt. No. CR 169455, 1982.

4. Hutzler, B. et al. "High Voltage Laboratory Testa and Lightning Phenomena," Proc. Intl. Conf. on Lightning, Paris, France, 1985.

5. Trost, T. F. et al. "Interpretation of F-106B In-Flight Lightning Signatures,"Report on NASA Langley Research Center grant No. NAG1-28, August, 1985.

ACKNOWLEDGEMENTS

The author wishes to thank M. E. Thomas of NASA Langley Research Center for supplying the digitized data used in this work and for providing much supporting information concerning the instrumentation of the F-106B aircraft. The author ia also grateful to M. G. Grothaus for help with the data analysis and to E. E. Kunhardt for useful discussions.

This research waa supported by the National Aeronautics and Space Administration through Langley Research Center grant No. NAG1-28.

Table 1. F-106B Aircraft Discharging Parameters

Strike No.	Max. E (kV/m)	Time Constant (ns)
82-38-02 (Aug. 8)	360	680
82-38-04	120	670
82-40-04 (Aug. 9)	190	500
82-40-07	440	370
82-42-06 (Aug. 11)	160	630
82-42-09	240	600

Table 2. Comparison of Discharges, F-106B Aircraft (84-17-01) and Typical Power-Supply Capacitor

	C (μF)	V (V)	Q (μC)	W (J)	P (W)
F-106B	0.0005	-632,000	-316	100	4.20 E+8
Capacitor	100	100	10,000	0.5	96.2

LOCATIONS OF ELECTROMAGNETIC SENSORS ON F-106B AIRCRAFT

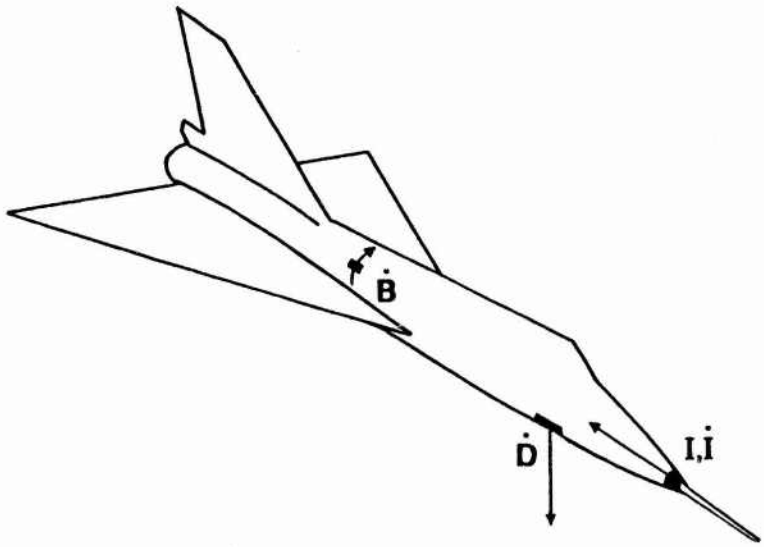

Fig. 1 - Sensor locations for 1982. Arrows give the directions for which the various quantities (B-dot, D-dot, I, I-dot) are defined to be positive

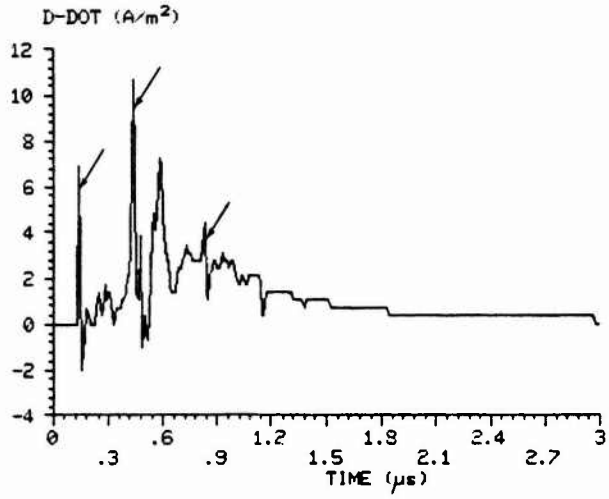

Fig. 2 - D-dot waveform showing three fast pulses, F-106B lightning strike No. 82-38-02

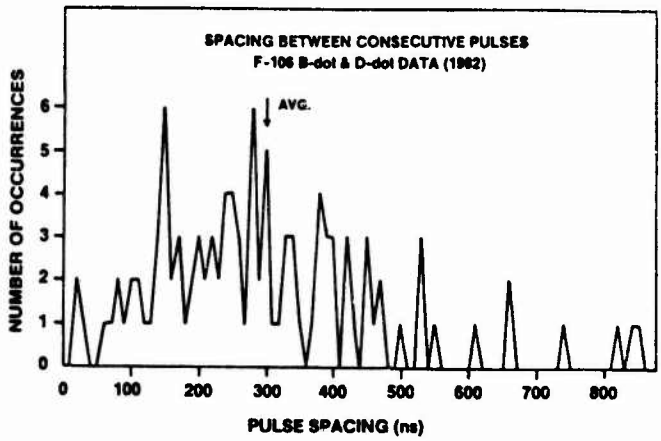

Fig. 3 - Distribution of time spacing between consecutive pulses

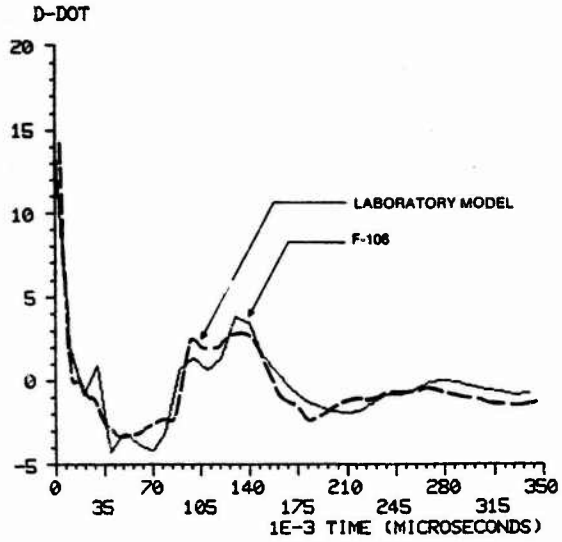

Fig. 4 - Comparison of D-dot double hump signature of F-106B (82-38-02) and laboratory model

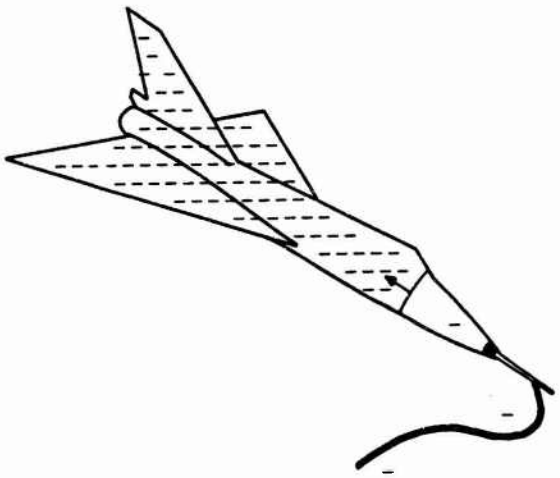

Fig. 5 - Channel attachment to noseboom, and abrupt loss of electrons at nose which propagates aft

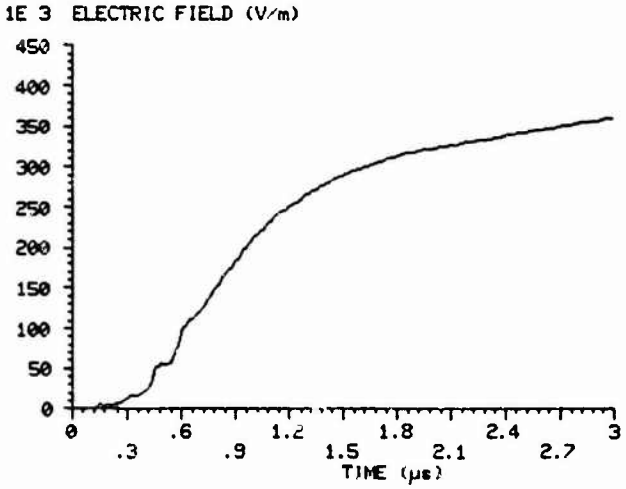

Fig. 6 - E waveform from time integral of D-dot in Figure 2 (82-38-02)

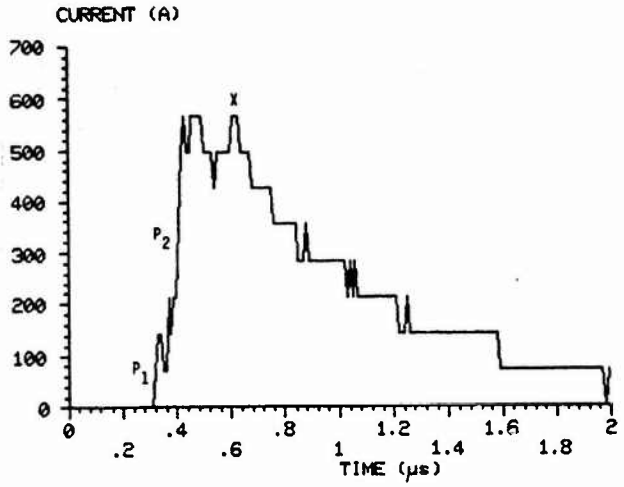

Fig. 7 - Lightning noseboom current waveform from I sensor, strike 84-17-01. Sharp increases occur at points P_1 and P_2, and a continuous decline follows point X

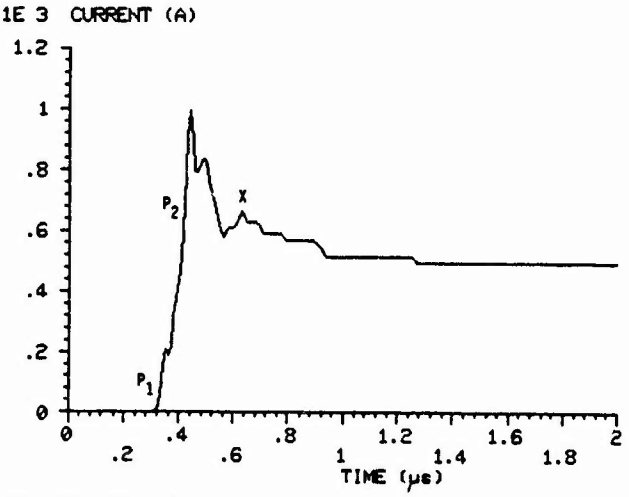

Fig. 8 - Time integral of I-dot waveform sensor for comparison with Figure 7 (84-17-01)

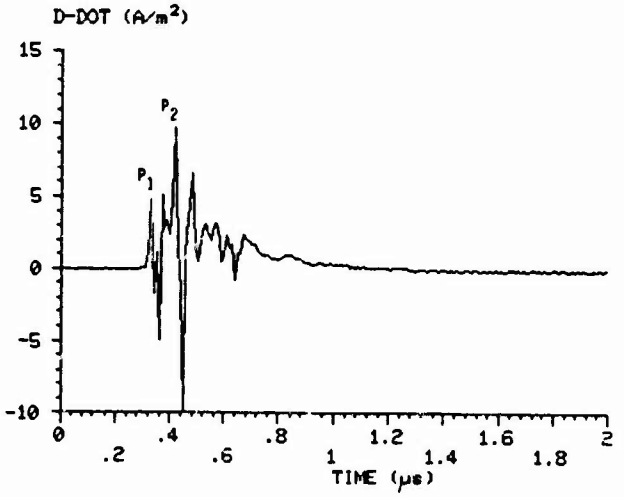

Fig. 9 - D-dot waveform, strike 84-17-01

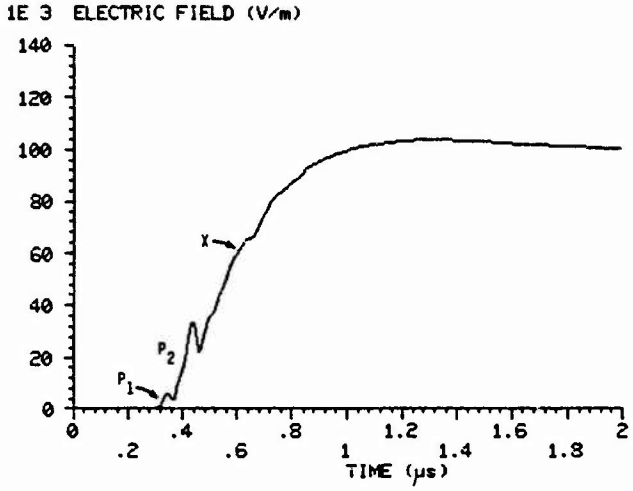

Fig. 10 - E waveform from time integral of D-dot in Figure 9 (84-17-01)

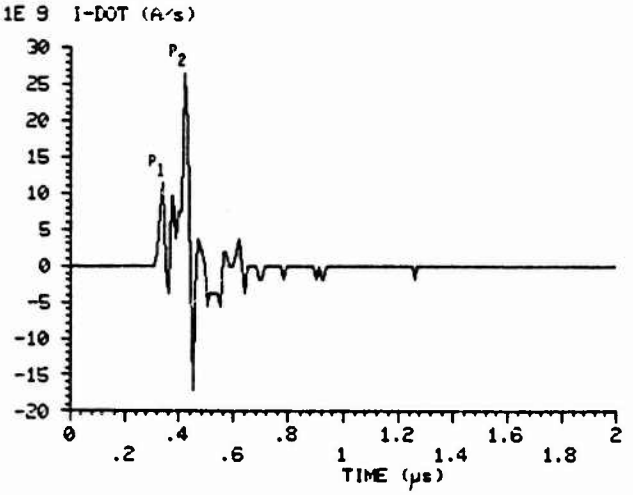

Fig. 11 - I-dot waveform used to generate Figure 8 (84-17-01)

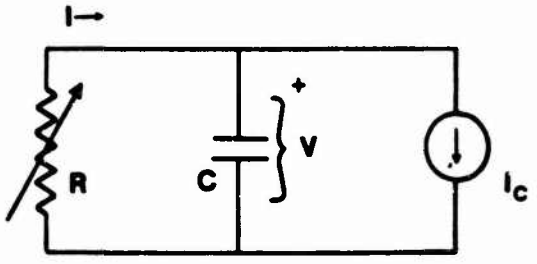

Fig. 12 - Equivalent circuit for aircraft charging and discharging scenario applied to strike 84-17-01

A THREAT-LEVEL LIGHTNING SIMULATOR

John L. Harrison, Y. G. Chen, Ed Galicki, and William Richardson
Maxwell Laboratories, Inc.
8888 Balboa Avenue
San Diego, California 92123

ABSTRACT

A threat-level lightning simulator having a low ripple output pulse with a peak current capability of 200 kA, and a peak rate of rise of current of 200 kA/μs is now in operation at Boeing Aircraft Corporation. The simulator is powered by a 4 MV Marx generator which drives a load with an inductance of 8 μH. The pulse is crowbarred when the circuit current is close to its maximum value by a laser-triggered crowbar switch. The decay time constant of the current pulse is determined by the load resistance.

The pulser generates a reproducible output waveform over a current range of 70 kA to 200 kA, and features a low prefire rate, and reliable precision triggering of its crowbar switch at close to the zero voltage ideal switching point. Consequently the machine operates with a reliability of over 90 percent.

This outstanding performance is achieved despite the severe duty enforced on the crowbar switch which carries a peak current of 300 kA, passes a charge of 40 C, and see an action level of approximately 2 MJ/Ω during each shot delivering the 200 kA rated current.

STATE-OF-THE-ART TECHNIQUES FOR LIGHTNING SUSCEPTIBILITY/VULNERABILITY ASSESSMENTS

John G. Schneider, Martin D. Risley,
M. Jean Reazer, Arturo V. Serrano
Technology/Scientific Services, Inc.

J. L. Hebert, 1Lt, USAF
Wright Aeronautical Laboratories (AFWAL/FIESL)

Abstract

State-of-the-art techniques to essess the susceptibility/vulnerability of aerospace vehicles, present and future, to the electromagnetic threats from lightning (LEMP) and electrostatic electricity discharges (ESD) ere described in this paper. These techniques are routinely used at the Atmospheric Electricity Research Laboratory (AFWAL/FIESL) of Wright Aeroneutical Laboratories. The techniques have evolved as a result of teste conducted on a wide variety of aerospece vehicles. Included ere cost-effective date acquisition, processing and storage systems and software that have been developed for high productivity and are based on microcomputer- controlled minicomputers capable of transient as well as CW meesurements; modular, reusable return path structures adapteble to aerospace vehicles covering wide ranges of sizes and shapes; programmable breakout box/cable combinations that permit induced voltage and current meaeurements or individual wires of aircraft cable bundles ueing non-contact probee; and wideband (DC to 50 MHz) analog fiber data links that are pneumatically controlled for use in the high electromagnetic noiee environment of high-voltage and high-current lightning eimulators.

These techniquee have been successfully ueed with test configuretione involving simuleted lightning current injection, rocket-triggered lightning experimente, high-voltage (shock) excitetion, radiated EMP, and swept (CW) frequency-test methods. The techniquee, equipment charecteristics, and procedures are preeented elong with known limitations.

INTRODUCTION

The rapid introduction of advanced composite materials and low level semiconductor based flight critical control systems into present and future aerospace vehicles has increased the need for efficient and accurate techniques for Lightning Susceptibility/Vulnerability Assessments. While analytical prediction of lightning protection is essential for the effective design of future aerospace vehicles, the geometric and parametric complexity of the vehicles will require that the vehicle undergo testing before final lightning qualification is achieved. In addition, design changes and modifications to enhance the capabilities of present aircraft will require testing to insure that these changes have not increased the inherent lightning susceptibility of a previously lightning hardened aircraft. The increased emphasis on lightning protection for future aerospace space systems has resulted in Military Standard MIL-STD-1757A and a new DOD Military Standard for indirect effects testing being developed by the SAE AE4L committee, since the need for effective and accurate lightning susceptibility/vulnerability test is paramount. Recognizing this need, the Atmospheric Electricity Hazards Group of the Flight Dynamics Laboratory, Air Force Wright Aeronautical Laboratories and the facility contractor Technology/Scientific Services, Inc. have undertaken an aggressive program to upgrade and enhance the ability to perform detailed lightning susceptibility tests on aerospace vehicles. These efforts cover the full spectrum of these assessment tests including: simulated threat generation; input waveform and induced transient data acquisition; and, data signal processing and analysis. This paper details recent advances in the state-of-the-art in each of these areas.

GENERATION

Advances in the area of generation include the development of a portable 4 MV prime power source for a new fast-rise, full/threat lightning simulator, the development of a pseudo coaxial modular return path system, and the development of frequency domain testing using a Swept Frequency Continuous Wave System to develop system transfer function.

The AEH Group has developed a Fast Risetime Generator which uses a NEMP-type peaking capacitor coupled to a high voltage marx to provide the fast current risetimes that have been observed during recent ground and in-flight lightning research program (1,2). This generator can produce a 40 KA 0.2x20 waveform, a full order of magnitude faster than generators routinely used for lightning simulation tests. The prime power source for this generator was an extremely long (84 foot) moveable marx designed in the 1960's by the Lightning and Transients Research Institute for the Air Force Weapons Laboratory (3). A new portable 4 MV marx generator has been designed to replace this aging generator in a truly transportable configuration. The generator's design is depicted in Figure 1. This generator has the distinct advantages of portability, operation in air and a rugged reliable triggering system. The generator consists of 40 100 KV capacitors arranged in eight banks of 5 capacitors each. Each leg is installed in a triangular structure to take advantage of the stability and ruggedness of that geometric shape. The total length of the generator is 25 feet allowing it to be transported on any standard 25 ft or longer flat-bed trailer. The generator operates in air saving the costs of oil or SF_6 and their associated house keeping systems. The in-air operation results in an increase in the inductance of the marx generator, but this is compensated for by the use of the NEMP-type peaking capacitor (2). The high voltage switches are spark gaps of the simple rugged design illustrated in Figure 2. They are numerically triggered taking advantage of the drop in their breakdown voltage due to a decrease in pressure when operating on the right-hand side of the Pachen curve. The operating range of these spark gaps for several pressures and distances is shown in Figure 3. The simple rugged design of the generator and its sparks gaps promises rugged reliable operation.

Return paths have typically been built in a unique manner for each particular aerospace vehicle being tested and either discarded or materials salvaged following the tests. The AEH group has designed a set of modular return paths which are reusable from test to test. Figure 4 shows the modular return paths being used on a CV-580 aircraft, and Figure 5 shows their use with an FAA experimental testbed. Return paths of this type have been shown to have an inductance as low as $3\mu H$ (4). The basic sections of the modular return path consist of wooden frames which measure 4 ft by 16 ft with wire screen permanently attached over the frames. Some of the sections have 45 degree angles on the edges which allows them to be mated to adjoining sections to form a coaxial type geometry. The sections are bolted together to form a continuous return path with compression connections between each adjacent section. Wire screen is suitable for lightning testing as the shortest wavelength of concern is much longer than the spacing in the wire grid. The modular design allows maximum flexibility for designing many different sizes and shapes of return paths. This approach is cost effective as it minimizes the costs of new materials and cost of construction for producing effective return path configurations.

The third advance in lightning simulation generation is the AEH Group in-house development of the ability to perform Swept Frequency Continuous Wave testing. This frequency domain determination of the transfer function of an aircraft is a powerful linear system test method that has been demonstrated to be an effective lightning susceptibility test method (5,6). The data processing in the frequency domain from one of these tests is illustrated in Figure 6. The aerospace vehicle being tested is subjected to various frequencies and the magnitudes of the induced transient voltages and currents is measured and recorded producing a Frequency domain transfer function which is limited in frequency by the ranges of the measuring instrumentation and the ability to produce responses which demonstrate an acceptable signal to noise ratio. Figure 6 shows a SFCW transfer function measured on a UH-60A Black Hawk helicopter (7) and its response to the $2x50\mu sec$ lightning waveform. This system developed by the AEH Group has the advantages: of compactness which makes it easily transportable; computer controlled acquisition, signal processing and graphics which speeds data acquisition and processing; the ability to make corrections for the characteristics of the measurement acquisition system; and the ability to combine the transfer function with a variety of different frequency domain threat waveforms. The AEH Group has extended the Frequency domain analysis techniques to

data acquired during moderate and severe simulated lightning susceptibility tests and data acquired during inflight lightning strikes (8).

DATA ACQUISITION

Advances in the acquisition and recording of measured lightning simulation induced voltages and currents transients on aircraft circuits include the development of a microprocessor controlled data acquisition system and the development of programmable breakout boxes.

Figure 7 show a Zenith Z-100 microprocessor which controls the acquisition of the data being recorded by two 2-channel transient digitizers/signal processors. In the past, data concerning the test being performed was logged on data sheets before and after the simulation test was performed. Between the test, the operator was required to set up and arm the digitizers as well as make all data entries. With the microprocessor controller, the computer prompts the necessary housekeeping information such as shot number, circuit being measured so that the operator cannot inadvertently forget to make these necessary entries between the tests. The computer also sets up the digitizers and arms them prior to the next shot. After the shot, the computer performs initial analysis on the signal and stores pertinent transient waveform parameters such as Peak maximum and minimum values. During lightning simulation tests on the F-16/LANTIRN systems (9), the computer provided time domain extrapolated values from the level at which the systems were tested up to the full severe level of 200 Kiloamperes. The computer then passed the data to a printer to provide immediate hardcopy feedback and documentation of the tests. An illustration of the data from several shots is presented in Figure 8. The computer controlled the storage of the waveforms recorded on a magnetic disk and then begau the entire series of events over again for the next shot.

Figure 9 shows a programmable breakout box which is capable of current and voltage measurements on 4 separate circuits without the necessity to open the compartment panel to gain access to change circuits. Figure 10 shows a schematic diagram of this breakout box. With 2 breakout boxes in operation, 16 measurements can be made on 8 circuits without gaining access to the compartment or circuits being measured. When a change is necessary 4 more circuits can be selected for each breakout box by simply plugging in a programmed plug which was constructed well in advance of the actual simulation tests. The breakout box is connected into the aircraft circuit using shielded cables with standard aircraft connectors. The cable lengths are minimized and identical gage wire as in the aircraft circuits are used to insure minimum perturbation of the circuit under test. The breakout boxes for the F-16 tests were pneumatically controlled to select the circuit to be measured. Transients measured were transmitted via analog fiber optics with a bandwidth of DC-30 MHz. The breakout boxes have since been upgraded to 100 MHz. Current measurements are made by a CT-1 Tektronix current transformer while voltage measurements are differential using two capacitive voltage probes (Ref 9). Transient induced currents were measured in one conductor of a wire pair while voltage measurements were made differentially on Hi/Lo signal lines or in reference to signal grounds for single ended circuits that use chassis ground as a return. For low level tests such as swept frequency continuous wave tests, the excitation signal is amplified.

The combination of the microprocessor controlled data acquisition systems and the programmable breakout boxes allows susceptibility tests to progress at a near real time pace with the time required to charge the simulation generator being the controlling factor. With this combination transient current and voltage measurements were made in over 200 separate circuits on the F-16/LANTIRN systems in a 2 working day period. The computer speeded up the acquisition of large volumes of data, and reduced the human errors that inevitably occur during long hours of testing.

DATA ANALYSIS

The addition of micro-computers and medium sized computers as integral parts of the lightning simulation test systems has greatly speeded up the acquisition, processing, and reduction of the simulation data; and resulted in a significant enhancement of the ability to perform thorough extensive post-test analysis.

The micro-processor integration into the simulation data acquisition system provides a substantial increase in the ability to perform timely simulation tests. Data reduction begins even as the data is acquired. The bookkeeping tasks or data logging is performed on line, initial data analysis is performed between shots and a hard copy of initial results in either graphic or tabular form is provided immediately following each test. The previous methods of data sheet logging and labeling of oscillogram photos and hand or visual measurements of the transient waveforms were costly in terms of time and were subject to human error. With sufficient sample rates the digitized waveforms allow computer processing of the signals which is accurate and immediate. The magnetic storage of the digital waveform data also allows post test reduction of the data. The data can be viewed and initial results obtain during the tests. Post-test computer aided reduction processing and analysis can be performed quickly and accurately. Computer-aided graphics allows customizing of the data presentation format for formal reports which were not previously possible with oscillogram photos.

One of the most exciting advances in simulation test data analysis has been the integration of frequency domain techniques for post-test simulation test data analysis. The time domain data acquisition and processing digitizers have been interfaced to the medium sized computer system developed for the Swept Frequency Continuous Wave System discussed earlier. Frequency domain techniques are illustrated in Figure 11 and basically consists of:

1) The transfer of the time domain lightning simulation test waveforms for the input and the induced circuit transient voltages and currents are transferred directly from the transient digitizers and magnetic disk storage system directly into the medium sized computer for frequency domain processing and analysis.

2) The time domain waveforms are transformed into the frequency domain via fast fourier transform.

3) The signals are corrected for the measured effects of the characteristics of the sensors,

breakout boxes and fiber optics systems used during the acquisition of the dsta. (Potentially, the configuration effects of the simulator return paths and generator which are not present during the in-flight situation could be removed at this time, however this procedure is in it development stages at publication time).

4) The induced transient voltage and current signals are returned to the time domain for preliminary analysis.

5) Additional processing continues in the frequency domain with the transient waveforms being divided by the input waveform. For the transient voltage waveforms this produces impedance transfer functions and for current waveforms direct trsnsfer functions.

6) These transfer functions are convolved with the lightning threat (For example: an actual in-flight measured lightning strike, or one of the standardized lightning threat simulation waveforms of the MIL-STD-1757A).

Lightning simulation tests are performed with generators which most closely produce injected current wsveforms specified for lightning simulation testing. Although these generators cannot exactly reproduce these waveforms, all of the information need to determine the aircraft systems response to the actual specified waveform haa been measured and recorded during the time domain tests. Frequency domain techniques allows this information to be brought out. This technique also allows linear extrapolation of system responses to any threat waveform, within the frequency limitations of the acquisition equipment, which is correct in amplitude and phase. Frequency domain techniques provides a powerful tool to analyze and exploit lightning simulation test generated transient data measurements.

SUMMARY

The need for accurate cost-effective lightning simulation techniques was diacuased. Advances by the AEH Group in the areas of generation, data acquisition and data analysis was presented. Theae included:

The design of a coat-effective portable 4MV marx bank for the AEH Group's Faat Risetime Generator and the development of a Swept Frequency Continuous Wave Lightning Simulation Test System in thc area of generation.

The development computer controlled data acquisition aystems and advanced programmable breakout boxea for induced transient voltage and current meaaurements in the area of data acquisition.

The development of micro-computer processing and reduction systems and the implementation of frequency domain techniques for post aimulation test data analysis.

The advances presented in this paper overviews techniques which greatly enhance the abilitу to perform detailed and accurate lightning simulation tests.

REFERENCES

1. J.L. Hebert, L.C. Walko, and J.G. Schneider, "Design of a Fast Risetime Lightning Generator", Presented at the International Aerospace and Ground Conference on Lightning and Static Electricity, Paris, France, June 1985.

2. J.D. Robb, "An Experimental and Theoretical Investigation on an NEMP Type Fast Rise Lightning Simulator", AFWAL-TR-84-3007, March 1983.

3. "Ten Million Volt Lightning and EMP Simulator", LTRI, AFAL-TR-64-340, February 1965.

4. B.J.C. Burrows, "Induced Voltsge Programme Theoretical Considerstions of Whole Aircraft Tests", Culham Lightning Studies Unit, May 1975.

5. L.D. Piszker, D.E. Young, "The Use of CW Test and Analysis Techniques in Lightning Vulnerability Assessment of Aircraft Systems", Paper Presented at FAA/GIT, Workshop on Grounding and Lightning Protection, May 1978.

6. D.B. Walen, "Lightning Simulation Tests on a Graphite Epoxy Airplane Mockup", Proc. of the IEEE 1985 National Aerospace and Electronics Conference (NAECON 85), Dayton, Ohio 20-24 May 1985.

7. J.G. Schneider, "Report of UH-60A Swept Frequency CW Tests", Under Contract F33601-85-D01D, Task 010, January 1986.

8. J. L. Hebert, J.C. Schneider, and J.S. Reazer, "Current Levels and Distribution on an Aircraft During Ground Lightning Simulation Tests and In-Flight Lightning Attachments", Paper to be Presented at the 11th International Aerospace & Ground Conference on Lightning and Static Electricity, June 1986.

9. J.L. Hebert, J.C. Schneider, M.D. Risley, and A. Serrano, "F-16D/LANTIRN Lightning Susceptibility Tests", AFWAL-TR-86-3006 , December 1985.

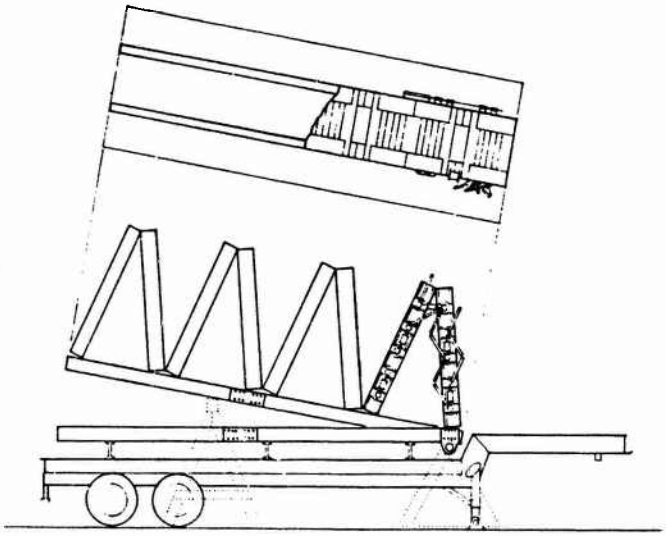

Figure 1. Drawing of the Portable Fast Rise Generator.

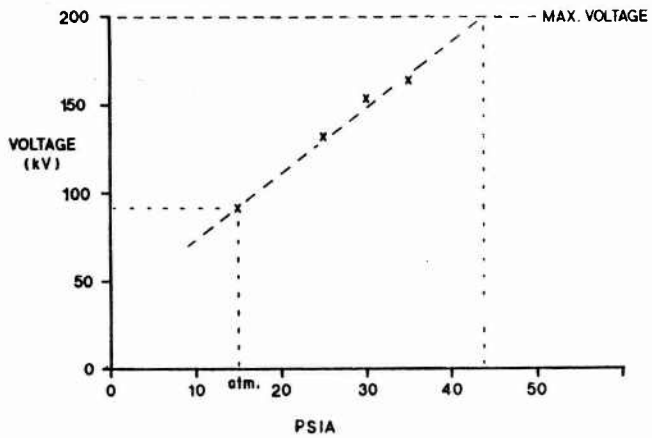

Figure 3. Graph Showing The Operational Limits of the 200kV Spark Gap. (X)-Indicate Measurements.

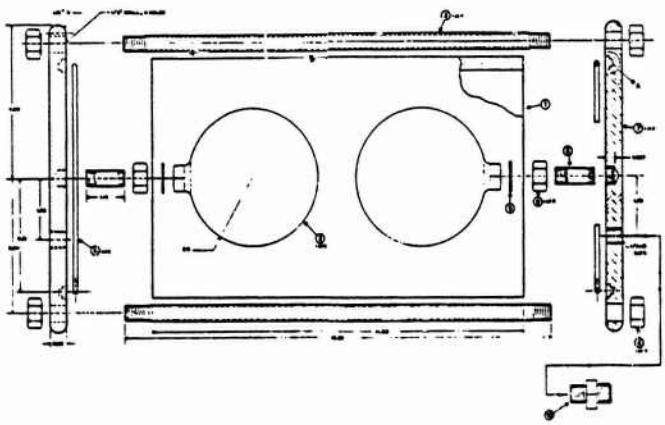

Figure 2. Drawing of the Spark Gap that is used in the New Fast Rise Generator.

Figure 4. The Modular Return Path Set Up Around the CV-580 Aircraft.

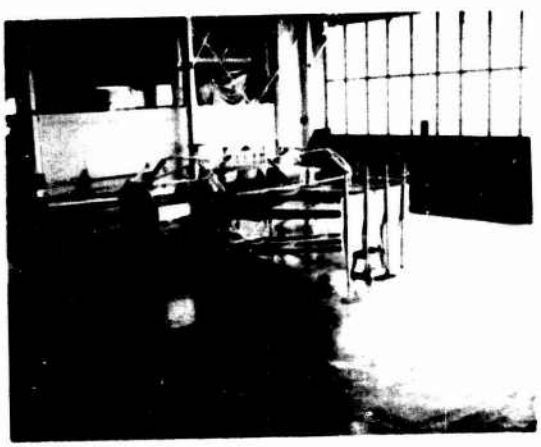

Figure 5. The Modular Return Path Set Up Around the FAA Research Test Bed.

DATA FLOW CHART

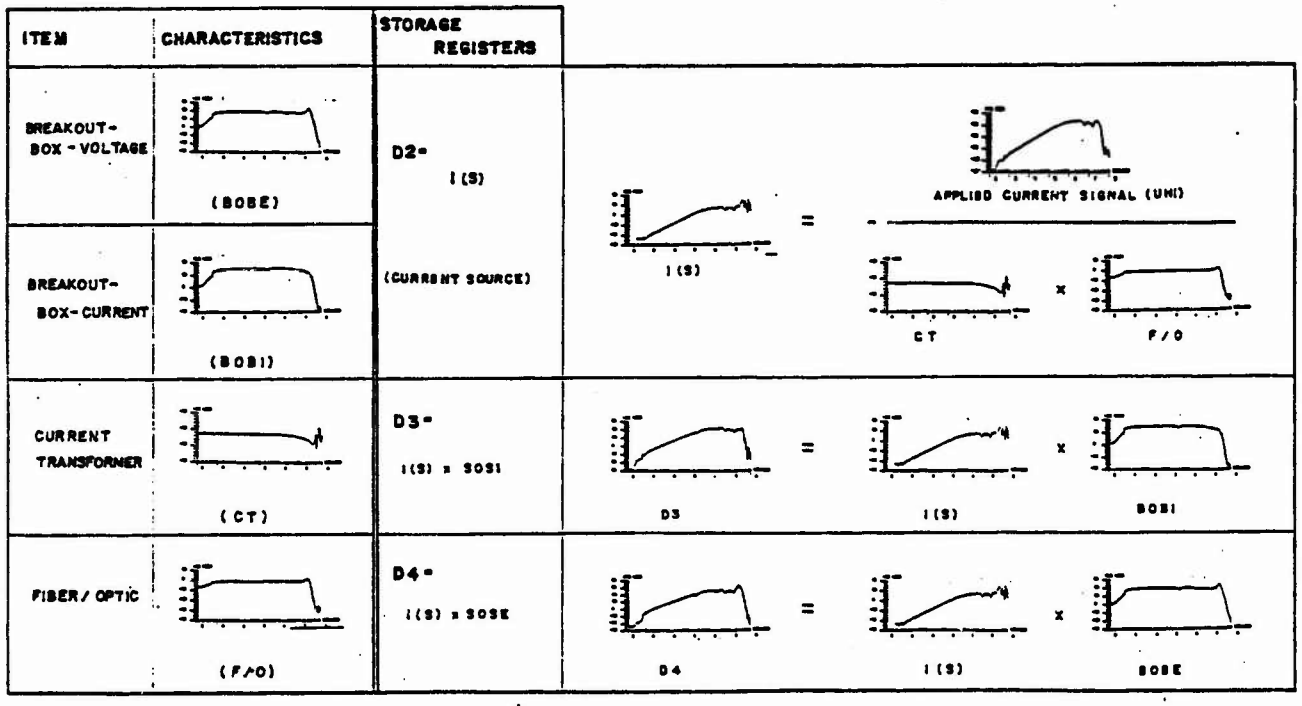

TRANSFER FUNCTIONS
from Breakout Box (SIGNALS AVERAGED 8 TIMES)

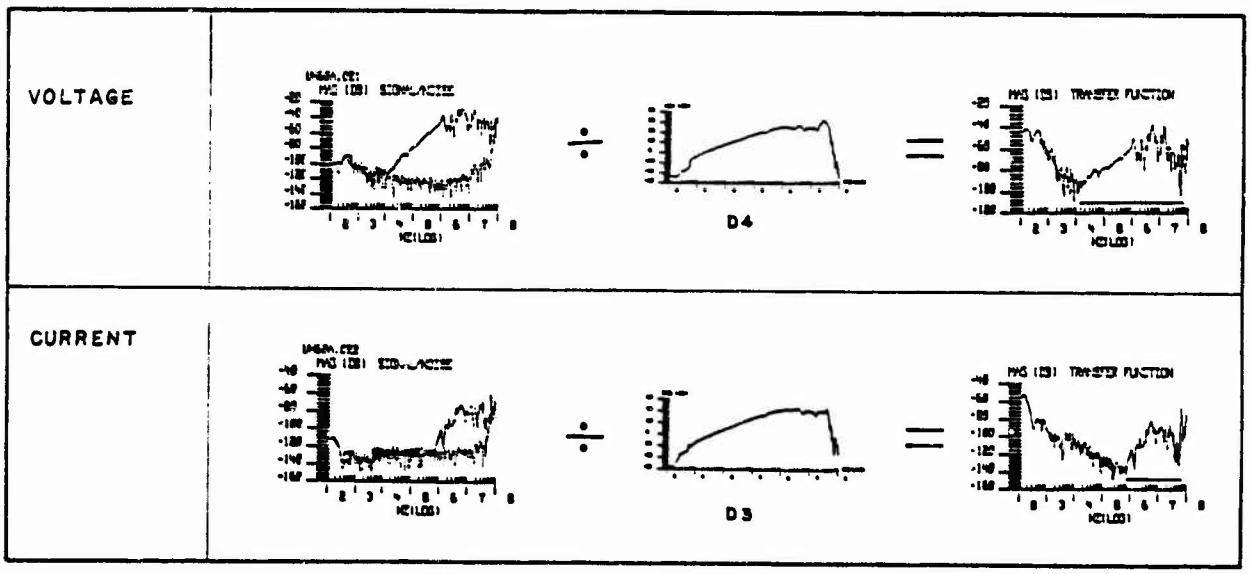

Figure 6. The SFCW Data Flow System Used to Acquire the UH-60A Data.

CABLE	PIN	PIN	APPLIED CURRENT 5KA		MEASURED		EXTRAPOLATED TO 30KA		APPLIED	MEASURED	EXTRAPOLATED TO 200KA	
			WITH	/ WITHOUT	WITH	/ WITHOUT	WITH	/ WITHOUT	30 KA	WITHOUT	WITH	/ WITHOUT
107	038	/ 039	4840.0	5020.0	V 1.0432	V 0.4164	V 6.4659	V 2.4881	29300.	V 1.1688	V 43.1059	V 7.9785
					V -1.0108	V -0.4854	V -6.2654	V -2.9005		V -1.1001	V -41.7494	V -7.5094
					I 0.0533	I 0.0699	I 0.3305	I 0.4177		I 0.1131	I 2.2033	I 0.7720
					I -0.0532	I -0.0765	I -0.3297	I -0.4571		I -0.1131	I -2.1979	I -0.7722
TYPE OF WAVEFORM (V)/(I)					C/B	C/B				A/A		

CABLE	PIN	PIN	APPLIED CURRENT 5KA		MEASURED		EXTRAPOLATED TO 30KA		APPLIED	MEASURED	EXTRAPOLATED TO 200KA	
			WITH	/ WITHOUT	WITH	/ WITHOUT	WITH	/ WITHOUT	30 KA	WITHOUT	WITH	/ WITHOUT
107	040	/ 079	5016.7	4960.0	V 1.1932	V 1.3714	V 7.1336	V 8.2948	28100.	V 3.5385	V 47.5708	V 25.1851
					V -1.2538	V -1.3412	V -7.4978	V -11.1363		V -5.2236	V -49.9854	V -37.2145
					I 0.0300	I 0.0399	I 0.1795	I 0.2416		I 0.1930	I 1.1965	I 1.3733
					I -0.0532	I -0.0565	I -0.3182	I -0.3420		I -0.2490	I -2.1210	I -3.9071
TYPE OF WAVEFORM (V)/(I)					C/B	E/B				E/B		

CABLE	PIN	PIN	APPLIED CURRENT 5KA		MEASURED		EXTRAPOLATED TO 30KA		APPLIED	MEASURED	EXTRAPOLATED TO 200KA	
			WITH	/ WITHOUT	WITH	/ WITHOUT	WITH	/ WITHOUT	30 KA	WITHOUT	WITH	/ WITHOUT
107	072	/ 073	5016.7	4856.7	V 1.2723	V 1.2913	V 7.6112	V 7.9765	27500.	V 3.6381	V 50.7415	V 26.4589
					V -1.2609	V -1.3269	V -7.5401	V -8.1964		V -3.1022	V -50.2671	V -22.5685
					I 0.0399	I 0.0666	I 0.2238	I 0.4112		I 0.1996	I 1.5921	I 1.4516
					I -0.0433	I -0.0765	I -0.2599	I -0.4726		I -0.6122	I -1.7260	I -4.4522
TYPE OF WAVEFORM (V)/(I)					F/B	F/B				F/H		

Figure 8. A Copy of a Data Sheet From the F-16/LANTIRN Tests.

Figure 7. Zenith Computer Controlling Two Digitizer Systems.

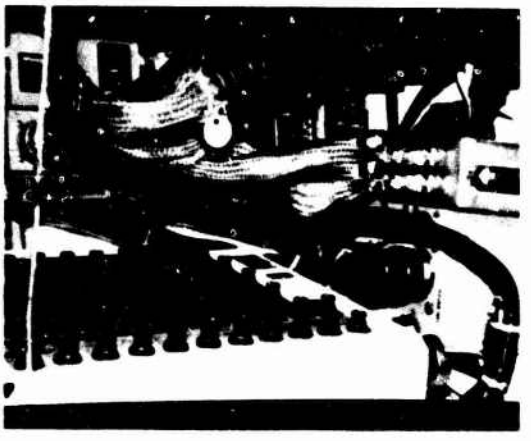

Figure 9. A Picture Showing the Breakout Box in a Compartment of the F-16.

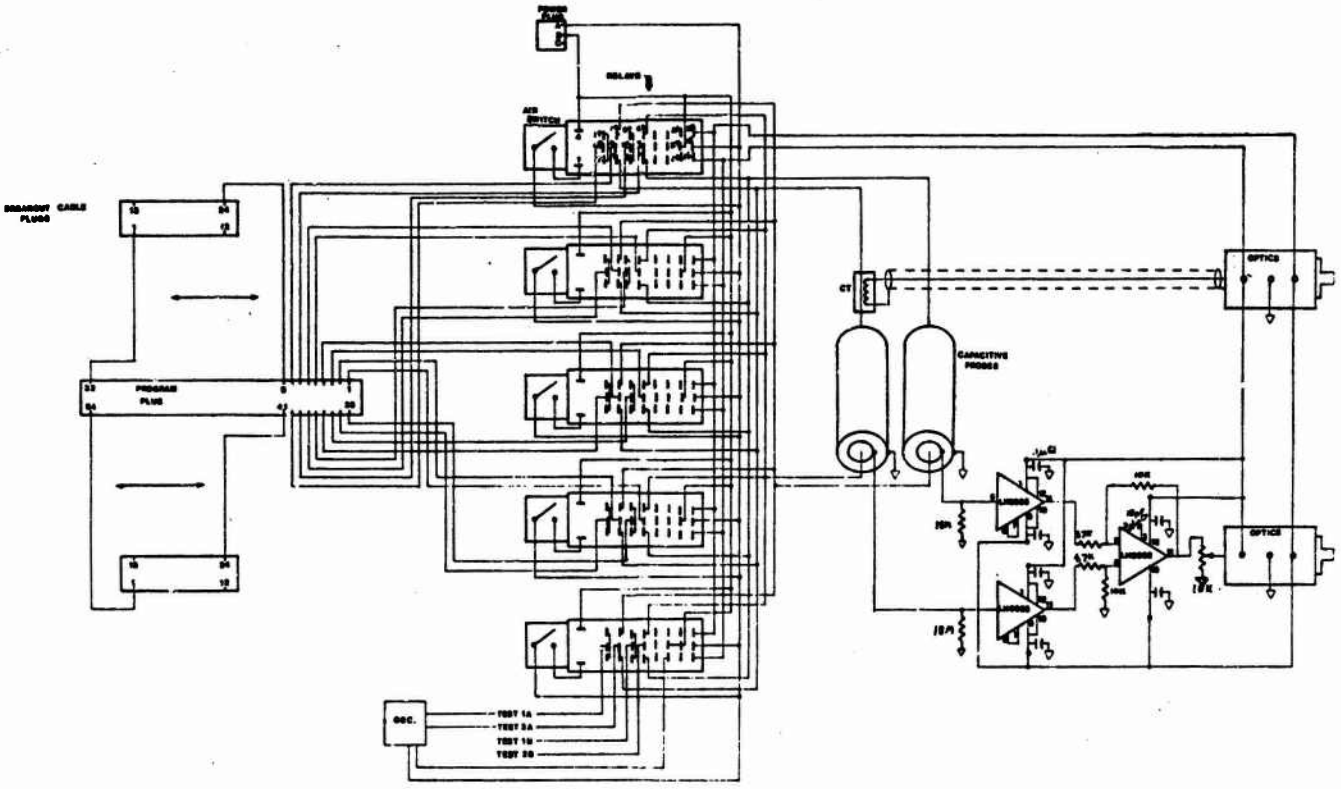

Figure 10. A Schematic Drawing of the Breakout Box Used During the F-16/LANTIRN Tests.

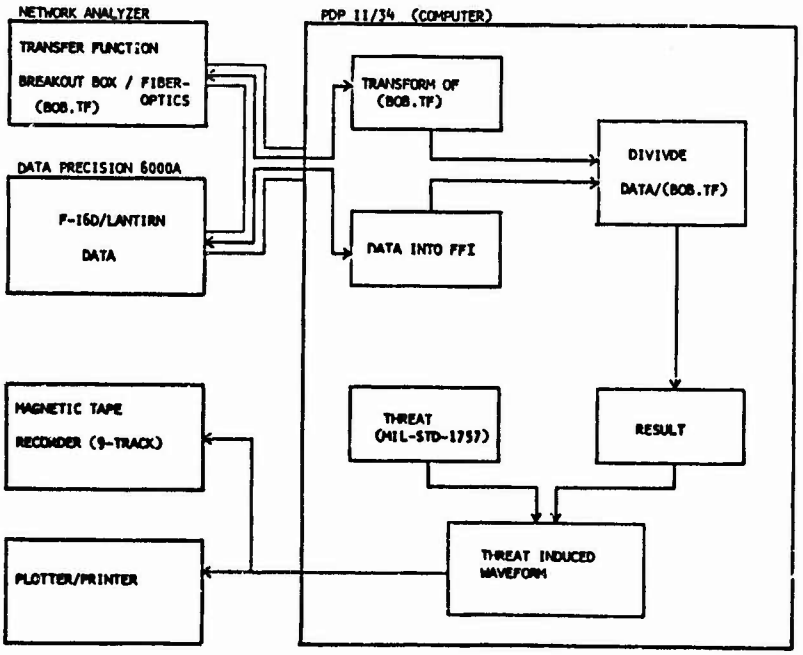

Figure 11. Data Flow Diagram for the Frequency Domain Analysis of the July 1985 F-16/LANTIRN Susceptibility Test Data.

COMPARISON OF LOW LEVEL FREQUENCY DOMAIN LIGHTNING SIMULATION TEST TO PULSE MEASUREMENTS

David B. Walen
Boeing Military Airplane Company
Seattle, Wasnington

ABSTRACT

Three lightning test tecnniques were used to measure induced transients on a modified F-14A airplane. The F-14A was modified by adding graphite/epoxy skin panels and by installing special avionics equipment. Test tecnniques demonstrated on tne F-14A included low current (less than 20A) swept frequency transfer function measurements, moderate current (28 kA) pulse tests and nigh current (200 kA) pulse tests. The results of the measurements were compared using Fourier transformations and linear extrapolation. Responses measured at lower current levels and extrapolated to nigner current levels were 25 percent lower to 32 percent higher than the responses measured at nigh levels.

INTRODUCTION

PROTECTING AIRCRAFT SYSTEMS from undesirable effects of lightning-induced transients requires careful protection design, installation and verification. Lightning simulation tests can be used to support the protection design and to verify the effectiveness of the protection design.

Results of three lightning simulation test techniques, performed on a modified F-14A airplane, were compared as part of the Atmospheric Electricity Hazards Protection program. The tests and evaluation showed the variations that resulted when induced transient responses were extrapolated from low drive current levels to higher drive current levels associated with the lightning environment. The magnitude of these variations can influence the safety margin requirements imposed during the lightning protection design, test and evaluation process. In addition, quantifying the variations will allow selection of cost-effective tests for the lightning protection verification.

DISCUSSION

The F-14A airplane used for the lightning simulation tests was modified by installing graphite/epoxy skin panels in place of aluminum panels. Other aluminum panels were removed to represent nonconducting composite skin materials. Special avionics systems were installed, including an automatic flight control system from an air-launched cruise missile, and an airborne computer and control panel linked by a MIL-STD-1553B data bus [1]*.

Three distinct sets of simulation equipment and techniques were used in the F-14A lightning tests to monitor the induced transient responses [2]. The techniques and equipment were:

a. Swept-frequency transfer function measurements using low drive currents (less than 20A) and network analyzers.
b. Current pulse response measurements using a moderate-level current (28 kA) pulse generator and transient digitizers.
c. Current pulse response measurements using a high-level current (200 kA) pulse generator and transient digitizers.

The F-14A was tested in the Boeing Military Airplane Company lightning test facility in Seattle, Washington. Figure 1 shows the arrangement of the F-14A and the lightning simulation equipment. Current was injected into the nose bulkhead of the F-14A and exited the airplane at the tail. Poultry netting was used to return the current from the tail to the nose drive point. The current injected on the airplane was monitored at the nose injection point during the transfer function tests and at the tail exit point for the pulse tests. The transient responses from the test probes were monitored using wide-bandwidth analog fiber optic systems. Network analyzers and transient digitizers were located in a shielded instrumentation room.

Transfer functions were measured using a computer-based swept frequency network analyzer system. The transfer functions were measured as responses relative to the drive current at the nose of the F-14A, so that

$$H(f) = \frac{R(f)}{I(f)}$$

where H(f) is the measured transfer function
R(f) is the test point response and
I(f) is the airplane drive current.

The transfer functions were corrected to compensate for the test probe characteristics and the reference current variations. The transfer function amplitude and phase were measured at 381 discrete frequencies between 100 Hz and 50 MHz. Below 1 kHz the signal to noise ratio was generally less than 10dB. For further analysis, the transfer function characteristics were estimated where the response was below the noise amplitude. The estimate was extrapolated from the trend of the measured transfer function amplitude and phase above 1 kHz.

A Fourier transform program was used to calculate the time response from the measured transfer function. An integration algorithm was used to allow unequally spaced frequency samples to be used for the transformation. The general operation is shown by the equation

$$r(t) = F^{-1}[H(f)I(f)]$$

where r(t) is the test point time domain response
H(f) is the test point transfer function
I(f) is the drive current spectrum and
$F^{-1}[\,]$ is the inverse Fourier transform operation.

A double exponential current waveform was used for the drive current function. The time constants of the double exponential equation were selected from the corner frequencies of the moderate level pulse generator current spectrum. The amplitude coefficient was determined from the moderate pulse generator output current peak amplitude. The double exponential spectrum is

$$I(f) = I_0 \left[\frac{1}{\alpha + j\omega} - \frac{1}{\beta + j\omega} \right]$$

where I(f) is the current spectrum
Io is 27.7×10^3 A
α is $4.35 \times 10^3 s^{-1}$
β is $2.5 \times 10^6 s^{-1}$
j is $\sqrt{-1}$
ω is the radian frequency ($2\pi f$)

This spectrum was used to simulate the moderate-level pulse generator output current for comparing the moderate-level pulse responses and the transformed transfer functions.

A fast rise time pulse generator was used to generate the moderate level (28kA) current pulse into the F-14A. The pulse generator produced a waveform to the peak amplitude that was approximately a quarter sine wave cycle at 208 kHz (figure 2). The peak current was 28 kA. The 530-kHz ripple occurring past the peak was due to the Marx generator ringing after the crowbar switch is closed. The 3.1-MHz ripple was due to the F-14A

* Numbers in brackets designate References at end of paper.

and return wire quarter-wavelength transmission line resonance. The major characteristics of the measured moderate-level current pulses are listed in table 1.

Current pulse tests were performed on the F-14A with peak amplitudes up to 200 kA. A high-energy crowbarred Marx generator was used for these tests. Maximum amplitude pulses from this generator represent the severe lightning threat defined for the AEHP program [3]. An example of the measured high-energy current waveform is plotted in figure 3. The significant characteristics of the measured waveform are listed in table 1. The measured waveform for the nose-to-tail current path shows ripple at 3.4 MHz caused by the airplane and return wire transmission line quarter-wavelength resonance.

TABLE 1. CURRENT PULSE CHARACTERISTICS

	Moderate	High
Peak current (kA)	28	200
Rate-of-rise (10-90%) (A/s)	3×10^{10}	1.7×10^{11}
Time to half value (μs)	80	40
Action integral (A^2-s)	3.5×10^{4}	2.5×10^{6}

The responses measured during the moderate and high level pulse tests were compared by simple extrapolation. The factor for extrapolating the 28-kA pulse responses to compare with high drive current responses was selected from the drive current peak amplitude or the ten to ninety percent rate of rise. Waveform and transfer function inspection was used to determine which factor to use for the extrapolation.

The results of four types of transient responses are presented in this paper. The responses include:

a) Magnetic flux measured on the outside of the F-14A skin panels.
b) Voltage measured across F-14A skin panels.
c) Voltage measured on individual wires that connected to avionics equipment.
d) Overall current measured on cable bundles that interconnected avionics equipment.

The responses shown were selected from many measurements on the F-14A [4]. The selected responses had signal to noise characteristics that generally exceeded 10dB and represent typical responses for the various airplane configurations.

The current density at various locations on the F-14A was determined by monitoring the rate of change of the magnetic flux ($d\phi/dt$). The measurements were made by measuring the voltage on small single-turn loops aligned parallel to the plane of the F-14A nose-to-tail axis. The $d\phi/dt$ responses measured during the moderate and high-level pulse tests were proportional to the time derivative of the drive current. The transfer function for the field probe voltage measured at TP1206 is shown in figure 4. An example of the response measured at fuselage station 313, test point TP1206, is shown in figure 5. This figure compares the response measured during the moderate-level pulse tests plotted with the response from the transformed transfer function. The two responses are proportional to the current rate of rise. The transfer function response peak amplitude is 11 percent higher than the measured moderate-level pulse response. The oscillation in both waveforms is caused by the quarter-wave airplane resonance.

The plots in figure 6 show the measured loop voltage versus the drive current rate of rise for TP1206. The straight line shows the extrapolation from the value measured at 28 kA. The amplitude extrapolated from the 28-kA drive current was 18 to 23 percent lower than the amplitudes measured at the higher drive currents.

Voltage was measured across a skin panel on the turtle deck. The voltage probe wire was attached to the aft fasteners on the panel. The voltage was measured between the forward fasteners and the probe wire at the front of the panel. The wire was routed adjacent to the panel to minimize loop-coupling effects. This probe measured the voltage caused by joint and panel resistance.

The transfer function in figure 7 shows the voltage response for the graphite/epoxy turtle deck panel. At low frequencies, the response increases at 20 dB per decade. This implies that at low frequencies the wire senses low voltage in the panel because most current would flow in the low-resistance aluminum panels and substructure. Above 30 kHz, the amplitude for the graphite-epoxy panel flattens out. The amplitude reflects a panel resistance of 7.9 mΩ for the turtle deck panel.

Figure 8 shows the waveforms of the structural voltage measured across the turtle deck panel. This figure compares the measured moderate-level pulse response and the response from the transformed transfer function. Both waveforms have very similar characteristics, including relatively fast amplitude decay at the later time. The amplitude of the transformed response was 13 percent higher than the measured pulse response amplitude.

The plot in figure 9 shows the peak measured amplitude versus the drive current for the structural voltage measured on the turtle deck panel. This test showed a linear scaling response, with amplitudes extrapolated from the 28-kA drive current exceeding the measured amplitude for higher drive currents by 9 to 17 percent.

One avionic system used in the F-14A tests consisted of an operational air-launched cruise missile automatic flight control system that included the flight control computer, sensors, and actuators. During the avionic transient response tests, the inertial navigation equipment (INE), radar altimeter (MRA), and flight control system equipment (FCSE) components were replaced with transient monitoring boxes. These monitoring boxes contained voltage test probes, attenuators, test point selector switches, and fiber optic transmitters. The voltage was measured on selected wires that connected to the avionic equipment.

Test point TP2202 was used to monitor the transients on the FCSE throttle actuator wire. The configuration includes the graphite-epoxy turtle deck panels and open forward avionics bays. The response was generally proportional to the time

derivative of the drive current waveform as indicated by the slope of the transfer function amplitude in figure 10. The waveform in figure 11 shows the response on this wire for the 28-kA drive current pulse. The figure shows the waveforms from the moderate-level pulse measurements and transformed transfer function measurements. The peak amplitudes of the measured pulse response was 3 percent higher than the transformed response peak. The oscillations at the airplane quarter-wavelength resonance dominate the response, which indicates the high-frequency coupling to the wire.

Figure 12 shows the peak voltage measured on the FCSE test point plotted versus the drive current rate of rise. The amplitude extrapolated from the 28kA drive currents ranged from 27 to 32 percent higher than the amplitude measured at higher drive current levels for the FCSE test point TP2202.

Currents on interconnecting cable bundles were measured using current transformers. The instruments monitored the overall current on the cable bundles, not individual wire currents. Figure 13 shows the current transfer function measured on wire bundle W3 (TP2501) during 28-kA pulse tests. This wire bundle is made up of twisted pair wires for the avionics equipment 28V-dc power. The transfer function for the current shows low amplitude below 5 kHz. For frequencies between 5 kHz and 1 MHz, the amplitude varies about 18dB, with no dominating response characteristic. The wire bundle current was generally proportional to the drive current in the early pulse times. Figure 14 shows responses for the moderate-level pulse measurement and the transformed transfer function. The peak amplitudes are within 12 percent, and the general waveshapes are similar. The measured moderate-level pulse response does not show the oscillations caused by the airplane quarter-wavelength resonance effects. However, the measured pulse response was not compensated for high-frequency-bandwidth limitations on the current probe, whereas the transfer function was compensated.

Figure 15 shows the currents for TP2501 plotted versus the airplane drive current. The amplitude extrapolated from the 28-kA drive current was 26 to 28 percent higher than the amplitude measured at higher drive currents.

SUMMARY

Transfer function responses were multiplied by the drive current spectrum, transformed into time responses using Fourier transforms, and then compared with responses measured during the 28-kA pulse tests. For four test points the pulse test responses were from 3 percent higher to 13 percent lower than the transformed transfer function responses. The mean pulse test amplitude was 8 percent or 0.7 dB lower than the transformed transfer function response amplitude. One factor affecting the quality of the transformed responses was the noise floor relative to the transfer function response. Noise measurements were taken for each specific test arrangement and the results were compared with the test point responses.

For eleven transient voltage, current, and field measurements, the high-level pulse response amplitudes ranged from 23 percent higher to 32 percent lower than the 28 kA responses extrapolated to the higher drive currents. The drive current amplitude or rate of rise were used for the scale factor. The extrapolated responses mean variation was 11 percent or 0.9 dB higher than the measured response amplitudes. The measurements were performed with 100-, 150-, and 200-kA nominal drive levels.

ACKNOWLEDGMENTS

This work was supported by the U. S. Air Force Wright Aeronautical Laboratories, Venicle Equipment Division, Wright-Patterson Air Force Base, Ohio under contract F33615-82-C-3406. The author would like to thank Rudy C. Beavin and Capt. M. Patricia Hebert of the Air Force program office for their support during this test and evaluation program.

REFERENCES

[1] D. L. Sommer and B. G. Melander, "Atmospheric Electricity Hazard Protection Design Evaluation - F-14A," Boeing report D180-27423-34, prepared under contract F33615-82-C-3406, December 1984.

[2] T. A. Prestwood and D. B. Walen, "Atmospheric Electricity Hazards Protection Validation Test Plan - F-14A," Boeing report D180-27428-38 prepared under contract F33615-82-C-3406, March 1985.

[3] B. G. Melander, "Atmospheric Electricity Hazards Threat Environment Definition," AFWAL-TR-85-3052, August 1985.

[4] D. B. Walen and M. M. Simpson, "Atmospheric Electricity Hazards Protection Assessment, Test and Analysis - F-14A," Boeing report D180-27423-44 prepared under contract F33615-82-C-3406, draft January 1986.

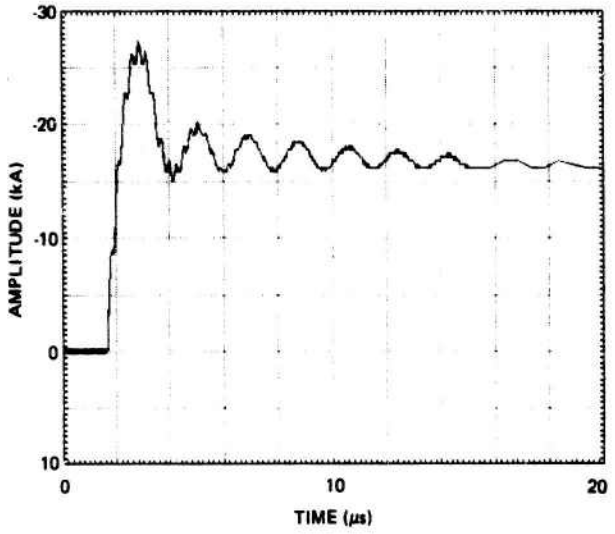

Figure 1. Moderate-Level Current Pulse Waveform

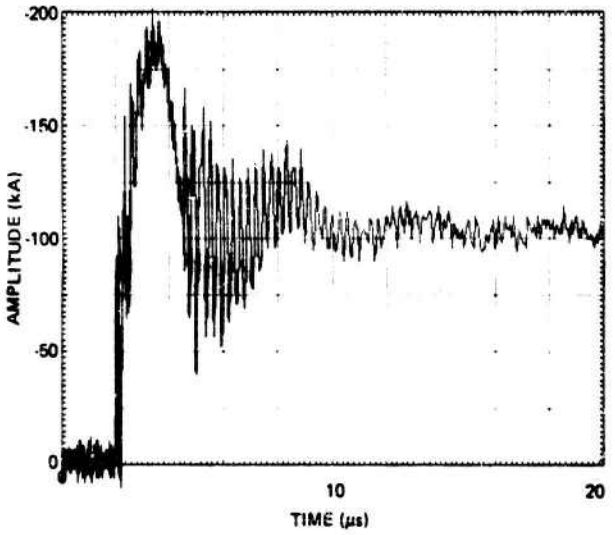

Figure 2. High-Level Current Pulse Waveform

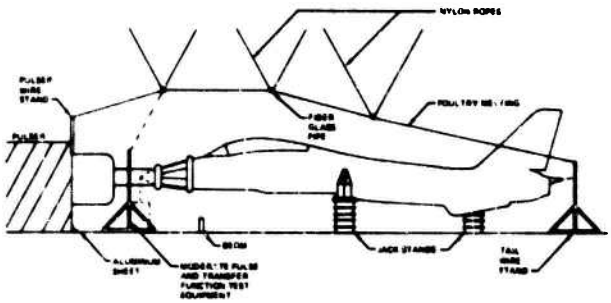

Figure 3. F-14A and Test Equipment Arrangement

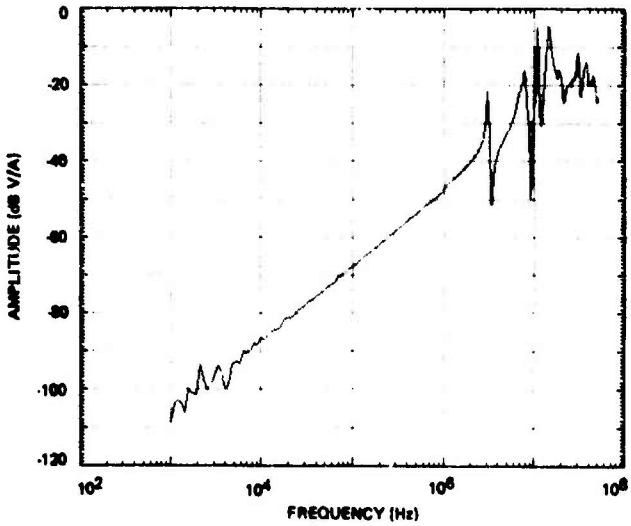

Figure 4. External Field Probe Voltage Transfer Function (TP1206)

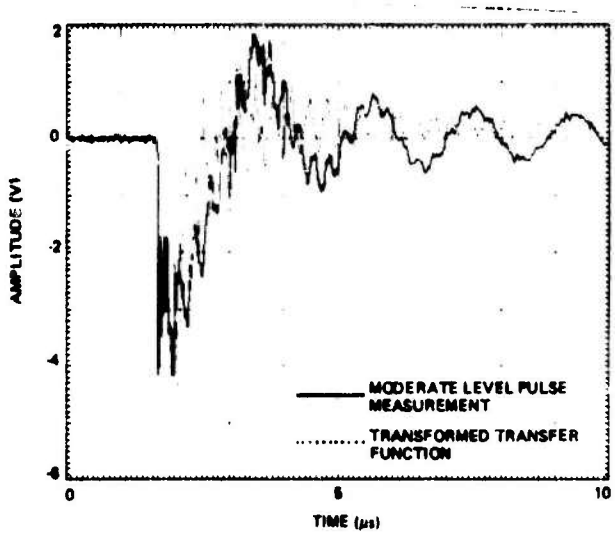

Figure 5. Field Probe Voltage (TP1206)

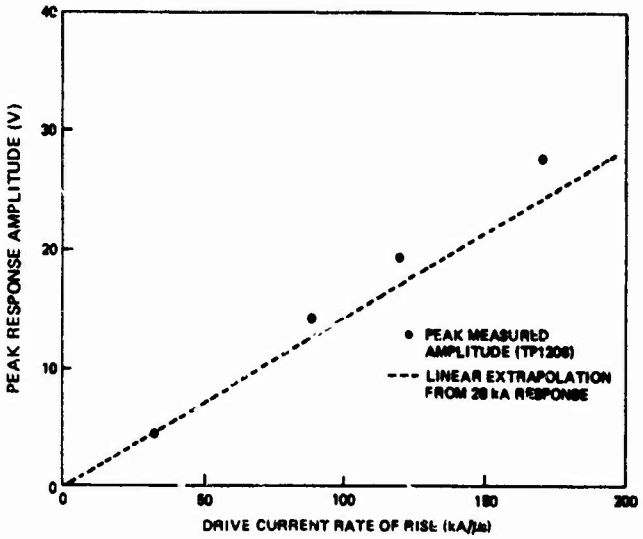

Figure 6. External Field Probe Amplitude Versus Drive Current (TP1206)

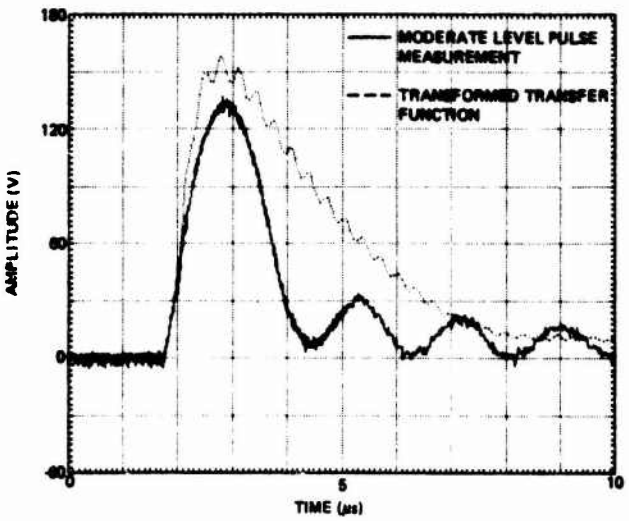

Figure 8. Structural Voltage on Graphite-Epoxy Panel (TP1402)

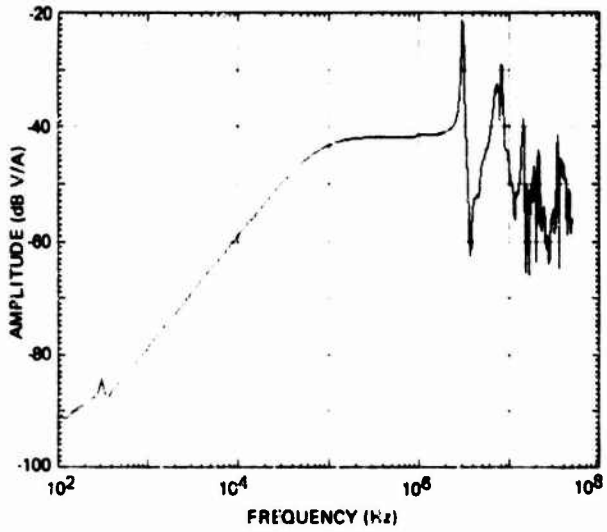

Figure 7. Structural Voltage Transfer Function (TP1402)

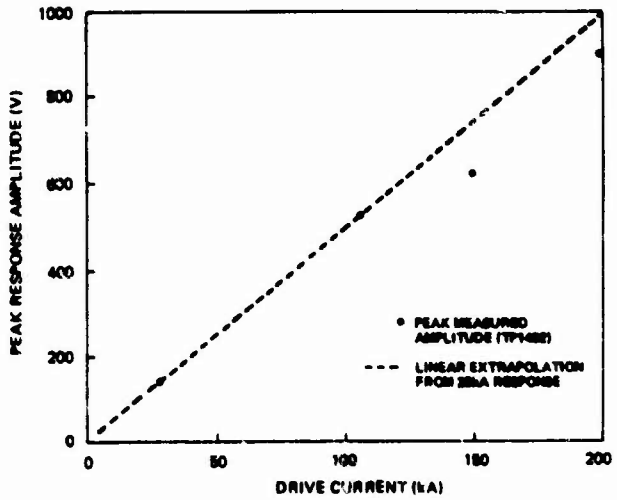

Figure 9. Structural Voltage Amplitude Versus Drive Current (TP1402)

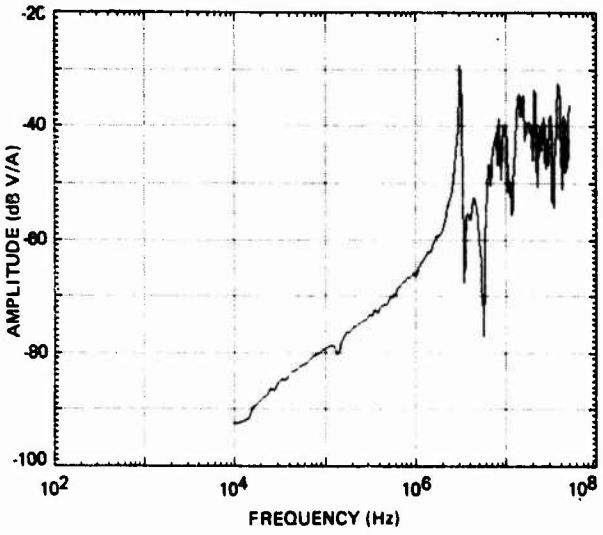

Figure 10. FCSE Throttle Control Pin Voltage Transfer Function (TP2202)

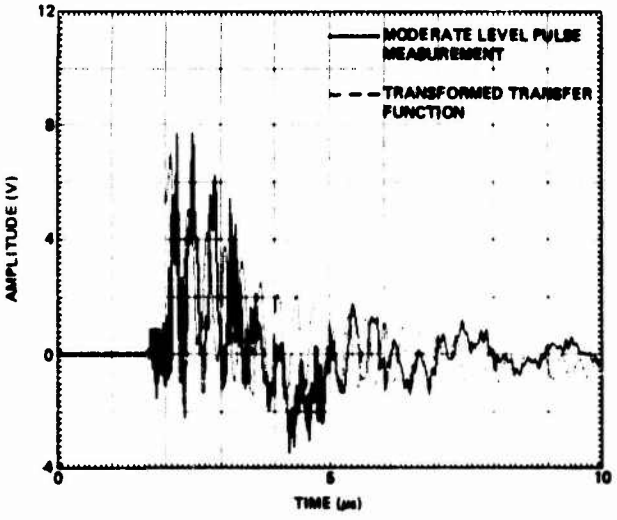

Figure 11. Voltage on FCSE Throttle Actuator Wire (TP2202)

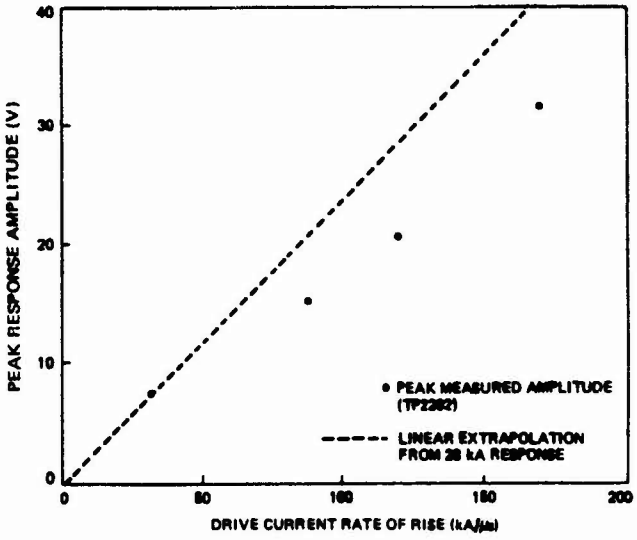

Figure 12. Circuit Voltage Versus Drive Current Rate of Rise (TP2202)

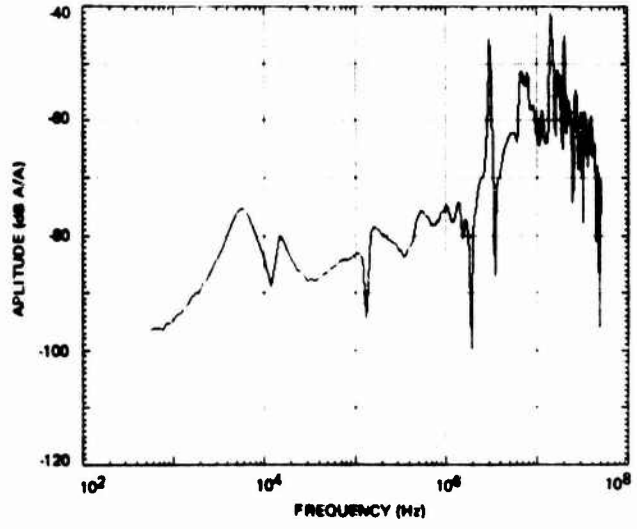

Figure 13. Cable Bundle Current Transfer Function (TP2501)

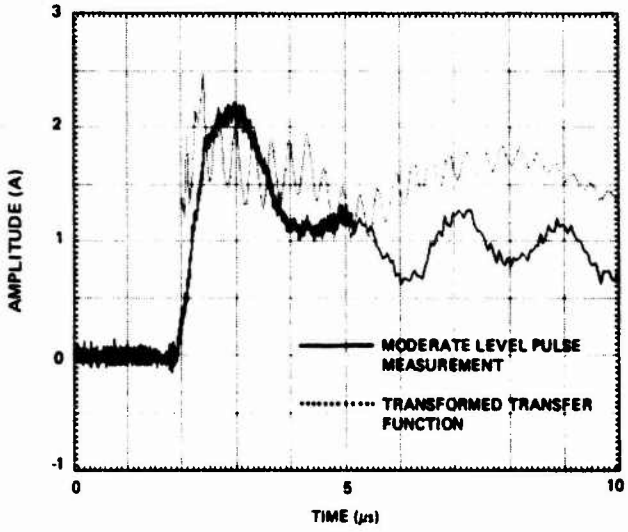

Figure 14. Current on Wire Bundle (TP2501)

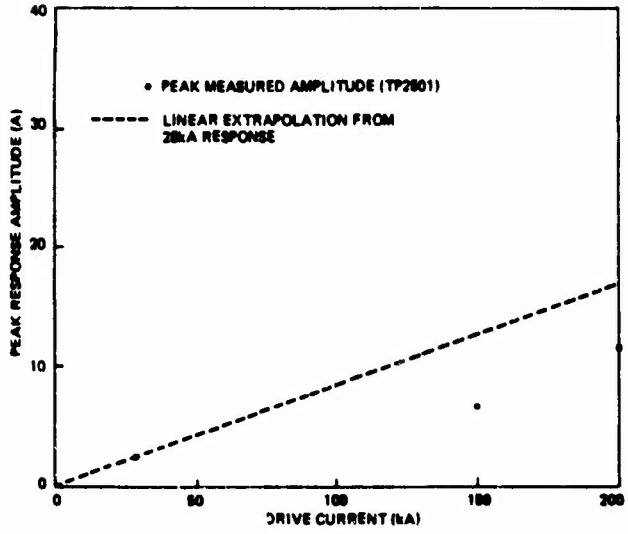

Figure 15. Cable Bundle Current Versus Drive Current (TP2501)

LIGHTNING STRIKES TO AIRCRAFT OF THE GERMAN FEDERAL ARMED FORCES

By

Wilfried Ziegler

Bundesamt fuer Wehrtechnik und Beschaffung
Leiter des Musterpruefwesens fuer Luftfahrtgeraet
der Bundeswehr (BWB-ML)

(Federal Office for Military Technology and Procurement
Director of Aeronautical Equipment Qualification
for the Federal Armed Forces)

ABSTRACT

A survey is given of the lightning strikes from 1973 through 1985. About 80% of the more than 345 lightning strikes reported involved the following four types of aircraft: F-104G "Starfighter", F-4 "Phantom", C-160 "Transall", and BR-1150 "Breguet Atlantic". For these four aircraft the lightning strike rates per year and the average rates for the whole period of 13 years will be shown. Since 1978 detailed evaluations of more than 230 incidents of lightning strike damage to aircraft are at hand. From this evaluation a statement on the safety hazards due to lightning strikes in flight will be deduced. The hazard to the respective aircraft at the time of the lightning strike will be assessed with respect to each incident of damage. Then this hazard will be classified according to four hazard severity categories, as specified: catastrophic, critical, tolerable and negligible. Finally, the lightning strike risk will be summarized and commented upon.

GENERAL SURVEY 1973-1985

This report is a continuation up to the end of 1985 of the statistical evaluation commenced in the previous report (1)*. By including the years from 1983-1985, the statistical information previously gained on lightning strike rates, distribution of the lightning strikes versus flight level, and attachment points has changed only slightly.

The statistical basis became broader, more than 345 lightning strikes occurred as compared to 260 strikes.

Also, the statements then made on damage are basically confirmed by the events of the following three years. Since 1978, detailed investigations and evaluations of more than 230 lightning strikes are now at hand.

This statistical basis now appears to be broad enough to deduce a statement on the safety hazards due to lightning strikes in flight.

LIGHTNING STRIKE RATE - From 1973 to 1985 more than 345 lightning strikes were reported. Of these, slightly more than 80% involved the following aircraft types:

F-104 G "Starfighter"
RF-4E/F4-F "Phantom"
-Fighter/Reconnaissance Aircraft (Mach 2+)
C-160 "Transall"
- Transport/Cargo Aircraft

BR-1150 "Breguet Atlantic"
- Long-Range Sea Reconnaissance Aircraft,

These 4 aircraft types are subsequently referred to in short as F-104, F-4, C-160, and BR 1150.

For these 4 types the lightning strike rates per year related to the respective flying hours and landings in that year are shown in the following Figures 1 and 2.

For all 4 aircraft types together it becomes apparent that the rate of lightning strikes related to landings is higher than that related to flying hours. This means that on an average more than one flight hour lies between two landings.

The great variation of the strike rate from one year to the next has no discernible relation to the number of flying hours.

Between two successive years, aside from a few exceptions, the number of flying hours or landings varies by $\pm$ 10% from the respective previous value. The number of lightning strikes, in contrast, varies 5 to 6 times from one year to the next.

Figure 3 shows the rates averaged over a period of 13 years for the 4 types of aircraft. The differences which become evident here are attributable to the different mission conditions in each case; the influence of individual years becomes less important. The F-104 and F-4 aircraft are subject to comparable conditions; in particular, however, training activities allow the meteorological conditions to be taken into account to a large extent. The respective tasks of the C-160 and BR-1150, on the other hand, do allow no or only little consideration of the meteorological conditions with respect to possible lightning events. It becomes evident that the selection of the reference magnitude for such strike rates is quite important, since the rates related to landings are comparable for both C-160 and BR-1150, but not those related to flying hours.

The lightning strike rates plotted in percent against the flight level in Figure 4 are close together for all 4 types of aircraft. The differences between the individual aircraft types cannot be definitely assigned to specific causes, the statistical basis still being too narrow.

But even the extremely few lightning strikes to the BR-1150 (less than 15) fit in well. From Figure 4 it can be generalized, however, that
-irrespective of the type of aircraft, type of propulsion, mission, and geographical location of the training aera-
the flight level is an essential factor with respect to the probability of lightning strikes.

This fact receives increased emphasis when a comparison is made of the flying hours accumulated by the 4 types of aircraft over a period of 13 years (rounding +/-10% max):

BR-1150 : C-160 : F-4 : F-104 =
1 : 4 : 7 : 9 .

These relations do not become evident at all from Figures 3 and 4.

ATTACHMENT POINTS AND AIRCRAFT WITH MULTIPLE LIGHTNING STRIKES - With respect to the F-104, F-4, and C-160 aircraft more than 270 lightning strikes were reported within the 13 years' period (1973-1985).

The evaluation of both F-104 and F-4 together shows the following results:

- More than 160 lightning strikes. As far as attachment points were detected, these were located in
  about 45% of the cases on pitot and radome,
  about 22% of the cases on wings including tips and tip tanks,
  about 21% of the cases on the horizontal/vertical tail.
- In some cases no definite attachment points were detectable, or none of these zones was affected.
- In 18 cases the aircrew felt electrical or mechanical shocks.
- In 9 cases the aircrew did not become aware of the lightning strike during flight.

The results for the C-160 aircraft were as follows:

- More than 110 lightning strikes. As far as attachment points were detected, these were located in
  about 42% of the cases on the radome,
  about 23% of the cases on the wings,
  about 16% of the cases on the horizontal/vertical tail.
- In some cases no definite attachment points were detectable, or none of these zones was affected.
- In 1 case the aircrew felt an electrical shock.
- In 1 case the lightning strike was not noticed by the aircrew during flight.

In these 13 years since 1973 some aircraft were hit several times:

*Numbers in parentheses designate references at the end of the paper.

F-104	1	a/c 3 times
	10	a/c 2 times each
F-4	1	a/c 3 times
	9	a/c 2 times each
C-160	1	a/c 7 times
	2	a/c 5 times each
	3	a/c 4 times each
	6	a/c 3 times each
	15	a/c 2 times each
BR-1150	2	a/c 2 times each.

Summarized in a somewhat different way:
Considering the F-104 and F-4 aircraft together, 21 a/c were hit by 44 lightning strikes, or about 2.8% of the total fleet by approximately 27.5% of the strikes.
As to the C-160 aircraft, 27 a/c sustained 77 lightning strikes, or about 28% of the fleet approximately 69% of the strikes.

LIGHTNING STRIKE RISK

Since 1978, the reported lightning strikes have been investigated and evaluated with respect to damage caused by the lightning strikes on the basis of uniform criteria.

As concerns the lightning strike risk, of first and foremost importance are the effects of a lightning strike damage on the safety of the aircraft during its continued flight following the strike, including the landing. The real extent of damage, for example judged by the expenditure for its repair, is second-rate under aspects of flight safety as long as the immediate loss of the aircraft due to the lightning strike as the greatest possible damage is not to be expected. Even minor damage the repair of which requires almost no expenditure may considerably affect the aircraft safety if systems essential to that effect have been involved.

It is the objective to deduce a statistically supported statement on the lightning strike risk for certain aircraft types in case of lightning strike.

DEFINITION OF HAZARD SEVERITY CATEGORIES - The more than 230 lightning strikes, investigation of which is now available, constitute a sufficiently broad and representative cross section of possible and typical lightning strike damage on the aircraft affected.

For the purpose of qualitative assessment of the effects of such damage on flight safety, four hazard severity categories were defined in accordance with MIL-STD 882.

For the aircraft there is a hazard of
- category 1 (Catastrophic Hazard)
  in the case of damage that may directly lead to a mishap;
- category 2 (Critical Hazard)
  in the case of damage with less effects than in category 1, but that does not permit continuation of flight after landing;
- category 3 (Tolerable Hazard)
  in case of damage that permits continuation of flight after landing, with certain conditions imposed, however;
- category 4 (Negligible Hazard)
  in the case of damage that does not have to be repaired before the next periodic maintenance action.

The ability of the aircraft to safely continue flight after the landing was chosen as a measure for distinction between categories 2-4. This appeared to be more adequate for the lightning strike damage classification and corresponds to the graduation of "major" - "minor" - "less than minor" aircraft damage in MIL-STD 882.

SELECTION OF LIGHTNING STRIKES 1978 - 1985 - Of the more than 230 evaluated lightning strikes in this period of time more than 180, or about 77% of the strikes, involved three types of aircraft, the rest being distributed among further 13 aircraft types.

Each aircraft struck by lightning during flight, or for which the suspicion of a lightning strike existed, was inspected immediately after its landing by BWB-ML for damage caused by lightning strikes.

This damage was then assessed by BWB-ML with respect to aircraft safety hazards at the moment of the strike and to the ability of the aircraft to continue flight after the landing.

This resulted in the classification of the incidents in one of the four categories.

The following three types were affected with almost equal frequency:
F-104 about 33%,
F-4 about 28%, and
C-160 about 39%.
With respect to the remaining types, the quantity of available data is insufficient to make a statistically significant statement. Therefore, only the above three types will be considered.

FREQUENCY OF CATEGORIES - The F-104 type of aircraft showed the following distribution:
Category 1 about 3%
Category 2 about 12%
Category 3 about 27%
Category 4 about 58%.
The F-4 type of aircraft showed the following distribution:
Category 1 about 15%
Category 2 about 13%
Category 3 about 37%
Category 4 about 35%.
The C-160 type of aircraft showed the following distribution:
Category 1 about 6%
Category 2 about 46%
Category 3 about 28%
Category 4 about 20%.
In each case the percentages are related to the total number of strikes to the respective aircraft type.

Summing up, the result is as follows:
Category 1 about 8%
Category 2 about 26%
Category 3 about 30%
Category 4 about 36%.
Consequently, it can be established that a total of about 8% of the lightning strikes clearly evidenced and investigated had influenced the aircraft safety at the moment of strike.

RISK ASSESSMENT - Generally, a risk is composed of the severity of a hazard and the probability of its occurrence.

To assess the risk associated with a lightning strike to an aircraft, impairment of its safety when

continuing flight, including the landing, is taken as a measure for the hazard severity immediately after the strike.

Therefore, the hazard severity categories 3 and 4 are negligible.

In case of a category 2 hazard, reduction of safety for flight continuation and landing may not be neglected. A safe landing is possible, but until such landing the probability of a crash caused by the lightning strike is considered extremely remote, or is excluded.

In case of a category 1 hazard, an immediate crash risk of the aircraft cannot be excluded.

Therefore, the risk assessment covers the hazards of categories 1 and 2. Relating the frequency of occurrence of these hazards to the respective flying hours, the rate thus obtained will be a measure for the probability of their occurrence. Now, the rate of category 1 and 2 hazards related to flying hours is designated as lightning strike risk.

The hazard rate of category 2 is designated as "Critical Lightning Strike Risk" (Critical LSR), and of category 1 as "Catastrophic Lightning Strike Risk" (Catastrophic LSR).

The results with respect to the three aircraft types were as follows:

Type	Critical LSR	Catastrophic LSR
F-104	0.174/10,000 FH	0.050/10,000 FH
F-4	0.161/10,000 FH	0.184/10,000 FH
C-160	1.780/10,000 FH	0.216/10,000 FH
All three types together :	0.460/10,000 FH	0.137/10,000 FH

Generally, it can be stated that in the past the Catastrophic LSR in flying operations amounted to 0.5 to 2.2/100,000 per one flying hour. Also, taking into consideration the fact that within the period of time investigated with more than 1,000,000 flying hours no crash due to a lightning strike occurred, the factual crash risk (greatest possible damage) within the Catastrophic LSR remained below 1/1,000,000 per flying hour. Presently, it is not possible to make an exact statement on the extent of the risk. A certain estimation, however, is possible by way of this statistically determined Catastrophic LSR taking into consideration the following facts:

a) The design criteria of the existing lightning protection correspond to the state of knowledge of lightning current parameters as of more than 10 years ago.
b) In all lightning strike incidents investigated, the aircraft involved showed no technical defect before the strike, neither were operating limitations exceeded.
c) In all incidents investigated, a safe landing was performed after the lightning strike.

Thus, in order to result in a crash, either a lightning strike more severe than so far experienced will be required, or, associated with the strike, further unfavorable circumstances must occur simultaneously, such as failure of an essential system independent of the lightning strike, or development of an explosive atmosphere.

In the more than 180 incidents investigated, so far none of the cases happened. Therefore, a probability of less than 1% is expected that more severe lightning strikes will occur or that such unfavorable circumstances will coincide with a lightning strike of hazard severity category 1.

Hence, the resultant crash risk probability per flying hour is less than 0.05...2.2/10,000,000.

This value is considered a limitation on the safe side for the case of a crash as the greatest possible lightning strike risk.

ACKNOWLEDGEMENT

The author wishes to acknowledge the help of Mr. M. Schirp, of BWB-ML, in collecting data reported herein and preparing the graphs.

REFERENCE

(1) Wilfried Ziegler,
"Lightning Strikes to Aircraft of the German Federal Armed Forces"
Proceedings of the 8th International Aerospace and Ground Conference on Lightning and Static Electricity, Fort Worth, Texas, U.S.A.,June 1983.

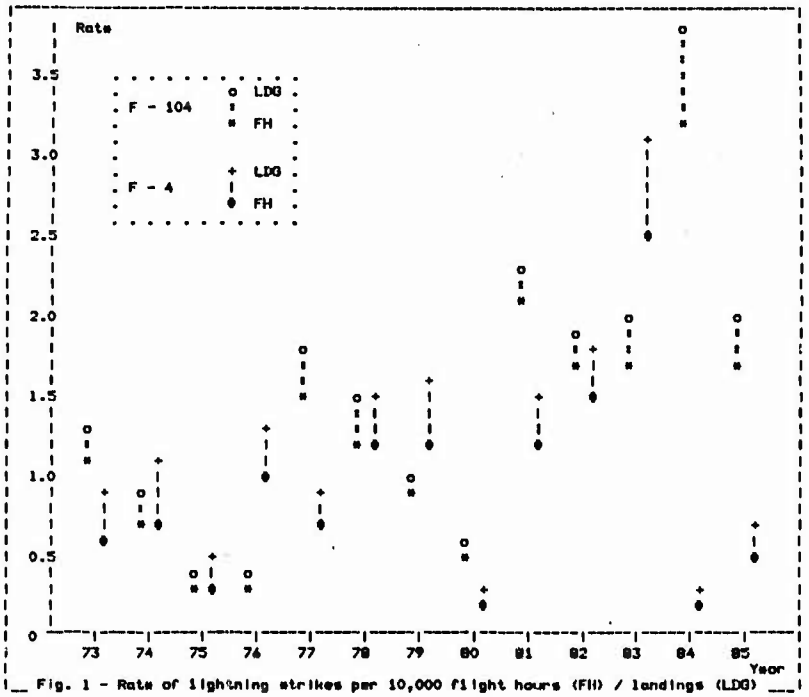

Fig. 1 - Rate of lightning strikes per 10,000 flight hours (FH) / landings (LDG)

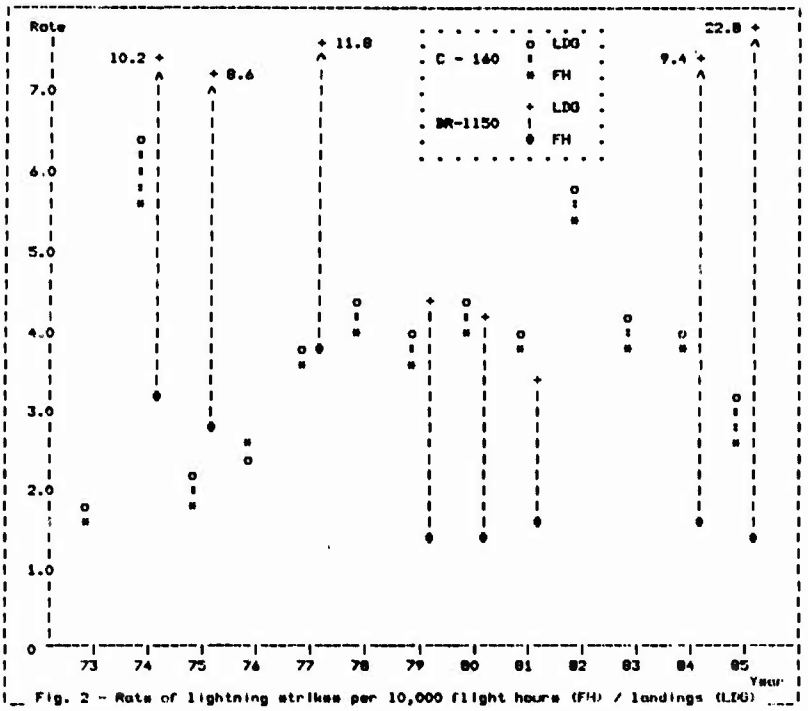

Fig. 2 - Rate of lightning strikes per 10,000 flight hours (FH) / landings (LDG)

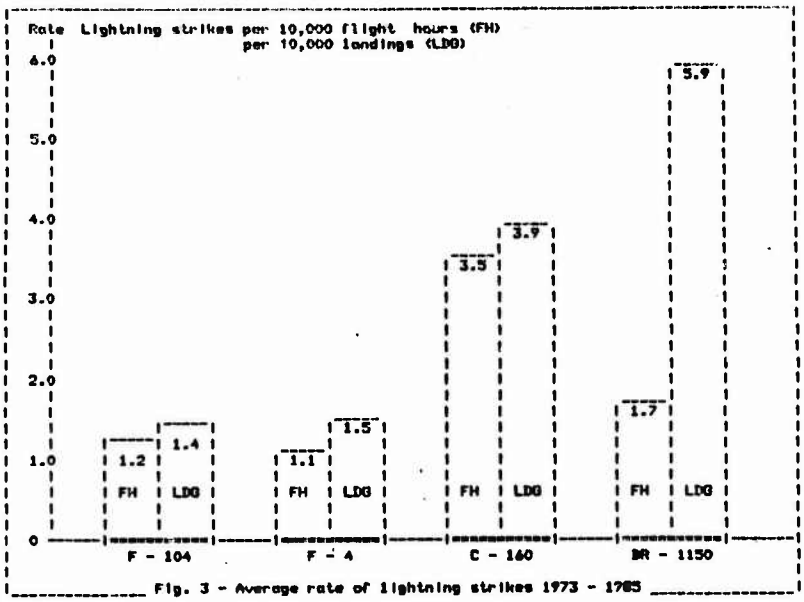

Fig. 3 - Average rate of lightning strikes 1973 - 1985

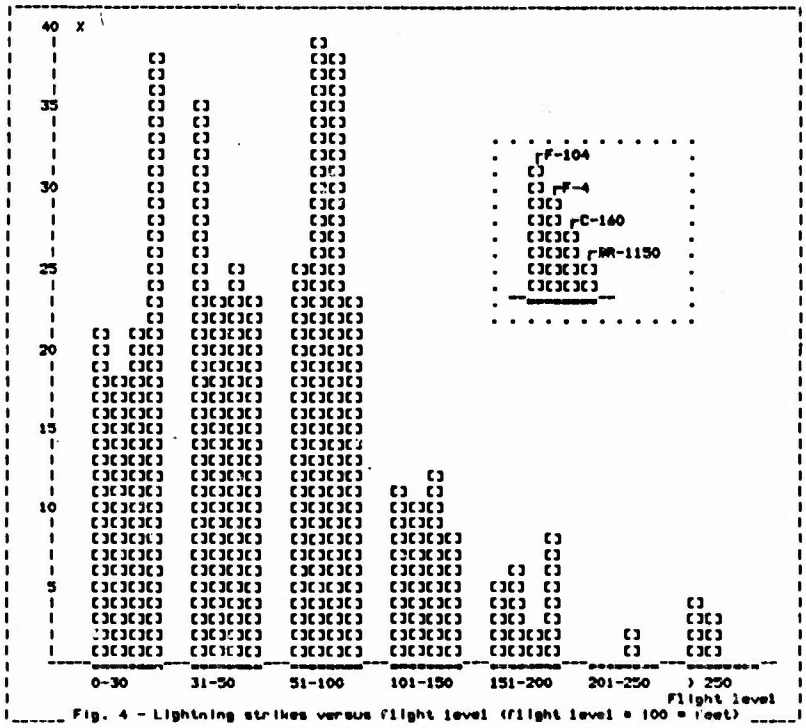

Fig. 4 - Lightning strikes versus flight level (flight level * 100 = feet)

ZONING OF AIRCRAFT FOR LIGHTNING ATTACHMENT AND CURRENT TRANSFER

C.C.R. Jones
British Aerospace, Military Aircraft Division (Warton),
A.W. Hanson
Private Consultant,
G.A.M. Odam
Royal Aircraft Establishment, Farnborough.

ABSTRACT

The zoning of aircraft surfaces into regions of different susceptibility to lightning attachment and current transport was defined many years ago on the basis of information on natural lightning strikes to in-service vehicles. The work was done for fixed wing aircraft only since the lightning experience to rotary winged aircraft was almost non-existant at that time. The observations on lightning attachment points were done by engineers and technicians involved in aircraft maintenance.

In this paper, the authors argue that the observations made for the original zoning work may have missed some vital evidence through lack of experience and understanding of what to look for. This assertion is based on recent experience of the authors in tracing attachments of natural lightning on aircraft. Since the original zoning work some new concepts have gained acceptance and understanding and these need interpretation of their effects on lightning zones. The zoning of helicopters, VTOL aircraft and delta winged aircraft is also discussed, and an alternative set of zones based on incident threat rather than the lightning component at an attachment point is presented.

ZONING OF AIRCRAFT FOR LIGHTNING ATTACHMENT AND CURRENT TRANSFER

by C.C.N. Jones (British Aerospace Military Division),
A.W. Hanson (Private Consultant)
and G.A.L. Odam (Royal Aircraft Establishment Farnborough).

1. INTRODUCTION

THE EXISTING RULES for dividing the surface of an aircraft into the probable lightning attachment zones (1,2,3,4)* were condensed from a great many records of natural lightning strikes to a variety of aircraft, mostly civil (as explained in references 5 and 6). An important feature of the recording method was that, for a number of operators and aircraft types, it was as near 100% as possible to preclude any bias towards the more severe events. The aeroplanes involved in the survey were, however of similar type and the currently popular wide-bodied types, delta-winged craft and rotor craft were not well represented. Another factor having a bearing upon the definition of rules through the recorded attachments is that the inspections were carried out, in general, by people without specific expertise in lightning. Arc burn damage is easily confused with mechanical or chemical erosion and minor arc marks might often have been discounted as arising from other causes or not observed at all. Therefore, a trailing edge burn mark might, for instance, be assessed to be a zone 1B attachment because the swept attachment points leading to it were not noted.

It is not, therefore, too surprising that experience of natural lightning strikes to these types has thrown-up some discrepancies in the application of the zoning rules as currently defined.

There is a real need for zoning rules as the protection levels designed into an aircraft structure are chosen according to the potential threats as indicated by the lightning attachment zones. Testing procedures, levels and the susceptibilities to be protected against are also selected according to the zoning. It is very important for safety of crew and passengers, and for mission accomplishment that the lightning protection levels are adequate. It is also important that lightning protection is not an unnecessary overkill for the following reasons:

a) minimum design and manufacturing costs,
b) minimum impact on other systems,
c) minimum weight penalty,
d) minimum operating costs and
e) for minimum maintenance and repair overheads.

The existing zoning rules appear to have worked quite well in practice over many years. This may be due to the inherent resistance to damage from lightning built into traditional structures and materials. The increasing use of composites is now demonstrating certain inadequacies. The new materials often lack the tolerance to lightning damage inherent in aluminium, and once the integrity of their surfaces is damaged due to lightning, there is a potential for rapid deterioration. Also, electronic systems might have ceased to function or merely have glitched in past aircraft with no repercussions on safety. Electronics in future aircraft will have executive authority over systems that are flight critical. Re-assessment of the zoning is necessary for the following reasons:

a) to tighten up the accuracy of zoning predictions because of the greater susceptibility of modern structures, materials and systems to the effects of lightning,

b) to accommodate shapes not covered by the existing rules, i.e. delta wings, foreplanes, wide bodies and large scale, rotor craft etc.,

c) to remove ambiguities and difficulties in the interpretation of the rules and provide guidance and examples of their use, and to indicate the implications of a zoning assessment.

This paper describes some of the shortcomings of the present zoning rules and suggests some possible areas of change. It is intended to provoke discussion on the subject which, it is hoped, will lead to better zoning specifications for all aircraft including rotor-craft.

2. THE CURRENT SPECIFICATIONS

In order to describe some of the difficulties and ambiguities in the use of existing zoning rules, the wording and presentation used in reference 1 are reproduced here for convenience.

"Zone 1 Surfaces of the aeroplane for which there is a high probability of initial lightning flash attachment (entry or exit).

"Zone 2 Surfaces of the aeroplane across which there is a high probability of a lightning flash being swept from a zone 1 point of initial flash attachment.

"Zone 3 Includes all of the aeroplane surface areas other than those covered by zones 1 and 2. In zone 3 there is a low probability of an attachment of the direct lightning flash. However, zone 3 areas may carry substantial lightning currents by direct conduction between two attachment points.

"Zones 1 and 2 may be further subdivided into A and B regions, depending on the probability that the flash will hang on for a protracted period of time. An A region is one in which there is a low probability that the arc will remain attached and a B region is one in which there is a high probability

* Numbers in brackets designate References at end of paper.

that the arc will remain attached. Some examples of zones are:

"Zone 1A Initial attachment point with low probability of flash hang on, such as a leading edge.

"Zone 1B Initial attachment point with high probability of flash hang on, such as a trailing edge.

"Zone 2A A swept stroke zone with a low probability of flash hang on, such as wing mid-cord.

"Zone 2B A swept stroke zone with a high probability of flash hang on, such as a wing inboard trailing edge.

"Figure 1 shows a diagram of a conventional aircraft where the zones have been identified. As indicated in the figure these zones have a finite width which is difficult to define. The existing specifications such as TSS Standard No 8-6 attempt to define the width of these zones, and their definitions are not in conflict with the present state of knowledge and are reproduced below:

"Zone 1 These areas are:

(a) within 0.5m of any trailing edge or tail extremity,

(b) within 0.5m of wing tip measured parallel to the tip,

(c) within 0.5m of any sharp leading edge which is likely to form a point of attaohment for lightning strikes,

(d) forward unprotected projections (e.g. nose, engine nacelle forward of wing), and

(e) any other projecting part may constitute a point of attachment.

"Zone 2 Extends 0.5m laterally to each side of fore and aft line passing through zone 1 forward projection points of stroke attachment. All fuselage surfaces and surfaces of nacelles not defined as zone 1 are included in zone 2 unless it can be shown, for example, that certain nacelle surfaces are adequately protected by their position relative to the wing.

"Zone 3 Surfaces for which there is only an extremely remote probability of direct or swept stroke. Ignition sources resulting from the aircraft contacting a lightning strike are either due to corona or streamering or sparking or poorly bonded joints due to the passage of lightning current through a zone 3 region. This zone includes all surfaces of the aeroplane not coming under the definition of zones 1 and 2."

The SAE AE4L Committee report(2) definitions are very similar but without the guidance on extents, and MIL-STD-1757A(3), though presenting the information differently and giving more guidance on interpretation, varies little in content. It incorrectly states that trailing edges aft of zone 1A should be in zone 1B but otherwise conforms and refers to the FAA Advisory Circular AC 20-53(4) as a source document. This last document uses very similar wording and presentation to reference 1.

3. INTERPRETATION OF EXISTING SPECIFICATIONS

The present zoning rules create considerable difficulties in interpretation for specific aircraft project applications. For instance, zone 1A and 1B are separately defined yet the extents are covered together yeilding a 0.5m band for zone 1B along a trailing edge of a wing or tail-plane surface. It is not clear to the authors whether the half metre extension of zone 1 from leading edges, trailing edges and wing tips is a genuine result of uncertainty of leader attachment or from some other cause. For example, in the case of the leading edge, initial attachments observed in this half metre band could be the result of swept leaders. At the trailing edge, apparent attachment points within the half metre zone may in fact have been mis-interpretation of the observed marks. These apparent attachment marks have been found at rivet heads and other surface discontinuities. Such marks have also been observed in hard-wired laboratory experiments in areas close to points of current input. This is clearly due to the very high zone 3 current densities in the area of the arc root.

Similarly, zone 1A is defined for a wing-tip as extending within 0.5m of the wing-tip measured parallel to the wing-tip. The extent of a zone 2A is that it should extend 0.5m laterally each side of a fore and aft line passing through zone 1A forward projection points. This it is sometimes interpreted to mean that the outermost 0.5m of a wing should be in zone 1A but that an area 0.5m wide inboard of that should be designated as zone 2A. It is difficult to conceive how aerodynamic forces might move an arc up the wing surface at a right angle to the direction of the air-stream.

Zone 3 is defined as surfaces for which there is only an extremely remote probability of direct or swept stroke attachment. The testing requirements are then defined in terms of zones and only zone 3 surfaces are specifically required to be tested using solid current connections and conducted currents. However, since most zone 1 and all zone 2 locations also have to survive zone 3 conditions, the test techniques (e.g. open arc or solid connection) must be chosen with respect to the specific hazards that might result and not just to the zone. Further, because zone 3 implies conduction of initial return strokes as well as subsequent return strokes, the test waveform parameters must be selected with due consideration for these test parameters as well as the current spreading and sharing that will result from the overall geometry of the conducting structure.

Probably the most misunderstood zone is 2B. Apart from being described as a swept stroke zone with a high probability of flash hang-on, they are more-or-less ignored. Especially confusing is the logic behind the recommended application of simulated lightning current. The present specifications implies that a long hang-on of 250ms to 1s must be simulated for a zone 2B

attachment, but in most circumstances some of the restrikes and continuing components will already have been spent on other surfaces. The application of current simulation pulses should take account of this. Specifying the residual duration of the continuing component of a lightning flash is difficult but some guidance is required or massive over-protection and over-testing will result.

4. OBSERVATIONS FROM NATURAL STRIKES

Another reason for considering a revision of the zoning rules arises from the observations of results of natural lightning strikes to aircraft inspected by two of the authors.

All of the zoning definitions put the main surface area of the vertical stabiliser in zone 3. However, several occurrences of swept stroke (zone 2A) attachments to tail fins, with zone 2B attachments to the rudder trailing edges have been observed. In one case, they were clearly swept from the fuselage, while in others, the swept attachment points formed a staight line from the fin leading edge to the rudder trailing edge. Similar occurrences have been recorded on attachments to the NASA F106 lightning research aircraft(7). Consequently, the leading edge of the fin should be considered as zone 1A with zone 2A to the rear, and the areas adjacent to the fuselage should also be considered as in zone 2A. This is especially important where a fin is used to contain fuel.

It has been found that any part of a delta wing can be subject to swept stroke attachments during natural lightning strikes(7). No forward projections or stress raisers are required on the wing skins to generate this condition. The experience of the NASA F106 flights indicate that this is usually due to sweeping of the lightning channel off the forward fuselage. The complex air flows over the wing surfaces probably account for the fact that no part of the surface can safely be said to be immune from attachment.

Two of the authors have also inspected the results of lightning strikes to several wide-bodied aircraft and noted attachment points well inboard from the wing tips, in areas which the existing zoning rules would designate zone 3. Typically, a swept stroke occurred across the upper surfaces of the wing some 2.5m inboard with a zone 2B attachment at the trailing edge. None of these attachments involved any forward projections that might have accounted for initial attachments. An occurrence of this type is predicted in the "Typical lightning strike zones" in a paper published in 1979(8), though the zone definitions included gave no means to establish that such areas were in zone 2A other than by attachment point testing.

It is difficult to theorise on the reasons for swept strokes in such areas. The straight lines of attachment points indicate that complex air flows sweeping the lightning channel up the wing are not responsible. Also, the absence of corresponding attachment points on the other surface of the wing precludes flying into an already existing lightning channel as the reason. Possible reasons are:

a) that significant space charge is fed into the volume of air around the areas on the aircraft highly stressed by the electric field between the cloud and ground before the start of the lightning discharge, and that this re-defines the high stress locations when the lightning leader approaches, and

b) that these types of aircraft are so large that, like very tall buildings, alternative rules are required to explain their interaction with the lightning phenomenon.

Though it is believed by the authors that the second is probably the more dominant factor, there is some evidence that the first may have an effect. An observation on an aircraft having sustained a natural lightning strike was that the first attachment to the nose of the aircraft was to a diverter strip on the underside of the radome. The swept stroke then tracked across the nose wheel bay door and up one side of the fuselage, then over the wing root fairing and along the fuselage above the wing. The fact that the sweeping tracked over the wing indicates a downcoming leader, as a horizontal or up-coming leader would have been intercepted during sweeping by the wing or engine nacelle, yet the initial attachment was to the underside of the radome. It is unlikely that this could result from local random variations in channel direction in such close proximity to a large conductive structure like an aeroplane. Charge scattered into the air around the tips of the diverter strips, may have caused an effective domed extension to the electrical shape of the aircraft structure re-defining the highest stress locations on the structure.

The probability that this will have an effect on attachment has been recognised for some time in the UK and high voltage attachment test techniques that account for it have been devised(9).

The second postulate might find support in the concept now applied to the protection from lightning strikes afforded by skyscaper buildings since the observation of strikes to the sides of the buildings formerly assumed to be in the "cone of protection". Applying a 25m rolling sphere(10) to the fuselage and wing of a large civil aircraft might produce the zones protected from initial attachment as shown in fig 2. As can be seen from the diagram, certain areas on the wing surfaces, leading and trailing edges and on the tail fin leading edges could all sustain direct initial attachment in agreement with the observed evidence. This technique has already been proposed in connection with the anomalous lightning attraction behaviour of a large radome with diverter strips(11).

5. SWEPT LEADERS

There has been some discussion in recent years concerning the swept leader phenomenon, and the implioations it has for zoning concepts.

The possibility of a leader channel being swept along the aircraft by virtue of its forward speed (fig 3) has long been oonsidered. It has been shown that under some extreme circumstances an aircraft could travel up to 12 metres in the time interval between the leader attachment and the arrival of the first return stroke(12). Consequently there is every reason to suspect that the leader attaohment point can also sweep at least a few metres under suitable conditions. On this basis it may be argued that the present limits set for zone 1A are no longer applicable, and under suitable conditions almost any part of the aircraft could be the point of attachment for the first return stroke. The inevitable question is - Should the limiting boundaries of the zones (especially zone 1A) be redefined?

If this were done then zone 1A would have to be extended at least into zone 2A and in most cases into zone 2B as well. But is this drastio step really necessary?

The main purpose, and oertainly the main usefullness, of the zoning concept is to determine the levels to which various parts of an aircraft should be protected and tested, and providing this criterion is still met there seems little point in far reaching ohanges which may only serve to create diffioult ambiguities without contributing anything significant to flight safety considerations.

In lightning ohannel modelling work by Little(13) the oalculated lightning ohannel parameters ohanged with altitude. Later, he considered how this could relate to the effects on airoraft at altitude(14). He conoluded that for a downward going leader, when an aircraft is struck at a significant altitude, "the (peak) current is likely to be reduced by a factor of two to four" whilst "the peak value of di/dt is likely to be one or two orders of magnitude less" than it would be at a much lower altitude. The action integral is a function of i^2. Although the duration of the pulse also changes with altitude and tends to inorease slightly, at significant altitude the action integral could be reduced by an order of magnitude.

More detailed consideration of this work suggests that both peak current and di/dt reduoe as the distance along the channel away from the meeting point of the upward and downward going leaders increases. The same oonclusion was reached in more recent work by Hoole and Allen(15), for both upward and downward going stepped leaders (fig 4).

The distance that the leader can sweep along the aircraft will increase with increasing altitude for a downwards going leader, and increase with decreasing altitude for an upward going leader. Similarly, the severity of the first return stroke (in respect of peak ourrent, di/dt and action integral) will decrease with increasing altitude for a downward going leader, and decrease with decreasing altitude for an upward going leader. Thus in a sub-sonic aircraft, the oonditions which might oause the leader attachment to sweep into an area at present regarded as a zone 2 area will also ensure that the levels of peak current, di/dt and action integral of the first return stroke will also be significantly reduced. This may be the reason why flight experience has not so far identified any problems arising from leaders swept beyond the present zone 1A extents. In view of this there seems little justification for changes in the present zoning for conventional sub-sonic aircraft. In special cases where flight critical failure meohanisms related to peak current or action integral are identified in zone 2 regions it may at first sight seem prudent to test with zone 1A oonditions. In such a case however it will be difficult to justify peak currents in excess of 50kA and action integrals greater than 0.2×10 A s, and this is less than the severity of a test current component D which is already a requirement for zone 2A testing.

In supersonic airoraft, because of their high forward speed, there could be some more significant sweeping of the leader in positions along the lightning channel where there is a less dramatic ohange of current parameters. There may, therefore, be some justifioation for a new look at the zoning of these airoraft. However, the geometry of most supersonio aircraft seems unsuitable for the zoning oonoepts that have been developed over the years for slower flying oraft, and so, perhaps, it is right for other reasons as well to reconsider the zoning of these aircraft.

6. HELICOPTERS AND AIRCRAFT CAPABLE OF HOVER

The possibility of hover requires a different analysis of the zones from that required for craft not capable of hover. A location or component on the surfaoe of a helioopter might be in one zone while hovering yet in another when in horizontal motion. It is neoessary to analyse the zones for all the modes of flight and allocate final zone delineations aooording to the worst case zone for each looation or oomponent on the surfaoe. In deoiding which is the worst oase zone, the threat severity should be considered as well as the susceptibility. For direct effeots damage the zones oould be considered in deoreasing order of severity from 1B, 1A, 2B to 2A and finally 3. Additional considerations to be taken into account are: a) that air stream will not stabilise a zone 1B attachment at the extreme edge of a structure during hover as it will during horizontal flight, so extension of zone 1B locations will have to be considered to allow for arc instability movement and redirection of leader attachment by corona shielding effecta, and b)

that under surfaces of the fuselage where there are projections like undercarriage and aerials, might still be subject to swept stroke conditions, but that slow forward flight will modify the hang-on time and therefore, the severity of component C to be allowed for. In certain circumstances, swept stroke zones will have to be considered as long hang-on zone 2B's.

Practical experience so far suggests that the rotor blades form a protective umberella over the top of the fuselage of a helicopter. Apart from the exposed tail boom and the possibility of side flashes from the rotor to the tail boom, the rest of the top surfaces might be placed in zone 3. For a fixed wing aircraft capable of hover, any upper surface conductive projections and their immediate environment, and large plain surfaces should be considered as zone 1B while the surfaces between these locations should be defined as zone 2A. Testing might be the only way to define this however. It should be noted that these aircraft use zero forward speed as seldom as possible owing to the high fuel consumption, and usually only for take-off and landing under restricted conditions. This should be taken into account when assessing protection needed for any additional hazards arising from the hover capability.

Helicopter blade tips will generally, by virtue of their constant motion, be in zone 1A. Where very wide blade tips are used there may be a case for defining zone 2A and 2B areas as well. It has been found in practice, and in model tests, that side flashing can occur between points on the blade root end or hub and the edge of the gearbox fairing. Though neither end of the side flash could be a primary lightning channel attachment point, the potential for damage will be exactly the same as if they were primary lightning attachment points and must be treated as such in all respects. It seems prudent to include these locations in the zoning definition to ensure proper consideration.

Figure 5 shows a suggested lightning damage zoning of a helicopter in hover while figure 6 shows the zoning suggested for the same craft in forward flight. These, with corrections to allow for sideways motion (if that is possible) should be superimposed and the worst case for each location used in the final zone definition.

7. DEFINITION OF ZONES.

One point arising out of the discussion in section 5 is that, though a certain region on the surface of an aircraft might under the present zoning rules be considered as a zone 2, it may see an initial return stroke albeit of reduced severity. These rules postulate a configuration of leader attachment points based upon the physical geometry of the aircraft and then assume that the first return stroke will always go to these initial attachment points: any sweeping action is assumed to take place only after the arrival of the first return stroke. The zones have come to be interpreted as regions where a specific type of attachment might occur or no attachment is likely, despite the origins of their definition. These origins were in the observed severity of the pitting caused by natural lightning strikes, often with no knowledge of the component of lightning that had caused the damage. In the treatment of helicopter zones discussed in section 6 it is shown that there are occasions when arc root damage might occur in areas where lightning channel attachment is inconceivable, yet side-flashing creates the need to protect against arc burn damage. In the opinion of the autnors, the protection requirements and simulation test levels required to demonstrate hardness to the effects of lightning should be defined in terms of the threat severity, and not simply on the basis of initial or swept attachment that can at best be inferred from physical position within the aircraft geometry.

A lightning protection and test requirement assessment should be made for each individual aircraft type taking into account the shape of the aircraft, flight envelope, speed and flight modes. The susceptibility should be expressed through the alternative zoning rules below, viz, in terms of the lightning threats for all modes and configurations. Where speed and flight envelope indicate, from figure 4, that there will be a transition zone (beta) between alpha and gamma, then suitable protection and testing should be devised commensurate with the threat and susceptibility. Once zones have been apportioned, the set of zone schemes should be condensed into the threat or threats against which each component must be protected.

8. AN ALTERNATIVE ZONING SPECIFICATION

The following wording is suggested to encompass the requirement that zone definitions should reflect attachment possibility and severity of the incident threat. This should ensure that the zones will guide a designer to provide appropriate protection and test using reasonable waveforms and severities.

ALPHA ZONE: Surfaces of an aircraft which must withstand the effects equivalent to the full threat severity associated with an initial lightning return stroke parameters, but with the expectation that subsequent return strokes will be swept to other surfaces by virtue of aircraft motion relative to the lightning channel.

BETA ZONE: Surfaces of an aircraft which will be subject to an initial return stroke attachment as a direct result of a swept leader. The threat parameters will be modified for the distance of the leader sweep in accordance with figure 4.

GAMMA ZONE: Surfaces of an aircraft which must withstand the effects equivalent to the full threat severity associated with a subsequent lightning return stroke parameters and intermediate and continuing

current, but with the expectation that further return strokes will be swept to subsequent attachment points by virtue of aircraft motion relative to the lightning channel. The whole continuing current may be divided between several swept attachments.

DELTA ZONE: Surfaces of an aircraft which must withstand the effects equivalent to the full threat severity associated with a subsequent lightning return stroke parameters and further components of the lightning flash since there is no expectation of lightning channel sweeping to other surfaces.

EPSILON ZONE: Surfaces of an aircraft which must withstand the effects equivalent to the full threat severity associated with an initial lightning return stroke parameters, and subsequent components of the lightning flash since there is no expectation of lightning channel sweeping to other surfaces.

ZETA ZONE: Surfaces of an aircraft for which the direct attachment of a lightning channel is extremely improbable.

NOTE: Since a lightning attachment to an aircraft implies an entry and an exit point, all zones must be capable of transferring all components of lightning current by conduction.

9. APPLICATION OF THE NEW ZONES

ALPHA ZONE includes all forward, upward, downward and sideways electrically conductive projections on a fixed wing aircraft not screened by other components of the structure, e.g. in the angle between fuselage and wing, or that are small relative to the structure around, e.g. small fin aerials or probes. It also includes exposed leading edges, and on large aircraft might include certain exposed surfaces such as the fuselage upper skin and outboard surfaces of the wing. Alpha locations should generally be considered to extend 0.5m back from the foremost extremity. Nose radome mounted pitot or diverter strips, wing tips, tail plane tips, fin tips, wing mounted engine nacelle lip-skins and fin aerials are typical examples. On a fixed wing aircraft capable of hover, and during hover only, there are no initial attachment zones from which sweeping is guaranteed and all attachment zones are designated epsilon. On rotary winged craft capable of hover, and during hover, the tips of the rotors are the only components whose motion guarantees sweeping and, therefore, only they can be designated alpha zone.

BETA ZONE includes areas in the airflow behind an alpha zone where a lightning leader might be swept by virtue of the aircraft's motion relative to the air before the first return stroke. However, the further back the sweep, the less the severity of the return stroke, and only those areas where the return stroke severity will be between the levels of current components A and D need be considered as zone beta. Such areas might be the fuselage behind the aircraft nose alpha zone or main wing surfaces aft of fore-planes.

GAMMA ZONE includes areas in the airflow behind an alpha or beta zone location where a lightning channel might be swept by virtue of the aircraft's motion relative to the air. Side-slipping and complex air flow over delta wings for instance, must be accounted for by 0.5m sideways extensions beyond the extent of the alpha zones from which sweeping can occur. The fuselage surfaces not already defined as alpha zone, wing roots and 0.5m onto the wing surface measured parallel to the fuselage would be defined as gamma zone on a conventional cruciform structure. On a delta wing, the whole wing surface would be considered as in gamma zone. Areas on the wing or vertical stabiliser surfaces behind leading edge initial attachment points would be in gamma zone as would the tail plane surfaces if sweeping from the wings were considered possible. Aircraft capable of hover have gamma zone locations on surfaces behind designated alpha zone locations. A rotary winged aircraft with very broad rotor blade tips might have narrow sections mid-chord in gamma zone also. In both cases, any conductive projections should be considered as in epsilon zone.

DELTA ZONE includes all trailing edges behind gamma zone locations that would not already be designated as epsilon zone, except where sweeping could continue onto other structure, from a wing to a tail plane for instance.

EPSILON ZONE includes all rearwards electrically conductive projections on a fixed wing aircraft or all projections on an aircraft capable of hover that are not screened from lightning attachment by other components of the structure. Trailing edges on the wing, tail plane and fin tips are typical examples. In normal forward flight, no extension beyond the extreme edge need be considered. In hover, however, the 0.5m extent of an alpha zone should be considered to account for any corona shielding or space charge effects.

NOTE TO ALPHA AND EPSILON ZONE DEFINITIONS: The projections refer only to conductive materials. A covering of insulating material would not normally be sufficient to modify likely attachments.

The application of the above concepts is depicted for a conventional aircraft in fig 7, for a delta winged aircraft in fig 8, for a fixed wing aircraft capable of hover in fig 9 and for a helicopter in fig 10.

10. APPLICATION OF SIMULATED CURRENT PULSES FOR TESTING.

Some changes are also necessary to the rules for applying test current pulses for the different zones. The suggested applications are recorded in table 1 below and encompass the correction to include component B and D (when simulation of the di/dt effects is required) in the zone 3 testing. Also incorporated is the range of continuing current component durations to allow for air-

craft speed and sweep distance.

TABLE 1. APPLICATION OF SIMULATED LIGHTNING CURRENT
(Current components A to D are in ref 1.)

Test Zone	Current Component			
	A	B (note 1)	C (note 1)	D
ALPHA	x	x	45ms	
BETA	x (note 2)	x	45ms	
GAMMA		x	45ms	x (note 4)
DELTA		x	45ms-1s (note 5)	x
EPSILON	x	x	250ms-1s	x (note 3)
ZETA (note 6)	x	x	250ms-1s	x (note 3)

Note 1: Components B and C need only be provided where the damage mechanism involves the maintenance of a current for a significant period.

Note 2: The normal ALPHA extent should be protected and tested to the full severity of 200kA and 2x10 A s, however, where the zoning analysis, by consideration of swept leaders, indicates a further extension or a transition region, the severity of the threat, and hence the protection and testing levels, should be modified in accordance with the data given in figure 4.

Note 3: Component D need only be provided for EPSILON or ZETA zone simulation when the peak di/dt parameter is of significance, or when more damage would be expected from the fast current component following the continuing current, e.g. when the continuing current has created a molten pool of metal on an aluminium component and the following fast current pulse causes the material to be splashed out of the way.

Note 4: For GAMMA zone simulations the fast current component would normally precede the continuing current as subsequent restrikes are expected to cause new attachment points.

Note 5: The duration of the continuing current pulse for EPSILON zone simulations should be selected according to the residual hang-on (up to 1 second) after the lightning channel attachment has swept from the initial attachment point. This should be calculated from the minimum time for a sweep to the point concerned taking account of the maximum likely speed of the aircraft.

Note 6: The current levels for all components for ZETA zone simulations should be scaled to the ratio of the test component size relative to the whole component making appropriate allowance for inductive current distribution. ZETA zone tests can be done using solid current connections.

11. ATTACHMENT POINT LOCATION BY TESTING

High voltage attachment point tests may, in certain circumstances, have value in predicting zoning, but, if some of the postulates recounted above are valid, then there is even greater reason to ensure that they are correctly devised and conducted. Effects such as corona shielding and the release of space charge into surrounding air require that DC electric fields are allowed to pre-exist the impulse and attachment. The effect of scale will require the use of large flat electrodes at considerable distance from the object when that object is large, and it may be necessary to do model tests in an SF environment in order to scale the whole discharge phenomenon

12. CONCLUSIONS

The authors have put forward some of the objections to and omissions from existing rules for zoning aircraft, and described experience gained from inspecting natural lightning strikes to aircraft. Cases have been put forward to justify suggested changes and areas where change is not recommended. A new set of rules for establishing zoning has been presented with guidance on their application and interpretation, also their impact on simulation current pulse application and on high voltage attachment testing has been described. Most importantly, the rewording has incorporated vehicles capable of hover, such as helicopters, for the first time. The main aims have been to make zoning more accurate, less arbitrary, less needful of interpretation and more widely applicable.

13. ACKNOWLEDGEMENTS

The authors would like to acknowledge the comments from Mr Mark Heseltine of Westland Helicopters Ltd and of Mr Alan Reed of British Aerospace Filton. The invitation to two of the authors to attend a meeting of the SAE AE4L Committee during which the zoning of helicopters was discussed is recognised as having crystallised views and requirements for these types of vehicles. The support of Culham Laboratory and British Aerospace (Warton) is also recognised.

14. REFERENCES

1. J Phillpott, "Recommended Practice for Lightning Simulation and Testing Techniques for Aircraft", CLM-R 163, 1977.

2. "Lightning Test Waveforms and Techniques for Aerospace Vehicles and Hardening", Report of the SAE Committee AE4L, 1978.

3. "Military Standard - Lightning Qualification Test Techniques for Aerospace Vehicles and Hardware", MIL-STD-1757A, 1983.

4. "Protection of Aircraft Fuel Sys-

tems Against Lightning", FAA AC 20-53A, 1983.

5. B.L. Perry, "Flight Experience", Short Course on Lightning Protection for Aircraft, Culham, 1983.

6. B.L. Perry, "British Researches and Protective Recommendations of the British Air Registration Board", Lightning and Static Electricity Conference Miami, 1968.

7. B.D. Fisher, G. . Keyser and P.L. Deal, "Lightning Attachment Patterns and Flight Conditions for Storm Hazards '80", NASA Technical Paper 2087, 1982.

8. J.A. Plumer, "A New Standard for Lightning Qualification Testing of Aircraft: Technical Overview, Definitions and Basic Waveforms", Certification of Aircraft for Lightning and Atmospheric Electricity Hazards Conference, 1979.

9. A.W. Hanson, "Recent Experimental Work on Lightning Attachment Point Location Tests", International Aerospace Conference on Lightning and Static Electricity, Oxford, 1982.

10. "British Standard Code of Practice for Protection of Structures against Lightning", BS6651:1985.

11. J. Bishop, A. Aked, C.W. Powell and H.M. Ryan, "Aspects of Lightning Protection Schemes for Radomes", 10th International Aerospace and Ground Conference on Lightning and Static Electricity, Paris 1985.

12. A.W. Hanson, "Lightning Protection Techniques for Radomes having Forward Mounted Pitots", Symposium on Lightning Technology, Hampton, Virginia, USA, 1980.

13. P.F. Little, "Transmission Line Representation of a Lightning Return Stroke", Journal of Applied Physics D, 11, 1978.

14. P.F. Little, "The Effect of Altitude on Lightning Hazards to Aircraft", 15th European Conference on Lightning Protection, Uppsala, Sweden, 1979.

15. P.R.P. Hoole and J.E. Allen, "Lightning Magnetic Field Calculations Using Finite Element Method", 10th International Aerospace and Ground Conference on Lightning and Static Electricity, Paris, 1985.

Copyright © Controller HMSO, London, 1986

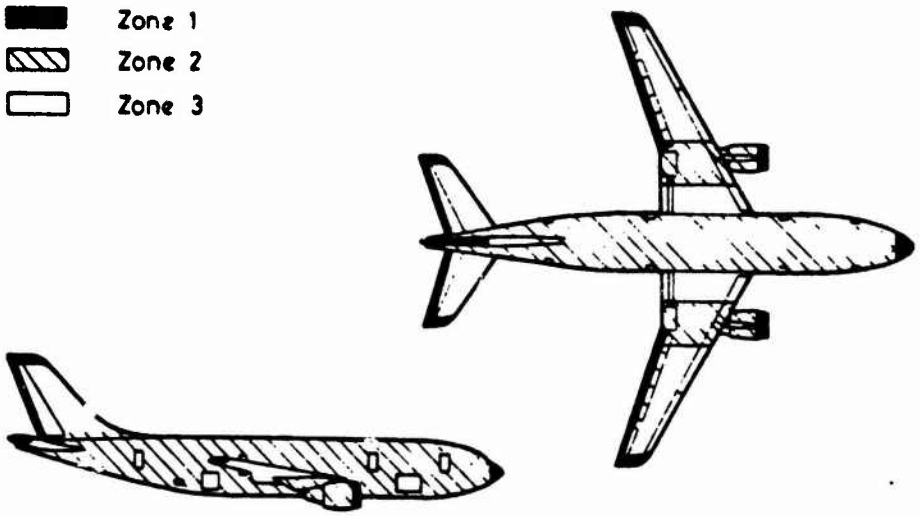

Fig 1. Existing Aircraft Zones.

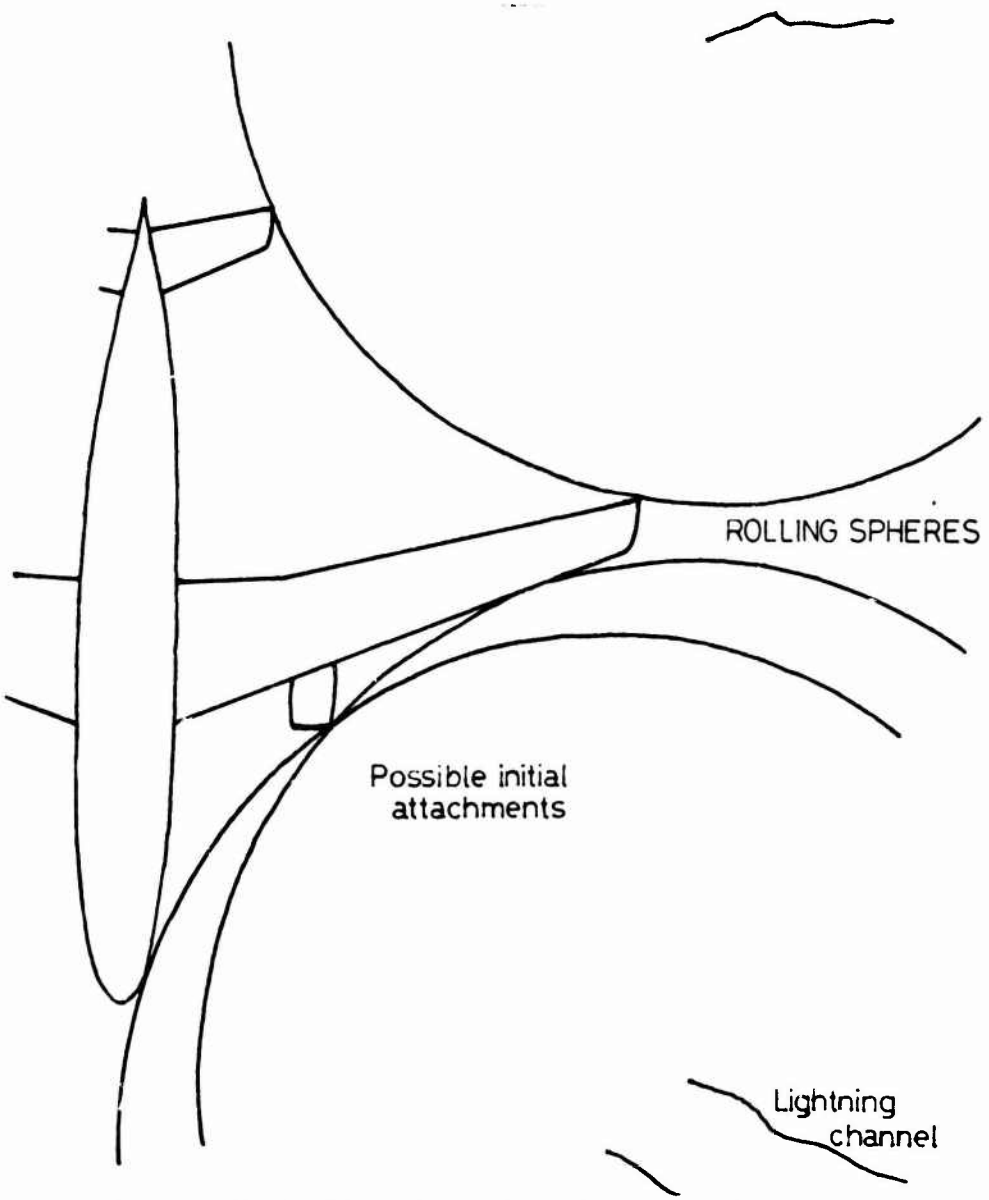

Fig 2. The Rolling Sphere Applied to a Fixed Wing Aircraft.

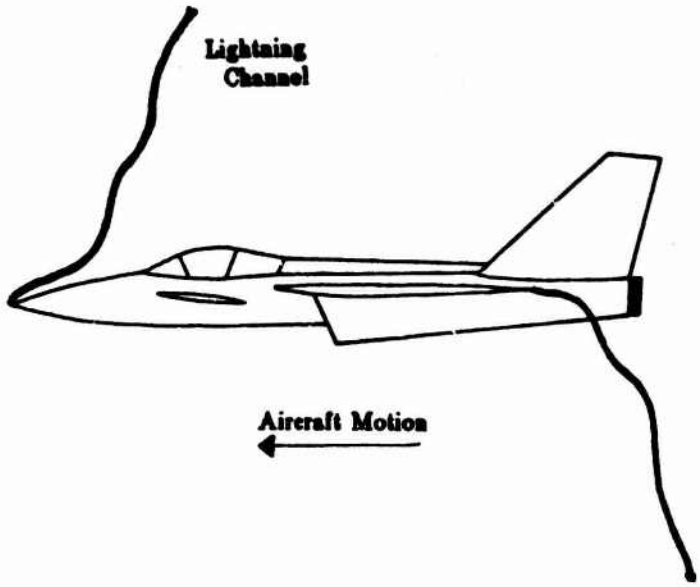

Fig 3. The Swept Leader Phenomenon.

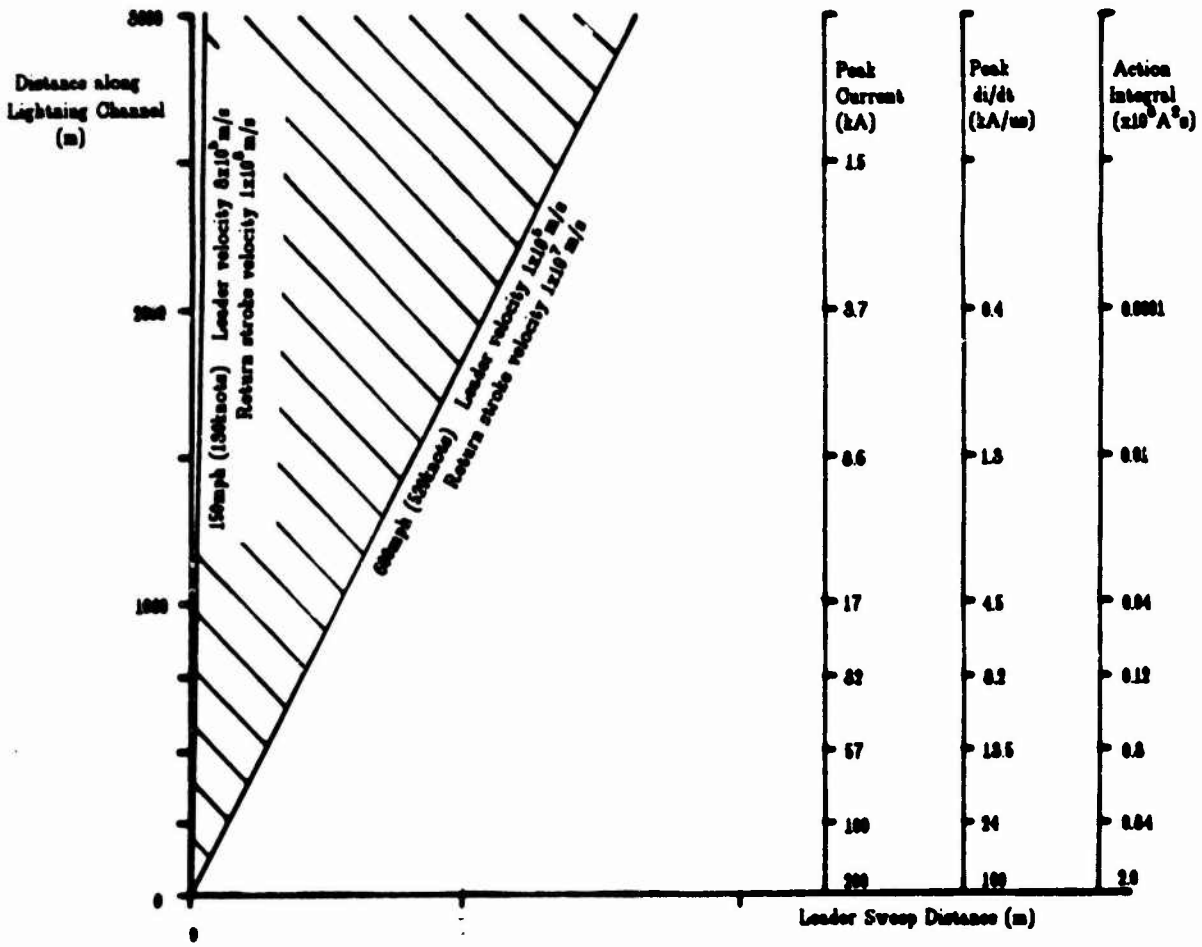

Fig 4. Change of Peak Pulse Parameters of Initial Return Strokes with Leader Sweep Diatance.

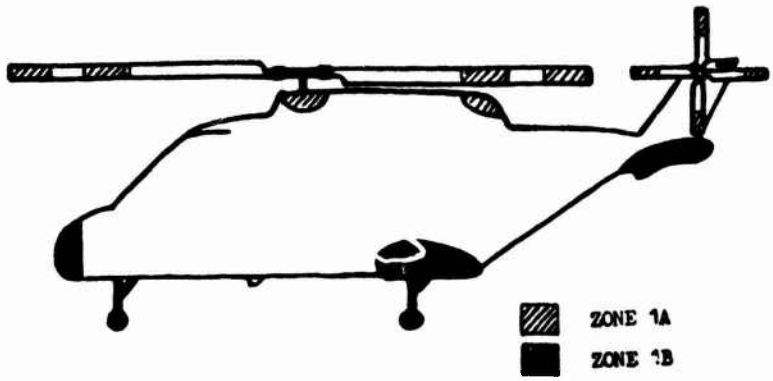

Fig 5. Zones on a Helicopter in Hover.

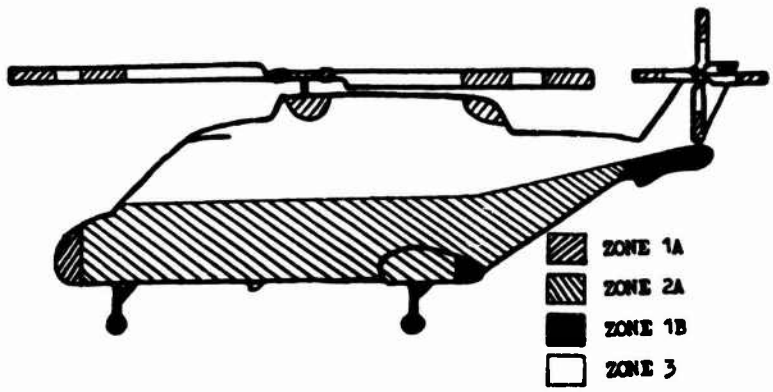

Fig 6. Zones on a Helicopter in Forward Flight

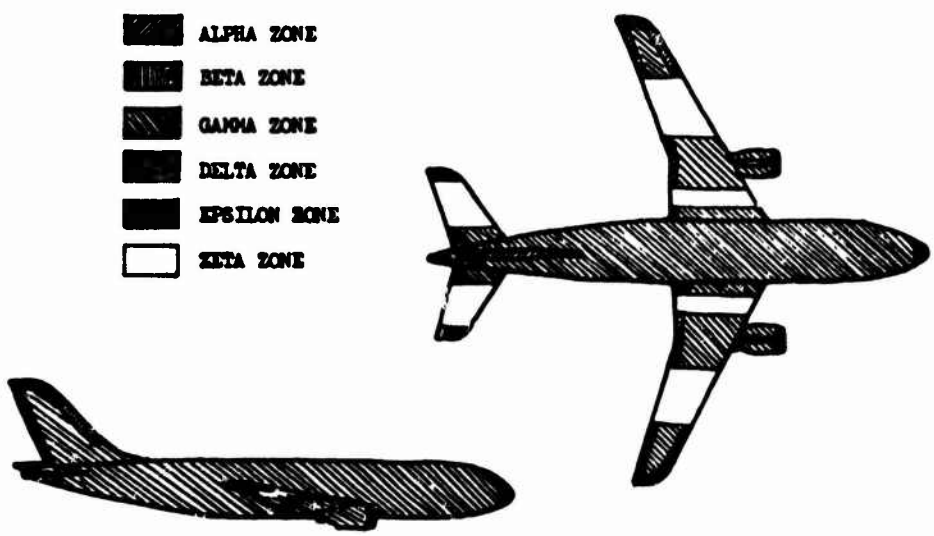

Fig 7. Suggested Zones for a Fixed Wing Aircraft.

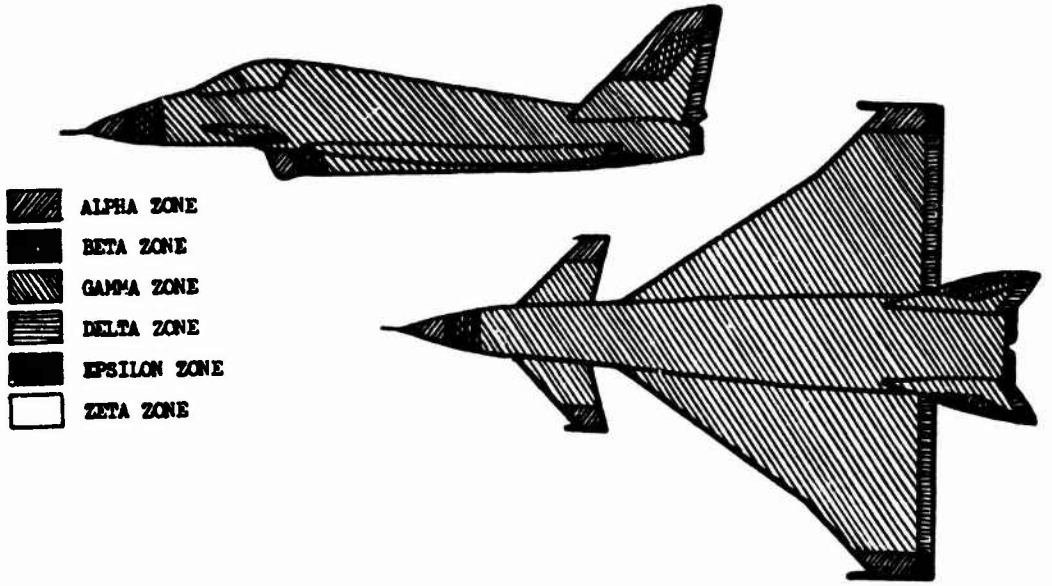

Fig 8. Suggested Zones for a Delta Winged Aircraft.

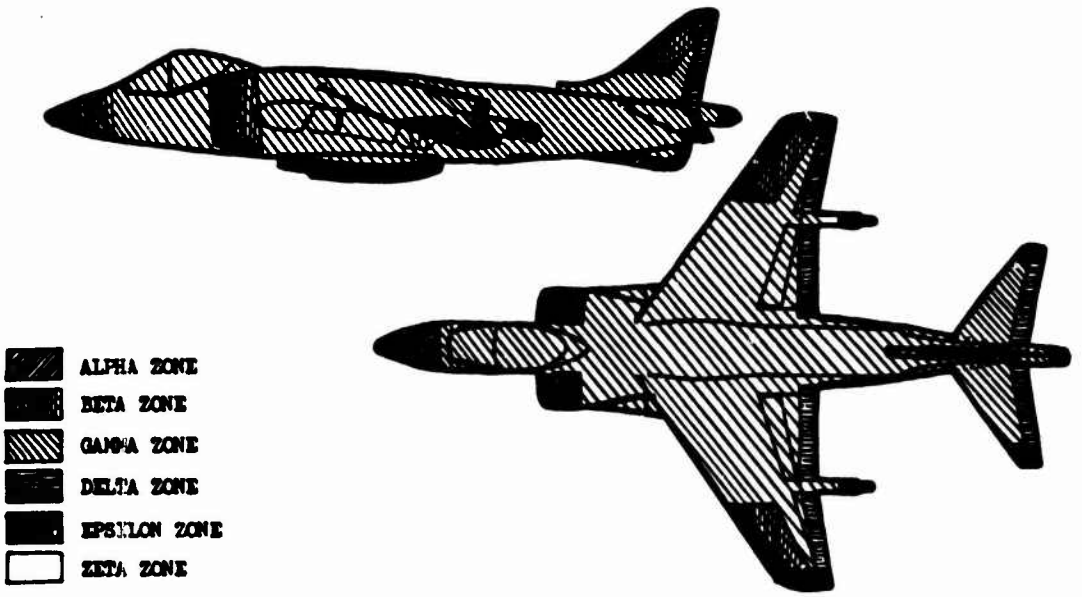

Fig 9. Suggested Zones for a Fixed Wing VTOL Aircraft.

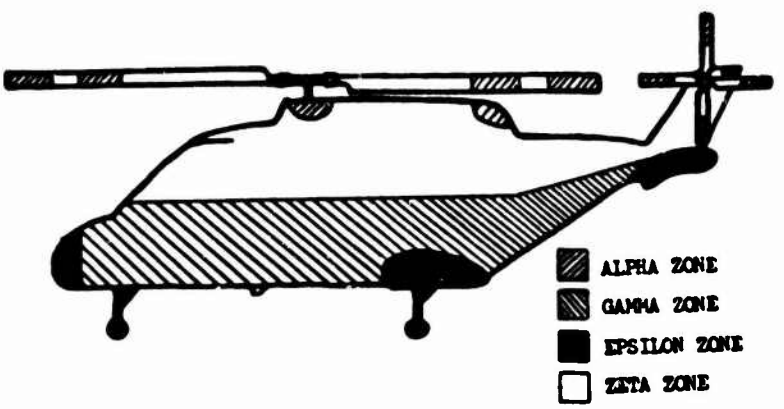

Fig 10. Suggested Zones for a Helicopter.

AIRWORTHINESS CONSIDERATIONS OF LIGHTNING STRIKE PROTECTION FOR HELICOPTER DIGITAL ENGINE CONTROLS

Richard L. Vaughn

Federal Aviation Administration - Rotorcraft Standards Staff

Fort Worth, Texas

ABSTRACT

The advent of "microprocessor technology" is resulting in functions in aircraft being implemented to a greater degree by digital process control rather than by conventional mechanical or electromechanical means. This change often results in an avionic unit performing a function having the possibility of hazardous or catastrophic effects, resulting from a failure of that system.

One such use of avionics is full authority digital engine control (FADEC) in transport category helicopters. These digital, processor-based controls are being installed in many civil helicopters because they offer many performance advantages (such as isochronous governing) which were not possible with conventional technology pneumatic or hydromechanical controls.

The use of FADEC in a Category A transport rotorcraft, especially one operated in an IFR environment, could result in a catastrophe to the rotorcraft if the system is not adequately protected from a lightning strike encounter. A discussion of the rationale and philosophy used for the development of guidance material and procedures for applicants seeking FAA approval of FADEC in transport category rotorcraft is contained in FAA Advisory Circular (AC) 29-2, "Certification of Transport Category Rotorcraft," paragraph 621. This information, incorporated into AC 29-2 on May 28, 1985, outlines acceptable means of demonstrating compliance with Federal Aviation Regulations (FAR), Part 29, § § 29.1309(a) and (h), considering protection against the possible catastrophic effects of a foreseeable lightning strike encounter. Advisory Circular 29-2 provides a characterization of the lightning environment and discusses the recommended types of tests and analyses to be used to demonstrate adequate protection.

These acceptable means of demonstrating airworthiness run the gamut from full-scale, full-level vehicle tests to a total vehicle analysis performed without a full-scale reduced level test on which to base or verify that analysis. In addition to "strike" type testing, consideration is given for the use of frequency domain analysis with low level swept CW testing. Also, the use of a formal certification (test) plan, with which the FAA concurs, is recommended.

INTRODUCTION

The U.S. airworthiness standard for transport category rotorcraft as provided in FAR Part 29, § 29.1309(h), requires that: "In showing compliance with paragraphs (a) and (b) of this section, the effects of lightning strikes on the rotorcraft must be considered in accordance with § 29.610." Section 29.610 requires that the rotorcraft must be protected against the catastrophic effects of lightning. Since the improper operation of FADEC could prove catastrophic to the rotorcraft, an applicant seeking approval for FADEC is required to demonstrate to the FAA that the installation complies with § 29.1309(a). Section 29.1309(a) requires that: "The equipment, systems, and installations whose functioning is required by this subchapter must be designed and installed to ensure that they perform their intended functions under any foreseeable operating condition." (The subchapter referred to is subchapter C which covers aircraft.) "Any foreseeable operating condition" is the regulatory basis for considering the environmental conditions caused by the meteorological phenomenon of lightning strikes to the helicopter during its operation. During the period of time before the 1970s, most helicopters operated in a visual flight rules (VFR) environment in which there was very little dependency on avionic equipment for the safe operation of the aircraft. Even with the advent of instrument flight rules (IFR) operations (due to the fact most avionics were analog devices installed in a mostly metal airframe), little consideration was given to lightning strike protection of the avionics beyond laboratory testing in accordance with the appropriate parts of RTCA Document DO-160 or similar standards.

Experience has indicated (8) that aircraft operating under IFR conditions are subjected to the environment of a lightning strike encounter. With the incorporation of digital, processor-based systems, such as FADEC, avionic systems are being installed where improper operation could have catastrophic effects. Because of these possible catastrophic effects, additional consideration is required to substantiate that FADEC's as installed can continue to operate properly when the helicopter is involved in a lightning strike encounter. Due to the performance advantages of FADEC operated engines in a transport category helicopter (13), various airframe manufacturers have been requesting approval of such an installation in their helicopters.

In order to discharge their responsibility to ensure consistency in the interpretation and

*Numbers in parentheses designate References at end of paper.

application of the U.S. airworthiness standards for rotorcraft, the FAA Rotorcraft Certification Directorate issued a change (May 28, 1985) to AC 29-2 to guide FAA certification engineers on an acceptable method of showing compliance with § 29.1309(a) and (h) for a FADEC installation considering the environmental condition of a lightning strike encounter of the helicopter. This paper discusses the philosophy and rationale utilized to arrive at the recommended "acceptable method."

DISCUSSION

CERTIFICATION PLAN - The use of a formal written plan outlining the proposed certification effort was incorporated into AC 29-2. The initial draft of the advisory material, presented at a public meeting, did not include a recommendation for this certification plan; however, because several commentors, from FAA and industry, recommended that this plan be included, consideration was given. After reviewing our experience on several certifications, the FAA concluded that the use of a certification plan would be very helpful to both the applicant seeking the certification and the FAA because the plan identifies and defines an acceptable resolution to the critical issues early in the certification. Additionally, the certification plan provides both parties with a complete outline of all the actions to be taken to demonstrate regulatory compliance. A discussion is contained in the advisory material of the salient points which should generally be included in the certification plan. A more complete discussion of these items is given in the following paragraphs.

DEFINITION OF ENVIRONMENT - In developing the advisory material to allow both industry and the FAA to determine that a FADEC installed in a transport category rotorcraft can continue proper operation in the environment of a lightning strike encounter, the first step is to quantify what constitutes a worst-case strike. This quantification is required because it is neither practical nor desirable to determine that an installation is acceptable by testing such an installation by exposing a helicopter to a sufficient number of natural lightning strike encounters prior to certification to convince the FAA of its acceptability.

There has been and continues to be a great amount of research accomplished to determine a value of currents and voltages reasonably representing what may be expected to be encountered in nature. While there is some agreement of what the numbers are, there is equally much disagreement. Even within the FAA, there is disagreement on the numbers. In particular, "Is the fastest instantaneous rate of rise 200 kiloamperes per microsecond or 100 kiloamperes per microsecond?"

Since there is some agreement both nationally (MIL-STD-1757A and SAE AE4L Committee Report) and internationally (Culham Laboratories CLM R 163 and Aerospatiale RE AERO 702 50) on the numbers for a 99 percentile strike, this value was chosen as a reasonable limit. The SAE AE4L committee report of June 20, 1978, "Blue Book" (3), was chosen as the characterization of a worst-case strike. This report describes what can be reasonably expected to be the operating condition of a worst-case lightning strike encounter by the helicopter.

It is the author's understanding that the SAE AE4L Committee is at this time taking action to revise the "Blue Book" to include an expanded mathematical definition of the "component A" and an expanded definition of the multiple strokes in a flash.

DETERMINE ZONES AND ATTACHMENT POINTS - The determination of zones and attachment points for helicopters is more complex than fixed-wing aircraft because the helicopter may be airborne with little airspeed, and the large amount of service experience which exists for fixed-wing aircraft is not available for helicopters (9). Recent studies (10) indicate the assumption that the lightning current is evenly distributed about the aircraft during a lightning strike, which has been used for anlysis performed for some cylindrical aircraft, is not valid for a helicopter. This is partially due to the unique shape of most helicopters.

The fact that a helicopter may be airborne with little airspeed causes a lack of swept stroke phenomenon, particularly on the bottom of the helicopter. There appears to be some agreement in the industry that the main and tail rotors are probable attachment points. In the case of FADEC, some of the current paths through the helicopter are more critical than others. The FAA has proposed research to provide guidance to certification engineers regarding the probable attachments of lightning to an average helicopter. Model studies have often been used in the past to provide data regarding attachment points. In addition to the use of models, corona discharge, method or testing of the full vehicle with drop wands from a Marx generator has been used to determine probable attachment points.

ESTABLISHMENT OF THE LIGHTNING ENVIRONMENT - Since not all of the "components" of the flash have an equal effect on FADEC, it is usually only necessary to use "component A" type testing. The use of component A at the attachment points of interest allows the investigation of the airframe responses to which FADEC system components are exposed. This internal environment may then be determined through the utilization of testing and/or analysis techniques.

FULL-LEVEL, COMPLETE VEHICLE TESTING - As a basically academic exercise, an FAA policy of testing a complete helicopter with a full-level strike, while demonstrating that the engine controls continue to function properly, is sufficient to prove compliance with § 29.1309. This policy is basically academic because testing the complete aircraft to a full level is very difficult. Therefore, it is preferable to determine the acceptability of the installation by the use of some analytical processes.

ANALYTICAL PROCESSES - When using various analytical methods to determine the airframe system responses to the full 200 kiloampere stroke, to make a determination of the protection adequacy, the system component hardness of susceptibility must be known.

It is recommended that the engine manufacturer supply this information; however, the final responsibility for the acceptability of the engine installation rests with the applicant. This recommendation is not meant to add a requirement to the engine manufacturer but to propose a more efficient method of certification. Unless full-scale, full-level testing is utilized, the system components' tolerance levels must be determined. If the engine manufacturer determines the tolerance levels of the system components, the data are available to all airframe manufacturers who wish to install the engine in their rotorcraft. If, however, the airframe manufacturer must determine the tolerance of the fuel control system components, then the data regarding the tolerances of the system components become the proprietary type data of the particular airframe manufacturer. The next airframe manufacturer seeking approval of the installation of the same engine in his airframe would be required to repeat the same tests on the system components to determine the component tolerance levels. The same situation would be true for the next manufacturer or STC applicant. It is easily possible that the same series of bench tests might be required to be repeated four or more times on the same system components by different airframe manufacturers. The SAE AE4L Committee Report AE4L-81-2 (4) is recommended to determine the levels and waveforms to be used for the testing accomplished in determining the tolerance level of the system components. When the computer unit is tested, it should be operating under software control. Several shots of the waveform should be made to determine if the system is susceptible to digital upset. If it is known that the processor being used has a particular susceptibility, then it may be necessary to synchronize the test shot with the particular program execution. This procedure is not foolproof and will not absolutely ensure that the susceptibility derived is correct. However, in view of the current technology, it represents a reasonable approach.

With the system component tolerance levels determined, an analysis must be performed to show the airframe responses do not exceed the tolerance level of the system components. The recommended method to complete the analysis is testing the complete vehicle system at some reduced level and linearly extrapolating the results to a full strike level. With this extrapolation of 50:1 at the recommended level, it is only prudent that a factor be added to account for the uncertainties which exist in doing such an analysis. A value of 6 dB was chosen as a result of discussions and recommendations of the National Resource Specialist for Advanced Avionics, the Transport Airplane Certification Directorate personnel, and a study accomplished by Chris Kendall Counsultants (1). Approvals have been made where no full-scale vehicle testing was accomplished to verify the airframe analysis. The policy for such an analysis was that it must be very rigorous and show a significant margin of protection. To provide guidance to the certification engineer on what constitutes a "significant margin," this was defined to be approximately 25 dB above the 6 dB uncertainty margin. Thirty-one dB is indeed a very large margin. However, when the analysis has no associated full-scale airframe testing to verify its correctness, a large margin is necessary. Even a small error in a basic assumption made for the analysis can result in a very significant error in the final results. This large margin is not intended to indicate a lack of confidence in utilizing analysis, rather a deep concern for the validity of the analytical results.

Note that the uncertainty or safety margin is applied as a function of the analytical process and not an adjustment to the quantification of the atmospheric environment.

Attention to the system configuration tested is important, because the configuration tested must represent the system as it will actually be configured in service. Due to the nature of the testing, it may be necessary and desirable to simulate some of the system components. This simulation should be shown not to derrogate the results of the test being performed.

Presently, there have not been any applicants for approval of FADEC who proposed to use a frequency domain coupling analysis and swept CW testing to predict the airframe system response to a lightning strike. Since this type of test and analysis has been used successfully for the approval of a transport category airplane, and because it was recommended to the Rotorcraft Directorate that this is a viable method to predict airframe response, this method is specifically mentioned in the criteria. This was done to make the certification engineer aware that this is a recognized method since most of the test procedures given imply "strike" testing.

PASS/FAIL CRITERIA - Due to the complexity of the system being tested and the fact that functions are performed by FADEC which are not necessarily required by the subchapter (subchapter C of 14 CFR; "Aircraft"), pass/fail criteria are needed to guide the certification engineer. These criteria help to ensure that a consistent after strike performance is required of the various FADEC's tested. The criteria recognize the fact that the FADEC computer may not be controlling the engine during strokes of the flash. If this occurs, it is acceptable only if no hazard is posed to the helicopter during the time the engine is not being controlled. Additionally, it is made quite clear that a manual reset cannot be used to recover FADEC from a digital upset. Some additional relief is given to provide that some ancillary functions of FADEC may fail during the test. If these features fail and they are of a nature that their absence without the crew's knowledge of this absence might create a hazard, then the crew must be alerted to this failure.

SYSTEM INSTALLATION CONSIDERATION - Design techniques, such as gross overbraid shielding or conduits, may be necessary to achieve acceptable system hardness. When such techniques are used, they must be verified by some type of periodic maintenance to ensure that operation and modification of the helicopter does not degrade the protection provided.

The advisory circular does not specify the exact method of making such information available. The method to be utilized is not specified because

any of the usual maintenance information channels (i.e., maintenance manuals, service bulletins, etc.) are an acceptable means of accomplishing this information exchange.

MISCELLANEOUS CONSIDERATIONS - The advisory circular recommends that the analysis should account for effects such as flashover and current diffusion effects which are triggered by the extremely high currents and fast rates of rise in the worst-case return stroke. These phenomena may have a significant effect on the current paths through the helicopter and therefore an effect on the system response of interest.

The term "alternate technology back-up fuel control" when written into the advisory circular assumes a mechanical reversion of some type. These mechanical reversion systems cannot meet the criteria of not requiring any immediate action. However, if automatic control of the engine was lost, the presence of the mechanical backup would provide a greater level of safety than an out-of-control engine. The term alternate technology is made deliberately vague so that the use of some other type of back-up system is not precluded. The material included is restricted specifically to transport category helicopters with Category A engine isolation with an alternate technology backup. This type of system is very comparable to other advanced digital avionic systems such as fly-by-wire flight controls. Because of this fact, a caveat is included to alert the certification engineer to the fact that the criteria may not provide sufficient protection for a fly-by-wire system. Since much activity exists in both industry and FAA to determine protection criteria for advanced digital systems, it is expected that the material will be revised or replaced as necessary to make it consistent with future FAA policy.

The advisory circular material in draft form was presented in a public meeting held in Fort Worth, Texas, on January 11, 1985. The final information, incorporated into AC 29-2 on May 28, 1985, was revised from the draft by the incorporation of some of the many fine comments which were rendered by interested individuals.

One such comment was a request for a definition of what constitutes "full authority" control. There was some confusion on this point since some manufacturers would term a control "supervisory," which the FAA would consider, for certification, as full authority. The term is not rigorously defined, but a sufficient definition is given to allow an applicant to determine if the fuel control of interest was considered full authority by the FAA.

CONCLUSION

The preceding discussion gives some of the rationale used in the formulation of the criteria included in AC 29-2. This advisory circular provides consistent criteria for FAA certification engineers to use in determining if FADEC in a transport category helicopter is installed in such a way as to ensure that the engine can continue to operate properly when the helicopter experiences a worst-case lightning strike encounter. Having this criteria published in an advisory circular provides the applicant with the knowledge of what is an acceptable method of showing compliance and should assist his design personnel. As with any advisory material, this approach to compliance is "an acceptable means but not the only means" and, thus, the applicant may use alternate approaches that are acceptable to the FAA to demonstrate compliance.

REFERENCES

1. Kendall, C., and Black, E., Chris Kendall Consultants, and Larson, W. E., and Rasch, N. O. FAA. Aircraft Generated Electromagnetic Interference on Future Electronic Systems, DOT/FAA/CT-83/49.

2. Fisher, J. A., and Plumer, J. A., Lightning Protection of Aircraft, NASA Reference Publication 1008, October 1977.

3. "Lightning Test Waveforms and Techniques for Aerospace Vehicles and Hardware," Report of SAE Committee AE4L, June 20, 1978.

4. "Test Waveforms and Techniques for Assessing The Effects of Lightning-Induced Transients," SAE AE4L Committee Report: AE4L-81-2, December 15, 1981.

5. Burrows, B. V. C., "Designer's Guide to the Installation of Electrical Wiring and Equipment in Aircraft to Minimize Lightning Effects," Culham Laboratory Report, CLM-R212.

6. Phillpott, J., "Recommended Practice for Lightning Simulation and Testing Techniques for Aircraft," Culham Laboratory Report, CLM-R 163.

7. "Aircraft Protection Against the Effects of Atmospheric Electricity, Lightning and Electrostatic Charges." Recommendations Pour Les Etudes De L'industrie Aerospatiale, RE. Aero 702 50, 1984.

8. Rasch, N. O., Glynn, M. S., and Plumer, J. A., "Lightning Interaction With Commercial Air Carrier Type Aircraft" Technical Papers of the International Aerospace and Ground Conference on Lightning and Static Electricity, June 26-28, 1984, pp. 21-1 - 21-11.

9. Albright, D. L., "Lightning Strike Qualification Testing of U.S. Army Helicopters" Proceedings and Minutes of the National Interagency Coordination Group Meeting, National Atmospheric Electricity Hazards Protection Plan for Aircraft, DOT/FAA/CT-82/45, December 8-9, 1981, pp. 111-115.

10. Heiderscheidt, G. A., "Protecting the World's Largest Commercial Helicopter from Atmospheric Hazards," Technical Papers of the International Aerospace and Ground Conference on Lightning and Static Electricity, June 21-23, 1983, pp. 97-1 - 97-17.

11. East, D. A., "Lightning-Induced Transient Protection For Commercial Aircraft, Using Frequency Domain Analysis and Low-Level Test Methods." Technical Papers of the International Aerospace and Ground Conference on Lightning and Static Electricity, June 26-28, 1984, pp. 52-1 - 52-7.

12. Belcastro, C. M., "Data and Results of a Laboratory Investigation of Microprocessor Upset Caused by Simulated Lightning-Induced Transients" International Aerospace and Ground Conference on Lightning and Static Electricity, NASA Conference Publication 2356, pp. 13-24.

13. Perks, M., and Brammer, P., "Helicopter Engine Control System Introduction of Digital Electronic System on Westland Lynx and Westland 30 with Rolls-Royce GEM Engines" Ninth European Rotorcraft and Powered-Lift Aircraft Forum, September 13-15, 1983, pp. 82-1 - 82-16.

SIMULATED LIGHTNING CURRENT TESTS ON A LYNX HELICOPTER

by C J Hardwick and V P Dunkley, Culham Laboratory, UK
R H Evans, J S P Hardy and R A Hobbs, Royal Aircraft Establishment, UK

ABSTRACT

Simulated lightning tests were carried out jointly by RAE and Culham Laboratory on a Lynx helicopter, involving the application of test current pulses up to 90kA peak. The test current was applied by discharging a capacitor bank into the rotor head in two alternative configurations to provide a current path from the rotor head to either the tail or the wheels, corresponding to the most likely paths for a lightning strike. Extensive measurements of skin current densities on the helicopter for both configurations were made. Measurement of transient-induced currents in seven wiring looms showed good linearity against amplitude of fuselage current; extrapolation to full-threat levels indicated somewhat higher levels than those previously experienced. Results varied considerably with current path and earthing arrangements. Examination of the frequencies present in the loom currents showed fair correlation with those present in the fuselage currents or corresponding to resonant peaks in the CW coupling characteristic.

INTRODUCTION

A PROGRAM OF SIMULATED LIGHTNING TESTS was carried out jointly by RAE and Culham Laboratory on a Lynx helicopter during the period October 1984 to January 1985. The main aim was the further development of test techniques and in particular to assess the extent to which facility effects with present techniques detract from the accuracy with which in-flight conditions are represented. A second aim was to compare the induced currents in cables during a low power CW test over the frequency range 1 to 50MHz, with those observed in the high current pulse test intended to simulate the effects of a lightning current pulse passing through the fuselage. Thirdly, it was intended to obtain information relevant to a helicopter to add to the data previously obtained on fixed wing aircraft such as the Jaguar (1)*.

In the pulse tests a transportable pulse generator applied a damped sinusoidal current of frequency about 30kHz through the helicopter fuselage. Transient skin currents were recorded at various parts of the fuselage and their frequency content was determined by Fourier analysis. The variation of frequency content when the system was earthed at three alternative points was the main criteria for assessing facility effects. The extent to which the induced cable currents varied with the earthing arrangements, in both the pulse and CW tests, was a further measure of facility effects.

EXPERIMENTAL ARRANGEMENT

Two of the most likely lightning current paths for a helicopter are "main rotor to tail rotor" and "main rotor to wheels".

The main rotor and tail rotor had been removed and the "rotor to tail" simulation was achieved by connecting the Lynx with a return conductor system of sheet Aluminium plates to the capacitor bank. The arrangement is shown schematically in Figure 1a-c.

The helicopter was placed on a ground plane made of sheets of Aluminium riveted together. The ground plane was connected to the building earth. The helicopter wheels were isolated from the ground plane and the generator-return conductor-helicopter system was connected to the ground plane at one of three points, namely the "cold terminal" of the generator, the tail, or the port under-side, also indicated in Figure 1.

The position of the return conductor above the tail was determined using a 2 dimensional inductive current mapping program so that an approximation to the free space current flow could be obtained. Because of the proximity of the ground plane, this return conductor could be quite close to the helicopter. (For a fixed wing aircraft, a quasi coaxial arrangement of return conductors is used, however, this is difficult to realise for a helicopter, especially for the "rotor to wheels" attachment.)

The "rotor to wheel" simulation was obtained by removing the tail return conductor and connecting the starboard wheel housing to the capacitor bank. This arrangement is shown in Figure 2.

*Numbers in brackets designate References at end of paper.

The generator had a capacitance of 6.46μF and could be charged to voltages from 20-80kV. The total inductance for both arrangements was between 4&5μH, giving an oscillating current waveform on the discharge of the capacitor of 27-31kHz. The maximum current and rate of change of current was 60kA and 11kA/μs for the rotor to tail configuration and 93kA and 20kA/μs for the rotor to wheels configuration respectively. The total resistance in the circuit was about 100mΩ.

METHOD OF MEASUREMENT AND ANALYSIS

MEASUREMENT OF TOTAL CURRENT, di/dt - The total current was monitored with a small coil placed underneath one of the return conductors near the capacitor bank. This coil produced a di/dt signal which was integrated to give the total current. The skin current measurements were made with small coils of cross sectional area of about 10^{-3} m^2. Signals from these coils were conveyed to the inner part of the fuselage with screened twisted pair cable taped to the fuselage body, then input to a differential fibre optic transmitter (FOL 100). These coils had a bandwidth of about 10MHz. Where possible, if apertures were available for cable and fibre optic transmitters (FOL 200), skin current measurements were made with an EG & G MGL-7A dB/dt probe of area $10^{-4}m^2$ which had a bandwidth of 1GHz. Measurements of free field dB/dt inside the cabin were made with an EG & G MTL-2A of area $0.01m^2$.

Signals were digitised in a remote screened room. The digitiser was a 2 channel Tektronix 7612 with 2048 samples per channel and a 200MHz maximum sampling rate.

INDUCED CURRENTS IN CABLES

General - Induced currents were measured in cable looms or other conductors at 7 positions in the avionic system, chosen to represent a range of degrees of exposure to electromagnetic fields, from well-shielded to completely open (the HF aerial); the positons are listed below:

A Fire detection box in rear bay
B Tail loom, rear bay
C Standby inverter, front bay
D Hydraulic valve
E Main power loom (bus bar)
F Loom near junction box, starboard door rear pillar
G HF aerial.

The induced current in each loom was monitored by linking to a Singer-Stoddart current probe of transfer impedance 1 ohm, the output being transmitted to the recording room by means of a fibre optic link type FOL 200. Since in most cases the loom comprised a number of wires, it was the bulk current that was measured; no attempt was made to determine the distribution of current between the individual wires or screens.

CW frequency reponse test - Low power sinusoidal current over a continuous frequency range of 1MHz to 50MHz was injected at the rotor head into the helicopter-return conductor system by means of a Network Analyser (NWA) through a power amplifier and ERA current probe. The level of injected current (which varied with frequency when the NWA output level was maintained constant) was monitored by a Singer Stoddart current probe and stored in the NWA. The monitoring probe was then transferred in turn to each cable under test and the process repeated with the same NWA level and frequency range. The NWA

plotted the ratio of cable current to rotor current. An example is shown in Figure 3. Both fuselage current paths were tested, each with two earthing configurations. The aim of the test was to investigate the relationship between the CW freqency response and the transient response to the high current pulse. It is of interest that some test facilities place considerable emphasis on low power CW testing, an inexpensive and safe method (2).

High current pulse test - By means of a current probe the bulk induced current was monitored, covering the 7 cables, the 2 current paths, and the 3 earthing points. In order to check the linearity of the coupling mechanism, measurements were made at 20, 40 and 60kV capacitor bank voltages (20 to 60kA fuselage current approximately). The signal from the current probe was transmitted by the fibre optic link to a storage oscilloscope and the display photographed. Emphasis was placed on recording the HF components rather than the LF corresponding to the injected fuselage test current (about 30kHz).

Induced bulk currents rather than voltages were measured because of the increasing tendency in the UK to specify and measure interference in these terms, for EMC, NEMP and lightning purposes.

SKIN CURRENT MEASUREMENTS

LOW FREQUENCY - Measurements of the peak amplitude of the low frequency skin currents were made for both current paths through the helicopter. The measurements were obtained by integrating the signal from the coils used for measuring the di/dt. The skin current density levels are dependent on the inductance of different current routes and were hence independent of the earthing point.

The results are shown in Figure 4a & b for the "rotor to tail" current path. For a voltage of 40kV, the maximum current density is 23kA/m at the top of the tail section. At this point the ratio between the current density at the top and bottom of the tail section is 8dB compared to a predicted value of 4dB. Without the ground plane, the predicted ratio was 18dB. For comparison, the total current of 41kA would give a uniform current density around the circumference at this position of 16kA/m.

The "rotor to wheel" current route results are shown in Figure 5. The maximum value is 21kA/m under the rotor head on the generator (starboard) side. The values on the port side are smaller by about 15dB.

HIGH FREQUENCY MEASUREMENTS - Coupling to cables can be proportional to di/dt but the high frequencies in the skin currents are reduced by a factor ω, therefore the study of high frequency effects was made on the di/dt waveforms. These waveforms were Fourier analysed and the frequency content was compared to the frequencies present in the cable bulk current measurements. Most of the measurements were surface di/dt but some measurements of free field dB/dt were made inside the fuselage.

Rotor to tail - These results showed quite complex spectra. In addition to the generator - helicopter system resonant frequency of 27kHz, there were bursts of HF oscillations in the range 2-20MHz, with a duration of about 5 μs. These frequencies appeared to fall into two categories.

The first was about 8MHz and 15MHz oscillations which were present on the tail section of the fuselage. These were believed to be the $\lambda/4$ resonance and its higher harmonic associated with the rotor to tail section/return conductor transmission line. The rotor-tail distance is only 6.3m which would imply a frequency of 12MHz for a $\lambda/4$ resonance. However, the inductance in the feed plates shown in Figure 1 was measured to be 1.7μH and the feed plates, about 10cm apart, will have a capacitance of 100 pF/m^2. This reactance is sufficient to lower the frequency to about 8MHz. This frequency was little changed in value and amplitude for the different earthing points.

The magnitudes of HF dB/dt on the tail section were up to four times larger than the LF value due to transmission line effects.

The second category had lower frequencies in the range 2-5MHz and these oscillations changed dramatically for different earthing points. For example, the cabin dB/dt (direction fore-aft) signal, circumferential skin current di/dt under the rotor, and the dB/dt signal on the surface of the ground plane all showed a prominent 2.5MHz resonance when the generator was grounded. This disappeared completely for the other two earth configurations.

Similarly the axial skin current di/dt on the underside of the fuselage/tail showed a 3.5MHz resonance only when the tail of the helicopter was grounded.

These effects are believed to be associated with LC resonances due to loops formed by the ground plane, helicopter and earth connection with stray capacitance between the helicopter and ground plane.

A summary of the frequencies and magnitudes of dB/dt for the "rotor to tail" configuration measurements is shown in Table 1.

Rotor to wheels - The data show little HF content compared to the other configuration, presumably as we have not created any specific transmission lines and the LF skin current in the region of the cabin is much larger than previously, so the HF effects due to LC ground resonances are less pronounced. The initial HF spikes decayed after about ½μs. Little change occurred for the different earth points. One exception is the axial skin current di/dt on the underside of the tail section, when the tail was grounded. As in the "rotor to tail" situation there was a strong 3MHz resonance, shown in Figure 6a, not present in the other configurations as shown in Figure 6b. The effect was more pronounced for "rotor to wheels" due to the absence of the 8MHz resonance. The capacitance between the ground plane and the helicopter/return conductor assembly was measured to be 1.48nF and the inductance in the tail section was estimated at 2μH giving a predicted LC resonance of 3MHz.

Both high and low frequency measurements varied linearly with the generator voltage to within 1dB.

RESULTS OF CABLE INDUCED CURRENT MEASUREMENTS

CW FREQUENCY RESPONSE - A typical plot showing how the ratio of induced cable bulk current to injected rotor head current varied with frequency in the 1-50MHz range is given in Figure 3. All measurements were of amplitudes only, no measurements being made of phase angle. The general trend was upwards with increasing frequency but levelling off to a constant mean level. Superimposed on the general trend were many resonant peaks starting at about 2MHz. With some cables, one resonance was dominant but in others there were a number of

resonances of approximately equal strength spread throughout the frequency range.

The general level varied widely between cables, being highest for the exposed HF aerial as would be expected, (34dB down at 1MHz for one configuration) and lowest for cable B (94dB down under the same conditions.) Variation between the two current paths, respresenting the most likely lightning current paths, was small for some cables but large for others (for example, 20dB at 1MHz for cable D). Variation with earthing point is a facility effect and should ideally be small; again it was small for some cables but large for others (for example, 14dB for cable D).

PEAK INDUCED CABLE TRANSIENTS - The peak induced bulk current transients in the cables showed good linearity against capacitor bank voltage, indicating that the tests were performed below the threshold of non-linear effects such as sparking. The peak amplitude varied widely between cables; for example, with one configuration at 40kV bank voltage the spread was from 24A (aerial) to 0.3A (cable B). Variation with current path and earthing point was not as wide as in the CW tests, being a maximum spread of 11dB (cable B) and 9dB (cable D) respectively.

For the purpose of estimating the full threat level of induced transient currents it was assumed that they were due to inductive coupling and proportional to the initial rate of rise of the applied test current. All amplitudes were extrapolated to 100kA/μs, and the results are shown in table 2 (the earthing arrangement which gave the maximum current was chosen for each entry in the Table).

For the internal cables the values are considerably higher than those for the FBW Jaguar which were about 3A (1), as would be expected from the open nature of the helicopter compared with the good shielding provided for critical systems of the FBW Jaguar. It may be noted that if a lightning current takes the path rotor/wheels the induced cable currents are likely to be lower than for the path rotor/tail, the only exception in these tests being cable C.

WAVEFORM OF TRANSIENTS AND RELATIONSHIP TO CW RESPONSE - The waveforms of the transient currents were complex and showed considerable variety, including forced oscillations at the frequencies of the LF and HF currents flowing in the fuselage (about 30kHz and mainly 8MHz respectively) and free oscillations at the resonances of the loom itself, initiated by the applied test current regarded as a shock excitation, and corresponding to the resonant peaks in the CW response. These 3 waveform types are illustrated in Figures 7 a-c.

For the forced oscillations the amplitude predicted from the CW response was simply the amplitude of the corresponding oscillation in the fuselage current multiplied by the current ratio at that frequency in the CW response. This could not be done directly for the LF fuselage current (about 30kHz) since the CW response was measured only down to 1MHz, but an estimate was made assuming that at low frequency the coupling between fuselage and cable was pure mutual inductance so that the coupling was proportional to frequency and the coupling at 30kHz was therefore determined by proportion from that at 1MHz. On this assumption the current ratio at low frequency may be expressed in the form ωT, where T is a coupling time-constant; values of T deduced from the ratio at 1MHz varied from 3.10^{-12}s to 3.10^{-9} s depending on cable, current path in the fuselage and earthing point.

For the free oscillations, use was made of the relationship that the CW response is also the Fourier transform of the transient response to a unit impulse excitation. It was expected that there would be an oscillation at the frequency of each of the main peaks in the CW response and the amplitude and damping of each were estimated by an approximate formula relating them to the peak amplitude and width of each resonant rise in the CW curve. However, the actual excitation in the transient test was the leading edge of a low frequency sinusoidal current (30kHz) which in relation to HF may be regarded as a ramp (linear rise). Since a unit ramp (1A/s) is obtained from a unit impulse by integrating twice, and this is equivalent to dividing by $(j\omega)^2$ in the frequency domain, the amplitude of the transient at frequency f obtained from the CW response was divided by $(2\pi f)^2$ and multiplied by the initial rate of rise of the test current to obtain the amplitude to be expected with the actual excitation employed. This division by ω^2 meant that although the resonant peaks in the CW response did not diminish substantially with increasing frequency they did become less important in the production of components of the transient response.

Where components of the expected frequency were actually present in the recorded transients, the procedure described for prediction from the CW response gave a reasonable estimate of their amplitude, but in the complex waveforms there were other frequencies not readily identifiable and some of the expected frequencies were absent.

CONCLUSIONS

Simulated lightning tests were carried out on a Lynx helicopter at severity levels of 93kA and 20kA/μs requiring factors of approximately 2 and 5 to extrapolate full threat values of i and di/dt respectively.

It was possible to measure the induced cable currents in an interference-free manner, by the employment of fibre optic links.

The amplitude of induced currents and skin currents scaled linearly with capacitor bank voltage to within 1dB. The peak induced current transients extrapolated to full-threat values varied from 1.5A to 22A in the internal cables, being considerably higher than in the FBW Jaguar (3A) as would be expected.

The induced current transients exhibited a variety of waveforms, being in general a mixture of damped sine waves, the frequencies including those of the LF and HF currents in the fuselage and those corresponding to the resonances of the loom itself, as indicated by the resonant peaks in the CW response. There were however, other frequencies not accounted for and some of the expected frequencies were absent.

There was fair correlation between the recorded transients and the CW response.

Variation of the transients and the CW response when the system was earthed at different points indicated the presence of significant facility effects, so that more work is needed to improve techniques with the aim of achieving better simulation of in-flight conditions.

The skin current transients could be understood in terms of transmission line resonances and LC resonances between the ground plane helicopter capacitance and loop inductance, the latter being a facility effect. There was fair correlation between the skin current and cable current transient frequency content.

REFERENCES

1 R H Evans and J Bishop, "Induced Transients in a Simulated Lightning test of the Fly-by-Wire Jaguar Aircraft" International Aerospace and Ground Conference on Lightning and Static Electricity, Fort Worth, Texas, USA, June 1983

2 D E Young and L D Piszker, "The Use of CW Test and Analysis Techniques in Lightning Vulnerability Assessment of Aircraft Systems" FAA and Georgia Tech Workshop on Grounding and Lightning Protection, Atlanta, Georgia, USA, 1978

Copyright: Controller, Her Majesty's Stationery Office London 1986'

Table 1

Table of magnitude and frequency content of B at various locations of the helicopter/generator system

If the largest component >x2 the next largest one, the largest component is underlined
Js refers to the small coil used for measuring surface current density

Earthing Point	System Current Coil	$\dot{B}$ in Cabin	Js 5m top	Js 1.5m top	Js 1.5m bottom	Js 0m stbd	Js Front stbd	$\dot{B}$ on ground plate
Bank f MHz	2.5,8.1	2.5	8.1	8.1,17,20	8.1,12.6,17	2.5,8.1	2.5, 10-12,16	2.5,12.8, 20,36
$\dot{B}$ KT/s	33	.13	12	4-7	2-5	5	2	1-2
Tail f MHz	7.6,9.3	7.6,9.3, 9.5	7.6	7.6,16	3.5,7.6,16	7.6,9.3	7.6,9.3, 9.8,16	-
$\dot{B}$ KT/s	33	.13	10	4-7	2-5	5	1.5-3	
Side f MHz	5.8,8.6 9.3	5.8,8.6, 9.5	8.6		5.6,8.6,9.3 13.6,16.6	5.6,9.6 13.8,16.6	5.6,8.6 20,36	5.8,8.6 16-20,36
$\dot{B}$ KT/s	27	.05	11		2-3	2	.5-1	

Table 2

Table of peak cable current transient extrapolated to a threat value of 100kA/μs

	Cable	A	B	C	D	E	F	G
Peak Current (A)	R/T path	7.5	4.2	9.7	15.6	22.3	111	329
	R/w path	3.3	1.5	14.1	7.0	18.4	29.2	105

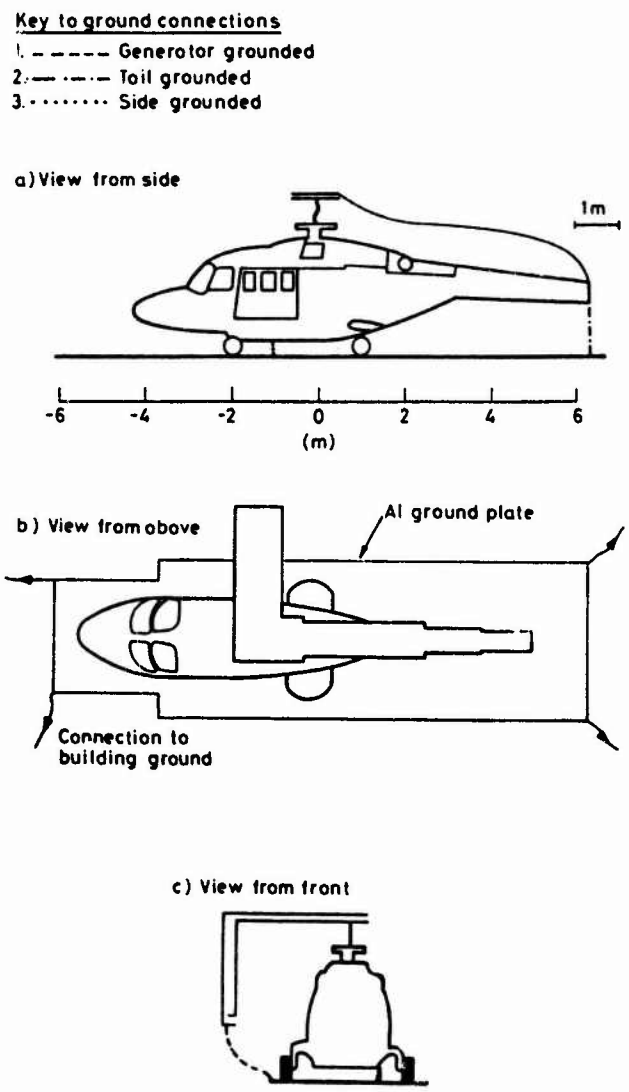

Fig. 1 - Return conductor arrangement for "rotor to tail" configuration

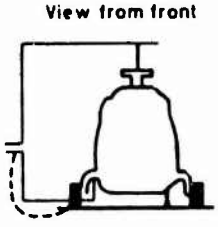

Fig. 2 - Return conductor arrangement for "rotor to wheels" configuration

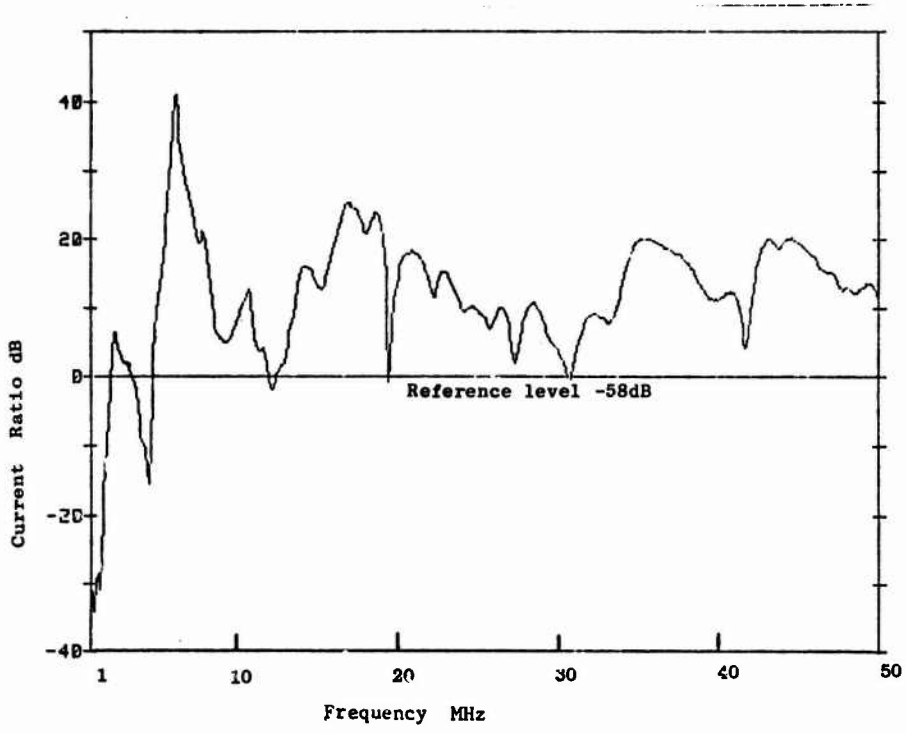

Fig. 3 - CW response for cable D, "rotor to wheels" current path, generator grounded

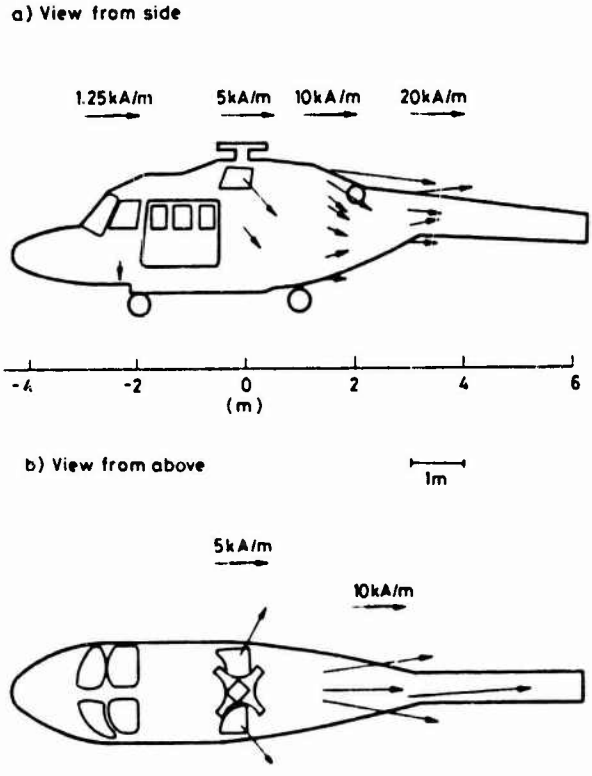

Fig. 4 - Skin current map for "rotor to tail"

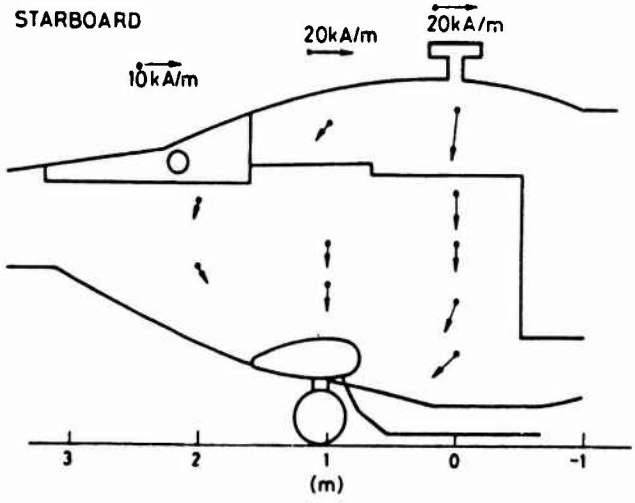

Fig. 5 - Skin current map for "rotor to wheels"

Note: For Fig 4&5 the magnitude of a skin current density vector at a particular section is defined by its length relative to the scale indicated directly above that section

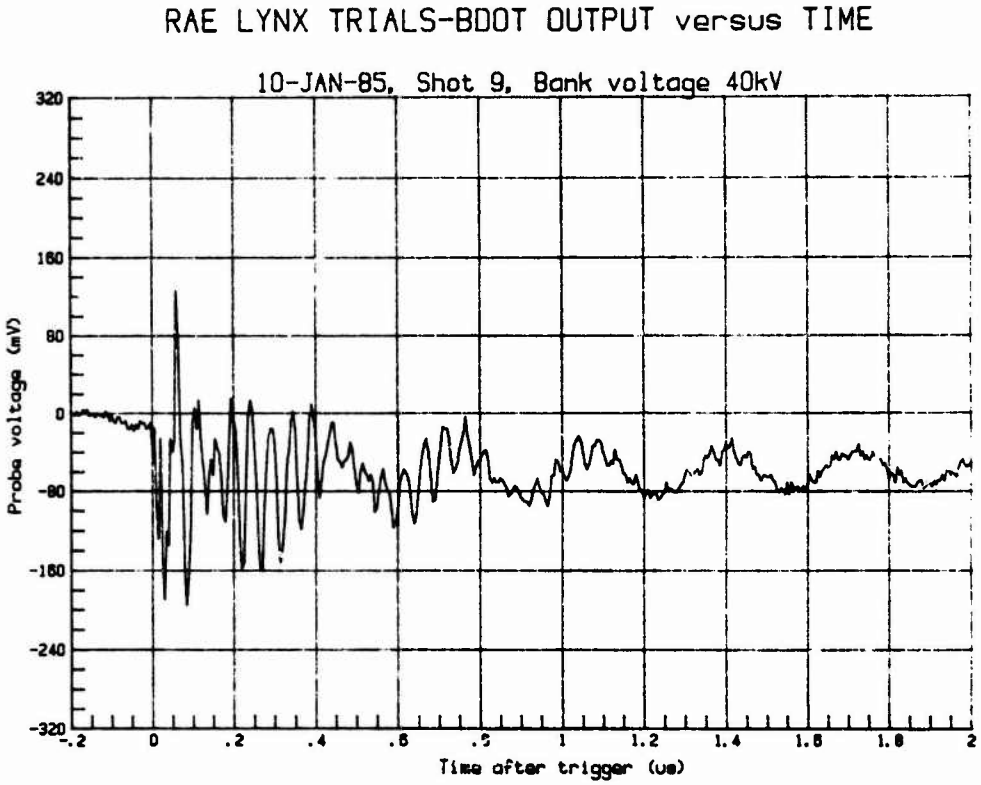

a) Tail grounded

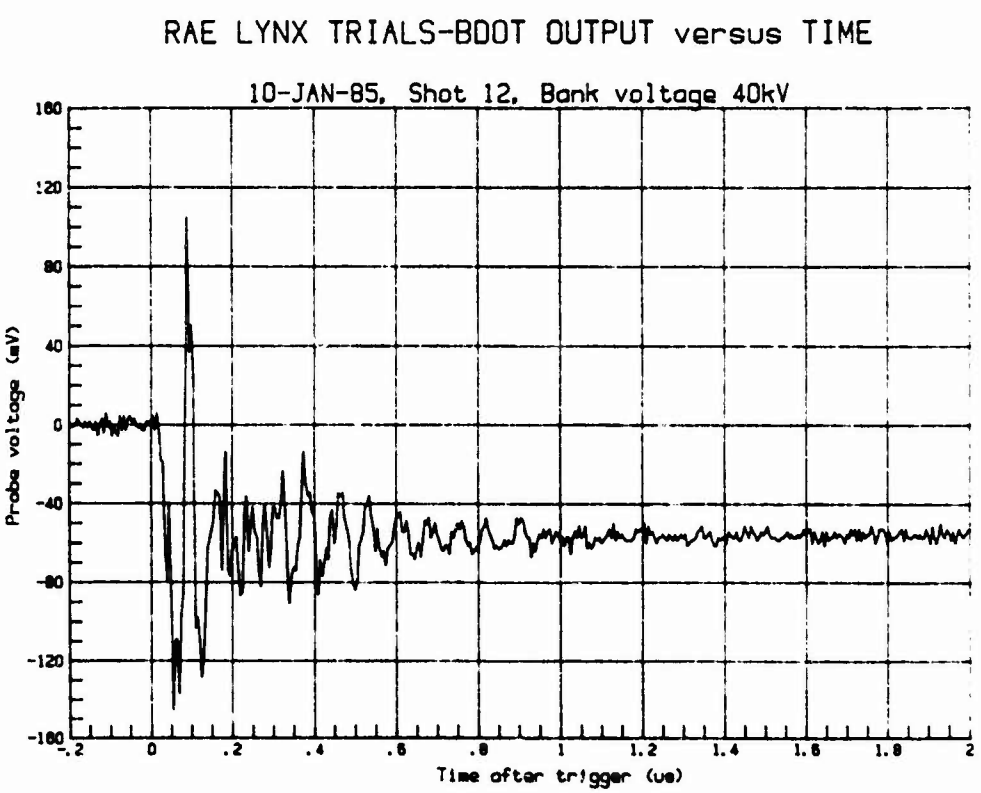

b) Generator grounded

Fig. 6 - Axial skin current di/dt on underside of fuselage tail

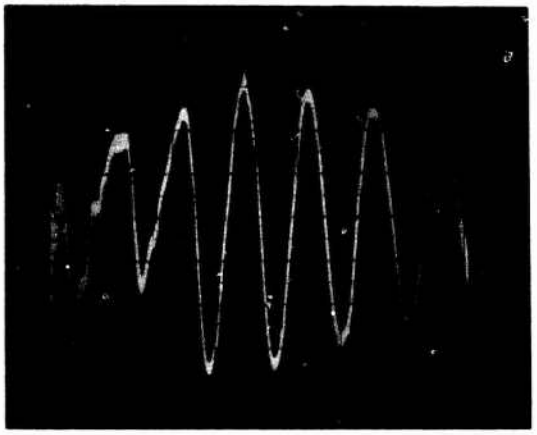

a) Cable C, 20μs/div, 0.18A/div, 31kHz oscillation

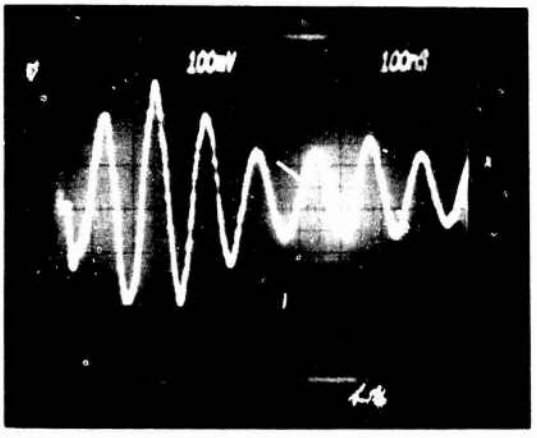

b) Cable F, 0.1μs/div, 2.8A/div, 8MHz oscillation

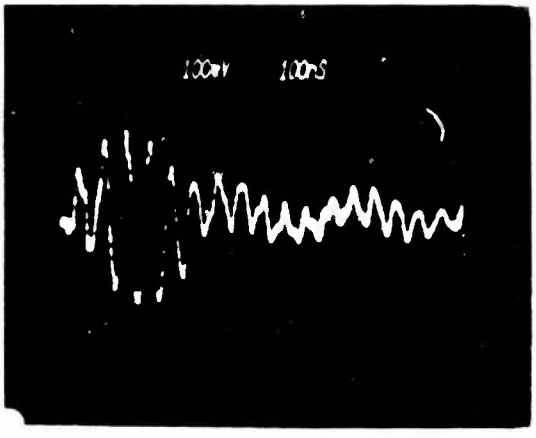

c) HF aerial, 0.1μs/div, 2.8A/div, 18MHz oscillation

Fig. 7 - Some waveforms of induced current transients

Prediction of skin currents flowing on a Lynx helicopter due to a simulated lightning strike.

A.Mallik

Kimberley Communications Consultants,
Nottingham, UK.

C.Christopoulos

University of Nottingham,
Nottingham, UK.

J.M.Thomson

Royal Aircraft Establishment,Farnborough,UK.

ABSTRACT.

A 3D Transmission Line Modelling(TLM) program has been used to model a simulated lightning strike on a Lynx helicopter.This TLM analysis has been used to identify the origin of the 3 principal resonances reported in measurements elsewhere. It is shown that all the 3 resonances are affected by the charging circuit,namely by the return conductor,ground plane and capacitor bank.

1.RAE AND CULHAM LABORATORY EXPERIMENTAL SETUP AND RESULTS

RECENTLY,SIMULATED LIGHTNING TESTS were carried out jointly by RAE and Culham Laboratories on a Lynx helicopter.Full details of these tests are reported elsewhere at this conference [1]. In these tests a large capacitor bank was dischargeo into the rotor head with return paths being provided at either the tail or the wheels. The helicopter was insulated from an aluminium ground plate and the system was earthed to the plate at one of 3 different points. These points were the bank,the helicopter tail and the underside near the port door. Thus with 2 different return paths and 3 different earthings a total of 6 different arrangements were studied. Skin current tranients were measured at 8 locations using B dot sensors. The principal resonances were found to be:

- -A low frequency 27KHz resonance associated with the overall inductance and capacitance of the circuit
- -A high frequemcy 8MHz resonance believed to be associated witn the rotor to tail length(quarter wavelength),modified by capacitance in the horizontal feed transmission plates
- -A low frequency 2 to 5 MHz resonance believed to be associated with stray capacitance between the helicopter and the ground.

Figure 1 shows details of the helicopter geometry, different current return paths and earthing variations.

2.COMPUTER PROGRAM USING 3-D TRANSMISSION LINE MODELLING(TLM).

TLM is a time domain numerical technique which has been used for solving electromagnetic fields[2], diffusion[3],lumped networks[4],and non linear wave propagation [5]. TLM models the propagation mechanism of EM waves by filling 3-D space with a network of transmission lines.This renders the problem discrete in both space and time since the exact solution is, in effect , a stable time stepping numerical routine.The advantage of the method lies in the simplicity of the modelling process and the efficiency in the use of computer resources.

The modelling of the geometry of an object is achieved by placing a 3-D mesh over it and part of the surrounding space volume. The mesh is then excited by field impulses modelling the physical situation. Meshes at present are restricted to graded orthogonal Cartesian ano polar types.After the initial excitation, iterations based on the TLM numerical algorithm commence.Thereafter, E and H field values at any location in the problem volume may be obtained in the time domain. The TLM model also provides complete information about the magnitude of the electromagnetic field components (at any specified frequency) around the helicopter. Graphic packages can then be used to provide field plots on any desired cross section through the helicopter.

Previous TLM modelling , eg aircraft responses [6],has been using E and H field excitations.This method of excitation is appropriate when an electromagnetic wave is incident on the aircraft. However in the Lynx tests a capacitor discharge was used to inject currents on the helicopter structure and the modelling was done using the recently developed 3-D condensed TLM node with 3 capacitance and 3 inductance stubs [7].This made it possible to model the capacitance and inductance elements in the bank and elswhere. The discharge of the capacitane bank was then modelled by placing an initial charge on the transmission line stubs modelling the bank.

3.COMPARISONS BETWEEN MEASUREMENTS AND TLM PREDICTIONS

All results presented in this section refer to the rotor to tail return path and bank earthed configuration. All TLM output refers to time differenced H field components so that comparisons with B dot experimental measurements could be made. An important part of the work has been to identify the origin of the measured resonances by varying the geometry used in the TLM simulations.

Figure 2 shows a discretised Lynx helicopter used in the TLM computer program. Eight output points are displayed corresponding to those in the RAE-Culham measurements. E and H field components in the time domain are calculated for each cell in the discretisation. The choice of stub parameters at each cell also makes it possible to vary the dimension of any slice of space in each of the 3 coordinate axes.This allows us to model separation distances of interest without having to substantially modify the input data files. Capacitance and inductance stubs are also available for each cell, to model lumped components, but here we only need to use the capacitance stubs to model the bank capacitance.

LOW FREQUENCY (27 KHZ) RESONANCE Measurements detailed in Reference [1] clearly show a damped LF resonance around 27 KHz This is believed to be an LC resonance arising from the capacitance C, and the inductance L, in the total system. Calculation shows that the inductance modelled by the geometry in Figure 2 is about 8.5uH instead of the 5.5uH corresponding to the 27 KHz measurements. Table 1 shows TLM predictions of LF resonances are inversely proportional to $\sqrt{C}$ and that the measured 27 KHz resonance is indeed an overall system LC resonance as expected.

HIGH FREQUENCY (8 MHZ) RESONANCE A strong 8 MHz peak reported in measurements is thought to be a quarter wavelength rotor to tail length resonance modified by capacitance in c the horizontal feed transmission plates. The results of the output from TLM simulations clearly demonstrate that the strengths of these 8 MHz resonances are critically dependant on the separation distance of these feed plates. Equivlantly it can be viewed that it is the capacitance provided by these plates that is responsible for the strength of the resonance. A TLM simulation was performed where a lumped capacitance of 400pF was introduced between the transmission line plates using capacitance stubs. The results of this modified a weak 8 MHz resonance to a strong 5 MHz resonance. TLM prediction of the B dot waveform at output point 3 in Figure 2 is shown in Figure 3.

OTHER HIGH FREQUENCY RESONANCES (2 TO 5 MHZ) These resonances are most evident in output points near the bottom of the fuselage.Some form of LC resonance associated with loops formed by the ground plate and helicopter bottom is suspected. To test this explanation the separation distance between the ground plate and helicopter was varied. In addition the ground plate was completely removed.The TLM output from these tests showed that the ground plate critically affects the strength of the measured 3 MHz resonance.Removal of the ground plate results in the complete disappearance of this resonance.In addition the output demonstrates that the separation distance between the ground plate and the helicopter also effects the strength of the resonance. TLM prediction of the B dot waveform at output point 6 in Figure 2 is shown in Figure 4.

4.CONCLUSIONS

A 3-D transmission line model (TLM) with the ability to model lumped capacitance and inductance elements has been used to model a simulated lightning test on a Lynx helicopter. Confidence in this TLM model has been shown by prediction of the 3 principal frequency components reported in measurements. Changes in the experimental configuration have been studied in the TLM model to show that all the 3 principal resonances are strongly affected by the configuration of the facility, such as the return conductor,ground plate and capacitor bank.

5. ACKNOWLEDGEMENTS.

This work has been carried out with the support of Procurement Executive, Ministry of Defence,UK.

6.REFERENCES

1 C.J.Hardwick et al,'Simulated lightning current tests on a Lynx helicopter',this conf.

2 S.Akhtarzad and P.B.Johns,'The solution of Maxwell's equations in three space dimensions and time by the TLM method of numerical analysis', Proceedings IEE 122,12, p.1344-1348,December 1975.

3 P.B.Johns, 'A simple explicit and unconditionally stable numerical routine for the solution of the diffusion equation'.Int.Journal Num. Meth. in Eng., Vol 11,p1307-1328, 1977.

4 P.B.Johns and M.O'Brien,'Use of the transmission-line modelling (TLM) method to solve nonlinear lumped networks'. The Radio and Electronic Engineer,Vol. 50 ,No.1/2,p.59-70,January 1980

5 C.Christopoulos, 'Propagation of surges above the corona threshold on a line with a lossy earth return'.Int Journal for Computation and Math. in Electrical and Electronic Eng.,Vol.4,No2, p.91-102,1985.

6 P.B.Johns and A.Mallik,'EMP response of aircraft structures using transmission-line modelling'. Proceedings of the 6th Electromagnetic Compatability Symposium and Exhibition,Zurich 1985.

7 P.B.Johns,'New symmetrical condensed node for three-dimensional solution of electromagnetic-wave problems by TLM',Electronics Letters,30th January 1986,Vol.22 No.3,p.162-164.

TABLE 1 - TLM predictions of LF resonance for different values of bank capacitance

CAPACITANCE, C	6.5uF / 1600	6.5uF / 400	6.5uF
INDUCTANCE, L (as modelled by TLM geometry in Figure 2)	8.5uH	8.5uH	8.5uH
TLM prediction of LF resonance (KHz)	880	442	22.2
$\frac{1}{2\pi\sqrt{LC}}$ (KHz)	856	428	21.4

Key to ground connections

1. – – – – – Generator grounded
2. — · — · — Tail grounded
3. · · · · · · · · Side grounded

a) View from side

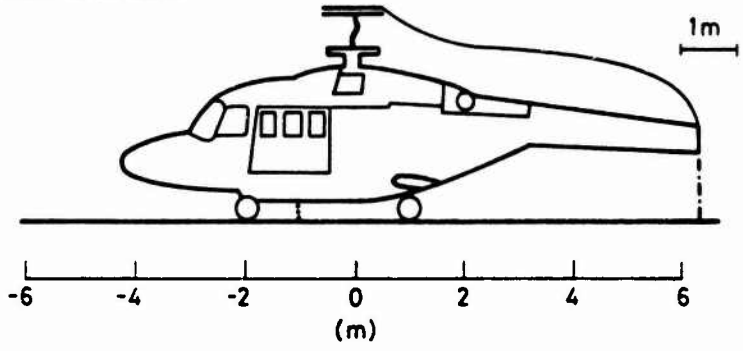

"Rotor to Tail" Return Conductor Arrangement

b) View from above

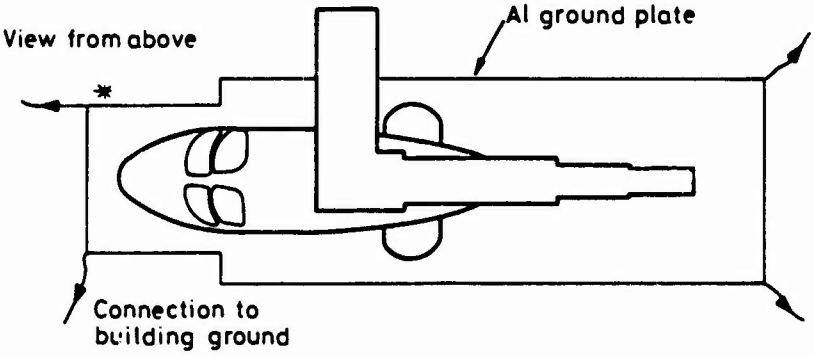

"Rotor to Wheels"

c) View from front

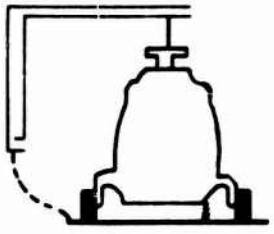

d) View from front

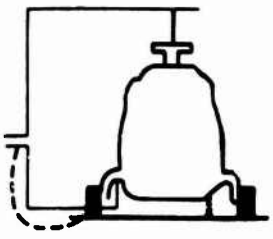

Fig. 1 - Experimental setup used in Reference 1

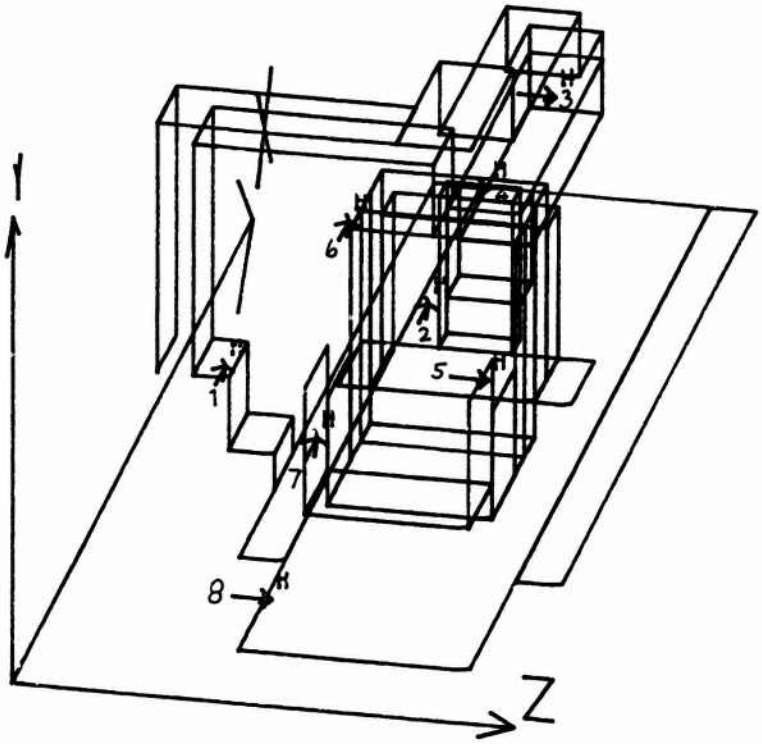

Fig. 2 - TLM discretisation of experimental setup in Figure 1

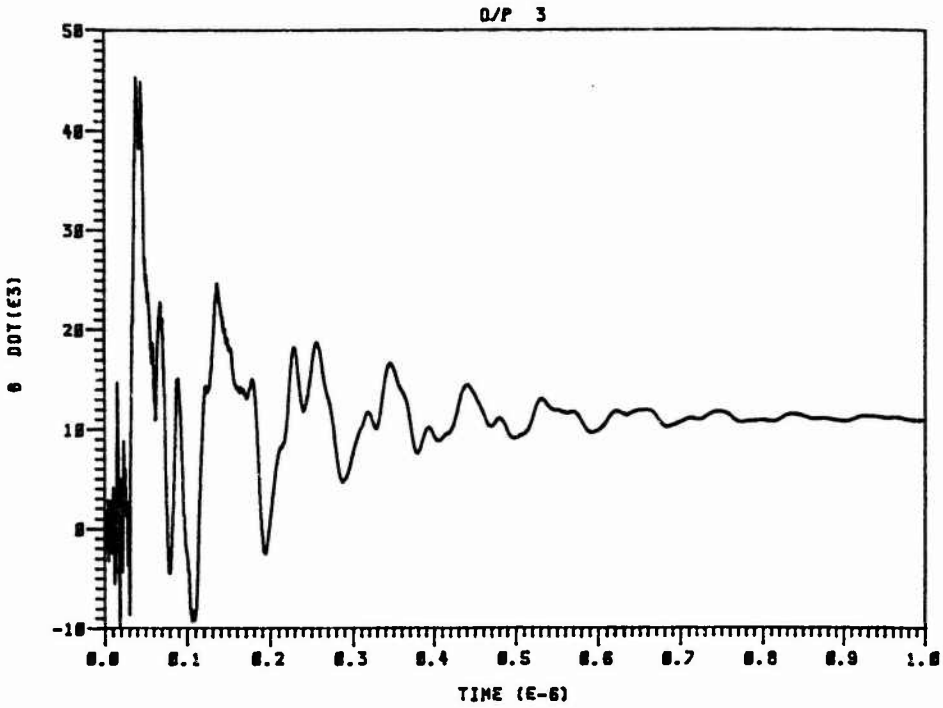

Fig. 3-TLM prediction of B dot waveform at output point 3

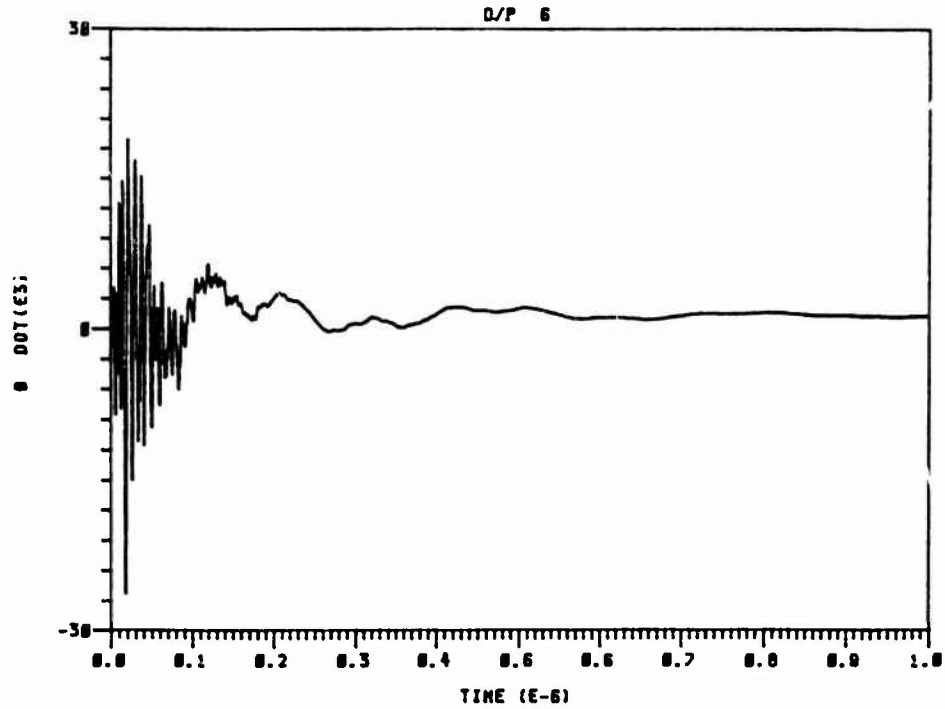

Fig. 4 - TLM prediction of B dot waveform at output point 6

SPATIAL AND TEMPORAL DESCRIPTION OF STRIKES TO THE FAA CV-580 AIRCRAFT

Jean S. Reazer and Arturo V. Serrano
Technology/Scientific Services, Inc.

Abstract

Spatial and temporal descriptions of strikes to the FAA CV-580, S/N 49, during the FY84 and FY85 lightning characterization program are presented in this paper. The aircraft was instrumented with wideband electromagnetic sensors and current shunts, then flown in Florida thunderstorms in 1984 and 1985 at altitudes from 2000 to 18000 feet. Waveforms were recorded digitally at a sample rate of five nanoseconds to give ten microsecond windows with a frequency response of 100 Megshertz. Wideband analog data were recorded continuously.

A technique for time correlating the digital waveforms to derive attachment points on the aircraft is discussed in detail. Current paths on the wings and fuselage are illustrated for several strikes and the inferred attachment points are correlated with video recordings from the four video cameras installed on the aircraft.

Information from analog recordings of slow field variations on the aircraft is then combined with the results of the above analysis to provide insight into the attachment process for cloud-to-ground, cloud-to-cloud and triggered lightning strikes to aircraft.

INTRODUCTION

During 1984, a Convair CV-580 aircraft provided by the Federal Aviation Administration (FAA) was instrumented with wideband electromagnetic sensors to measure the effects of lightning attachments. The aircraft was flown in central Florida thunderstorms in 1984 and 1985 at altitudes of 2,000 to 18,000 feet, collecting fifty strikes in approximately 100 hours of flying time.

In this paper, a technique for time correlating the outputs of the sensors is described which allows determination of the point where the strike attached to the aircraft. Measurements recorded on the wings and fuselage are illustrated for several strikes and the attachment points derived from these data are correlated with photographs from the video cameras installed on the aircraft.

Once the attachment point is known and the direction of current flow on the aircraft established, the polarity of the sensor outputs can be used to determine whether negative charge is flowing onto the aircraft, as would be expected during a cloud-to-ground event, or is flowing off the aircraft, indicating an interaction of the aircraft with a positive charge center. Negative charge flow onto or off the aircraft is shown to be correlated with altitude, with strikes at low altitude (2,000 to 4,000 feet) indicating negative charge flow onto the aircraft and strikes at high altitude (14,000 to 18,000 feet) generally producing negative charge flow off the aircraft.

METHOD

Consider a hypothetical aircraft fuselage instrumented with two loop type sensors to measure surface current. One sensor is mounted forward on the fuselage about 15 feet ahead of the wing axis, while the second is aft on the fuselage about 15 feet behind the wing axis. Since the sensors are 30 feet apart, assuming a current velocity equal to the speed of light through the aircraft, a current pulse applied to the nose of the aircraft will reach the forward sensor 30 nanoseconds (ns) before it reaches the aft sensor. With sufficient time resolution in recording the two waveforms, it is possible to tell whether the current pulse was applied to the nose or to the tail.

Assume that both sensors have been oriented so that negative charge flow from the nose to the tail will produce a positive output. Conversely, then, current flow from the tail to the nose will produce a negative output on both sensors. Figure 1 shows four simple scenarios in which lightning attaches to an aircraft. In 1A, negative cloud charge is lowered to the aircraft and there is a strike to the nose producing negative charge flow toward the tail and two positive waveforms as sensor outputs. In 1B, negative charge is lowered to the aircraft and there is a strike to the tail, producing negative charge flow toward the nose and two negative waveforms as sensor outputs. In 1C, it is assumed that the charge lowered to the aircraft is positive. In this case, the strike to the nose results in negative charge flow off the aircraft and negative waveforms as sensor outputs. Finally, as in 1D, negative charge flow off the aircraft during a strike to the tail produces positive sensor outputs. Thus identifying the attachment point of the lightning event and recording the polarities of the resulting sensor outputs allows determination of whether negative charge was moving onto or off the aircraft during the flash.

AIRCRAFT INSTRUMENTATION

Sensors

Magnetic Field Sensors

The four magnetic field sensors on the aircraft were of the Multi-Gap Loop (MGL) type manufactured by EG&G, and designed to measure the rate-of-change (derivative) of the magnetic field resulting from surface currents on the skin of the aircraft. A sensor was placed underneath each wing between the engine nacelle and the fuselage. The remaining two sensors were placed on top of the fuselage, one forward of the wing and one aft of the wing. The outputs of these sensors were split into two by power splitters. One output was sent to a waveform digitizer whose output was recorded on digital 9-track tape. The second output was integrated by signal conditioning components and recorded on direct channels of an analog recorder. The sensors were oriented so that a positive output would occur for negative charge flow from nose to tail, or from the right wingtip to the left wingtip.

Electric Field Sensors

The electric field sensors were of the Flush Plate Dipole (FPD) desig manufactured by EG&G. These sensors respond to the rate of change (derivative) of the electric field. One sensor was mounted underneath each wingtip, one sensor was mounted on the forward upper fuselage ahead of the wing, and one sensor was mounted on the left surface of the vertical stabilizer. The output of the fuselage sensor was integrated and recorded in an FM channel of the analog recorder. The outputs of the three other sensors were split into two by power splitters. One output was directed to waveform digitizers and recorded on digital 9-track tape and the second output was integrated by the signal conditioning components and recorded on the analog recorder. The wingtip sensors, which looked down, produced a positive output in a negative electric field. The fuselage sensor produced a negative output in a negative electric field since it was mounted on top of the fuselage.

Television Cameras

Two of the cameras were of the CID type manufactured by General Electric. These cameras were equipped with modified Nikon wide angle lenses (180 degree field of view) and were installed on the fuselage, one viewing up and one viewing down. The remaining two cameras were of the vidicon type manufactured by RCA. These two cameras were installed on the left and right side of the fuselage so that each one viewed one wing. The camera outputs were recorded in VHS format using RCA video recorders.

Recording Syatems and Timing

Waveform Digitizers

The waveform digitizers were Tektronix 7612D's with programmable plug-ins. The digitizers were

controlled by special software developed in the AFWAL/FIESL Research Facility by T/SSI, and a PDP-11/35 minicomputer. The digitizers were triggered simultaneously by a common pulse from the trigger system so that all the digital records were time synchronized. After the waveform was digitized, it was transferred to 9-track tape for storage under the automatic control of the computer system. The digitizers were operated at the fastest sampling rate to produce a ten microsecond (μa) window with 2,048 samples at five ns intervals.

Analog Recorder

The analog recorder was a Honeywell 101, 28-channel recorder. FM channels had a bandwidth of DC to 500 kiloHertz (kHz) while direct record channels had a bandwidth of 400 Hertz (Hz) to two megaHertz (mHz).

Trigger System and Time Synchronization

The trigger system was activated by the un-integrated output of the surface current sensors. It was set to detect a level change, either positive or negative, from any of their inputs. It would then output a common pulae to each of the digitizers, the system controller and the analog recorder. Time synchronization between the analog and digital recordings was via the trigger pulse recorded on one analog channel. Time synchronization with the video recording systems was accomplished by recording IRIG B time code on each recorder.

A more detailed explanation of the aircraft instrumentation is provided in Reference 2.

RESULTS

Two strikes, one of each polarity, are analyzed in detail to show how the method was applied. The results are then tabulated and correlated with altitude.

Negative Charge Flow Onto the Aircraft

On 17 August 1984, the aircraft was flying at 4,000 feet when it was struck. The video camera on the top of the aircraft showed a strike in the direction of the nose (Figure 2).

The integrated outputs from the four surface current sensors are shown in Figure 3. Their polarities are consistent with either negative charge flowing onto the aircraft from nose to tail, or negative charge flowing off the aircraft from tail to nose. Figure 4 shows an overlay of the fuselage sensor derivative outputs which indicates that the current pulse reached the forward fuselage sensor approximately 50 ns before it reached the aft fuselage sensor. Figure 5 is an overlay of the derivative outputs from the wing sensors, with one reversed in polarity to facilitate the comparison. As expected for a strike to the nose, current reaches both sensors at the same time and the resulting peaks coincide. Finally, the current peak at the electric field sensor on the vertical stabilizer occurred 45 ns after the peak on the aft fuselage surface current sensor, consistent with fore to aft current flow.

Consistent evidence thus exists for an initial attachment point to the nose of the aircraft, establishing that this strike resulted in negative charge flow onto the aircraft. This is corroborated by positive waveforms on the electric field sensors at the wingtips and the negative waveform on the electric field sensor on the fuselage.

Negative Charge Flow Off the Aircraft

On 13 July 84, the aircraft was struck while flying at 14,000 feet. The upper camera shows a flash heading toward the tail. (See Figure 6.) The attachment point was also confirmed by physical inspection after the flight. A 3/8 inch hole was found on top of the vertical stabilizer. Since there was only one strike recorded during this flight, it was evident that the damage was from this attachment.

As before, the fuselage surface current sensors both show positive polarities, indicating negative charge flowing onto the aircraft from nose to tail, or negative charge flowing off the aircraft from tail to nose (Figure 7). In this case, the impulse appears first on the electric field sensor on the vertical stabilizer, arriving 24 ns later at the surface current sensor on the aft fuselage and 16 ns later at the sensor on the forward fuselage. The pulse appears simultaneously on both current sensors on the wings and, 40 ns later, appears on the electric field sensors near the wingtips. Since the attachment apparently was to the tail, the polarities of the sensor outputs indicate negative charge flow off the aircraft.

Analysis of Results

Similar analysis were performed on nine strikes, seven from 1984 and two from 1985. The results are shown in Table 1, which lists the polarity of the waveform and its time of arrival at the sensor for the surface current (I-FF, I-AF, I-RW, I-LW) and wingtip electric field sensors (E-RW, E-LW) for each strike. The table also lists the attachment point determined from this data, whether where was video evidence substantiating it, the altitude and the direction of charge flow (+ for negative charge flow off of the aircraft, - for negative charge flow onto the aircraft). The final column in the table shows the initial 35 ns of the electric field change on the aircraft measured at the forward upper fuselage.

A review of this table shows that all three of the strikes at low altitude (2,000 - 4,000 feet) had polarities consistent with negative charge flow onto the aircraft. Of the six strikes at high altitude (above 14,000 feet), five had polarities consistent with negative charge flow off the aircraft, while only one had a polarity consistent with negative charge flow onto the aircraft.

The polarities of the strikes at low altitude are consistent with the well known model of a thunderstorm dipole and the lowering of negative charge to ground during a negative cloud-to-ground flash (Reference 3). Since cloud-to-ground strikes lowering positive charge to ground are rare in most thunderstorms (Reference 3), this result is to be expected at low altitude. It also suggests that the aircraft is actually involved in a cloud-to-ground event, rather than acting in some way to trigger a strike which would not otherwise have occurred.

The preponderance of strikes indicating interaction with positive charge centers at high altitudes is interesting. In an earlier paper, Rustan and

Moreau (Reference 1) presented data showing that many of the high altitude strikes to the CV-580 had a common initial electric field signature. This signature is seen on all the high altitude strikes which appear to be interacting with positive charge centers. It is not seen on the one strike which showa motion of negative charge onto the aircraft. Rustan and Moreau postulated that this signature indicated that the aircraft initiated the discharge by means of a negative leader propagating out from the aircraft for distances not greater than 300 meters.

In esrlier work, it has been suggested that an aircraft charged to a high potential by triboelectric processes had a higher probability of triggering a strike (References 4, 5). Since triboelectric charging generally produces a negative charge on the aircraft and an aircraft at 14,000 - 18,000 feet is flying at an altitude in the thunderstorm where positive charge centers become more visible, our data may support this suggestion.

CONCLUSIONS

1. Although the sample is limited, there sppears to be a correlation of aircraft altitude with the type of charge motion on the aircraft. A strike at low altitude generally results from interaction with a negative charge center while a strike at high altitude usually results from interaction with a positive charge center.

2. The strikes at high altitude indicating interaction with poaitive charge centers appear to share a common initial field change, which suggeats they are triggered strikes. This field change is not seen on the one high altitude strike indicating interaction with a negative charge center, or on the strikes at low altitude.

3. The results presented indicate that with a minimum of four (4) well placed surface current sensors, enough spatial information is available to identify current paths resulting from lightning attachments to the aircraft. Further, the polarity of the signals from the sensors can be used to infer the type of charge flow.

4. If the data from each of the four sensors is time-correlated with sufficient resolution, the time of arrival at each sensor can be combined with the spatial data to identify the entry and exit points and whether charge is flowing onto or off the aircraft.

REFERENCES

1. Rustan, P.L. and Moreau, J.P. "Aircraft Lightning Attachment at Low Altitudes", 10th International Aerospace and Ground Conference on Lightning and Static Electricity, Paris, France, June 1985.

2. Rustan, P.L., Kuhlman, B.P., Burket, H.D., Reazer, J. and Serrano, A., "Low Altitude Lightning Attachment to an Aircraft", AFWAL-TR-86-3009 in Process, February 1986.

3. Uman, M.A. and Krider, E.P., "A Review of Natural Lightning: Experimental Data and Modeling", IEEE Transactions on Electromagnetic Compatibility, May 1982.

4. Vonnegut, B., "Electrical Behavior of an Aircraft in a Thunderstorm", Rep. FAA-ADS-36, February 1985.

5. Clifford, D.W. and Kasemir, H.W., "Triggered Lightning", IEEE Transactions on Electromagnetic Compatibility, May 1982.

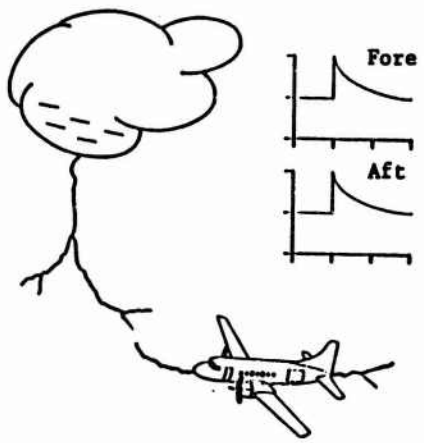

1A Negative Charge Flow onto Aircraft - Strike to Nose

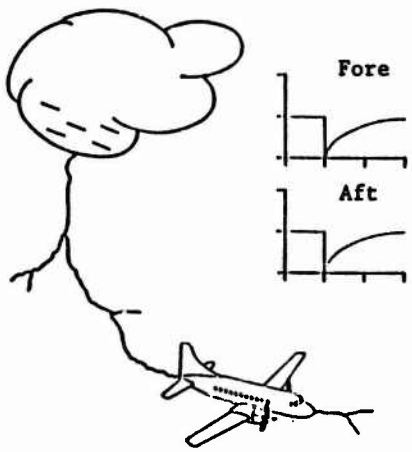

1B Negative Charge Flow onto Aircraft - Strike to Tail

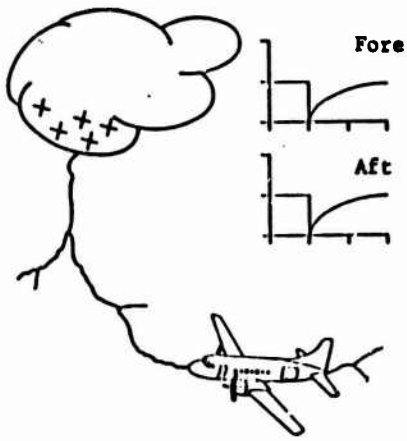

1C Negative Charge Flow off Aircraft - Strike to Nose

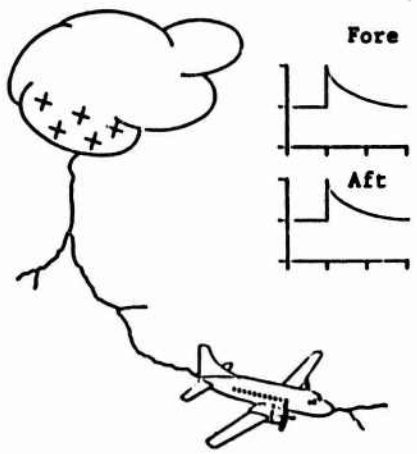

1D Negative Charge Flow off Aircraft - Strike to Tail

Figure 1. Outputs Expected from Fore and Aft Loop Sensors on Aircraft Fuselage during Four Different Lightning Attachment Scenarios

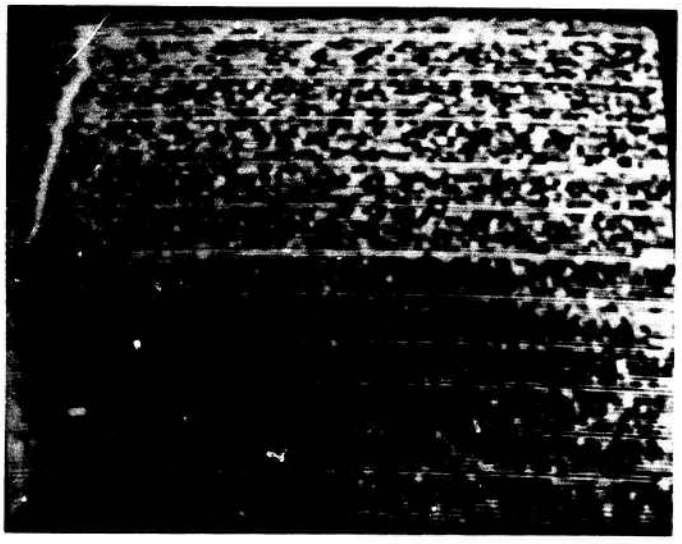

Top Camera - Lens Viewing Upward

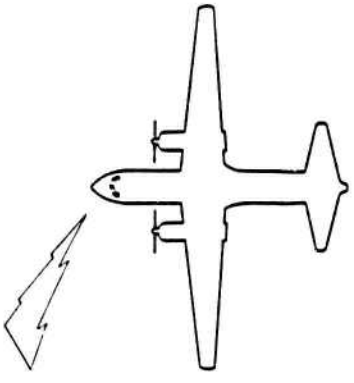

Figure 2. Strike to the Nose of the CV580 Aircraft
17 August 1984

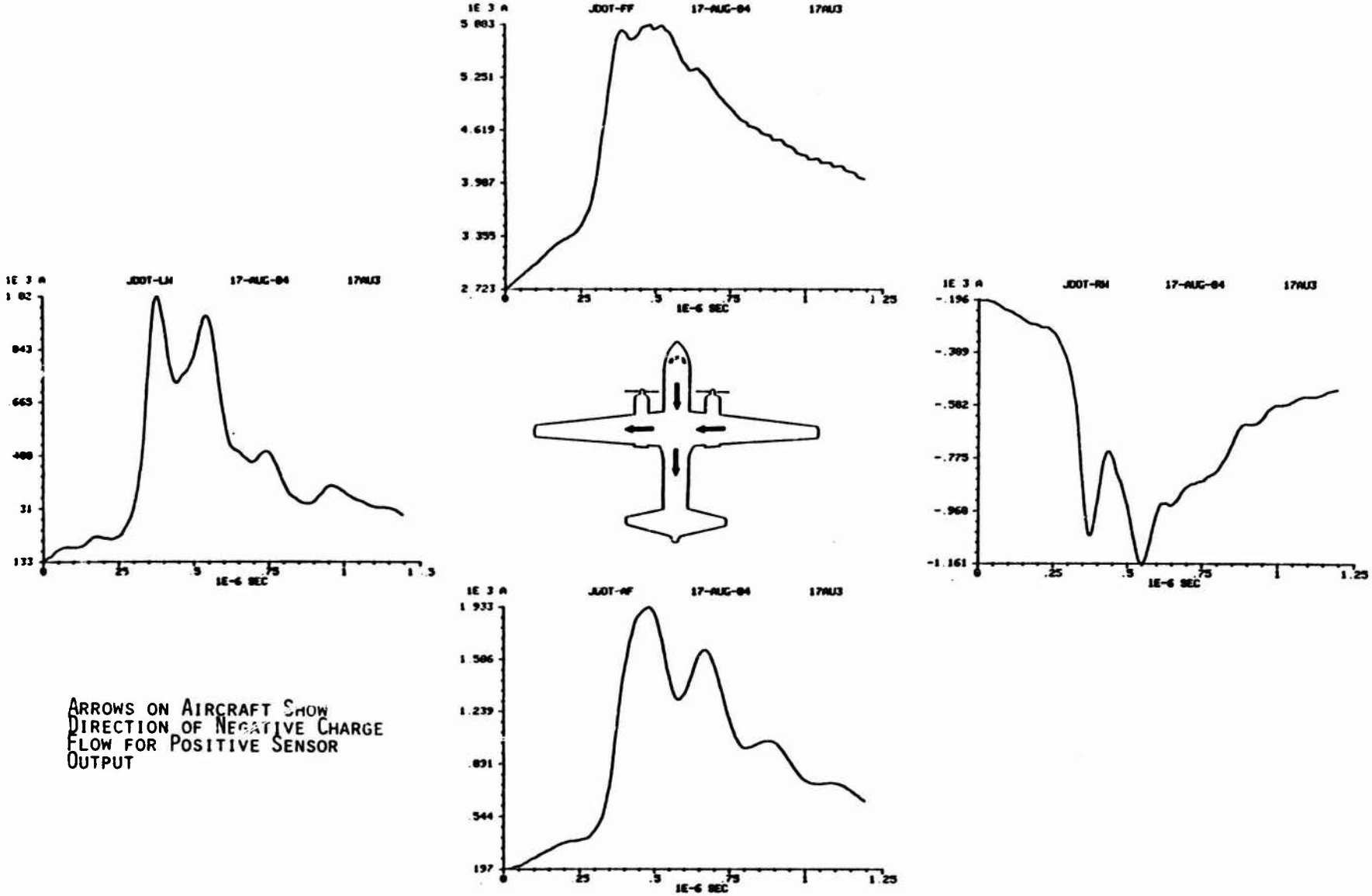

FIGURE 3. OUTPUTS, CLOCKWISE FROM TOP, FOR THE FORWARD FUSELAGE, RIGHT WING, AFT FUSELAGE AND LEFT WING SURFACE CURRENT SENSORS DURING A STRIKE TO THE AIRCRAFT NOSE

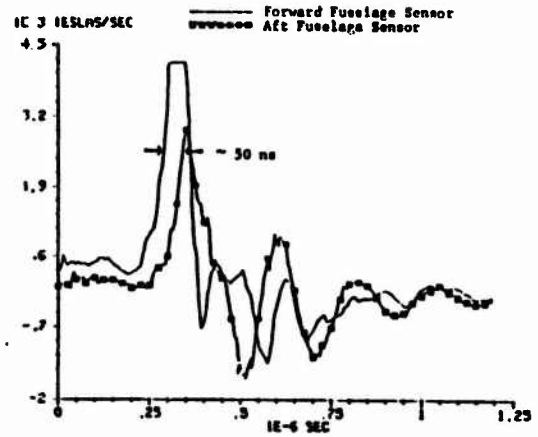

Figure 4. Overlays of the Derivatives of the Surface Current at the Forward and Aft Fuselage Sensors Showing the Time Delay for an Attachment at the Nose - 17 Aug 84

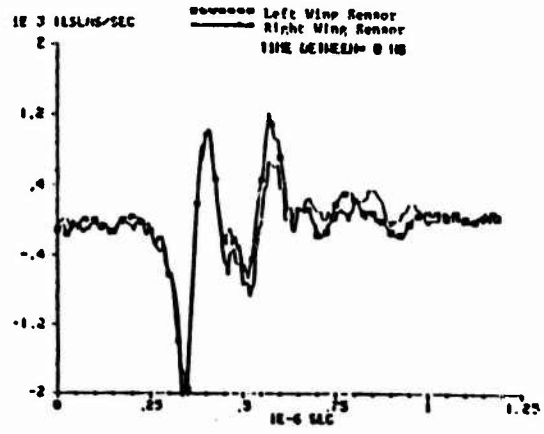

Figure 5. Overlays of the Derivatives of the Surface Current at the Left and Right Wing Sensors Showing the Time Delay for an Attachment at the Nose - 17 Aug 84

Top Camera - Lens Viewing Upward

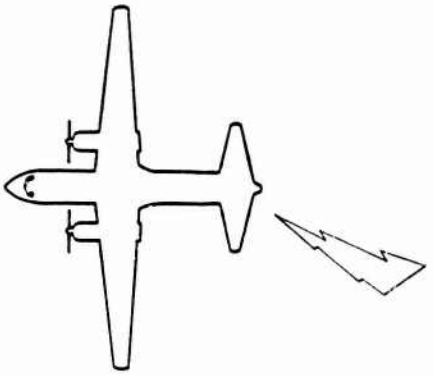

Figure 6. Strike to the Tail of the CV580 Aircraft
13 July 1984

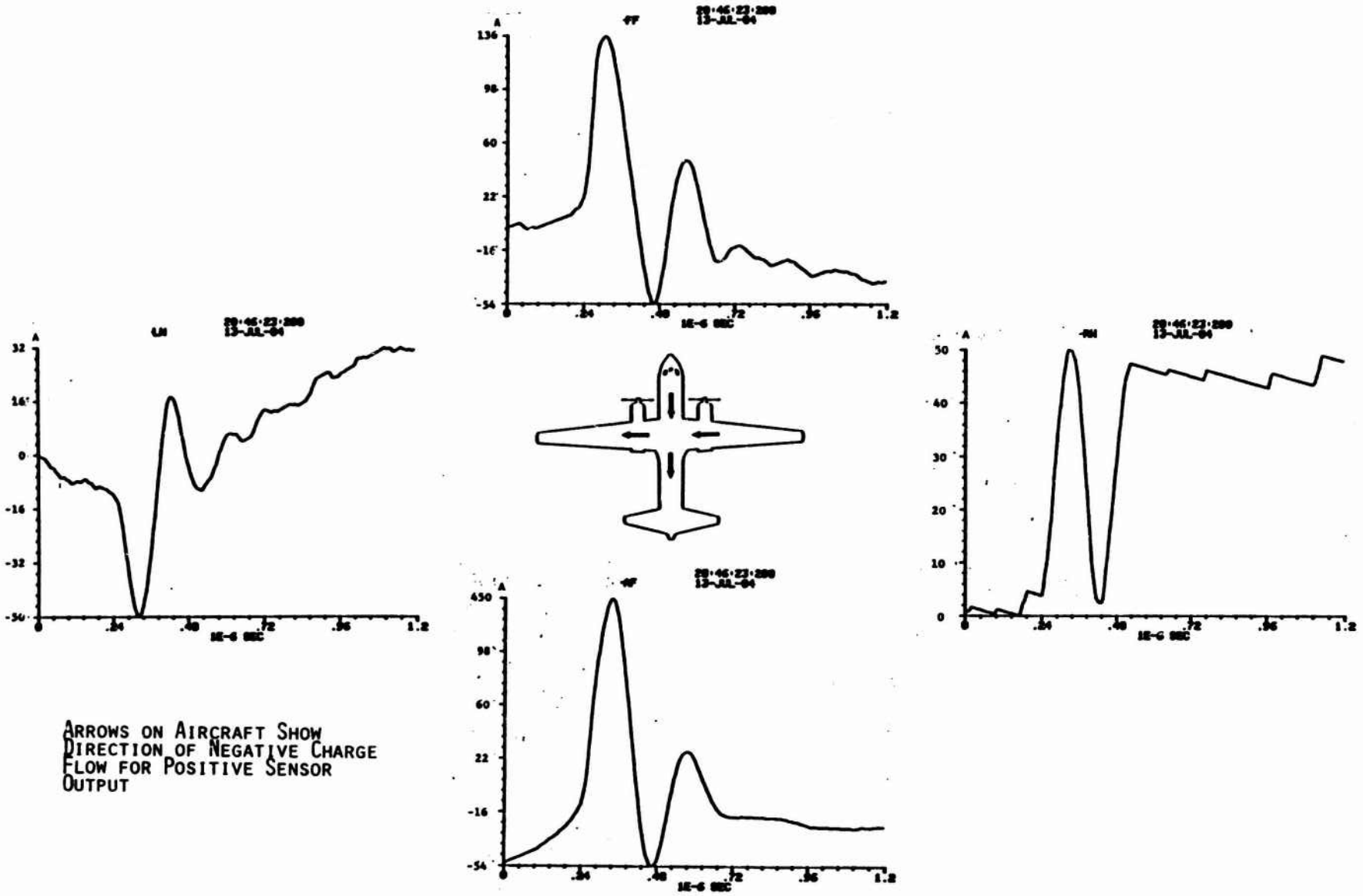

FIGURE 7. OUTPUTS, CLOCKWISE FROM TOP, FOR THE FORWARD FUSELAGE, RIGHT WING, AFT FUSELAGE AND LEFT WING SURFACE CURRENT SENSORS DURING A STRIKE TO THE AIRCRAFT TAIL

DATE	I FF		I AF		I RW		I LW		E RW		E LW		Attachmt Point	Video Evid	Altitude	Charge Flow	Initial Field Change
	Pol	TOA	Pol	TOA	Pol	TOA	Pol	TOA	Pol	TOA	Pol	TOA					
13 Jul 84	+	270	+	254	+	273	-	273	N/A	N/A	-	304	Tail	yes	14000	+	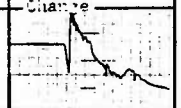
6 Aug 84	N/A	N/A	-	347	-	331	-	360	N/A	N/A	-	410	Right Wing	yes	14000	+	N/A
7 Aug 84 #1	+	233	+	258	N/A	N/A	N/A	N/A	-	305	-	295	Tail	yes	18000	+	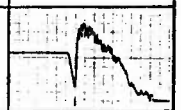
7 Aug 84 #2	+	277	-	277	-	269	N/A	N/A	-	233	-	382	Right Wing	yes	18000	+	
17 Aug 84	+	295	+	343	-	343	+	343	+	395	+	391	Nose	yes	4000	-	
20 Aug 84	+	283	+	301	-	288	+	288	+	328	+	323	Nose	yes	2000	-	N/A
5 Sep 84	+	278	-	278	-	283	+	299	-	240	-	336	Right Wing	yes	18000	+	
27 Jun 85	-	665	-	650	-	670	+	665	+	700	+	695	Tail	no	14000	-	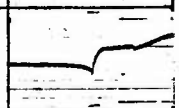
29 Jun 85	N/A	N/A	+	750	+	750	N/A	N/A	+	707	+	815	Right Wing	yes	1800	-	

Table 1

Data Used to Determine Charge Flow during Nine Strikes to the CV580 Aircraft in 1984 and 1985

Time of Arrival (TOA) in Nanoseconds

Simultaneous Airborne and Ground Measurement of Low Altitude Cloud-to-Ground Lightning Strike on CV-580 Aircraft

Jean S. Reezer
Technology/Scientific Services, Inc.
Deyton, Ohio

Richerd D. Richmond
Wright Aeronautical Laboretories
AFWAL/FIESL
Wright-Pattereon AFB, Ohio

Abstrect

During the 1984-85 Airborne Lightning Characterizetion Program conducted by the Atmospheric Electricity Hazards Group of the Air Force Wright Aaronautical Laboratories (AFWAL/FIESL), the CV-580 eircraft was struck three times while flying at low altitude (twice in '84 and once in '85). For the avant recorded in '85, eimultanaous ground meesurements of the alactric and magnetic fielde were also recordad.

Tha measured fielda at the ground eita are usad to astimate the paak current in the channel et the point of impact, and the current et the aircraft altitude (600 metars ebove ground) ie pradicted. Thase rasults ere comperad with the dete obteined on the eircraft. The current emplitudee, poleritiee, end peths as well as the predicted currents are uead to determine the portion of the cloud-to-ground lightning stroka intercepted by the eircraft. Similar enalysis ere conducted on the low eltitude evants from 1984.

INTRODUCTION

During the summers of 1984 and 1985, a CV-580 aircraft provided by the Federal Aviation Administration (FAA) and instrumented by the United States Air Force Wright Aeronautical Laboratories (AFWAL) was flown in or near Florida thunderstorms at altitudes of 1800 to 18000 feet (550 to 5500 meters). The sensors and instrumentation on the aircraft recorded the electromagnetic fields and currents produced when the aircraft was struck by lightning.

Ground stations were set up during both summers to monitor the fields while the aircraft was flying. In 1985, the ground station was equipped with two flush plate dipole electric field sensors and two magnetic field loop sensors to monitor fields produced by lightning within 100 kilometers (km) of the Kennedy Space Center site.

On 29 June 1986, a direct lightning strike to the aircraft was recorded simultaneously by the airplane instrumentation and by the instrumentation at the ground station. The aircraft was flying at an altitude of 1800 feet (550 meters). The data recorded for this event and the conclusions drawn from that data are presented in this peper. Based upon these conclusions, a similar discussion is presented for two low altitude strikes recorded during the 1984 project.

INSTRUMENTATION

AIRCRAFT SENSORS - A total of 27 sensors were installed on the aircraft, of these only those pertinent to this discussion are described. Four resistive current shunts and booms were mounted on the aircraft. One was attached to each wing tip. A third shunt was located at the tail boom and the fourth was mounted at the top of the vertical stabilizer. The tail boom also contained a derivative current sensor.

Four derivative magnetic field (or surface current) sensors were also on the aircraft. Two were mounted on the top of the fuselage, one fore and one aft of the wing. The remaining two were mounted, on the lower surface of each wing, between the fuselage and the engine pod.

Each wing tip contained a flush plate dipole electric field (or displacement current) sensor. These sensors were also derivative sensors and were mounted on the bottom surface of the wing.

Video cameras were used to record the scene across the top of each wing as well as above and below the fuselage. These records were useful in confirming aircraft attachment points.

DATA ACQUISITION - Signals from the sensors were recorded in discrete digital windows using Tektronix 7612 waveform digitizers. These digitizers recorded a 10 microsecond (s) window at five (5) nanosecond (ns) intervals, providing an upper frequency response greater than 50 MHz. Signal levels of either polarity from either the current shunts or the surface current sensors triggered the digitizers when any signal exceeded a preset level. A detailed description of the aircraft instrumentation is given in Ref. 1.

GROUND STATION - The ground station equipment was located near the edge of a lagoon at the northern end of Kennedy Space Center. Two flush plate electric field antennas and a pair of crossed-loop magnetic field sensors were mounted on the roof of the ground station trailer. The outputs from the sensors were electronically integrated and recorded on an analog tape recorder.

Irig-B timing signals were used to time synchronize recordings on the aircraft and at the ground station.

LOW LEVEL STRIKE

On 29 June 1985 at 18:49:49.6 (Z), the aircraft instrumentation recorded a lightning attachment. The aircraft was over the ocean near Melbourne, Florida at an altitude of 1800 ft (550 m). The location of the aircraft was 28:17:02 N, 79:57:07 W, placing it about 48 nautical miles (nm) or 90 km from the ground site. The outside air temperature was 20 degrees Centigrade (C) and the aircraft was in clouds, rain, and moderate turbulence.

Figure 1 shows a 164 microsec window of the electric field recorded at the ground station at 18:49:49. This was the only event recorded within several seconds of the time of the attachment to the aircraft.

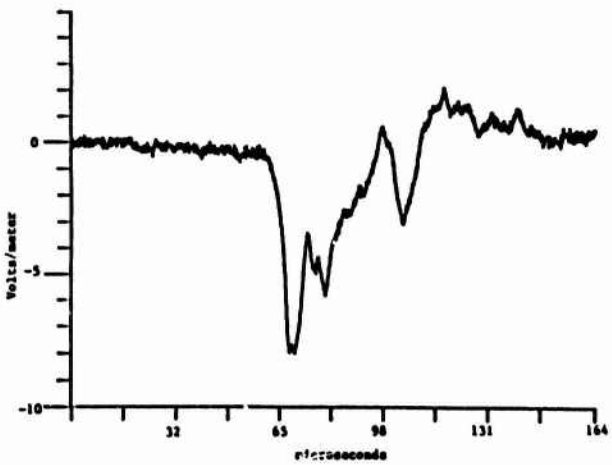

Fig 1. Ground Station Electric Field (18:49 29 June '85)

The polarity of the field indicates that this flash lowered negative charge to ground (in this case, to sea). The measured electric field peak was nine (9) volts/meter (V/m). Since the actual distance to the flash is known (90 km), an estimate of the ground level return stroke current can be calculated. Dropping the retardation time term in equation 5 of Ref 2, we have

$$I = \frac{2\pi CR}{\mu_o v} \, 8 \qquad (1)$$

where R is the distance (in meters) from the flash and v is the return stroke velocity. From Ref. 3, a nominal value of 1.2×10^8 meters/second (m/s) is used for v. Because there are essentially radiation fields at this distance, the relationship E/B=C can be used to rewrite Eq. 1:

$$I = \frac{2\pi R}{\mu_o v} E \qquad (2)$$

with the measured value of E=9 V/m, equation 2 provided a peak current of 33.75 kiloamps (kA) at sea level. Assuming an exponential decay of current with height, z, of form

$$I(z) = I(s) \exp(-z/n) \qquad (3)$$

with $n = 2 \times 10^3$ meters (m) (2), the current in the main channel at an altitude of 550 m should be 25.6 kA.

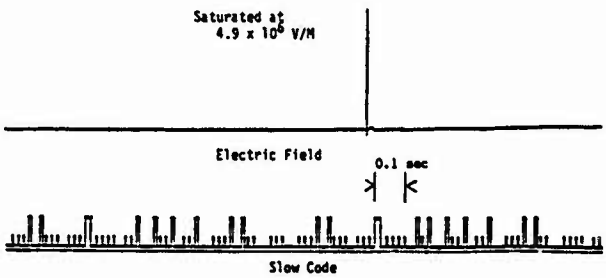

Fig 2. Slow Electric Field - Strip Chart (18:49 29 June '85)

Figure 2 shows the electric field recorded on the aircraft stripchart at 18:49:49. It indicates a short, single stroke flash which saturated the sensor electronics and, therefore, the actual amplitude cannot be determined. The digital data recorded at the time of the flash is shown beginning in Figure 3, which shows that a current of 2.8 KA flowed into the right wing current shunt and a current of about 1.5 KA flowed out through the tail.

Expansions of these waveforms in Figure 4 show the delay between the time when the current pulse reached the two sensors, confirming the direction of current flow from right wing to tail. The outputs from two surface current sensors are shown in Figure 5. They show currents of 2100 A on the right wing and 1100 A on the aft fuselage. The polarities of all the sensor outputs are consistent with negative charge flow onto the aircraft (Reference 4). The digital data set was incomplete, so current levels from the left wing sensors are not available for this event. The video cameras, however, show streamers at both wing tips.

In summary, the aircraft digital data is consistent with negative charge movement onto the aircraft, as would be expected during a negative cloud-to-ground flash. Current levels apparently ranged from 1.5 to 3 KA at the time of the attachment.

CONCLUSIONS

Sufficient information was available for the 29 June low altitude strike to the CV-580 so that a reasonable estimate could be made of the current in the cloud-to-ground flash. A peak current of 25 KA was calculated for the single return stroke at the aircraft altitude.

Sensors on the aircraft recorded approximately 3 KA of current. Although video records show a definite attachment to the aircraft, it does not appear that the aircraft intercepted the main return stroke current. It is suggested that, instead, the aircraft was involved with one of the branch leaders attached to the main channel.

Two low altitude strikes in 1984 both also show sensor output polarities consistent with negative charge flow onto the aircraft. Maximum current levels recorded during these strikes were 3.5 KA and 1.3 KA, respectively. Although the CV-580 apparently has been struck by cloud-to-ground flashes while flying at lower altitude, these events do not seem to have involved the main return stroke channel. Thus the current levels experienced during these flashes cannot be regarded as representative of the full threat from a cloud-to-ground flash.

REFERENCES

1. Rustan, P.L., Kuhlman, B.P., Burket, H.D., Reazer, J. and Serrano, A., "Low Altitude Lightning Attachment to an Aircraft", AFWAL-TR-86-3009 (in process), February 1986.

2. Uman, M.A., "Lightning Return Stroke Electric and Magnetic Fields", Journal of Geophysical Research, Vol 90, No. Du, 30 June 1985.

3. Idone, V.P., and Orville, R.E., "Lightning return stroke velocities in the the Thunderstorm Research International Program (TRIP)", Journal of Geophysical Research, Vol 87, 4903-4915, 1982.

4. Reazer, J. and Serrano, A., "Spatial and Temporal Description of Strikes to the FAA CV-580 Aircraft", to be published, proceedings, International Aerospace and Ground Conference on Lightning and Static Electricity, Dayton, OH, 1986.

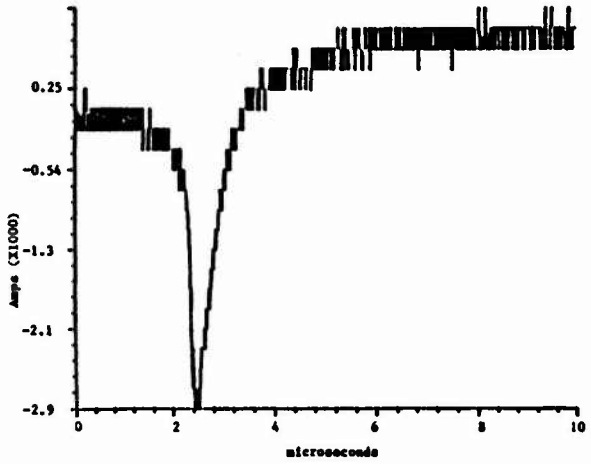

Fig 3A. Current Shunt - Right Wing (18:49 29 June '85)

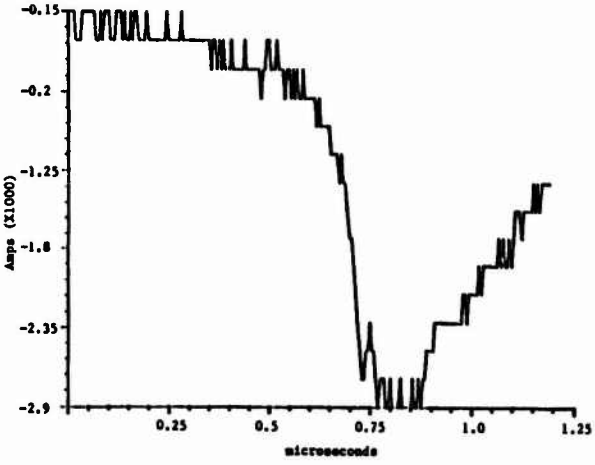

Fig 4A. Current - Right Wing (Expanded)

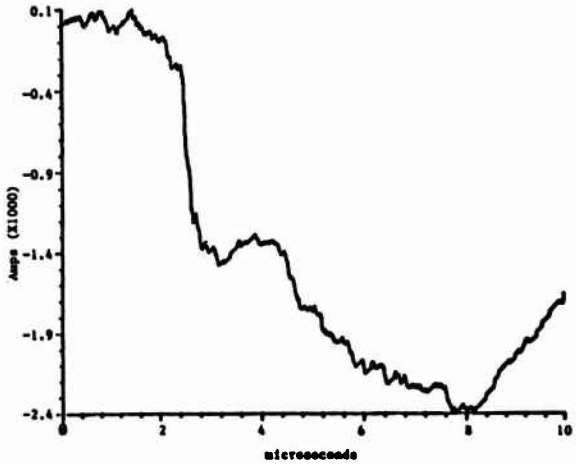

Fig 3B. Integrated dI/dt-Tail Boom (18:49 29 June '85)

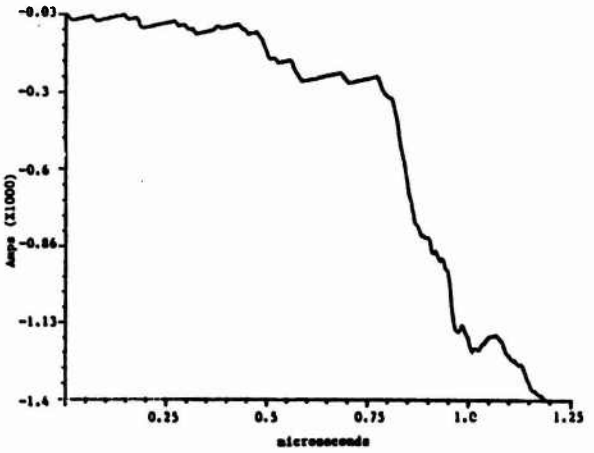

Fig 4B. Tail Current (Expanded)

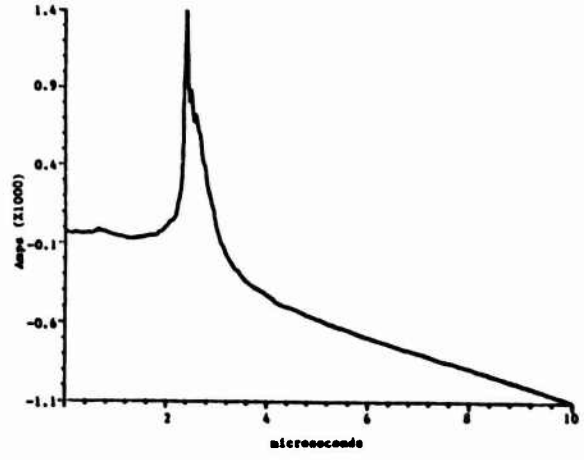

Fig 5A. Surface Current - Right Wing (Integrated)

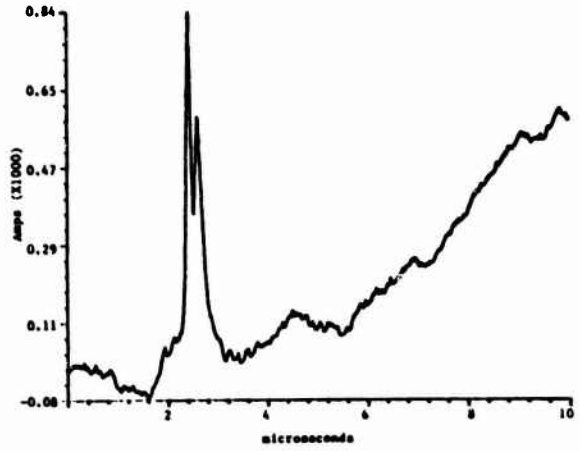

Fig 5B. Surface Current - Aft Fuselage

Comparison of Electromagnetic Measurements on an Aircraft from Direct Lightning Attachment and Simulated Nuclear Electromagnetic Pulse

Harold D. Burket, 1Lt, USAF
Air Force Wright Aeronautical Laboratories
AFWAL/FIESL
Wright-Patterson AFB, OH 45433

ABSTRACT

A Federal Aviation Administration CV-580 aircraft with wideband instrumentation was flown in Florida thunderstorms during the summers of 1984 and 1985 to measure the aircraft response to direct lightning attachments. Electromagnetic field and current levels were recorded continuously with a 28-channel analog recorder having a two megahertz bandwidth. Ten microsecond windows of digital data with five nanosecond sample intervals were obtained and time-synchronized with the analog data.

The aircraft was then subjected to simulated nuclear electromagnetic pulse (NEMP) tests at the Patuxent River Naval Air Test Center. In addition, extrapolated responses of the aircraft to simulated NEMP were prepared by the Air Force Weapons Laboratory. The extrapolations were based on responses obtained from scale model tests performed by the University of Michigan.

This paper compares electromagnetic field levels measured on the aircraft during simulated NEMP tests with scale model extrapolations and with responses from two direct lightning attachments.

INTRODUCTION

During the summers of 1984 and 1985, the U.S. Air Force Wright Aeronautical Laboratories (AFWAL) and the Federal Aviation Administration (FAA) conducted a lightning measurement program to expand the limited existing data base on low altitude lightning attachment to aircraft and to define and validate lightning characterization models by which lightning hazards protection for aircraft is developed. An instrumented FAA CV-580 aircraft was flown in central Florida thunderstorms at altitudes between 2,000 and 18,000 ft where 50 direct lightning strikes to the aircraft were received. Analog and digital records of electromagnetic field and current levels on the aircraft surface were collected for each attachment.

In addition to lightning characterization and lightning model validation, AFWAL was also interested in determining the comparable levels of simulated nuclear electromagnetic pulse (NEMP) radiation on the same aircraft. To identify the commonalities and differences in the threats of lightning and simulated NEMP, tests were performed on the CV-580 using the EMP simulator located at the Naval Air Test Center in Patuxent River, MD. In addition, extrapolated aircraft responses for a reciprocal double exponential excitation were provided by the Air Force Weapons Laboratory (AFWL) based on small scale model tests. This paper will compare simulated NEMP responses with extrapolated predictions and with measurements recorded during two lightning attachments to the aircraft.

AIRCRAFT INSTRUMENTATION

Five surface current density (J_S) rate-of-change sensors and five displacement current (J_N) sensors were mounted on the aircraft surface. The J_S sensors were located on the top of the forward fuselage (J_SFF) and aft fuselage (J_SAF), on the bottom of the left wing (J_SLW) and right wing (J_SRW), and on the top left wing (J_STLW). The J_STLW sensor was designed in France and was provided by the Office National d'Etudes et de Recherches Aerospatiales (ONERA). The other J_S sensors were modified versions of the radial multigap loop (MGL) ground plane B-dot Model 5 (MGL-5) sensor designed by EG&G (1). The J_S outputs were scaled to indicate the magnetic flux density rate-of-change (dB/dt) and, when integrated, the magnetic flux density (B). Consequently, these measurements are expressed in teslas/second (T/s) and teslas (T) instead of units normally associated with surface current density.

The five J_N sensors were mounted on the top of the forward fuselage (J_NFF), on the bottom of the left wing (J_NLW) and right wing (J_NRW) tips, on the vertical stabilizer (J_NVS), and on the top right wing (J_NTRW). The J_NTRW sensor was a hollow spherical dipole (HSD) type sensor provided by ONERA. The remaining four were flush plate dipole (FPD) sensors designed by EG&G. The J_N outputs were scaled to indicate the displacement current (dD/dt) expressed in amperes per square meter (A/m^2).

Current shunts were also mounted to the left wing (ILW) and right wing (IRW) tips. Following the first summer of lightning acquisition flights, additional instrumentation was mounted on the aircraft. A current shunt was placed on top of the vertical stabilizer (IVS) and a boom was mounted behind the vertical tail. The tail boom contained a current shunt (ITB), a current rate-of-change sensor (I-Dot TB), and a magnetic field rate-of-change sensor (B-Dot TB). Figure 1 shows the sensor locations during the 1985 portion of the program. However, only J_S and J_N measurements are presented for the comparisons made in this paper.

Tektronix 7612 waveform digitizers capable of recording 2048 samples at 5 nanosecond (ns) intervals were used to obtain 10 microsecond (μs) windows of digital data. Twenty-eight channels of continuous analog data with a 2 megahertz (MHz) bandwidth in the direct channels were also recorded. The analog records, therefore, were recorded to correlate digital data with particular events during lightning flashes and lacked the frequency response necessary for measurement of high frequency simulated NEMP responses.

SCALE MODEL EXTRAPOLATIONS

Small scale model studies of the aircraft were performed during 1985 for AFWL at the University of Michigan Radiation Laboratory (2). A 1:74 scale model of the CV-580 was tested to determine the external electromagnetic response of the aircraft at nine model test points corresponding to actual sensor locations on the aircraft. Excitation fields were applied in nine orientations and polarizations corresponding to configurations commonly used in F-106B NEMP tests performed at AFWL. Figure 2 shows the location of the points tested on the model and Figure 3 indicates the directions of incidence and the polarizations for which measurements were made in determining the aircraft response for the comparisons of this paper.

AFWL used the aircraft response from the scale model tests to extrapolate responses expected for excitations from their vertically polarized dipole (VPD-II) and Horizontally Polarized Dipole (HPD) EMP simulators as well as for a reciprocal double exponential input. This was done using techniques developed for similar extrapolations made for an instrumented F-106B aircraft used by the NASA Langley Research Center to conduct lightning research (3). The CV-580 extrapolations were presented to AFWAL for comparison with simulated NEMP tests.

SIMULATED NEMP TESTS

The CV-580 aircraft was then subjected to simulated NEMP tests in January 1986 at the Naval Air Test Center in Patuxent River, MD. The TACAMO EMP Simulator (TES) facility was used to pulse the aircraft with the fuselage parallel and then perpendicular to the direction of the incident electric field. The TES, an HPD simulator similar to the one at AFWL, produced a 60-65 KV/m electric field with a 7-8 ns rise time at a point corresponding to the top of the fuselage. Figure 4 shows the relative positions of the aircraft and the TES pulser and Figure 5 indicates field directions for both the parallel and perpendicular configurations.

Data recorded from J_S and J_N sensors were compared directly to extrapolated predictions obtained from scale model responses using a reciprocal double exponential excitation for orientations corresponding to both aircraft configurations used during simulated NEMP testing. The reciprocal double exponential extrapolations were expressed in terms of

dB/dt and dD/dt and could be compared directly to actual aircraft measurements.

COMPARISON OF EXTRAPOLATED AND MEASURED RESPONSES

Figure 6 shows a typical reciprocal double exponential waveform used to predict aircraft responses and a representative excitation received during simulated NEMP tests. The reciprocal double exponential input assumed a 60 kV/m peak field strength with a 5 ns rise time and a 250 ns decay time to 50 percent of the peak value. Typical simulated NEMP excitations had comparable peak magnitudes with 7-8 ns rise and decay times.

Four sets of responses were available for comparison from sensors mounted on the fuselage and vertical stabilizer for configuration 1 in which the electric field vector was parallel to the fuselage. The J_NFF sensor was designed for analog recordings only and the J_NVS responses had insufficient signal-to-noise ratios. Figures 7 and 8 compare extrapolated and typical responses measured digitally for the J_SFF and J_SAF sensors.

Figure 7 shows that both J_SFF responses have negative polarities, as should be expected, since the sensor orientation was opposite that of the applied electric field in both cases (See Figures 1,2,3, and 5). The waveforms have similar characteristics and amplitudes except that the measured response contains approximately 80 ns of pre-event sampling. Fast Fourier Transforms (FFTs) of both signals indicated spectral components near 4.5, 6.5, and 14.5 MHz. The 6.5 MHz frequency corresponds to reflections between the nose and tail of the aircraft. The 4.5 and 14.5 MHz components seem to correspond to resonances in the wings and horizontal stabilizer, although the effect of such resonances should be minimal for this configuration. The 31.5 MHz component in the measured response compares closely to resonances from the tail boom.

The J_SAF responses are compared in Figure 8 and indicate similar general characteristics and amplitudes on the same order of magnitude. The extrapolated waveform has a positive polarity because the J_SAF sensor was aligned with the incident electric field in the scale model case (See Figures 2 and 3). The measured simulated NEMP response has a negative polarity because the sensor orientation was opposite that of the applied excitation (See Figures 1 and 5). The same aircraft resonances are visible in both FFTs although the measured response appears to contain additional frequencies between 8 and 14 MHz. Reflections between the tips of the horizontal stabilizer fall into this range and would likely have a stronger effect on measurements from the J_SAF sensor.

Analogous measurements were available from two sensors in configuration 2 where the direction of the applied electric field was perpendicular to the fuselage. Figure 9 shows the J_SLW responses which have comparable magnitudes and similar general characteristics. The J_SLW sensor had the same orientation with respect to the applied field in both instances (See Figures 1,2,3, and 5) and the waveform polarities match accordingly. The extrapolated responses predict primary spectral components near 4.5 and 10.5 MHz corresponding approximately to reflections between wing tips and between the wing tips and the fuselage.

The J_NLW responses are compared in Figure 10 in which both sensors had orientations that were nearly perpendicular to the incident electric field vector (See Figures 1,2,3, and 5). The waveforms have either the same polarity and general characteristics, excluding the first large negative pulse in the measured response, with magnitudes differing by a factor of two; or, the waveforms have opposite polarities but comparable levels of magnitudes. The two largest frequency components in both responses correspond to the primary wing resonances seen by the J_SLW sensor. The source of the 16 MHz component in the measured response is not immediately apparent but corresponds approximately to the frequency of the large negative pulse in the measured response of Figure 10.

COMPARISON OF LIGHTNING AND SIMULATED NEMP

Two lightning attachments recorded in 1984 were selected for comparison with the simulated NEMP test measurements. Current propagation along the aircraft in these strikes most closely matched the two NEMP test configurations. A flash on 17 August 1984 attached near the front of the fuselage and approximately 67 percent of the current propagated to the rear of the fuselage. Another strike attached to the right wing on 5 September 1984 and most of the current propagated to the left wing of the aircraft. Detailed descriptions of the lightning attachments are given by Rustan, et al (4).

The nose-to-tail current propagation in the 17 August attachment makes this event similar to configuration 1 of the simulated NEMP tests. Figure 11 shows the J_SFF and J_SAF lightning responses which can be compared to those shown in Figures 7 and 8. The J_SFF sensor saturated and the estimated current through the forward fuselage exceeded 2.6 kA. Due to the saturation, sharp discontinuities and a DC component were introduced into the FFT of the J_SFF signal. It is believed that the attachment occurred in a branch of a cloud-to-ground discharge in which negative charge was transferred to the aircraft (5). Consequently, the direction of the current propagation is opposite that of conventional current and accounts for the difference in polarities of the lightning and NEMP responses. The lightning measurements saturated and the effects are reflected in the corresponding FFTs. The J_SFF signal shows an apparent oscillation 200 ns after the beginning of the discharge. Figure 12 gives 1 s expansions of the J_NLW and J_NRW measurements for this event and the corresponding simulated NEMP responses. The lightning measurements saturated and the effects are reflected in the corresponding FFTs. Peak lightning and NEMP magnitudes of this nose-to-tail or parallel configuration are summarized in Table 1.

Current propagated primarily from the right wing to the left wing during the 5 September attachment thus making this event analogous to configuration 2 of the simulated NEMP tests. Over 1.2 kA of current were measured on the IRW sensor. Once again, it is believed that negative charge flowed through the aircraft in the direction opposite that of conventional current. Figure 13 shows the J_SLW and J_NLW lightning responses which can be compared to the NEMP measurements in Figures 9 and 10. The lightning responses for the J_SRW and J_NRW sensors are given in Figure 14 along with the corresponding NEMP measurements. Peak measurements for this wing-to-wing or perpendicular configuration are listed in Table 2.

Lightning and NEMP responses both contained frequencies corresponding to wing and fuselage resonances in the two configurations. However, lightning measurements often contained spectral components below 4 MHz that were not present in simulated NEMP. Furthermore, lightning responses seldom indicated significant frequencies higher than 10 MHz. Peak amplitudes for simulated NEMP measurements were 4 to 20 times higher than those of the two lightning attachments compared.

DISCUSSION

Several factors detract from the quality and detail of the extrapolated predictions for the CV-580 responses to simulated NEMP. First of all, the scale model used to determine the aircraft responses did not include the extra instrumentation added to the aircraft prior to the 1985 portion of the program. It seems reasonable that the 15 ft tail boom, in particular, would cause additional resonances in the measured responses. Another factor concerns the differences between the actually applied excitation and the reciprocal double exponential used for the extrapolations. The faster rise time and slower decay time of the reciprocal double exponential waveform tends to elevate the magnitude of the extrapolated predictions at the lower frequencies. Another significant factor that may affect the comparisons, however, relates to configuration effects involved with the test methods used during simulated NEMP testing. The scale model tests were performed in an anechoic chamber to simulate flight in free space. During NEMP tests, however, the aircraft was on the ground. No adjustments were made for ground effects or for variations in the applied field that might affect the results since these data were unavailable.

Despite the dissimilarities in fine detail and though only a limited number of corresponding measurements was available for comparison, the extrapolated and observed responses are quite similar and seem to possess the same general characteristics. Predicted and measured magnitudes were very comparable and both responses indicated dominant aircraft resonances. Additional frequencies in the measured responses could be attributed to actual aircraft structures in most cases.

Caution must be taken when trying to draw conclusions based on lightning and simulated NEMP measurements. The peak magnitudes in Tables 1 and 2 have little value unless the relative threat levels of lightning and NEMP are taken into consideration. Military Standard 1757 (MIL-STD-1757A) establishes the lightning levels to which aerospace vehicles must be protected (6). It projects a peak current amplitude of 200 kA. The two lightning attachments used in this study contained peak current levels that were two orders of magnitude lower. The applied field during simulated NEMP tests, however, represents a moderate NEMP threat.

If the lightning amplitudes measured in the 17 August and 5 September events were extrapolated to the 10-20 kA peak current levels in typical return strokes (7), the peak magnitudes would be comparable to those measured during simulated NEMP tests. Extrapolation to the 200 kA full threat level defined in MIL-STD-1757A would make the aircraft response to lightning one order of magnitude more severe than the moderate NEMP threat. The value of such extrapolations based on a single parameter, however, is subject to debate. Although extrapolations can prove useful when done within certain constraints, scales used to extrapolate peak current to higher levels may not apply for rate-of-change measurements. In fact, large amplitude current pulses often have slower rates-of-rise.

CONCLUSION

Extrapolated simulated NEMP responses based on small scale models appear reasonably accurate for the limited number of measurements available for comparison. The responses of J_S sensors mounted on the fuselage agree more closely with scale model predictions when the incident electric field is parallel to the fuselage. Extrapolated and measured J_SFF responses show magnetic flux density rate-of-change levels near 50 and 44 kT/s, respectively, on the forward fuselage. The J_SAF extrapolated and measured responses on the aft fuselage are about 50 and 57 kT/s, respectively. All J_S fuselage responses contain spectral components near 4.5, 6.5, and 14.5 MHz corresponding to major aircraft resonances. Wing responses are quite comparable when the applied field is perpendicular to the fuselage. Peak extrapolated and measured J_SLW responses on the left wing are approximately 14 and 11 kT/s, respectively. These responses contain frequencies near 4.5 and 10.5 MHz corresponding to primary wing resonances. Scale model extrapolations should become more accurate as models are improved to include additional aircraft resonances and when effects peculiar to simulated NEMP test methods are taken into account.

Direct comparisons of the responses from two lightning attachments to the aircraft and from simulated NEMP tests indicate that both contain frequency components corresponding to wing and fuselage resonances. However, the lightning responses often contain frequencies below 4 MHz that are not present in simulated NEMP and seldom include significant frequencies above 10 MHz. Although peak response magnitudes for simulated NEMP are 4 to 20 times higher than that of lightning, the simulated NEMP level tested represents a moderate NEMP threat whereas the lightning attachments analyzed involved the relatively low current levels of 1.2 and 2.6 kA. Extrapolation to higher lightning current levels is tempting but subject to certain constraints. Simulated NEMP responses should be compared directly to the lightning responses of higher current attachments that represent a comparable level lightning threat.

REFERENCES

1. EG&G Washington Analytical Services Center Inc., Standard EMP and Lightning Instrumentation, Albuquerque, NM.

2. V. Liepa, M. Mikesell, and L. Pierce, "Exterior Electromagnetic Response of CV-580 Aircraft", Report to Air Force Weapons Laboratory prepared by the University of Michigan under Subcontract DC-SC-4088-3 for Dikewood, Division of Kaman Sciences Corporation, October 1985.

3. D. Andersh, J. Steil, K. Lee, and F. Yang, "Comparison of F-106B Responses to Natural Lightning and Simulated EMP", Fourth Annual IEEE Hardened Electronics and Radiation Technology Conference, Monterey, CA, July 1985.

4. P.L., Rustan, et al, "Low Altitude Lightning Attachment to an Aircraft", Air Force Wright Aeronautical Laboratories Technical Report AFWAL-TR-86-3009, in publication process.

5. J.S. Reazer and A.V. Serrano, "Spatial and Temporal Description of Strikes to the FAA CV-580 Aircraft", Eleventh International Aerospace and Ground Conference on Lightning and Static Electricity, Dayton, OH, June 1986.

6. Military Standard 1757A (MIL-STD-1757A), "Lightning Qualification Test Techniques for Aerospace Vehicles and Hardware", July 1983.

7. M.A. Uman, "Lightning", New York: McGraw-Hill, 1969.

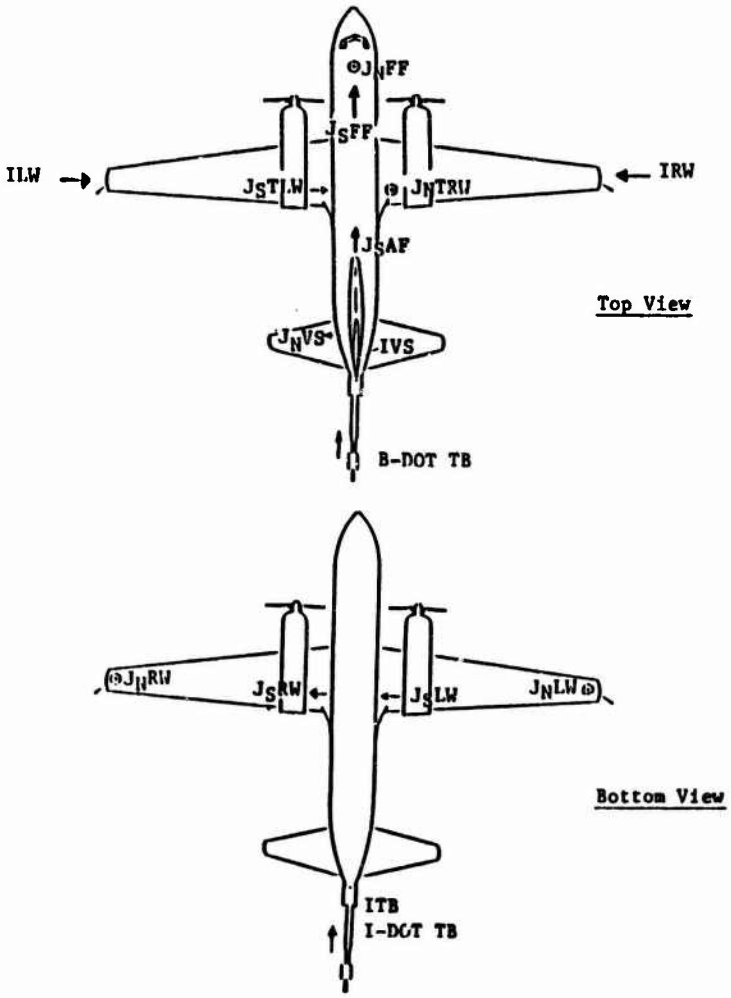

Fig. 1. 1985 Sensor Locations for CV-580 Aircraft. Arrows Indicate Positive Direction of Current Flow

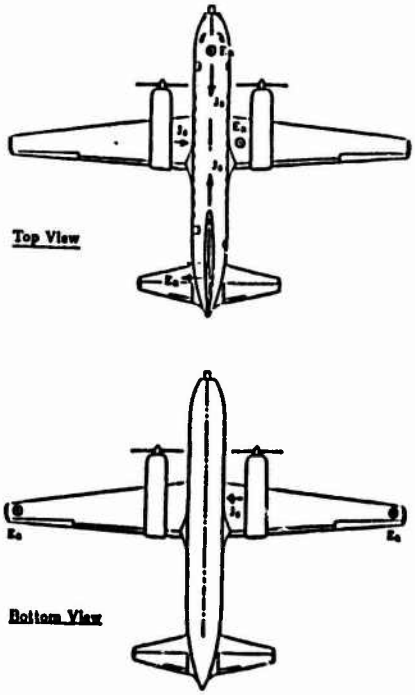

Fig. 2. Scale Model Test Point Locations

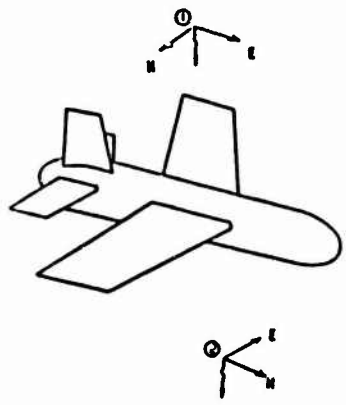

Fig. 3. Scale Model Excitation Field Directions and Polarizations

TES TEST FACILITY

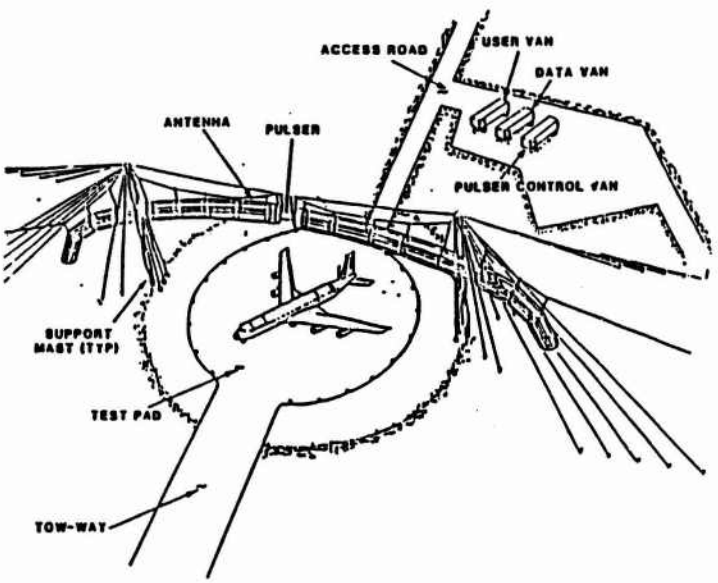

Fig. 4. Relative Positions of CV-580 Aircraft and TES Pulser

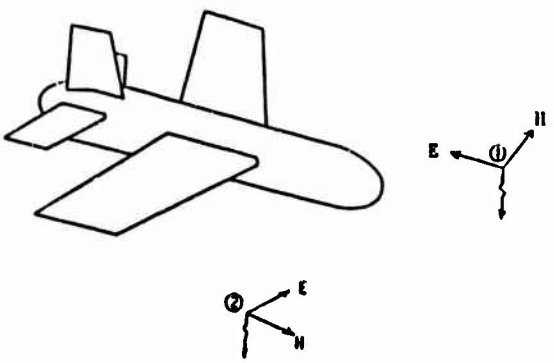

Fig. 5. Field Directions for Parallel (1) and Perpendicular (2) Configurations

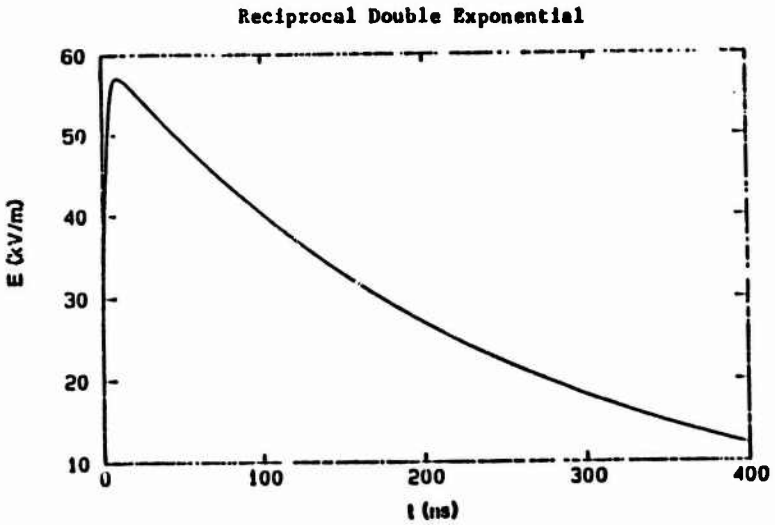

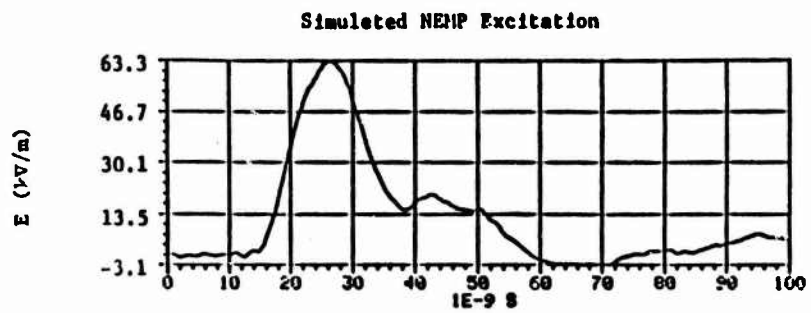

Fig. 6. Reciprocal Double Exponential and Simulatad NEMP Input Waveforms

Extrapolated Scale Model Response

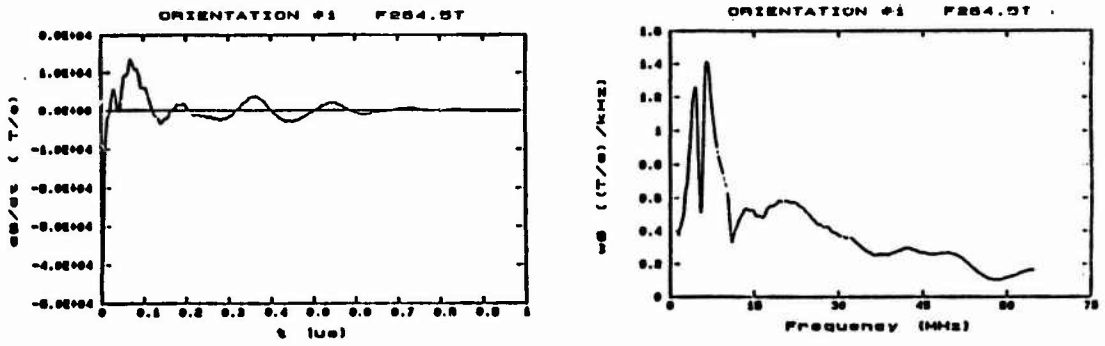

Measured Response

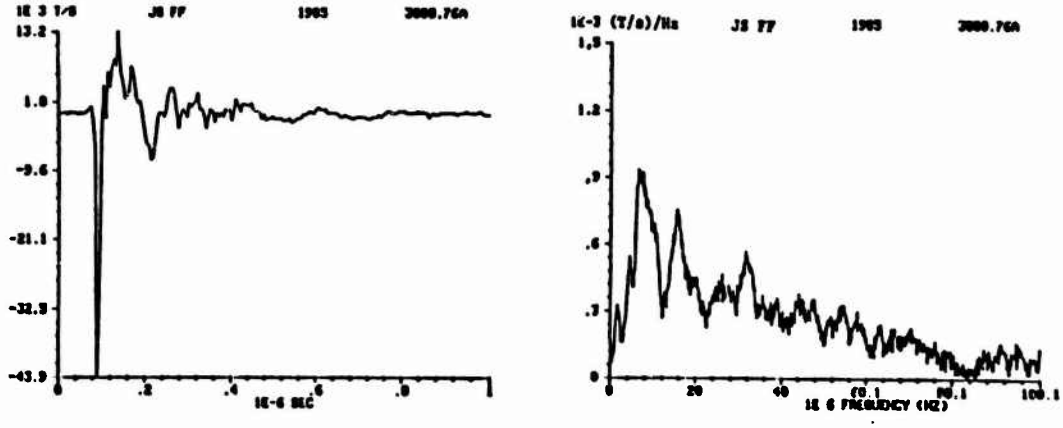

Fig. 7. Extrapolated Scale Model and Measured Responses of J_SFF Sensor Parallel Configuration

Extrapolated Scale Model Response

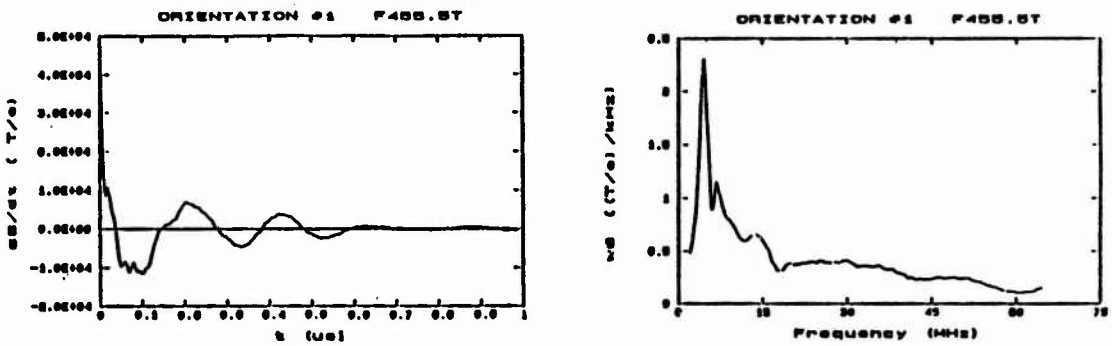

Measured Response

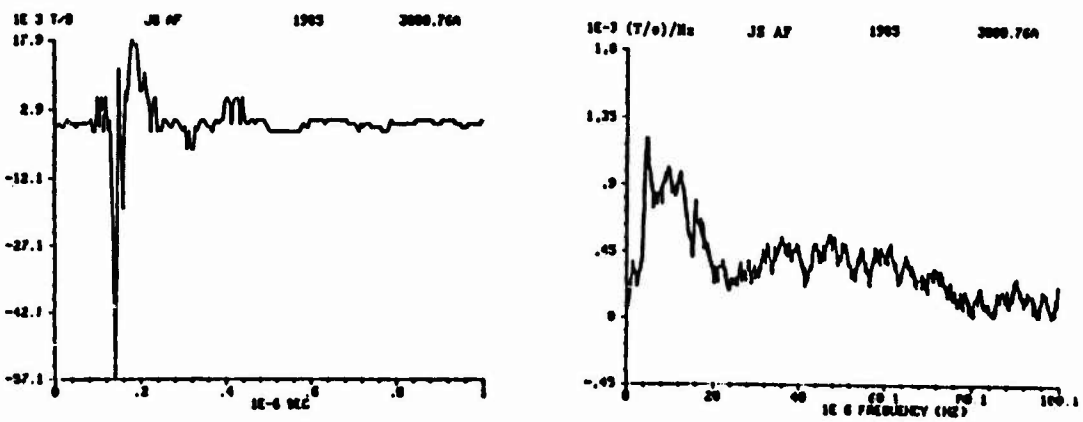

Fig. 8. Extrapolated Scale Modal and Measured Responses of $J_S AF$ Sensor Parallel Configuration

Extrapolated Scale Model Response

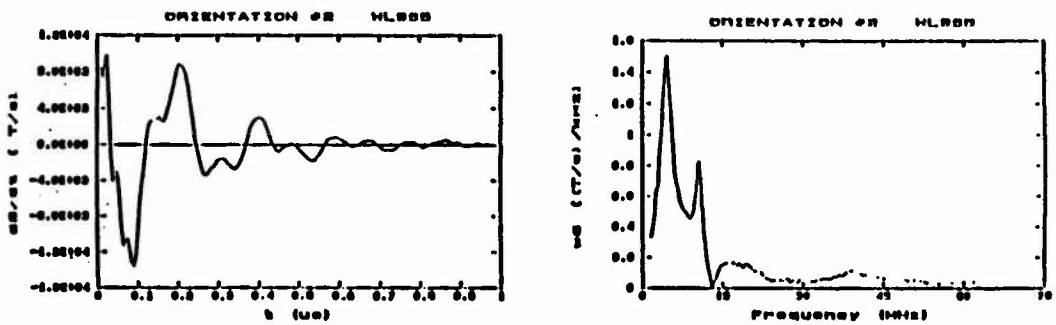

Measured Response

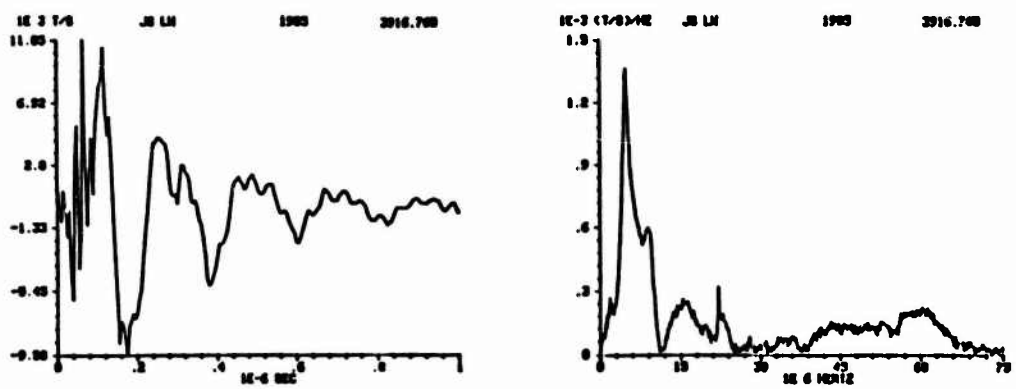

Fig. 9. Extrapolated Scale Model and Measured Responses of J_SLW Sensor Perpendicular Configuration

Extrapolated Scale Model Response

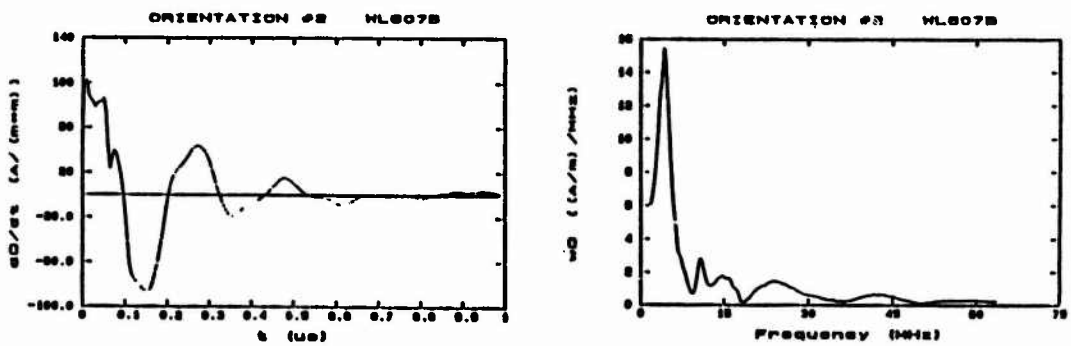

Measured Response

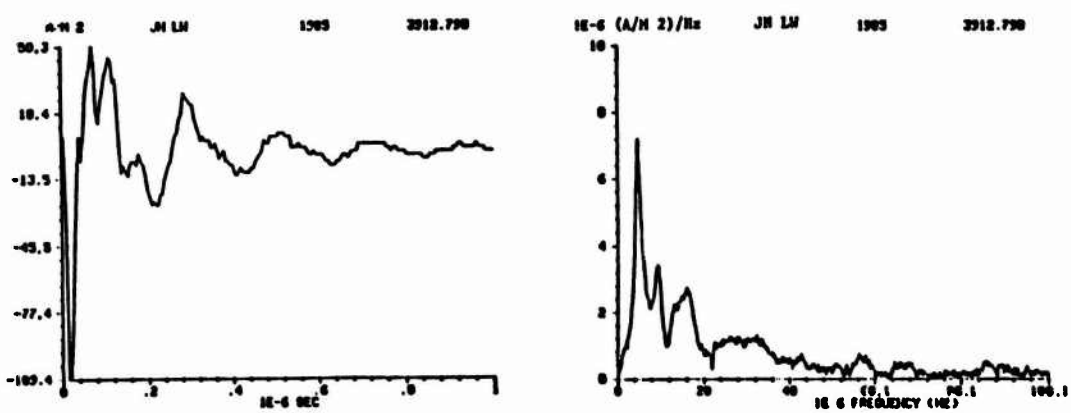

Fig. 10. Extrapolated Scale Model and Measured Responses of J_NLW Sensors Perpendicular Configuration

J_SFF Lightning Response

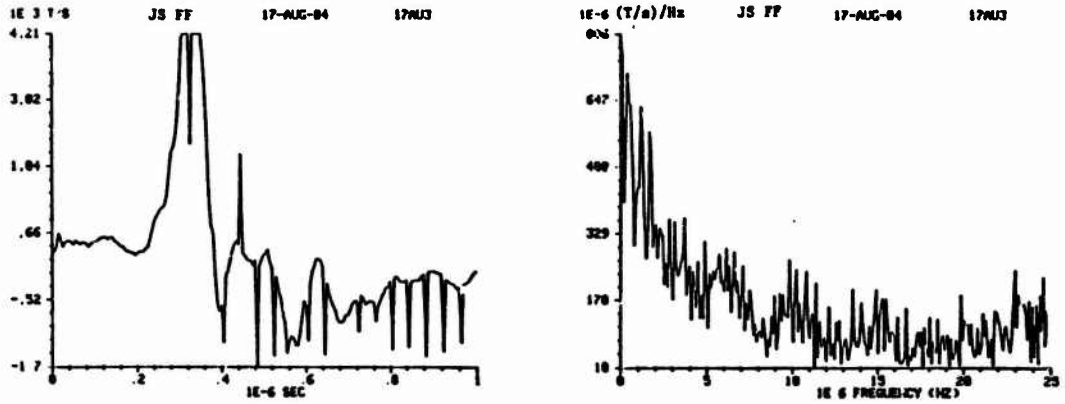

J_SAF Lightning Response

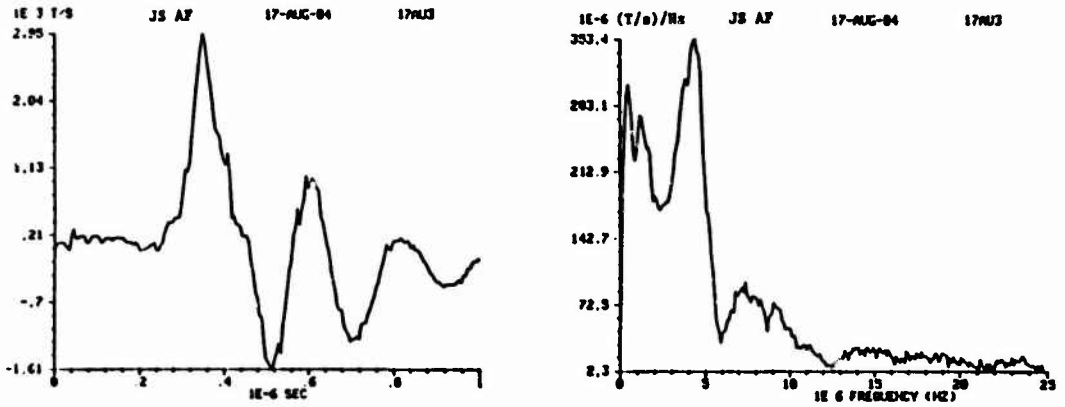

Fig. 11. J_SFF and J_SAF Lightning Responses to Nose-to-Tail Attachment

J_NLW and J_NRW Lightning Responses

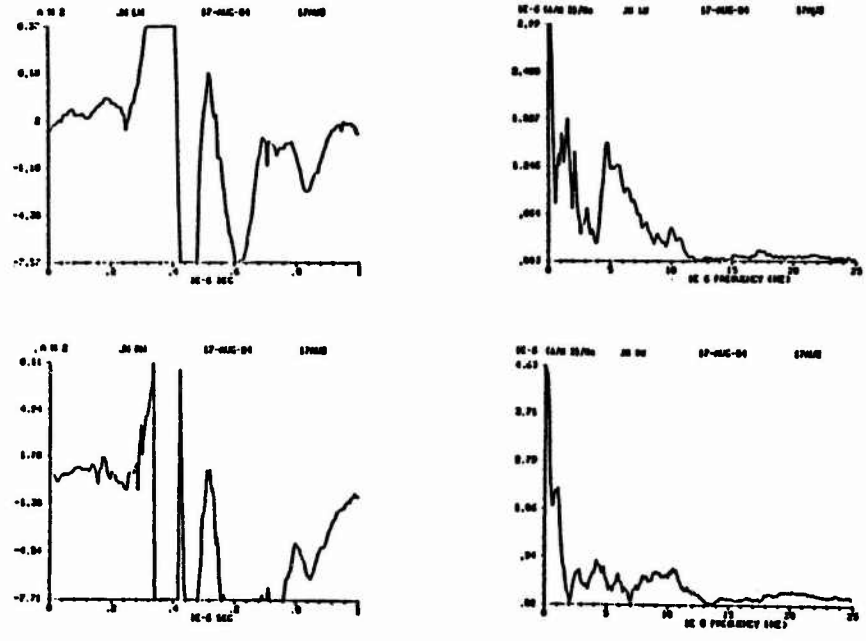

J_NLW and J_NRW Simulated NEMP Responses

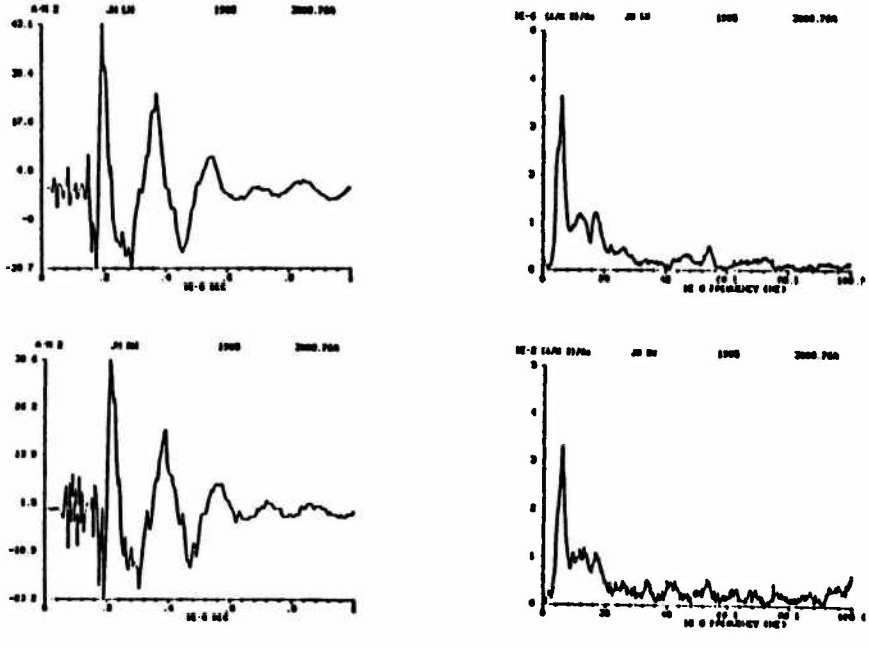

Fig. 12. J_NLW and J_NRW Lightning and Simulated NEMP Responses
Nose-to-Tail/Parallel Configuration

J_SLW Lightning Response

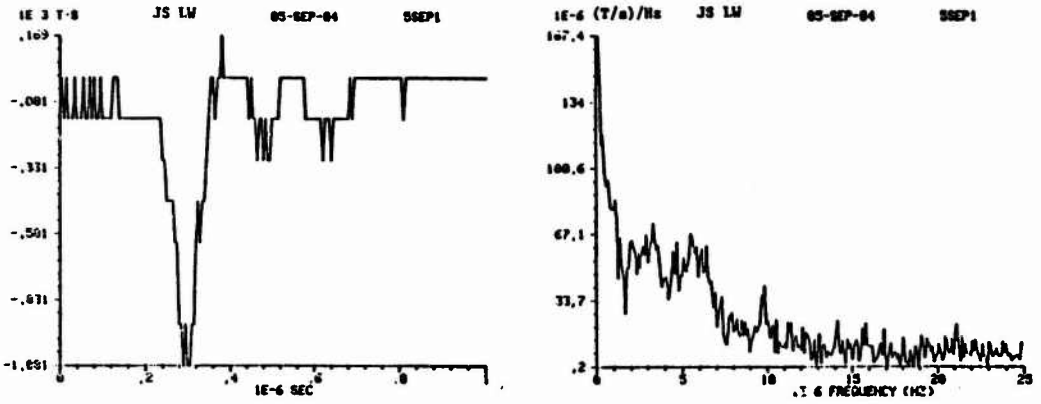

J_NLW Lightning Response

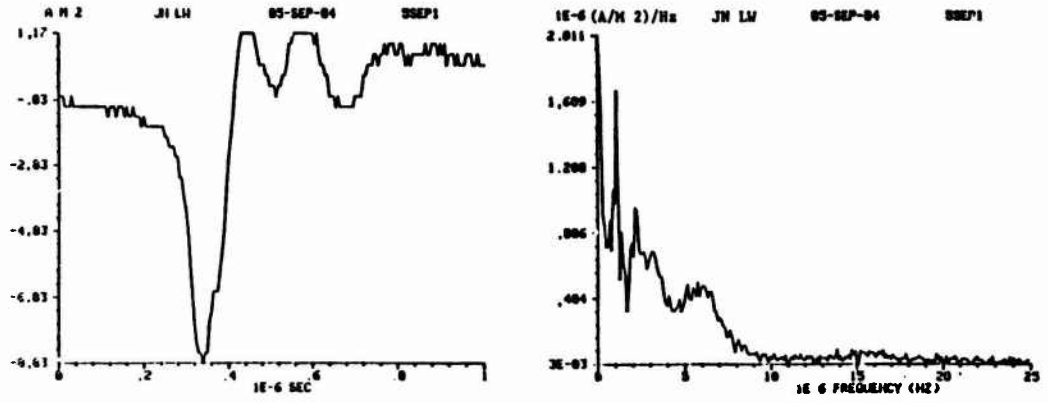

Fig. 13. J_SLW and J_NLW Lightning Responses to Wing-to-Wing Attachment

J_SRW and J_NRW Lightning Responses

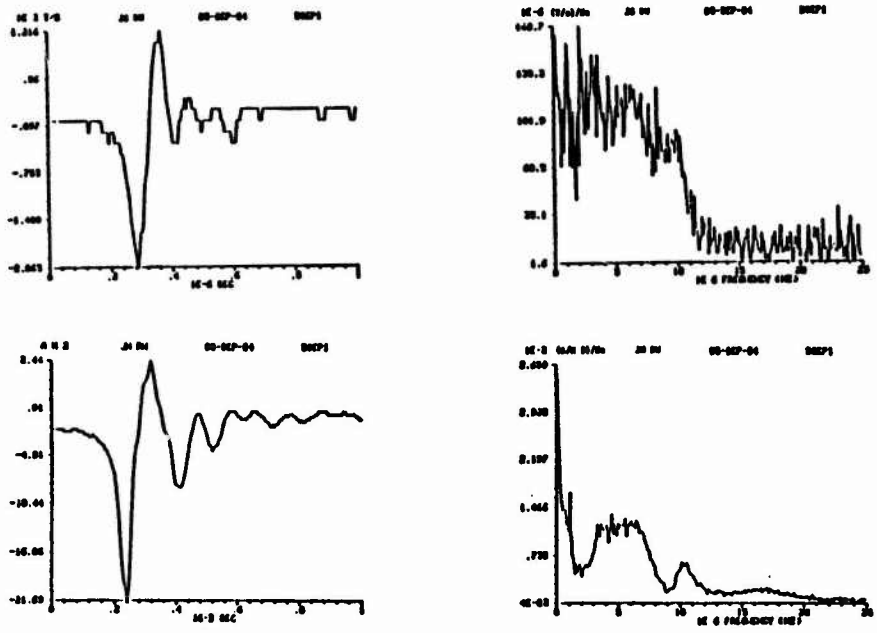

J_SRW and J_NRW Simulated NEMP Responses

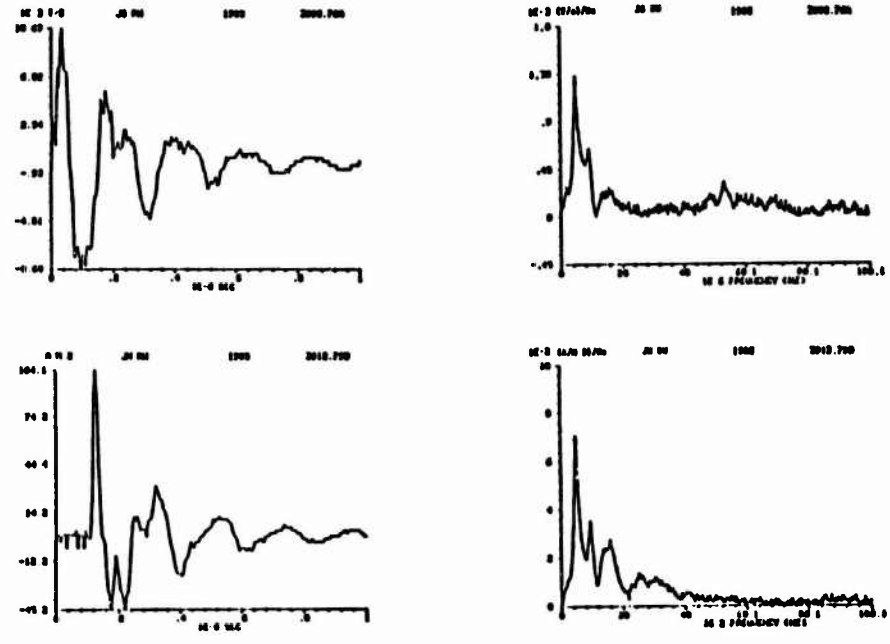

Fig. 14. J_SRW and J_NRW Lightning and Simulsted NEMP Responses
Wing-to-Wing/Perpendicular Configuration

Table 1

Summary of Responses for Nose-to-Tail/Parallel Configuration

Sensor	Measured Peak Amplitudes	
	Lightning	Simulated NEMP
J_SFF	* > 4.2 E 3 T/s	43.9 E 3 T/s
J_SAF	2.9 E 3 T/s	57.1 E 3 T/s
J_NLW	* > 8.4 A/m^2	43.1 A/m^2
J_NRW	* > 8.1 A/m^2	38.6 A/m^2

* Measurement was ssturated

Table 2

Summary of Responses for Wing-to-Wing/Perpendicular Configuration

Sensor	Measured Peak Amplitudes	
	Lightning	Simulated NEMP
J_SLW	1.1 E 3 T/s	11.0 E 3 T/s
J_SRW	2.1 E 3 T/s	10.7 E 3 T/s
J_NLW	8.8 A/m^2	109.4 A/m^2
J_NRW	21.7 A/m^2	104.1 A/m^2

ANALYSIS OF THE FIRST MILLISECONDS OF AIRCRAFT LIGHTNING ATTACHMENT

J.P. Moreau and J.C. Alliot

Office National d'Etudes et de Recherches Aérospatiales,
BP 72, 92322 Châtillon Cedex, FRANCE.

Abstract

This paper presents a characterisation of the lightning attachment to an aircraft based on the study of field and current measurements made during the first milliseconds of the phenomenon. The data have been collected during the C 580 1984 program (20 strikes), the C 160 program (12 strikes) and the C 580 1985 program (30 strikes). The paramaters being characterized are the current and the electric and magnetic field on the aircraft surface. We shall show how the pulse repetition rate of the tens of electromagnetic pulses we found during this first period indicates that the aircraft sustains different physical processes. This phenomenology will be the one encountered in a laboratory experiment using a 6 MV generator sparking over a floating 4 m cylinder. All these studies lead to some conclusions about lightning simulation for indirect effects on aircraft. This work has been supported by DRET (Direction des Recherches, Etudes et Techniques).

INTRODUCTION

THREE AIRCRAFT LIGHTNING EXPERIMENTS were conducted during the summers of 1984 and 1985 to determine the characteristics of lightning strikes to a flying aircraft. Data from 61 lightning strikes were collected and analyzed during these programs. These experiments were performed in the C160 french aircraft in 1984, and in the CV-580 research aircraft in 1984 and 1985. The main parameters recorded in these programs were the current flow through the aircraft and the electromagnetic fields at the aircraft surface during lightning attachment. The instrumentation used in these aircrafts will not be described here because it was done in the last conference [1] [2]

This paper will provide a description of the electromagnetic pulses during the initial aircraft lightning attachment process. The study of the simultaneous electric and magnetic field during the beginning of the discharge showed that the aircraft sustains different physical processes. Additionally, our analysis provides an insight into the understanding of the development of the streamers and leaders during the initial channel formation in the aircraft lightning discharge

This analysis has been compared to the results of an indoor experiment conducted in december 1985 in the EDF LEHT (Electricite de France, Laboratoire d'Essais a Haute Tension) facilities of the "Renardieres". This experiment, fully described in [3], provided electromagnetic and photographic data for the phase of connection in which the plasma is of high resistivity and during which the object is floating between impulsive streamers at both ends. This paper will provide a comparison between this laboratory experiment and the actual situation of an aircraft struck by lightning.

AIRBORNE LIGHTNING DATA

We studied the reationship between the electric and magnetic field pulses measured during the first 10 ms of the lightning strikes in the C160 and CV-580 programs. Fig. 1 shows the overall characteristics of these pulses for a two milliseconds interval during one of the strikes in the C160 program. The main characteristics of these pulses is that a repetition rate can be found (between 10^3 and 10^4 pulses/second). Fig. 1a shows the evolution of the electric field pulsea separated by some 200 µs. Fig. 1b shows the correlated magnetic field. On these pictures the electric field pulses have a magnitude roughly constant, except for one or two pulses, or slightly decreasing whereas the corresponding magnetic field pulses are increasing. Looking at both pictures it is clearly seen change of physical process at time 1.6. Same constatation can be made on Fig. 2 around time 1.2. Fig. 2 represents the evolution of the electromagnetic field on the skin of the C 160 during a 2 ms interval. Also on these pictures around time 1.6 on fig. 1 and 1.2 on fig. 2 there is an increase of the pulse repetition rate. On tne C 160 the signal of current was not available but it is believed, from the observation of similar data of the CV-580 that the main current had flown since these times. We will

csll this period "presttachment" process or "predischarge" snd call arbitrarily the attachment period, the period during which a continuing current above 100 A is flowing through the current sensor. The 10% - 90% rise time of these pulses measured on digital recorders [2] rsnged from about 50 ns to sbout 10 µs. Table 1 shows a summary of the rise time measured for these strikes. Nine out of the 12 strikes in the C 160 aircraft showed this pattern. The remaining three strikes in the aircrsft showed one large correlated electric snd magnetic field for the entire discharge.

Fig. 3 shows the overall charscteristics of the electric field pulses induced on the aircraft skin during the first millisecond prior to the sctual attachment in the 1985 program. Fig. 4a shows the current signal on the right wing shunt. Fig. 4b shows the fast vsriations of the electric field on this wing

On these pictures it is easy to distinguish a preattachment period where there sre electric field varistions between time -2 and time 4 or 5. During this period the electric field variations marked by letters on fig. 4b are impulsive. these impulses are not noise becsuse they are correlated with others pulses seen on others sensors not shown here. The time intervals between pulses are a little longer than in the C 160 and are about 500 µs. Like in the C 160 data we can notice an increase of the pulses repetition rate between point j and point k on fig. 4b which corresponds to the beginning of the attachment, that is the apparition of significant values of current on the wing. As for the C 160 experiment we can conclude that a new physical process is in progress. Also we can notice that the amplitude of the electric field pulse is roughly constant all over the process whereas the pulses of current sre increasing. Table 2 summarizes the characteristics of the electromagnetic pulses somehow comparable to the C 160 data.

Table 2.

On fig. 5 which represents signals measured on the skin of the CV-580 during another right wing attachment similar constatations can be made. here the predischarge activity lasts less than 1 ms. After this period, ss observed previously, the current is impulsive.

INTERPRETATION OF THE LIGHTNING DATA

Lightning data seen on the C 160 and on the CV-580 aircraft show that there is a predischarge activity charscterized by an impulsive process. We will suggest different interpretations of what may happen to the aircraft before the main current flows through it and will recall a laboratory experiment fully described in [3] in which some similarities may be found with the actual situation. Three scenarios may be thought to achieve the connection between the aircraft and the discharge. We shall analyse the consequences on the electromagnetic fields induced on the skin of the aircraft of these three scenarios and see how well the repetition rate of pulses observed during the preattachment period snd during the attachment itself may be explained. A lightning leader has been often described as a low resistivity channel preceeded by a zone of high resistivity called streamer. The progression of such s system of discharge is stepped and the time interval between steps is around tens of microseconds.

One of the scenarios is the following: the sircraft may initiate the discharge by sending leaders of opposite polarities away from it. These leaders may propsgate without making any connections with others leaders coming from the cloud, this configuration corresponds to the scheme of fig. 6. This configuration should induce leader currents on the surface of the aircraft of hundreds amps at the very beginning of the discharge. In this hypothesis the propagation of the merging leaders has to be stepped as usual and the repetition rate of this proceas is of tens of microseconds which is roughly an order of magnitude less than what is observed during the predischarge period. In this case, the propagation of the lightning is not disturbed by the presence of the aircraft if the impedance of tha metallic structure of the aircraft is neglected. Airborne dats does not show usually significant current before the attachment snd when some magnetic field pulses are detected during that period the time interval between pulses seems a little too long for a leader process. Besides there is some controversy about the value of the electric field necessary for such a propagation sway from the aircraft. Since this suggestion does not cover entierely the actual dats, we shall examine the others possibilities.

The second possibility is that the aircraft sends streamers and lesders of positive and negative polarities induced by an approaching leader issued from the cloud; this scensrio will lesd to the connection between two resistive streamers. This configuration corresponds to the scheme of fig. 7. As in the previous suggestion a leader current has to be observed since the

beginning. Also when the leader coming from the aircreft reaches the leader issued from the cloud high value of $\Delta E/\Delta t$ haa to be observed due to the voltage drop induced in the resistive connection. For the same reeaona that for the previoua auggestion this hypothesis is not clearly confirmed by the airborne data, so we shall examine the laat possibility.

The scheme of this auggeation is given on Fig. 8 in which a leader chennel reachea the aircraft. In this configuration the aircreft enters in zone of streemers and sends also streamers which are not yet leaders fig. 8a [5]; when the connection ia achieved with the leader issued from the cloud, others streamers are issued from another extremity of the aircraft end become leaders fig. 8b. Since thia time, current can flow through the aircreft. In thia configuration the connection is achieved during the preettachment period by a resitive path which may induce high $\Delta E/\Delta t$ and time intervals between pulaes related both to the physics of the streamer process and to the electrical characteristics of the equivalent circuit that is the resistance of the connecting path and the capacitance of the leader channel and of the aircreft. In the last two suggestions the introduction of this resistive connection will affect the progression of the lightning discharge until the streamer zone becomea leader: then the situation is equivalent to the first configuration. The laboratory experiment described below helps to understand what could be the scheme of the connection and what effect it could have on the measured fields. The set-up corresponds to fig. 9 and consists of an aluminium cylinder of 4 m length and 0.5 m in diameter suspended by means of dielectic ropea inaide the 12 m gap of the 6 MV, 450 kJ EDF generetor. Thia generator provides rise time of 800 ns and the inductance of the return path allows current risetime of 200 na with an amplitude of 30 kA.

The interpretation of the laboratory experiment was greatly simplified by the presence of the streak camera. The camera hed an UV capability which allowed the displey of the streamer. By studying the data displayed on fig. 10 we can interpret the fields variations of fig. 11. The cylinder is first connected by resistive atreamers issued from the negative rod of the generator (point a on fig. 10) the potential of the cylinder then increases (phase a on fig. 11). The value of the potential geta so high that the conditions for the onset of streemers at the bottom end are immediatly established (point b on fig. 10 to which correaponds the field variation of point b on fig. 11). The potential of the cylinder then decreases because of the voltage drop in the high resistance of the upper gap. The extinction of the lower streamer (see fig. 10) induces a process of recharging the capecitance of the cylinder. This mecheniam will take place again, point c end point d, inducing faat electric field variations superimposed to the low frequency drift aeen between point b and c on fig. 11. This process could last for a while aa long ea the streamers do not reach the ground. In thia experiment streamers reach the ground at point d. So only two pulaes are observed. After thia period the field on the aurface of the cylinder depends on the relative evolution of the reaitivity of the top and bottom gaps.

The main concluaion of this laboratory experiment ia that the fast electric field variations observed on a floating structure can be explained in terma of connections to the source through resistive paths and thet relaxation proceaaea can take place [3]. The presence of thia resistance has an effect on the evolution of the ratio between electric end the magnetic fielda meaaured on the akin of the cylinder. Besides it has also en effect on the development of the diacharge itaelf. We believe that a aimilar process may happen during the predischarge in the actual situation of an aircraft atruck by lightning.

CONCLUSION

It haa been shown from experimental data that an aircraft sustains electromagnetic field variations prior to the main current flowa. The probability of the highest $\Delta E/\Delta t$ occurs during that period. However the level of the diaplacement current denaity induced is in general compliance with the A or D component of MILSTD1757A. We have described a poasible process of the preattachment involving charge and discharge of both the capacitance of the aircraft and the capacitance of the approaching channel through a resistive path. During the laboretory experiment we found that the capacitive effect of the approaching leader was negligeable end alao that streamera of oppoaite polarities merging from the aircraft had no aignificant effect on the potentiel and field veriationa of the cylinder. In the actual situation also theae effects are small although this phase is important for the rest of the discharge. From a simulation point of view the importance of the reproduction of right values of $\Delta E/\Delta t$ has been already mentionned [6], [7] we have shown that these

values may be obtained through high resistivity paths. The effect of the pulse repetition rate has never been considered for testing. This effect depends on the type of circuitry which can be upset either by an integrating process, either by interference between the operational frequency and the lightning pulses repetition rate. The study of the preattachment process shows a great interest because it may answer the question of the influence of the predischarge on the main discharge. There may be a relation between the peak value of the current and how well the channel has been heated. This may lead to some conclusions about aircraft protections if the preliminary process can be dominated.

REFERENCES

[1] - P.L. Rustan Jr., B.P. Kuhlman and J.M. Reazer, "Airborne and ground electromagnetic field measurements of lightning", 10th ICOLSE, Paris, 10-14 juin 1985.

[2] - J.P. Moreau and J.C. Alliot, "E and H fields measurements on the Transall C 160 aircraft during lightning flashes", 10th ICOLSE, Paris, 10-14 juin 1985.

[3] - G. Labaune, J.P. Moreau, J.C. Alliot, B. Hutzler, G. Ricquel, "Experimental study of the interaction between an arc and an electrically floating structure". in this conference.

[4] - P.L. Rustan Jr and J.P. Moreau, "Aircraft lightning attachment at low altitudes", 10th ICOLSE, Paris, 10-14 juin 1985.

[5] - J.A. Bicknell and R.W. Shelton, "The energy requirements of an aircraft triggered discharge", 10th ICOLSE, Paris, 10-14 juin 1985.

[6] - W.G. Butters, D.W. Clifford, K.P. Murphy, K.S. Zeisel, and B.P. Zuhlman, "Assessment of lightning simulation test techniques", Proceedings of the International Conference on Lightning and Static Electricty, Oxford, 23-25 mars 1982.

[7] - P. Levesque, J. Taillet, G. Labaune, S. Larigaldie and J.C. Alliot, "Study of the physical mechanisms and the perturbations created by the attachment of an arc to a conducting cylinder, 10th ICOLSE, Paris, 10-14 juin 1985.

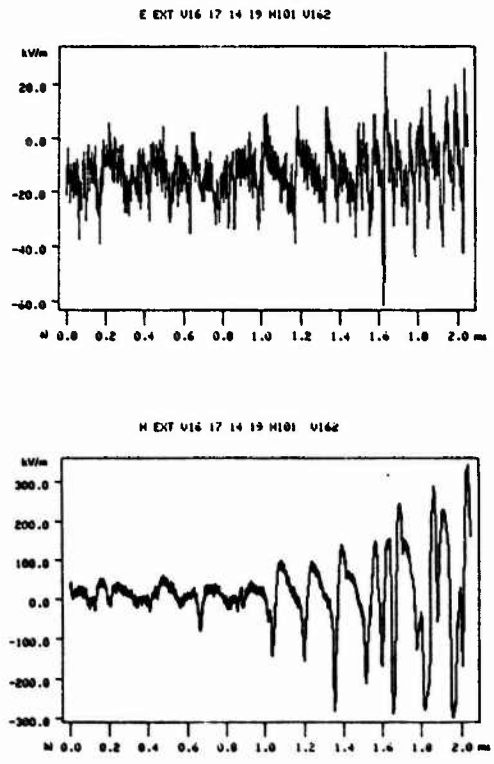

Fig. 1 - Electromagnetic field on the C160

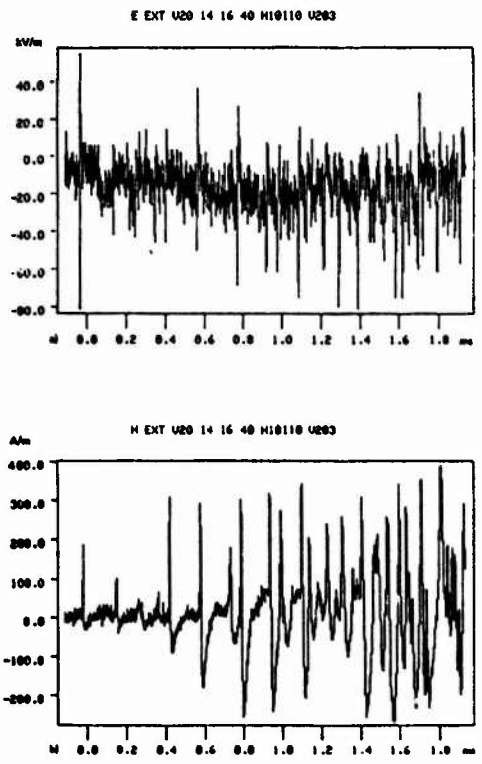

Fig. 2 - Electromagnetic fields on the C160

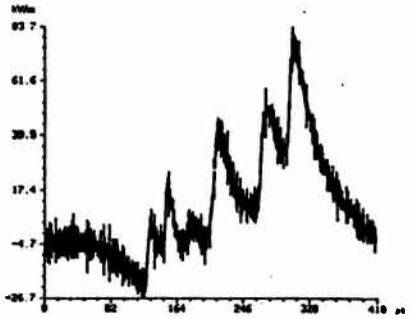

Fig. 3 - Electric field pulses on the CV580 1984 program

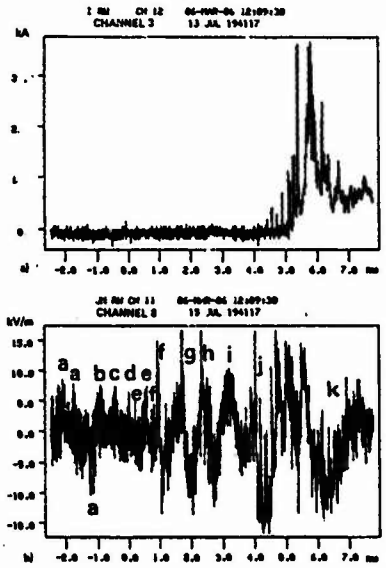

Fig. 4 - Current a) and electric field b) on the Right Wing of the CV580

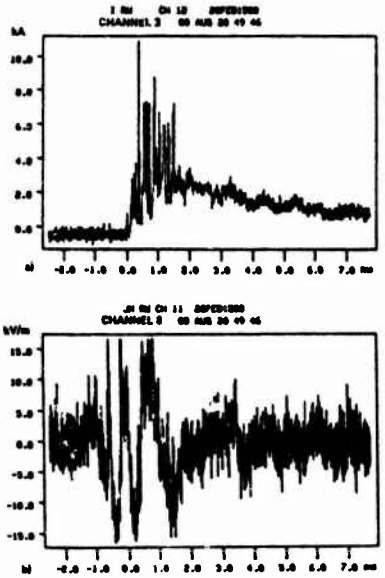

Fig. 5 - Current a) and electric field b) on the Right Wing of the C-580

Fig. 6 - Leaders merging from the aircraft

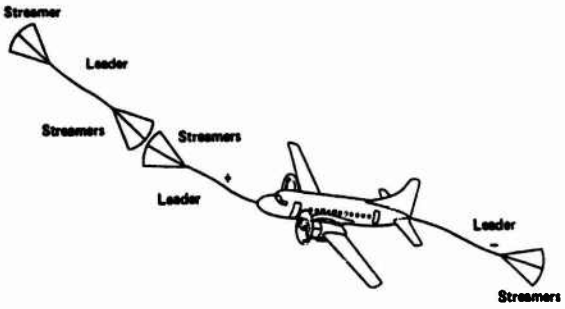

Fig. 7 - Leader coming to the aircraft

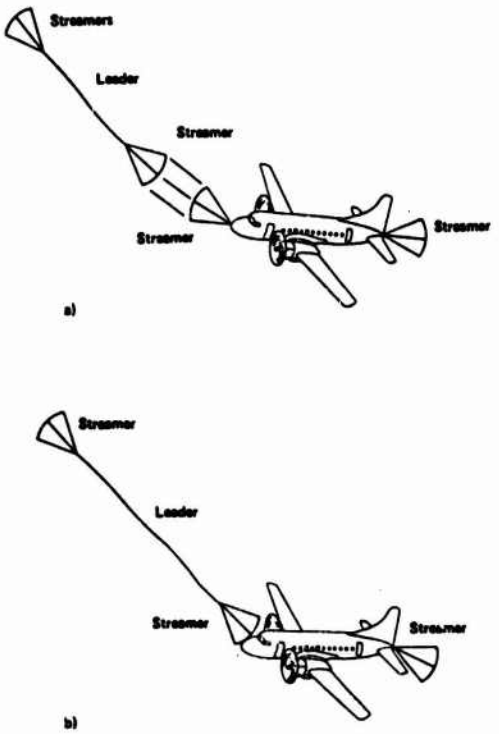

Fig. 8 - Leader coming to the aircraft

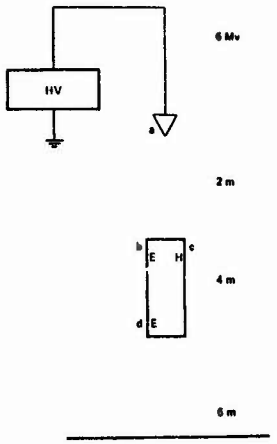

Fig. 9 - Set up of high voltage experiment

Fig. 10 - Discharge configuration on the cylinder

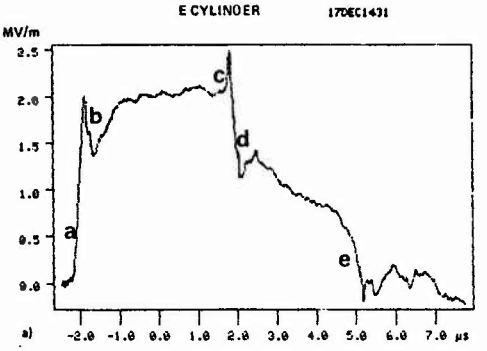

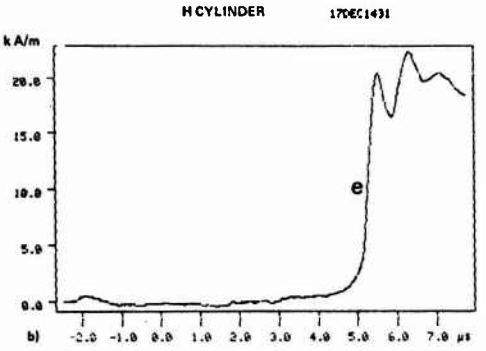

Fig. 11 - Fields on the cylinder
a. Electric field
b. Magnetic field

	RISE TIME		REPETITION RATE	TIME BEFORE ATTACHMENT	MAX VALUE		MAX SLOPE
PULSES CHARACTERISTICS ON THE C 160							TABLE 1
	min	max		max	min	E	ΔE/Δt
Electric	50 ns	200 µs	10^4	1 ms	100 µs	50 kV/m	1.5 x 10^{12} V/m/s
						H	ΔH/Δt
Magnetic	50	200	10^4	1 ms	100 µs	300 A/m	6 x 10^3 A/m/s
PULSES CHARACTERISTICS ON THE CV-580							TABLE 2
	min	max		max	min	E	ΔE/Δt
Electric	30 ns	200 µs	10^4	3 ms	100 µs	500 kV/m	5 x 10^{12} V/m/s
						H	ΔH/Δt
Magnetic	30 ns	200 µs	10^4	3 ms	100 µs	500 A/m	2 x 10^{10} A/m/s

TABLE 1 - TABLE 2

Current Levels and Distributions on an Aircraft During Ground Lightning Simulation Tests and In-Flight Lightning Attachments

1Lt James L. Rebert
Air Force Wright Aeronautical Laboratories (AFWAL/FIESL)
Wright Patterson AFB, Ohio 45433

Jean S. Reazer, John G. Schneider,
Martin D. Risley and Arturo V. Serrano
Technology/Scientific Services, Inc. (T/SSI)
Dayton, Ohio 45431

ABSTRACT

Current levels and distributions recorded during in-flight lightning strikes on a specially instrumented CV-580 aircraft are compared with those resulting from ground simulation tests with two generators and two return path configurations. Current levels and distributions were measured on the CV-580 aircraft equipped with wide-band acquisition systems during thunderstorm flights over Florida in 1984 and 1985 and during ground tests at Wright Patterson AFB, Ohio.

The aircraft was instrumented with current shunts at each wing tip during 1984 and 1985 and with shunts at the tail and top of the vertical stabilizer in 1985. During both years, the aircraft was equipped with four multigap loop magnetic field sensors, one on each wing, one on the forward upper fuselage and one on the aft upper fuselage.

During three separate test periods, the CV-580 was subjected to extensive ground lightning simulation tests with a four microfarad, 200 kilovolt pulse simulation capacitor bank and a fast risetime generator capable of currents up to 45 kiloamperes. Two return path configurations were used, one a flat plate design and the other coaxial.

Current levels and distributions on the aircraft during ground tests with currents applied nose-to-tail and wing-to-wing are compared with results obtained for two lightning attachments in flight where strikes attached to the nose and right wing respectively. This comparison is performed first in the time domain where waveform temporal characteristics are compared for the ground and airborne cases. The electromagnetic interaction is then compared in the frequency domain where the spectral content is analyzed via the use of measured transfer functions.

INTRODUCTION

This paper presents the initial results of an experimental investigation of the currents measured on a specially instrumented CV-580 lightning research aircraft during lightning simulation tests as compared to those experienced during actual in-flight lightning strikes.

During 1984 and 1985, a CV-580 aircraft supplied by the Federal Aviation Administration and instrumented hy the Atmospheric Electricity Hszards (AEH) Group of the Air Force Wright Aeronautical Laboratories (AFWAL/FIESL) was flown in and near active Florida thunderstorms to measure the electromagnetic interaction of the aircraft with lightning strikes and to characterize the significant parameters of lightning which contribute to this interaction.

Before and after the 1984 summer thunderstorm flights and prior to the 1985 summer program, the CV-580 was subjected to extensive lightning simulation tests to provide a lightning susceptibility assessment of the aircraft, to allow lightning measurement and scquisition system check-out, to perform system calibration and to allow data acquisition trigger levels to be set. The CV-580 was ground tested with two lightning simulation generators and two return path configurations.

Recent lightning characterization programs have had a significant impact on the validity of lightning simulation threat waveforms which are accepted as adequate to ensure lightning protection for aerospace vehicles. The specially instrumented CV-580, its in-flight lightning strike data and the extensive ground simulation tests performed on this aircraft present a unique opportunity to compare the electromagnetic interactions of simulsted lightning on the aircraft with those experienced during an in-flight lightning strike. This paper presents general overviews of lightning simulation, the CV-580 in-flight characterization program, and the ground simulation tests performed on that aircraft. This is followed by a comparison of the airborne and ground results in the time and frequency domains.

GROUND SIMULATION

The goal of lightning simulation is to ensure flight safety (1). The military must also ensure mission completion in hostile electromagnetic environments including adverse weather conditions and lightning. The adequacy or realism of s lightning simulation test is limited by our knowledge of the complexities of the natural lightning environment during attachment to the aircraft, the capacities of the lightning simulstion generating equipment, and the configuration or facility effects of the simulation test set-ups. The introduction of advanced composite materials and sophisticated low level flight critical electronics has resulted in the possibility of increased inherent susceptibility/vulnerability of aircraft, and hence, increased interest in performing more accurate lightning simulation tests. The heart of the lightning simulation test is the waveform used to simulate the natural lightning event, while the soul is the ability to simulate the most significant effects of the in-flight aircraft and lightning electromagnetic interaction.

Because of its significance to lightning simulation and to the lightning protection of aerospace vehicles, several lightning characterization programs have heen undertaken to characterize the natural lightning environment and to measure its interaction with aircraft. The most recent include in-flight programs with the NOAA WC-130 aircraft (2), the NASA F-106 aircraft (3), and the FAA CV-580 aircraft (4,5,6); and ground programs such as the rocket triggered lightning experiments (7). Lightning measurements made during these programs have shown that natural lightning is a complex and variable phenomena. While it is extremely difficult to simulate a complete natural lightning flash, it has been accepted that most of the current and voltage characteristics of lightning can be produced separately with pulsed power impulse generators (8); and that the direct and indirect effects of lightning can be simulated by the production of four of its parameters (9). They are:

- The current peak amplitude (Imax)
- The maximum current rate of change (dI/dt)
- The action integral ($\int i^2 dt$)
- The charge transfer ($\int i dt$)

Lightning characterization programs involving in-flight strikes are intended, in part, to characterize a balanced threat based on the statistical probability of combinations of these parameters. Traditionally, during lightning simulation tests, the most severe of the four parameters are simulated to attain a lsrge safety margin, even though measurements to date have never shown these levels of each psrameter to occur within a single lightning strike. The levels of these parameters and their significance to the aircraft/lightning interaction event must he continually evaluated as they have a profound effect on the levels of lightning protection which must he added to an aircraft and this protection directly affects the cost, weight and performance of the aircraft.

Since each of the four parsmeters is responsible for certain effects during the lightning simulation, much effort has been expended to develop standardized current waveforms for use in simulation tests. Widely accepted are the MIL-STD-1757 waveforms which were developed and categorized by the SAE AE4L Committee (10,11,12). Since then, further characterization programs (2,13) have shown that some lightning flashes, and in particular subsequent return strokes, have much faster risetimes and efforts have been made to build simulation generators capable of producing these faster risetimes (14,15). An extensive effort by the Atmospheric Electricity Hazards Protection Advanced Development Progrsm (AFWAL/FIEA) resulted in the development of two waveforms to simulate the indirect effects of lightning, one for the severe lightning threat and one for the average moderate lightning threat (16). The SAE AE4L committee continues to review the standardized lightning simulation test waveforms in light of data from on-going lightning characterization programs (17).

While characterization programs advance the simulation waveforms, other research has provided break throughs in aircraft and lightning interaction simulation and analysis. Two of the most exciting advances have been the development of frequency domain lightning simulation test techniques and the extension of frequency domain analytical techniques

to traditional time domain high level current injection lightning simulation tests.

The frequency domain lightning simulation test incorporates the Swept Frequency Continuous Wave (SFCW) Test (18,19) to develop a frequency domain transfer function for the aircraft circuit being tested by injecting a known frequency waveform and measuring the systems response to that frequency. As the frequency is swept, typically from DC to 100 MHz for lightning simulation, additional measurements are made at set frequency intervals. The magnitude of the input waveform at zero phase is divided out of the system's frequency domain responses, producing a transfer function of the system's response over the entire range for which it is tested. This technique is extended to time domain high level current injection simulation tests via the Fourier Transform. The time domain injected current waveforms and the resulting measured induced transients are transformed into the frequency domain where, by dividing the response by the input, the transfer function of the circuit is obtained. These transfer functions offer a method by which:

1. The measured data may be corrected to compensate for the response of the transient messuring sensors and the characteristics of the fiber optics data transmission links.

2. Simulation configuration effects may he identified and accounted for.

3. The circuit's induced transient responses may be linearly extrapolated to determine the circuit's susceptibility to either MIL-STD-1757A waveforms, actual in-flight measured lightning strikes or any other desired threat wsveform.

Time domain lightning simulation induced transients on aircraft contain not only the characteristics of the aircraft but also those of the measuring or data acquisition devices. The latter may hc measured and divided out of the frequency domain transfer function.

McCormick, et. al. (20) has shown that a lumped RLC generator model coupled to a transmission line model of the aircraft and return paths can be used to predict their first order configuration or facility effects. When a more accurate prediction or analysis of these effects is needed, a boundary condition solution to Maxwell's equations is required. These may be performed either in the frequency domain or in the time domain. The AEH Group uses the three dimensional finite difference time domain code (21) for this purpose and is presently developing the capability to perform this analysis in the frequency domain using the General Electromagnetic Model for the Analysis of Complex Systems (GEMACS) code (22). Once these configuration effects are analyzed, the differences between the in-flight and ground simulation configuration effects may be accounted for in the circuit's transfer function.

Extrapolation of low level SFCW and moderate level simulation data has its advantages and disadvantages. The primary advantage is the ahility to determine linearly the circuit's response to any threat waveform by multiplying the circuit's transfer function with the frequency spectral content of the threat waveform, then performing an inverse Fourier transform. Practical experience in the lightning simulation testing of aerospace vehicles has shown that it is not always possible to exactly reproduce the MIL-STD-1757 waveforms (23,24). Most of the circuit's response is uniquely determined regardless of the waveform used as long as the injected waveform contains sufficient spectral content to excite the natural modes of the vehicle (i.e. the risetime is fast enough and the fall time is slow enough). Using the measured transient responses and input waveforms to produce the circuit's transfer function allows the determination of the circuit's linesrly extrapolated response to the MIL-STD-1757 or any other threat waveform. Another advantage is that low level swept frequency testing may be performed in a laboratory environment where noise sources may be strictly controlled. Operation of high current lightning simulation generators characteristically is accompanied hy an extremely noisy electromagnetic environment due to high voltage pulsed power switching within the generator. The control of noise sources results in an improvement in the signal-to-noise ratio for the measured circuit transient data. In the frequency domain tests, the noise sources are measured and can be accounted for whereas in time domain tests they are random sources which are extremely difficult to control. The primary disadvantage of the low level SFCW method, as is the case with any low level test method, is that linear extrapolation does not account for non-linear effects which may occur during the lightning aircraft interaction. Sparking at panel edges or fasteners or component breakdown in electronic circuits due to transient voltages or currents cannot be accounted for in linear extrapolation, although in some cases they may be predictable. Because the aircraft is not being subjected to lightning's parameters at full threat levels, careful analysis must accompany the extrapolation. The AEHP ADP has shown that in many, but not all cases, linear extrapolation is conservative in that it predicts higher responses than those which occur at the higher levels (25). In any case, the integration of frequency domain techniques as described above, results in a substantial enhancement of the ability to perform lightning susceptibility/vulnerability tests and anslysis on aerospace vehicles. These frequency domain techniques are used extensively in the comparison of the in-flight lightning/aircraft electromagnetic interaction with that experienced during ground simulation tests as presented in this paper.

IN-FLIGHT LIGHTNING MEASUREMENTS

During 1984 and 1985, the CV-580 aircraft supplied by the FAA and instrumented by AFWAL/FIESL measured and recorded the electromsgnetic fields and skin current distributions on the aircraft due to direct lightning attachments. Lightning currents were measured at the base of booms equipped with current shunts installed at the wing tips in 1984 and at the tail and the top of the vertical stabilizer in 1985. The shunts were oriented to produce a negative polarity waveform when conventional current flowed onto the aircraft. The skin current distributions on the aircraft were measured by four EG&G Multi-gap Loop (MGL) derivative magnetic field sensors located: one under each wing between the engine and the fuselage, one on the top forward fuselage and one on the top aft fuselage. These magnetic field sensors were oriented so that a negative output would occur for conventional current flow from the nose to tail or from the right wing tip to the left wing tip. The electric fields present on the aircraft during the

lightning attachments were measured by three EG&G Flush Plate Dipole (FPD) derivative electric field sensors located: one under each wing tip and one on the left surface of the vertical stabilizer. The wing tip electric field sensors were oriented to produce a positive output in s negative electric field. Video cameras viewing both wings and wide angle video cameras viewing the hemispheres above and below the fuselage surfaces visually recorded the entry and exit locations during the lightning attachments and were used to verify the lightning current paths on the aircraft as determined by sensor measured polarities and delay times (6).

The outputs of the sensors were recorded in the following ways.

1. Shunts - signal split in two: one output to Tek 7612 digitizer and onto digital 9 track tape; other output directly to an analog recorder.

2. Magnetic Field Sensor - signal split in two: one to Tek 7612 digitizer and onto digital 9 track tape; other integrated by signal conditioning components and recorded directly on analog tape.

3. Electric Field Sensors - signal split in two: one to Tek 7612 digitizer and onto digital 9 track tape; other integrated by signal conditioning components and recorded on analog tape.

The same instrumentation used to measure the in-flight electromagnetic interaction of the CV-580 with lightning was used during the ground simulation tests and these measurements form the basis for the experimental comparison of the airborne and ground electromagnetic interaction events.

GROUND LIGHTNING SIMULATION MEASUREMENTS

The ground lightning simulation measurements were made on the CV-580 during 1984 and 1985 using two generators and two return path configurations.

The aircraft was tested with a four microfarad 200 KV, Pulse Simulation Unit (PSU), capacitor bank and flat plate return paths during early 1984. This generator and a 40 KA, 200 nanosecond Fast Risetime Generator were used with modular coaxial return paths in Octoher 1984. Specific descriptions of the test set-ups and simulation tests performed in 1984 are detailed in a previous conference paper (24), as was the fast risetime generator (15). The modular return paths are discussed in another paper at this conference (26). Figures 1 and 2 show the test set-ups for two of the generator/return path configurations.

The injected current waveforms were measured by a Pearson current transformer and recorded on magnetic disks for each shot during each of these simulation tests. These waveforms' shapes and peak amplitudes were varied to provide the broadest range of measurements on the aircraft. The purposes of these tests were: safety of flight lightning susceptibility/vulnerability assessment, lightning electromagnetic field data acquisition system check-out, aircraft measurement system calihrstion and trigger level adjustments, and the measurement of the aircraft system's responses to a wide range and variety of simulated lightning waveforms. The on-board in-flight lightning measurement systems were used to measure and record the electromagnetic interaction of the CV-580 to simulated lightning strikes on the ground.

TIME DOMAIN ANALYSIS AND COMPARISON

The time domain skin current distributions measured on the CV-580 during two in-flight lightning strikes, one on 20 Aug 1984 and one on 5 Sept 1984, are compared with those measured during the ground simulation tests using two generators snd two return path configurations. The 20 Aug 1984 strike was selected because temporal analysis of the polsrities and time delays in the output waveforms of the magnetic field sensors showed that the primary current path through the aircraft was from nose-to-tail (6). The same analysis of the current shunts and magnetic field sensor's output waveforms showed that the primary current path through the aircraft during the 5 September 1984 strike was wing-to-wing. As the current paths of these two lightning strikes most closely matched the ground simulation test configurations, they were chosen for comparison.

The four temporal characteristica necessary to simulate the direct and indirect effects of lightning are compared in tables 1 and 2. Table 1 lists the current amplitudes, risetimes, rates of rise, charge transfer and action integral vslues recorded on each of the aircraft's four multigap loop magnetic field sensors during the ground tests with esch of the generator/return path combinations. Table 2 presents the same data as measured during the two airborne strikea.

These measured parameters show that the most severe conditions were produced by the fast risetime generator with the coaxial return path. In the nose-to-tail configuration these produced: risetimes of 341 to 453 nanoseconds (ns), rates of rise 3.2 x 10^{10} A/S, amplitudes of 13 kiloamperes (KA) and action integrals of 105 and 128 A^2S on the fore and aft skin current sensors, respectively. In the wing-to-wing configuration the generator was set up to produce amplitudes of about 5 KA and risetimes of 200 ns for rates of rise of sbout $2.5x10^{10}$ A/S and action integrals of 4.4 A^2S.

The airborne measured dsta was at lower levels which are representative of the in-flight data obtained in the AFWAL/FIFSL airhorne programs to date. Current amplitudes were 1088 A on the forward fuselage sensor for the nose-to-tail strike and 816 A at the right wing for the wing-to-wing strike. Risetimes of 104 to 305 ns on the four sensors produced a maximum rate of rise of $4.3x10^{9}$ A/S and action integrals of less than 1 A^2/S.

The CV-580 was flown for 50 hours below 20,000 ft in the vicinity of Florida thunderstorms in 1984 and collected data from 21 lightning strikes. A complete review of the analog records shows the highest current pulse recorded to have a peak amplitude of 6 KA. On-going analysis of 1985 data, while still unfinished, preliminarily shows that after 50 more flying hours and 29 more strikes, the highest peak amplitude measured was 12 KA. In both years the average peak current amplitudes recorded were much lower than these values. No risetimes faster than 100 ns have been seen.

In addition to the four current parameters, considerable information may be gleaned hy comparing the current distributions in the airborne case as

compared to those experienced with the four gencrator/return path configurations. Figure 3 illustrates the current waveforms recorded on the aircraft by the skin current sensors during the wing-to-wing strike, together with the injected current as measured at the right wing boom current shunt. Figure 4 shows similar data for the nose-to-tail strike (no shunt data). In each of these strikes it is shown that some of the current redistributes onto and excites resonances on those portions of the aircraft which are not in the direct path of the lightning current. This is, some current is distributed on the wings during the nose-to-tail strike and onto the fore and aft fuselage during the wing-to-wing strike.

The fast risetime generator with the coaxial return path configuration was found to most sccurately simulate the in-flight event in terms of the current parameters and the current distrihutions produced on the aircraft. With this return path this generator is capable of producing currents up to 40 KA with risetimes of 200 ns for a rate of rise of 2x10" A/S. This is more than adequate to simulate the most aevere parameters of the 50 airborne strikes below 20,000 feet which have heen measured to date. Figures 5 and 6 show the current waveforms recorded at the input and the responses at the four sensors during tests with the fast risetime generator/coaxial return paths for the wing-to-wing and nose-to-tail configurations, respectively. These distributions are most representative of those expcrienced during the airborne strikes.

The fast risetime generator with flat plate return path is not capable of producing the fast risetimes which were possible with the coaxial return paths due to the increased inductance of this return path configuration. The flat plate return paths do not produce the same current distributions on the aircraft, but instead cause the current to flow more directly from the entry to exit points with less distribution on those portions of the aircraft not in this direct path.

The pulse simulstion unit was not capable of producing fast enough risetimea to simulate the lightning strikca in either return path configuration.

FREQUENCY DOMAIN ANALYSIS AND COMPARISON

Frequency domain techniques as described in a paper at this conference (26) were applied to the airborne and ground data to analyze and compare further the adequacy of the generator/return path combinations in simulating the airborne event in terms of transfer functions.

The first step in the frequency domain analysis was to remove the effects of measurement system components from the measured data responses. The frequency domain transfer functions of the aircraft's derivative magnetic field sensors, the ground input current transformer sensor and fiber optics links were measured and recorded from DC to the component's upper frequency limit using a Hewlett Packard 3577A network analyzer. The network analyzer produces a swept frequency continuous wave output and measures the component's response. By dividing the component's output responses to the input at discrete frequencies a transfer function for the component is produced. The time domain measured ground and airborne transient waveforms were transformed into the frequency domain by Fast Fourier tranaform. The transform was corrected by dividing out the transfer function of the measuring components leaving a more accurate representation of the source which produced the sensor's meaaured response. This corrected Fourier transform is inversed back into the time domain to produce the time domain signal. All time domain signals were corrected in this manner. An interesting side benefit of this procedure is that responses measured by derivative field sensors are automatically integrated to display the source excitation which caused the sensor's output. This is illustrated in Figure 7 for the multigap loop magnetic field sensors mounted on the aircraft. Figure 7a shows the original time derivative waveform and 7b its Fast Fourier transform as recorded during a ground test with the fast risetime generator. Figure 7c shows the transfer function of the multigap loop sensor as measured using the Hewlett Packard 3577A network analyzer. Figure 7d shows the corrected Fourier transform which results when the original tranaform is divided by the transfer function of the sensor and Figure 7e the resulting inverse transformed time domain signal. This benefit can be appreciated by those who have experience with the software integration of time derivative digital sensor data. This process eliminates common problems with zero reference values and with integration error drift. The procedure is also more accurate as software integration assumes that the sensor is a perfect derivative sensor. The transfer function illustrated in Figure 7c showa this is definitely not the case as a perfect derivative sensor would produce a transfer function which has a straight line from zero with a slope of times the frequency. Frequency domain processing allows the sensor's effects to be removed whether the sensor response is perfect or, more commonly, is less than perfect.

The next procedure in the frequency domain analysis was to produce the transfer function of the aircraft at the four sensor locations for the airborne and ground cases. These were formed using the following relationship:

$$T(\omega) = R(\omega)/S(\omega)$$

Where $T(\omega)$ is the frequency domain transfer function, $R(\omega)$ is the corrected Fourier transform of the multigap loop sensor response and $S(\omega)$ is the Fourier transform of the applied source current. The source current was the injected current for the ground tests and the right wing boom shunt current for the airborne wing-to-wing data. No airborne source data was available for the strike to the nose and preliminary attempts to use the forward fuselage's sensor data as the source reference have only produced limited success.

This procedure is illustrated in Figure 8. The corrected frequency domain response of the forward fuselage sensor to the airborne wing-to-wing strike, $R(\omega)$, is shown in the upper left hand corner. The Fourier transform of the right wing boom current shunt, $S(\omega)$, is shown in the upper right hand corner. The aircraft's transfer function at the location of the forward upper fuselage is shown in the middle log-log plot, while the lower plots illustrate this same transfer function in linear-linear form from 97 KHz to 1 MHz (left) and 1 MHz to 25 MHz (right).

Figure 9 shows the aircraft transfer functions at the locations of each of the four multigap loop aensors during this airborne strike.

Many of the prominent peak magnitudes in these transfer functiona occur at frequencies which relate quite closely to dimensiona of the aircraft. The spike at 4.7 MHz represents a half wavelength of approximately 105 feet, the distance from wing tip to wing tip. At 5 MHz or 98 feet the frequency may correspond to the distance from the wing tip to the tip of the vertical atabilizer, the diatance from the wing tip to the tip of the horizontal stabilizer or from the wing tip to aircraft tail. Nine MHz (55 feet) corresponda to the diatance from the wing tip to the fuselage and 7.2 MHz (68 feet) to the distance from thc wing tip to the far engine mount. The 11-12 MHz frequencies correspond to the distance from the wing tip to the closer engine mount. The left wing, right wing and aft upper fuselage transfer functiona show peaks at 1.5, 2.5 and 3.6 MHz which are too low to correspond to direct aircraft dimensions. These frequencies correspond well, however, to frequencies which are multiples or combinations of aircraft distances. For example, 2.5 MHz is 197 feet or twice the distance from the wing tip to the tail or roughly the combined distance of wing tip to wing tip and nose to tail; and 3.6 MHz ia 137 feet, twice the distance from the wing tip to the far side of the fuselage or the combination of the distance from wing tip to tail and the distance from the wing tip to the near engine mount. The frequency 1.5 MHz could relate to the combination of several aircraft dimensions. Thc transfer functions are particularly interesting to the lightning protection electromagnetic analyst aa they clearly show that the interaction of lightning produces resonances which are more complex than the those predicted simply by wing to wing or nose to tail dimensions and may cloaely correspond not only to direct aircraft dimensions but also to combinations of theae dimensions.

Figure 10 ahows the tranafer functions at the four sensor locations for the ground test with the fast risetime generator and the coaxial return paths in the wing-to-wing configuration. The overall distribution of the transfer functiona peak magnitudes corresponds well to the airborne case for the ranges of 4 to 13 MHz, 20 MHz and at 23 to 25 MHz. These transfer functions show additional reaonancea st 16-17 MHz which were not present in the airborne strike.

Figure 11 showa the same tranafer functiona for the fast risetime generator with the flat plate return paths in the wing to wing configuration. These transfer functions have peaks at about 10 MHz which are not found in either the airborne case or with the coaxial return paths. In this configuration the transfer functions do not diaplsy as many peak magnitudes at frequencies below 10 MHz. Above 15 MHz, the flat plate return path provides a very faithful reproduction of the airborne measured transfer function with spikes at 19 MHz and in the 23-24 MHz range. Preliminary analyais with a three dimensional finite difference electromagnetic code indicates that these high frequency spikes may be more a function of noise than of particular resonances on the exterior of the aircraft (27). Figure 12a showa a model of the CV-580. Figure 12b showa the source (S_w), Figure 12c the predicted resonsnces on the forward fuselage during a wing-to-wing-strike where one third of the current flowed out of the tail, and Figure 12d the Fourier transform of this signal. Figure 12e is a log-log plot of the transfer function with the right wing boom current, Figure 12a, taken as the source, and the forward fuselage current taken as the responae. Figure 12f ahows the same linearly for 97 KHz to 25 MHz. This analysis would tend to indicate that the resonances above 19 MHz are cauaed either by noiae, internal coupling, or resonances within the data acquisition coaxial wirc networks rather than by natural modea on the aircraft's exterior.

Figure 13 compares the transfer functions obtained using the 4 microfarad 200 KV capacitor bank in the wing-to-wing configuration. Figure 13a shows the aource waveform (upper left) and the resulting transfer function at the left wing senaor location (upper right) for a coaxial return path. Figure 13b shows the same waveforma for a flat plate return path. With the exception of the spike at 5.5 MHZ, neither transfer function showa evidence of the pronounced, discrete frequencies seen in the airborne data or produced by the fast risetime generator. The alower risetimes in this configuration do not provide sufficient high frequency content to excite several of the natural modea of the aircraft which are evident in the airborne tranafer functions and ground tests with the fast risetime generator.

CONCLUSIONS

1. The choice of lightning simulation generators and return path configurations has a pronounced effect on the current levela and diatributions experienced on the aircraft as evidenced by the transfer functions resulting from each configuration.

2. While the fast risetime generator and coaxial return paths provide the most realiatic simulation of the airborne event, they too produce their own configuration resonances at 16-17 MHz which are not evident in the airborne event.

3. Electromagnetic anslysis with codes such as the three dimensional finite difference code provides a method by which the configuration effects of the simulation set-up may be distinguiahed from the natural modes of the aircraft in flight. This provides a viable means by which these effects may be identified and eliminated from the responae data.

4. Frequency domain analysis of in-flight lightning strike dsts, lightning simulation test dsta and data derived by electromagnetic analysis provides transfer functions by which the aircraft'a interaction with aeveral lightning threat waveforms may be determined (i.e. the multiplication of the aircraft's transfer function with a threat waveform's frequency spectral content will predict the aircraft'a linear response to that waveform).

5. Resonances experienced on aircraft during lightning atrikes cannot all be sssociated with simple, individual aircraft dimensions. Particularly interesting are low frequency resonances which correapond to either multiples of aircraft lengths or to combinations of aircraft lengths.

6. Ground aimulation tests at 20 KA with the faat risetime generator/coaxial return path configuration produced more scvere current parameters on the aircraft than any strike experienced during 50

lightning strikes below 20,000 feet. Over 90% of the strikes could be simulated with 5 KA at 200 ns.

7. Slow (high inductance) lightning generators do not excite the aircraft modes which were present in the transfer functions of the airborne data and in simulation tests with the fast risetime generator.

REFERENCES

1. E.H. Schultze, "Updating the MCAIR Lightning Simulation Laboratory", Proc. of 8th International Aerospsce and Cround Conference on Lightning and Static Electricity, Ft. Worth, TX, 21-23 June 1983.

2. P.L. Rustan, B.P. Kuhlman, G. DuBro, and J.S. Reazer, "Airborne Measurements of the Risetimes in Lightning Return Stroke Fields", Proc. of 8th International Aerospace and Cround Conference on Lightning and Static Electricity, Ft. Worth, TX, 21-23 June 1983.

3. K.A. Zaepell, B.D. Fisher, and M.S. Ott", Direct-strike Photographs, Swept-Flash Attachment Patterns, and Flight Conditions for Storm Hazards '82", NASA Technical Memorandum 86347, Feb 1985.

4. P.L. Rustan, B.P. Kuhlman, and J.S. Reazer, "Characterization of Fast Rise Time Electromagnetic Pulses Recorded in Airborne Measurements During Florida Thunderstorms", Proc. of the 9th International Aerospace and Cround Conference on Lightning and Static Electricity, Orlando, FL, 26-28 June 1984.

5. P.L. Rustan and J.L. Hebert, "Lightning Measurements on an Aircraft Flying at Low Altitude", Proc. of 2nd International Conference on the Aviation Weather System, Montreal, Csnada, 19-21 June 1985.

6. J.S. Reazer and A.V. Serrano, "Spatial and Temporal Description of Strikes to the FAA CV-580 Aircraft", Proc. of 1986 International Conference on Lightning and Static Electricity, Dayton, OH, June 1986.

7. R. Richmond, "Rocket Triggered Lightning - A Comparison with Natursl Lightning", Proc. of 9th International Aerospsce and Cround Conference on Lightning and Static Electricity, Orlando, FL, 26-28 June 1984.

8. E. Gockenbach, M. Morreau, and H. Sutter, "An Impulse Generator to Simulate Lightning Effects on Aircraft", Proc. of 8th International Aerospace and Cround Conference on Lightning and Static Electricity, Ft. Worth, TX, 21-23 June 1983.

9. F.A. Fisher and J.A. Plumer, "Lightning Protection of Aircraft", NASA Reference Publication 1008.

10. "Lightning Test Waveforms and Techniques for Aerospace Vehicles and Hardware", SAE-AE4L Report, 20 June 1978.

11. "Lightning Qualification Test Techniques for Aerospace Vehicles and Hardware", Military Standard MIL-STD-1757A, 20 July 1983.

12. N. Rasch, "User's Manual for AC-20-53A Protection of Aircraft Fuel Systems Against Fuel Vapor Ignition due to Lightning", Federal Aviation Administration Report DOT/FAA/CT-83/3, October 1984.

13. D.W. Clifford, E.P. Krider, and M.A. Uman, "A Case for Submicrosecond Risetime Lightning Current Pulses for Use in Aircraft Induced Coupling Studies", IEEE International Symposium on Electromagnetic Compatibility", 79CH1383-9 EMC, San Diego, CA, October 1979.

14. R.A. Perala, T.H. Rudolph, P.M. McKenna, and J.D. Robb, "The Use of a Distributed Peaking Capacitor and a Marx Generator for Increasing Rise Rates and the Electric Field for Lightning Simulation", Proc. of 9th International Aerospace and Ground Conference on Lightning and Static Electricity, Orlando, FL, 26-28 June 1984.

15. J.L. Hebert, L.C. Walko, and J.G. Schneider, "Design of a Fast Rise Time Lightning Generator", Proc. of the 10th International Aerospace and Ground Conference on Lightning and Static Electricity, Paris, France, 10-13 June 1985.

16. B.C. Melander, "Atmospheric Electricity Hazards Threat Environment Definition", The Boeing Military Airplane Co., AFWAL-TR-85-2052, AFWAL/FIEA, Wright Patterson AFB, OH 45433.

17. Personal Conversation with L.C. Walko and R.C. Beavin, Members of SAE-AE4L Committee, Jan. 1986.

18. L.C. Walko and J.L. Hebert, "Lightning Simulation Tests on a FAA CV-580 Lightning Research Aircraft", Proc. of the 10th International Aerospace and Cround Conference on Lightning and Static Electricity, Paris, France, 10-13 June 1985.

19. D.W. Clifford, K.E. Crouch, and E.H. Schulte, "Lightning Simulation and Testing", IEEE Trans. on Electromagnetic Compatibility, Vol. EMC-24, NR 2 ISSN 0018-9375.

20. W. McCormick, K.J. Maxwell, and R. Finch, "Analytical and Experimental Validation of the Lightning Transient Analysis Technique", by Technology Incorporated AF Wright Aeronautical Laboratories Technical Report, AFFDL-TR-78-47, Wright Patterson AFB, OH 45433, Mar. 1978.

21. J.L. Hebert, J.C. Schneider, MM.D. Risley, J.S. Reazer, and A. Serrano, "Swept Frequency Continuous Wave Lightning Susceptibility Tests on s UH-60A Black Hawk Helicopter", Air Force Wright Aeronautical Laboratories Technical Report currently in publication, (AFWAL/FIESL) Wright Patterson AFB, OH 45433.

22. E.L. Coffey and J.L. Hebert, "Implementation of CEMACS for Lightning Interactions Analysis", paper presented at this conference.

23. D.W. Clifford, K.E. Crouch, and E.H. Schulte, "Lightning Simulation and Testing", IEEE Trans on Electromagnetic Compatibility, Vol EMC-24, No.2, May 1982.

24. L.C. Walko and J.L. Hebert, "Lightning Simulation Tests on a FAA CV-580 Lightning Research Aircraft", Proceedings of the 10th International Aerospace and Ground Conference on Lightning and Static Electricity, Paris, France, 10-13 June 1985.

25. D.B. Walen and M.M. Simpson, "Atmospheric Electricity Hazard Protection Assessment, Test and Analysis - F14A", The Boeing Military Airplane Company, AF Wright Aeronautical Laboratories Technical Report (AFWAL/FIEA) Presently in Publication, Wright Patterson AFB, OH 45433.

26. J.G. Schneider, M.D. Risley, J.S. Reazer, A.V. Serrano, and J.L. Hebert, "State-of-the-art Techniques for Lightning Susceptibility/Vulnerability Assessments", Paper presented at this conference.

27. C.F. Williford, R. Jost, and J.L. Hebert, "Comparison of Absorption and Radiation Boundary Conditions in 3DFD Code", Paper presented at this conference.

Figure 1. Picture Showing the Fast Risetime Generator with the Modular Coaxial Return Paths.

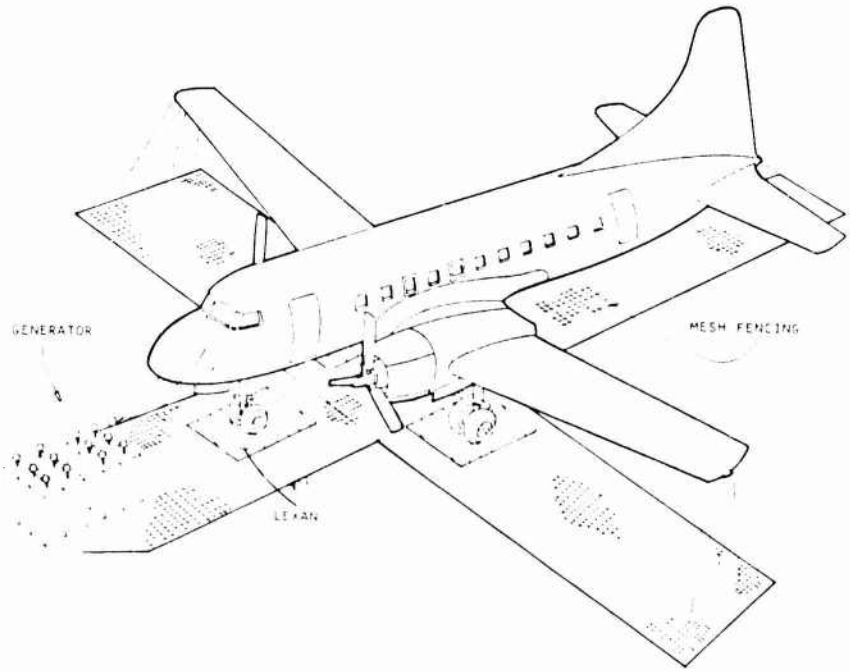

Figure 2. Illustration of the Four Microfarad, 200 Kilovolt Generator with Flat Plat Return Paths.

Table 1

Waveform Paramters Measured on the CV580 Aircraft Surface Current Sensors during Simulation Tests with Various Generator/Return Path Configurations

Generator	Ground Plane	Configuration	Sensor	Amplitude (A)	Rise Time (NS)	Rate of Rise (A/S)	Charge Transfer[1] (A S)	Action Integral[1] (A^2S)
Fast Rise	Coaxial	Nose to Tail	FF	13950	341	3.2×10^{10}	.0091	128
			AF	12567	453	2.2×10^{10}	.011	105
			LW	1600	*	*	*	.45
			RW	1300	*	*	*	.29
Fast Rise	Coaxial	Wing to Wing	FF	600	*	*	*	.23
			AF	1390	*	*	*	.95
			LW	5400	200	2.6×10^{10}	.001	4.3
			RW	4200	220	2.4×10^{10}	.002	4.4
Fast Rise	Flat Plate	Nose to Tail	FF	3255	482	4.3×10^{9}	.004	7.6
			AF	4185	236	1.0×10^{10}	.003	8.6
			LW	*	*	*	4×10^{-7}	.15
			RW	*	*	*	5×10^{-7}	.07
Fast Rise	Flat Plate	Wing to Wing	FF	*	*	*	*	.26
			AF	*	*	*	*	.16
			LW	4400	336	8.2×10^{9}	2.5×10^{-6}	13.5
			RW	4440	210	1.5×10^{10}	3.7×10^{-6}	13.7
Pulse	Coaxial	Nose to Tail	FF	5022	358	8.3×10^{9}	.01	33.9
			AF	3255	393	6.3×10^{9}	.008	14.6
			LW	N/A	N/A	N/A	N/A	N/A
			RW	280	197	1.0×10^{9}	.002	.81
Pulse	Coaxial	Wing to Wing	FF	*	*	*	.0007	.08
			AF	1162	*	*	*	*
			LW	1456	1700	6.5×10^{8}	.006	5.4
			RW	N/A	N/A	N/A	N/A	N/A
Pulse	Flat Plate	Nose to Tail	FF	1162	3500	2.7×10^{8}	.009	6.7
			AF	930	1700	4.7×10^{8}	.007	4.5
			LW	*	*	*	*	*
			RW	480	*	*	*	*
Pulse	Flat Plate	Wing to Wing	FF	279	*	*	*	*
			AF	232	*	*	*	*
			LW	6240	2600	2.0×10^{9}	1.4×10^{-5}	92.5
			RW	7200	3100	2.0×10^{9}	1.9×10^{-5}	135.4

* Not proceasable due to low aignal-to-noise ratio

1 Integrated over a 10 μs window

Table 2

Waveform Paramters Measured on the CV580 Aircraft Surface Current Sensors during Lightning Attachments to the Nose and Right Wing

Strike	Sensor	Amplitude (A)	Rise Time (NS)	Rate of Rise (A/S)	Charge Transfer (A S)	Action Integral (A^2S)
N - T	FF	1088	217	3.8×10^{9}	.0006	.71
	AF	521	187	1.9×10^{9}	.0001	.15
	LW	216	110	2.5×10^{9}	4.5×10^{-5}	.09
	RW	240	125	1.5×10^{9}	7.8×10^{-5}	.06
W - W	FF	279	*	*	*	.02
	AF	558	104	4.3×10^{9}	.0001	.03
	LW	544	350	1.7×10^{9}	.002	.63
	RW	816	215	3.4×10^{9}	.0005	.31

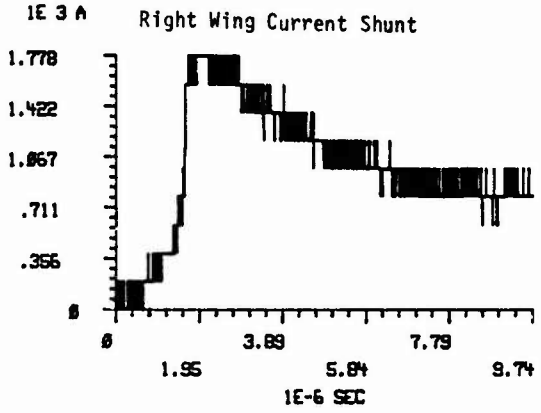

A.

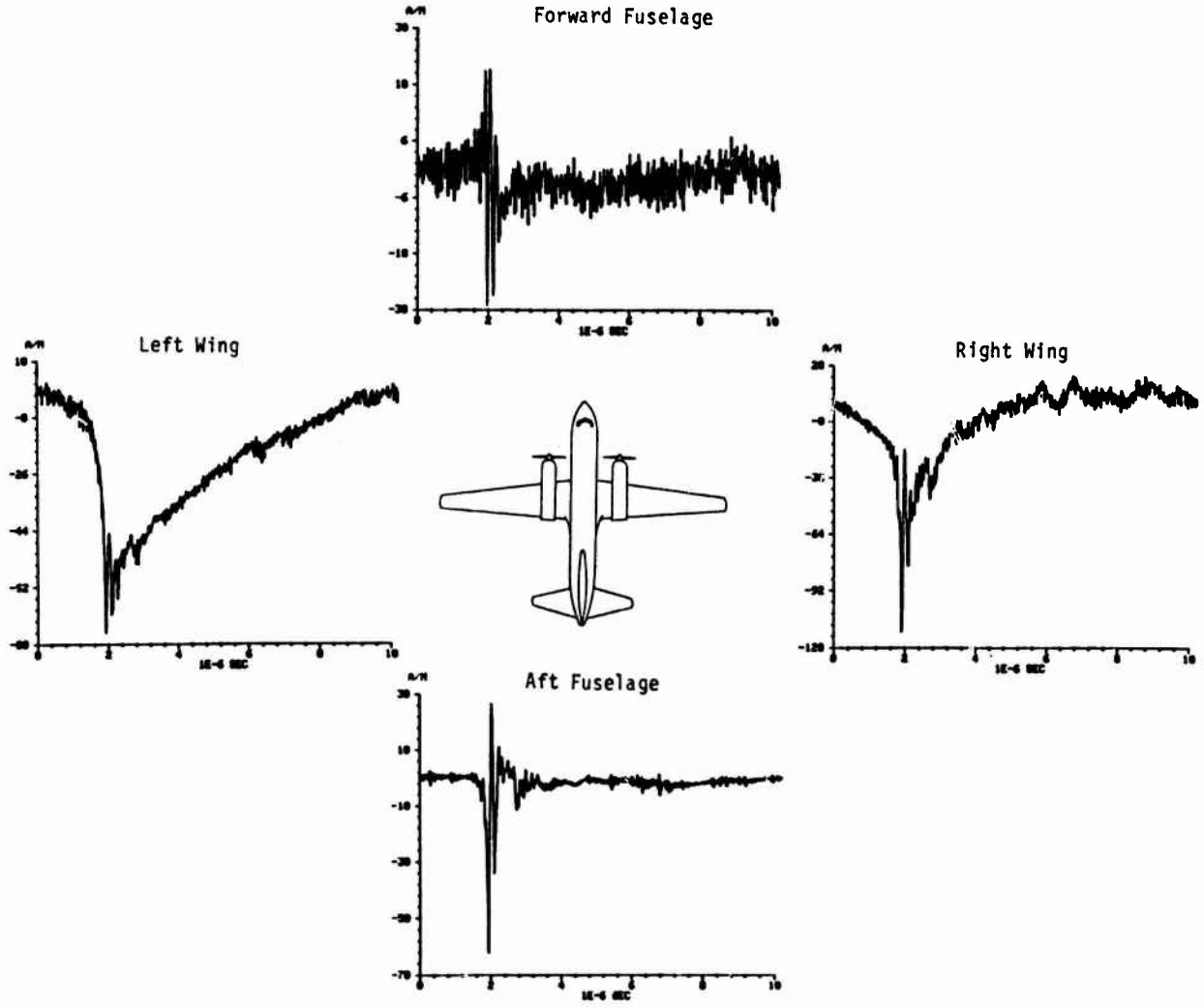

B.

Figure 3. Injected Current Measured at the Right Wing Current Shunt (A) and Surface Current Waveforms Recorded on the Aircraft Skin Current Sensors (B) for an Airborne Lightning Strike to the Right Wing Boom

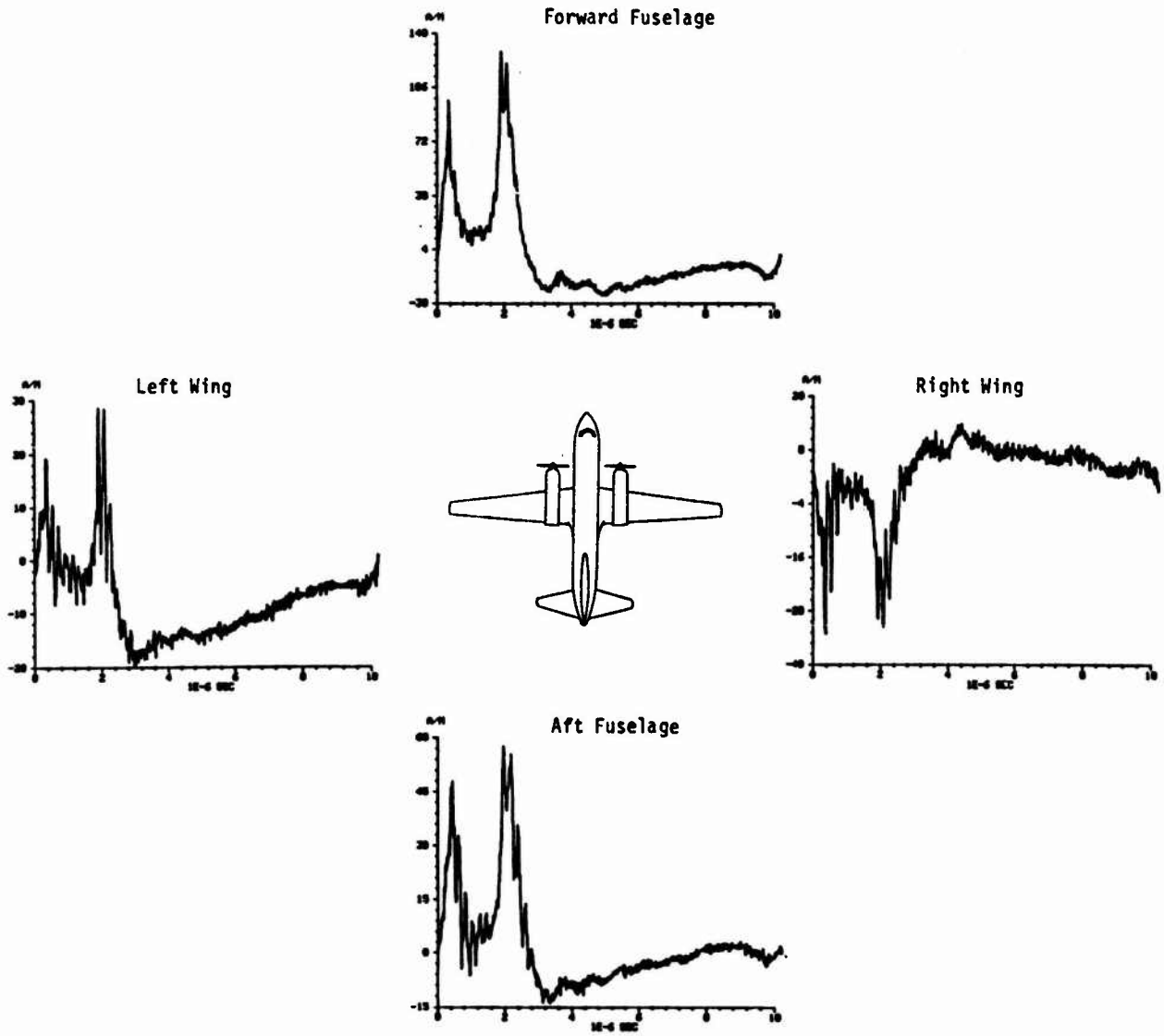

Figure 4. Surface Current Waveforms Recorded on the Aircraft Skin Current Sensors for an Airborne Lightning Strike to the Nose

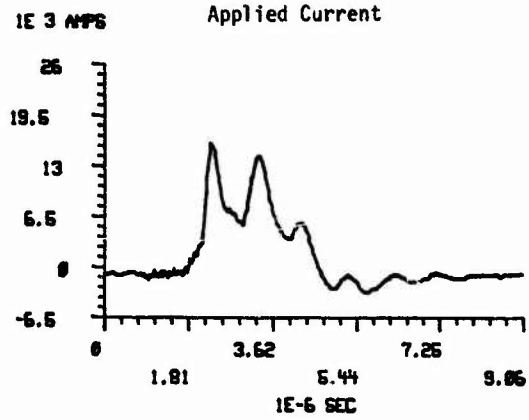

A.

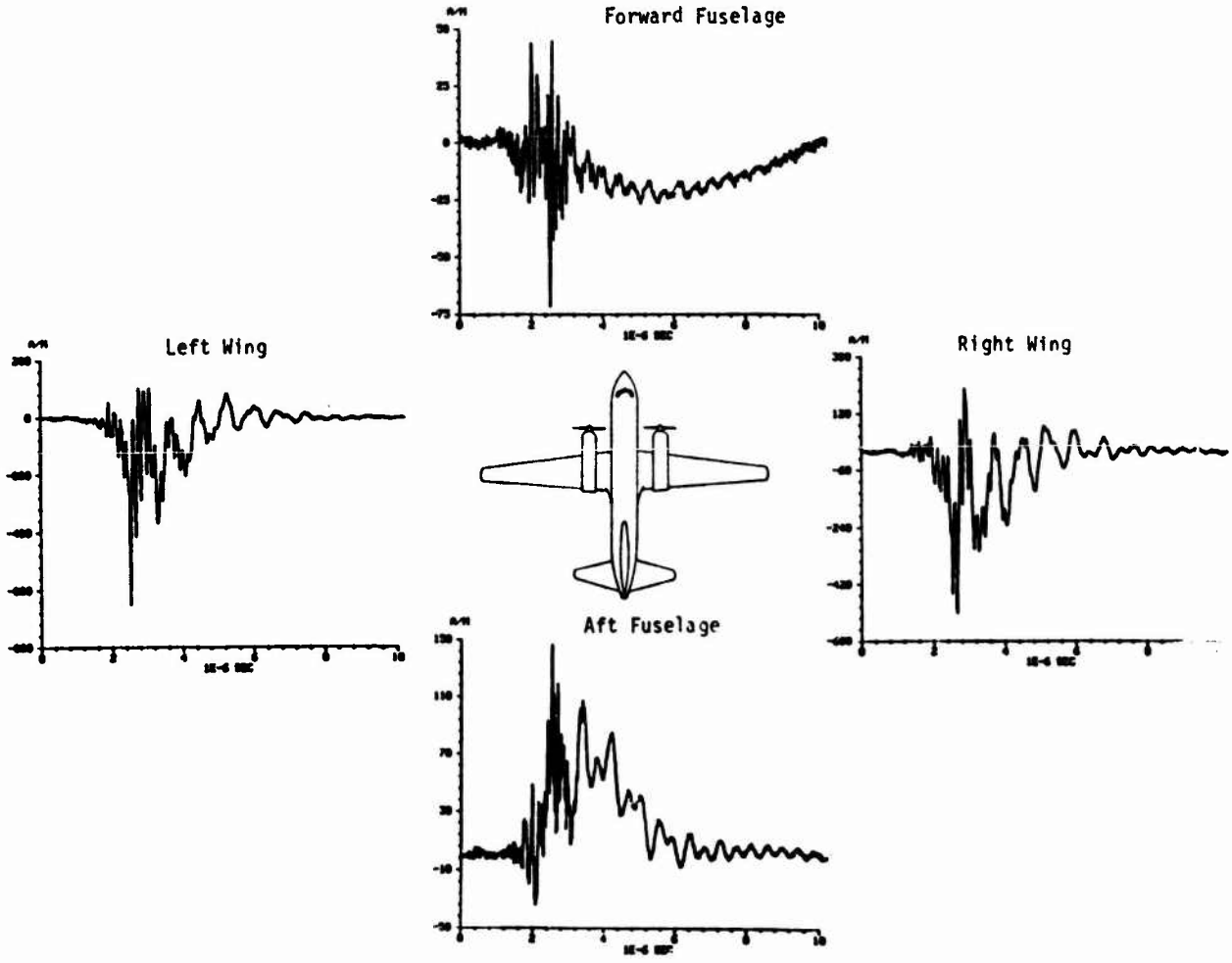

B.

Figure 5. Injected Current (A) and Surface Current Waveforms Recorded on the Aircraft Skin Current Sensors (B) during Ground Testing with the Fast Rise Time Generator and Coaxial Return Path - Current Applied Wing-to-Wing

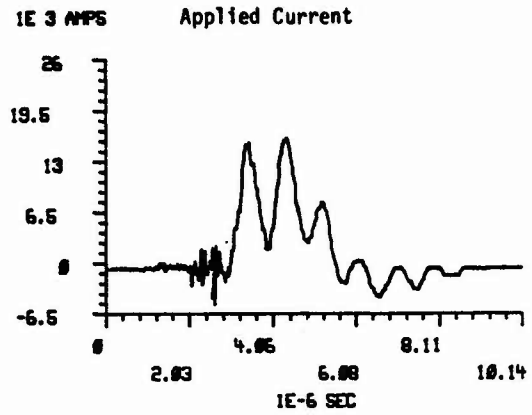

A.

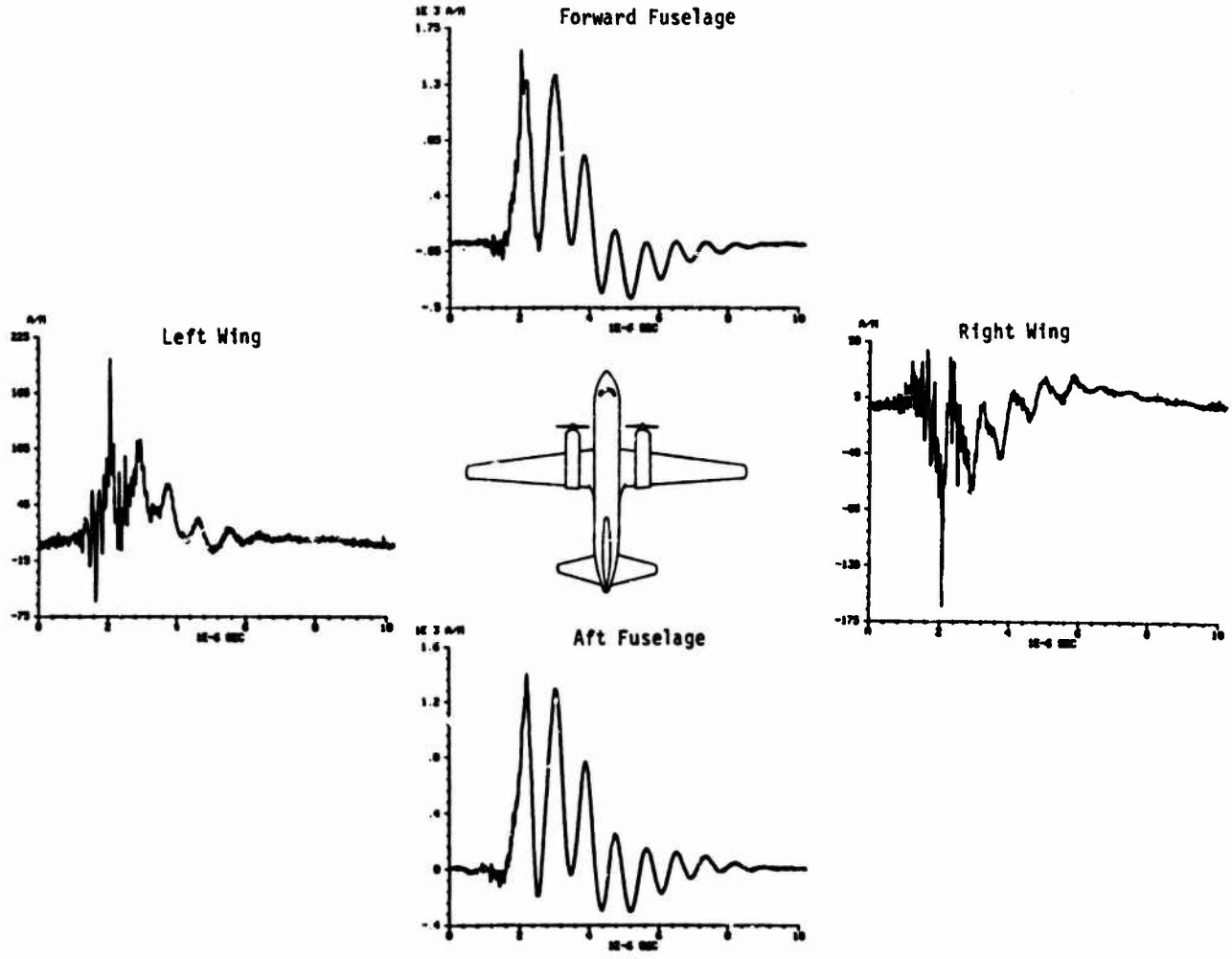

B.

Figure 6. Injected Current (A) and Surface Current Waveforms Recorded on the Aircraft Skin Current Sensors (B) during Ground Testing with the Fast Rise Time Generator and Coaxial Return Path - Current Applied Nose-to-Tail

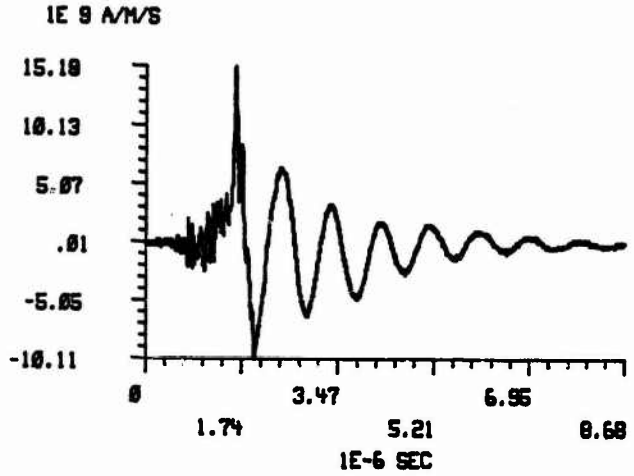

A.

Time Domain Derivative Waveform from Multi-Gap Loop Sensor on Aircraft

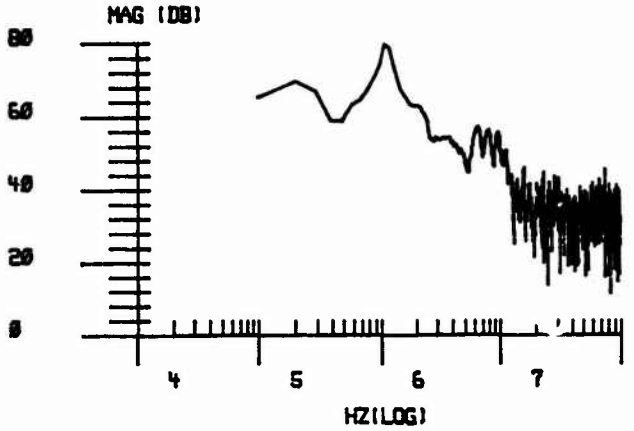

B.

Log-Log Polar Plot of Fast Fourier Transform of (A)

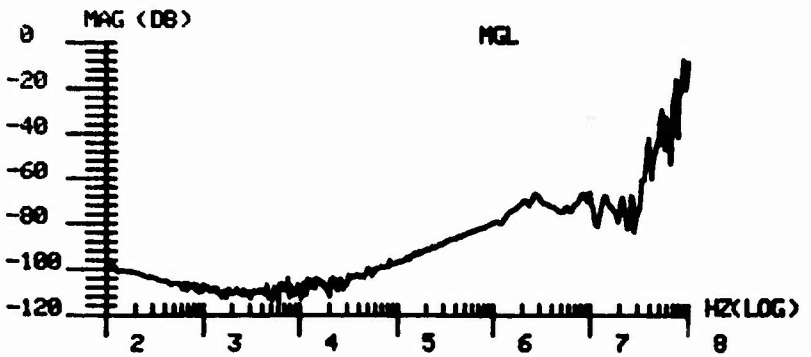

C.

Frequency Response of Multi-Gap Loop Sensor from 100 Hz to 100 MHz

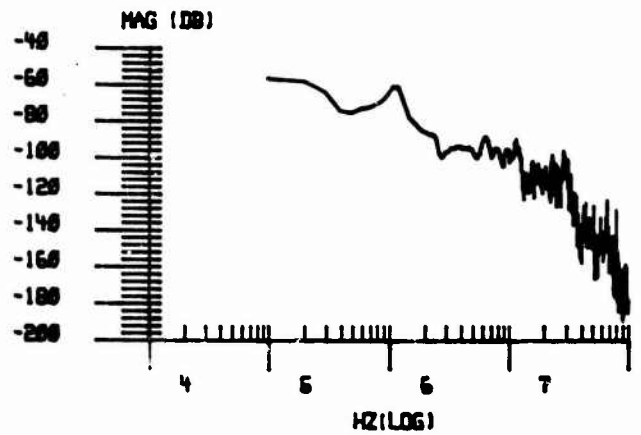

D.

Log Log Polar Plot of Corrected Fast Fourier Transform of (A)

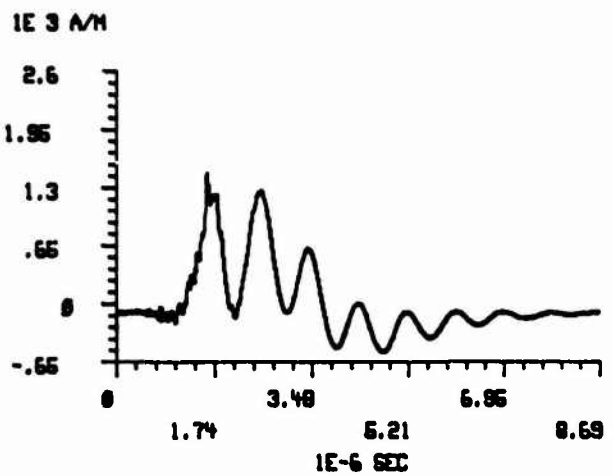

E.

Inverse Transform of (D) to Produce Integrated, Corrected Multi-Gap Loop Sensor Output

Figure 7. Illustration of Technique Used to Correct Data for Nonlinearity in Measurement Systems

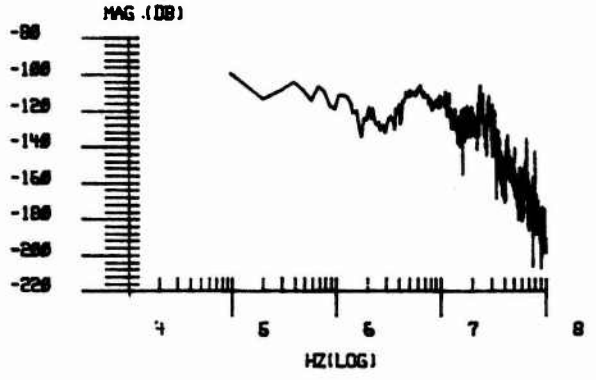

A.

Fast Fourier Transform of Sensor Response on Forward Fuselage

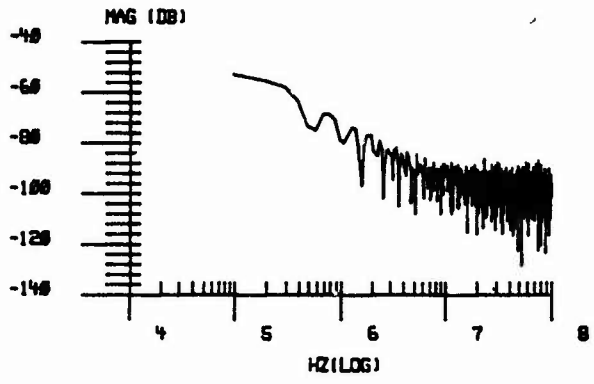

B.

Fast Fourier Transform of Current Source

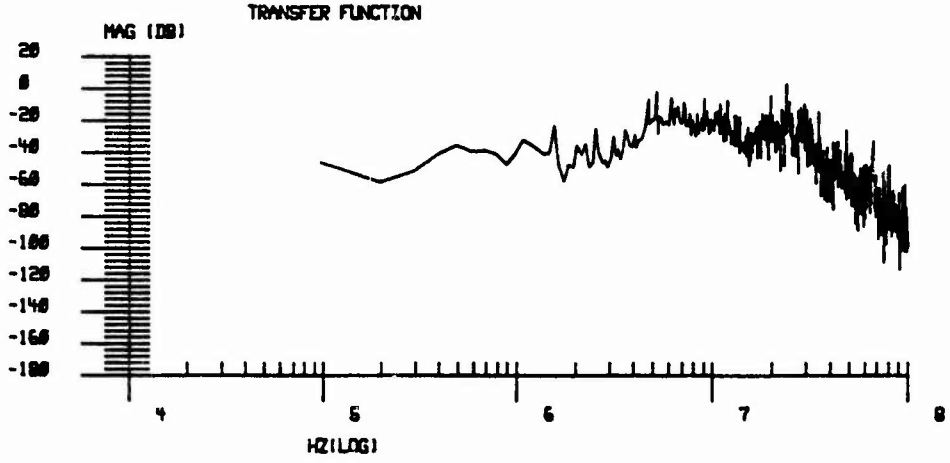

C. Log-Log Polar Plot of Transfer Function - $R(\omega)/S(\omega)$

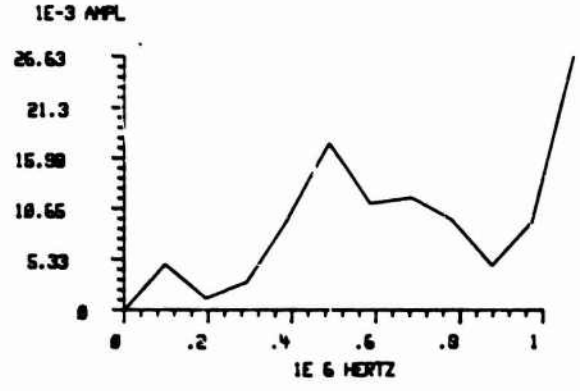

D.

Linear Plot of Transfer Function 0-1 MHz

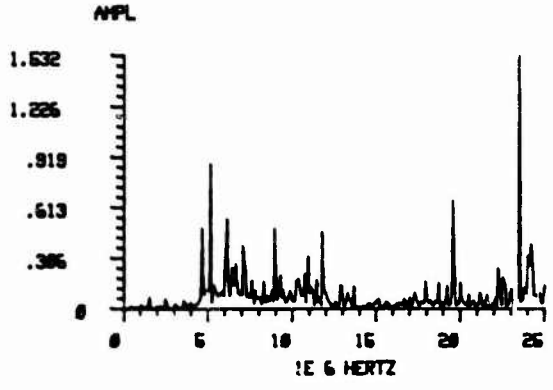

E.

Linear Plot of Transfer Function 0-25 MHz

Figure 8. Transfer Function at the Forward Surface Current Sensor Location - Strike to Right Wing

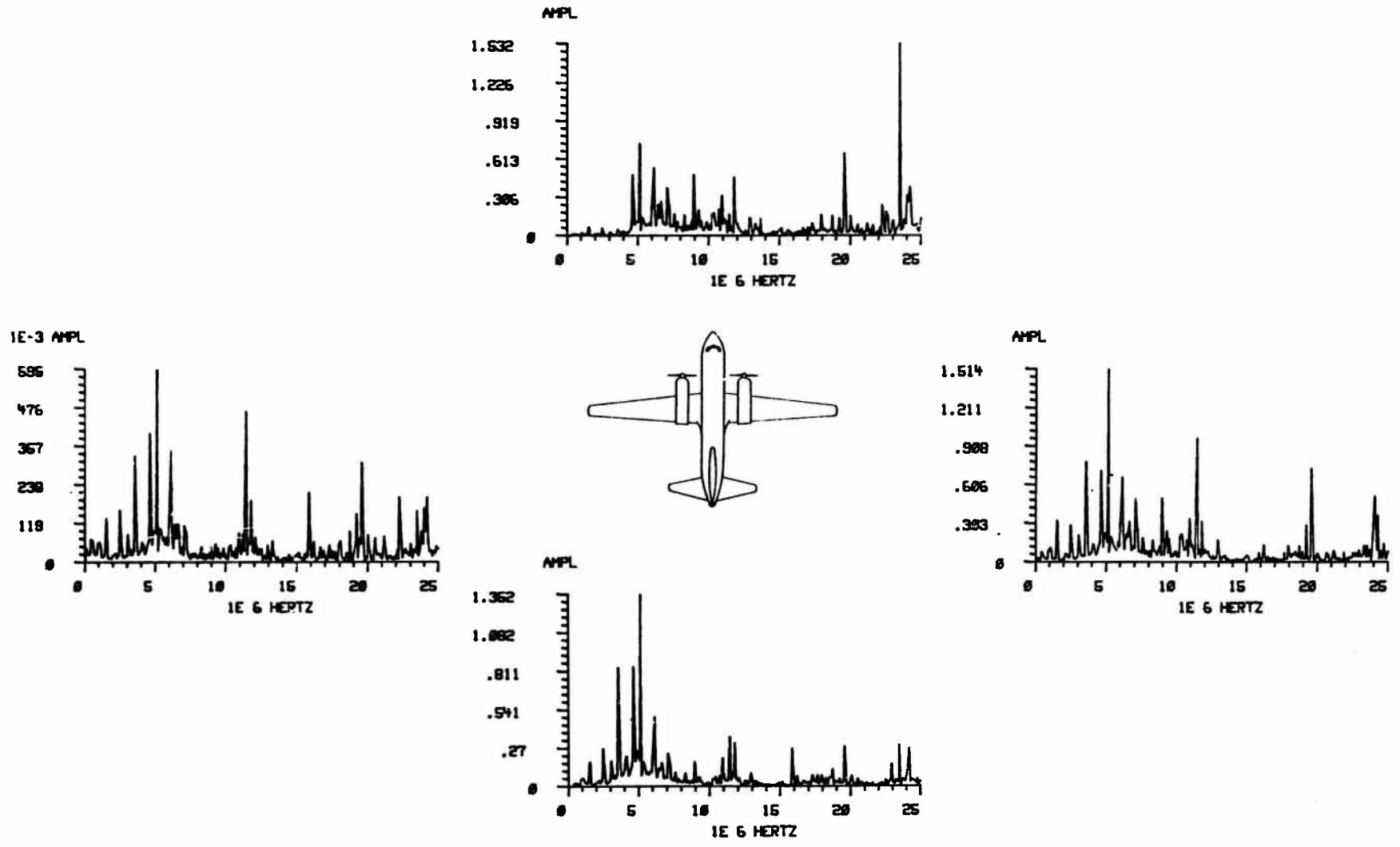

Figure 9. Aircraft Transfer Functions at the Four Surface Current Sensor Locations - Strike to Right Wing

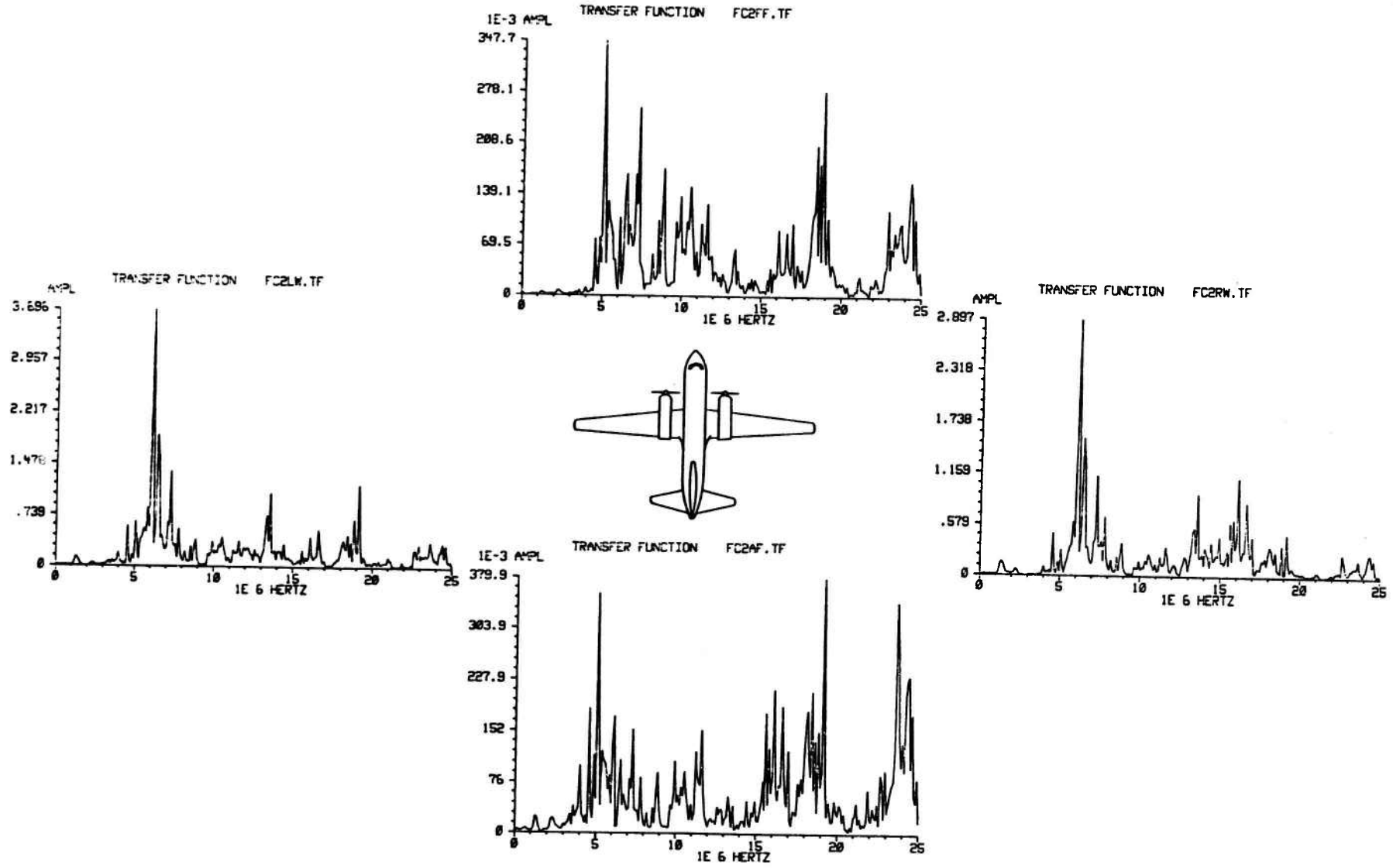

Figure 10. Aircraft Transfer Functions at the Four Surface Current Sensor Locations - Ground Test with Fast Rise Time Generator and Coaxial Return Path - Wing to Wing Configuration

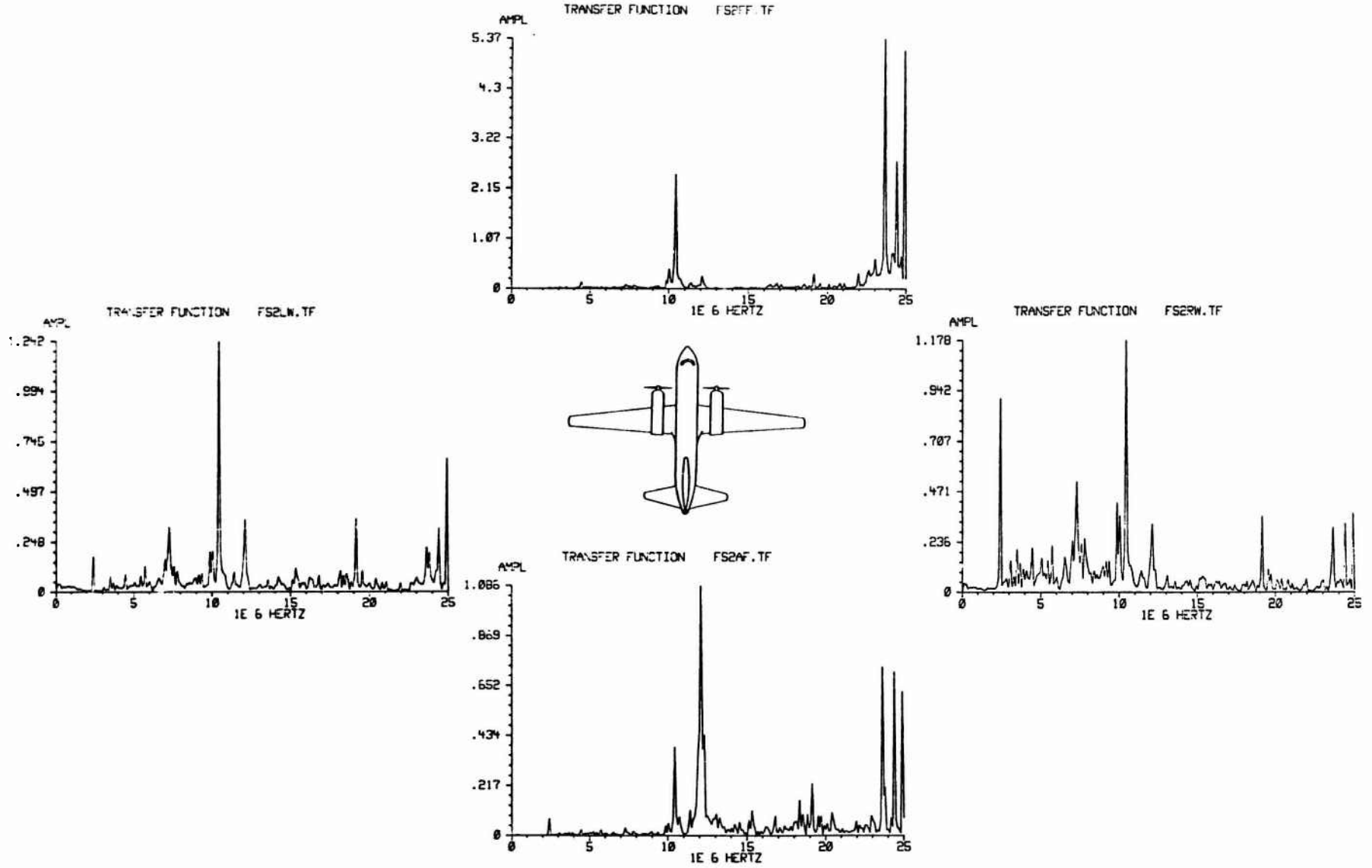

Figure 11. Aircraft Transfer Functions at the Four Surface Current Sensor Locations - Ground Test with Fast Rise Time Generator and Flat Plate Return Path - Wing to Wing Configuration

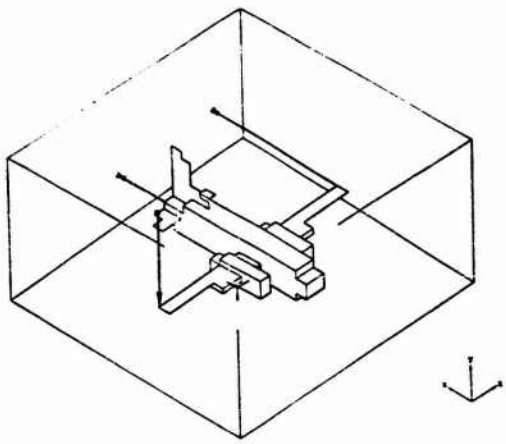

A.

T3DFD Code Model of the CV580 Aircraft

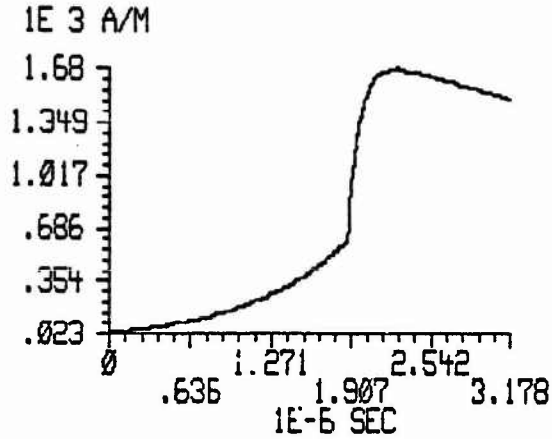

B.

Source Waveform for T3DFD Code Application

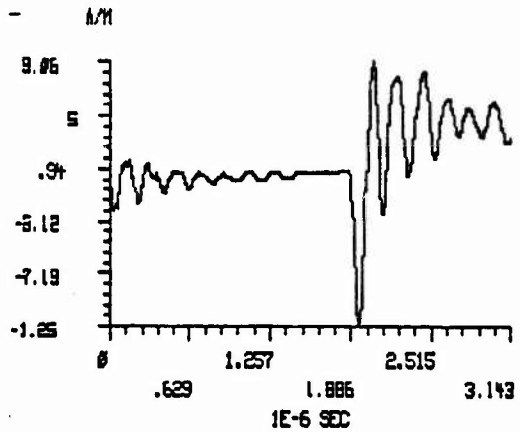

C.

Response at the Forward Fuselage Surface Current Sensor to the Source in 12B

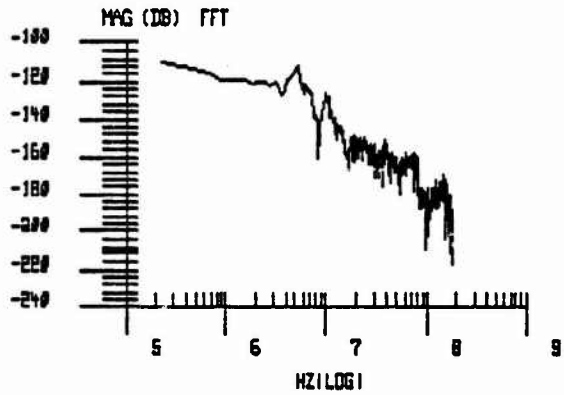

D.

FFT of Response in 12C

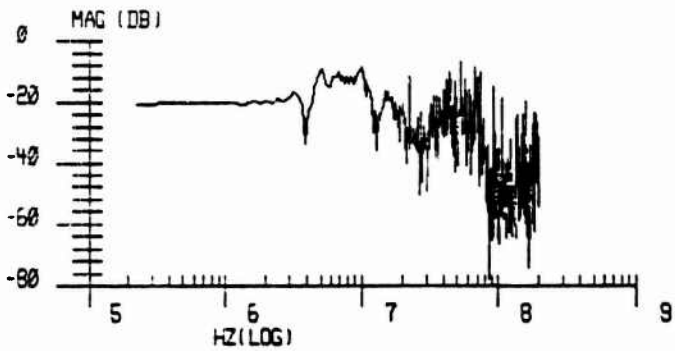

E.

Log-Log Plot of Transfer Function When Response in 12C is Divided by Source in 12B

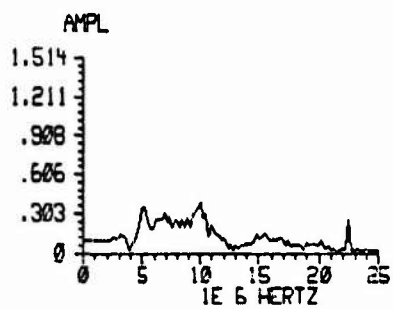

F.

Linear Plot of 12E from 97 kHz to 25 MHz

Figure 12. Prediction of the Aircraft Transfer Function at the Forward Fuselage Current Sensor Using the T3DFD Electromagnetic Code

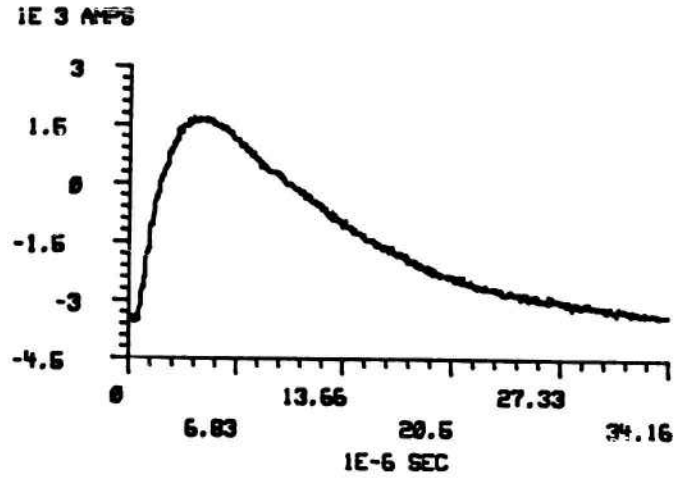

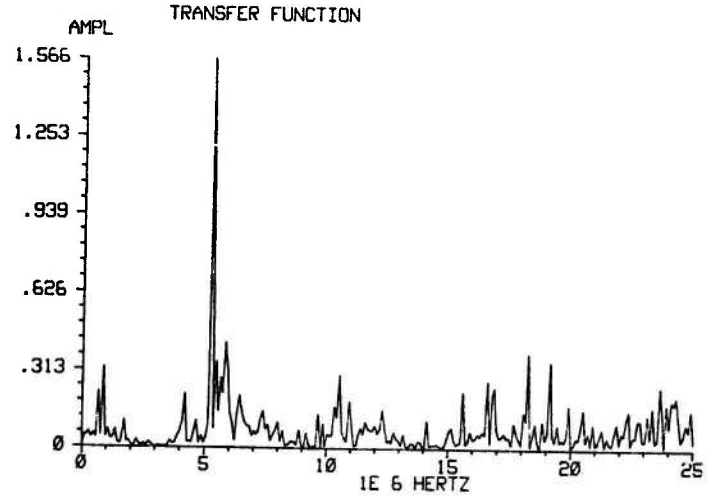

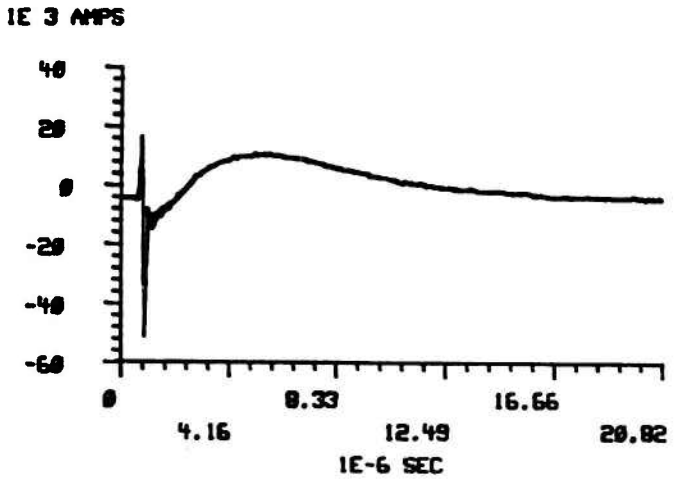

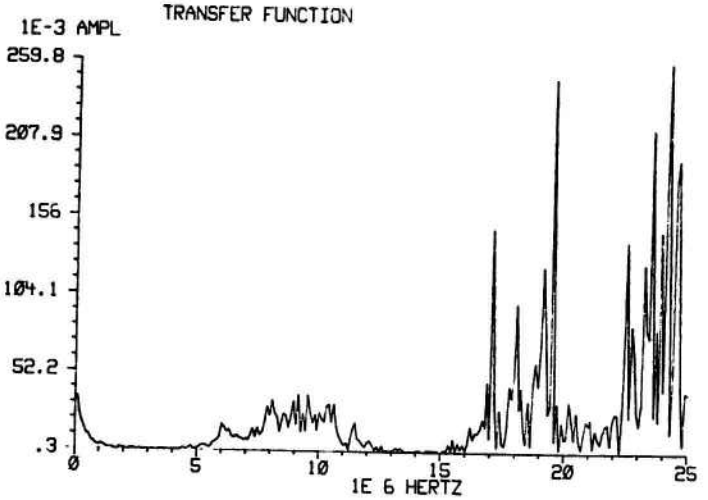

Figure 13. Injected Current Waveforms (A) and Aircraft Transfer Functions at the Left Wing Surface Current Sensor (B) for the Pulse Simulation Unit with a Coaxial Return Path (Top) or a Flat Plate Return Path (Bottom)

JOINT THUNDERSTORM OPERATIONS USING THE NASA F-106B AND FAATC/AFWAL CONVAIR 580 AIRPLANES

Bruce D. Fisher and Philip W. Brown
NASA Langley Research Center
Lt. Col. Alfred J. Wunschel, Jr.
Air Force Systems Command
1Lt. Harold D. Burket
Air Force Wright Aeronautical Laboratories
Jesse S. Terry
FAA Technical Center

ABSTRACT

During the 1985 thunderstorm season, three joint thunderstorm research flights were conducted within 100 n.mi. of NASA Langley Research Center by the NASA Storm Hazards F-106B and the FAA/USAF CV-580 research airplanes with ground-based weather radar measurements by the NASA Wallops Flight Facility. This paper discusses the thunderstorm penetration capabilities of each airplane and the techniques used to safely place the two airplanes into the same thunderstorm cell for collection of correlated electromagnetic data. It is concluded that joint thunderstorm research operations of two aircraft with significantly dissimilar thunderstorm penetration capabilities are counterproductive to both airplanes in terms of gathering electromagnetic data while maintaining range safety.

INTRODUCTION

The NASA LANGLEY RESEARCH CENTER Storm Hazards Program and the FAA/U.S. Air Force Low Altitude Lightning Characterization Program conducted joint thunderstorm research operations in the vicinity of the NASA Wallops Flight Facility in Virginia during the 1985 thunderstorm season. The NASA Storm Hazards Program was in the sixth season of using an F-106B fighter-type aircraft to penetrate thunderstorms in Oklahoma and Virginia in order to gather direct lightning strike data at altitudes from 5000 ft to 50 000 ft (1)*. The second research aircraft was a Convair 580 transport-type aircraft owned and operated by the FAA Technical Center (FAATC) with lightning instrumentation and research personnel provided by the Air Force Wright Aeronautical Laboratories (AFWAL). The CV-580 airplane was in the second year of a program to characterize low altitude lightning strikes to aircraft in which penetrations of Florida thunderstorms were made at altitudes between 2000 ft and 20 000 ft (2 and 3). The program objectives of the joint missions were to: a) investigate aircraft lightning strikes at low altitudes and during different stages of storm development; b) investigate the effect of aircraft size and shape factor on the probability of direct strikes to aircraft in the same environmental conditions; c) compare the probability of direct strikes for different altitude regions of the same storm; and, d) measure electromagnetic waveforms of common lightning events from two airplanes.

At the conclusion of the 1985 Florida research season with the CV-580 airplane, one practice flight and three joint thunderstorm flights were made by the two airplanes in conjunction with ground-based support from NASA Wallops. The NASA F-106B airplane experienced four direct lightning strikes and the FAATC/AFWAL CV-580 airplane experienced two strikes during these flights. Unfortunately, the six strikes were not correlated with events on the other airplane. It was concluded that joint thunderstorm research operations of two aircraft with significantly dissimilar thunderstorm penetration capabilities are counterproductive to both airplanes in terms of gathering electromagnetic data while maintaining range safety. The purpose of this paper is to summarize the operational procedures that were developed for conducting coordinated thunderstorm operations and to describe the difficulties of implementing these procedures. The discussion includes a comparison of airborne and ground-based weather radar data from one penetration in which the F-106B airplane overflew the CV-580 airplane.

TEST EQUIPMENT

F-106B RESEARCH AIRPLANE - The NASA Storm Hazards Program utilized a specially-instrumented and lightning-hardened F-106B "Delta Dart" airplane (Fig. 1) to make thunderstorm penetrations (1). Prior to each thunderstorm season, the lightning hardening procedures (1 and 4) were verified during ground tests (1 and 4) at NASA Langley. The onboard data systems included instrumentation to record the electromagnetic waveforms from direct lightning strikes and nearby lightning flashes (1 and 5), and several photographic systems for documenting the locations of the lightning attachments to the airplane (1, 6, and 7). The airplane altitude, Mach number, attitude angles, ambient temperature, and other flight conditions were measured by the Aircraft Instrumentation System (AIS) and an Inertial Navigation System (INS) (8). The parameters from the AIS and INS were telemetered in real time to receiving sites at NASA Langley and NASA Wallops by a pair of L-band telemetry transmitters installed on the F-106B. No additional instrumentation, flight systems or lightning hardening procedures were required for the joint flight operations with the CV-580 airplane.

CV-580 RESEARCH AIRPLANE - A Convair CV-580 transport aircraft (Fig. 2) was instrumented to make lightning strike measurements in and near Florida thunderstorms at altitudes below 20 000 ft (2, 3 and 9). As was the case with the F-106B airplane, the CV-580 airplane was lightning-hardened (2), and these procedures were verified during extensive lightning simulation tests at Wright-Patterson AFB, Ohio (10). The onboard data systems were similar to those installed on the F-106B, including instrumentation for lightning characterization (2, 3 and 11), field measurements (2, 3 and 11), turbulence measurements, and a four camera video monitoring system for documenting lightning attachment patterns. For the joint operations with the F-106B airplane, NASA Langley loaned the FAATC the L-band telemetry hardware and data interface cards necessary to transmit the CV-580 position information from its onboard Inertial Navigation System (INS) to the NASA Wallops Main Base Telemetry Station.

THUNDERSTORM PENETRATION CAPABILITIES OF THE TWO AIRPLANES - The thunderstorm penetration capabilities of the F-106B and CV-580 airplanes are summarized in Table 1. The lightning hardening provisions were taken to better insure that the aircraft could withstand the effects of a full threat cloud-to-ground strike with a peak current amplitude of 200 kA (12). The g-limits are those of the basic aircraft, with the limits for the F-106B airplane being higher than those for the CV-580 airplane, because the former was designed as a fighter while the CV-580 airplane was designed as a transport. The precipitation reflectivity limits were set by the researchers to keep the aircraft out of thunderstorm regions in which there was damaging precipitation. The NASA Storm Hazards researchers chose a limiting value of 50 dBZ, as values of this magnitude usually indicated the presence of damaging hail. The FAA and U.S. Air Force researchers chose a lower limiting value of 35 dBZ in order to avoid areas of moderate rain rate, which could cause excessive erosion to the radome on the CV-580 airplane. The penetration speeds of 300 knots indicated airspeed (KIAS) for the F-106B airplane and 185 KIAS for the CV-580 airplane were the best gust penetration speeds given in the handbooks for each airplane. The altitude limits for the F-106B airplane were 5000-50 000 ft; corresponding limits for the CV-580 airplane were 2000-20 000 ft. The upper altitude limits for both airplanes were just below the service ceilings of the airplanes. The lower altitude limits were selected to insure an adequate margin of safety considering each airplane's respective performance.

*Numbers in parentheses designate References at end of paper.

GROUND-BASED SYSTEMS AT NASA WALLOPS FLIGHT FACILITY - Instrumentation from the Atmospheric Sciences Research Facility at NASA Wallops (1 and 13) was used to provide guidance to the flight crews of the two aircraft during the joint thunderstorm penetration missions. The facility included the following:

- O Two C-band tracking radars, which tracked the C-band beacons mounted on the airplanes.
- O S-band radar (SPANDAR), which monitored the precipitation reflectivity of the storms.
- D UHF-band radar, which obtained the range, elevation and azimuth angle of echoes from lightning channels.
- D Cloud-to-ground lightning mapping system for mapping the geographical locations of cloud-to-ground lightning strikes.
- D Telemetry receivers for receiving the INS position data from the CV-580 airplane and the AIS and INS data from the F-106B airplane.

SPANDAR and the UHF-band radar conducted horizontal and vertical scans of the storm cell(s) of interest before and after each penetration. During the actual penetration, the SPANDAR made horizontal scans at the altitude of the CV-580 airplane to provide range safety information, while the UHF-band radar was "slaved" to the CV-580 airplane position via inputs from the C-band tracking radar which was dedicated to that airplane. Photographs of the NASA Wallops radars are shown in Fig. 3.

NASA LANGLEY FLIGHT SERVICE STATION - As was the case for operations with the F-106B airplane alone (1 and 6), the primary responsibility to launch and recall the two airplanes, select the storms and altitudes of interest, and provide real-time flight support and guidance to the aircrews was carried out by the Storm Hazards project personnel located in the NASA Langley Flight Service Station. The real-time interfaces with the NASA Wallops personnel were also the same as for the F-106B missions (1).

The equipment installed at NASA Langley to support the joint mission was nearly identical to that described in (6), and included communications systems, lightning detection systems, time displays, and an integrated video display which tied much of these data together. The equipment is listed in Table 2, which includes a key for locating these systems in Fig. 4(a), which is a photograph of the NASA Langley control room. The integrated video display system, Table 2 and Fig. 4(b), superimposed the following data onto a single display: color-coded precipitation reflectivity factor and geopolitical maps from three National Weather Service (NWS) S-band weather radar sites; cloud-to-ground lightning locations from the NASA/SUNY-Albany cloud-to-ground lightning mapping system (13); and, the ground track from the F-106B airplane and discrete digital read-outs of several key flight parameters which were telemetered to the ground from the airplane. A simulated example of the integrated display is shown in Fig. 4(b). During joint operations with the CV-580 airplane, the cloud-to-ground lightning locations were not displayed, and the CV-580 airplane position from its onboard INS was substituted. The position update rates were 2 sec and 30 sec for the F-106B and CV-580 airplanes, respectively. The CV-580 data were transmitted over telephone lines from the NASA Wallops telemetry receiver site. Although some solo F-106B flights were made without NASA Wallops support, all joint flight operations were made with both NASA Langley and NASA Wallops real-time support.

A map of the joint test area is shown in Fig. 5. The three NWS weather radar sites used by the integrated video display were located at Patuxent River, MD (NHK), Volens, VA (VQN) and Cape Hatteras, NC (HAT). The three direction finder sites for the cloud-to-ground lightning mapping system were located at NASA Wallops, NASA Langley, and Charlottesville, VA (CHO). The home base for the CV-580 airplane was the FAA Technical Center (FAATC) at Atlantic City Airport, NJ (ACY).

JOINT OPERATIONS PROCEDURES

A schematic showing the flight procedure used to safely place the F-106B and CV-580 airplanes into the same thunderstorm cell for collection of correlated electromagnetic data is given in Fig. 6. Basically, the procedure was an asynchronous, coordinated orbit along a radial to SPANDAR at NASA Wallops, intending to put both aircraft in the storm at the same time, over the same geographical point, separated by a safe altitude margin. The basic guidelines used were as follows:

1) Each airplane was tracked independently at NASA Wallops by C-band tracking radars; both ground tracks were plotted in real time on a plot board in the SPANDAR control room.
2) Each airplane was tracked in real time in the project control room at NASA Langley on the integrated video display, which received INS position data from the two airplanes via telemetry.
3) The F-106B airplane flew at the altitude of the lower flash density center (14), as determined by the UHF-band radar, in hopes of triggering a lightning strike which would be detected by the instrumentation onboard the CV-580 airplane, or would actually strike the CV-580 airplane.
4) The CV-580 airplane flew at an altitude lower than that of the F-106B airplane, with a minimum separation between the two airplanes of 4000 ft. The 4000 ft minimum altitude separation was selected to insure adequate separation of the two airplanes during the altitude excursions that would likely be experienced in thunderstorms. The minimum penetration altitude for the CV-580 airplane was set at 20DD ft.
5) The NASA Wallops SPANDAR was used to define "safe" zones for the CV-580 airplane, in which the peak precipitation reflectivity values were less than 35 dBZ. The SPANDAR data were supplemented with the data from the onboard X-band radar installed on the flight deck of the CV-580 airplane.
6) The crew of the F-106B airplane avoided thunderstorm areas where the precipitation reflectivity values exceeded 50 dBZ by using the data from their onboard X-band weather radar and

the data from the NASA Wallops SPANDAR, even though the latter data were taken at a lower altitude than that of the F-106B airplane.

7) The NASA Wallops UHF-band radar was "slaved" to the CV-580 airplane position via inputs from the C-band tracking radar which was tracking the CV-580 airplane.
8) Both airplanes, SPANDAR and the control room at NASA Langley were on the same VHF radio frequency.
9) Holding areas on each side of the storm and escape headings were chosen by the pilots with concurrence by the personnel at SPANDAR and NASA Langley prior to each penetration.
10) Because neither aircraft had any cockpit display of the other airplane's position (such as radar beacon information), ranges and bearings from radio navigation aids, INS fixes, and time-to-go to the storm, were verbally passed between the CV-580 and F-106B flight crews.
11) The F-106B airplane, because of its speed and maneuverability, was responsible for adjusting the relative positions of the two airplanes.
12) From the practice mission, it was determined that the additional communications required to provide the CV-580 airplane with the proper head start to the target point in the storm on each coordinated, synchronous penetration interfered with the passing of safety information from the ground to the airplanes. Also, it was determined that if the orbits of the two airplanes were asynchronous, but on the same radial, that both airplanes, in fact, spent a good deal of time in the storm at the same time, although going opposite directions at times. Therefore, asynchronous penetrations were used, with the F-106B pilots minimizing the time spent outside the storm, thereby eliminating the holding patterns for the F-106B airplane in most instances.

RESULTS OF JOINT OPERATIONS

Following the flight test operations with the CV-580 airplane in Florida in 1985, the airplane returned to Atlantic City, NJ to conduct joint thunderstorm research operations with the NASA F-106B airplane as part of the NASA Storm Hazards '85 Program (1). Joint missions were conducted in three thunderstorms which occurred within 100 n.mi. of NASA Wallops. The locations of these storms are shown on the map in Fig. 5, along with the location of each airplane at the time of each direct strike. As can be seen in Fig. 5 and in Table 3, which is a summary of the joint operations, there were four direct strikes to the F-106B airplane and two direct strikes to the CV-580 airplane. None of these strikes were correlated with events on the other airplane. The lack of correlated electromagnetic data reflected the difficulty experienced in coordinating the operations of the two airplanes.

A typical example of the problems encountered in conducting joint operations was flight 85-041 (see Fig. 5 and Table 3), in which the F-106B airplane made 12 penetrations totalling 31.4 mins, while the CV-580 airplane accumulated 76 mins of "penetration" time. On only three occasions were the two airplanes able to simultaneously cross the same geographical point at the same time. On the third occasion, at 21:17 GMT, both airplanes were heading north as the F-106B airplane overtook and overflew the CV-580 airplane from the south. Photographs of the ground-based weather radar displays at NASA Langley and NASA Wallops for this penetration are shown in Figs. 7 and 8, respectively. The integrated video display at NASA Langley, Fig. 7, was photographed at 21:17 GMT; the precipitation data were transmitted from the NWS radar at Patuxent River, MD at 21:15 GMT. The radar was sampling the storm at an altitude of 3100 ft in the vicinity of the two airplanes (40 n.mi. range at a tilt angle of 0.4 deg.). The airplane ground tracks have been enhanced and the discrete status data from the F-106B airplane have been removed for clarity. For comparison purposes, the airplane ground tracks have been graphically superimposed on the SPANDAR photograph, Fig. 8, which was taken at 21:16:24 GMT. The SPANDAR tilt angle was set so that the radar would sample the storm at the nominal CV-580 penetration altitude of 14 000 ft (1.5 deg. at 120 n.mi.). Comparing Figs. 7 and 8, it can be seen that there are significant differences in the appearances of the same storm on the two displays. These differences are due to the difference in altitudes at which the radars were sampling. However, both displays showed extensive areas where the precipitation reflectivity values exceeded 35 dBZ, the maximum permissible level for the CV-580 airplane. These areas also were seen on the airborne weather radar display in the CV-580 cockpit (not shown), and the pilot of that airplane turned to the northeast to avoid those areas. This turn caused the paths of the two airplanes to diverge, since the F-106B airplane was able to proceed into areas of heavier precipitation (see Table 3).

A photograph of the airborne weather radar display in the F-106B cockpit is shown in Fig. 9. This photograph was taken at 21:15:47 GMT while the F-106B airplane was approximately 5 n.mi. away from the leading edge of the 30 dBZ contour. The position and heading of the F-106B airplane at the time of this photograph are indicated in Fig. 8. A small area with a precipitation reflectivity value of 50 dBZ or greater is visible in the center of the storm cell; as the airplane penetrated further, this area became larger, and the airplane flew through an area of small hail. No storm areas with precipitation reflectivity values of 50 dBZ or greater are visible in the vicinity of the F-106B airplane in Figs. 7 and 8. The differences in storm appearance on the three radar displays are caused by the following: differences in radar sampling altitude; actual differences in storm characteristics between the sampling altitudes of the ground-based radars and the F-106B penetration altitude; loss of detail in the two ground-based radar displays because of the large size of the radar sample volumes of these radars (sample volume, in turn, is a function of radar beam width, pulse width and range to the target); and, the attenuation of the X-band weather radar in the F-106B airplane. (The ground-based S-band radars - SPANDAR and the NWS radars - are not subject to attenuation.) The true extent of the 50 dBZ core

in the storm cell shown in Fig. 9 was masked by the intervening rainfall between the core and the airborne radar, with the true extent and intensity of the core only becoming apparent as the airplane penetrated further into the storm and approached the core. The different appearances of the same storm on different radars (both real and apparent) made it difficult to provide precise guidance information from the ground to the airplanes, and contributed to the divergence problem in the joint operations.

The differences in penetration capabilities of the two airplanes were major factors in the divergence problem. The effect of the lower precipitation reflectivity limit for the CV-580 airplane has already been discussed. Although turbulence was not a factor in the penetration shown in Figs. 7-9, the difference in gust load limits between the two airplanes (see Table 3) was also important. For example, in Florida the CV-580 crew typically avoided the south and west sides of afternoon thunderstorms because of the likely occurrence of turbulence. (In Florida thunderstorms, hail was not a frequent hazard.) On the other hand, the F-106B personnel flew on the south and west sides of the thunderstorms in order to be upwind of the hail, which was frequently present in the Virginia storms.

The final factor which complicated the conduct of joint operations was the need to coordinate the flight operations with normal air traffic through the air traffic control (ATC) system. On flights 85-041 and 85-043, the airplanes were handled in the standard ATC fashion, with each airplane in communication with the controller for that altitude. On these two flights, the pilots had to communicate with each other and the personnel at NASA Langley and NASA Wallops on the VHF radio, and to their respective controllers on the UHF radios in order to coordinate the optimum path for data, flight safety and air traffic control. In one mission, however (flight 85-042, see Fig. 5), both research airplanes were able to transit the storm simultaneously with frequent crossings over the same geographical point. During this one flight, the pilots were permitted a great deal of freedom in selecting altitudes and radial headings to SPANDAR since they were operating with a single air traffic controller in an offshore military warning area in which there were no other aircraft. Unfortunately, the storm was weak and decaying by the time both airplanes could be cleared into the area, and neither airplane was struck.

In summary, the two airplanes used in these joint thunderstorm operations frequently diverged because of the following four reasons: the differences in storm environments between the two airplane penetration altitudes; the real and apparent differences in the appearance of the storm on the different radar displays; the dissimilar penetration capabilities of the two vehicles; and, the air traffic control coordination problem. The divergence of the two airplanes' paths, in turn, led to four adverse circumstances. First, the divergence of the paths minimized the chances of making common airborne measurements because of the large distances between the two airplanes. Second, there was a loss of ground-based range safety coverage because the NASA Wallops radars were trained on the airplane with the lower penetration capabilities (the CV-580) and were not able to survey the altitude/area being penetrated by the F-106B airplane. This left the F-106B to make penetrations using its own onboard X-band radar, which was subject to attenuation. Third, since the NASA Wallops radars were dedicated to the CV-580 airplane, there was a loss of correlated ground-based science measurements for the airborne measurements on the F-106B airplane. Finally, there was a potential for placing one or both airplanes in unproductive or even dangerous thunderstorm areas.

Operationally, the pilots felt that both airplanes could be operated in the same storm at the same time only when the storm's strength was less than the lower of the two maximum precipitation reflectivity limits. This limitation on storm strength, coupled with the proven low strike rates at low altitudes (1 and 9), and the F-106B airplane's relatively limited low-altitude station time (45 mins), resulted in a very low probability of making common electromagnetic measurements. Therefore, it is concluded that coordinated thunderstorm research operations of two airplanes with significantly dissimilar thunderstorm penetration capabilities are counterproductive to both airplanes in terms of gathering electromagnetic data while maintaining range safety.

SUMMARY OF RESULTS

During the 1985 thunderstorm season, three joint thunderstorm flights were conducted with the NASA F-106B and the FAA/USAF CV-580 airplanes. The results of these flights were:

1. The F-106B and CV-580 airplanes experienced four and two strikes, respectively. These strikes were not correlated with lightning events on the other airplane.
2. Although operational techniques were developed for safely placing both airplanes in a thunderstorm at the same time, it was concluded that coordinated thunderstorm research operations of two airplanes with significantly different thunderstorm penetration capabilities were counterproductive to both airplanes in terms of gathering electromagnetic data while maintaining range safety.

ACKNOWLEDGEMENTS

The authors would like to acknowledge the contributions of Mr. Norman L. Crabill, the Storm Hazards Program Manager; Dr. John C. Gerlach and the staff of the Atmospheric Sciences Research Facility at NASA Wallops; and, the other crew members who flew onboard the two airplanes.

REFERENCES

1. Bruce D. Fisher, Philip W. Brown, and J. Anderson Plumer, "Summary of NASA Storm Hazards Lightning Research, 1980-1985." Presented at International Conference on Lightning and Static Elec., Dayton, OH, June 1986.

2. Maj. Pedro L. Rustan, Brian P. Kuhlman, ILt. Harold D. Burket, Jean Reazer, and Arturo Serrano, "Low Altitude Lightning Attachment to an Aircraft." AFWAL - TR-86-3009, in publication.

3. Harold D. Burket, "Comparison of Electromagnetic Measurements of an Aircraft from Direct Lightning Attachment and Simulated Nuclear

Electromagnetic Pulse." Presented at International Conference on Lightning and Static Electricity, Dayton, OH, June 1986.

4. Bruce D. Fisher, Gerald L. Keyser, Jr., Perry L. Dea`, Mitchel E. Thomas, and Felix L. Pitts, "Storm Hazards '79 - F-106B Operations Summary." NASA TM-81779, March 1980.

5. Mitchel E. Thomas, "Direct Strike Lightning Measurement System." AIAA-81-2513, November 1981.

6. Bruce D. Fisher, Philip W. Brown, and J. Anderson Plumer, "NASA Storm Hazards Lighting Research." Proceedings, Flight Safety Foundation, 30th Corporate Aviation Safety Seminar, Dallas/Ft. Worth Airport, TX, April 1985, pp. 117-155.

7. Philip W. Brown, "Development of and Results From Camera Systems for Recording Daytime Lightning Strikes to an Airplane in Flight." AIAA-86-0020, January 1986.

8. Jimmy W. Usry, R. Earl Dunham, Jr., and Jean T. Lee, "Comparison of Wind Velocity in Thunderstorms Determined from Measurements by a Ground-Based Doppler Radar and a F-106B Airplane." NASA TM-86348, April 1985.

9. P. L. Rustan, Jr., and J. L. Hebert, "Lightning Measurements on an Aircraft at Low Altitude." Preprints, Second International Conference on the Aviation Weather System, Montreal, Canada, June 1985, pp. 220-225.

10. L. C. Walko, and Lt. J. L. Hebert, "Lighting Simulation Tests on FAA CV-58D Lightning Research Aircraft." Proceedings, 10th International Aerospace and Ground Conference on Lightning and Static Electricity, Paris, France, June 1985, pp. 137-147.

11. P. L. Rustan, Jr., B. P. Kuhlman, and J. M. Reazer, "Airborne and Ground Electromagnetic Field Measurements of Lightning." Proceedings, 10th International Aerospace and Ground Conference on Lightning and Static Electricity, Paris, France, June 1985, pp. 253-258.

12. "Protection of Aircraft Fuel Systems Against Lightning." AC No. 20-53A, FAA, April 1985.

13. John C. Gerlach, and Robert E. Carr, "Wallops Severe Storms Measurement Capability." Preprint Vol. - 5th Symposium on Meteorological Obs. and Instrumentation, Toronto, Canada, April 1983. American Meteorological Society and Canadian Meteorological and Oceanographic Society, pp. 449-453.

14. Vladislav Mazur, John C. Gerlach, and W. David Rust, "Lightning Flash Density Versus Altitude and Storm Structure from Observations with UHF and S-Band Radars." Geophysical Research Letters, Vol. 11, No. 1, January 1984, pp. 61-64.

Table 1 - Thunderstorm penetration capabilities of the F-106B AND CV-580 airplanes

Criteria	F-106B	CV-580
Peak current, kA	200	200
Gust limits, g	6 to -2.4	3.24 to -1.24
Precipitation reflectivity limits, dBZ	50	35
Penetration speed, KIAS	300	185
Altitude limits, kft	5 to 50	2 to 20
Nominal low-altitude station time, min.	45	120

Table 2 - Equipment at NASA Langley for real-time Storm Hazards flight support

Key to Figure 4	Equipment
	o Communications
A	- VHF radio - Conversations with both aircrews
B	- UHF radio - Transmissions to Air Traffic Controllers from F-106B
C	- Dedicated land line to Wallops - Conversations with Wallops researchers
D	- Voice via telemetry - All VHF and UHF radio transmissions and receptions onboard F-106B
	o Lightning
E	- Cloud-to-ground lightning mapping system remote display processor and plotter - Cloud-to-ground lightning strike locations
F	- Stormscope - Azimuth and range to lightning discharges
G	- Strip chart recorder - Real-time output of onboard field mill system via telemetry
	o Time
H	- Greenwich Mean Time display
I	- Elapsed time display
	o Satellite Imagery
J	- GOES satellite receiver - Visual and infrared images of mid-Atlantic states

Table 2 - Equipment at NASA Langley for real-time Storm Hazards flight support, concluded

Key to Figure 4	Equipment
	o F-106B Airplane Status
K	- DLite trigger lights panel - Status of DLite digitizers; transmitted via telemetry
L	- Computer terminal CRT display - Airplane position, altitude, temperature, airspeed, heading, and trigger status; raw data transmitted via telemetry and then converted to engineering units by ground-based microcomputer
	o Integrated Displays
M	- Plot board - Preprinted map with operating areas and Air Traffic Control areas; airplane position and storm locations manually superimposed during the flight
	o Integrated Video Display
N	- Color-coded precipitation reflectivity factor and geopolitical maps via dedicated phone numbers (Patuxent River, MD; Volens, VA; Cape Hatteras, NC) or dial-up numbers at National Weather Service radar sites
O	- F-106B airplane position from onboard INS; transmitted via telemetry
P	- Digital displays of F-106B airplane magnetic heading, pressure altitude, ambient temperature and fuel state (pounds remaining) from onboard AIS; transmitted via telemetry
Q	- Cloud-to-ground lightning locations from cloud-to-ground lightning mapping network/or CV-580 position from onboard INS; relayed to Langley from Wallops telemetry site
R	- Video cassette recorder
S	- VHF radio uplink of integrated display to F-106B

Table 3 - Summary of joint operations

NASA Flight No. 85-	Date	Location	Strikes		Penetration Time, mins (Penetrations)		Nominal Altitudes, kft	
			F-106B	CV-580	F-106B	CV-580	F-106B	CV-580
040	Aug. 30	Easton, MD	2	2	32.2 (16)	66 (a)	19	10,14
041	Sept. 9	Bay Bridge, MD	2	0	31.4 (12)	76 (a)	19	14
042	Sept. 10	Dam Neck, VA	0	0	6.0 (12)	51 (a)	17,19,21	14

NOTE = (a) No count of penetrations are made for the CV-580, since many passes are made on the fringe of the storm or beneath the storm

Fig. 1 - NASA Langley Research Center F-106B research airplane

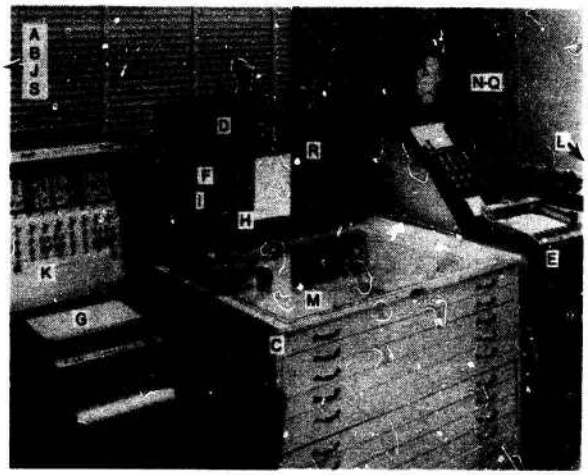

(a) Overview of the control room

Fig. 4 - Storm Hazards mission control room at NASA Langley

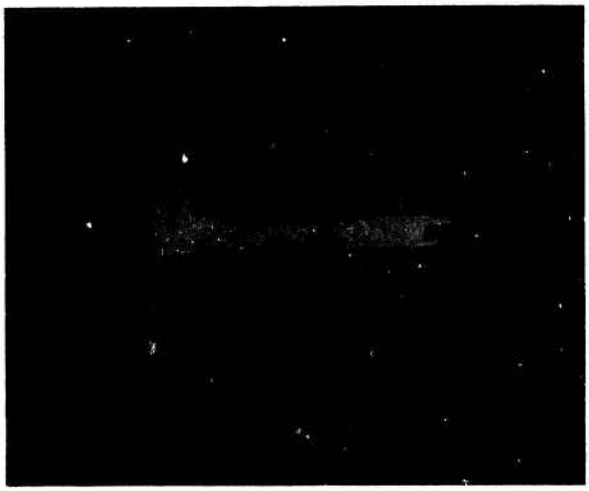

Fig. 2 - FAATC/AFWAL CV-580 lightning research airplane

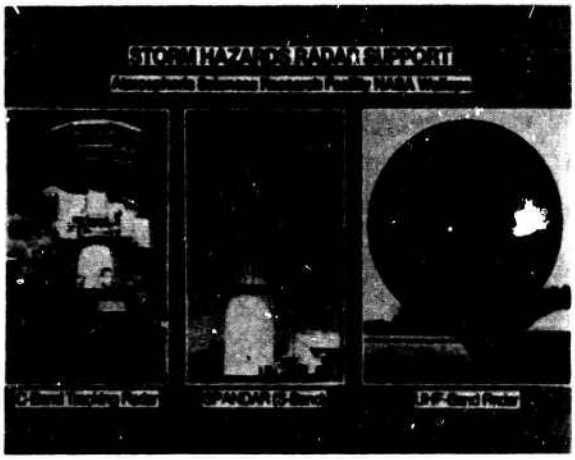

Fig. 3 - Storm Hazards radar support at NASA Wallops

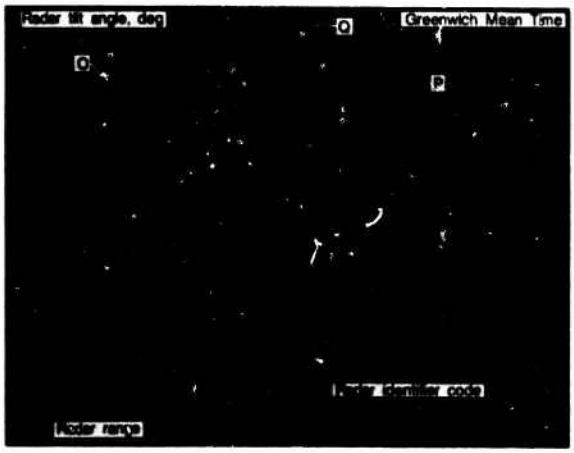

(b) Detail of integrated video display. Simulated data have been superimposed on weather radar data from Cape Hatteras, NC

Fig. 4 - Concluded

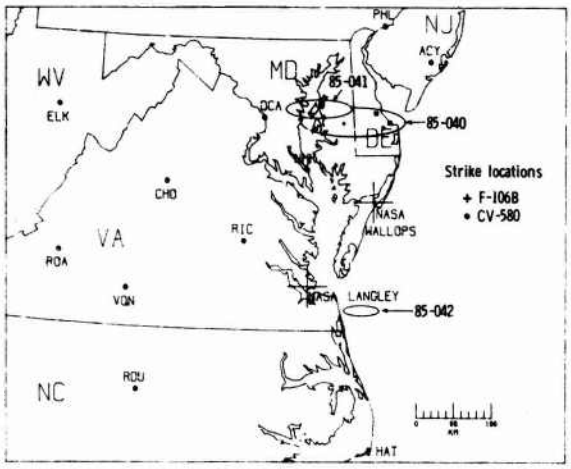

Fig. 5 - Map of area used for joint thunderstorm research flights

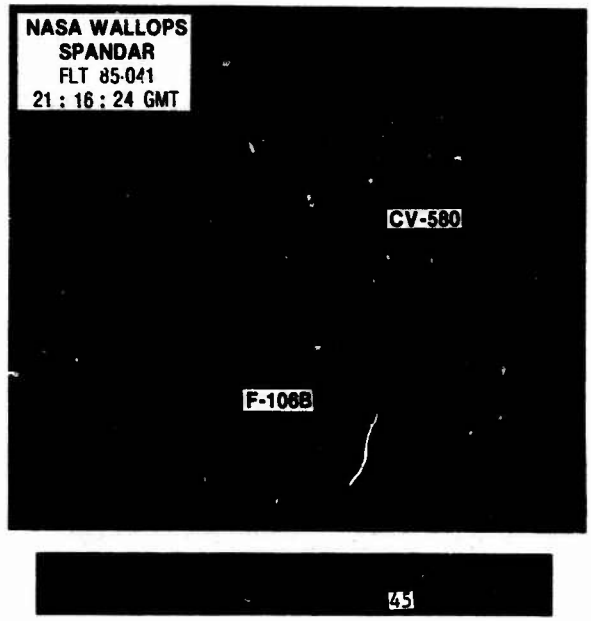

Fig. 8 - NASA Wallops SPANDAR video display at 21:16:24 GMT, flight 85-041. Thunderstorm outline and airplane ground tracks have been graphically superimposed. Cross ticks on ground tracks indicate 21:16 and 21:17 GMT. Dart indicates location and heading of F-106B at 21:15:47 GMT

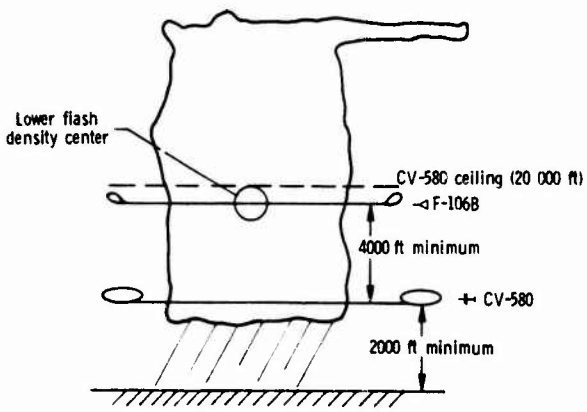

Fig. 6 - Schematic of procedure used for coordinated thunderstorm operations

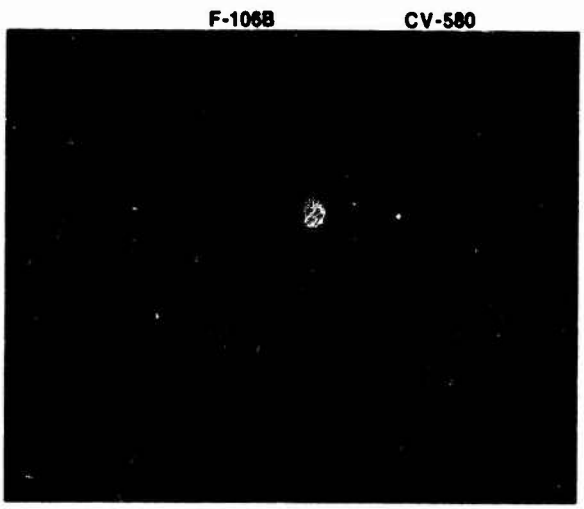

Fig. 7 - Integrated video display at NASA Langley at 21:17 GMT, flight 85-041. Airplane ground tracks have been enhanced

Fig. 9 - Airborne X-band radar display in F-106B airplane at 21:15:47 GMT, flight 85-041

INTERNATIONAL CONFERENCE ON LIGHTNING AND STATIC ELECTRICITY

CURRENT AND CURRENT-DERIVATIVE IN TRIGGERED LIGHTNING FLASHES - FLORIDE 1985 -

J. HAMELIN - C. LETEINTURIER - C. WEIDMAN
Centre National d'Etudes des Télécommunications - LANNION - FRANCE

A. EYBERT-BERARD - L. BARRET
Centre d'Etudes Nucléaires de Grenoble - FRANCE

Abstract : Current (I) and Current-derivative (dI/dt) measurements with submicrosecond time resolution were made on triggered lightning return-strokes at the Kennedy Space Center during the summer of 1985. The current was measured using a coaxial shunt and the current-derivative with a wideband inductive sensor. Both sensors were located at the base of the lightning channel and were connected through fast analog fiber optic links to several fast transient digitizers and a magnetic tape recorder. It was thus possible to record triggered lightning current variations over a large frequency range (I : DC to 30 MHz ; dI/dt : DC to 90 MHz).

The experimental set up is described in detail ; I and dI/dt measurements are presented and discussed in order to better characterize triggered lightning currents. Current records are comparable with Florida 1983-84 /1/ ; the peak-currents of the return-strokes were varying between a few kA and 50 kA and the peak current-derivatives between a few tens of kA/μs and 260 kA/μs.

1. INTRODUCTION

The last experimental campaign RTLP* 35 took place at Kennedy Space Center from June 15 1985 to August 20 and was initiated by NASA. About 10 American and French scientific groups were participating in this experiment.

Most of the groups were recording triggered lightning signals at short range (50 m), mean range (500 m to 5 km) and about 1-2 km up.

The triggered lightning technique has been used in France since 1973 and was modified for Florida experiments in 1983. /1/

Among the main characteristics of a lightning discharge, currents and current-derivatives are fundamental ; they are the two parameters we will discuss in this paper.

After a general description of the experiment : technical features of the sensors and the recording systems, the general and some specific I and dI/dt records will be presented. Finally we will discuss the data, their limits and the main consequences.

*RTLP : Rocket triggered Lighting Program

2. EXPERIMENT

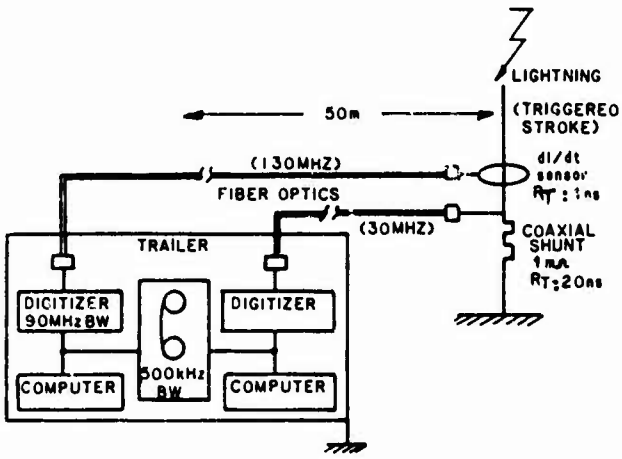

Fig. 1 A block shematic diagram of the measuring system

2.1. Current-measurement

Lightning current is measured through a coaxial shunt : 10^{-3} ohms ; rise time $\leq$ 20 ns and characteristic impedance 50 ohms. The signal is attenuated, then transmitted to the recording system through 3 fiber optics (diameter 200 µm, length 100 m ; 30 MHz bandwidth). The recording system is located inside a metallic grounded truck, 50 meters from the discharge. In this way, there are 3 measurement channels :

- DC - 1 MHz, bipolar, logarithmic, 80 dB dynamic with 0.1 Amp. accuracy ; the signal is recorded on a magnetic tape in FM mode (500 kHz BW)

- DC - 1 MHz, linear, 33 dB dynamic, maximum range + 24 kA - This channel has been used to visualize the signal on a scope with a camera.

- 30 Hz - 30 MHz, linear, 36 dB dynamic, maximum range + 60 kA - The signal is digitized (Le Croy 8928) with 200 MHz sampling rate, 3 bits, 64 kbytes memory - The triggering threshold was about + 5 kA ; the signal was delayed by 220 ns.

2.2. Current - derivative measurement

The current-derivative sensor was located at the base of the triggered lightning and the recording system inside a grounded metallic truck 50 meters from the impact point of the discharge - Fig. 1 shows a shematic diagram of the measuring equipment.

The current-derivative sensor is an inductive current probe of which the output voltage is $V = M \frac{dI}{dt}$

M is the mutual inductance : 10^{-9} Henries

I is the total current through aperture

The sensor rise time is 1 nanosecond and dI/dt max is 500 kA/µs. The sensor was joined to the digitizer through a fiber optics (130 MHz). The digitizer (Tektronix 7612 - 200 MHz sampling rate) has two channels, one for dI/dt measurement and the other one for dE/dt measurement (an antenna was mounted on the roof of the grounded trailer ; see paper "Submicrosecond structure .....by J. HAMELIN et al. Dayton conference"). The digitizer was triggered by the dI/dt signal (with different thresholds throughout the summer between 5 and 40 kA/µs).

The experiment was set up in order to obtain four return - strokes in a flash ; which means 4 return-strokes dI/dt signatures during 512 x 5 ns = 2.5 microseconds.

The trigger time was recorded with the magnetic recorder, in synchronization with the IRIG B time and the analogical current signal ; so it has been possible to correlate current and current- derivative for each dI/dt record.

2.3. The set up on the triggering site

The choice and the general set up of the triggering site (fig. 2) is based on the NASA decisions to carry out several simultaneous experiments on that site :

- current and current-derivative measurements of the triggered lightning flashes (CENG* and CNET*)

- lightning strike object (L.S.O., instrumented metallic cylinder to simulate an aircraft fuselage (U.S.A.F*)

- test of a metallic mesh cage (NASA)

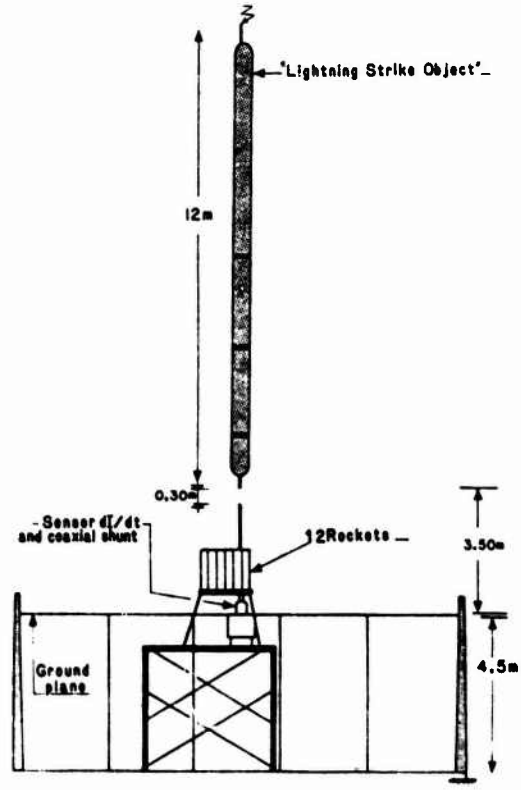

Fig. 2 : triggering site

The I and dI/dt sensors were located above the ground plane (20 cm above ; the ground plane was materialized by the metallic mesh cage, 4.5 m above the ground an 3.5 m under the L.S.O. ; the L.S.O. was either connected or disconnected (gap 0.3 m) to the rod above the sensors to which it was attached.

*CENG : Centre d'Etudes Nuclaires de Grenoble

CNET : Centre National d'Etudes des Télécommunications

USAF : US Air Force

DATE	TIME		CONTINUOUS CURRENT			RETURN-STROKES			OBSERVATIONS
REFERENCE	UT	10+(mS)	Duration (mS)	mean (A)	Q (C)	L.S.T.N.	I max (kA)	dI/dt max (kA/us)	
17 July	19h09	10	360	50	22.5				
		400				S	20.5	186.25	
8504		425				S	7.2	43.75	
		534				S	10.9	98.75	
5RS		653				S	11.2	118.75	
		723				S	17.6		
2 August	19h48	10	325						
8508		354				H	10.4		
		378				H	15	80	
3RS		430				H	9	72.5	
2 August	19h53	10	325	80	27				
		430				L	19.76		
		495				L	17.64		
8509		519				H	5		
		532				H	5		
		548				H	5		
		588				L	17		
12RS		735				H	3		
		758				H	5		
		784				L	8		
		924				T	24		
		1037				H	10		
		1177				H	2.5		
2 August	19h59	10	467	100	50				
		586				L	19.76	182.5	
8510		675				H	7.5	66.25	
		699				H	6.5	70	
5RS		827				L	16	170	
		960				H	5		
2 August	20h05	10	400	40	25				
		447				L	17.6		
8511		488				L	15		
		553				L	20		
		586				L	16		
7RS		782				H	5		
		910				L	23		
		983				H	7.5		
2 August	20h09	10	475	100	45				
		570				L	49.4	260	
8512		638				L	27.5	188.75	
		704				L	14.8		
4RS		808				H	7.5	107.5	
8 August	01h02	10	95(+)	+1000	75	H	45		
			135(-)	- 80	10				Gap L.S.O.-Rod : shorted
8518		420				S	16.5	133.75	
		495				S	11.75	96.25	E field at ground level + 2.5 kV/m
4RS		535				H	5		before the flash
		585				S	10.1	63.75	
10 August	16h26	10	170	25	2.8				
8522		204				T	10.6		
2RS		266				T	7		
10 August	19h45	10	750			H	2.5		
8523		802				H	12	87.5	
2RS		927				H	5		
10 August	20h09	10	300	30	8.2				
8525 1RS		346				L	13.8	103.75	
13 August	23h13	10	300	30	8.6				
		340				S	6.15	65	Gap L.S.O.-Rod : shorted
		392				L	12.3	96.25	
8532		445				S	7.45	130	
		452				S	6.40	106.25	
		515				L	14.5		
10RS		525				L	10.5		
		567				L	17		
		628				L	9.5		
		678				L	6.9		
		689				S	5.6		
14 August	14h46	10	317	90	28				
		380				L	30	175	Gap L.S.O.-Rod : shorted
		407				S	5.4	100	
8535		435				L	10	110	
		459				S	14.4	141.25	
		500				S	5.9		
12RS		525				S	8.8		
		650				S	19.7		
		712				S	19.7		
		783				S	10.4		
		897				H	3		
		960				H	7.5		
		1067				H	3		
14 August	15h36	10	495	50	26				
		527				L	10	90	Gap L.S.O.-Rod : shorted
		618				H	7.5		
8536		682				S	13.6	129.6	
		693				S	5.95	111.6	
		705				H	3		
9RS		727				S	9.87	147.6	
		949				S	23.46		
		1052				S	7.47		
		1095				S	9.06		
15 August	18h19	10	275						
		330				T	12		
8539		356				T	12		
3RS		388				S	9.6	92.5	
15 August	18h21	10	300						
		391				H	7.5		
		396				S	8	71.87	
		391				S	11.73	96.25	
		422				L	19	142.5	
		438				S	7.47	71.87	
		466				S	8.27		

Fig. 3 : General data

3. DATA

Throughout the experimental campaign, about 30 lightning flashes were triggered ; 15 of them had one or several return strokes for which there were I and dI/dt data.

The maximum magnitudes were 49.4 kA and 260 kA/μs (same return-stroke) ; on average, each flash presents at least a return-stroke exceeding 20 kA and the mean value of dI/dt is 11^ kA/μs (Fig. 4-5).

The general characteristics of the discharges are similar to those triggered during the previous campaigns in Florida /1/, considering the current magnitude, the electrical charge moving along the lighting channel, the strokes number (12 maximum with a mean = 6) and the total duration (1.15 sec maximum with a mean = 561 ms).

The general data are shown in fig. 3. The return strokes have been mentioned when the current exceeded 2 kA.

(1) when it has been possible, the current maximum value has been determined by the 30 Hz - 30 MHz system marked "L" ; if not by the DC-1 MHz system recorded with a digitizer (10 MHz sampling rate) marked "S", and with the DC- 1 MHz system recorded with the magnetic recorder "H" or the scope "T".

(2) the time TO corresponds to the beginning of the current, called "continuous current" preceeding the return-strokes.

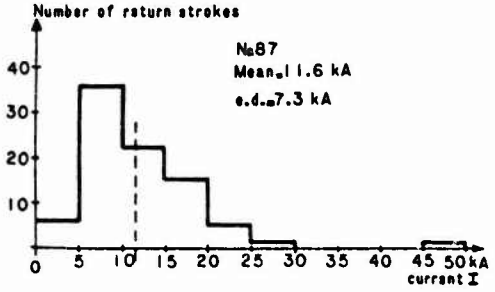

Fig. 4 : Peak-current histogram

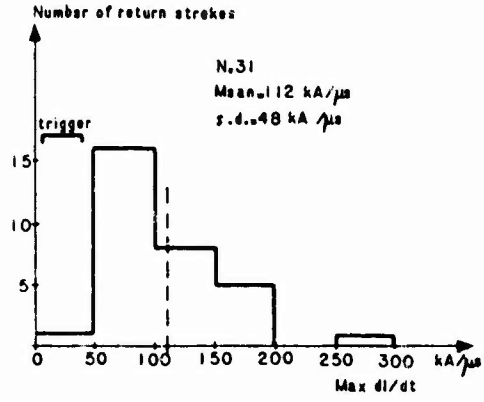

Fig. 5 : Peak current-derivative histogram

In fig. 3, the negative sign has been omitted on front of current peak value. There is only one time (8513) that there is a positive pulse (marked + 5)

4. FLASHES 8512 and 8518

4.1. Flash 8512 (fig. 6)

This flash was triggered on august 2 at 20 : 09 UT ; the electric field at the ground level was - 4.3 kV/m. There were 4 return-strokes. The first one had a peak-current of 49.4 kA.

Despite the fact that the magnitude of the peak current was double that of what we usually obtain in a flash in Florida ($\overline{I}$ max in a flash = 20 kA), current waveform is similar to those recorded before. /1/

Fig. 6 shows the dI/dt waveforms for the first two return-strokes. The first one has the largest peak dI/dt (260 kA/μs) with a full width at half maximum 165 ns. These dI/dt peaks are fairly narrow. This triggered flash is very significant since it provides proof that we can observe very large current-derivatives.

4.2. Flash 8518 (fig. 7)

This flash was triggered on august 8 at 01 : 02 UT ; it is interesting in the fact that the triggering conditions were quite unusual.

The electric field at the ground level before triggering was + 2.5 kV/m ; note that 95 % of flashes are triggered when the E field is negative (between 4 and 6 kV/m in Florida, 8 and 10 kV/m in New-Mexico and St Privat d'Allier).

The storm activity was almost non existant over the site. The electric field record shows a few intra-cloud discharges (1 flash about every 2 minutes with a negative electric field 1 - 2 kV/m). The electric field inverted about eight minutes before the triggering ; during this period there was no lightning discharge at all over the site.

The current record shows a strong positive pulse (+ 5 kA - duration 95 ms) followed by a negative pulse (-30 A) ; the channel was still illuminated.

The current passed zero. This bipolar continuous current was followed by 4 negative return-strokes (16.5, 11, 5 and 10 kA peak-currents). Fig. 7 shows two dI/dt pulses recorded during the first two return-strokes (134 and 96 kA/μs peak-current derivatives).

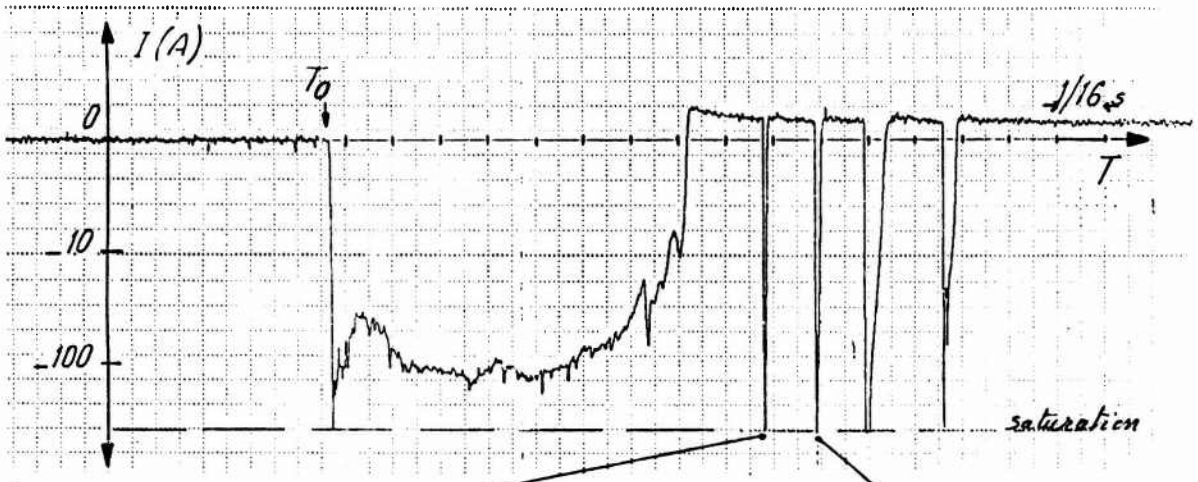

6-a

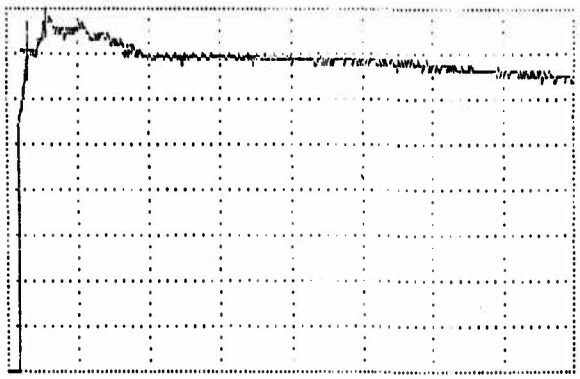

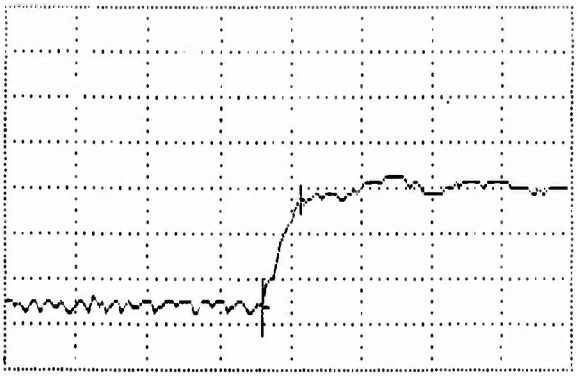

8512 : 6 kA/div., 1 μs/div., I = 49.4 kA

8512 : 6 kA/div., 200 ns/div., I = 27.5 kA

6-b

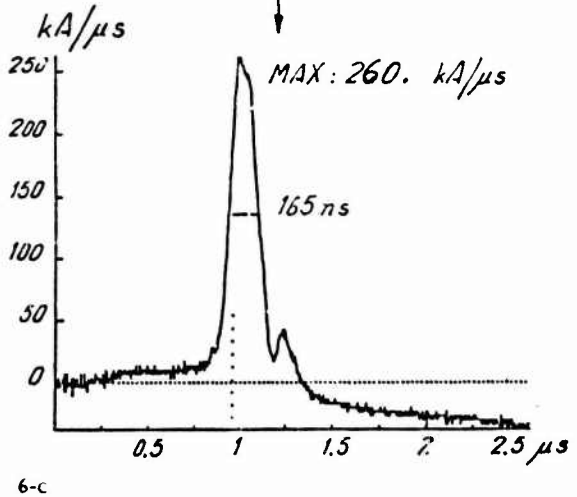

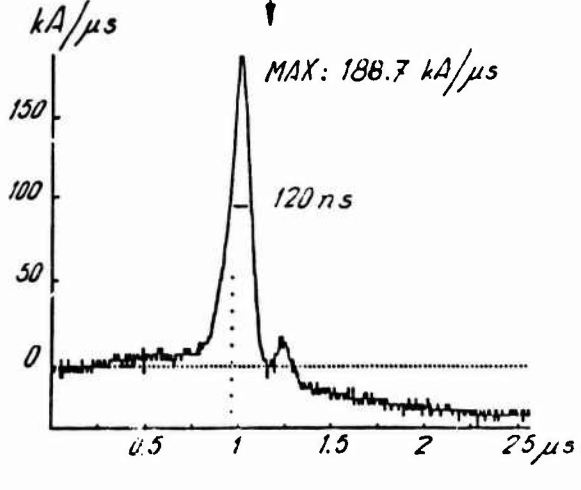

6-c

Fig. 6 : Flash 8512

6-a : logarithmic current record

6-b : current records of the first two return-strokes

6-c : current-derivative records of the first two return-strokes

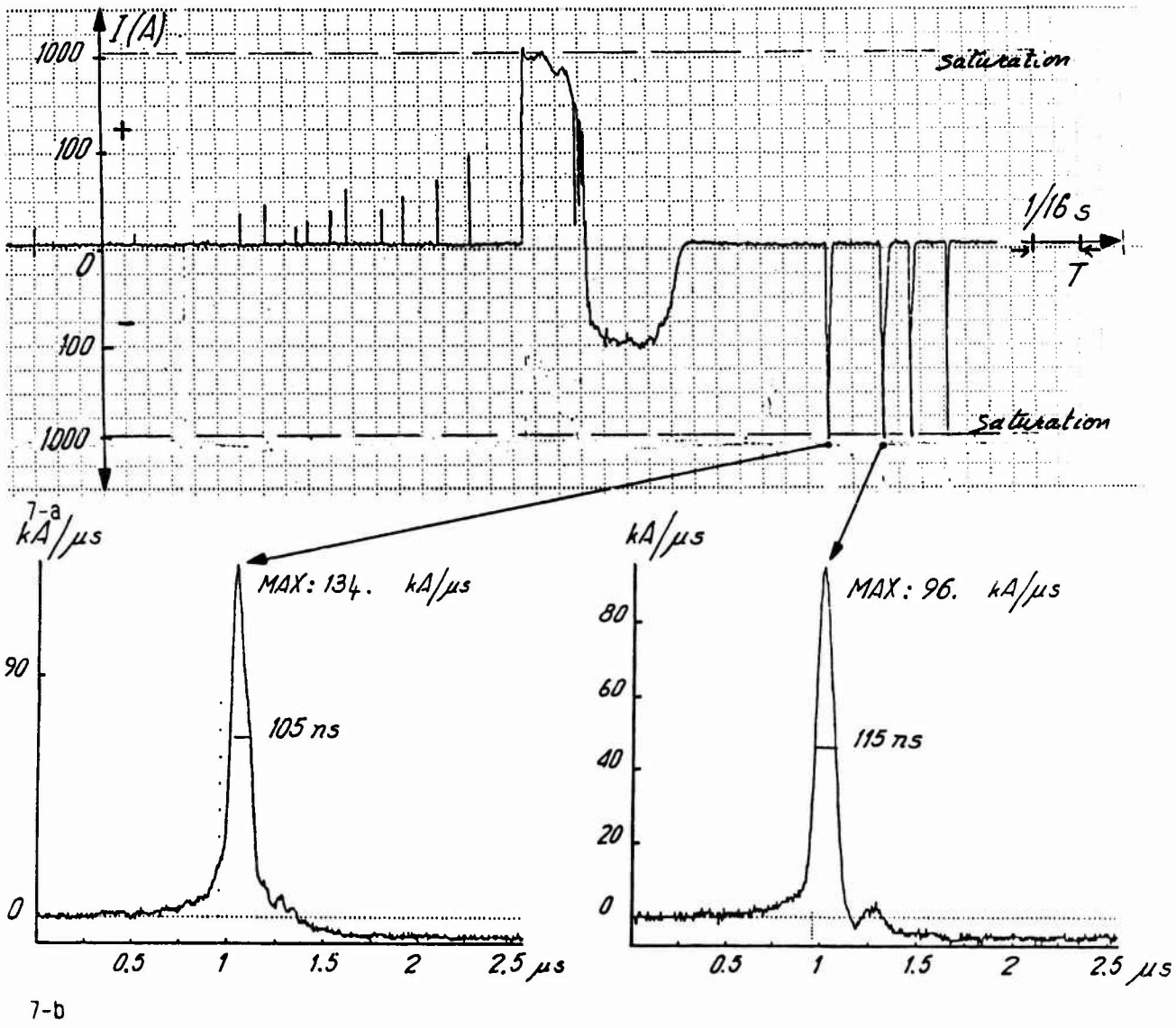

Fig. 7 : Flash 8518

7-a : logarithmic current record

7-b : current-derivative records of the first two return-strokes

5. DISCUSSION

5.1. Limits

As shown in fig. 2, the way the experiment was set up leads us to ask several questions :

1st : In order to observe a possible difference in the current and current-derivative waveforms, we have shortened the gap (between the rod and the L.S.O.) for part of the triggered flashes. We cannot see any significant difference either in the waveforms or in the magnitudes ; for example :

$\overline{\frac{dI}{dt}}$ gap open = 112.9 kA/µs

$\overline{\frac{dI}{dt}}$ gap shorten = 108.7 kA/µs

2nd : Some "anomalies" exist in parts of I and dI/dt waveforms : oscillations in I waveforms (fig. 8a) and existence of a double peak on the main one of the dI/dT waveform (fig. 8b)

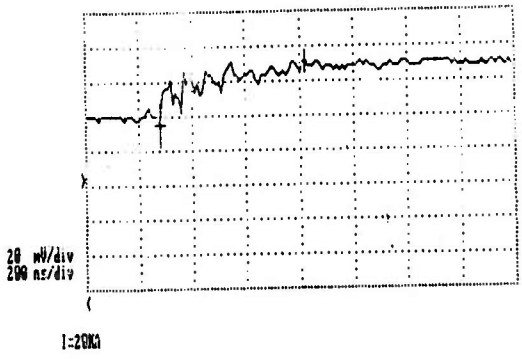

Fig. 8a : I Waveform - triggered lightning 8511

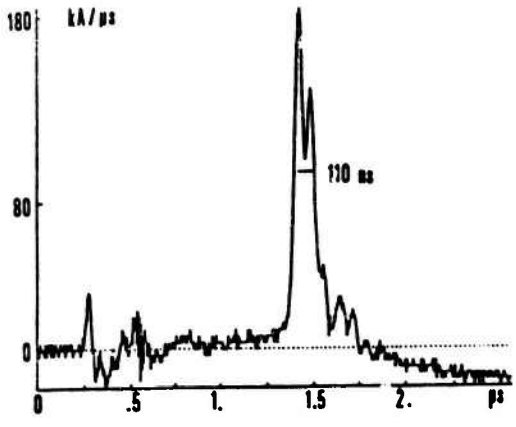

Fig. 8b : dI/dt waveform - triggered lightning 8504

Possible reasons for these perturbations :

- the instrumentation trailer was probably not an electromagnetic-proof shelter in such a perturbed environment, although the measurements entered through fiber optics

- the cylinder (total length with the rod : 15 m) could cause a resonant phenomenum with a 100 ns period - we can see (fig. 8 a-b) 60-70 ns oscillation periods and 30 ns on dI/dt and I records respectively.

We should note that simultaneous measurements of the electric field-derivative dE/dt at 50 m (the trailer mentioned above) and at 5 km, both show a double peak, similar to dI/dt peak (fig. 9).

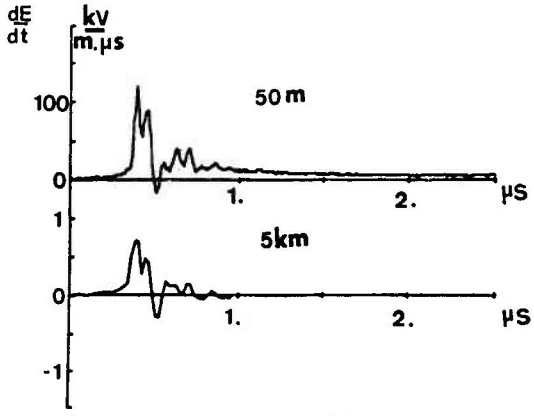

Fig. 9 : Simultaneous records dE/dt at 50 m and 5 km range from triggered lightning 8504

- the ground plane was probably not very efficient;one could observe arcs between meshes of the metallic mesh cage during a flash, revealing a bad equipotentiality.

5.2. Current records

Current records in 1985 are similar to those obtained in Florida in 1993 and 1984.

	1983	1984	1985
Number of flashes	19	8	15
maximum current	55 kA	30 kA	49.4 kA
I max	14.8 kA	13.2 kA	20 kA

In 1985, we noticed that the mean electric field at the ground level before triggering was lower than before :

1983-84 : $\bar{E}$ = 4.5 kV/m ; 1985 : $\bar{E}$ = 3.5 kV/m

This is probably due to the electric field sensor environment : the field was likely attenuated by vegetation.

We should note the discharge which was triggered with a low positive electric field (+ 2.5 kV/m) ; this leads us to reconsider the field threshold criterium to trigger flashes.

Source	First Reurn-Strokes				Subsequent return-strokes			
	N	95 %	50 %	5 %	N	95 %	50 %	5 %
Anderson and Eriksson (1980) /3/	75	9.1 kA/µs	24.3 kA/µs	65 kA/µs	113	9.9 kA/µs	39.9 kA/µs	162 kA/µs
Garbagnati et al. /4/ (1981)	42	3.6 "	14 "	55 "	33	7.5 "	33 "	145 "

Fig. 10 : Summary of previous lightning current-derivative measurements

5.3. Current-derivative records

5.3.1. Comparison with literature

Part of current measurements have been carried out on the top of mountains with towers by Berger /2/, Garbagnati /4/ and for more than ten years, with triggered lightning /5/.

The current derivatives had been obtained by measuring the slope of the steepest portion of current waveforms. Values of the maximum dI/dt are log-normally distributed. The values at the 95 %, 50 % and 5 % levels are listed in fig. 10.

In the Anderson and Eriksson (1980) and the Garbagnati et al. (1981) data, the maximum first and subsequent stroke dI/dt are, for the most part, larger than first stroke current-derivatives.

In any case, these dI/dt values come from I records. The dI/dt records (§ 3.1) are obtained from direct measurements ; they only concern subsequent strokes (the triggered lightning process does not make it possible for us to carry out any measurement on a common first return-stroke).

The first and main conclusion is that those values are much larger (mean dI/dt max : 112 kA/µs) than the ones presented in fig. 10.

We can compare these with previous estimates of dI/dt from dE/dt measurements /6/ and /7/ which give 154 kA/µs and 227 kA/µs respectively. These values have been obtained by assuming the relation :

$$\frac{dI}{dt}(t) = \frac{2\pi D\, \varepsilon_0\, c^2}{v} \frac{dE}{dt}\left(t + \frac{D}{c}\right)$$

(D : range - v : return-stroke velocity)

for far field with a propagation above a good conductive ground (salt water) and assuming only one current propagating along the lightning channel.

Our dI/dt measurements are smaller (mean dI/dt max : 112 kA/µs) than the ones estimated by /6/ and /7/ but much larger than /3/ and /4/. The correlation between dE/dt and dI/dt measurements is dicussed in /8/.

5.3.2. Full-width at half-maximum and rise-time

A histogram of the full-width at half-maximum (FWHM) of the dI/dt signal is shown in fig. 11. The FWHM is 100 ns with a standard deviation 45 ns. The s.d. is quite large due to the existence of one or two peaks on the dI/dt waveform.

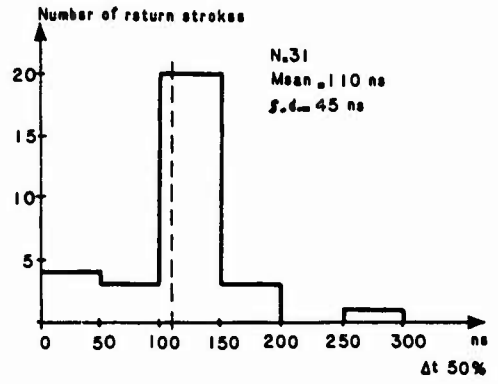

Fig. 11 : Full-width at half maximum histogram of dI/dt records

In comparison with FWHM distribution, fig. 12 shows the histogram of $\int \frac{dI}{dt}$ risetime (10 % - 90 %) - The dI/dt signals have been integrated, thus giving us the current waveform ; Fig. 13 shows an example ; we have considered the risetime between 10 and 90 % from the break point to the maximum. $\overline{\Delta t}$ = 162 ns ; the standard deviation (69 ns) is also quite large ; there are two possible explanations for this : a negligeable offsett on dI/dt signal may introduce a more substantial difference on the integral and although the break point is usually determined quite precisely, its location can be at times more ambiguous to determine.

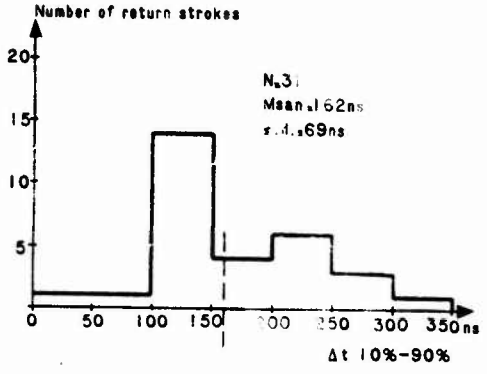

Fig. 12 : Rise time history of $\int$ dI/dt waveform

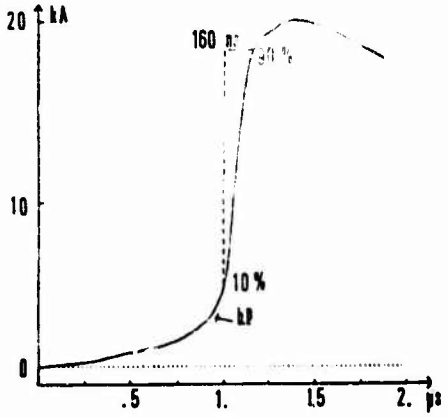

Fig. 13 : An example of $\int$ dI/dt signal - 8504
BP is the break point.

5.3.3.

When one observes most current-derivative waveforms (fig. 8b), one can see a glitch between one and five microseconds before the main peak ; this glitch exists also on electric field waveforms recorded at 50 m and 5 km from the discharge (fig. 14). This glitch only appears on triggered lightning signals and it might be due to the attachment process between the downward leader and the leader rising upward from the top of the wire.

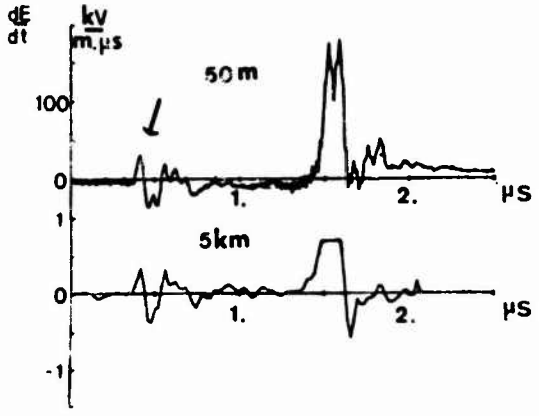

Fig. 14 : Electric field-derivative measurement at 50 m and 5 km from the flash 8504.

5.4. Correlation between current and current-derivative

The current-derivative integrations have been obtained by a trapezoidal method ; the sampling interval was 5 ns and the window 2.5 µs. Fig. 15 compares the maximum value of current measurements with the integral of the current-derivative records. We can see that there is a fair similarity between the two values, considering that some I measurements have been made with less accuracy (⊐ symbol) and that the integration method emphasized quite substantially a negligeable offsett on the dI/dt values.

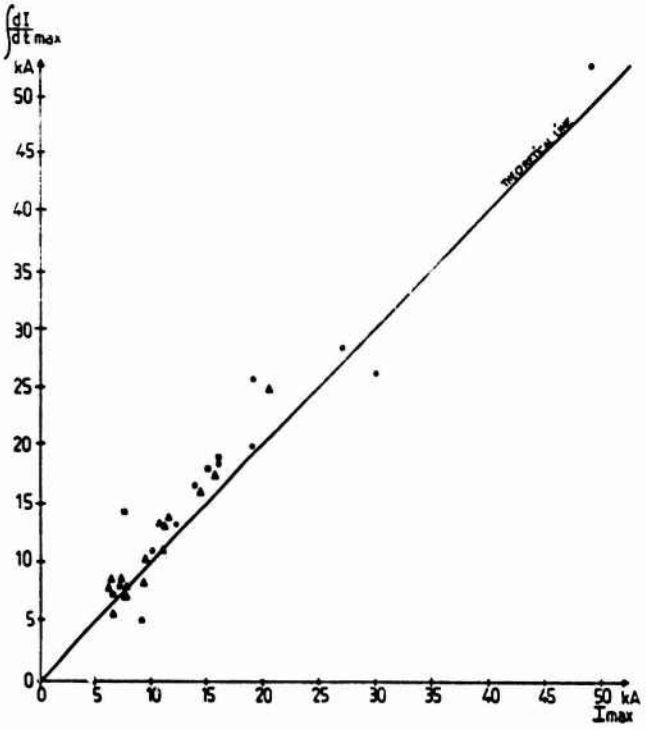

Fig. 15 : Relation between I max measurements and I max estimated from dI/dt measurements

Note the relation between I max and dI/dt max in fig. 16. The dI/dt max increases with I max. This is an important point, considering that the mean-value of I max (11.6 kA) was not very high and that there might be some much larger lightning currents : the Saint-Privat d'Allier Research Group /5/ records that 10 % of triggered flashes have a peak current greater than 29 kA.

The mean-value of dI/dt max (fig. 5) is 112 kA/us but dI/dt max reaches 260 kA/us corresponding to a maximum current of 49.4 kA. Therefore, we can expect very large current-derivatives associated to very large lightning currents.

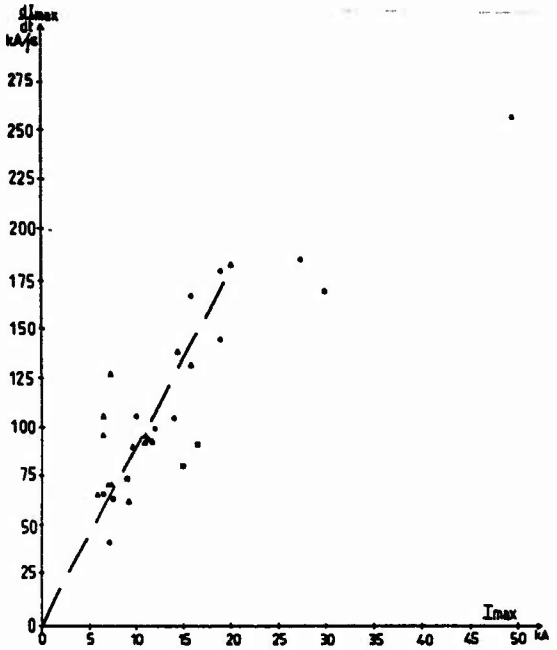

Fig. 16 : Relation I max with dI/dt max records.

6. CONCLUSION

The Rocket Triggered Lightning Program in Florida 1985 made it possible to obtain 15 flashes with return-strokes. Most of them were triggered in the presence of negative electric field at the ground level and gave a negative continuous current followed by one or several negative return-strokes. The current values (Imax R.S = 11.6 kA) and waveforms are similar to those obtained in Florida in 1993 and 1984. /1/

Two flashes were triggered in the presence of a positive electric field, with a low value (+ 2.5 kV/m) ; the continuous current of one of them began with a positive pulse (+ 5 kA), changing to a negative polarity and was then followed by negative strokes. Flashes have never before been triggered in the presence of such a low positive electric field ; this highlights the possibility of obtaining lightning under the anvil with fairly large currents (5 to 16.5 kA - flash 8518).

Considering the current-derivative measurements, it has been very important to measure this parameter which reveals itself as being much larger than previous current measurements could predict. The dI/dt mean value is 112 kA/µs with a peak of 260 kA/µs which is almost 5 times higher than has been recorded in previous works /3, 4/. Some other measurements will be necessary to eliminate or to answer some questions due to the set up of the experiment itself. But, even if the dI/dt measurements are lower than those predicted by /5, 7/ this dI/dt value is still very large and this parameter is very important for the protection of electronic systems (aircrafts, telecommunications..).

REFERENCES

/1/ P. LAROCHE - A. EYBERT-BERARD - L. BARRET

"Triggered lightning flash characterization"

10th international Aerospace and ground conference on lightning and static Electricity - ICOLSE - Paris-june -1985

/2/ K. BERGER - R.B. ANDERSON - H. KRONINGER

"Parameters of lightning flashes".

Electra - N°. 41, 23-37 - 1975

/3/ R.B. ANDERSON - A.J. ERIKSSON

"Lightning parameters for engineering application"

Electra - N° 69, 65-105 - 1980

/4/ E. GARBAGNATI - F. MARINONI - G.B. LO PIPERO

"Parameters of lightning currents, interpretation of the results obtained in Italy"

16 th Lightning Conf. on Lightning Protection, Szeged - Hungary - july - 1981

/5/ SAINT-PRIVAT d'ALLIER RESEARCH GROUP

"Eight years of lightning experiments at Saint-Privat d'Allier"

Revue Générale de l'Electricité - n° 9 - september 1982

/6/ C.D. WEIDMAN

"The submicrosecond structure of lightning radiation fields"

PHD dissertation - University of Arizona - USA - 1982

/7/ C. LETEINTURIER - E.P. KRIDER - J.C. WILLETT

"Submicrosecond structure of the radiation fields produced by lightning".

10 th International Aerospace and ground Conference on Lightning and Static Electricity - ICOLSE - Paris - june - 1985

/8/ J. HAMELIN - C. LETEINTURIER - L. NICOT - C. WEIDMAN

"Correlated current-derivative (dI/dt) and electric field-derivative (dE/dt) emitted by triggered flashes".

1986 International Conference on Lightning and Static Electricity - Dayton - OHIO- june 1986

ACKNOWLEDGMENTS

We are grateful to W. JAFFERIS of the NASA Kennedy Space Center for his support.

ELECTRICAL ONSET CONDITIONS OF UPWARD FLASHES TRIGGERED BY THE ROCKET AND WIRE TECHNIC (*)

P. Laroche
Office National d'Etudes et de Recherches Aerospatiales
BP 72, 02322 Chatillon Cedex, France

A. Eybert-Berard, L. Barret
Centre d'Etudes Nucleaires de Grenoble
85 X, 38041 Grenoble Cedex, France

ABSTRACT

An experiment on flashes triggered by the rocket and wire technic was held on the Kennedy Space Center during the summer 85. Close electric field measurements from DC to more than 1 MHz were performed simultsneously with a wide band (DC to 30 MHz), wide dynamic (about 100 dB) current measurement at the lightning flash foot. The onset of an upward triggered flash consists in positive streamers emitted from the tip of the conductive wire and followed by an upward positive leader.

After a brief presentation of the overall experiment results, we present and discuss the current pulses corresponding to streamers emission and the related cloud electric field measurements.

The behaviour of the first stages of the triggered flashes will also be discussed in terms of the general electrical atmospheric conditions at the rocket launching time. Simultaneous electrostatic field measurements at ground performed in different location, emphasize the point that this parameter is greatly influenced by space charge near ground.

(*) This work was supported by DRET (Direction des Recherches, Etudes et Techniques

1985 Rocket Triggered Lightning Investigation
Lightning Strike Object Results

Richard D. Richmond
Atmospheric Electricity Hazards Group (AFWAL/FIESL)
Air Force Wright Aeronautical Laboratories
Wright-Patterson AFB, Ohio 45433

Abstract: During the 1985 summer thunderstorm season, AFWAL participated in a Rocket-Triggered Lightning program at NASA Kennedy Space Center, Fl. Fourteen (14) triggered flashes struck the Lightning Strike Object (LSO). The characteristics of those flashes, as measured on the LSO, are discussed in this paper. The durstion of the attachment and the number and frequency of return strokes are also presented. The rise times and amplitudes of the magnetic fields produced on the LSO are tabulated. Finally, LSO resonance effects are briefly discussed.

INTRODUCTION

As part of a continuing effort to characterize the lightning threat to aerospace vehicles, the Atmospheric Electricity Hazards Group of the Air Force Wright Aeronautical Laboratories (FIESL) participated in a Rocket Triggered Lightning Investigation at Kennedy Space Center (KSC), Florida during the summer of 1985. The electromagnetic fields produced on a Lightning Strike Object (LSO) when the object was struck by lightning were measured.

EXPERIMENT DESCRIPTION

The RTLI experimental set up was composed of three parts; the strike object (LSO), the sensors on the LSO and the fiber optic system used to transfer the sensor outputs, and data recording instrumentation. A brief description of each part follows.

LIGHTNING STRIKE OBJECT (LSO): The LSO is an aluminum cylinder 17 meters long by one half meter in diameter. The LSO was suspended from wooden poles, using mylar lines, so that the top of the object was approximately 22 meters above ground level. A gap of one half meter normally isolated the bottom of the object from the grounded grid work and rocket launch platforms below the LSO. Figure 1 illustrates the experimental setup.

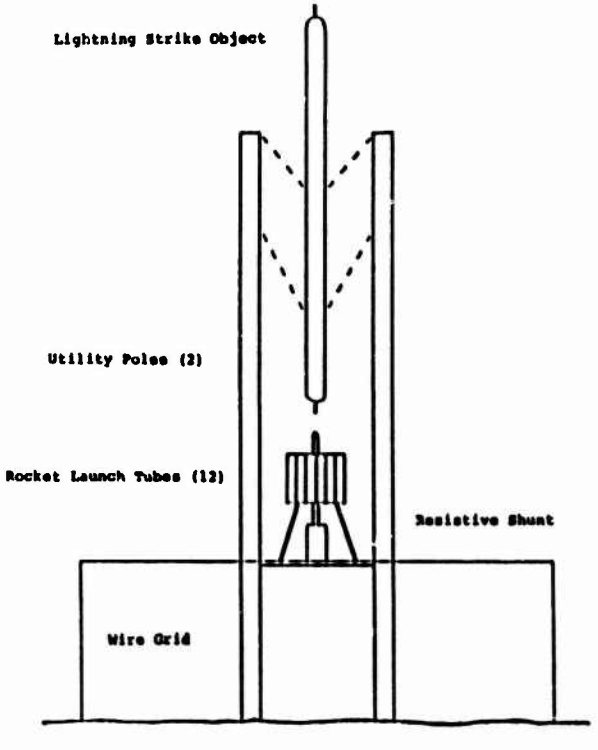

Fig.1 - 1985 Rocket Triggered Lightning Scaffold

LSO SENSORS/FIBER OPTIC SYSTEM: Sensors for measuring the magnetic fields and displacement currents along the length of the LSO were mounted near each end and at the middle of the cylinder. These sensors were derivative sensors; loops for magnetic field and capacitive plate for displacement current. A derivative current sensor was at the top of the LSO and a resistive shunt was at the bottom. The signals from these sensors were input to fiber optics transmitters for relay to the recording instrumentation. Fiber optics were used to provide isolation and noise immunity. Pneumatic (air) lines were used to turn on internal calibration pulses and to select attenuator in the fiber optic transmitters.

INSTRUMENTATION: The data recording instrumentation was housed in a shielded trailer located about 50 meters from the LSO. The main component of this instrumentation was the 10 channel digitizer with a sampling interval of 20 nanosecond and a 164 microsecond window. This digitizer provided detailed data for the first stroke of the triggered event. Low pass filters with a cut-off frequency of 20 MHz were installed on the fiber optics receivers to prevent aliasing of the digital data. The signals were also integrated in the fiber optics receivers. These integrated outputs were input to an analog tape recorder to provide a record of the entire triggered event. Fiber optic attenuators and digitizer trigger levels were selected to insure that a comprehensive record of a direct stroke attachment would be made. Still, movie and video cameras were also used to record the events.

EXPERIMENTAL RESULTS

GENERAL: During the 1985 experiment, over thirty (30) flashes were triggered. However, only 14 of these flashes contained return strokes that attached to the LSO. Table 1 is a synopsis of those attached flashes. Figure 2 is a histogram of the time between successive return strokes in multi-stroke flashes. The currents measured by a ground shunt for these flashes are presented in another paper at this conference. (1)

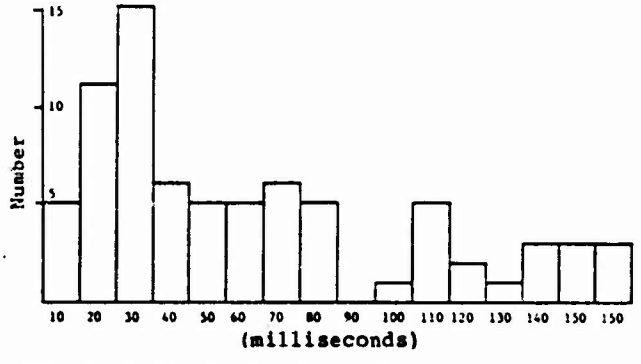

Fig.2 1985 RTL Time between Return Strokes

Table 1 - Synopsis of '85 RTL Flashes
'Flashes Attaching to Strike Object'

Date	Time (UT)	Number of Return Strokes	Duration * (milliseconds)
17 July	19:09:51	7	553
2 Aug	19:48:39	4	88
"	19:53:52	11	608
"	19:59:40	7	375
"	20:05:02	13	543
"	20:09:58	4	480
7 Aug	01:02:04	4	165
10 Aug	19:45:36	3	439
13 Aug	23:13:07	8	348
14 Aug	14:46:49	16	686
"	15:36:57	2	14
15 Aug	18:17:52	3	58
"	18:21:56	6	124

* Times are from first attachment to last return stroke.

For the flashes triggered in '85, there was an initial period of continuing current along the vaporized wire path. This current was not usually attached to the LSO except for a few flashes where the path was close enough to the LSO that the plasma engulfed the object. For these flashes, the highly ionized column of air (plasma) through which the lightning current was flowing would be blown against the LSO by the wind. The continuing current would then flow along the LSO. These lower level (about 1000 Amp), slowly varying currents would not produce measurable signals on the LSO sensors. After the continuing current, individual subsequent strokes would then attach to the cylinder. For all but one of the attached flashes, the return strokes attached to the hemispherical top of the LSO and exited out the bottom. The one different flash, triggered on 2 Aug, attached near the middle of the LSO. For this flash, the return strokes followed the original current path until turning at nearly right angles to attach near the middle of the LSO. At least one flash during the 1983 experiment exhibited a similar 90 degree turn, but it attached to the top of the LSO. No other triggered flash has shown this mid point attachment.

MAGNETIC FIELDS ON THE LSO: Using the analog records, the integrated magnetic fields measured by the loop sensors were tabulated. An average waveshape of the measured magnetic field is shown in Figure 3. The rise-time of the leading edge based on 10%-90% of the peak magnitude was measured and these values are summarized in the histograms of Figure 4. In the configuration shown in Figure 1, the cylinder and grid can be considered a tower system. Melander (2) shows that current rates of rise are consistently higher at the bottom of a tower. This would mean a correspondingly higher rate of rise for the magnetic field at the bottom. Figure 4 shows a somewhat faster averaged rise-time measured at the bottom of the LSO than at the higher sensors. Although by no means conclusive, it does seem reasonable to conclude that the mounting configuration was partly responsible for the variations in rise-time.

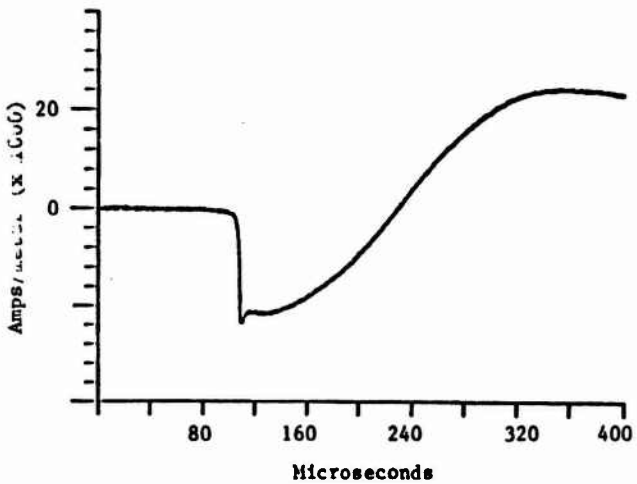

Fig. 3 - Magnetic Field Waveshape on LSO

A similar rise-time increase has been observed in previous experiments. One of the flashes triggered to the LSO on 5 August 1982 was a very active flash lasting over 700 milliseconds. Shown in Figure 5 are the magnetic field (dB/dt) waveforms recorded on each of the LSO sensor loops for one of the subsequent strokes of that flash. Although the peaks are saturated, an estimation of the rise-time is still possible. The rise-times (from top to bottom) are 2, 1, 0.7 microseconds respectively.

Figure 6 is a histogram of the peak magnetic fields measured on the middle. The values listed in Amps/meter can be converted to kiloamps by multiplying by a factor of 1.6. This factor is based on an assumed uniform current distribution around the circumference of the LSO. Because this sensor is near the middle of the LSO, it is reasonable to expect that the distribution would be uniform. Direct comparison with an external sensor such as the French shunt (1) would be necessary to verify calculated current levels.

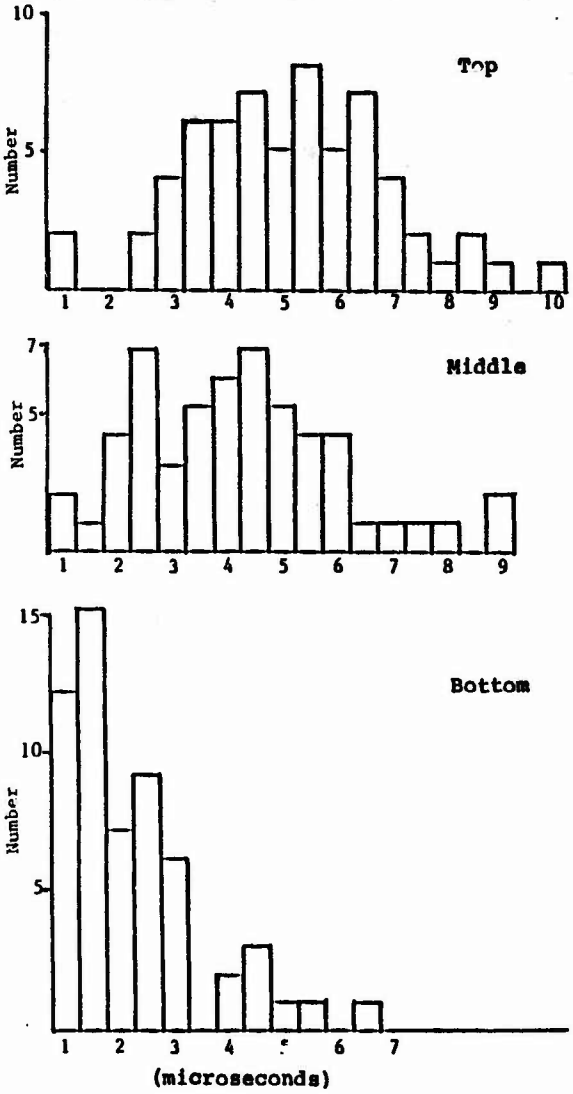

Fig.4 Magnetic Field Risetimes

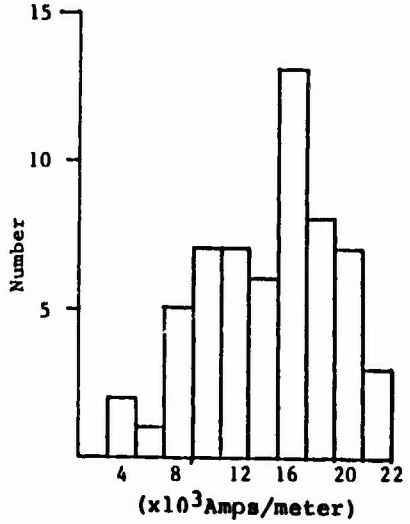

Fig 6 - Middle Magnetic Field Peak Values

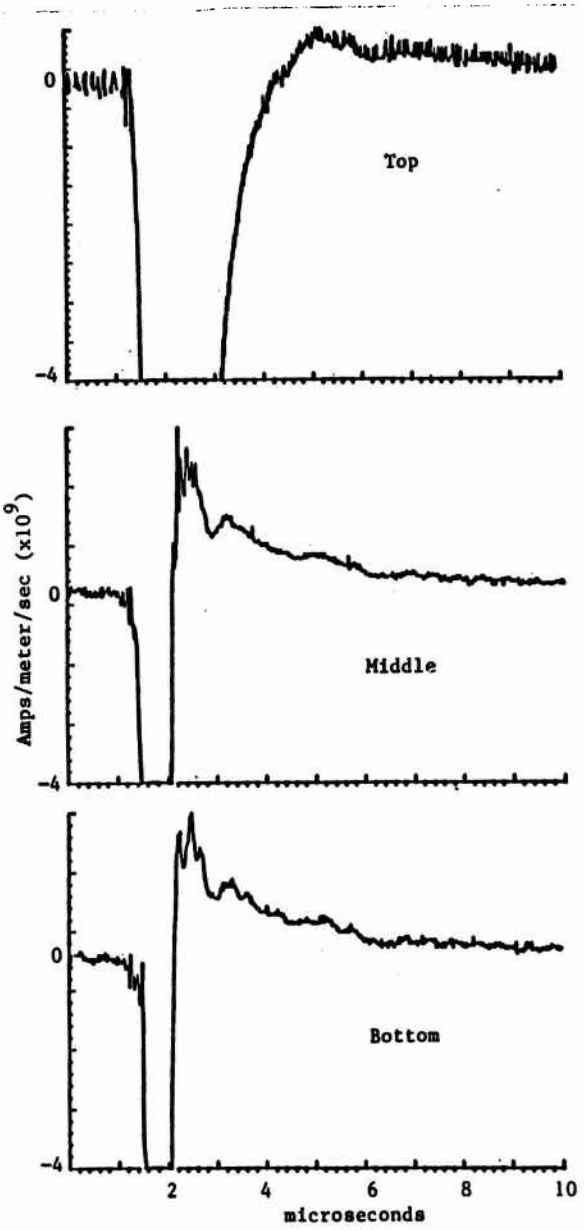

Fig 5 - Magnetic Fields (5 Aug 1982) (dB/dt)

Although not a direct current measurement, P. Hubert measured the magnetic fields produced by the triggered flashes at a diatance of 180 meters (3). By making some first order approximation, an estimate of the currents in the flash can be calculated. While the currents derived from the ground system and from the LSO are not in exact agreement, they are comparable (usually within 50% of the peak value).

For most of the flashes measured during the 1985 program, the lightning attachment point was at the top of the LSO, often at the location of the current probe. Such attachments would directly involve the entire cylinder length in the lightning channel As stated earlier, one flash (19:48:39 - 2 Aug) attached to the middle of the LSO. For this flash, signala obtained from sensors at the top of the LSO could only come from reflected signals traveling from end to end along the cylinder length. Shown in Figure 7 is the waveform for the first stroke of this flash obtsined from the dI/dt at the top of the LSO. A 10 microsecond portion of the signal is expanded and shown in Figure 8. As the LSO was configured for 1985, quarter and half wave resonances would be expected at 6.25 and 12.5 MHz. The Fast Fourier Transform (FFT) of the waveform, Figure 9, does show these resonances. Also visible in Figure 9 is a very strong, completely unanticipated, signal at 7 MHz. It was initially thought that this frequency may be associated with the scaffolding and grid system within which the LSO was suspended. However, suhsequent laboratory testa have shown that this is not the case. For these laboratories tests, the LSO was mounted in a coaxial return path and injected with pulses of up to 20 kiloamps. Analysis of the waveforms obtained still produced a very dominant resonant type signal at 7 MHz. This was true even when a completely different sensor, fiber optics and transient recorder system were used to measure skin currents on the LSO. The reason for this response has not yet been determined and testing continues. There seems to be little doubt though that this is a real LSO-related response. One possible explanation for thia involves the internal wiring of the LSO. The quarter-wave resonant length at 7 MHz is approximately 10 meters. Thia is the length of the metal conduit inside the LSO that houses the fiber optics transmitter power cablea. The LSO had been assembled in the 1985 configuration for almost two years and a certain amount of corrosion had taken plsce. The capacitive plate antennas directly connect the trsnsmitter boxes to the outer skin of the LSO. It is possible that the combination of corrosion and direct coupling had created a tuned circuit at 7 MHz.

The LSO was mounted in two configurations for 1985. The first was with a half meter gap between the LSO and the grounded shunt. The second was with the gap shorted. The data in Figure 4 is for all of the return strokes measured during 1985. Separating the data from the two configurations shows little or no statistical differcnce.

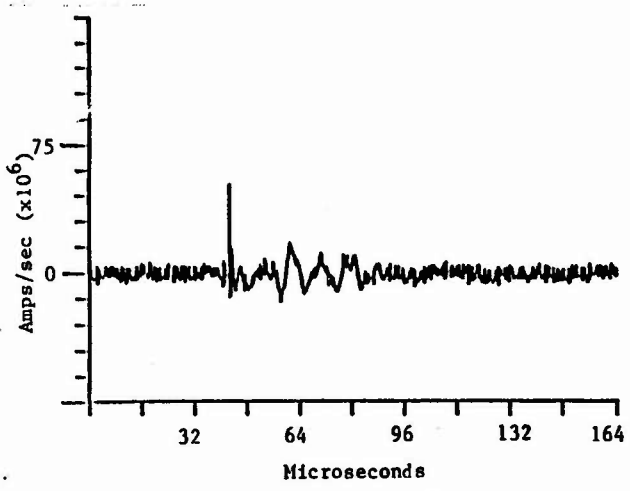

Fig 7 - dI/dT (Triggered 2 Aug 85, 19:49)

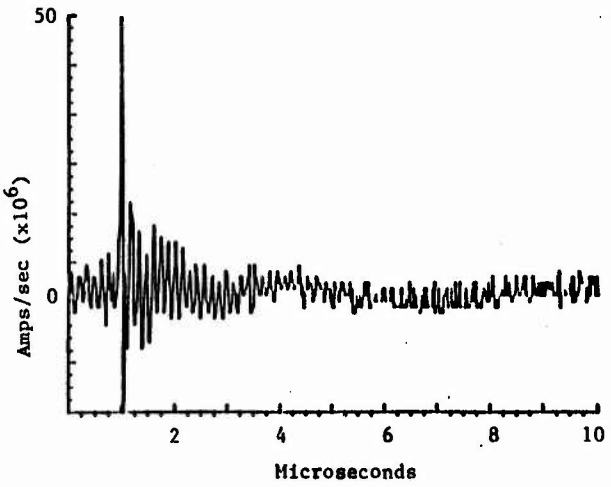

Fig 8 - dI/dT (Expanded)

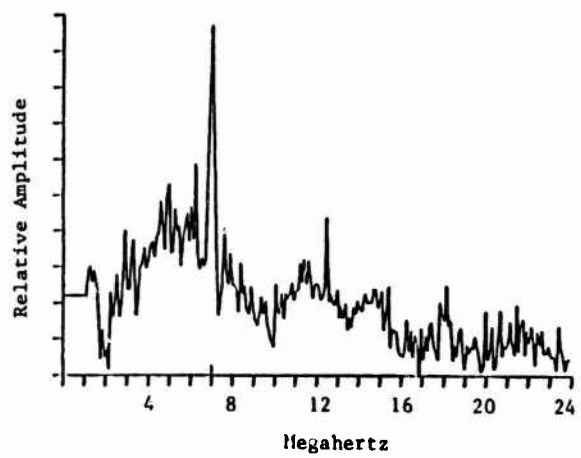

Fig 9 - FFT of dI/dT (2 Aug 85, 19:49)

SUMMARY

The data obtained from the LSO during the 1985 Rocket Triggered Lightning Program has been briefly described. The general characteristics - flash duration, number of return strokes, return stroke currents - have been discussed. The values reported for 1985 are similar to those from previous years and compare well with natural lightning (4).

Substantial currents have been recorded on portions of the LSO not directly in the path of the lightning currents. These signals could only result from effects induced on the LSO - probably from reflections at the ends of the cylinder. Simple antenna calculations are only partially successful in predicting the frequency content of these induced signals. Such signals can be significant and should be anticipated during any analysis of aerospace type structure responses.

REFERENCES

1. J. Hamelin, "Currents and Current-derivatives in Triggered Lightning Flashes - Florida 1985", these proceedings.

2. B.G. Melander, "Effects of Tower Characteristics on Lightning Arc Measurements", Proceeding - International Aerospace Conference on Lightning and Static Electricity, Orlando, Florida, 1984.

3. P. Hubert, B. Hubert, "Some Results of Observations on Triggered Lightning at Kennedy Space Center in July, August 1985", DPHG/SAP, CEN Saclay, France, 17 Jan 1986.

4. R. Richmond, "Rocket Triggered Lightning, A Comparison With Natural Flashes", Proceedings - International Aerospace Conference on Lightning and Static Electricity, Orlando, Florida, 1984.

ATMOSPHERIC ELECTRICITY HAZARDS PROTECTION (AEHP) DEMONSTRATION

Rudy C. Reavin

Captain M. Patricia Hebert

THE ATMOSPHERIC ELECTRICITY Hazards Protection (AEHP) Advanced Development Program being conducted by the Air Force Wright Aeronautical Laboratories (AFWAL) is conducting AEHP demonstration investigations through contract with Boeing Military Airplane Company (BMAC). Appropriate AEHP schemes for the fighter, transport/bomber, helicopter and cruise missile classes of air vehicles are being demonstrated with modified F-14 and All-Composite Airframe Program (ACAP) testbeds. Other Government agencies are participating with AFWAL in support of the AEHP program, which is being conducted to provide design criteria to define appropriate AEHP against the moderate 20kA peak amplitude, $5x10^{10}$A/sec maximum rate-of-rise and the severe 200kA peak amplitude $2x10^{11}$A/sec maximum rate-of-rise attached lightning threats. To demonstrate effective AEHP for air vehicle electrical/electronic systems representative of mid-90s technology, a lightning simulator capable of providing a lightning stroke with the parameters of the severe stroke has been prepared by Maxwell Laboratories, Inc for use on the AEHP program. Various protection concepts developed during the initial part of the AEHP program will be applied to configure the AEHP systems required by the demonstration testbeds of the latter phase of the ADP. These AEHP concepts include circuit and system shielding, terminal protection, conducting floors and cable protection which have been demonstrated to be effective for establishing the protection required against induced electromagnetic (EM) energy or electromagnetic energy directly coupled to electrical/electronic systems. In addition to the induced EM threat, AEHP investigations have been initiated to assure appropriate protection against physical and thermal damage to air vehicles as the result of direct attachment of lightning flashes with composite, as well as metal airframes. Full advantage will be taken of synergistic benefits realized between induced and direct AEHP protection systems. The application of both swept frequency continuous wave (CW) and time domain pulses (moderate and severe) to AEHP program testbeds are discussed.

INTRODUCTION

The two-phase AEHP Advanced Development Program (ADP) enjoys the application of financial and program resources by an assembly of military/civilian agencies. This support is suggested on the logo for the ADP shown as Figure 1. The Flight Dynamics Laboratory (AFWAL/FI) provides the ADP office for interagency coordination and AEHP program direction. Other federal military agencies contributing to the program include other Air Force laboratories and the Aeronautical Systems Division, as well as the Army, the Naval Air Systems Command and the Defense Nuclear Agency. In addition, the Federal Aviation Administration and the National Aeronautics and Space Administration are participating in the program. BMAC is the prime contractor for the program. The National Interagency Coordination Group (NICG) for the National AEHP program meets annually to review the work accomplished,

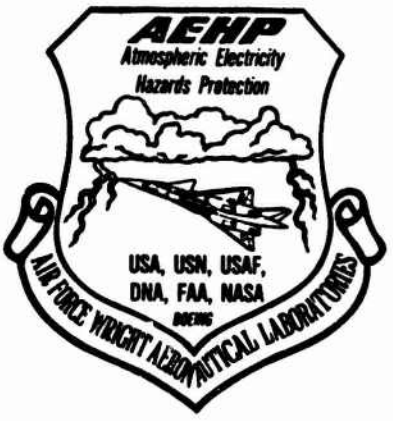

Figure 1 - AEHP ADP Logo

underway and planned by various agencies to encourage a coordinated application of federal resources for AEHP investigations. In addition to the agencies identified in the AEHP logo, the National Severe Storms Laboratory of the National Oceanographic and Atmospheric Administration (NOAA/NSSL) is also a member of the NICG.

The first phase of the AEHP program produced design guidelines defining balanced protection concepts to provide confidence for all-weather application of advanced avionic and structural concepts in military and civilian scenarios. Balanced protection concepts appropriate for each of four classes of aircraft; e.g., fighters, transports/bombers, helicopters and missiles, were developed. This phase was initiated on 1 Apr 82. During Phase One of the program, the electromagnetic environments incident on aircraft electrical/electronic systems were defined and appropriate protection schemes established. In order to achieve this result, the interaction of AE environments with modern aircraft structure(s); e.g., advanced composite materials, high resistance metals; were determined. This permitted characterization of the AE associated threat incident on advanced electrical/electronic elements; e.g., fly-by-wire, power-by-wire, et al. Appropriate hardening concepts were then evaluated experimentally to assure confident operation of flight/mission critical elements under AE threat conditions. The hardening employed includes a balanced set of: system, power and information shielding; passive/active system protection; et al. The AEHP concepts prescribed were also evaluated for their contribution to protection against other EM threats; e.g., EMI, NEMP.

The second phase is utilizing testbeds configured from modified airframes and special test electronics to evaluate the effectiveness of the AEHP concepts developed. Tests with a modified F-14A have been completed and testing with a specially configured helicopter testbed are scheduled to begin in July of 1986. The helicopter testbed has been fabricated from a tool-proof airframe produced during the US Army's All-Composite Airframe Program (ACAP) and special test electronics

repreaentative of aircraft ayatema of the 1990a. The effectivenesa of AEHP applied will be demonatrated/evaluated uaing ground-haaed lightning aimulation facilitiea. The results of initial teats will be evaluated and appropriate adiustmenta performed on the AEHP achemes employed to improve the balanced protection provided. In addition to the demonstration of balanced protection effectiveness, techniquea for qualification of protection and continued assessment of the integritv of the AEHP provided will he identified and demonstrated. Finally, design guides for the application of AEHP will be provided.

The AEHP AFP invitea contributions from the aeroapace technical community to improve the effectiveness of the program and aid tranaition of program reaults to aerospace ayatem application. Your constructive criticism of the AEHP program is encouraged. Continuing interactiona will improve the quality of the AEHP program and yield a maximum return oo the program investment.

AEHP DEMONSTRATION

To demonstrate the effectiveness of AEHP coocepts developed during the program, protection schemes for the F-14A and ACAP baaed testheds were developed. Teat plana were then eatablished for the demonstration using appropriate atmoapheric electricity simulatora. The lightning threat simulators and the testbeds together with teat results will be discussed helow.

LIGHTNING SIMULATION - The AEHP of electrical/electronic systems on modern aircraft can he partially assesaed uaing a awept frequency continuous wave (CW) signal generator and network aoalvzer operating at low current levels; e.g., 20A. Thia procedure will allow definition of a frequency domain transfer function for analytically asaeaaing the impact of lightning aaaociated currents and fields on electrical/electronic ayatema of interest. In the time domain, lightning pulse aimulators mav be employed to determine ayatem responae to the lightning threat. For the AEHP program, a full-threat (aevere) level simulator was prepared and used. It is also poasihle to uae other pulsers to simulate the lightniog threat at lesser intenaities aod perform appropriate scaling of impacts to coosider the full-threat level, aa waa done for the AEHP program using a 28kA pulaer (moderate threat simulation).

The awept frequencv CW aystem uaed for the AEHP program functiooal diagram ia shown in Figure 2.

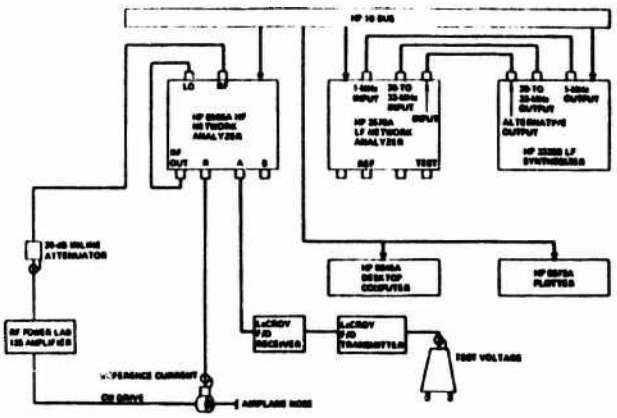

Figure 2 - Swept Frequency Transfer Teat Equipment

Thia syatem allowed meaaurementa from 50Hz to 100MHz. To accommodate for measurement probe characteriatic variationa, a reference tranafer function meaaurement waa performed using a standard calibration fixture prior to performing teat noint tranafer function measurements. Tranaforma of the tranafer function for aelected lightning threat current levels can then he produced to analytically predict the responae of points of interest to the lightning threat aelected.

Using a lightning pulae simulator, the time domain reaponae of pointa of interest can be measured directlv. Theae measurementa were performed uaing threat current levels of 28kA, and alao valuea from 100kA to 200kA. The former aimulation waa performed with the BMAC 28kA aimulator while the latter aimulations were done with the 200kA aimulator developed for the AEHP program by Maxwell Laboratoriea, Inc. The functional diagram for the 28kA (moderate threat level) pulser is shown in Figure 3. The 200kA (severe threat level) pulser is ahown connected to the F-14A teathed and return circuit atructure in Figure 4.

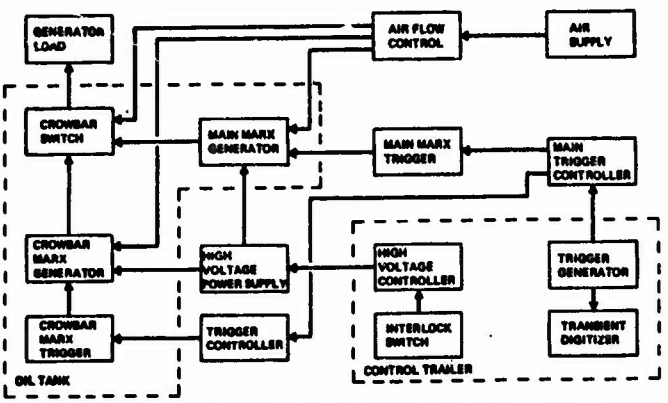

Figure 3 - Moderate-Level Pulse Generator Functional Diagram

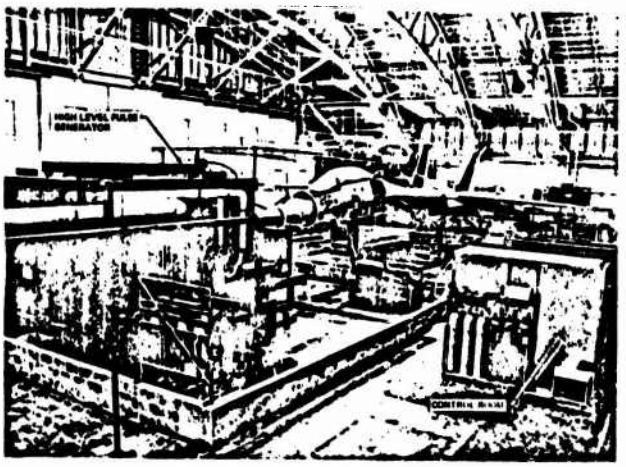

Figure 4 - F-14A and High-Level Pulse Generator

With the moderate level pulser, the AEHP achemes are demonstrated/evaluated againat the defined moderate lightning threat: 20kA peak amplitude with a peak rate-of-riae of $5x10^{10}$ A/S, time-to-peak current of 2μs and fall time to 1/2 peak current of 50μs, aod a minimum action integral of $1.5x10^{4}A^{2}S$. Meaaured "moderate lightoing pulae"

characteristics are shown in Table 1. With the severe level pulses, the protection schemes were demonstrated/evaluated with simulated lightning pulses having up to a peak current amplitude of 200kA with a peak rate-of-rise of 2×10^{11} A/S, time-to-peak of 4.3μs and fall time to 1/2 peak current of 50μs, and an action integral of 1.5×10^{6} A^2S into a 8μH load. Measured "severe lightning pulse" characteristics are shown in Table 2. Figure 5 compares the frequency spectrum of the severe threat simulator (solid line) with the AEHP defined severe threat (dashed line).

	Measured waveform		Defined double exponential waveform
	Nose-to-Tail	Nose-to-Wing	
Peak current (kA)	28	26	20
Rate of rise (10-90%) (A/s)	3×10^{10}	2.4×10^{10}	1.9×10^{10}
Time to half value (μs)	80	30	80
Action integral (A^2-s)	3.5×10^{4}	2.4×10^{4}	1.5×10^{4}

Table 1 - Moderate-Level Current Pulse Characteristics

	Measured waveform		Defined double exponential waveform
	Nose-to-Tail	Nose-to-Wing	
Peak current (kA)	200	195	200
Rate of rise (10-90%) (A/s)	1.72×10^{11}	1.4×10^{11}	8×10^{10}
Time to half value (μs)	80	80	80
Action integral (A^2-s)	2.8×10^{6}	1.8×10^{6}	1.8×10^{6}

Table 2 - High-Level Current Pulse Characteristics

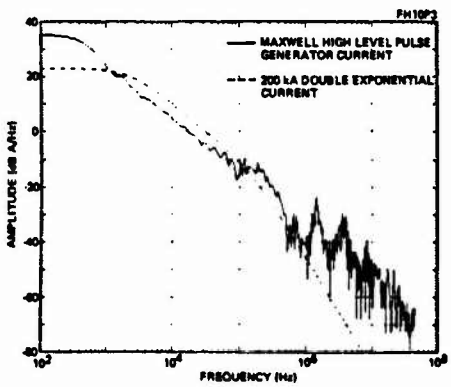

Figure 5 - High-Level Current Pulse Spectra

F-14A TESTBED AEHP DEMONSTRATION/EVALUATION

For the F-14A testbed, AEHP was provided against the defined moderate level threat shown in Figure 6. The AEH protected electrical/electronic

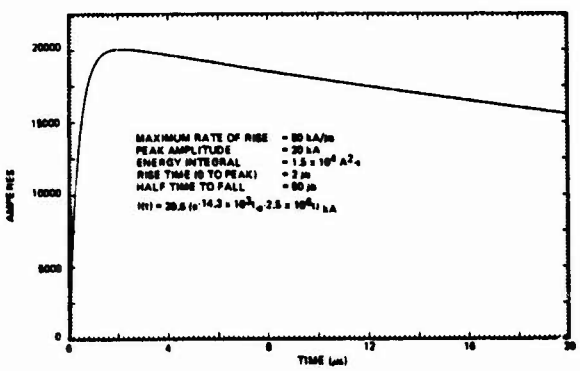

Figure 6 - Defined Moderate-Level Threat

equipment and cables evaluated are shown in Figure 7 and Figure 8 with test points (TP) designated. These equipments were located in the testbed as shown in Figure 9. In addition to the data gathered for the AEHP of electrical/electronic equipment listed above, several measurements of the "lightning threat associated" environment were made to characterize the aircraft testbed response to attached lightning. Test points for testbed characterization are shown in Figure 10. Various test points were monitored when some or all of the lightning threat simulation techniques listed in Table 3 were applied to the testbed.

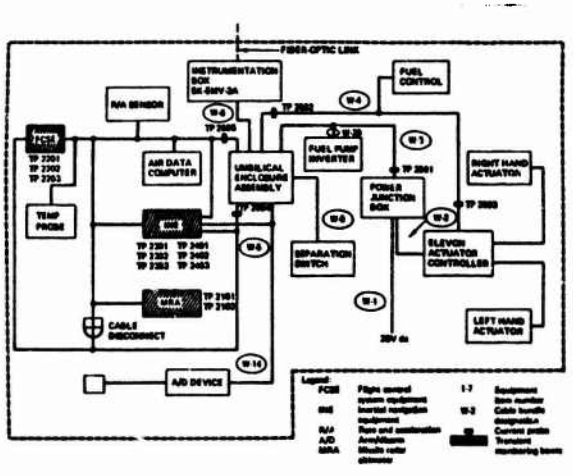

Figure 7 - ALCM Equipment Test Points

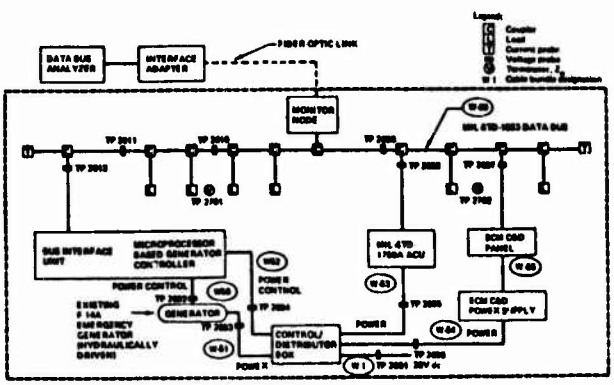

Figure 8 - Advanced Avionics Cable Current Test Points

Type of Evaluation	Designation
CW transfer function measurements (20A)	C
Moderate-level pulse measurements (28kA)	M
Intermediate-level pulse measurements (65kA and 150kA)	I
High-level pulse measurements (200kA)	H

Table 3

The testbed characterization work was performed for several cases of panel coverings; e.g., aluminum, Gr/Ep, open.

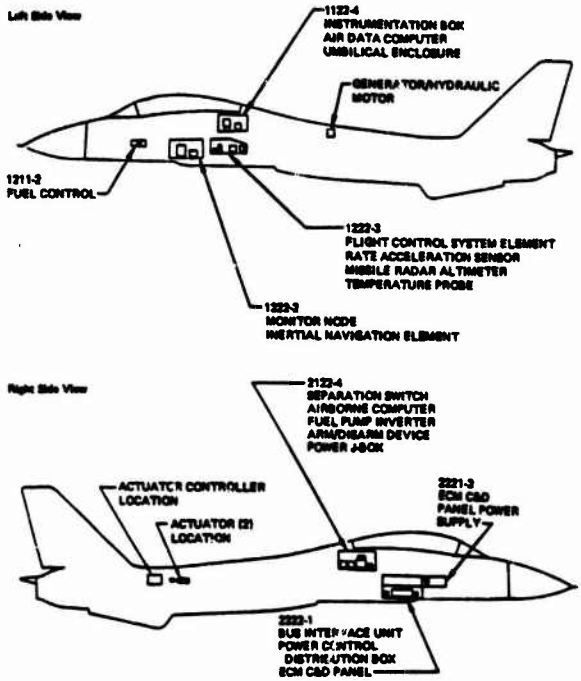

Figure 9 - Equipment Locations

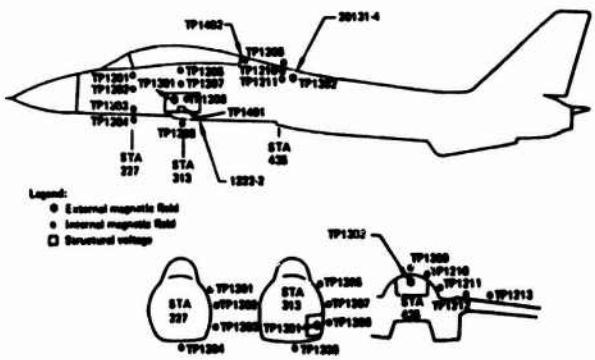

Figure 10 - Airplane Characterization Test Point Locations

The induced levels of voltage/current at various equipment pins and on selected cable bundles were compared with specified avionics susceptibility limits to measure AEHP effectiveness. The moderate-level lightning waveform had been used as the design point for the AEHP so the measured transient response amplitudes were compared with that threat to determine the safety margin for the unit being evaluated; e.g., SM=20 log V_s/V_m where SM is the safety margin in decibels, V_m is the measured pin voltage, and V_s is the specified pin voltage. The safety margins experienced for selected units associated with the special ALCM avionics suite employed are shown in Table 4. Protection techniques employed to achieve this AEHP included cable and box shielding and/or circuit protection in addition to cable routing away from apertures.

Test circuit	Pin voltage limit (V)	Nose to tail		Nose to wing	
		Measured voltage (V)	Safety margin (dB)	Measured voltage (V)	Safety margin (dB)
MRA 28V dc	350	57.3	16	39.4	19
FCSE inverter	100	7.7	22	7.7	22
INE squib enable	100	6.4	24	8.3	22
INE 28V dc	350	22.4	24	23.3	24

Table 4 - ALCM Avionics Safety Margins

In addition to measuring induced transients and structural voltage drops for aircraft stations and equipment of interest, we also performed functional evaluations of AEH protected equipments. In this instance, the operation of the test electronics was monitored during pulse tests to identify system upset or failure. During this portion of the testing, the special ALCM avionic suite performed an automatic flight control sequence, while the data bus system ran error detection sequences using the MIL-STD-1553B bus for data interchange. The avionics systems experienced no upset or damage when subjected to their design level, the moderate-level attached lightning threat with 20kA peak amplitude. The results of tests with the special ALCM avionics is shown in Table 5. It is to be noted that for threat levels up to 100kA, 14db over design level, for both the nose-tail and nose-wing attachment configurations, the operation of the test electronics was normal.

Current path	Number of pulses	Pulse amplitude (kA)	Response
Nose-to-tail	20	28	Normal operation
	15	100	Normal operation
	5	130	Normal operation
Nose-to-wing	7	28	Normal operation
	12	100	Normal operation
	4	140	First upset required restarting ALCM equipment. Could not restart equipment after second upset

Table 5 - ALCM Avionics Functional Responses

ACAP TESTBED AEHP DEMONSTRATION

A tool-proof article from the Bell helicopter ACAP presently under contract with the US Army has been modified to incorporate lightning protection for the vehicle, which is made from Gr/Ep structure with Kevlar skin panels. The avionics suite to be used in AEHP demonstration/evaluation will include elements from the F-14A testbed's avionics suite and other Government-furnished elements. "Lightning" testing of the ACAP is scheduled to begin in July 1986. The tests will include demonstration/evaluation of the AEHP provided up to threat levels of: 200kA with peak rate-of-rise of 2×10^{11} A/sec; and action integral of 2×10^{6} A^{2}sec.

LIGHTNING DIRECT EFFECT EVALUATION

In order to limit protection penalties, the techniques for protecting and verifying the protection of aerospace vehicles fabricated from advanced materials against direct attachment effects of lightning are being reviewed to identify technical voids and contributions to indirect effect protection, as discussed above. It is believed that significant synergism may be realized from appropriate application of the AEHP against induced and direct; i.e., physical/thermal effects.

CONCLUSION

The AEHP program has established a lightning threat for moderate and severe encounters with lightning, established appropriate test technology

for AEHP testing, and identified and demonstrated successful AEHP for various classes of air vehicles. The demonstration program will be continued to treat the challenging case of the ACAP helicopter. The need for physical/thermal protection, as well as synergism available between indirect and direct atmospheric electricity hazards protection schemes will also be documented.

REFERENCE

AEHP program documentation from Contract F33615-82-C-3406, Atmospheric Electricity Hazards Protection (AEHP) of Advanced Technology Aircraft (Electrical/Electronic Subsystems)

AIRCRAFT LIGHTNING-INDUCED TRANSIENT TEST AND PROTECTION COMPARISON

Mark M. Simpson
Boeing Military Airplane Company
P.O. Box 3707, M/S 33-03
Seattle, Washington 98124-2207

ABSTRACT

Ten transfer function and nine moderate-level pulse comparisons were made between test responses and predicted responses for a modified F-14A. The predicted responses were calculated prior to the test using a distributed parameter network model consisting of transmission line models and lumped parameter networks. The moderate-level peak amplitude predictions selected for these comparisons were from 1.2 to 7.4 times greater than the measured peak amplitudes.

INTRODUCTION

This paper gives an overview of a distributed parameter network model that was used to calculate the moderate level current pulse responses of a modified F-14A testbed. This model was developed to support and evaluate the modified F-14A testbed lightning protection design. This model was also developed to evaluate the distributed parameter network modeling technique. The F-14A was modified by removing five forward avionics bay access panels and replacing the turtle deck panels with graphite-epoxy panels. Air-launched cruise missile (ALCM) avionics and test equipment were installed in the forward avionics bays. Moderate-level current pulse responses of the ALCM avionics, airborne computer, and test equipment were predicted.

MODEL DESCRIPTION

The F-14A transient analysis incorporated a distributed parameter network model with previous test data and analysis results (1), (2), (3). The PRESTO modeling programs were used to calculate the network responses (4). PRESTO is a set of computer programs which calculate the transient response of transmission lines and lumped parameter networks. TRAFFIC, a PRESTO system subprogram, calculated the frequency domain response of the distributed parameter network models.

The TRAFFIC network models produced test point transfer functions, with the test point response relative to the total drive current on the airplane. TRAFFIC used a linear solution of the network equations. The test point transfer functions were multiplied by the drive current spectrum and the product was Fourier transformed to produce the test point pulse response. A transmission line model was developed to represent the current distribution along the F-14A and return conductors. Coupling to internal wires was modeled with lumped parameter networks. The general sequence of the calculations is illustrated in figure 1.

LIGHTNING MODEL - The drive current on the airplane was modeled using a double exponential current waveform. The waveform equation in amperes is listed below.

$$I(t) = 27.7 \times 10^{3} (e^{-14.3 \times 10^{3} t} - e^{-2.5 \times 10^{6} t}) \quad A$$

This waveform represents the peak current and rate of rise generated by the Boeing moderate-level pulse generator.

AIRCRAFT CURRENT DISTRIBUTION MODEL - Current distribution along the airplane was represented with a series of coaxial transmission line segments. The dimensions of the airplane and the return conductors were used to develop an equivalent coaxial transmission line. Then the electrical parameters of the coaxial transmission line were used in the network analysis. The transmission line model of F-14A and return conductors is illustrated in figure 2.

The PRESTO TRAFFIC program was used to calculate the response of the transmission line current distribution model (4).

Each transmission line segment was represented by an impedance block composed of distributed resistance, inductance, and capacitance. TRAFFIC then calculated the network response using transmission line equations. A 1A current source drove the airplane model at 425 frequencies ranging from 100 Hz to 100 MHz. The ac resistance incorporated into the transmission line model was set to produce a quality factor of 36, a value based on results of previous F-16 tests (6).

Circumferential current variations on the airplane were determined from an F-14A model developed by the Syracuse Research Corporation (5). Method-of-moment calculations performed on the F-14A model produced the current distribution. The circumferential current distribution was incorporated into the transmission line model in terms of a current density factor (J_S).

The drive point impedance and external magnetic fields were calculated from this airplane model. The drive point impedance was calculated by dividing the voltage at the airplane nose by the current. Magnetic fields were calculated by determining the current density at points along the transmission line model.

INTERNAL MAGNETIC FIELD MODELS - Separate internal magnetic field models were developed for the forward avionics bay and for the turtle deck. The fields inside a trough in an infinite plane were used to model the fields inside the avionics bays (7). A factor relating the internal magnetic field to the external magnetic field was multiplied by the external current density to calculate the internal magnetic field.

The turtle deck internal magnetic field was modeled with measured data on an F-16 graphite-epoxy mockup (6). This F-16 diffusion transfer function was used because the F-16 graphite-epoxy mockup is similar in shape to the F-14A. Craft found that current will distribute over the surface of graphite-epoxy structures the same as for aluminum structures (8). The measured diffusion transfer function was a constant up to 64 kHz, where it started to decrease at 20 dB per decade. A resistance of 0.32Ω in parallel with a 7.81-μF capacitance modeled this transfer function. The transfer function of the circuit model was then multiplied by the transmission line external magnetic field transfer function.

STRUCTURAL VOLTAGE MODELS - The structural voltage drop coupling models were developed for the forward avionics bay and for the turtle deck panel. The forward avionics bay structural voltage drop was modeled as an inductor because the avionics bay was open and therefore the coupling mechanisms were inductive. The value for the inductor was obtained from the inductive contour lines in a slotted cylinder determined by Burrows (9). The rectangular avionics bay was mapped into the slotted cylinder. The inductive contour value was then multiplied by the length of the voltage probe and a factor to take into account the difference in current density between the cylinder and the F-14A. The voltage probe was located 0.051 m below the top of the avionics bay. The inductive contour value was 0.04 μH/m. The probe length was 1.12m. Taking into account the difference in current density between

the slotted cylinder and the F-14A, the inductance was calculated to be 0.06μH. The transfer function of the circuit model was multiplied by the external magnetic field transfer function.

The turtle deck structural voltage drop was modeled as loop and joint coupling. The joint coupling and the loop coupling were 180 degrees out of phase. The circuit model for the loop coupling accounted for the diffusion through the turtle deck. The voltage drop probe was a wire 4.24m long situated 0.01m above the aircraft structure. The joint coupling was modeled as a resistance in series with an inductance. The values for the resistance and inductance were taken from a panel voltage transfer function measured on a graphite-epoxy F-16 mockup (6).

CABLE COUPLING MODELS - For cables in open avionics bays, the coupling was modeled as the transfer function of an inductor whose value was obtained from the model of the open forward avionics bay structural voltage drop. This value was then multiplied by the wire length and a factor to correct for the differences in current distribution between the slotted cylinder and the F-14A. The coupling to cables beneath the turtle deck was determined by the turtle deck structural voltage drop coupling.

The avionics coupling diagram is shown in figure 3. Cables W3 and W6 were multiconductor cables. However, to simplify the modeling, the cables were modeled as a single twisted-pair cable of the predominant wire gauge. Cables W3 and W6 also had several branches. To simplify the model, the cable branch effects were not included. Only common-mode cable coupling was calculated.

The coupling sources were grouped into one source for each type of coupling and placed at the end of the cable closest to the missile radar altimeter (MRA). Each coupling source was added separately with the others open circuited. The coupling source consisted of the transfer function of the coupling source multiplied by the external magnetic field transfer function. The MRA 28V-dc power line open-circuit voltage transfer function for each coupling source was superimposed to compute the total transfer function for the MRA 28V-dc power line open-circuit voltage and the core currents on cables W51 and W1. The aperture sources were modeled as inductors whose values were obtained from Burrows M_{TF} contours using the same method that was used to calculate the coupling for the forward avionics bay structural voltage drop (9). The diffusion and joint source were modeled using the same model that calculated the turtle deck structural voltage drop. The cable impedance values were calculated from the equation for two cables 2 in above a ground plane. The impedance of the cable inside the shield was calculated from the formula for a coaxial cable. The shield transfer impedance was based on previously measured data. The shield transfer impedance was modeled as two pigtails with an impedance of 11.4 mΩ and 602 pH (1).

TEST AND PREDICTION COMPARISON

After the tests the predictions were compared to the test data (3). The predictions and test data comparisons are shown in table 1. This table was generated from figures of the measured test responses plotted on the predicted test responses. Figures 4 through 9 are typical of those figures.

The turtle deck external magnetic field transfer function comparison (figure 4) shows variations of six decibels up to the second resonance. The variations after the second resonance are within 15 decibels. The 15 decibel variation is the result of the F-14A and return conductors being more lossy and radiating more energy than predicted by the transmission line model of the F-14A testbed. The turtle deck external magnetic field comparison (figure 5) shows peak amplitudes within 1.2 times of each other and shows the same rates of rise. The predicted response does not decay as fast as the measured response because the lightning model used does not model decay that fast. The predicted response has a slightly different shape because the lightning model does not model the moderate-level pulser ringing. The missile radar altimeter 28 V-DC power open circuit voltage transfer function comparison (figure 6) shows variations up to 10 decibels below the second resonance. The variations above the second resonance are within 30 decibels. The 30 decibel variation is the result of the F-14A and return conductors being more lossy and radiating more energy than predicted by the transmission line model of the F-14A testbed. The missile radar altimeter 28 V-DC power open-circuit voltage comparison (figure 7) shows peak amplitude within 4.9 times of each other and shows the same envelope shapes. The oscillatory nature of the predicted response is the result of the F-14A and return conductors being more lossy and radiating more energy than predicted by the transmission line model of the F-14A testbed.

The cable W1 core current transfer function comparison (figure 8) shows variations within 40 decibels up to first resonance. Between the first resonance and the second resonance the variations are within 20 decibels. Above the second resonance the variations are within 40 decibels. The 40 decibel variation is the result of the F-14A and return conductors being more lossy and radiating more energy than predicted by the transmission line model of the F-14A testbed. The cable W1 core current comparison (figure 9) shows peak amplitudes within 1.5 times of each other and shows the same envelope shapes. The oscillatory nature of the predicted response is the result of the F-14A and return conductors being more lossy and radiating more energy than predicted by the transmission line model of the F-14A testbed.

The pretest peak amplitude predictions were from 1.2 to 7.4 times greater than the measured peak amplitudes. Both the pretest predicted responses and the measured responses decayed quickly. The pretest peak amplitude predictions and the measured peak amplitudes depended on the current rate of rise. However, the pretest predicted responses had a damped sinusoid riding on top of the waveforms. The sinusoid had a frequency corresponding to the F-14A testbed quarter-wavelength resonance.

PREDICTION SUMMARY

The F-14A test point responses were predicted before the lightning simulation tests. After the tests, the F-14A test point predicted responses were then compared to the measured responses.

The peak amplitude predictions were an average of three times greater than the measured peak amplitudes. The peak amplitude predictions were from 1.2 to 7.4 times greater than the measured peak amplitudes. Both the predicted responses and the measured responses decayed quickly. Peak amplitude of the predicted responses and the measured responses depended on the rate of rise in th current. However, the predicted responses were more oscillatory than the measured response. The predicted responses had a damped sinusoid riding on top of the waveforms. The damped sinusoid had a period corresponding to the F-14A testbed first resonance.

ACKNOWLEDGEMENT

The work described in this paper was performed under sponsorship under Atmospheric Electricity Hazards Protection (AEHP) Advanced Development Program, Vehicle Equipment Division, Wright-Patterson Air Force Base, Ohio contract F33615-82-C-3406. The author would like to acknowledge the support of the following people: Air Force Program Manager Rudy C. Beavin, Air Force Technical Manager Captain M. Patricia Hebert, Boeing AEHP Program Manager Stanford D. Schneider, and Boeing Technical Manager David B. Walen.

REFERENCES

1. O. L. Sommer and B. G. Melander, "Atmospheric Electricity Hazards Protection Design Evaluation-F-14A," Boeing report D180-27423-34, under contract F33615-82-C-3406, December 1984.

2. M. M. Simpson, "Atmospheric Electricity Hazards Protection Evaluation Test Predictions-F-14A," Boeing report D180-27423-41, under contract F33615-82-C-3406, September 1985.

3. D. B. Walen and M. M. Simpson, "Atmospheric Electricity Hazard Protection Assessment, Test and Analysis-F-14A," Boeing report D180-27423-44, under contract F33615-82-C-3406, draft - January 1986.

4. "PRESTO Digital Computer Code User's Guide", ONA 3898F-1, -3, -5 and -6, under contracts DNA001-78-C-0271 and DNA001-78-C-0138, October 1980.

5. O. T. Auckland, et al., "Electromagnetic Hardening of Composite Structures - Susceptibility Analysis of the F-14 Aircraft to Nuclear Electromagnetic Pulse and Lightning Threats," SRC report TR82-1276, Volume 2, under contract N0019-79-G-0584, June 1982.

6. D. B. Walen, "Atmospheric Electricity Hazards Vulnerability Test and Assessment," number D180-27423-24 AFWAL-TR-84-3103 and F33615-82-C-3406, December 1984.

7. K. S. H. Lee, "EMP Interaction: Principles, Techniques, and Reference Data," AFWL-TR-80-402 under contract F29601-76-C-0149, December 1980.

8. W. L. Craft, et al., "Protection Optimization for Advanced Composite Structures," AFWAL-TR-81-3039, under contract F33615-77-C-5169, May 1981.

9. B. J. C. Burrows, "Designer's Guide to the Installation of Electrical Wiring and Equipment in Aircraft to Minimize Lightning Effects," Culham Laboratory report CLM-R212, January 1981.

Test point	Test point ID	Measured		Predicted	
		Peak amplitude	Time to peak μs	Peak amplitude	Time to peak μs
Forward avionics bay external magnetic field	TP1206	3.67 kA/m	1.20	9.84 kA/m	2.05
Turtle deck external magnetic field	TP1209	3.29 kA/m	1.20	3.84 kA/m	2.05
Forward avionics bay internal magnetic field	TP1301	3.11 kA/m	1.20	4.20 kA/m	2.05
Turtle deck internal magnetic field	TP1302	532 A/m	5.40	3.83 kA/m	11.90
Forward avionics bay structural voltage drop	TP1401	992 V	0.40	6.63 kV	0.05
Turtle deck structural voltage drop	TP1402	137 V	1.10	1.01 kV	0.90
MRA 28V dc power open circuit voltage	TP2101	57.3 V	0.36	283 V	0.10
Cable W1 core current	TP2601	1.09 A	2.00	1.6 A	0.25

Table 1. Predicted and measured response peak amplitude comparison

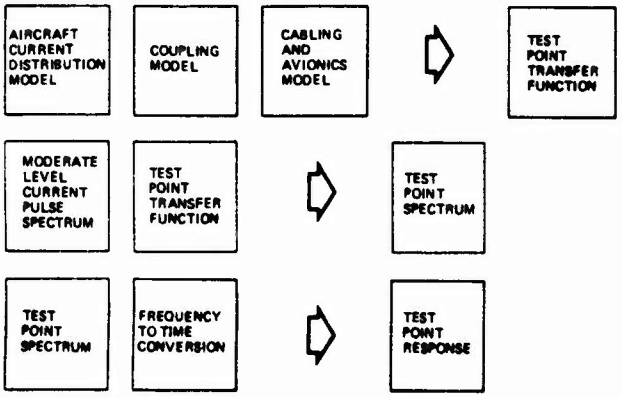

Figure 1. Predictions model flow

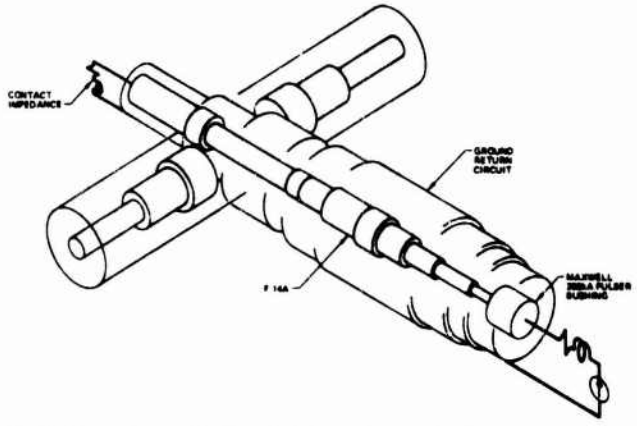

Figure 2. Transmission line model of F-15A and return conductors

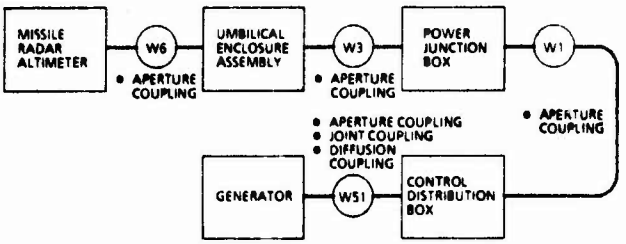

Figure 3. Avionics coupling diagram

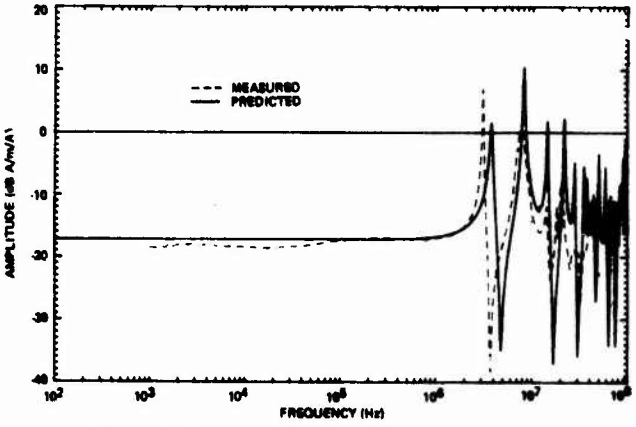

Figure 4. Turtle deck external magnetic field transfer function comparison

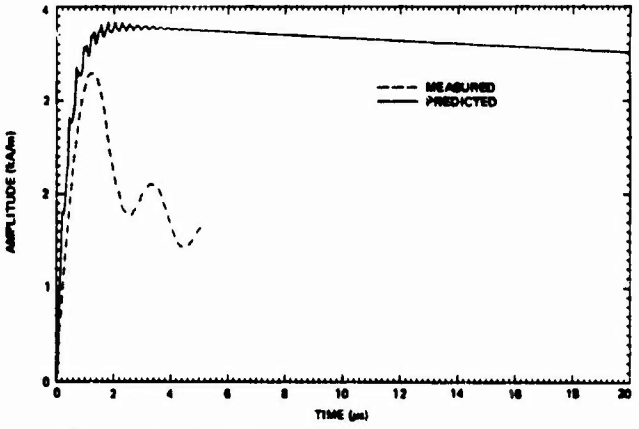

Figure 5. Turtle deck external magnetic field comparison

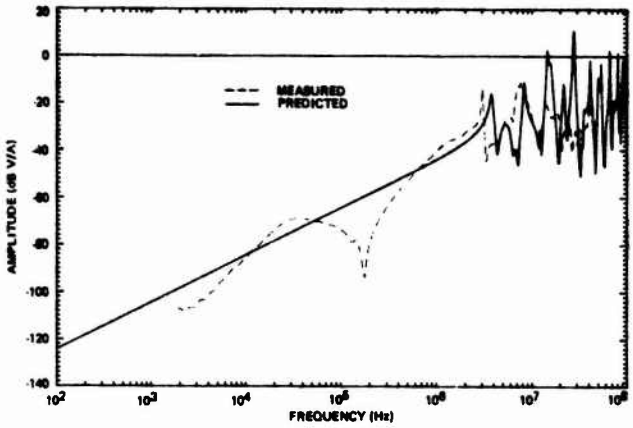

Figure 6. MRA 28V-DC power open-circuit voltage transfer function comparison

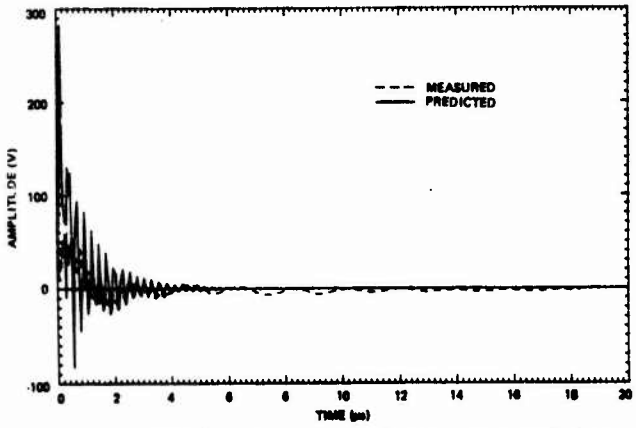

Figure 7. MRA 28V-DC power open-circuit voltage comparison

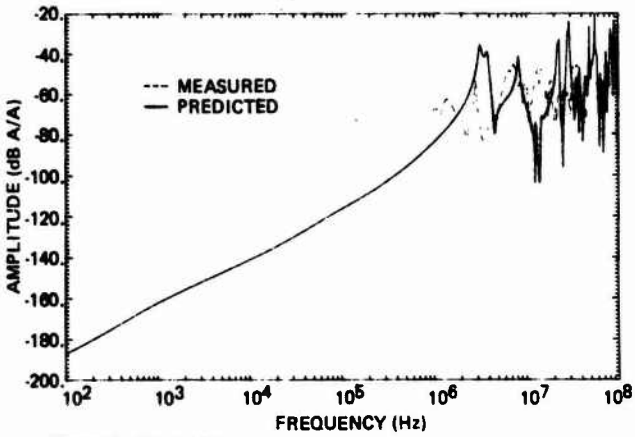

Figure 8. Cable W1 core current transfer function comparison

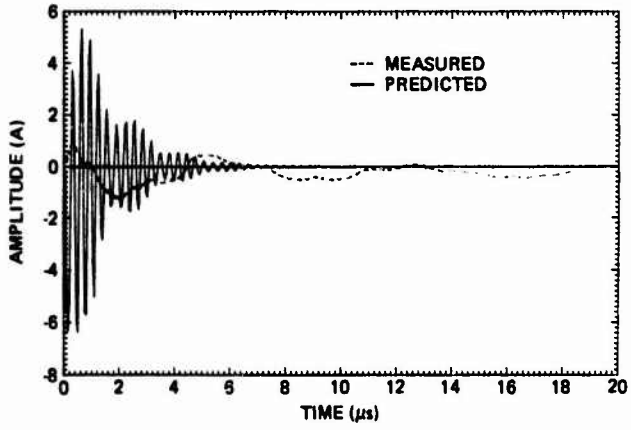

Figure 9. Cable W1 core current comparison

SUBMICROSECOND STRUCTURE OF THE RADIATION FIELDS PRODUCED BY LIGHTNING CORRELATED CURRENT DERIVATIVE (dI/dt) AND ELECTRIC FIELD DERIVATIVE (dE/dt) EMITTED BY TRIGGERED FLASHES

J. Hamelin, C. Leteinturier, L. Nicot, and C. Weidman
Centre National d'Etudes des Telecommunications
Lannion, FRANCE

ABSTRACT

During the summer of 1985, an experiment on triggered lightning flashes was conducted in Florida; several French and American Research groups were involved in the lightning characterization. The National Center of Telecommunications (CNET) was particularly interested in the measurement of the lightning derivative current dI/dt, one of the main lightning parameters in order to design efficient protections. The dI/dt sensor, located at the base of the lightning channel, has a risetime response of about one nanosecond; through a 130 MHz anslog fiber optic link, that sensor was connected to a transient digitizer, giving a dI/dt value every 5 nsec.

The derivative electric field dE/dt was simultaneously measured, 50 m from the triggered lightning discharge.

In that report, the experiment is described in detail. We investigate the validity of return-stroke model expressions correlating dE/dt and dI/dt and we also compare these dE/dt measurements at 50 m to those obtained at various distances. (1, 2).

/1/ C.D. WEIDMAN and E.P. KRIDER, Geophys. Res. Lett. 7(1980) 955-958

/2/ C. LETEINTURIER - E.P. KRIDER and J.C. WILLETT, 10th internation. Aerosp. and Ground Confer. on Lightning and Static Electricity - Paris - June 1985.

EXPERIMENTAL STUDY OF THE INTERACTION BETWEEN AN ARC AND AN ELECTRICALLY FLOATING STRUCTURE(*)

by G. Labaune, J.P. Moreau, J.C. Alliot, V. Gobin
Office National d'Etudes et de Recherches Aérospatiales,
BP 72, 92322 Châtillon Cedex, France

and B. Hutzler, G. Riquel, R. Garabedian
Electricité de France, Les Renardières,
BP 1, 77250 Moret-sur-Loing, France

We describe an experiment allowing the study of the connection between an arc and an electrically floating structure.

The high voltage set-up is the 6 MV generator of the EDF Research Center "Les Renardières". Gaps both side of the structure are about 4 m.

Data presented concern currents on the high voltage rod and at the earth, electric and magnetic fields at the surface of the structure, and voltage appearing on various kind of lines inside the structure.

The phenomenology of the connection is also studied by the way of an electronic image converter.

An important part of the analysis deals with the phase of the connection during which the plasma each side of the structure is of high resistivity (predischarge). We show that during this phase, the structure is in electric equilibrium between impulsive positive and negative streamers which induce fast and strong variations of the electric field at its surface.

An attempt will be made to compare laboratory results with in-flight measurements in the case of the connection between an aircraft and an atmospheric lightning channel.

(*) This work was supported by DRET (Direction des Recherches, Etudes et Techniques.

INTRODUCTION

This experimental work is performed within the framework of the study on the connection of aircraft and atmospheric lightning chanels. In-flight measurements on an aircraft [1, 2] show up the existence of complex attachment mechanisms during the period preceeding the passage of the return stroke. The process involves phases of electric and magnetic field pulse variations at the structure surface. The difficulty of accessing the parameters defining the discharge on the outside of an aircraft in flight led us to study these connection mechanisms on a cylindrical laboratory model. Previous experiments made with short arcs [3] (a few tens of centimeters) have shown the existence of a phase during which the high resistivity of the plasma channels formed in the gaps leads to strong variations of the structure potential, hence of the electric field at its surface.

Nevertheless, for short gaps, the initial streamers from the electrodes are long enough to cross these gaps and form a conduction condition which gives a preponderant significance to the electrical circuit. Hence, this configuration does not allow study of the influence of the discharge attachment process on the structure electric balance. To remove this problem, we have set up an experiment which uses air gaps which are several meters long, so that the phases during which the discharge channel propagates can be observed. A priori, this configuration seems to yield a nearer representation of the electrical behavior of an aircraft from which a leader propagates.

We have also examined the behavior of typical lines placed in the cylinder so as to determine which of the physical mechanisms appearing during connection, are the most dangerous to on-board equipment.

EXPERIMENTAL DEVICE AND EXPERIMENTS RUN

The experiments were run at the EDF's Renardières Testing Center. Figure 1 shows the high voltage test hall and the experimental set-up.

The shock generator (1) can deliver a maximum voltage of 6 MV and an energy of 450 kJ.

The rise time of the pulses can be set from two to several hundreds of microseconds.

The test model is a cylinder made of AG5 length 4 m, dia. 0.5 m, wall thickness: 2 mm). The cylinder has four square openings (20 x 20 cm) which can be blanked with metallic or composite material plates.

The experimental equipment consists of:

- a Thomson electronic imag converter operating in streak mode in the visible and ultraviolet spectra,
- a Hadland image converter operating in streak mode and frame mode in the visible and ultraviolet spectra,
- a current measuring coaxial shunt (2) located at the extremity of the high voltage rod,
- a current measuring coaxial shunt (3) placed on the ground. It is fitted with a rod ensuring attachment with the arc,
- a capacitive divider (4) ensuring voltage measurement at the high voltage rod.

Fitted to the cylinder are:

- two Ḋ sensors (5) with a equivalent area of $0.82 \times 6.10^{-3} m^2$,
- one Ḃ sensor (6) with a equivalent area of $1.5 \times 10^{-4} m^2$
- one line inside the model, placed parallel to the model axis. The distance to the opening can vary from 5 to 45 cm.

Line measurement impedance is 50 Ω; the terminal impedance is interchangeable and can vary from short circuit to open circuit. The length of the line can also be changed.

The set of measurements is transmitted via optical fibers (bandwidth 200 MHz). Digitization is performed by 8-channels, Tektronix 7612 D. The digitizers and data storages are controlled by a Tektronic 4041 calculator.

The use of very wideband analog integrators has proved to be difficult, hence, we opted for storing the signals in a derivative form for this experiment, the values of the electric and magnetic fields were then obtained through digital integration. The digitizer dynamic measurement range (30 dB) is a constraint given the very large spectral content of the signals recorded. However, it proved adequate for the tests using fast rise time voltage shocks (< 50 µs).

The tests were run in negative polarity with voltage shock rise time of 2 to 50 µs. The choice of polarity was dictated by previous experiments performed by the Groupe des Renardières which showed that the gap that can be crossed by 6 MV voltage is around 12 m (given the presence of the model) and that typical streamer size is around 2 m. These values have proved to be coherent with the analysis of the model electrical behavior before establishing a resistive junction in the two gaps.

CONNECTION PHENOMENOLOGY

REVIEW OF THE GENERAL PHENOMENOLOGY OF DISCHARGES IN LARGE AIR GAPS [4]

Traditionally, a distinction is drawn between the positive discharges developing in the direction of the electric field and negative discharges developing in the opposite direction. The phenomenology associated with these two polarities is fundamentally different.

POSITIVE DISCHARGES - In accordance with the preceeding convention, positive discharges develop from positive electrode. A leader extends out from the rod due to the energy drained by the streamers at its tip. This type of streamer is a medium in the process of thermalization. It radiates in the red spectrum. The streamers at the tip are strong electric field media where electrons are accelerated in a cold gas and make ionizing collisions; The associated radiation is purely ultraviolet (electronic recombination). The orders of magnitude of the electric fields are from 0.5 to 1 $kV.cm^{-1}$ in the region of the leader and 4 to 5 $kV.cm^{-1}$ in the region of the streamers.

The general properties of the discharge (speed, current, etc.) depend on the electrode-plane geometry and the shape of the pulses, hence, propagation can be continuous or discontinuous.

NEGATIVE DISCHARGES - There are discharges which propagate from negative electrode. Their breakdown threshold in a given gap is two to three times higher than that for positive discharges. A negative discharge is always discontinuous. In certain rising time or geometric configurations, a highly complex phenomenology arises involving negative streamers, spatial stems, spatial leaders and positive leaders.

If an electrically floating metal object is introduced into the breakdown gap, the

phenomenon becomes even more complicated because discharges from the high voltage rod the ground rod and the two ends of the object come into play. This configuration has already been the subject of a specific study [4].

Not all the phases of connection will be treated fully in this paper, our purpose is simply to determine those inducing variations in the electric and magnetic fields on the surface of the cylinder which are likely to created interference on the equipment inside it.

DESCRIPTION OF CONNECTION ON THE MODEL

Figure 2 shows the simultaneous development of luminous phenomena (in the visible and ultraviolet spectra) observed in the two rod voltage gaps and the electric and magnetic fiels on the surface of the cylinder.

The event chronology is as follows: when the voltage of the rod becomes high enough, negative streamers appear at its extremity. Their structure is filamentary. They carry a pulse-like current. The peak value of the pulses can reach several hundreds of amperes. A negative streamer-leader system propagates in the direction of the model. We observe that this approach phase does not give a significant variation in the electric and magnetic fields on the surface of the structure. In the configuration used, the capacitive effects related to the approach of the negative streamers and the effects of the positive streamers from the top surface of the cylinder are negligible Moreover, it has been shown that during the whole experiment, the capacitive effects (associated to a change in the field geometry) are negligible and that the measurement of the E field gives a good picture of the cylinder potential.

When the junction is made with the top surface of the cylinder or with the positive streamers extending from it (point 1 on the curve showing the electric field variations), a variation in the electric field at the surface of the structure is observed, which shows that its potential has increased. This variation depends on the capacitance of the structure and the impedance present in the medium in the top gap.

The appearance of a large electric field in the bottom gap gives rise to the appearance of negative streamers at the base of the cylinder. They have the same morphology as those observed previously at the high voltage rod (their appearance corresponds to point 2 on the graph of the electric field).

The current they carry across the high impedance of the top gap provokes a drop in the potential of the cylinder and the extinction of the negative streamers at its base (point 3).

The extinction of the streamer leads to the relaxation of the RC circuit set up by the cylinder capacitance and the resistance of medium in the top gap.

Figure 3 is a detailed view of this phase which shows up systematically and which is one of the major causes of the variations in the electric field at the surface of the structure.

The next period (segment 4-5 on the electric field graph, figure 3) appears as a period of extinction on the cameragram, the electric field is stable at point 5, there is a sudden reignition of the top gap. This brings complex phenomenology into play which induces an increase in the surface electric field on the structure.

The process is the same as for phases 2-3-4: appearance of a negative streamer at the base of the cylinder, drop in the electric field (or cylinder potential) associated with the flow of current through the strong impedance of the top gap, extinction of the streamer (point 6) and relaxation of the RC circuit between points 6 and 7.

An additional phenomenon shows up on the cameragram, figure 3. It is a strong corona effect emanating from the edge of one of the openings. We will see later that these local effects are one of the major causes of interference on the line.

Afterwards, a negative downward leader-positiveupward leader system develops in the bottom gap. Their junction brings us back to the short gap configuration (3); the cylinder is equilibrium between the two resistive media, the circuit is closed.

Starting at this instant, and during the period as follows (up to point 8), there is no short circuit (arc phase) in either one of the two gaps. As we have seen previously, the surface electric field is a correct representation of the potential of the structure. If one of the gaps was in short-circuit, it would remain stable (at high voltage or at ground) and if both gaps were in short-circuit, a strong current would flow.

This phenomenon has already been observed in the study of short gaps and which showed that the passage to arc could not occur until after a critical density of energy is deposited in the medium; this threshold can be reached first in one of the gaps or the other;

This property also appears here. It should be remarked that the passage to the arc occurred in the bottom gap when cylinder was placed near the high voltage rod (1 to 2 m).

Finally, when the medium reaches the arc phase in the two gaps, the current (surface magnetic field) can be established in the circuit (point 8).

COMPARISON WITH THE DATA RECORDED IN-FLIGHT

a) The propagation phase of the discharge between the electrode and the cylinder does not provoke any significant variation in the electric and magnetic fields on its surface. The variations only occur when a junction has been set up by a resistive medium in the top gap.

b) Except for the effect of the first contact with the negative streamers, the strongest variations in the surface electric field are related to the fact that negative streamers tend to propagate the discharge towards the ground provoking the flow of a strong current across the resistive medium in the top gap. These variations are impulsional as is the propagation mode of negative streamers. The variations in potential occurring on the surface of the structure reinforce this character.
Therefore the basic parameter driving the variations in the surface electric field is the impedance of the top channel.

c) The variations in the surface magnetic field are associated to the current flow caused by the negative streamers forming the bottom channel (a few hundreds of amperes) and the arc current (a few tens of thousands of amperes in our case).

d) Figure 4 shows the simultaneous development of the electric and magnetic fields at the surface of an aircraft in flight. The sequence presented was recorded before the passage of the arc current. It would seem reasonable to assume that the mechanism causing the field impulsions is the same as the one described in b). It can be observed that over time and for relatively constant variations in the magnetic field, variations of the electric field become smaller and smaller. This property can be explained by the fact that the medium of the upper gap, which is in the process of thermalization, becomes more and more conductive.
The number of pulses obtained in-flight can be large by comparison to what we have observed in our experiment where connection at the ground is obtained very rapidly.

e) Finally, we would like to indicate the magnitudes of ariationso f the surface electric and magnetic fields:

$$dE/dt = 10^{12} - \text{V/m/s}$$

$$dH/dt = 4.10^{9} - 7.10^{9} \text{ A/m/s}$$

These values are fully comparable with those recorded in flight [1, 2].

INTERFERENCES INDUCED ON THE INTERNAL LINES

In this section we will describe the influence of the various phases of attachment on the lines located inside the structure.

First of all, let us state that the diffusion time of the magnetic field through the testcylinder wall is around 10 µs. This value removes any possibility of interference on the lines by this mechanism during the period of development of the observed phenomena.

We have already observed [3] that the sensitivity of internal lines to variations of external electric and magnetic fields is strongly related to their load impedance.

All the results given further on were obtained with only one opening unblanked.

INFLUENCE OF LINE LOAD IMPEDANCE

LINE LOADED WITH HIGH IMPEDANCE - Figure 5 shows the simultaneous development of parameters outside the cylinder and the voltage on the line.

It can be observed that interference appears on the line during periods of variation of the external electric field. Figures 5d, e, f show that when the variations of the electric and magnetic fields occur simultanoously on the outer surface, interference on the line perfectly follows the derivative of the external electric field and not that of the magnetic field. The oscillation (8 MHz) that shows up simultaneously after passage of the arc on the external electric field and on the line voltage (figure 5d, e) is effectively due to the outside circuit after connection in the two gaps. It has been observed on several records that the oscillation that appears on the line at each sudden change of the external electric field represents its excitation. Tests run with lines of different lengths show that the lines act as quarter-wave antennas. During these phases, the structure itself is not excited, no oscillation appears on the records of the external electric field.

LINE LOADED WITH A LOW IMPEDANCE - As already shown (3), the lines in short circuit orlocated with a low impedance are sensitive to variations of the external magnetic field (figure 6a).

LOCAL EFFECTS

In certain cases, a line loaded with a high impedance (hence sensitive only to external electric field variations) undergoes strong interference whilst the records of the external electric field show no variation (figure 7, point A).

The image converter cameragrams systematically reveal the simultaneous appearance of a corona effect on the edge of the opening left unblanked.

The interference on the line is generally of high amplitude whilst the lines loaded with low impedances are completely insensitive to the appearance of this type of phenomena.

It should also be observed that the associated currents should be of low amplitude since the surface electric field is not affected even though the upper gap medium is in a resistive phase. The strong intensity of the interference can therefore be attributed to a strong coupling between the discharge and the line.

TESTING WITH COMPOSITE MATERIAL COVERS

A certain number of tests were run to determine the interference induced on the line when the openings on the cylinder are blanked with composite material plates (thickness 3 mm).

It seems that the internal lines, whether they be loaded with high or low impedances, undergo interference related to the variations of the external magnetic field (figure 8). We will not give an interpretation of their coupling mode here. However, the respective spectral content of the external magnetic field and the interference on the line (figure 8b) when compared with those when the opening is not blanked, would infer that the interference is associated with the diffusion of the magnetic field across the composite material.

REVIEW OF THE ORDERS OF MAGNITUDE OF THE OBSERVED VALUES

The table hereafter lists the main orders of magnitude of the outside parameters and the interference they induce on the various lines. All these values were reproduced during the few hundred firings made during the experiment.

Moreover, the derivatives of the external electric and magnetic fields are thoroughly representative of the records obtained in-flight during lightning strikes.

All the results are given for the case where a single access allows penetration of the field, the other three openings are blanked with metallic plates.

CONCLUSIONS

The study of the connection of an electrically floating structure via electric arcs a few meters long has confirmed the existence of a strong resistive phase of the medium during the formation of the discharge channel. In addition, the greater distance separating the gaps (longer than the streamers) allowed observation of the propagation phases in the two gaps. Under our experiment configuration, the upper discharge propagation phase did not cause significant interference on the surface of the structure. Conversely, propagation in the bottom gap provoked strong electric interference due to the rise in the potential of the structure in association with the flow of streamer current across the gap which is still highly resistive.

It would seem that the results obtained are comparable with those obtained during lightning and in-flight experiments.

From the standpoint of internal interference, the variations in the surface electric field provoke the appearance of relatively strong voltages on the internal lines when they are loaded with high impedance.

It was also observed that local effects (corona effects appearing on the asperities of the structure) can provoke the same type of strong lines of interference if they occur in the immediate proximity of the openings.

Finally, the tests run using the composite materials showed that their used lead to a significant penetration of the magnetic field.

REFERENCES

[1] - J.P. Moreau, J.C. Alliot, *E and H fields measurements on the Transall C160 aircraft during lightning flashes*, 10th International Aerospace and Ground Conference on Lightning and Static Electricity, Paris, 1985.

[2] - P.L. Rustan, J.P. Moreau, *Aircraft lightning attachment at low altitude*, 10th International Aerospace and Ground Conference on Lightning and Static Electricity, Paris, 1985.

[3] - P. Levesque, J. Taillet, G. Labaune, S. Larigaldie, J.C. Alliot, *A study of the physical mechanisms and the perturbations created by the attachments of an arc to a conducting cylinder*, 10th International Aerospace and Ground Conference on Lightning and Static Electricity, Paris, 1985.

[4] - B. Hutzler, G. Riquel, J.P. Riu, *High voltage laboratory tests and lightning phenomena*, 10th International Aerospace and Ground Conference on Lightning and Static Electricity, Paris, 1985.

[5] - J.P. Moreau, *Analysis of the first milliseconds of aircraft lightning attachment*, 11th International Aerospace and Ground Conference on Lightning and Static Electricity, Paris, 1985.

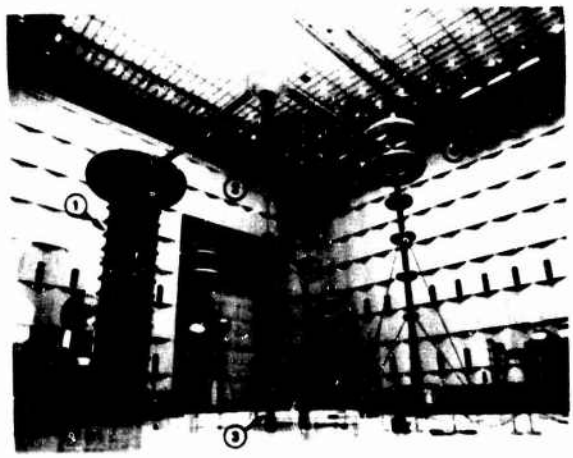

Fig. 1 - Overall View of the Experimental Device

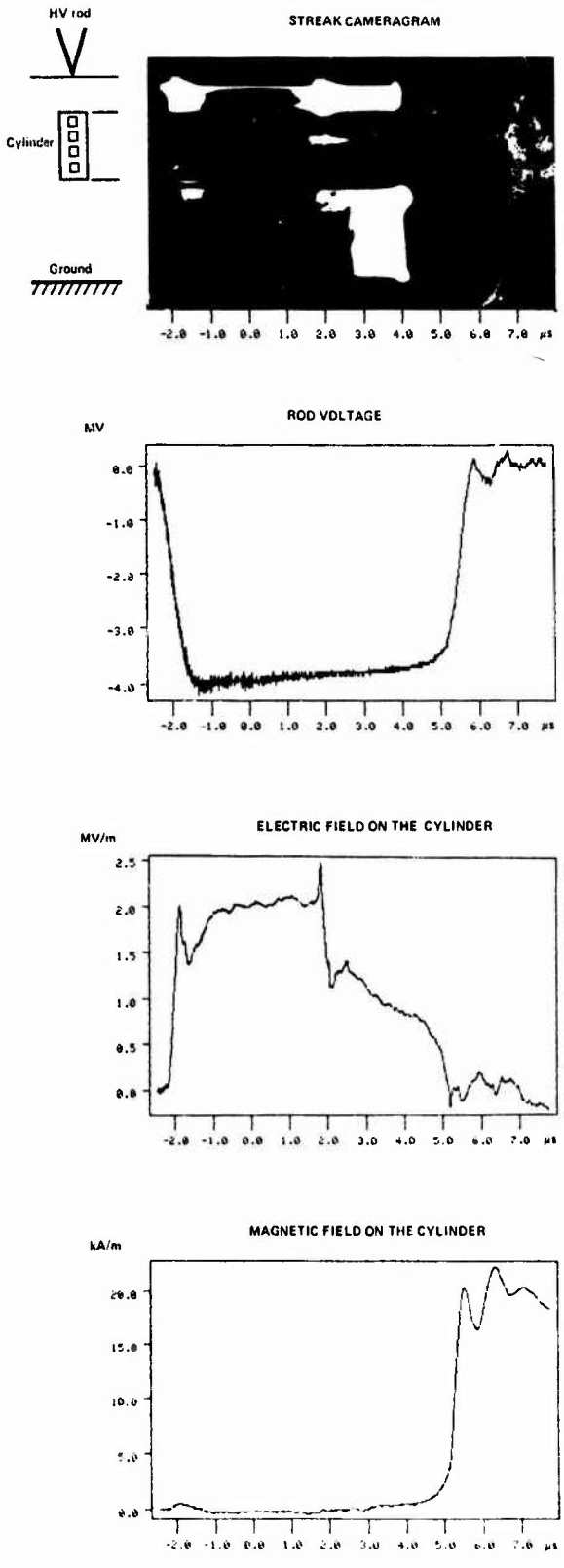

Fig. 2 - General Connection Phenomenology

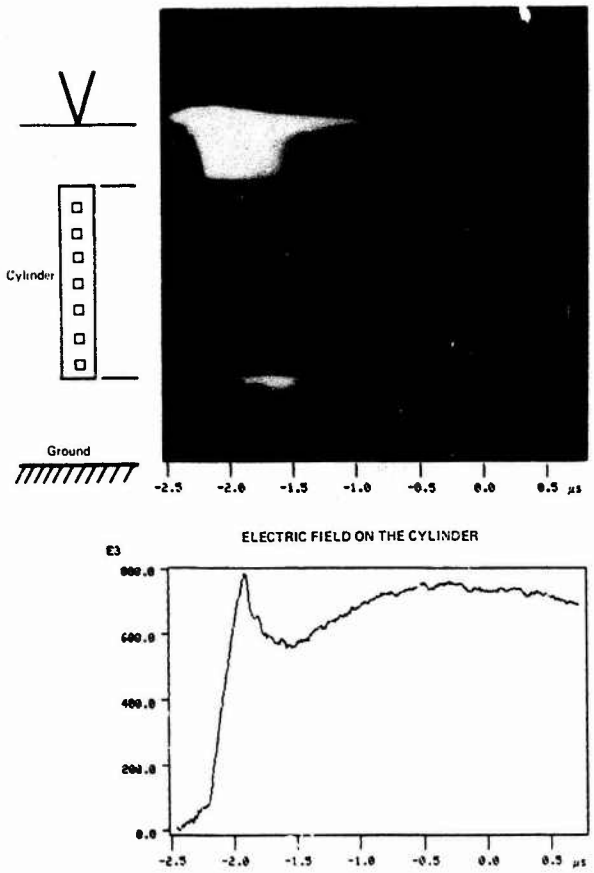

Fig. 3 - Electric Interference associated with Streamers appearing at the Base of the Cylinder.

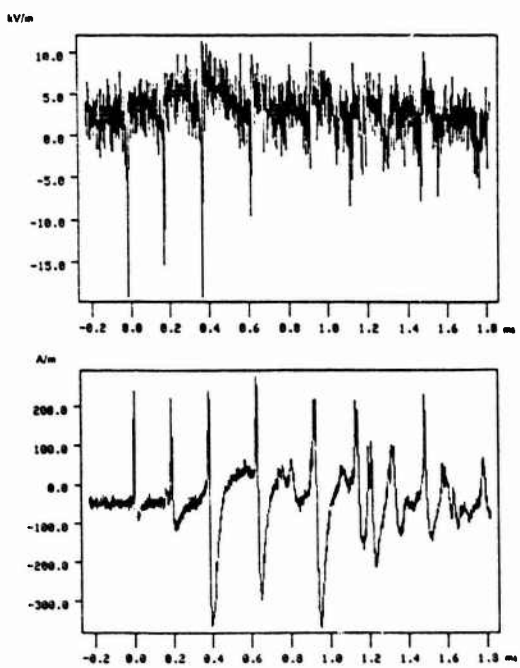

Fig. 4 - Electric and Magnetic Field records obtained from an Aircraft struck by Lightning

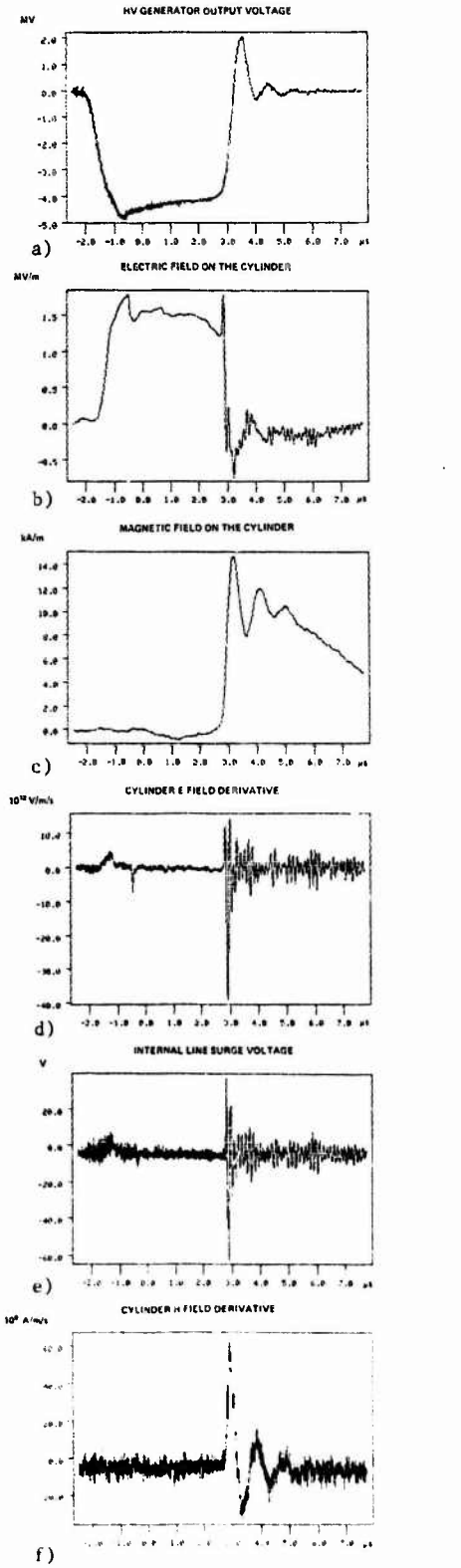

Fig. 5 - Line loaded with a High Impedance
a. HV Generator Output Voltage
b. Electric Field on the Cylinder
c. Magnetic Field on the Cylinder
d. Cylinder E Field Derivative
e. Internal Line Surge Voltage
f. Cylinder H Field Derivative

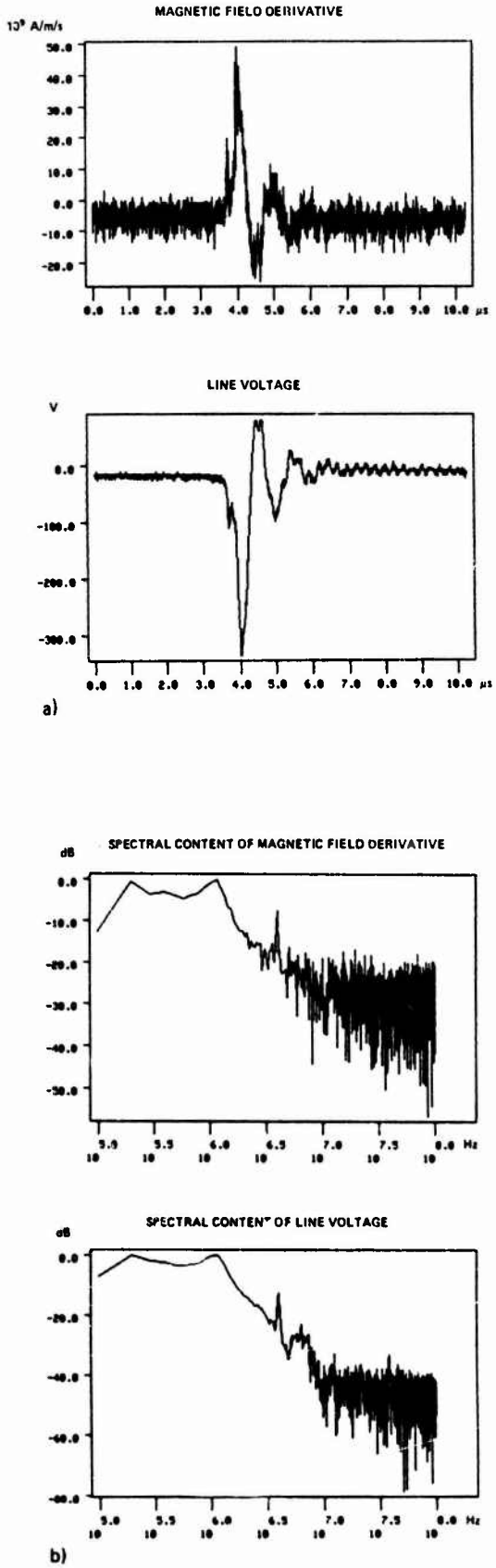

Fig. 6 - Lines loaded with Low Impedance

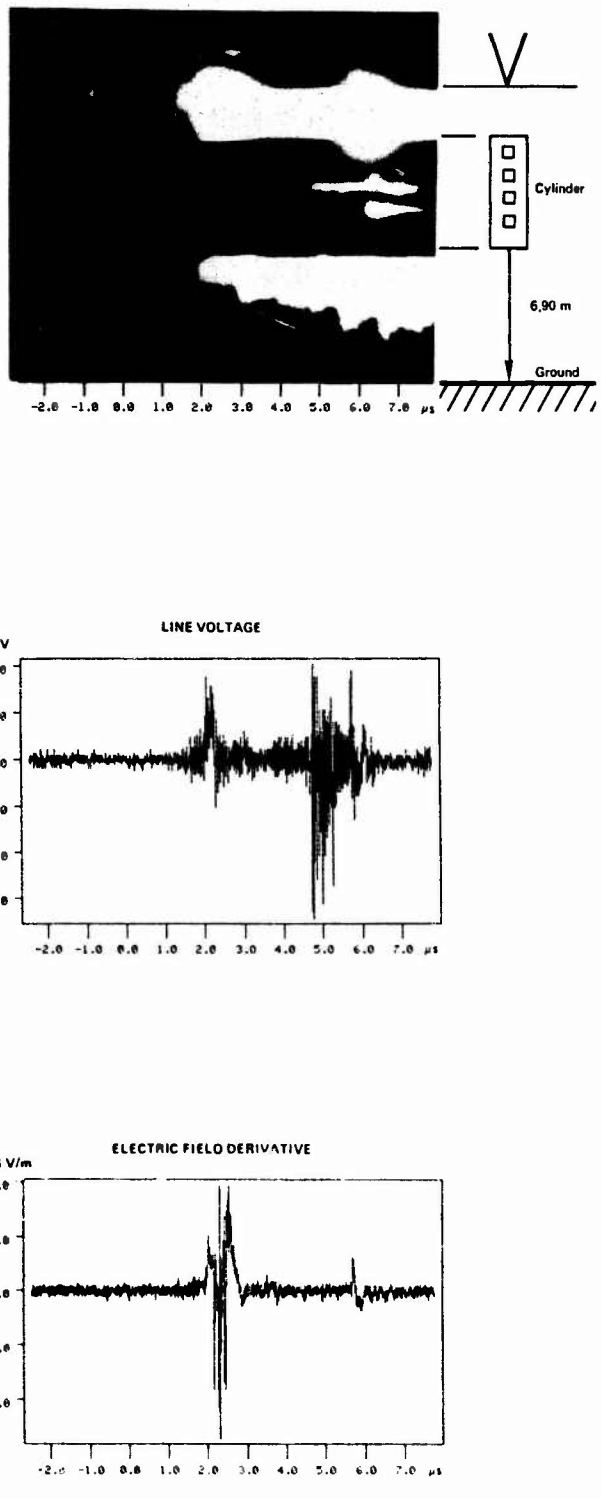

Fig. 7 - Interference associated with Corona Effect near the Openings

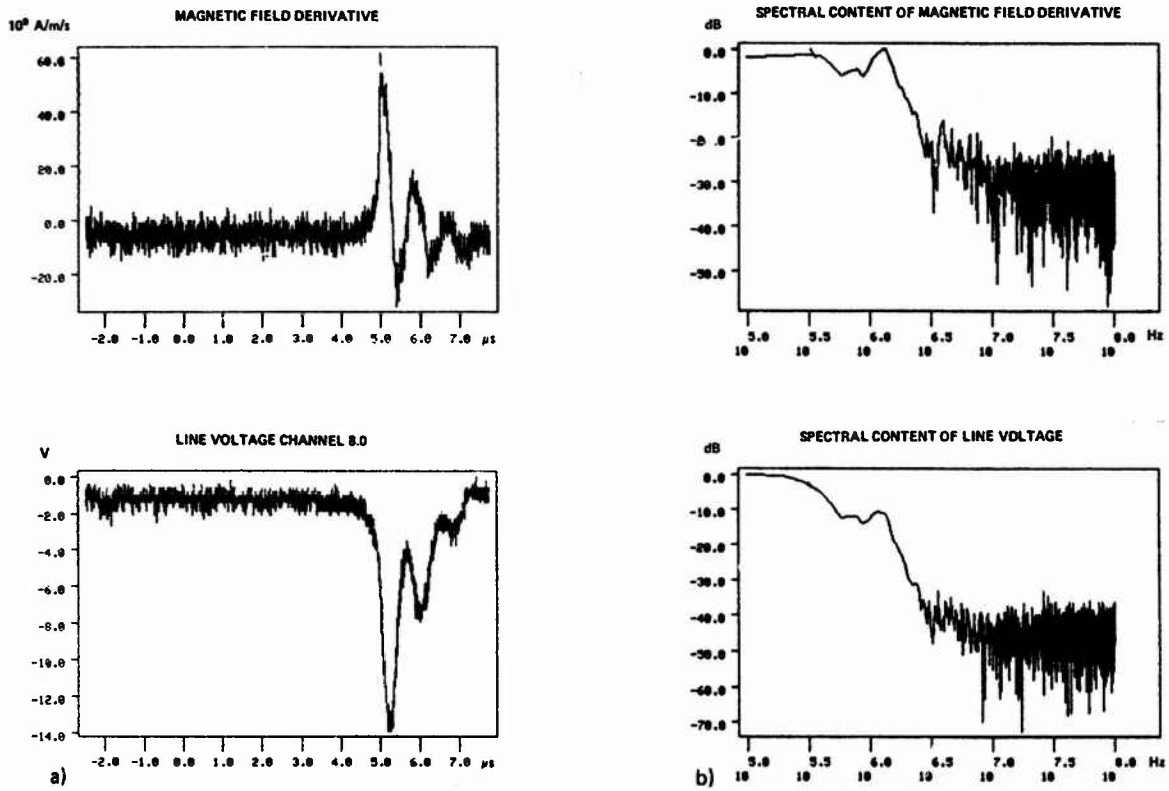

Fig. 8 - Tests using Composite Material Blank. Low Impedance Line

CONFIGURATIONS	DISTANCE BETWEEN LINE AND APERTURE	EXTERNAL PERTURBATION	PEAK VALUE ON LINE
LINES LOADED BY HIGH IMPEDANCE			
Free aperture	5 cm	$\frac{dE}{dt} = 4.10^{13}$ V/m/s	60 V
	Local effect	0	40 V
	35 cm	$\frac{dE}{dt} = 10^{13}$ V/m/s	2 V
Composite material	5 cm	$\frac{dH}{dt} = 50.10^{9}$ A/m/s	400.10^{-3} V
	35 cm	$\frac{dH}{dt} = 40.10^{9}$ A/m/s	50.10^{-3} V
LINES LOADED BY LOW IMPEDANCE			
Free aperture	5 cm	$\frac{dH}{dt} = 55.10^{9}$ A/m/s	300 V
Composite material	5 cm	$\frac{dH}{dt} = 50.10^{9}$ A/m/s	80 V
	35 cm	$\frac{dH}{dt} = 55.10^{9}$ A/m/s	6 V

TABLE I

CORONA FROM SIMULATED AIRCRAFT SURFACES AND THEIR CONTRIBUTION TO THE TRIGGERED DISCHARGE

by

Sheiton R W and Bickneii J A

Physics Department,
University of Manchester, Institute of Science and Technology
Manchester M60 1QD, U.K.

ABSTRACT

Evidence that aircraft may trigger an high current discharge, inciuding the iightning strike, has been accumulating in recent years. The results of some experiments designed to simuiate this type of breakdown suggest that a cruciai part of the mechanism invoiv=s the interaction of postive corona streamers with the precipitation. Based on this idea the required breakdown fields have been estimated experimentaily as a function of aititude.

INTRODUCTION

Experimental work has been carried out to evaluate the important parameters that govern the behaviour of those high current discharges which are triggered by and from isolated conductors in an electrically active region; the relevant example here is the aircraft or missile triggering discharges ranging from local breakdown of a few amperes to the lightning stroke itself. Although some similarities exist between aircraft discharges and those commonly studied using long gap rod-plane electrodes at ground level, there are sufficient differences to justify a rather different experimental approach; these differences arise mainly because of the absence, in the aircraft case, of the very highly stressed electrode (the rod) and a second discrete electrode (the plane). In this study, the reason for the chosen experimental approach was dictated by that feature of the electrostatic environment which is believed to expose the aircraft to the greatest risk - the space charge field

Briefly there appear to be two important preconditions for electrical breakdown namely:-

(i) corona production
(ii) sufficient available energy to convert the low current corona to a high current discharge.

Electric charge may reside on the aircraft or contribute to the space charge of the surrounding medium; although both forms can lead to corona, the energy is quite different in the two cases. An aircraft in flight inevitably becomes charged via a variety of possible mechanisms (e.g. p-static, engine); because the aircraft capacitance is quite small ($C \gtrsim 1000pF$), and assuming zero space charge, relatively little deposited charge is required to raise the potential of the aircraft by tens or hundreds of kV. At only a few kV, however, corona develops which, limits the growth in electric potential - a process encouraged by static wicks - so that the total available energy of $\frac{1}{2}CV^2$ remains quite small; condition (i) but not (ii) holds and high current events are precluded.

Should the aircraft now fly through a region where space charge provides a significant ambient field, independent of aircraft charge, then the electrostatic picture is transformed as is the magnitude of the electrostatic potential energy although the availability of this energy is a separate issue. The ratio γ of this energy (for a space charge field E in a spherical volume of radius R in the vicinity of the aircraft) to that provided by a charged aircraft of dimension L and potential V is given approximately by

$$\gamma = \left[\frac{R^3}{L}\right] \cdot \left[\frac{E}{V}\right]^2$$

so that even for a large potential (V~100kV) and a small field ($E \sim 10^3$ Vm^{-1}) R~100m provides a value for the ratio γ of 10^4.

Naturally, in practice, both types of charge distribution will be present but without an adequate space charge field it is assumed here that a breakdown would not occur. There is the additional factor concerning energy availability.

A space charge field induces ambipolar corona rather than the monopolar corona resulting from only the aircraft charge, so that positive corona, in particular, is necessarily always present at some aircraft surfaces. (1). The reason for believing that it is just this corona polarity which is of key importance was presented in detail at ICOLSE 1985 (2). In essence, the argument depends upon the unusual propagation characteristics of positive corona streamers; provided the space charge ambient field exceeds the stability field then there is no apparent theoretical limit to the distance over which the streamer can travel. This stability field is $\sim 4 \times 10^5$ Vm^{-1} at atmospheric pressure but decreases with decreasing pressure and, therefore, increasing altitude. The propagating streamer system then provides the basis of a possible mechanism for making the field energy, which is known to be present, actually available to the discharge. Since most charging processes leave the aircraft with a net negative charge - and negative corona does not propagate in the same way - this method of energy release would not be available to a negatively charged aircraft.

The experimental arrangement attempts to simulate the streamer propagation and growth in a quasi-uniform field variable in extent and magnitude from onset to breakdown with the effect of altitude represented by changes in gas pressure.

EXPERIMENTAL

Electrode arrangement This is shown schematically in Fig.1. The (lower) unstressed plane electrode is 0.42m in diameter and is earthed through the resistor R_d. The (upper) stressed electrode may be either 0.42m or 0.25m in diameter; the smaller electrode is used at high fields and/or low pressures. A 100kV DC power supply of negative polarity provides the variable and quasi-uniform field in the interelectrode space; the power supply may be decoupled from the electrode

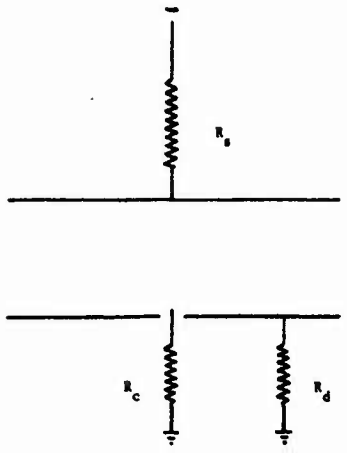

Fig 1
The Electrode Arrangement

by the optional HV resistor R_s of 200MΩ. A third needle electrode is located at the centre of a 2cm. diameter hole drilled in the middle of the unstressed electrode. One end of the needle protrudes a few mm into the gap whilst the opposite end is earthed through the resister R_c. In normal operation, the applied field induces positive corona streamers from the tip of the needle electrode from which they propagate in the field to the cathode. Streamers are produced at a frequency of between 1 and 10 kHz depending upon field strength and pressure. The whole electrode system is contained within a cylindrical GRP vessel fitted with a throttled pump on the outlet and a gas mixing facility on the inlet so that dynamic pressures from 1 atmosphere down to a few torr may be maintained. Humidity may also be varied and monitored.

Data Acquisition The currents i_c and i_d flowing in the resistors R_c and R_d are measured simultaneously. The conduction current i_c is a measure of the current flowing in the streamer channel adjacent to the needle electrode which is a consequence of the streamer propagation; it is analagous to the current flowing from the aircraft. The displacement current i_d depends upon the evolution of space charge in the gap and so is a valuable aid in the interpretation of the various events leading to breakdown. Both currents are recorded on a Philips digital storage oscilloscope (Type PM 3315) which has a maximum sampling rate of 125 MHz. The digital data is stored on disc for subsequent analysis.

RESULTS

The time dependence of typical conduction currents is illustrated in Fig 2 for a range of fields increasing from streamer onset; the higher field is still well below breakdown. Some corresponding displacement currents are shown in Fig 3. Air pressure

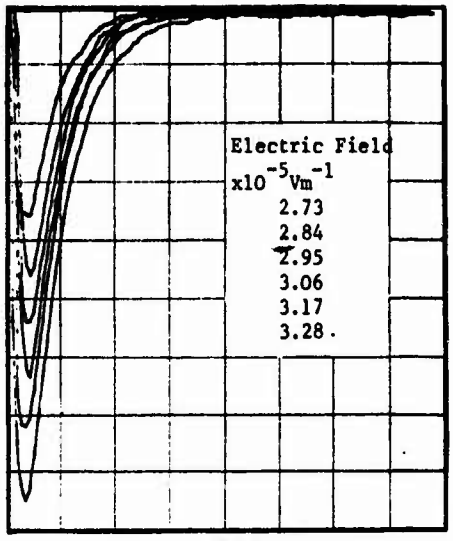

Fig 2
Typical Conduction Current Profiles
Vertical Scale: 1.75mA/div
Horizontal Scale: 250ns/div
p=600 torr

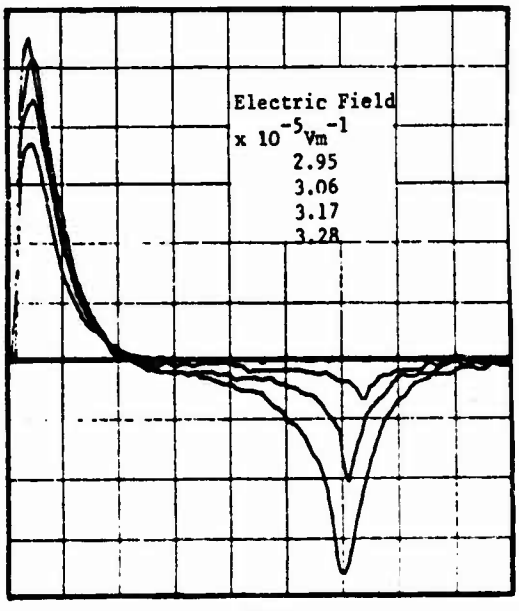

Fig 3
Typical Displacement Currents
Vertical Scale: 1.75mA/div
Horizontal Scale: 250ns/div
p=600 torr

was 600 torr and the electrode spacing 18.3 cm. All the traces shown here are analogue reconstructions from digital data. A negative going conduction current is equivalent to an electron current into the needle electrode and therefore removal of negative

charge from the gap, in this case from streamer channels adjacent to the needle electrode. A positive going displacement current implies a net increase in positive space charge (or decrease in negative charge) in the gap and, of course, the opposite polarity for a negative going current. These current profiles may be conveniently discussed in three stages corresponding to three successive events.

Stage I	The streamer transit
Stage II	The streamer arrival at the cathode
Stage III	Post arrival development

Stage I

The propagation of the streamer creates a channel linking the active head of the streamer to its source - the needle electrode in this case. More realistically a streamer system would be a multi-head, multi-channel arrangement. The head of the streamer consists of a dense positive space charge and the channel, a weakly ionised plasma. At the stability field, when no growth in the head charge occurs then, because the net charge remains constant, the net channel charge will be zero. At higher fields, when an increase in head charge is expected, the channel will be left with a net negative charge - equal, of course, to the increase in the head charge. However, because the field gives rise to an electron current along the channel towards the source (the conduction current), negative charge is removed leaving the channel with a net positive charge and, therefore, a net positive charge in the gap. This behaviour accounts for the initial negative going conduction current and positive going displacement current during the first 100ns or so. Because of electron attachment, in air predominantly to oxygen molecules to form negative ions

$$O_2 + e \longrightarrow O_2^-$$

electrons produced locally by the streamer propagation mechanism have a decreasing probability of reaching the needle electrode as the point of production extends into the gap. So the conduction current peaks and decays away at a rate dependent upon the electron attachment rate ν. A similar decay is observed in the displacement current as the initially high rate of growth in net positive charge is moderated by the increasing negative ion population caused by electron attachment. For the large propagation lengths anticipated in the case of airborne streamers local ionisation would make no contribution to the measured conduction current at source because of local attachment, so that the current profiles shown in Fig 2 for a propagation length L_s=18.3 cm would be little affected for larger values of L_s. This point is discussed quantitatively later.

Stage II

The arrival of the streamer at the cathode has no discernable effect upon the conduction current for the fields relevant to Fig 2. The displacement current, by contrast, exhibits a charge of polarity which peaks after a time which depends inversely on the field. The transit time of the streamer has been estimated using the data of Tang (3) who measured streamer velocities in air as a function of field and pressure although his data was obtained using only single streamer systems rather than the repetitive systems discussed here. The calculated transit time of the streamers correlates reasonably well with the time to negative peak of the displacement current
(Table 1). This negative peak implies an increase in net negative space charge which grows with field; the correlation with streamer arrival strongly suggests this is caused by electron injection at the cathode produced by the very high local fields associated with the head space charge. This view is supported by the absence of a negative peak for the lowest field of Fig 3; this field is just below the stability field so that the streamer does not arrive at the cathode. The injected electrons become attached as before to form negative ions which, because of their low mobility, should contribute a small ion current, detectable as a conduction current to the unstressed electrode, for a time comparable with the ion transit time; this is indeed observed.

Stage III

At fields greater than those so far considered, an additional feature appears on the conduction current record. This is illustrated in Fig 4 which shows the conduction currents obtained over a narrow field range ($1.75 - 1.95 \times 10^5 Vm^{-1}$) at a pressure of 300 torr; the additional feature, a second peak, can be clearly seen becoming more pronounced at the high fields. Again using the Tang data, these second peaks correlate with the streamer arrival at the cathode. At only marginally higher fields a large increase in the conduction current may be observed (Fig 5) which occurs a finite, but variable, time following this second peak; the delay is significantly shorter than the electron transit time. Coincident with this increase in conduction current is a similar rapid increase in displacement current pointing to a large increase in net positive charge in the gap (Fig.6). A further sequence is shown (Fig. 7) where, for the same experimental conditions, two events show markedly different behaviour; the first exhibiting what we may refer to as a current regeneration, whilst the second does not. In this case the first and second conduction

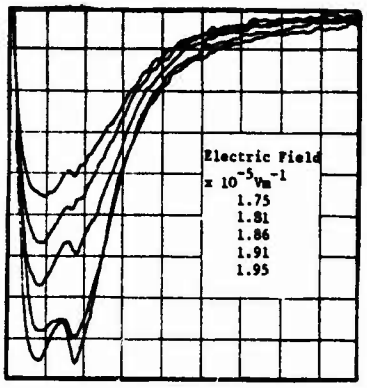

Fig 4
Current Profiles Showing Second Peak
Vertical Scale: 1.75mA/div
Horizontal Scale: 500ns/div
p=300 torr

current peaks have merged - with the second peak dominant - so that the current front appears distinctly non-linear. The occurrence of the current regeneration is normally associated with at least a partial breakdown of the gap.

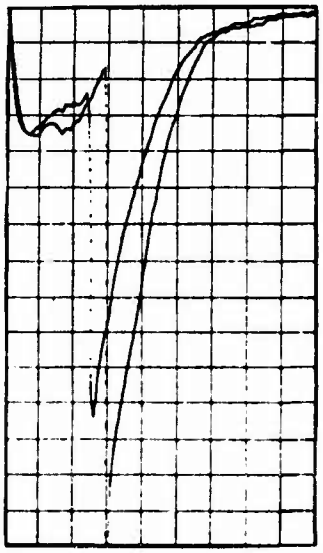

Fig 5
Current Regeneration
E= 1.91, 1.99 x 10^5 Vm^{-1}
Vertical Scale: 3.5mA/div
Horizontal Scale: 500ns/div
p=300 torr

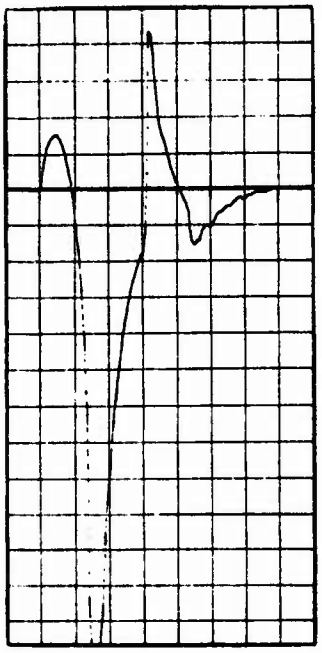

Fig 6
Displacement Current for a Regeneration
Vertical Scale: 7.0mA/div
Horizontal Scale: 500ns/div
p=300 torr. E = 1.99 x 10^5 Vm^{-1}

Interpretation

The coincidence of the second peak in the conduction current with the streamer arrival at the cathode - in this case some 18 cm distant from the electrode - indicates the presence of a very fast ionising wave generated at the cathode and travelling along the partially ionised streamer channel. These waves, observed by Suzuki (4) and others, increase the local electron density either by increasing the impact ionisation coefficient or by some other mechanism such as that suggested by Barreto (5). The net effect is to sustain the current in the channel which would otherwise decay due to electron attachment - as in Fig 2. This additional current , if sufficient, may then lead to breakdown after a delay time which, in the present experiment, is ~250ns. The breakdown machanism, caused essentially by gas heating, has been studied by Marode(6) and more racently by Bayle (7). The gas heating causes an expansion of the neutral species out of the channel, an increase in E/p and therefore the effective ionisation coefficient (α-η) leading to a runaway breakdown. Visually, the onset of the current regeneration may be identified with the appearance of highly luminous filamentary channels extending well into the gap closely followed by gap breakdown (Fig. 8).

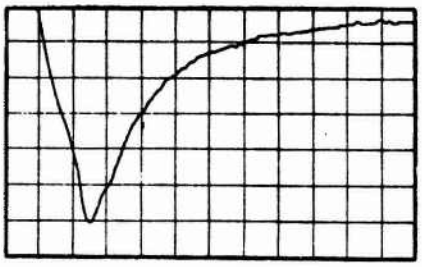

(a)
Conduction Current for $E = 1.5 \times 10^5 Vm^{-1}$
Vertical Scale: 7.0mA/div
Horizontal Scale: 500ns/div
p=200 torr

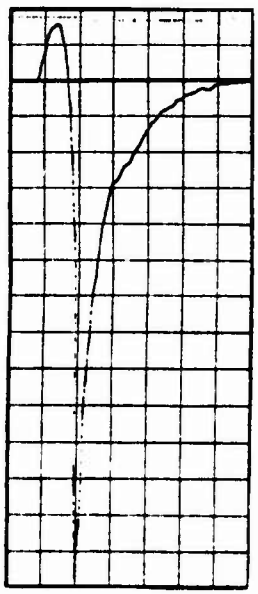

(b)
Displacement Current for (a) same scales

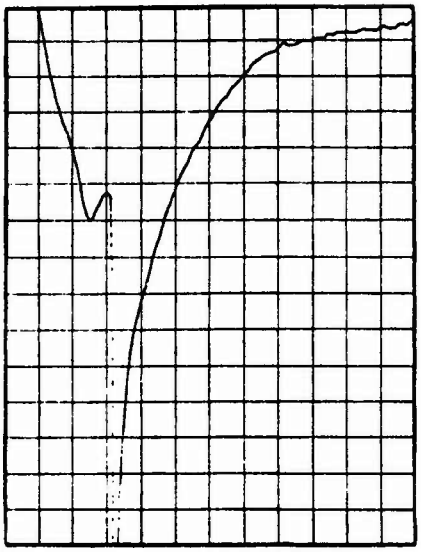

(c)
Conduction Current showing a regeneration.
Same conditions as at (a)

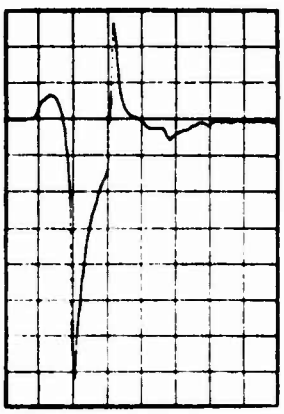

(d)
Displacement Current for (c)
Vertical Scale: 17.5mA/div
Horizontal Scale: 500ns/div
note the different vertical scale
Fig 7

Discussion

Comparisons between the behaviour of streamers produced in the laboratory and those

(a)
Visual Appearance of a Current Regeneration.
2 Regenerations can be seen here

(b)
The breakdown
Fig 8

Discussion

Comparisons between the behaviour of streamers produced in the laboratory and those developing from aircraft surfaces must be carefully made bearing in mind the differences in the two experimental circumstances. Stage I might be reasonably expected to be common for both depending, as it does, only upon the existence of a sufficiently large propagation field. As mentioned earlier, the conduction current measured in the laboratory should be similar to the current flowing from the aircraft for a similar field and pressure.

A simple model of the streamer propagation suggests that the conduction current I is given by

$$i(t) = Q(x)V\exp(-\eta Vt)$$

where Q(x) is the charge/unit length of channel created by the streamer propagation. V is a modified velocity $v_s v_e/(v_s + v_e)$ where v_s and v_e are the streamer and electron drift velocities respectively for the prevailing condition and η the attachment coefficient. Q(x) basically reflects the increasing number of streamer channels resulting from streamer branching. Representing this as a power law of form Ax^n leads to a time to peak current t_p where

$$t_p = n/\eta V$$

or, since $v_e\eta = \nu$ and $v_s \gg v_e$

$$t_p = n/\nu$$

Measurements by Sadik (8) suggest $n \sim 0.5$ so that with ν in the range 1 - 10 MHz, t_p is 500 - 50 ns. depending upon field and pressure. Clearly for streamer propagation lengths $L_s < v_s t_p$ (i.e 0.5-5.0 cm), the peak current would coincide with the streamer arrival at the cathode as implied, for example, by Bayle (7) but for aircraft streamers ($L_s \gg v_s t_p$), the current maximum is independent of L_s as suggested earlier.

Stage II, the streamer arrival at the cathode, represents an obvious difficulty in making a comparison with aircraft streamers since no obvious discrete cathode exists. The laboratory work indicates principally that the streamer arrival is accompanied by two effects namely

(i) the generation of a fast ionising wave
(ii) the production at the cathode of significant electron emission.

The relative contribution of each to the subsaquent breakdown is of crucial importance here in view of the difficulty of envisaging event (ii) for aircraft streamers. Whilst in short gaps (1 cm) it is quite possible that the appearance of a large negative space charge could enhance the field and hence contribute to the breakdown, this contribution must diminish with increasing gap size. The electron drift velocity v_e may be approximated by

$$v_e = 10^6 \left[\frac{E}{p}\right]^{0.713} \text{ cm/s}$$

For the appropriate values of E/p this yields a drift velocity $\sim 3 \times 10^6$ cm/s so that during the time delay of typically 250 ns. between the streamer arrival at the cathode and the current regeneration the space charge would have travelled only 0.75 cm. even without any electron attachment. For the present observations in an 18.3 cm. gap this should be insignificant so that effect (ii) above can be ignored.

By contrast if the streamer-hydrometeor interaction is similar to the streamer-cathode interaction, so that the precipitation particles may be regarded as a distributed cathode, then ionising waves are as likely to lead to a local breakdown developing from the aircraft as from the equivalent point in a laboratory gap. The mean free path of a streamer in a thundercoud has been treated by Bickneil (2) and shown to be significant.

Although a more complete analysis of the data obtained so far is required to fully justify this conclusion, if the interpretation is valid then it should follow that the field required to produce a current regeneration is sufficient for the breekdown of aircraft streamers providing that adequate streamer-hydrometeor interactions are available and the required energy input is sufficient (9). For a given (adequate) field and pressure not every streamer leads to a regeneration - e.g. Fig. 7. To illustrate this point, the percentage of regeneretions is shown as a function of the field at different pressures in Fig. 9. Also represented are the breakdown fields for the 18.3 cm. gap pressures. Above 400 torr. breakdown occurs as soon as a regeneration appears - the percentage figures for fields in excess of breakdown were obtained by decoupling the gap from the power supply with the 200MΩ series resistor and so reducing the energy available. However, et the two lower pressures, 200 and 300 torr, 100% regeneretion levels are ettained before breekdown occurs. This difference in behaviour is attributed to the amount of energy evelisbie for the fields prevailing at these lower pressures. Since the energy input is not obviously linear then for airborne streamers with an extensive

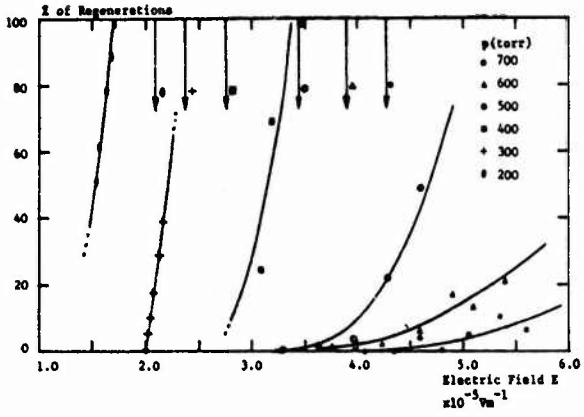

Fig 9
The Field Dependence of the Current Regeneration. The breakdown field at each pressure is indicated by the arrow

field and therefore energy available, this limitation may not be serious. The appearance of a current regeneration would then represent a criterion for estimating the lower limit of the breakdown field. Fig. 10 shows the variation of this field with pressure - represented here by altitude - based on this proposition.

SUMMARY AND CONCLUSIONS

Energy considerations lead to the conclusion that positive streamers make an important contribution to triggered discharges. In fair weather conditions the production of the streamers by and from aircraft would lead only to currents flowing from the aircraft of a few milliamperes because most of the ionisation resulting from streamer propagation occurs at distances sufficiently large to ensure that electron attachment remains the dominant process. Experimental results obtained in gaps of relatively small dimensions - although these dimensions may be considered large enough to similarly allow attachment to dominate - indicate that the streamer interaction with the cathode generates fast ionising waves which are responsible for reviving the streamer conduction current and ultimately the thermalising of the streamer channel leading to e high current breakdown. The same process could arise from streamer-hydrometeor interactions which take place when aircraft are flying in electrically active clouds. On this basis minimum breakdown fields for aircraft are proposed which depend critically on pressure and therefore altitude. Maintaining a negative charge on the aircraft may therefore help prevent high current discharges.

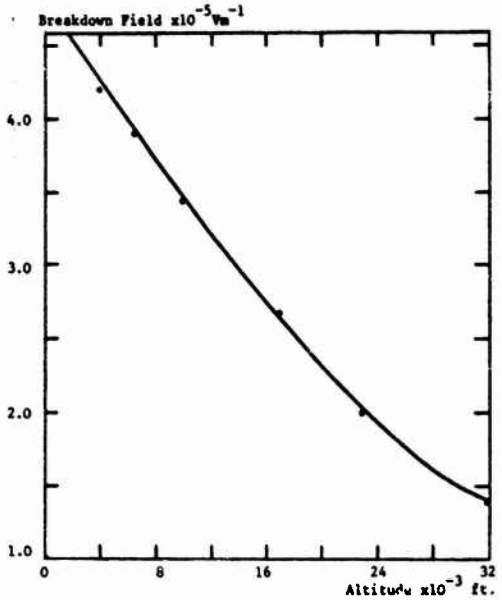

Fig 10
The predicted dependence of the breakdown field on altitude

REFERENCES

(1) Humood, B. Y. PhD Thesis (1984) UMIST Manchester UK

(2) Bicknell, J. A. and Shelton, R. W. ICOLSE Paris 1985

(3) Tang, T. M. PhD Thesis (1982) UMIST Manchester UK

(4) Suzuki, T. J. Appl. Phys, 48, 5001, 1977

(5) Barrett, E. Jurenka, H. and Reynolds, S. I. J. Appl. Phys, 48, 4510, 1977

(6) Marode, E. Bastien, F. and Bakker, M. J. Appl. Phys, 50(1), 140, 1979

(7) Bayle, P. Bayle, M. and Forn, G J. Phys D: Appl Phys 18, 2395, 1985

(8) Sadik, A. Bicknell, J. A. and Tang, T. M. VI Int. Conf. on Atmospheric Electricity, Manchester 1980

(9) Bicknell, J. A. and Humood, B. Y. 8th IAGCLS, (1983), Fort Worth, Texas

ACKNOWLEDGEMENT

This work is supported in part by the European Office of Aerospace Research and Development (EOARD) on Grant AFOSR 83-0083.

LIGHTNING PROTECTION OF ADCOCK ANTENNA SYSTEMS

J.L. ter Haseborg
Technical University Hamburg-Harburg, Germany
Department of Electrical Measurement Techniques

F. Wolf
C. Plath GmbH Company for Nautical Electronics
Hamburg, Germany

ABSTRACT

In opposition to receiving antennas for regular receiving systems, electronic equipment for direction-finder antennas as e.g. Adcock antennas can be destroyed not only by direct lightning strokes, but also by induced lightning pulses which cause the response of arresters in the antenna bases. This response produces interfering pulses which may damage sensitive components in the central electronic unit (goniometer).

A protection circuit has been developed which provides a sufficient protection against lightning-induced currents and minimum interferences concerning the incoming signals.

INTRODUCTION

Electronic Systems which are connected to transmission lines or to antennas are endangered in a particular manner concerning electromagnetic interferences as produced e.g. by lightning or NEMP [1]*. In this case the exclusive application of shielding measures for sensitive components against interfering electromagnetic fields is not sufficient. Special protective measures are necessary against interfering signals-induced in transmission lines and antennas-penetrating the shield via cable entries and applying sensitive input circuits. Protective measures in terms of protection circuits against surges on a line generally have to show two characteristics:

- sufficient suppression of interfering pulses
- largely non-attenuated transmission of the signals.

There is a basically difference between protection circuits for power supply lines and protection circuits for communication lines [2], [3]. Normally protection circuits for power supply lines are dimensioned for comparatively high useful currents. In case of communication lines the transmission of signals in a specified frequency range is required. Concerning high frequency receiving systems, protection circuits against interfering currents have to show the following important characteristics:

- reproducible response dependent on edge steepness of the interfering pulses
- sufficient current-carrying capacity (in case of protection semiconductors: sufficient peak pulse power dissipation)
- minimum insertion loss for incoming signals
- minimum intermodulation distortions caused by protection components with a non-linear characteristic.

In this paper protective measures for suppressing lightning induced currents in a special antenna system, here: Adcock antenna system, are described. For these antenna systems intermodulation distortions are of special interest because the incoming signals show values of the order of microvolt up to several hundred millivolts and in case of diodes as protective components, these values are identical with the voltages in the curved part of the diode characteristic.

ADCOCK ANTENNA SYSTEMS, APPLIED BY LIGHTNING INDUCED SURGES

The essential parts of an Adcock direction-finder system are the antenna system (Adcock antenna system) and the central electronic unit (reduction goniometer). An Adcock antenna system consists of rod antennas which are arranged on the peripheries of two concentric circles as shown in fig. 1 and 2. The diameters show values of 4o m or 1o m respectively. According to fig. 2 the antennas on the outer circle are dimensioned for a frequency range between 3oo KHz and 8 MHz and the antennas on the inner circle for a frequency range between 8 MHz and 3o MHz.

Concerning the function of this system a direction finding is carried out by subtraction of the voltages of two antennas which are arranged diametrically on the circles [4].

The rod antennas and the central electronic unit (reduction goniometer) are interconnected by a balanced transmission line (twinax cable). By means of this twinax cable a common-mode rejection is obtained. Special baluns are installed in the antenna bases and in the input circuits of the goniometer as shown in figs. 3 and 4. Induced surges in the antennas, e.g. caused by lightning, may strike the spark gaps and the gas arresters which are installed in the antenna bases (s. fig. 3). Caused by these striking protective devices which serve as coarse protection, threshold pulses with comparatively steep edges occur. These pulses-penetrating the shielding of the goniometer via the twinax connectors - may propagate largely non - attenuated because the complete system-consisting of antennas, twinax cables and goniometer-is dimensioned for incoming signals with frequencies up to 3o MHz. This frequency range and the frequency spectrum of the residual pulses - caused by the striking arresters and spark gaps - are overlapping. Particularly the sensitive hybrid-power dividers of the goniometer according to fig. 4 may be damaged by these infering pulses. Quite often these damages are not visible but there occur irreversible variations concerning electrical data and parameters of the hybrid-power dividers.

By means of the test facility as shown in fig. 5 the test object is applied by LEMP-simulated pulses. The test object consists of an antenna base (fig. 3) and a goniometer (fig. 4) which are interconnected by a twinax calbe with a length of 2o m. According to fig. 5 the input test pulse u_1 (s. fig. 3) and the currents i_2 at three different points M1, M2 and M3 in the reduction goniometer (s. fig. 4) have been measured. Figure 6 shows the test pulse $u_1'(t)$ (without test object). The oscillograms of fig. 7a represent the response $u_1(t)$ caused by the striking gas arrester, and the currents $i_{2H}(t)$, $i_{2C}(t)$ and $i_{2A}(t)$, whereby $\hat{i}_{2H} > \hat{i}_{2C} > \hat{i}_{2A}$. These results clearly illustrate that the pulses i_2 with a rise time of approx. 1o ns are caused by the striking gas arresters; by way of contrast fig. 7b shows the results which have been obtained without gas arresters. The highest interfering pulse is the input current i_{2H} of the hybrid power divider PD5 with an amplitude of $\hat{i}_{2H} = 4A$; in case of an input impedance of 5o Ω an interfering input voltage of 2oo V is valid. Dependent on the lightning surge it is possible that these interfering currents or voltages respectively which damage the power dividers may even still be higher.

PROTECTIVE MEASURES FOR THE SENSITIVE POWER DIVIDERS

The power dividers are applied by interfering pulses which are penetrating the shielding of the goniometer via the twinax connectors. Special protection circuits for suppressing these pulses with characteristics as discussed in the introduction have been developed. Figure 8 shows the insertion of suppressor diodes in the circuitry of the reduction goniometer. In this case the peak pulse power dissipation of the diodes is of secondary significance because the spark gap and the gas arrester in the antenna base are dimensioned for a comparatively high current-carrying capacity. Figure 9 represents the currents $i_{2A}(t)$, $i_{2C}(t)$ and $i_{2H}(t)$ when applying the LEMP-simulated pulse $u_1(t)$. A comparison shows that the maximum current pulses $\hat{i}_{2A}$, $\hat{i}_{2C}$ and $\hat{i}_{2H}$ of fig. 9 are considerably lower than the pulses represented in fig. 7a (without protection circuits).

NON-LINEAR DISTORTIONS OF THE PROTECTION CIRCUIT

Receiving - and direction finder - antennas in the HF-band are usually employed as wideband systems; a wide frequency spectrum with high dynamic signal range is to be worked on.

* Numbers in parentheses designate References at end of paper.

If non-linear devices are used in protection circuits, there may be the danger of generating distortions at the antenna output. Beside the low insertion-loss, which becomes noticeable by the increase of the system noise figure, the protection circuit must display a transfer function as linear as possible within the normal operating amplitude level range of the system. Therefore, interfering distortions are of special interest because the incoming signal levels show values of the order of microvolts up to several hundred millivolts.

When two signals $x_1(t)$, $x_2(t)$ whose frequencies

$$f_1 = \omega_1 / 2\pi \quad , \quad f_2 = \omega_2 / 2\pi$$

are simultaneously applied to a non-linear device whose transfer-function is of the form:

$$H = a_o + a_1 x + a_2 x^2 + a_3 x^3 + ... + a_n x^n \quad (1),$$

output terms result which include all possible products, see fig. 1o.

The most significant output terms are:

$$a_1 (A \cos \omega_1 t + B \cos \omega_2 t), \quad (2)$$

which represents the two signals,

$$o.5\ A^2\ a_2 \cos 2\omega_1 t + o.5\ B^2 a_2 \cos 2\omega_2 t \quad (3) \text{ and}$$

$$o.25\ a_3\ A^3 \cos 3\omega_1 t + o.25\ a_3\ B^3 \cos 3\omega_2 t \quad (4),$$

which represent the harmonic distortion;

$$a_1\ a_2\ AB \cos (\omega_1 t \pm \omega_2 t) \quad (5)$$

represent the 2nd-order-intermodulation - IM2.

$$o.75\ a_3\ A_1^2\ A_2 \cos (2\omega_1 t \pm \omega_2 t) \quad (6)$$

$$o.75\ a_3 A_1\ A_2^2 \cos (2\omega_2 t \pm \omega_1 t) \quad (7)$$

$$1.5\ a_3\ AB^2 \cos \omega_1 t + 1.5\ a_3\ A^2 B \cos \omega_2 t \quad (8)$$

represents the 3rd order intermodulation IM3 and cross-modulation of interest.

Beside the signals requested, intermodulation terms of 2nd and 3rd order appear at the output of the device. Since these products have different input signal to output signal ratio slopes, they will cross at some point for a given input signal level. This intersection is termed the intercept point - fig. 11. In case of 2nd and 3rd order intermodulation signals non-existing in the input frequency spectrum are generated, which are received by the receiver subsequent to the antenna. Through cross-modulation the received modulation of a signal is superimposed by the modulation of a stronger disturbing signal.

In case these products have already been developed in a protection circuit, there are no possible measures to eliminate them afterwards. The intermodulation and cross-modulation values of the lightning protection circuit must distinctly range below the performance values of the following receiver, i.e. it must displaya distinctly higher intercept point. In order to test the quality of a protection circuit and compare it to the values of the subsequent receiver, a measuring equipment set-up according to fig. 12 is used. Mainly the 3rd order intermodulation is measured. The cross-modulation can be calculated with the knowledge of the 3rd order intercept point [5]. According to fig. 12a two isolated signal generators; apply their outputs to the device under test; its output is connected to a spectrum analyser. The output signal level of the fundamental frequency and the difference to the intermodulation products are measured. The 3rd order intercept point is either calculated from these values or read from a nomogram [5], [6] or constructed graphically - s. example fig. 13. Another method with similar measuring equipment set-up is shown in fig. 12b. There the influence of the non-linearity effects of the protection circuit on the subsequent receiver with given noise figure and intercept point is measured. The associated spectrum shows the possible reduction of receiver performance specifications.

Measurement example of the developed lightning protection circuit.

Since the proposed protection circuit probably has high intercept point values, it was tried to measure the reduction of the system specifications according to method fig. 12b.

The receiver used in this example had the following specifications:

noise figure 11 dB (noise factor 12.59)

3rd order intercept point + 3o dBm

The protection circuit presents an insertion loss of o.2 dB in the worst case. The overall noise factor is described by:

$$F = F(\text{Protection}) + \frac{F(\text{Receiver})-1}{G(\text{Protection})} = 13.19 \quad (9)$$

(corresponds to 11.2 dB)

where: F = noise factor; G = gain

The calculated or graphically constructed 3rd order intercept point (according to fig. 13) of the output spectrum in fig. 12 is:

IP3 = 3o dBm.

The protection circuit does not cause any measurable reduction of the intermodulation figures of the system.

Measuring directly as per measurement equipment set-up in fig. 12 a no products could be observed - with the exception of internal products of the measuring equipment itself.

Since the IP3 of the measuring equipment amounted to about 45 dBm, it must be concluded, that the IP3 of the protection circuit is greater than 5o dBm and the protection circuit causes no reduction of intercept figure system specifications. The developed antenna protection circuit is of very high quality.

CONCLUSIONS

By means of these protection measures against induced lightning surges the interfering pulses at the inputs of the hybrid-power dividers are reduced to values of approx. 2oo mA. Interferences in this order of magnitude don't cause the above mentioned damages.

The research work concerning protection of antenna systems is going on. Particularly protection circuits for Adcock antenna systems against comparatively steep interfering pulses (steepness up to 1o kV/ns) as caused e.g. by NEMP will be developed.

REFERENCES

1. J.L. ter Haseborg and H. Trinks, "Protection Circuits for Suppressing Surge Voltages with Edge steepness up to 1o kV/ns", 5th Symposium on EMC, Zurich, March 8-1o, 1983

2. J.L. ter Haseborg and H. Trinks, "Protection of Electronic Systems against Surge Voltages caused by lightning", 17th International Conference on Lightning Protection, The Hague, Sept. 6-9, 1983

3. J.L. ter Haseborg and H. Trinks, "Problems concerning EMP- and Lightning Protection of High Frequency Transmission Lines", International Conference on Electromagnetic Compatibility", University of

Surrey, UK, Sept. 18-21, 1984
4. Informations on direction finders and direction finder antennas, C. Plath GmbH, Hamburg, West-Germany
5. Erst, Stephan J., "Receiving Systems Design", Artech House, Inc. 1984
6. Norton, David E., " The Cascading of High Dynamic Range Amplifiers", Anzac Electronic, USA

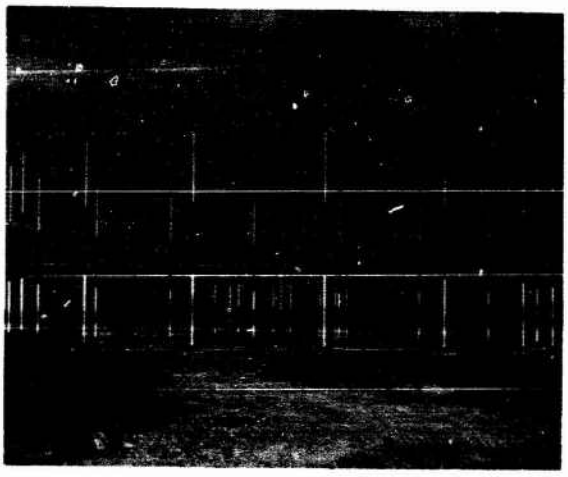

Fig. 1 - Adcock antenna system

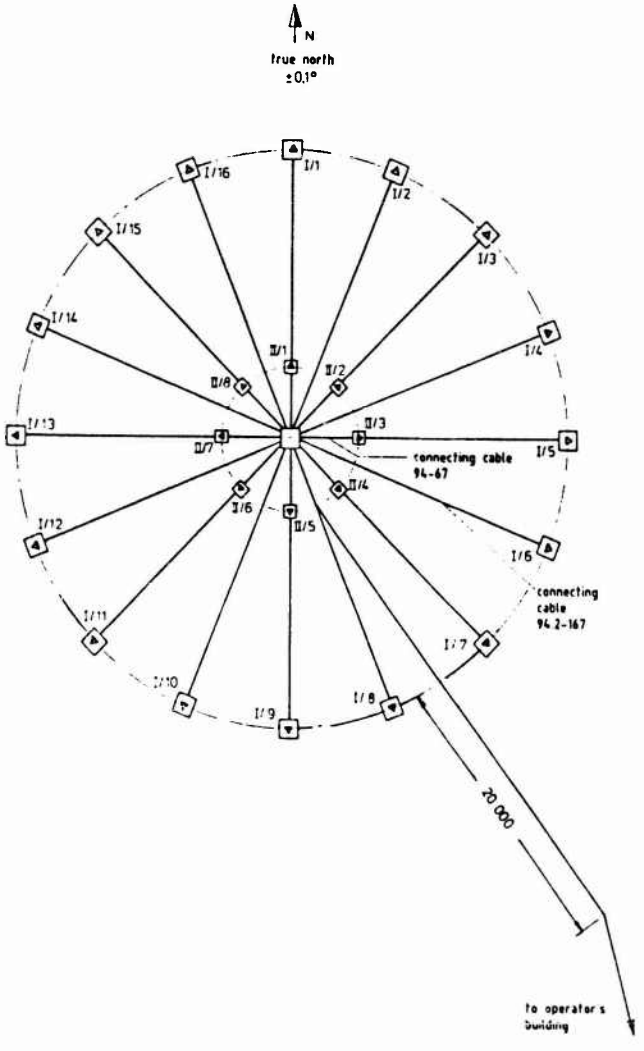

Fig. 2 - Arrangement of the rod antennas

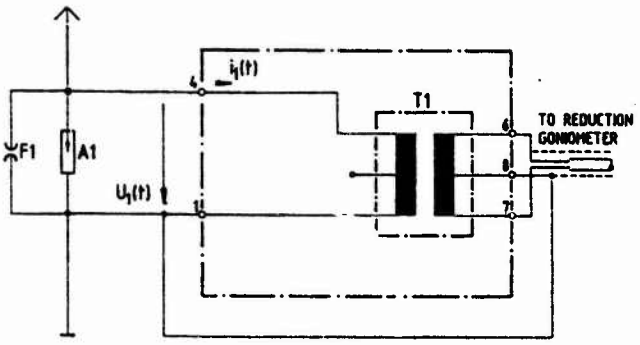

Fig. 3 - Antenna base of a rod antenna

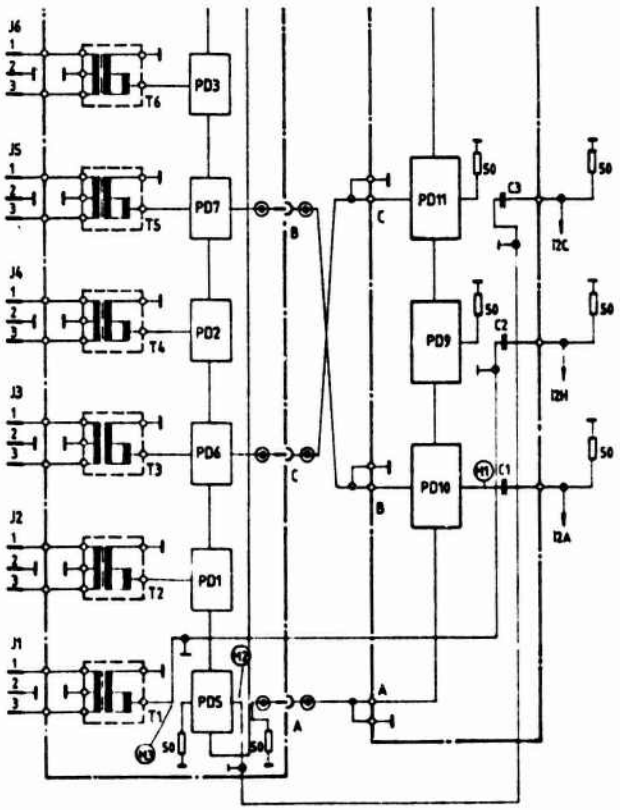

Fig. 4 - Part of circuitry of reduction goniometer

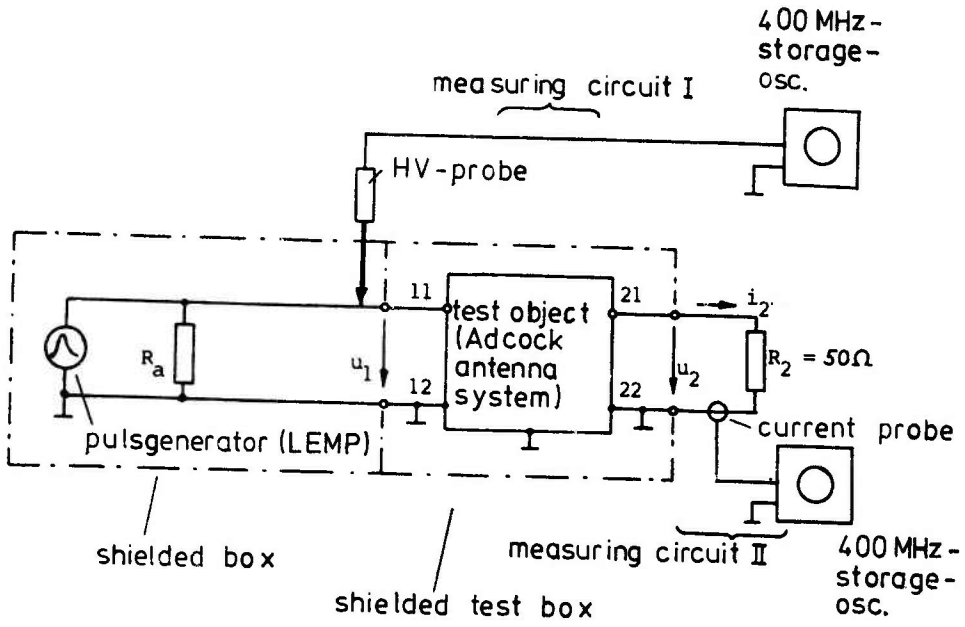

Fig. 5 - Test facility for applying the Adcock antenna system with lightning - simulated pulses

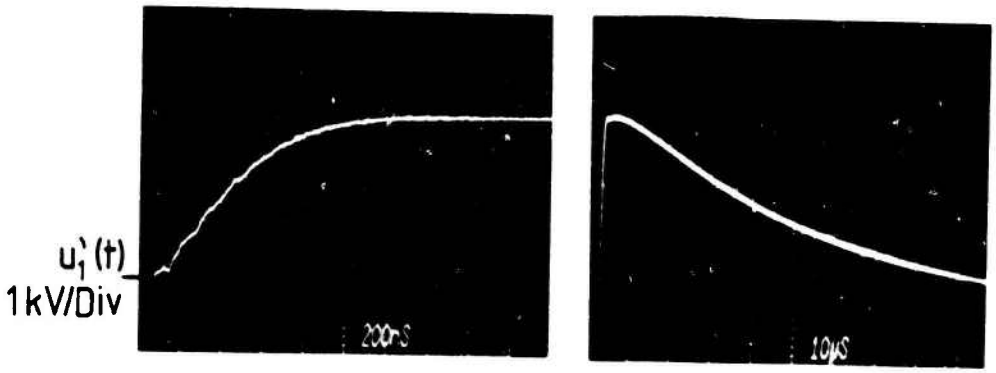

Fig. 6 - Test pulse $u_1'(t)$

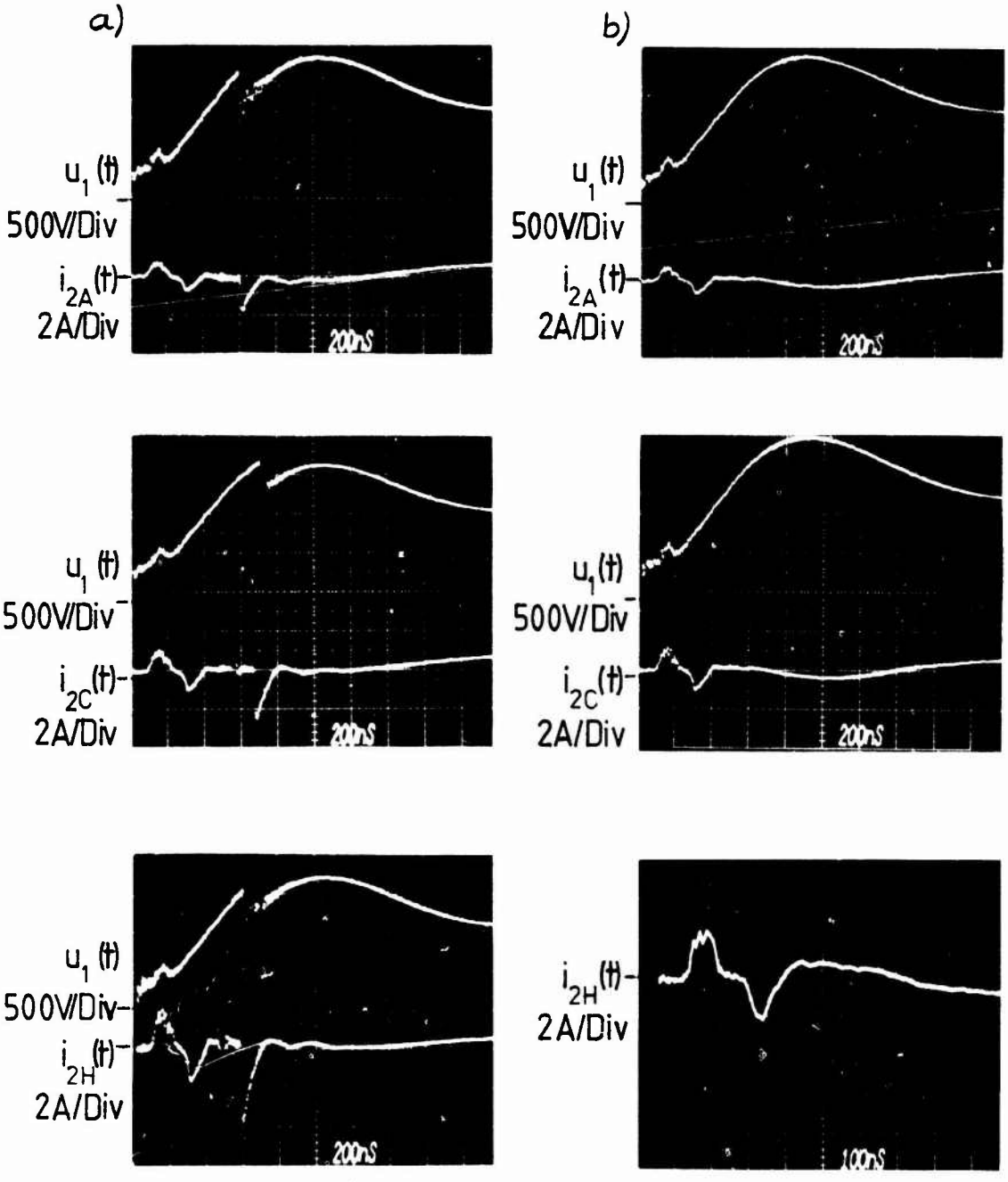

Fig. 7 - Currents $i_{2H}(t)$, $i_{2C}(t)$, $i_{2A}(t)$ according to Figures 4 or 5 respectively (without protection circuits in the goniometer) when applying $u_1(t)$:

a) with striking gas arrester
b) without striking gas arrester } in the antenna base

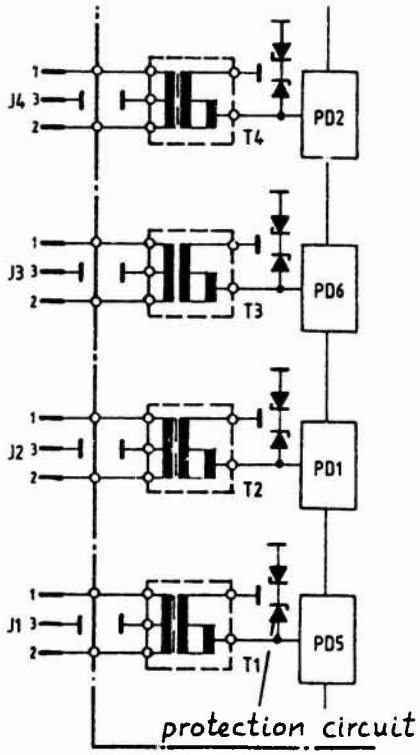

Fig. 8 - Part of circuitry of reduction goniometer with protection circuits

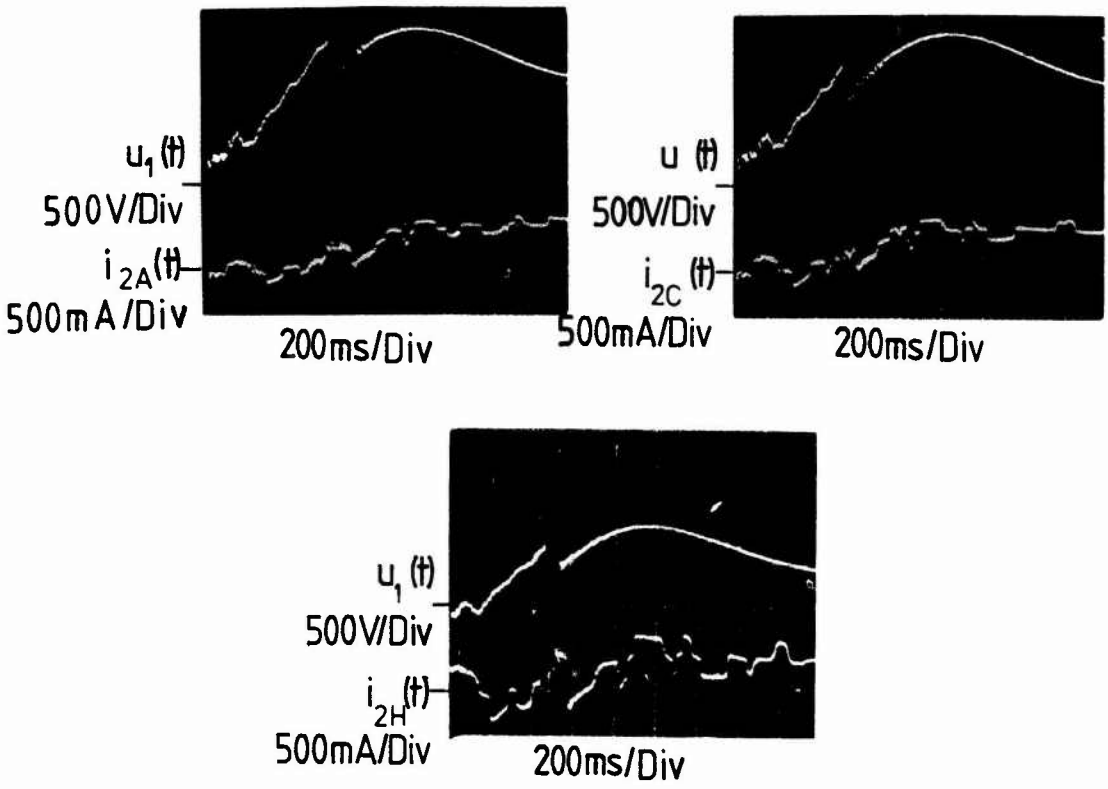

Fig. 9 - Currents $i_{2H}(t)$, $i_{2C}(t)$, $i_{2A}(t)$ according to Figures 4 or 5 respectively with protection circuits in the goniometer according to Figure 8

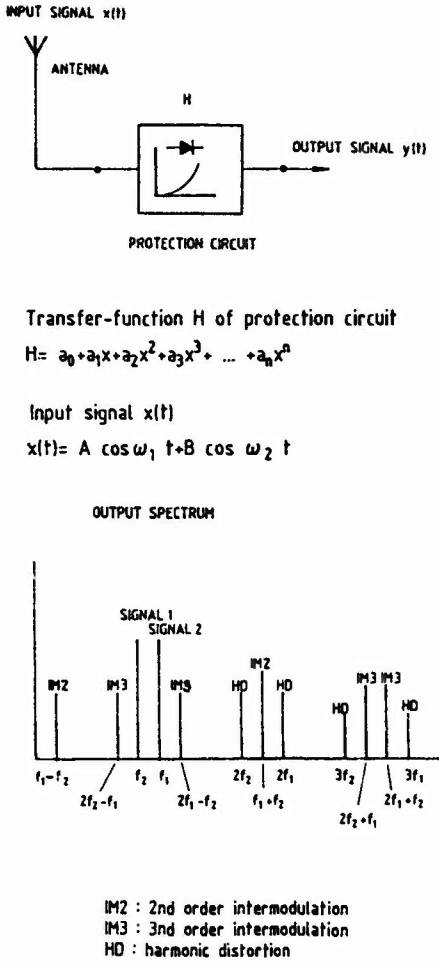

Fig. 10 - Distortion products of 2nd and 3rd order

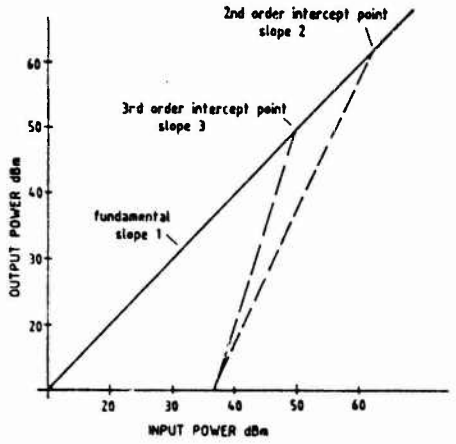

Fig. 11 - Device outputs showing the fundamental and 2nd and 3rd order distortion products

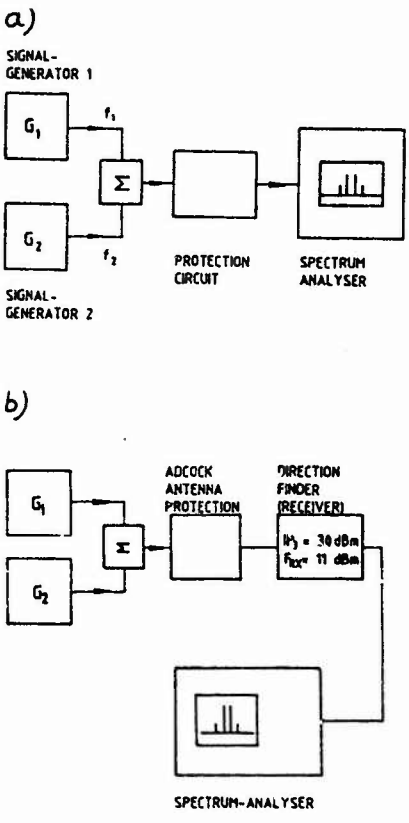

Fig. 12 - Intermodulation measurement techniques with an example

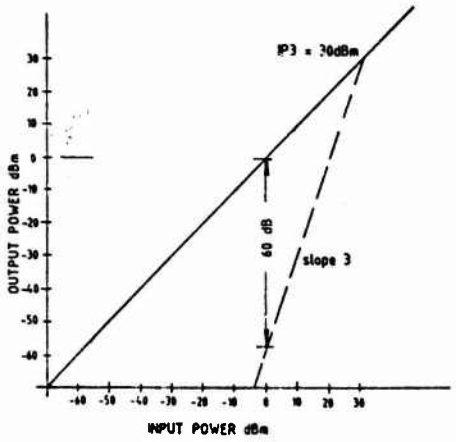

Fig. 13 - Graphical construction of 3rd order intercept point

EMI/EMP - THE CONNECTOR SOLUTION

By L. A. Krantz
Engineering Manager
EMI/Transient Suppression Connectors

Allied Corporation
Amphenol Products
Bendix Connector Operations
40-60 Delaware Street
Sidney, NY 13838

Abstract

With the advent of sophisticated electronics and severe EMI/EMP environments, it has become necessary to solve these problems in the connector rather than inside the system to avoid using space in the equipment and keep the effects outside the enclosure. In order to meet these requirements, Bendix Connector Operations of Amphenol Products has been in the business of supplying EMI filter pin connectors to the Aerospace Industry for about 20 years.

Using this technology base, BCO has developed a line of connectors which contain transient protection devices with or without EMI filtering. This paper will discuss the existing technology base that was used to design, manufacture and qualify the filter connectors. It will expand upon this base to show how transient suppression devices are packaged into the same connectors and how the connectors can be built using filters or transient protection devices alone or in parallel or series combinations. The paper will discuss the development of metal oxide varistors into sleeves for use in connectors and the packaging of unipolar and bipolar diodes onto connector pins. Some connector pins are as small as Size 22 (0.030).

The paper will discuss the EMP testing and results. The data used to qualify the connector design will also be presented and discussed.

DISCUSSION

BCO (BENDIX CONNECTOR OPERATIONS) has been a manufacturer of filter pin connectors for 20 years. These connectors are designed to replace discrete filter networks. They provide a compact sealed package designed to intermate with a designated connector series and be terminated to the internal electronics using standard practices; see Figure 1. The basic design has not changed over the past years, while design modifications have improved the product and increased manufacturing yields. The filter devices in the connector are not removable but encapsulated in an oven-cured epoxy system. The filter system is based on a selectively plated barium titanate capacitor and a ferrite bead. The capacitor is manufactured by BCO from purchased ceramic sleeves. Each ceramic sleeve is plated to form two isolated capacitors with the common electrode the external ground of the capacitor. Internal in the capacitor is a margin separating the two hot electrodes. With a ferrite bead mounted on a solid pin and the capacitor surrounding it, a single-turn transformer is formed with the capacitor solder terminated to the pin; see Figures 2 and 3.

By manufacturing the capacitors, we are able to control the design requirements of the ceramic. The ceramic sleeve is purchased from our suppliers to a Procurement Specification. This document requires that the sleeve meet certain mechanical features and specific electrical tests. These include ID, OD, length and minimum wall thickness. The electrical tests involve IR, DWV, dielectric constant and temperature coefficient. The dielectric withstanding voltage test is performed at 1000 V to assure dielectric integrity. Because of this, our standard plated capacitors will meet the MIL-STD-702 600-V spike test for aircraft power supplies. By coating the capacitor margin areas, we can significantly improve this voltage capability. Conformal coated capacitors will meet the FCC 1500-V 10x223-us spike voltage test for equipment that must interface on telephone lines. The quality of coated capacitors is verified by testing their IR at 1000 V with a 15-second electrification time. The typical breakdown voltage has been measured to be 2500 V.

By controlling the dielectric constant, the cutoff frequency can be controlled. This has enabled a family of filter capacitors to be established to satisfy industry needs. This family covers the frequency ranges of MF, HF, VHF and UHF. There are at least two different levels of cutoff frequency in each range; see Figure 4. The connector design is such that any one connector can be assembled with a mix of filters having different cutoff frequencies, ground pins or insulated feedthru contacts. The termination of the contacts can be one of several popular types: solder cups, PCB, thermocouple weld termination or UTS (universal termination system) removable crimp contact. The contact style can be either pin or socket. The contact size can be 16, 20 or 22; see Figures 5 and 6.

The connector types into which these filters can be installed covers the complete range of popular MIL types to include: MIL-C-38999, MIL-C-26482, MIL-C-24308, MIL-C-5015, MIL-C-28840, MIL-C-83723, MIL-C-26500, MIL-C-27599 and others; see Figure 7. These include many series within these specifications. For a number of years, there was no MIL specification to cover filter pin connectors. BCO created their own MIL-type specification. This document, BSF1, was written in MIL spec format to include qualification requirements and inspection tests for outgoing product. When a customer required a filter pin connector, they would write their own procurement specification. The F-18 aircraft program required a great many filter pin connectors on all avionics equipment in order to meet the EMI specification for the system. McDonnell Douglas wrote a procurement specification for all of their subcontractors to use when purchasing filter pin connectors. BCO participated with E Binghamton and MDAC in writing this specification. BSF1 was used in the preparation of this specification. This document included many new requirements and some standard features. The most notable are that the filters are to be nonremovable and terminated using a crimp insertable contact (UTS). EMI performance was specified over a broad temperature range. There was a new requirement for RF current. This was 3 A at the resonant frequency of the filter. Prior to this, the requirement was 0.25 A. A pin bending test was added to assure that if the mating pin were bent 90 degrees to touch the insert that the capacitor was not damaged and that the pin material was malleable enough to be bent without breaking.

This document was used by MDAC subcontractors. It eventually was published as 25M24. This was used as the basis for MIL-STD-2120. Both documents attempted to provide the using industry and the manufacturers a system of standardization. They both address the same needs, the difference being that the 25M24 spec was set to a specific program whereas the MIL-STD attempted to satisfy all manufacturers and users alike. Consequently, some of the needed performance limits became too general. However, it is a very good start in attempting to have everyone meet the same criteria.

It was during the preparation of the MDAC specification that a series of tests was run to determine the ability of the connector to withstand the power supply transients of MIL-STD-702. This transient was a 600-V pulse of about 50 microseconds long. It was found that standard plated product would always withstand this pulse until the magnitude was increased to 1000 V. At 1000 V, it became necessary to conformally coat the margins to suppress corona, hence flashover. Many different connectors have been tested by various customers to the limits of 600 to 1500 V. Many of these have been specified to survive EMP threats.

The internal design of the connector is the same regardless of the type of MIL spec connector. A mechanical ground system commons the ground electrode of the filter to the connector shell. The ground plate is a precious metal plated molding of high-temperature plastic. The ground plate contains integral fingers that surround the capacitor ground electrode. The ground plate is grounded to the connector shell through a ground spring that the plate nests into and has peripheral spring fingers that are trapped between the perimeter of the plate and the shell of the connector. The plate at the termination end of the connector is covered with a silicone potting seal which prevents encapsulant from entering the ground fingers. The front of the connector is also sealed with an oven-cured encapsulant behind a glass-filled epoxy insert. This encapsulant is designed to match the thermal coefficient of the ceramic, act as a heat sink and stress isolate the capacitor from external mechanical loads; see Figure 8. This assembly is designed and tested to the MIL spec environments. This design meets and exceeds the requirements of MIL-C-38999. The only exceptions that have been taken to the applicable MIL spec are:

a. Working voltage is reduced from 600 V to 200 V.

b. Dielectric withstanding voltage is reduced to 500 V from 1300 VAC rms for Size 22 contacts.

c. Temperature range is reduced to -55°C to +125°C from -65°C to +200°C.

These changes are required because of the temperature characteristics of the titanate capacitor. However, there are some significant product improvements that are gained with the fixed contact design. They are:

a. Pin bending - The pin contact can be bent to the interface and restraightened without damage to the ceramic capacitor inside the connector.

b. RF current - The BCO design is guaranteed to 3 A but tested without failure to 5 A.

c. Environmental seal - Because of the epoxy seal, all BCO connectors can meet a requirement for immersion into 3 feet of water, unmated front and rear, without water penetration or effect on insulation resistance at 500 V. This connector design with PCB tails is also being used in mass termination wave reflow soldering processes. The connector as designed can be immersed into trichloroethene at 160°F with a hot water wash and rinse with temperatures up to 250°F. With proper thermal shielding, BCO filter connectors are being solder terminated to PC boards in a vapor phase soldering process.

d. Increase in minimum insulation resistance from 5 Gohms to 10 Gohms.

All of the above is based on the filter being designed using tubular capacitors. There is another method that is gaining in popularity. This is the use of planar capacitor arrays. A planar capacitor is based on the use of a disk of ceramic with a pattern of holes in it. The pattern of holes corresponds to the pin pattern of the connector arrangement. The array is designed so that between each hole and the edge of the array is a discrete capacitor. Each capacitor is equal to half of the total capacitance of the filter required for that line in the connector; see Figures 9 and 10. The connector is assembled with two arrays separated by a ferrite bead of the appropriate length. When installed into the connector, a ground ring that surrounds the ground electrode will connect the ground of the array to the shell of the connector. In this design, the ground plane is in the array itself and not a separate element; see Figure 11. The pins are soldered to the holes of the array in a vapor phase process. At this time five arrangements are in production. Three of these are two years old and are being made in significant volume.

Our experience has shown us that there are certain economies in using the planar. The most significant are:

a. Multilayer construction with the ability of mixing different value capacitors, insulator or grounded holes using a low dielectric constant stable ceramic that has a low temperature coefficient. It also has a lower decade hour aging and a lower voltage coefficient. The ratio between the highest and the lowest capacitor in the same array cannot exceed 10 to 1 at present. The dielectric grade ceramic used is X7R. By using NPO, ceramic capacitances as low as 50 pF per hole can be designed into the array.

b. Easier to control lot integrity of each capacitor in the connector, since all in the array are made from the same raw ceramic and fired simultaneously. Because of this, they will have the same temperature and voltage coefficient.

c. Reduced overall length of the filter because the wafer-like construction of the filter array will allow reductions in the length of the connector shell. By using reduced length ferrite beads with minimal reduction in insertion loss, a filter planar can be packaged into a connector shell no longer than the MS connector it replaces.

d. Increased strength because the array is thicker than the wall of the tubular capacitor.

e. Higher capacitance filter does not mean extremely high cost, as with the tubular capacitor. Capacitance values up to 400,000 pF per hole are being made with working voltages at 50 VDC. This will allow a 1-uF balanced Pi filter to be packaged into a standard length filter connector shell.

f. Higher filter efficiency because Pi imbalance between input and output capacitor can easily be held to less than 2:1, which is the best achievable with tubular capacitors.

g. In a properly designed filter connector, planars can handle RF currents up to 9 A at resonance.

h. By consideration in the initial design, planars can handle voltage spikes up to 1500 V, as with the tubular capacitor.

With all of the above, BCO has been able to establish a complete EMI filter connector line that is capable of meeting the entire MIL spec environment with the exceptions listed previously. They provide some significant advantages to the using industry, they are sealed to moisture penetration, can be wave soldered using MIL-approved soldering and cleaning processes. They can withstand EMP and transient pulses up to 1500 V without failure. Insertion loss performance as a filter in a connector has been tested out to 18 GHz and can be guaranteed to levels of 70 dB between 1 and 18 GHz. The connector design allows specification of crosstalk or isolation levels of 85 dB between filter contacts and/or connector shell.

Using this technological base, BCO has had the capability to produce connectors that are able to suppress transient pulses as well as EMP pulses since 1974. A report has been issued regarding the work performed with GE, Harry Diamond Labs and BCO connectors using metal oxide varistor sleeves; HDL-TR-179-1 dated Aug 1974 on contract DAAG39-72-C-0179. This report made several important recommendations regarding the success of the connectors containing metal oxide varistor sleeves. The sleeves tested were supplied by GE for assembly into BCO connectors. They were handmade for Size 16 pins and 130-V line operation. The report recommended developing smaller sleeves, lower operating voltages and better methods of manufacture. No further work was done on those recommendations at that time.

In the intervening years, BCO developed a Lightning Arrestor connector that was capable of absorbing primary lightning currents. This connector is a gas discharge hermetic connector designed for an Army Communications Van. It will break down at 230 V and handle currents up to 200,000 A. There is a filter connector designed to mate to its output and absorb transients up to 2500 V for 200 ns. Because of the use of a gas (tritium) in a sealed chamber, the ionization requirement of the gas limited the response time to milliseconds. This is unsuitable for nanosecond response times required for EMP.

To satisfy the needs for EMP events, BCO designed a connector using commercially available transient response diodes; see Figure 12. This connector was designed again for an Army Communications

Van that in this case was the satellite down link and switching matrix for a combat telephone network. Because of the size of the diodes, 1500 W, the connector was designed with the diodes mounted outside the perimeter of the contacts. A multilayer PCB was designed to interconnect to each pin and diode. The diodes were commoned to a ground plate that formed the forward bulkhead of the connector. In application, the connector was mounted with a jam nut thread to a bulkhead with mating plug connectors on each end. A cable was mated to each end so that if a pulse in excess of the energy rating of the diode destroyed the diode, a new connector could be installed immediately. This connector meets all test requirements as verified by independent test facilities. The most significant feature of the design was its ability to control overshoot during pulse injection tests with a very fast 5000 V/ns rise time pulse. In all EMP connector designs, control of ground impedance is the most critical feature that will spell success or failure. If not controlled, the system will see voltages that can cause failures immediately or at some later unknown time. There were other applications for this design, but all were limited by the physical size of the package.

This design had the following diodes:

Stand-off voltage	± 11 V
Leakage current	± 5 μA
Breakdown voltage	± 13.5 to 16.5 V
Maximum clamping voltage	± 22 V @ 68 A
Wattage	1500 W

When tested with a 5000 V/ns rise time pulse:

Maximum overshoot was	45 V
Maximum current was	450 A

In 1983, contact was made again with GE regarding metal oxide varistor sleeves for connector applications. A purchase order was signed with GE to develop and manufacture two sleeves that would operate at 47 V and 53 V. One was to be used on a Size 20 pin and the other was for a Size 22 pin. This effort was to develop a family of sleeves for the full range of contact sizes and voltages from 8 to 240 V. These sleeves were designed to be interchangeable with the full line of tooled filter connector components. They were designed to replace the capacitor and ferrite on an existing filter pin; see Figure 13. Initial prototype sleeves were delivered in Feb. 1985. In the summer of 1985, a complete qualification of connectors containing metal oxide sleeves was completed. The testing was to the requirements of MIL-C-26842, Series II. Device characteristics of leakage current, clamping voltage at 1 mA and capacitance were measured before and after each environment.

These tests were performed on eight (8) single-hole jam nut mount receptacles, Shell Size 22, Arrangement 55P. They were divided into three test groups. The connectors were further subdivided by having contacts with two different voltage devices. The voltages were 41 and 220 V. These voltages refer to the nominal clamping voltage at 1 mA for the sleeve. There is now a family of devices that covers 22, 39, 47, 200 and 240 V. Each test group consisted of the following:

a. Group 1 - Device characterization
   - Clamping voltage
   - Leakage current
   - Capacitance
   - Insertion loss
   - Pulse current capability
   - Pulse energy capability
   - RF Current

b. Group 2 - Mechanical environment
   - Thermal shock
   - Random vibration
   - High G shock
   - Contact retention
   - Humidity

c. Group 3 - Life test
   - 1000 h at 125°C with voltage

The criteria used to judge the components on test were as follows:

Metal oxide varistor type	41 V	220 V
Leakage current	<200 μA	<1200 μA
Varistor voltage at 1 mA	39/44 V	198/242 V
Capacitance at 1 MHz	3000 pF	250 pF
Clamping voltage at 10 A	80 V	400 V
Energy rating	0.1 J	0.4 J
Current rating	40 A	180 A
Life test voltage	28 VDC	130 VAC

The only test where there were any problems was the life test. This was because of high leakage during the test. As a result of this, the sleeve was changed. The changes resulted in a varistor body much more stable than an existing comparable device. The powder formula was changed. The wall of the sleeve was increased to provide much more strength. This reduced the capacitance. The major improvement was a dramatic decrease in the leakage current. All of the above changes were incorporated into the 41-V device. The 200-V devices will also be changed, but data is not available at the time of publication. The specification for the 47-V device is as follows:

Maximum Rating @125°C

Continuous RMS	Continuous DC	Transient Energy	Peak Current	Max Leakage @ 20 V
30 V	36 V	0.5 J	250 A	5 μA

Maximum Rating @25°C

Capacitance @ 1 MHz	Varistor Voltage Min	Varistor Voltage Max @ 1 mA	Clamping Voltage(8x20) Peak Voltage	Clamping Voltage(8x20) Peak Cur
1000 pF	42 V	52 V	100 V	10 A

These specifications are for a Size 22 device that will mount on a Size 22 pin in a BCO EMP connector.

There have been a number of tests performed by customers to verify the reliability of the varistor and its ability to meet or comply with their particular requirements. The information which follows is a brief summary of some of these results. As a result of these tests, the tubular varistor connector has been specified for three major programs. For these programs, the varistor will be used alone or in combination with EMI filtering. The contact sizes will be 16, 20 and 22. These programs will be using the following connector series: MIL-C-38999, Series III and MIL-C-83723, Series II.

MOV F47-20, -22
Exponential Pulse

	Peak Current	V Clamp	Frequency	Results
25°C	0-198 A	78-111 V	8x340 μs	25 times at max voltage of 1100 V at each polarity--no deterioration
	0-452 A	80-130 V	1x6 μs	Same as above except max voltage was 2400 V
85°C	0-198 A	55-66 V	8x340 μs	Same as above
	0-460 A	36-60 V	1x6 μs	Same as above except one pin pulsed 500 times

The same series tooled for the filter connector line can be used for EMP connectors. The EMP connector is designed exactly like the filter connector except that the capacitor/ferrite is replaced by the MOV sleeve. The sleeves are soldered to the pin at each end of the hot electrode to ensure low circuit impedance; see Figure 14. The contacts are sealed in the connector. All connectors will be factory tested to ensure leakage current, capacitance and varistor voltage are within limits. A sample test for clamping voltage will be performed; see Figures 15 and 16.

There has been considerable concern regarding the response time of varistors, especially to nanosecond rise time pulses. BCO has conducted considerable investigation into this area. We have been able to determine that with the leadless varistor mounted into a connector, the response time is faster than the comparable disk device currently on the market. In fact, comparative tests have been performed which show the effect of the leads on response time. In comparison to diodes, MOV devices will have more capacitance, handle far more energy (for a given device capable of being mounted on the same size pin), inherently are bipolar and have a higher clamping voltage. The clamping ratio for a varistor compared to a diode will be higher. The clamping voltage ratio is the ratio between the voltage at 1 mA and at 10 A with an 8x20 μs pulse. The ratio will be about 2:1 for a varistor and 1:25 for a diode.

Some applications cannot tolerate the clamping ratio or high capacitance of the varistor and need the characteristics of the diode. In order to satisfy these needs, an epoxy sealed bipolar chip that is small enough to mount on a Size 22 pin was developed. The device has been tested by our customers. It has met MIL STAR EMP criteria. The device is designed for TTL logic networks and must tolerate the damped exponential decaying sine pulse that peaks at 1000 V and 10 A between the frequencies of 100 kHz and 100 MHz. The device characteristics are as follows:

Stand-off voltage	$\pm$ 8.2 V
Max clamping voltage	$\pm$ 13.5 V @ 10 A
Capacitance	500 pF
Breakdown voltage @ 1 mA	$\pm$ 10 V $\pm$10%
Power rating	600 W
Max leakage current	2 μA

The application also requires that the diode be packaged with a high capacitance planar Pi filter. The filters will be of two different cut-off frequencies, 200 kHz and 2 MHz. There are four other diode voltages, +15, -15, +28 and $\pm$45. All of these devices are provided in the same package capable of being mounted on a Size 22 pin. To meet a higher energy rating would require a larger chip. This would mean that it will require the next size pin, Size 20. The diode itself is leadless and mounts directly on the pin. The second lead of the diode is terminated to a ground sleeve. The geometry of this assembly is such that it will directly replace a filter pin in the same pattern with diode pins or MOV pins. They can be mounted in series or in parallel within the pattern of the connector.

The connector is designed with a separate ground for the diode and filter. The diode contact is assembled separately from the connector and tested before being assembled into the connector. The filter elements in this case are planar capacitors. They are not soldered to the pin but are a solderless design with individual springs to make contact with the pin and electrode of the array. The arrays are assembled into the shell individually (this is a Pi filter which requires two capacitors per pin) with a ferrite bead separating the arrays. Each array has its own ground spring. Prior to encapsulation, the assembly is checked. After filling, all contacts are tested for diode characteristics and insertion loss. Max clamping is checked to a sampling plan.

At the time of publication, there are a group of 10 diode connectors being assembled. These will be divided into two groups of five each. Five will be tested by our customer and five by BCO. The customer tests are primarily for the EMP capabilities. The BCO tests will be to the MIL specification requirements of thermal shock, random vibration, high G shock, humidity, durability, contact retention, fluid immersion and whatever else relates to a satisfactory design. These tests will be completed by June of 1986.

With the capabilities described here, BCO does feel that the using industry has available the connector solution to EMI/EMP. A design that offers many different alternatives to choose from; provides a compact package solution; uses known designs that have a field proven history; provides sufficient design safety limits to assure that the system will be reliable and interface to the external connector environment without compromising performance, even though it in itself is a complex electronic subsystem. The most important consideration is that these connectors are cost effective when compared to the alternatives of space, larger number of junctions and problems of internal shielding if the EMP event is allowed to invade the enclosure before it can be suppressed.

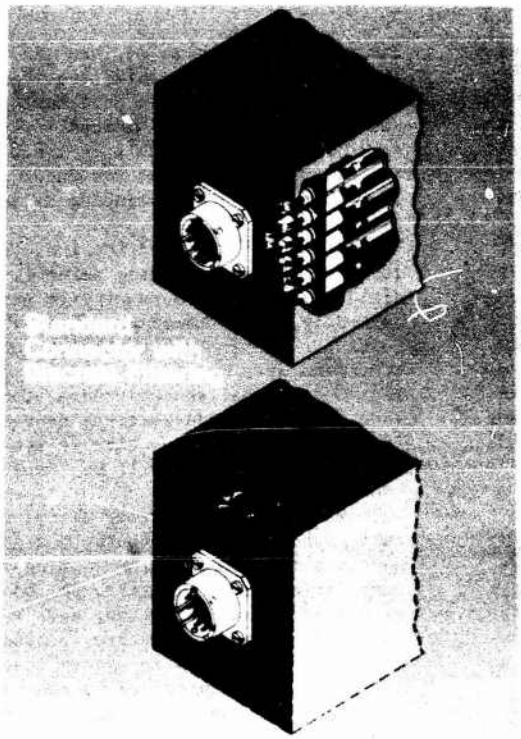

BENDIX® FILTER ADVANTAGES

- **Eliminates External Filter Circuits**
- **Eliminates Excessive Assembly Times Associated with External Filtering**
- **Increased Reliability – Fewer Solder Junctions**
- **Physically Protected Filter Elements Factory Pre-tested**
- **Reduction of Weight and Space**
- **Reduced Installation Cost**

Figure 1

TUBULAR CAPACITOR

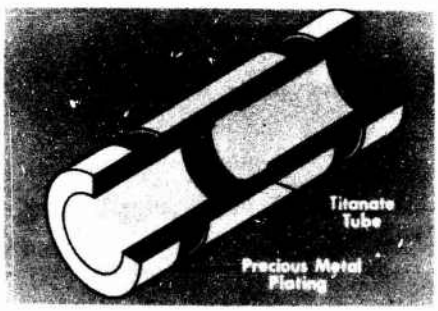

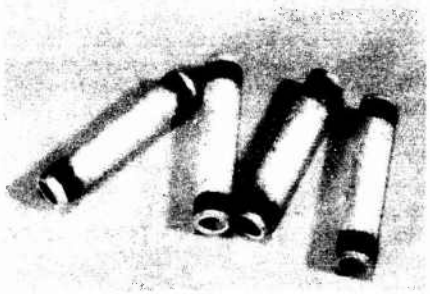

Figure 2

TUBULAR CONTACT ASSEMBLY

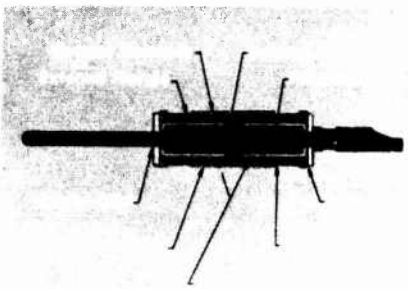

Figure 3

WHY A LOW PASS FILTER CONNECTOR

Typical Filter Attenuations

as a function of frequency at +25°C

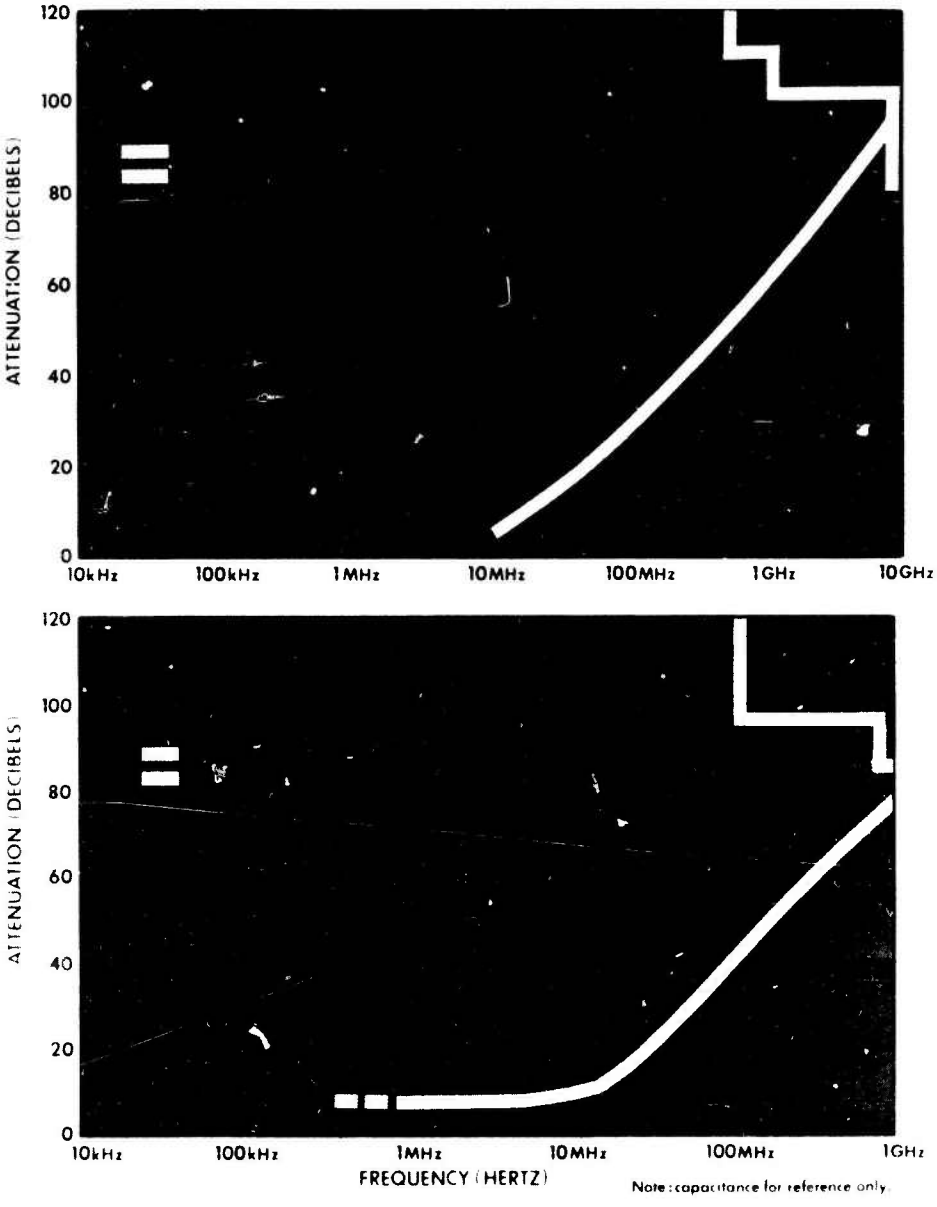

Figure 4

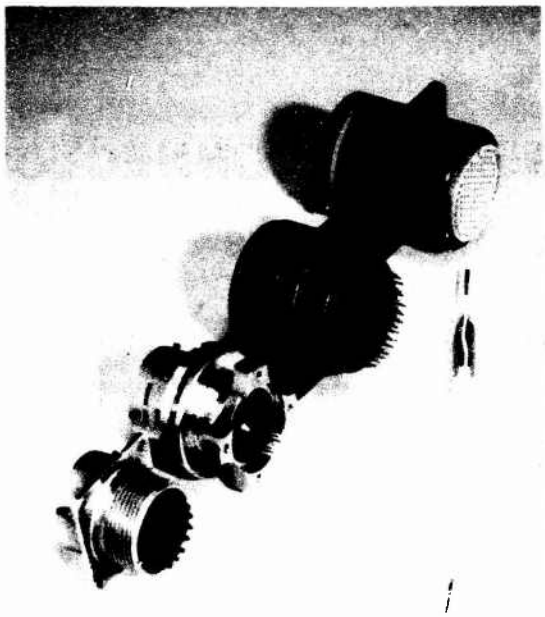

CONTACT TERMINATION OPTIONS

- Solder Cups
- Crimp Removable
- Printed Circuit Board Termination
- Wire Wrap
- Coaxial
- Fiber Optic Hybrid
- Thermocouple
- Grounded
- Feedthrough
- Insulated
- Combinations of the Above

Figure 5

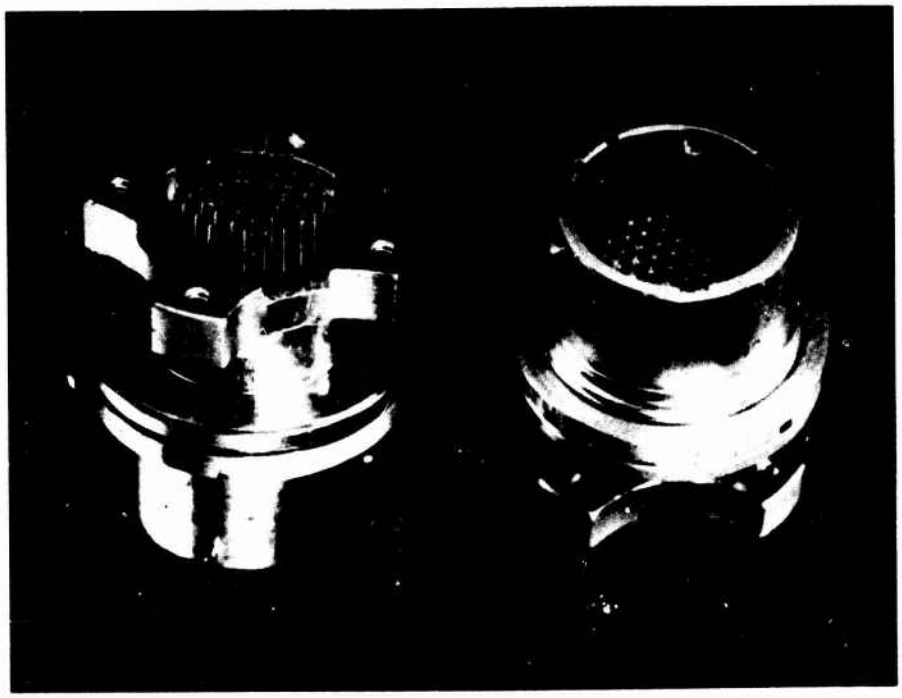

Figure 6

MIL-C-38999 (Series I, II, III)

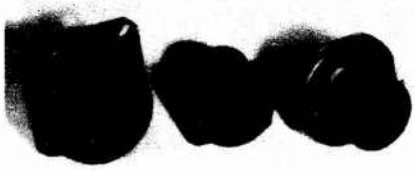

MIL-C-26482 (Series I, II)

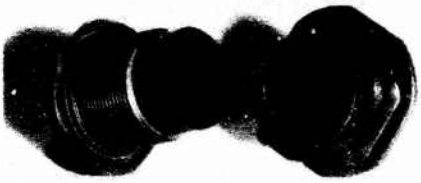

MIL-C-5015 and MIL-C-22992

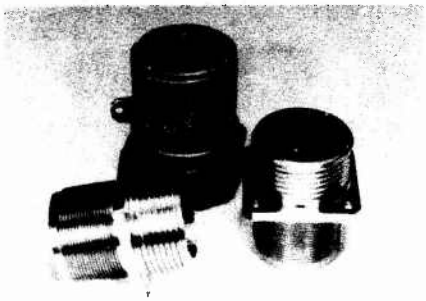

Others:
- MIL-C-28840
- MIL-C-26500
- MIL-C-27599
- MIL-C-83723

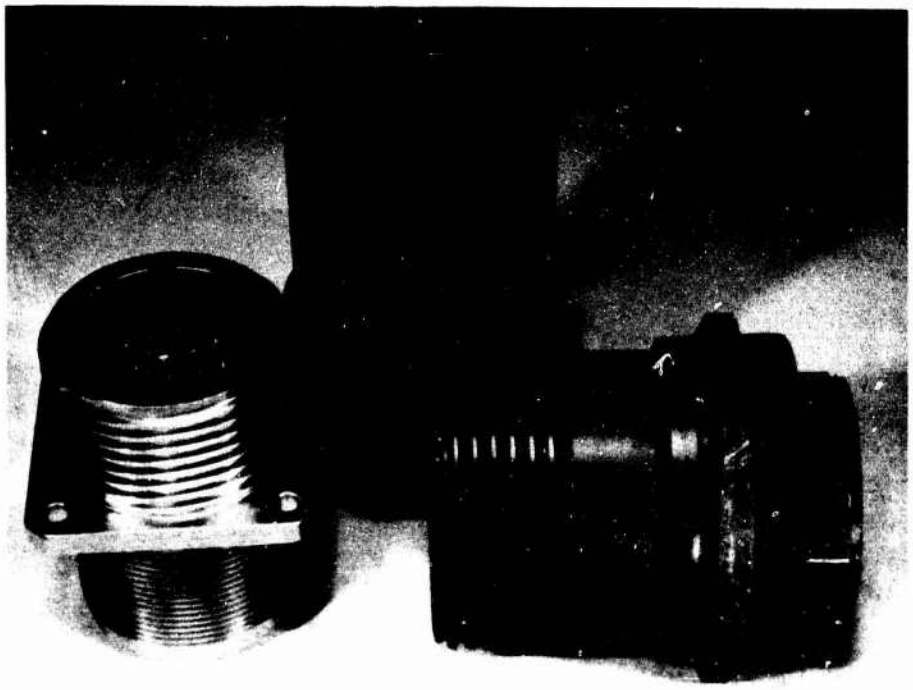

Figure 7

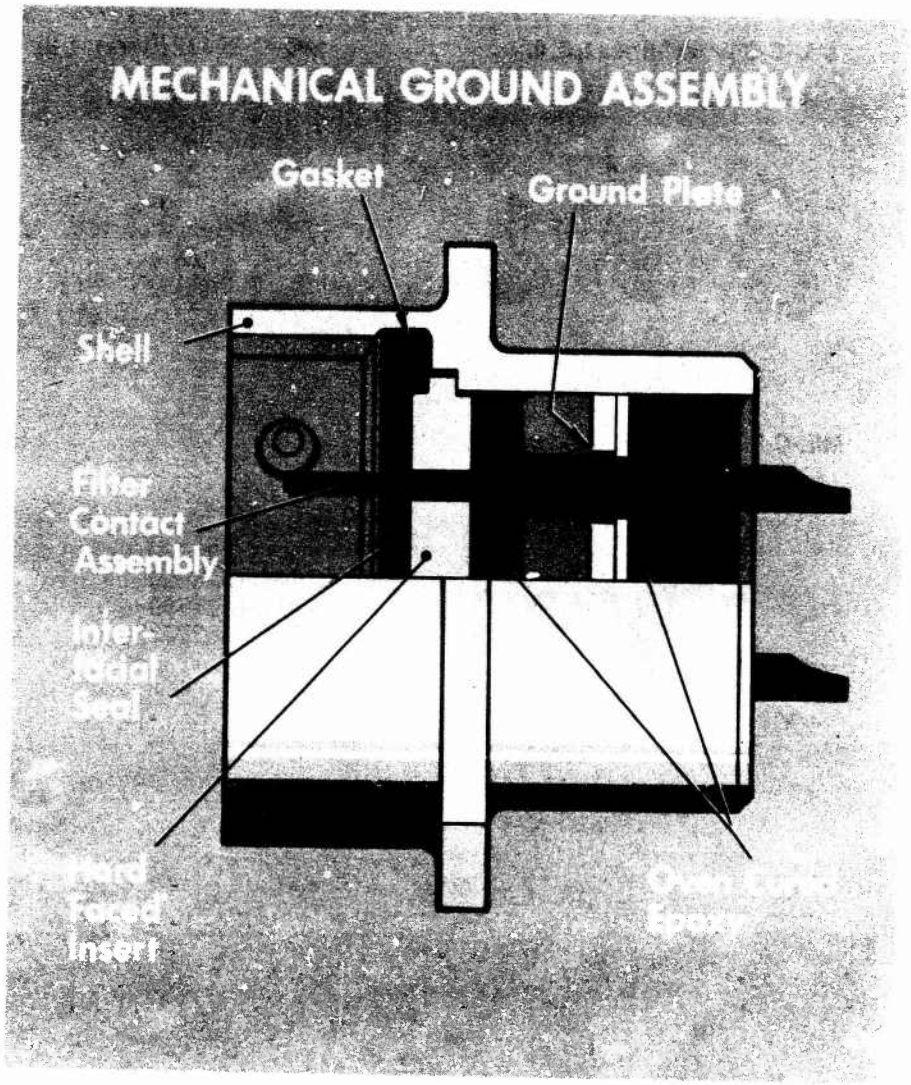

Figure 8

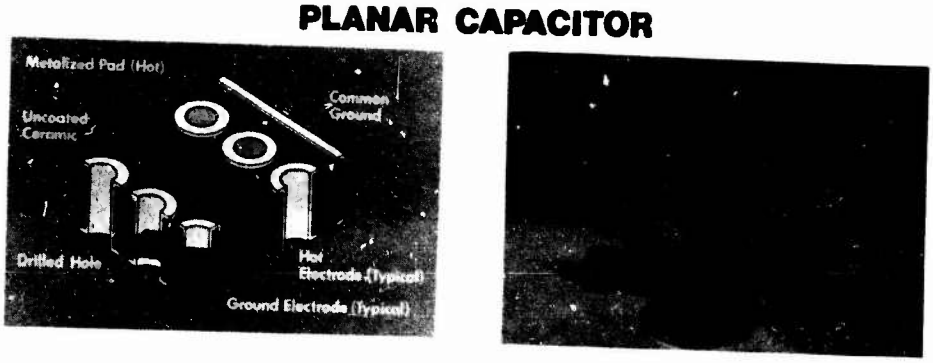

Figure 9

PLANAR CONTACT ASSEMBLY

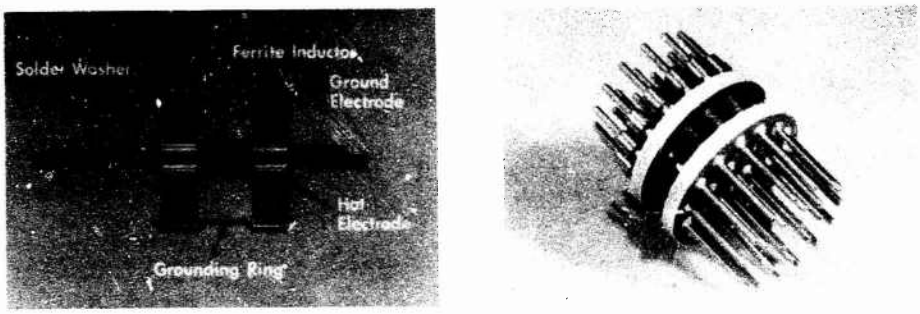

Figure 10

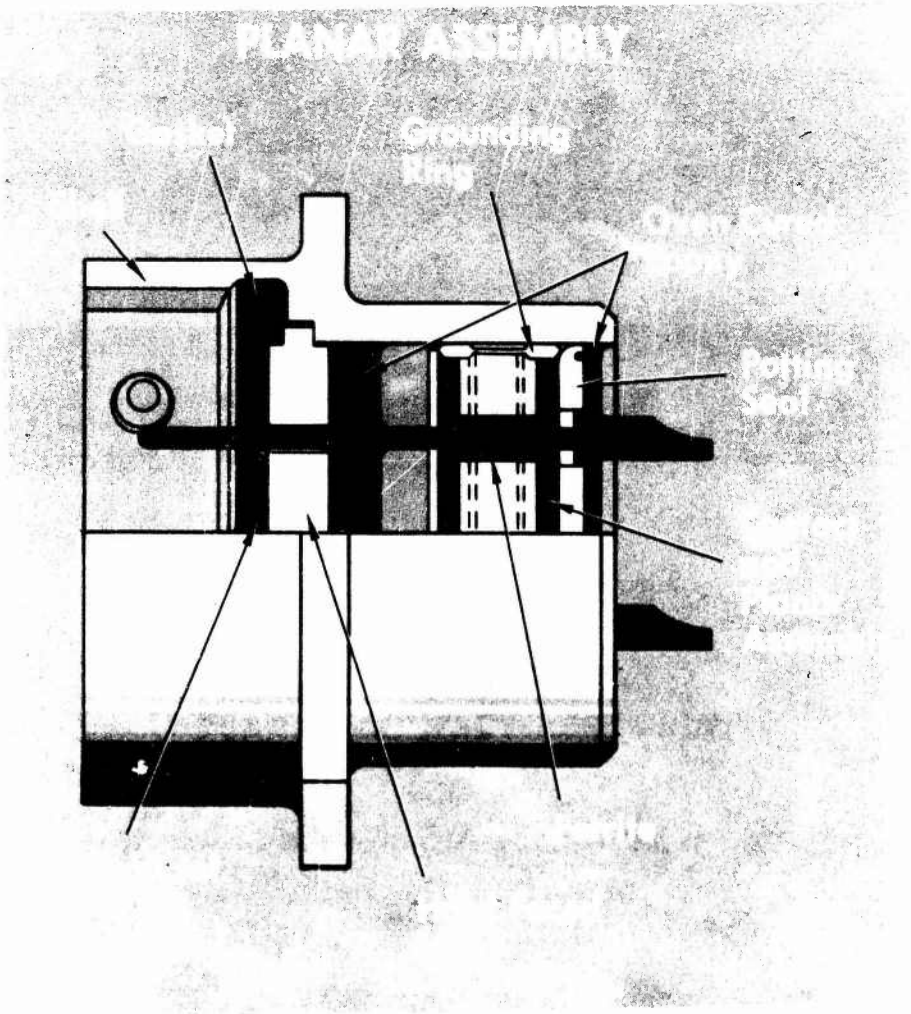

Figure 11

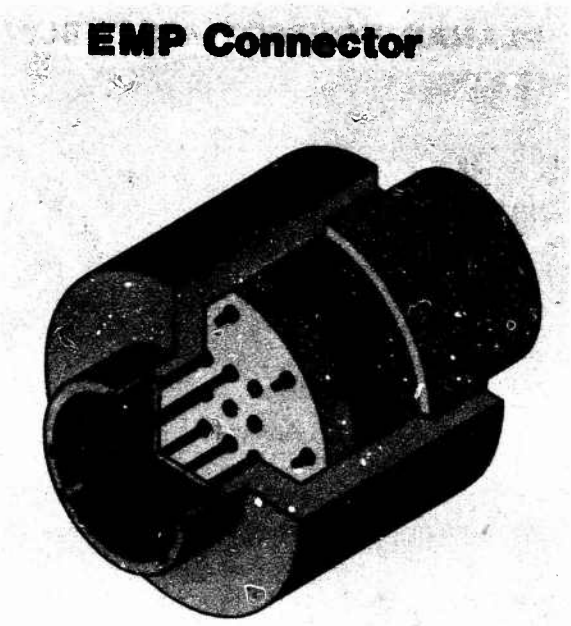

Figure 12

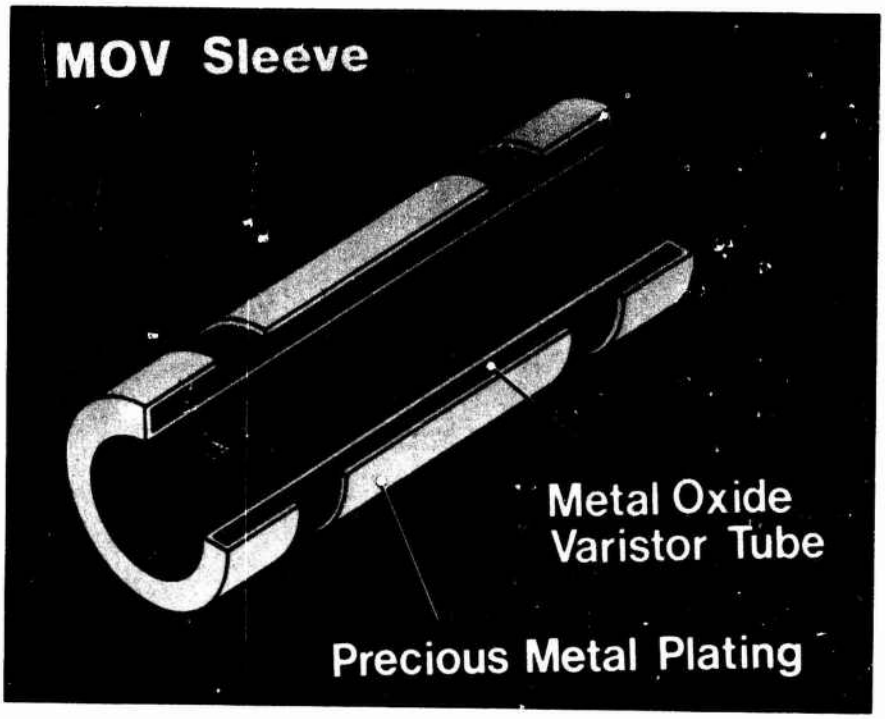

Figure 13

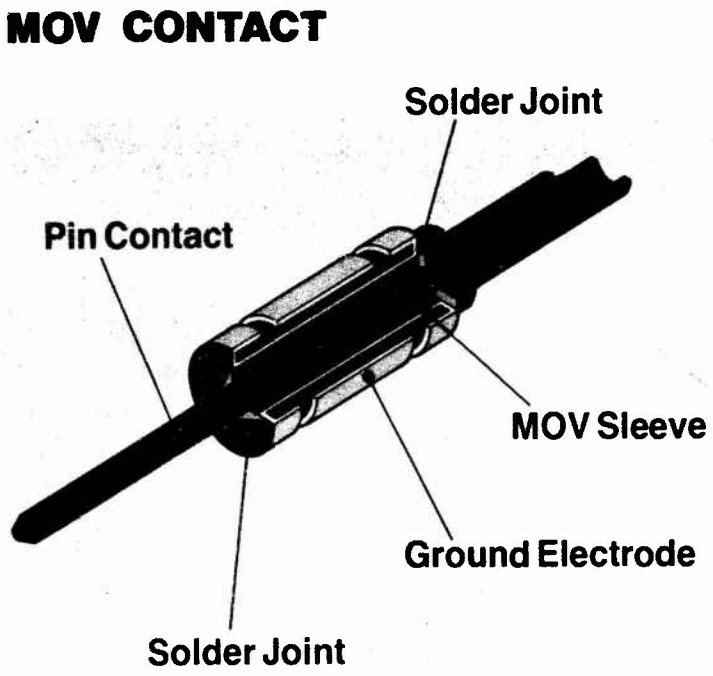

Figure 14

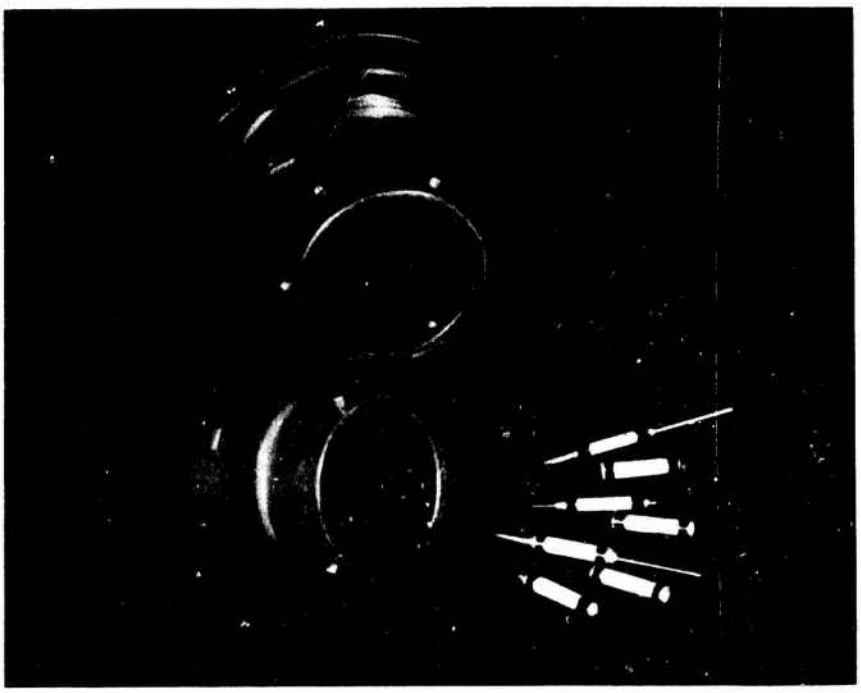

Figure 15

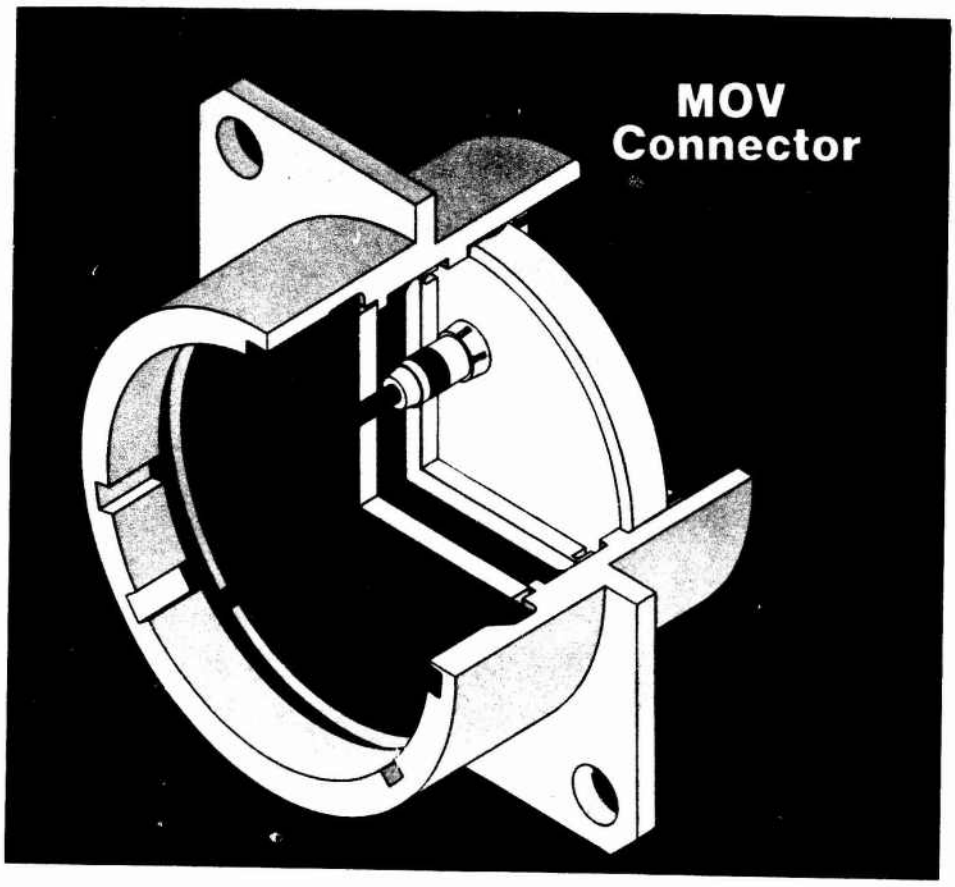

Figure 16

EFFECT OF E-FIELD MILL LOCATION ON ACCURACY OF ELECTRIC FIELD MEASUREMENTS WITH INSTRUMENTED AIRPLANE

Vladislav Mazur
NOAA/National Severe Storms Laboratory
Norman, OK 73069

Lothar H. Ruhnke
Naval Research Laboratory
Washington, DC 20375

Terry Rudolph
Electromagnetic Applications, Inc.
Denver, CO 80226

Abstract

It is common in airborne observations to measure the ambient electric field and self-charge of the instrumented airplane with four field mills. In this case, the sensors' locations on the airplane are critical for accurate measurement. It is shown that positioning sensors on or near crossing points of the lines of the airplane's electrical symmetry (neutrality) decreases significantly the amplification of errors in the signal processing system that are transferred into errors in the ambient field estimates. The calculations are made using the computer simulated model of the NASA F-106B research airplane placed in a uniform electric field. Two new calibration procedures for the net charge on the airplane are suggested.

Introduction

An interest in vertical electric field profiles was responsible for the initiation of early measurements from airplanes of the ambient field, in addition to measurements made with instrumented balloons (Rossmann, 1950, Markson, 1977). The influence of the airplane's self-charge on these measurements required the use of sensors placed at symmetrical points on the airplane, in particular on the left and right wings. The sum of readings from these two sensors indicated the magnitude of the self-charge, while their difference yielded the external (horizontal) component of the ambient electric field. To obtain the vertical field in the assumed absence of a horizontal field component, the airplane was tilted at a known angle; the absence of a horizontal field was verified in level flight. Clark (1958), Fitzgerald (1958) and others used the wing tips as sensor locations because of the high enhancement factor of local electric fields at these points. The importance of electric field structure in thunderstorms to cloud physics and lightning research prompted attempts to measure all three vector components of the ambient electric field and the self-charge of the airplane. Fitzgerald (1965) and Anderson (1966) employed additional field sensors, and Kasemir (1951, 1964) introduced the cylindrical field mills to obtain the vector components of the electric field. However, it has always been difficult to adequately calibrate these sensors to convert the obtained readings into meaningful interpretations of ambient field conditions.

The procedure that is widely used to determine calibration coefficients consists of flights with known pitch and roll in predetermined electric field. The analytical estimates of the airplane form factor using a small-scale model of an airplane in a parallel-plates electric field were described by Evteev (1972). Not much has been said in the literature about the success or failure of either these calibration procedures or of the accuracy of airborne electric field measurements in general. Therefore, the credibility of the airborne electric field data obtained near or within thunderstorms is limited to gross estimates of magnitudes and polarities.

Recent advances in thundercloud modeling have increased the need for systematic measurement of the electric field in and around thunderstorms during different stages of their development. Such a task can be handled only with instrumented airplanes. Also, from studies of lightning hazards to aircraft, it has been determined that most, if not all, lightning strikes to aircraft in thunderstorms are triggered by the aircraft itself (e.g., Mazur et al., 1984, Rustan et al., 1985). This has put a new emphasis on the accuracy of ambient field and self-charge measurements during storm penetrations. Together with the electromagnetic parameters of lightning strikes to the airplane recorded on board, the parameters of the electrical environment provide complete information needed for the interpretation of electrical interaction between the airplane and the thundercloud. It may be assumed that triggered lightning is associated with particular but defineable electric field environments and, when determined, the knowledge of these environments may be used to avoid lightning strikes to aircraft flying through clouds of different types, as well as to provide a reliable warning to pilots of impending lightning strikes. It is, therefore, important to evaluate the accuracy of airborne electric field measure-

ments. This might also include reviewing calibration algorithms. Our paper deals generally with this subject for an airplane equipped with four shutter type field mills. We will use as an example the NASA F-106B research airplane to illustrate several aspects of problems discussed in detail in sections to follow.

Optimum Position of E-field Sensors on the Airplane

An airplane with metallic skin has influence charges on its surface from the three components of the ambient electric field, and an additional self-charge resulting from triboelectricity and engine exhaust (for a certain type of aircraft). While we cannot measure an ambient electric field without an airplane present, we can measure the local fields on the level of the airplane skin in places where the field mills are installed. Because the intensity of the local field varies in different parts of the airplane, our measurement is affected by the sensor's position. It must also be assumed that the self-charge will contribute to the output of each field mill. A set of four linear equations in matrix form (1) describes the local fields for four sensors (E_1, E_2, E_3 and E_4) as a function of three orthogonal components of ambient field (E_x, E_y, E_z) and the self-charge Q.

$$\begin{bmatrix} E_1 \\ E_2 \\ E_3 \\ E_4 \end{bmatrix} = \begin{bmatrix} a_{11} & a_{12} & a_{13} & a_{14} \\ a_{21} & a_{22} & a_{23} & a_{24} \\ a_{31} & a_{32} & a_{33} & a_{34} \\ a_{41} & a_{42} & a_{43} & a_{44} \end{bmatrix} * \begin{bmatrix} E_x \\ E_y \\ E_z \\ Q \end{bmatrix} \quad (1)$$

In order to transfer the local field values into the sensor voltage outputs, a set of four additional calibration coefficients (one per sensor) should be determined. The sensitivity of each field mill is easily estimated by independent calibration of each mill on a flat ground in a known electric field. Therefore, we will operate in our analysis with only the matrix (1) consisting of coefficients a_{ij} that reflect the airplane form factor.

Let us assume that the homogeneous part of the ambient field is larger than the size of the airplane. In the following examples the direction of the E-field is considered, for the sake of simplicity, to be an orthogonal one relative to the airplane axes. Figure 1 shows a fuselage cross-section in a horizontal E-field, E_y. The E-field in the proximity of the airplane skin decreases with the distance (up or down) from the horizontal axis of symmetry. Therefore, the place to install a field mill to maximize its sensitivity to E_y is on the horizontal plane of symmetry. In order to make the mills for measuring E_z insensitive to the E_y component, they should be on the vertical plane of symmetry, where vertical components of the E_y field lines compensate each other (see part of Figure 1 enlarged in Figure 2), since they are of the opposite sign. Figure 3 shows a portion of a fuselage in the vertical, E_z, field. As in the previous case, the positioning of the field mill for measuring E_y in the horizontal plane of symmetry makes it insensitive to the horizontal component of the E_z-field in close proximity to the airplane skin, while the positioning of the field mill for measuring the E_z component in the vertical plane of symmetry maximizes its sensitivity to the E_z-field. Figures 4 and 5 show views of the airplane in a horizontal, E_y, electric field, in the horizontal and vertical planes. Using the same considerations as previously, the ideal position for the E_y mills (E_1 and E_2 in Fig. 4) would be at points where the lines of electrical symmetry of the E_x and E_z-fields cross. The mill for measuring E_x (E_y in Fig. 4) should be installed on the plane of horizontal symmetry to minimize the influence of E_y and E_z. To maximize its sensitivity to E_x, the mounting should be somewhere in the nose or tail section. The E_4-mill would be mounted most effectively in the aft section of the aircraft, as indicated in Figure 5, and pointed toward the rear.

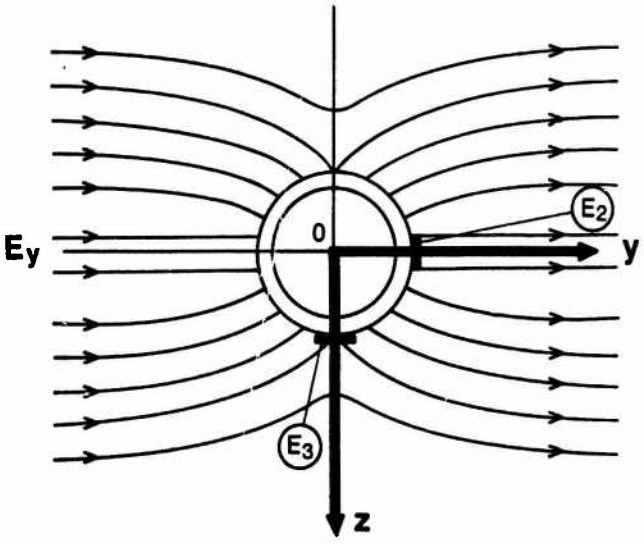

Fig. 1 Cross-section of a cylindrical fuselage in E_y-field. E_2 and E_3 are sensors of the corresponding ambient field components E_y and E_z.

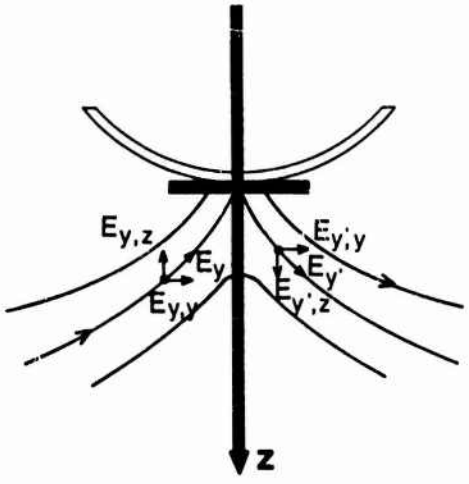

Fig. 2 E_3-mill in E_y - field. $E_{y,z} + E_{y',z} = 0$, thus, no contribution from E_y in E_3 mills.

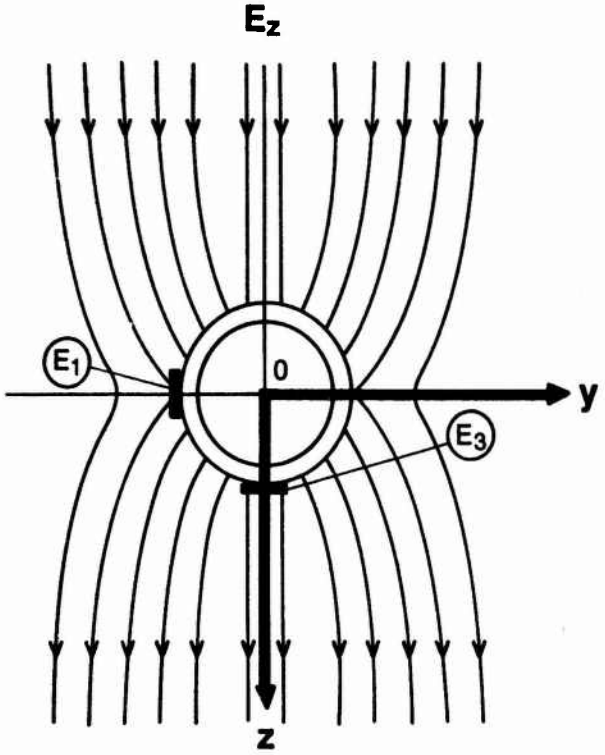

Fig. 3 Cross section of a cylindrical fuselage in E_z-field. E_1 and E_3 are mills of the corresponding ambient field components E_y and E_z.

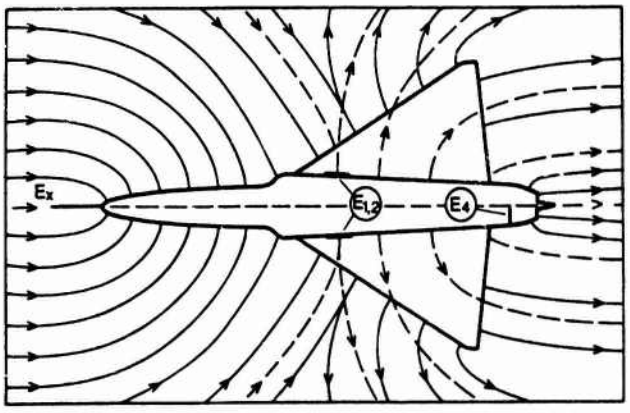

Fig. 4 Sketch of airplane fuselage in horizontal plane in E_x - field.

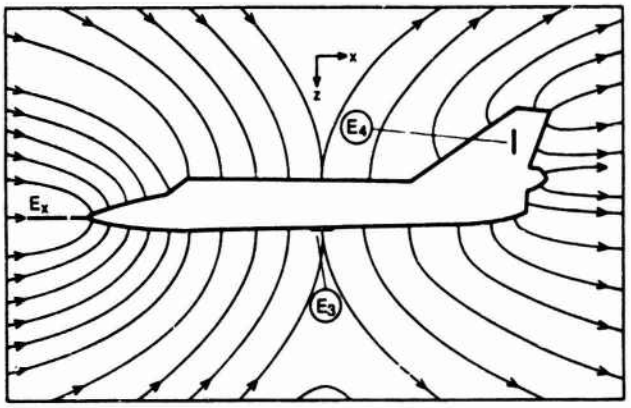

Fig. 5 Sketch of vertical profile of airplane fuselage in E_x - field.

The horizontal symmetry of airplanes makes it possible to convert the 4 x 4 matrix of the type shown in (1) into a 3 x 3 matrix (2). This is done by positioning field mills for measurements of the E_y-component on both sides of the fuselage symmetrically, and the rest of the mills along the horizontal axis of symmetry. The E_y component of an ambient field is equal in such a case to $(E_1 - E_2)/2a_{12}$.

$$\begin{bmatrix} \frac{E_1+E_2}{2} \\ E_3 \\ E_4 \end{bmatrix} = \begin{bmatrix} a_{21} & a_{23} & a_{24} \\ a_{31} & a_{33} & a_{34} \\ a_{41} & a_{43} & a_{44} \end{bmatrix} \times \begin{bmatrix} E_x \\ E_z \\ Q \end{bmatrix} \quad (2)$$

To keep the field mill output unaffected by the other orthogonal components of the ambient electric field which we do not wish to measure, the matrix coefficients a_{ij} in the equation (2) should be equal to zero for $i \neq j$ (except for a_{i4}). Even in the case of ideally located sensors, the coefficients a_{i4} resulting from the airplane charge will remain greater than zero. In reality, the locations for mounting field mills are always less than ideal; and therefore, the effect of the sensors' location on measurements should be estimated.

We can group all potential errors into two independent categories: (1) errors in values of matrix coefficients, i.e., in the link between ambient and local field, and (2) errors in signal processing, i.e., in the link between local field and signal output. One widely used method of calculation for the matrix coefficients is the airplane calibration in a known electric field. Then, both the accuracy of calibrational procedure and errors in signal processing will contribute to the accuracy of the matrix coefficient determination. The other recently introduced method uses the mathematical model of aircraft in a homogeneous electric field in computer simulated calculation of matrix coefficients (Figure 6). The accuracy of this method depends upon the size of the grid in the model and skills with which the details can be simulated by the model. The new method provides the researcher with an opportunity to quickly evaluate the performance of field mills at chosen locations. Signal processing errors are affected, among others, by the accuracy of local field mill calibration, signal-to-noise ratio, non-linearity of amplifiers, and DC-offset. An additional error which might result from nonhomogeneity in the ambient field would also appear on the signal output.

Our purpose in this paper is to evaluate the effect of potential errors in signal processing on the ambient field and self-charge with different locations of the sensors on the airplane. The matrix coefficients in this analysis are considered to have fixed values. We will define the matrix as being stable if the variance of field mill outputs (E_1, E_2, E_3, E_4) is less or comparable with the variance of ambient field components (E_x, E_y, E_z, Q). It is otherwise defined as being unstable.

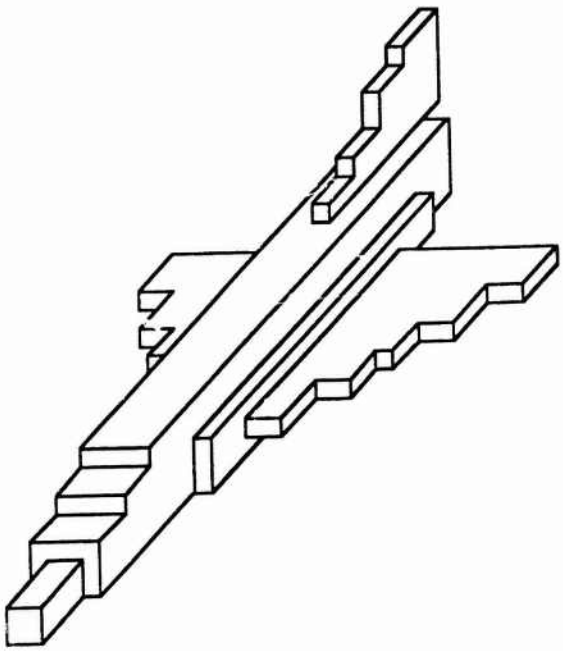

Fig. 6 Block model of F-106B airplane used in computer simulated calculations of matrix coefficients.

Evaluation of the Field Mill Locations on the F-106B

The matrix equation (3) for the F-106B airplane, in terms of the local fields at the four field mill locations (Fig. 7), has been calculated from computer simulation studies (Rudolph and Perala, 1985). Because of the dislocation of sensor E_4 relative to the horizontal axis of the airplane, the obtained matrix is of the 4 x 4 type.

$$\begin{bmatrix} E_1 \\ E_2 \\ E_3 \\ E_4 \end{bmatrix} = \begin{bmatrix} -4.38 & 1.46 & 0.08 & 507 \\ -4.38 & -1.46 & 0.08 & 507 \\ -2.47 & 0 & 1.52 & 464 \\ 0.89 & 0.15 & 1.03 & 276 \end{bmatrix} \times \begin{bmatrix} E_x \\ E_y \\ E_z \\ Q \end{bmatrix} \quad (3)$$

The inverted matrix is:

$$\begin{bmatrix} E_x \\ E_y \\ E_z \\ Q \end{bmatrix} = \begin{bmatrix} -0.005 & 0.041 & -0.306 & 0.449 \\ 0.342 & -0.342 & 0 & 0 \\ -0.310 & -0.360 & 1.017 & -0.478 \\ 0.001 & 0.0014 & -0.0028 & 0.004 \end{bmatrix} \begin{bmatrix} E_1 \\ E_2 \\ E_3 \\ E_4 \end{bmatrix} \quad (4)$$

Let us assume a signal processing error of a certain maximum level, e.g., 10%. Using matrix equations (3) and (4), we will calculate the ambient field values and estimate their variance resulting from the 10% variance of local fields. Three cases of electrical environment are considered. These cases closely approximate natural conditions inside the storm for (1) an arbitrary field and an average self-charge defined as type A ($E_x = E_y = E_z = 10$ kv m^{-1}, $Q = 100$ μc), (2) a dominating self-charge in the relatively weak electric field defined as type B ($E_x = E_y = E_z = 1$ kv m^{-1}, $Q = 100$ μc), and (3) a dominating component of the ambient field and an average self-charge, type C ($E_x = E_y = 10$ kv m^{-1}, $E_z = 100$ kv m^{-1}, $Q = 100$ μc). The value of self-charge $Q = 100$ μc has been chosen because its contribution to the local field is comparable with those from the ambient field. The field mills E_1 and E_2 are always adjusted to work identically in pairs. Therefore, we will consider the variance of outputs of both sensors as being related rather than independent. The results of calculations for the electrical environment of type A are presented in Table 1.

Table 1. Test of matrix stability for the F-106B, type A field condition.

Ambient field: $E_x = E_y = E_z = 10$ kv m^{-1}, $Q = 100$ μc

Local field: $E_1 = 22317.8$ v, $E_2 = -6921.9$ v, $E_3 = 36753.7$ v, $E_4 = 48200.5$ v.

Local field	$E_1, E_2,$	$\underline{0.9}E_1, \underline{0.9}E_2,$	$E_1,$	$E_2,$	$E_1,$	$E_2,$
Amb field	E_3, E_4	$E_3,$ E_4	$\underline{0.9}E_3, E_4$		$E_3,$	$\underline{0.9}E_4$
E_x(v)	10000	10039.1	11125.2		7833.2	
E_y(v)	10000	9012.2	10013.6		10013.6	
E_z(v)	10000	10345.6	6163.3		12204.4	
Q(μc)	100	98.3	110.3		80.9	
Var E_x	(%)	0	11		22	
Var E_y		10	0		0	
Var E_z		0	38		22	
Var Q		2	10		19	

As seen in Table 1, the variance in the value of one local field measurement leads to variances in more than one component of the ambient field and/or self-charge. This means both amplification in the absolute value of the error, and an an shift in the total vector of the ambient fiel Considering the ambient field error as a vect with three orthogonal components, the coe cient α_E, calculated as the ratio of the ab value of this vector to the corresponding variance of the local field (see Equation 5), represents the error amplification.

$$\alpha_E = \frac{\sqrt{(\mathrm{Var}E_x)^2+(\mathrm{Var}E_y)^2+(\mathrm{Var}E_z)^2}}{\mathrm{Var}E_i} \quad (5)$$

The self-charge amplification is $\alpha_Q = \frac{\mathrm{Var}Q}{\mathrm{Var}E_i}$.

Results of the matrix stability test in Table 1 may be converted into the error amplification coefficients in Table 2.

Table 2. Error amplification coefficients for the F-106, type A field condition.

	Local field variance		
	E_1, E_2	E_3	E_4
α_E	1.0	4.0	3.1
α_Q	1.2	1.[illegible]	1.9

For initial field conditions identified as types B and C, the error amplification coefficients are shown in Table 3.

Table 3. Error amplification coefficients for the F-106, Type B and C field conditions.

Field Type		Local field variance		
		E_1, E_2	E_3	E_4
B	α_E	30.0	49.1	18.7
	α_Q	1.0	1.3	1.2
C	α_E	1.0	5.6	6.3
	α_Q	<1.0	5.0	5.5

The analysis of error amplification coefficients in Tables 2 and 3 indicates that the matrix for the F-106B field mill configuration is unstable. The absence of symmetrical pairs for E_3 and E_4 mills makes ambient field components E_x and E_z especially sensitive to self-charge Q.

Testing the optimum positioning of field mills

Employing the concept of electrical symmetry and the block modeling of the F-106B, we produced the 4 x 4 matrix (6) for optimum location of four field mills on the F-106B (see Fig. 8).

$$\begin{bmatrix} E_1 \\ E_2 \\ E_3 \\ E_4 \end{bmatrix} = \begin{bmatrix} 0.011 & 0.405 & -0.373 & 120 \\ 0.011 & -0.405 & -0.373 & 120 \\ 0.064 & 0 & 1.47 & 270 \\ 0.113 & 0.016 & 0.003 & 9.25 \end{bmatrix} \times \begin{bmatrix} E_x \\ E_y \\ E_z \\ Q \end{bmatrix} \quad (6)$$

The three types of electrical environment, described earlier as types A, B, and C, are applied for testing the matrix stability. The results are presented in Table 4.

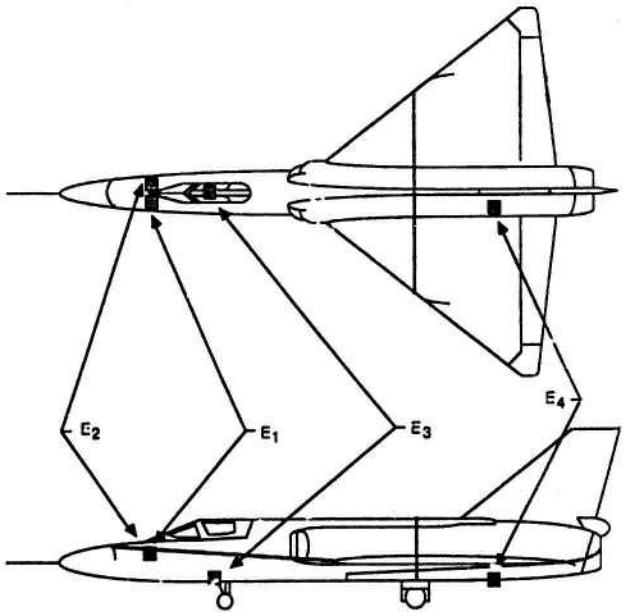

Fig. 7 Location of electric field mills on F-106B airplane (1985 season).

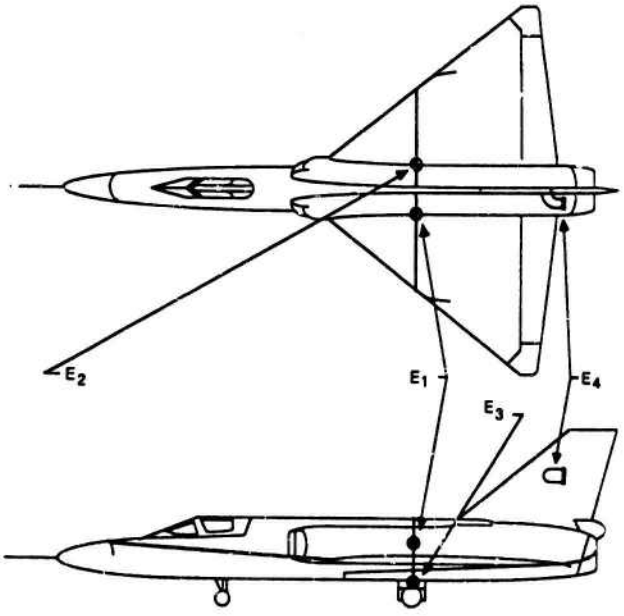

Fig. 8 Optimum location of electric field mills on F-106B airplane. Shadowed lines are lines of electrical symmetry.

Table 4. Error amplification coefficients for the optimum field mill locations, Type A, B, and C field conditions.

Field Type		Local field variance E_1, E_3	E_3	E_4
A	α_E	1.0	2.1	2.2
	α_Q	<1	<1	<1
B	α_E	11.0	12.6	10.8
	α_Q	<1.0	<1.0	<1.0
C	α_E	1.7	1.9	2.8
	α_Q	2.4	1.2	1.2

The analysis of ambient field and self-charge variances for optimum field mill configuration shows that the matrix (6) is stable in two out of three types of electrical environment (types A and C), and unstable in the case of dominant self-charge (type B). It should be realized, however, that with always significant input into the local field measurements from self-charge, and without a symmetrical pair of sensors for E_3 and E_4, the matrix can never be stable under the domination of self-charge. The comparison of the two field mill configurations on the F-106B, current and optimim, definitely proves that the accuracy of ambient field measurements increases considerably when the sensors are placed according to the principal of electrical symmetry.

Determination of the Matrix Coefficients Due to self-charge on the Airplane

The traditional way to determine the matrix coefficients that result from the ambient field components is still the calibration flight in the known electric field. The determination of the matrix coefficient from the self-charge by calibration is a more complicated procedure, owing to the difficulties of measuring the charge value in flight.

When the charged airplane is insulated from the ground (e.g., by teflon blocks), the airplane and its mirror-image charge (a result of the conductive earth) make a capacitor of capacitance C. This capacitance can be measured using available techniques. Because of nonuniformity in the charge distribution on the airplane when in the position described above, the outputs of field mills cannot be used for calculation of the matrix coefficients associated with self-charge. If the aircraft is elevated (e.g., by a crane with electrically insulated cables) to a height sufficient to exclude the mirror-image charge effect, this would simulate a clear sky flying condition. The necessary height may be calculated using the computer simulated model of the airplane. This height for the F-106B should be at least 10 m above the ground (Fig. 9). With the measured capacitance C of the airplane (in its lifted position), the quantitative net charge Q may be applied to the airplane by bringing its potential to a value $V = \frac{Q}{C}$. Because the ambient field is negligible, the recorded outputs of the field mills will be equal to the products of the applied net charge Q and the corresponding matrix coefficients. Thus, these coefficients may be determined.

The other method of calculating the matrix coefficients resulting from self-charge is based on actual records of the field mills during descent and landing of the airplane with an undetermined charge Q (Anderson, personal communication). With the assumption of a negligible ambient field, these records will indicate some steady values until the airplane reaches a certain

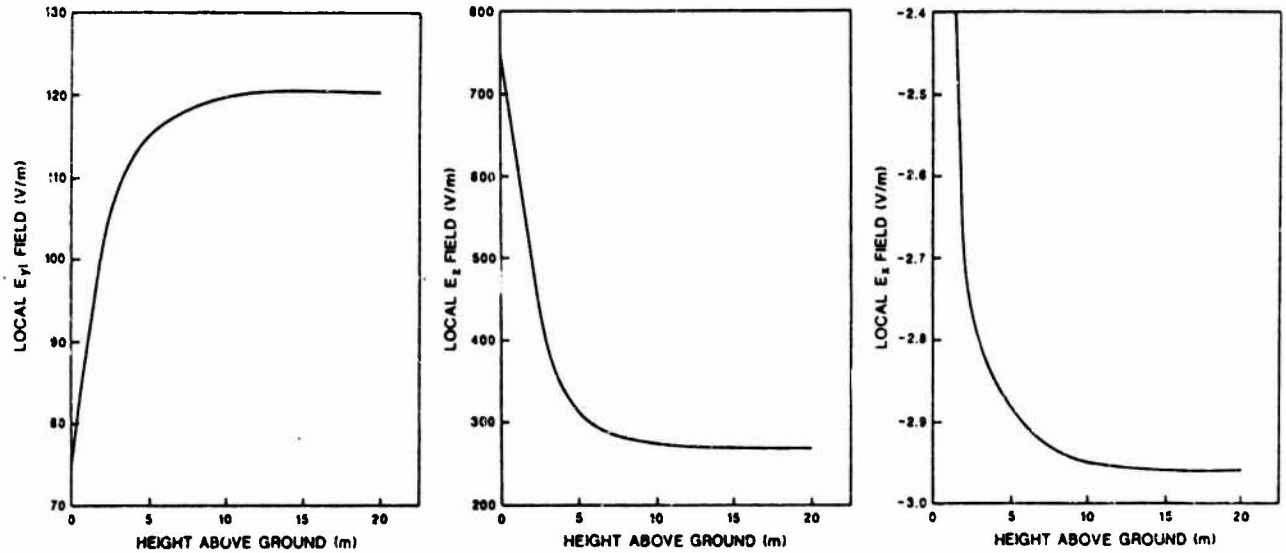

Fig. 9 E-field mill records on the F-106B, elevated. Plateaus in curves occur at the height of 10 m above the ground, that is indicative of the flying condition without the mirror-charge effect.

height above the ground, where the airplane mirror-image charge begins to affect the field mill readings. At this time, the record of all field mills start changing rapidly. On airplane touchdown, all field mills outputs drop to zero. By charging the airplane when it is electrically insulated from the ground, we bring the field mill readings to values equal to those of the steady record during the descent. With the measured capacity C on the ground, we can now calculate the charge Q on the airplane at the time of its descent. Because the steady field mill values during descent are equal to the products of Q and the corresponding coefficients, the matrix coefficients may be determined. The difficulty of utilizing this technique is probably to maintain a constant value of charge on the airplane during its final approach to the ground.

Discussion

There are, as we have shown, significant errors when interpreting electric field records from aircraft-mounted field mills. The most severe errors are due to poor location of field mills on the aircraft. The proper and optimum location for the four sensors is at any of the six cross points of the three electrical symmetry lines. To utilize this for the measurement of E_y component of the ambient electric field is fairly easy, because of the usual left-to-right symmetry of aircraft. The other symmetry points are often not accessible, and a compromise must be applied. Random errors in the field mills readings produce an amplified error in the ambient field and self-charge depending on matrix of form factors. The problem is increased if one attempts to measure the ambient field in the presence of a strong self-charge.

The uncertainty of the form factor matrix affects the accuracy of the ambient field mostly through the dominant matrix coefficients a_{ij} ($i \neq j$) for the stable matrix and through all matrix coefficients for the unstable matrix. This makes the ambient field measurement less susceptible to errors in the matrix coefficient values for the optimum location of field mills on the airplane. The matrix coefficients can be determined with carefully designed calibration procedures or with computer simulation. As in our example, at least rough values of matrix coefficients can be obtained by computer simulation to find optimum locations. It is customary and worthwhile that a significant part of available flying time is used for these calibrations. The greatest problem there is the experimental determination of the form factors for the self-charge.

References

Anderson, R.V., "Measurements of total current density above active snowstorms," J. Atm. and Terr. Phys., 28, pp. 789-793, 1966.

Clark, J.F., "The fair-weather atmospheric electric potential and its gradient," in: Recent Advances in Atmospheric Electricity, pp. 61-73, edited by L.G. Smith, Pergamon Press, New York, 1958.

Evteev, B.F., "Electric field strength measurements at the surface of an aircraft model," in: Studies in Atmospheric Electricity, pp. 118-121, edited by V.P. Kolokolov and T.V. Lobodin, Leningrad, 1972.

Fitzgerald, D.F. and H.R. Byers, "Aircraft observations of convestive cloud electrification," in: Recent Advances in Atmospheric Electricity, pp. 245-268, edited by L.G. Smith, Pergamon Press, New York, 1958.

Fitzgerald, D.F., "Measurement techniques in clouds," in: Problems in Atmospheric and Space Electricity, pp. 199-214, edited by S.C. Coroniti, Elsevier Publishing Company, Amsterdam, 1965.

Kasemir, H.W., "Die Feldkomponentenmuhle," Tellus, Vol. 3, No. 4, pp. 241-247, 1951.

Kassemir, H.W., "The cylindrical field mill," Technical Report ECOM-2526, U.S. Army Electronics Command, Ft. Monmouth, New Jersey, 1964.

Markson, R., "Airborne atmospheric electrical measurements of the variation of ionospheric potential and electrical structure in the exchange layer over the ocean," in: Electrical Processes in Atmospheres, pp. 450-459, edited by H. Dolezalek and R. Reiter, Steinkopf, Darmstadt, 1977.

Mazur, V., B.D. Fisher, and J.C. Gerlach, "Lightning strikes to an airplane in a thunderstorm," J. of Aircraft, 8, 607-611, 1984.

Rossman, F., "Luftelektrische Messungen mittels Segelflugzeugen," Oeutscher Wetterdienst Berichte, No. 15, 1950.

Rudolph, T.H. and R.A. Perala, "Studies in increasing the probability that the NASA F-106B thunderstorm research aircraft will be struck by lightning at low altitudes," Report prepared for NASA, Feb. 1985.

Rustan, P.L. and J.P. Moreau, "Aircraft lightning attachment at low altitudes," Proc. 10th International Aerospace and Ground Conference on Lightning and Static Electricity, Paris, France, 259-265, 10-13 June 1985.

A WIDE BANDWIDTH ELECTROSTATIC FIELD SENSOR FOR LIGHTNING RESEARCH

Klaus P. Zaepfel
NASA Langley Research Center
Mail Stop 130
Hampton, Virginia 23665

ABSTRACT

Data obtained from UHF Radar observation of direct-lightning strikes to the NASA F-106B airplane have indicated that most of the 690 strikes acquired during direct-strike lightning tests were triggered by the aircraft. As an aid in understanding the triggered lightning process, a wide bandwidth electric field measuring system was designed for the F-106B by implementing a clamped-detection signal processing concept originated at the Air Force Cambridge Research Lab in 1953. The detection scheme combines the signals from complementary stator pairs clamped to zero volts at the exact moment when each stator pair is maximally shielded by the rotor, a process that restores the dc level lost by the charge amplifier. The new system was implemented with four shutter-type field mills located at strategic points on the airplane. The bandwidth of the new system was determined in the laboratory to be from dc to over 100 kHz, whereas past designs had upper limits of 10 Hz to 100 Hz. To obtain the undisturbed electric field vector and total aircraft charge, the airborne field mill system is calibrated by using techniques involving results from ground and flight calibrations of the F-106B, laboratory tests of a metallized model, and a finite-difference time-domain electromagnetic computer code.

EXPERIMENTAL CALIBRATION OF AN AIRCRAFT VECTOR ELECTRIC FIELD METER SYSTEM

R. V. Anderson and J. C. Bailey
Naval Research Laboratory
Washington, D. C. 20375

ABSTRACT

Although numerous aircraft have been instrumented for the measurement of electrostatic field, and there have been a few instances of calibration on an absolute basis, the absolute calibration of an airborne system for the measurement of s full three dimensional vector field has not been reported. This report outlines the problems inherent in such a calibration. The design of field meters which are simultaneously suitable for lightning measurements and for calibration is summarized. A description of the calibration accomplished is provided, and the inherent errors are estimated. It is concluded that the process described is viable, and possible improvements are suggested.

BACKGROUND

THE MEASUREMENT OF ELECTROSTATIC FIELD from aircraft is seen to present two layers of difficulty. First the measurement system must be designed and installed to operate in an aircraft environment. In this context the designer must address the issues of electrical noise, mechanical vibration, remote location of sensors, and adequate dynamic range in a satisfactory manner. If this is accomplished, then the questions of aircraft charge, separation of components, determination of enhancement ratios, and establishment of an absolute calibration reference remain to be addressed. The process of implementing a calibrated aircraft field meter system consists therefore of a number of procedures which must be finished sequentially. In the sections to follow, these sequential procedures are described in the order of their requirement, and a summary section is provided in which the accuracy of the process is evaluated and in which suggestions are given for further improvement of the process. Although the work described was primarily concerned with the CV-580 aircraft used in the Direct Strike Program, an attempt has been made to address the calibration problem in general terms, with results specific to the CV-580 used to illustrate the techniques employed.

FIELD METER DESIGN

The electric field meter is a device in which mechanical energy is modulated by the electric field being measured. It thus functions as a parametric amplifier with the pumping frequency determined by the mechanical motion employed. A successful field meter was apparently first reported by Matthias [1]* in 1926. Subsequent developments are summarized and/or referenced in [2]. The two principal limits on field meter sensitivity are noise and drift in offset potentials. Noise denotes the net spurious signal created by electronics, stray couplings, mechanical imbalances, and contact imperfections. It is both broadband and specific to the signal frequency depending on the generation mechanism.

As will be seen, calibration is dependent on measurement of fair weather electric fields which are often no more than 10 V/M in magnitude; so measurement noise forms a significant limit on system calibratibility.

Electronic noise is addressed by the use of standard low-noise circuitry and components. Shielding and grounding must be vigorously prosecuted. Care is exercised in the sensor head design to insure that there is no capacitive coupling between the stator or the signal leads and anything except the external field being measured. This level of shielding is accomplished by the addition of a shield plate covering the stator mounting bolts, a shield tube which is integral with this plate through which the output coaxial cable is led, application of braid around the connector, the use of an unbroken cable between the head and the preamplifier, and the provision of a totally enclosed preamplifier module. System grounding is exclusively at the head location, and extensive use is made of decoupling networks.

A recent study [3] concluded that 304 stainless steel was an optimum material for field meter construction. The entire sensing system (all components exposed to the ambient field) was consequently made of this material. The rotor and stator were made of 1/8" thick stock to guarantee that there would be adequate rigidity upon exposure to the airstream, and 1/4" electrode spacing was maintained to reduce the effect of Volta potentials. It is possible to increase signal to noise ratio through the use of larger head area [4], but this option was precluded by considerations of the available space at the selected aircraft locations.

The completed head is shown in Fig. 1. An available 8000 rpm synchronous motor was selected because of its size and the availability of accurate 400 Hz power on the CV-580 aircraft. The two bladed design used with a three-pole motor gives a signal frequency of 266.7 Hz which is near the optimum value for operation in a 400 Hz environment. Phase reference is provided by a magnetic rotor (416 stainless steel) mounted on the rear extension of the motor shaft and a permanent magnet pickup coil. The rotor is insulated from the motor shaft to preclude the introduction of bearing noise; it is grounded by silver-graphite brushes on a coin silver slip ring.

Two additional considerations are worthy of mention in this discussion. The design should facilitate maintinance operations. If this is not done, necessary cleaning and repair will be deferred to the detriment of the measurement. The heads were built so that rotor and stator could be removed from the outside without the removal of the head unit. This facilitated cleaning of the Teflon (TM) stator insulators after exposure to wet environments. The removal of the entire head assembly was possible with extraction of only four machine screws; so repair and/or replacement was possible in a few minutes. The second consideration concerns the coaxial cable used to carry the signal from head to the amplifier. In the author's experience, cables designed for RF service can introduce

*Numbers in brackets designate References at end of paper.

excessive microphonic voltages at audio frequencies. RG-149/U has proven to be a good cable for minute audio frequency signals, and its use (or that of an equivalent) is mandatory.

The amplifier design is conventional; so little need be said with the exception of a few specific features which contribute significantly to the utility of the final product. The preamplifier, in its fully shielded enclosure, is in the form of a current to voltage converter. This keeps the stator element at ground potential and reduces the effect of insulator contamination. Its schematic is shown in Fig. 2. The protective diodes at the input were crucial to reliable operation of the amplifier. It is seen that there is provision for the introduction of a DC voltage on the stator for use in calibration. This voltage makes an artificial field in the head which is useful for overall system calibration and as will be seen later is also of value in reducing self charge fields. The remainder of the amplifier provides a gain variation in the ratio of 10000:1 in decade steps, low pass filters in signal and phase reference channels to provide sinusoidal signals to the following stages, a half-lattice phase shifter in the reference channel with which to adjust the phase relationship between channels, and a phase sensitive rectifier. The entire amplifier is shown in Fig. 3. DC filters at the output of the synchronous rectifier provide time constants of 10 and 157 mS for lightning and calibration data, respectively.

AIRCRAFT INSTALLATION

An aircraft in flight must resolve the three components of the field vector and a fourth independent contribution produced by the net charge on the aircraft. Therefore, a minimum of four field meters is needed to define and resolve these four components. Although it may be theoretically possible to obtain vector component separation with almost any random location of four electric field meters on an aircraft, it is obvious that there are locations which greatly simplify this process. "Nodal surfaces" can be defined on which the effect of one of the vector components of the external field vanishes. In theory, a solution of LaPlaces equation defines these surfaces; in practice it is better to derive an approximation of these surfaces from considerations of symmetry; and locate the sensors as well as possible on intersections of such surfaces. One symmetry which immediately suggests itself is the location of two of the four meters symmetrically with respect to a vertical plane through the center of the aircraft. In this manner, the difference of these two meters will be solely dependent on the horizontal field component which is transverse to the direction of flight. The wing tips are attractive for this location because of the obvious symmetry and also because of the significant field augmentation at such an extremety. The measurement of small fair weather fields which, as will be seen is needed for calibration, is significantly aided by this augmentation.

The other two field meters are best located on the vertical plane of symmetry already mentioned. Upward facing locations were rejected upon consideration of water droplet impaction; so the last two meters by default had to be installed on the centerline of the belly. Maximum component separation was achieved by locating one of the meters as far forward as possible (the obvious nose location was unavailable because of the existing radar installation) with the other one as far aft as possible. The locations are shown in Fig. 4. A system of coordinates attached to the aircraft is used in the ensuing discussion and is shown in Fig. 5. X is defined in the forward direction, Y is transverse, and Z is the vertical axis.

It should be noted at this time that the aircraft charge in flight was orders of magnitude greater than previously experienced with reciprocating engine aircraft. This fact has independently been found to apply to most if not all turbine engine aircraft by several other investigators. In the measurement of thunderstorm fields, this large value of charge is of little consequence; but in fair weather fields, it forces operation of the system at a level of sensitivity too low to enable observations with useful accuracies. Consequently, a scheme of discharge wicks was implemented which successfully reduced the net charge on the aircraft to a value more suitable for fair weather use. This development is described in a companion paper [5]; so it will not be described further here. As has been mentioned, further removal of fields produced by aircraft charge can be effected during calibration flights through the use of DC "bucking" voltages applied to the stator of the head. These bucking voltages were continuously recorded for use in data analysis.

DERIVATION OF AIRCRAFT ENHANCEMENT FACTORS

If the external field is defined in terms of the coordinate system given in Fig. 5, and if the four meters are denoted by P (=Port wing), S (=Stbd wing), F (=Forwardmost belly location), and T (=Tailward belly location), it is possible to write a system of equations for the response of the four

meters as:

$$Ep = Px\,Ex + Py\,Ey + Pz\,Ez + Pq\,Q$$

$$Es = Sx\,Ex + Sy\,Ey + Sz\,Ez + Sq\,Q$$

$$Ef = Fx\,Ex + Fy\,Ey + Fz\,Ez + Fq\,Q$$

$$Et = Tx\,Ex + Ty\,Ey + Tz\,Ez + Tq\,Q$$

where Q is the net aircraft charge and Px ... Tq are the enhancement coefficients (note that they are dimensionless except for the charge coefficients). If the wing tip locations are symmetric and if the belly locations are on the centerline and are not appreciably influenced by protruding objects (such as antennas), then it is possible to to re-write these equations in a simplified form as:

$$Ep = Px\,Ex + Py\,Ey + Pz\,Ez + Pq\,Q$$

$$Es = Px\,Ex - Py\,Ey + Pz\,Ez + Pq\,Q$$

$$Ef = Fx\,Ex + Fz\,Ez + Fq\,Q$$

$$Et = Tx\,Ex + Tz\,Ez\ \ Tq\,Q$$

It has been found convenient to define, display, and record two derived quantities:

$$Y = (Ep - Es)/2 = Py\,Ey$$

$$Q' = (Ep + Es)/2 = Px\,Ex + Pz\,Ez + Pq\,Q$$

In general, Q' will be primarily a measure of the net charge, Q, on the aircraft, although it is somewhat contaminated by the X and Z components of the external field.

There are ten coefficients in the set of equations listed above. Two sets of equations exist: one for external field and one for charge. Only the relative values of the one are required to determine values of the other. In each set one value must be determined on an absolute basis; and the ratios of the others to this absolute value then define the entire set. From the definition of Y above, it is obvious that Py should be the absolute term of that set. For similar but less compelling reasons Pq was chosen from the set of charge coefficients for the absolute determination.

The ratios of the external field augmentation factors are determined by maneuvers of the aircraft in the fair weather field. The fair weather field is probably the best test field for calibration since it is reasonably stable with time, it consists solely of a vertical component, and it exhibits considerable horizontal homogeneity. As has frequently been alluded, the fair weather field is, however, small in magnitude and in general is at the lower limit of the measurement capability.

An aircraft roll in fair weather provides a known exposure of the aircraft Y and Z coordinates to the vertical external field. A roll through an angle of θ has the effect of:

$$Ey = E \sin(\theta)$$

$$Ez = E \cos(\theta)$$

where the (vertical) external field is given by E. The result of a precision roll is that an Ey field appears (from 0) and the Ex field is reduced by $(1 - \cos\theta)$. Thus

$$Ey = E \sin(\theta)$$

where E is the (vertical) ambient field, and therefore

$$E = [Ep(\theta) - Es(\theta)]/2Py \sin(\theta)$$

while the forward meter gives

$$E = [Ef(0) - Ef(\theta)]/[Fz\,(1 - \cos(\theta))]$$

Equating these two expressions yields the ratio Fz/Py. In practice, both left and right banks are made giving a doubled data value for greater accuracy. Similarly, the ratio Tz/Py is obtained from data from the tail meter.

Somewhat more difficult is an experimental determination of the ratios Fx/Py and Tx/Py. The maneuver used for this consists of a shallow climb (at an angle of exactly 15 degrees) until the aircraft is near stall followed immediately by a dive of the same amount. If engine power is maintained constant throughout, it is a good supposition that aircraft charge is invariant and, with climb/dive angle of ϕ:

$$Ex = E \sin(\phi)$$

$$Ez = E \cos(\phi)$$

with E defined as before. Note that the cosine of 15 degrees is nearly unity; so Ez is unchanged with negligible error. This measurement suffers not only from the shallow angles which must be employed but also from the vertical variation of the fair weather field. Consequently, care must be exercised to insure that such variation does not significantly affect the measurements.

The ratios Fx/Py and Tx/Py are derived in an entirely analogous manner to that for Fz/Py and Tz/Py. The ambient vertical field is still determined from observed differences in the wing tip meters in a precision roll maneuver, and this is equated to the vertical field sensed by the belly meters by

$$E = [Ef(+\phi)-Ef(-\phi)]/[2\ Fx \sin(\phi)]$$

and

$$E = [Et(+\phi)-Et(-\phi)]/[2\ Tx \sin(\phi)]$$

from which the required ratios can easily be determined.

By far the most difficult of the coefficients to determine are the wing tip "contamination" terms Px/Py and Pz/Py. They appear in the equation defining Q' and nowhere else. The method employed to determine Pz/Py was to measure the change in Q' between a roll and the straight and level flight attitude. This difference involves Py and Pz. Similarly, the change in Q' between climb and dive is related to both Px and Py and can be used to assign a value to their ratio. Expressions for the vertical field in terms of changes in Q' during maneuvers can be written as

$$E = [Q'(+\phi)-Q'(-\phi)]/[2\ Px \sin(\phi)]$$

and

$$E = [Q'(0)-Q'(\theta)]/[Pz\ (1-\cos(\theta)]$$

which, again, can be equated to the value obtained from the wing tip meters in a roll.

In practice, it is found that the level of noise in the raw data was so high that most of these differences were undetectable. A further examination of the data indicated that this noise strongly correlated with the recording of Q'. Therefore, derived recordings were made in which a variable fraction of Q' was linearly mixed with the F and T data streams. The fraction for each was varied until the apparent correlations vanished. It was observed that this experiment could be repeated with a precision of the order of 3%. Typical maneuver recordings with and without this Q' removal are shown in Fig. 6. Although Q' is not a pure charge indication, its utility in data enhancement is obvious.

Another source of information on the ratios of the augmentation coefficients is found in the data on lightning discharges which occur near the aircraft without actually contacting the aircraft. Examination of the charging of the aircraft after a typical takeoff as seen in Fig. 7 shows that there is a charging time constant of the order of 5 seconds. Consequently, it is reasonable to suppose that there can be no significant change in net charge during the short duration of a lightning event. If it is reasonable that $\Delta Q=0$ in such an instance, it is theoretically possible to derive all the external field coefficient ratios from a sufficiently large number of distant lightning events. From a typical such recording, shown in Fig. 8, it is seen that there is little change in Q' and that the data values are large and well defined. The solution of this problem in the indicated manner requires the treatment of a large system of non-linear algebraic equations which is presently under study. Alternatively, it is possible to formulate an iterative approach which should at least test the coefficient matrix for reasonableness. This, too, is still under study.

Calibration coefficients may also be derived with other techniques. Analytic modeling is often mentioned. It appears that a numerical simulation in a digital computer is a straightforward problem presenting few substantive difficulties. Aircraft geometries are quite complex, however; so modeling with any accuracy is a formidable task. It has also been observed that small changes (of the order of a few mm) in sensor mounting can produce changes in the augmentation of as much as a factor of two. It has also been suggested that the large quasi-stable fields observed under thunderstorm anvils might be useful for calibration. In two years' effort, one, and perhaps two, anvils have been observed which might have been useful for calibration purposes.

The ratios of the charge coefficients Pq/Fq and Pq/Tq can be determined in three ways. The experimental removal of correlations between the F and T recordings and the Q' channel provides values for these ratios directly. In flight changes in engine power setting effect a variation in the aircraft charge; the resultant steps in the data recordings also provide these ratios. It is also possible to derive ratios of the charge coefficients from observation of static readings (against a "zero" value) in level flight since the high self charge produces the only field of significance. This last technique, while viable, suffers from the fact that it is not a difference technique and requires that a zero level be determined.

The absolute coefficient for external field, Py, must be determined by comparison with a known field. There are several ways in which a "known" field may be determined. The ionospheric potential is a relatively well-known 290 KV with a diurnal variation which has been extensively studied for many decades [6]. Therefore, if a vertical profile of field measurements is obtained from ground level to the aircraft ceiling (of the order of 6 KM), and if this profile is integrated, a potential (for 6 KM) is obtained. A typical profile is shown in Fig. 9. Extrapolation from this height to ionospheric altitude can be done in accord with well defined rules (such as the exponential increase of conductivity with altitude and charge conservation) to yield an apparent potential [7]. The ratio of this augmented apparent potential to the true potential is then Py. Comparison with an already calibrated aircraft is possible and depends on

the accuracy of calibration of the known aircraft, the horizontal homogeneity of the fair weather field being measured, and the navigational precision of both aircraft.

The ultimate absolute calibration is of course a comparison with field measuring instrumentation on the ground. Since maneuvers are impossible at altitudes of 10-20 meters, the aircraft measurements must be made with vertical-looking meters; and it has been observed that such data are not reliable unless some in flight zero check apparatus is included in the installation. It is also theoretically possible to construct an artificial field much larger than the ambient fair weather field and which is sufficiently large and spatially homogeneous to allow the aircraft to fly through it. In the absence of such a facility, its construction was not a reasonable option at the present time.

The absolute charge coefficient, Pq, was experimentally determined through measurement of the field observed upon the application of a known DC voltage to the aircraft resting on electrically insulating mats. This ratio relates aircraft potential to field in the presence of the image aircraft below the surface. The effect of the image can be evaluated from examination of data recordings taken during the landing process. Immediately prior to touchdown, the image effect is identical to that seen on the insulating mats (the geometries are identical). If the reasonable assumption is made that the aircraft charge is invariant during the final landing approach (the Q' recording is observed to be constant and there are no engine power changes), then the ratio of charge sensitivities aloft and in the presence of the image aircraft is equal to the ratio of the fields measured aloft and prior to touchdown. Charge and voltage are related through capacitance by

$$Q = C\ V$$

$$Pv = (Epg/Vg)*(Epa/Epl)*(Ca/Cg)$$

where Epg is the field produced on the ground by voltage Vg, Epa and Epl are the field values observed aloft and at landing, respectively, and Ca and Cg are aircraft capacitances aloft and on the ground (or just prior to touchdown). A typical landing data recording is shown in Fig. 10.

The capacitance ratio Ca/Cg is yet to be determined. This is addressed by modeling. An expression for the capacitance of a conducting sphere above an infinite conducting plane has been derived [6]. It is obvious that the sphere underestimates the true capacitance of an aircraft at small heights. Another simple model which should overestimate the capacitance of the aircraft at small heights is a circular disk parallel to the plane. At small heights, it is possible to use the parallel plate formula for capacitance with little error; while the capacitance of the disk at infinite height is available in analytic form. The capacitance variation with height for the sphere and disk models is plotted in Fig. 11 normalized to the values at infinite height. Both sphere and disk were assigned a radius of 6.759 meters which gives the same horizontal cross sectional area as the CV-580 aircraft. Also indicated on the figure is the height of the CV-580 at landing. A value for the capacitance ratio of 0.54 is seen to be quite consistent with either model and is therefore a reasonable value.

It should be noted that a value for Pv has been obtained, not Pq. Pq is available if an absolute aircraft capacitance is known. Pv, which relates self-charge field to voltage on the aircraft, is certainly a useful quantity; but Pq could be estimated from the 752 pF capacitance at infinity of a sphere of 6.759 meter radius (this estimate is probably high - the disk model gives a value of 479 pF). So, finally the measured values are:

$$Epg/Vg = 2.044\ (V/M)/V$$

$$Epa/Epl = 1.273$$

and

$$Ca/Cg = 0.54$$

so

$$Pv = 1.41\ (V/M)/V$$

and

$$Pq = Pv/C = 1868\ (V/M)/Coul\ (C=752)$$

or

$$Pq = 2933\ (V/M)/Coul\ (C=479)$$

where a realistic value might be the mean value of 2400 (V/M)/Coulomb. It should be noted that the terms Pq Q and Pv V are numerically and dimensionally identical.

CALIBRATION RESULTS

The equations of field meter response to external vector field and self charge were previously given in terms of charge coefficients Pq, Fq, and Tq. The voltage coefficients Pv, Fv, and Tv are equally useful and more accurately known. These equations rewritten in terms of voltage become:

$$Ep = Px\ Ex + Py\ Ey + Pz\ Ez + Pv\ V$$

$$Es = Px\ Ex - Py\ Fy + Pz\ Ez + Pv\ V$$

$$Ef = Fx\ Ex + Fz\ Ez + Fv\ V$$

$$Et = Tx\ Ex + Tz\ Ez + Tv\ V$$

where V is the aircraft voltage with respect to its surroundings. The measured values for the coefficients then are:

Px=2.69±1.6 Py=18.1±2 Pz=.4±.8 Pv=1.41±.07

Fx=1.16±.16 Fz=-1.87±.3 Fv=.24±.01

Tx=-.92±.15 Tz=-1.23±.4 Tv=.32±.02

Inversion of the matrix gives:

Ex = .028 Ep +.028 Es +.340 Ef -.497 Et

Ey = .028 Ep -.028 Es

Ez = .055 Ep +.055 Es -.394 Ef -.176 Et

V = .285 Ep +.285 Es -.528 Ef +1.00 Et

as the best available estimate. The charge coefficients are probably valid to within 5% while the uncertainties in the external field coefficients depend strongly on their method of derivation. All the coefficients are dimensionless except in the bottom row where a dimensionality of meters pertains.

Error estimates were given on the first set of coefficients (Px, ...,Tv) which are the directly measured values. The important estimate, however, is the accuracy to which an external vector field can be determined. Since the matrix inversion process is nonlinear and involves all the values, an estimate was obtained by using a Monte-Carlo analysis in which each parameter was allowed to deviate within its estimated error in a random Gaussian manner. The conclusion is that fields can be determined at least to within 25% at this time with further improvments possible.

CONCLUSIONS

The obvious primary conclusion of this study is that a vector field calibration is possible and that it has successfully been achieved. It may also be concluded that the measurement of the vector field from an aircraft is fraught with pitfalls which must be avoided if success is to be expected. Aircraft charge variations are seen to be perhaps the single most severe source of noise in fair weather measurement, and the effort expended in its removal is well repaid. There are many aspects of instrument design which contribute to the success or failure of the calibration effort, and many of these have been described in some detail along with viable solutions to problems.

It is also seen that the fair weather field used for calibration must be stable with time and horizontally homogeneous. The requisite aircraft maneuvers must be executed with precision or the calibration results will be vitiated. Enough cannot be said about the necessity of truly fair weather for a calibration program. Even the existence of small "fair weather" clouds in the vicinity of the flight path can wreak havoc with the results. Finally it must be noted that these results could be materially improved with additional calibration flights both because better weather could be selected and because of the additional data base then available. It is a pleasure to acknowledge the invaluable contribution made by Jesse Terry and the other pilots of the FAA Technical Center. Without their willingness to perform unseemly acts with accuracy and good grace, this calibration would have been impossible.

REFERENCES

1. A. Matthias, "Fortschritte in der Aufklarung der Gewittereinflusse auf Leitungsanlagen." Elektrizitatswirtschaft,25, July 1926.

2. S. Gathman and R. Anderson, "Improved Field Meter for Electrostatic Measurements.", Rev Sci Inst.,36,Oct 1965.

3. J.C. Willett and J.C. Bailey, "Contact-Potential and Surface-Charge Effects in Atmospheric-Electrical Instrumentation.", NRL Memorandum Report 5063, April 1983.

4. R.V. Anderson, "Absolute Measurements of Atmospheric Charge Density.", J. Geophys. Res.,71, Dec 1966.

5. R.V. Anderson and J.C.Bailey, "Improved Electrostatic Discharge Wicks for Aircraft.", International Aerospace and Ground Conference on Lightning and Static Electricity, June 1986 (This volume).

6. R. Anderson, "Measurement of Worldwide Diurnal Atmospheric Electricity Variations", Monthly Weather Review,95,Dec 1967.

7. J. H. Kraakevik, "Electrical Conduction and Convection Currents in the Troposphere.", in "Recent Advances in Atmospheric Electricity", L.G. Smith,Ed.,Pergamon Press,1958.

8. R.V. Anderson, "Electrostatic Theory Applied to Helicopter Discharging.", International Aerospace and Ground Conference on Lightning and Static Electricity.", DOT/FAA/CT-83/25, June 1983.

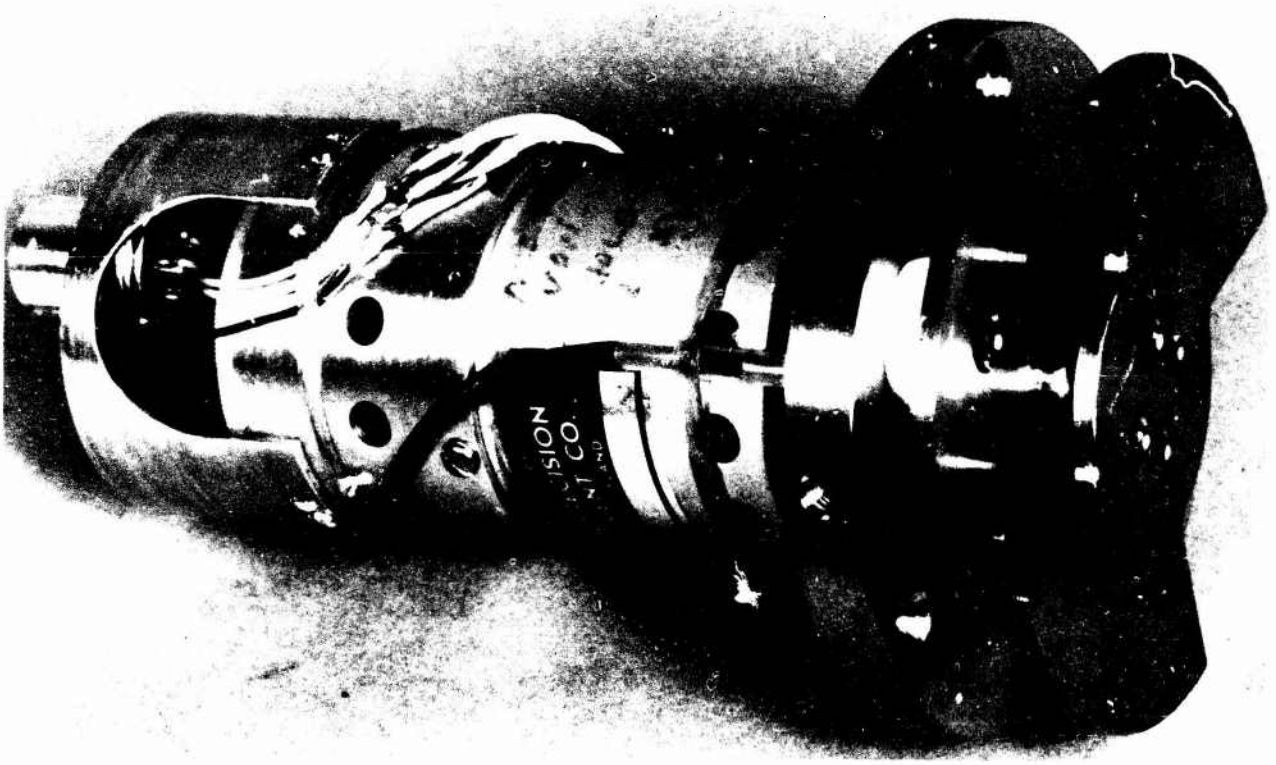

Fig. 1 - Photograph of complete electric field meter head showing element spacing, shielding, and insulators

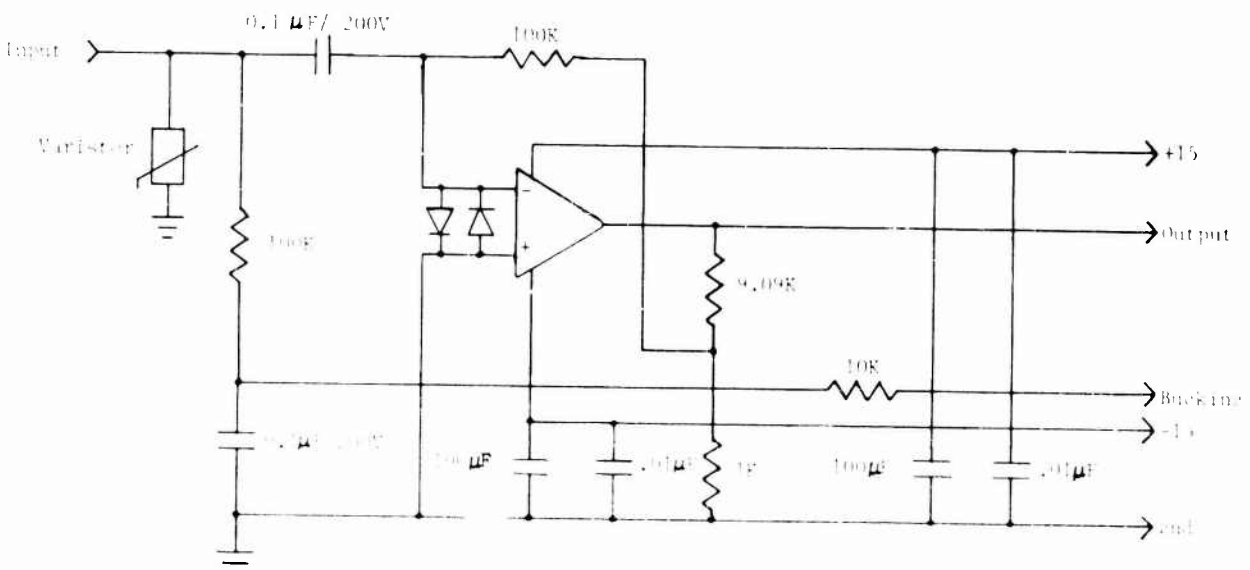

Fig. 2 - Preamplifier schematic shown, having voltage offset, offset trim, and buckout compensation

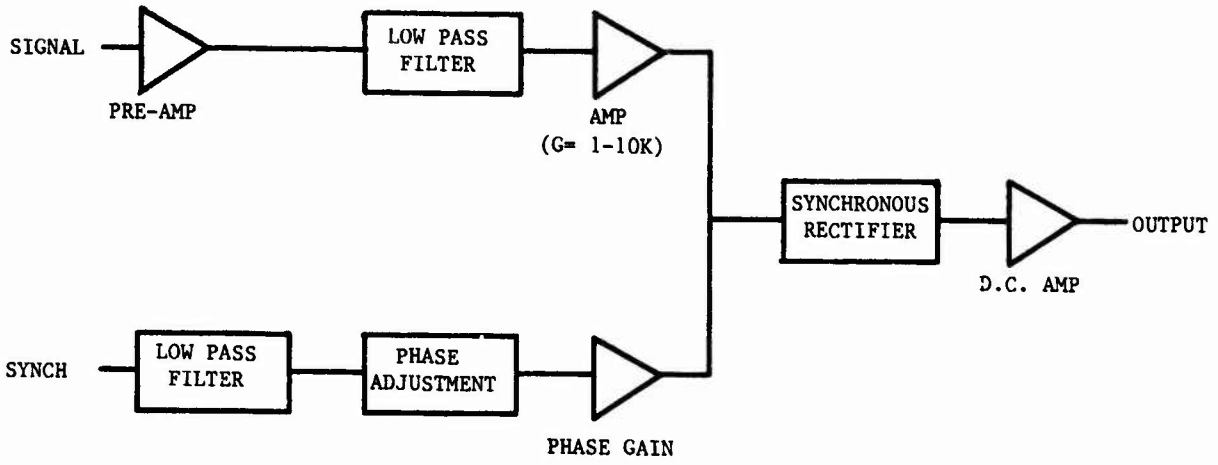

Fig. 3 - Block diagram of complete electric field meter amplifier

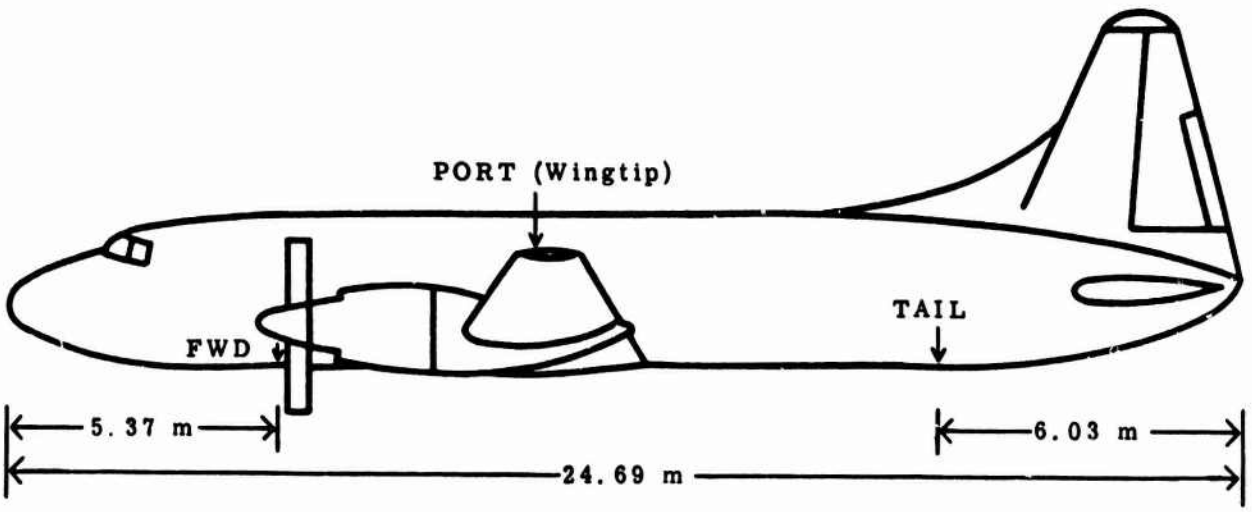

Fig. 4 - Outline drawing of CV-580 aircraft with field meter locations indicated

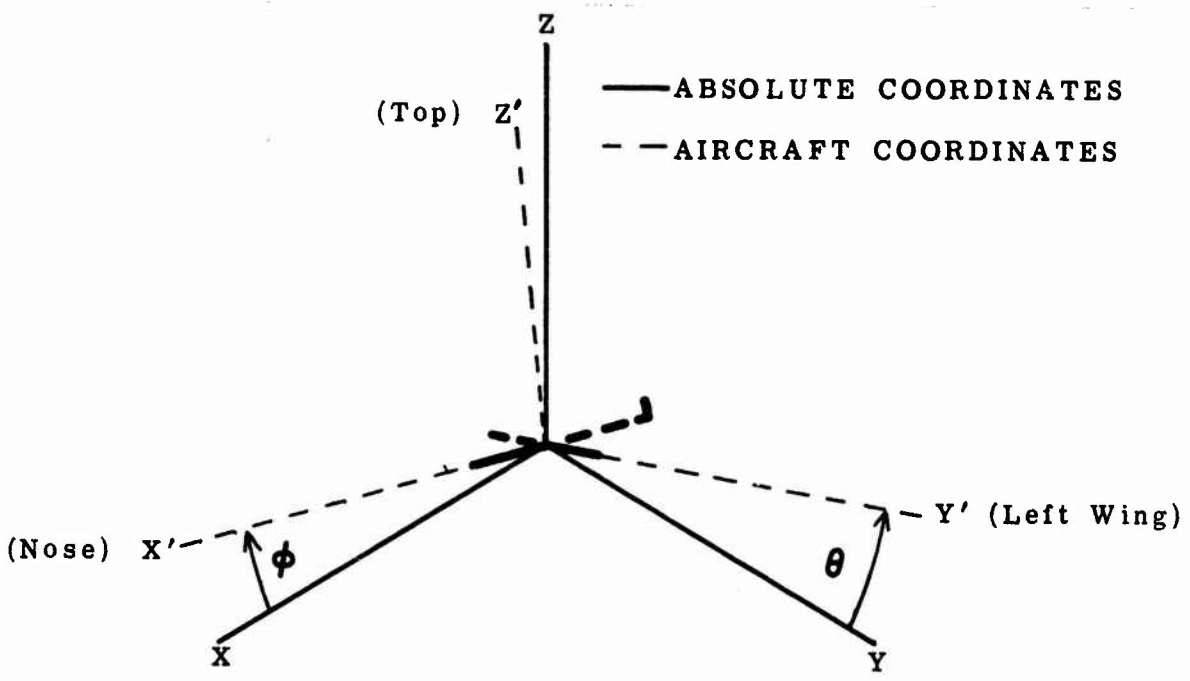

Fig. 5 - Cartesian coordinate system attached to aircraft

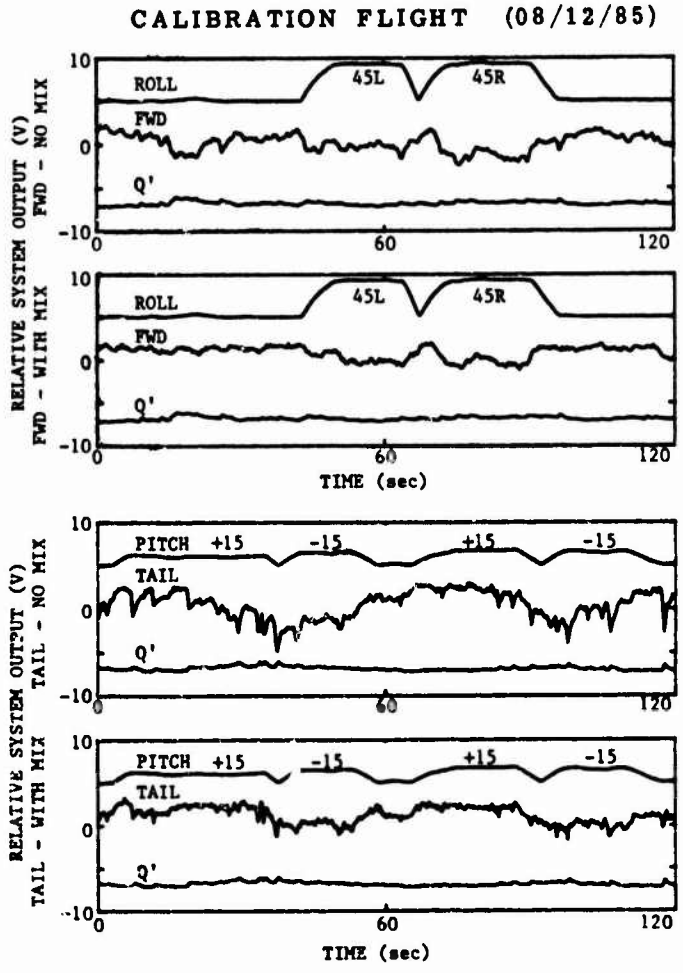

Fig. 6 - Data chart showing the effect of bank and dive maneuvers and the effectiveness of Q' removal in enhancing data readability

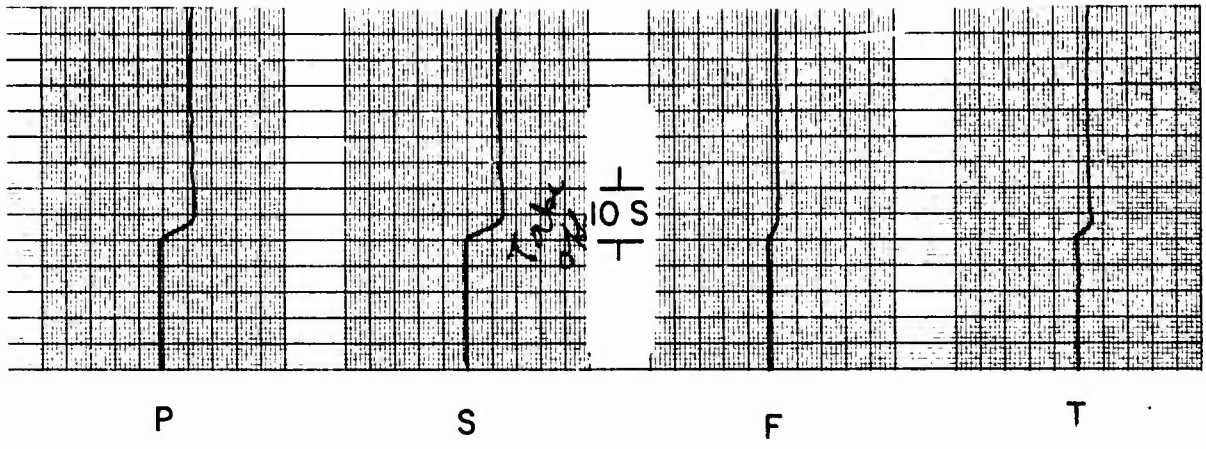

Fig. 7 - Aircraft charging rate as seen in a typical data recording taken during a takeoff

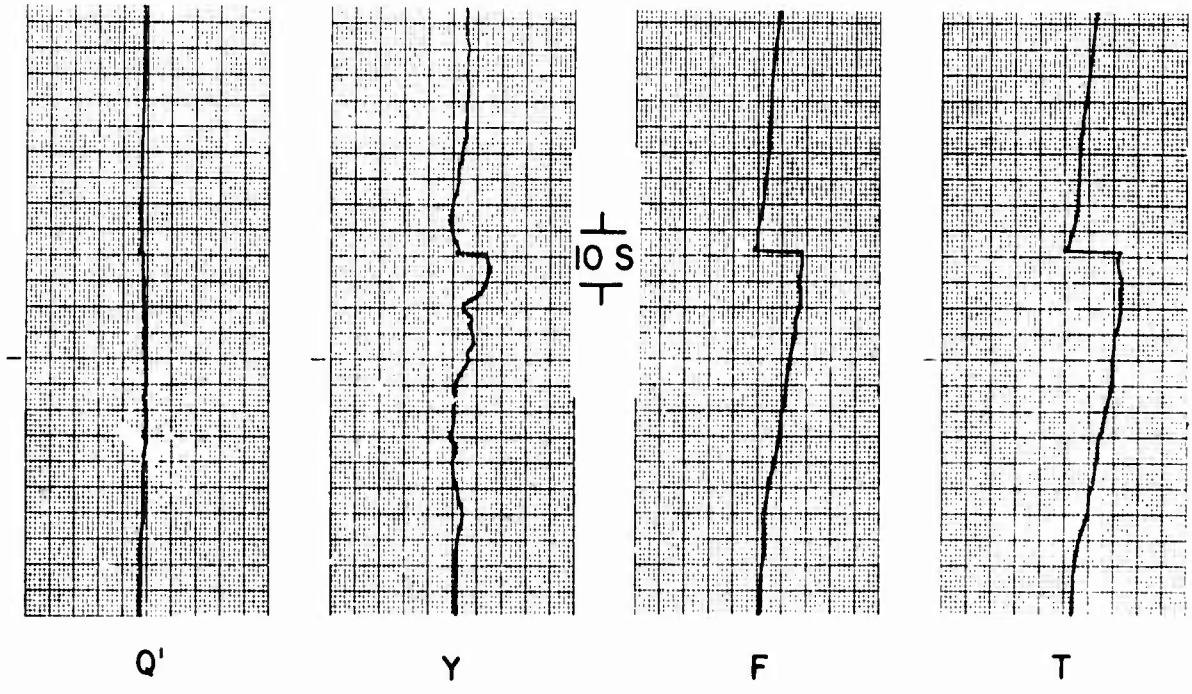

Fig. 8 - Electric field changes produced by a distant lightning discharge

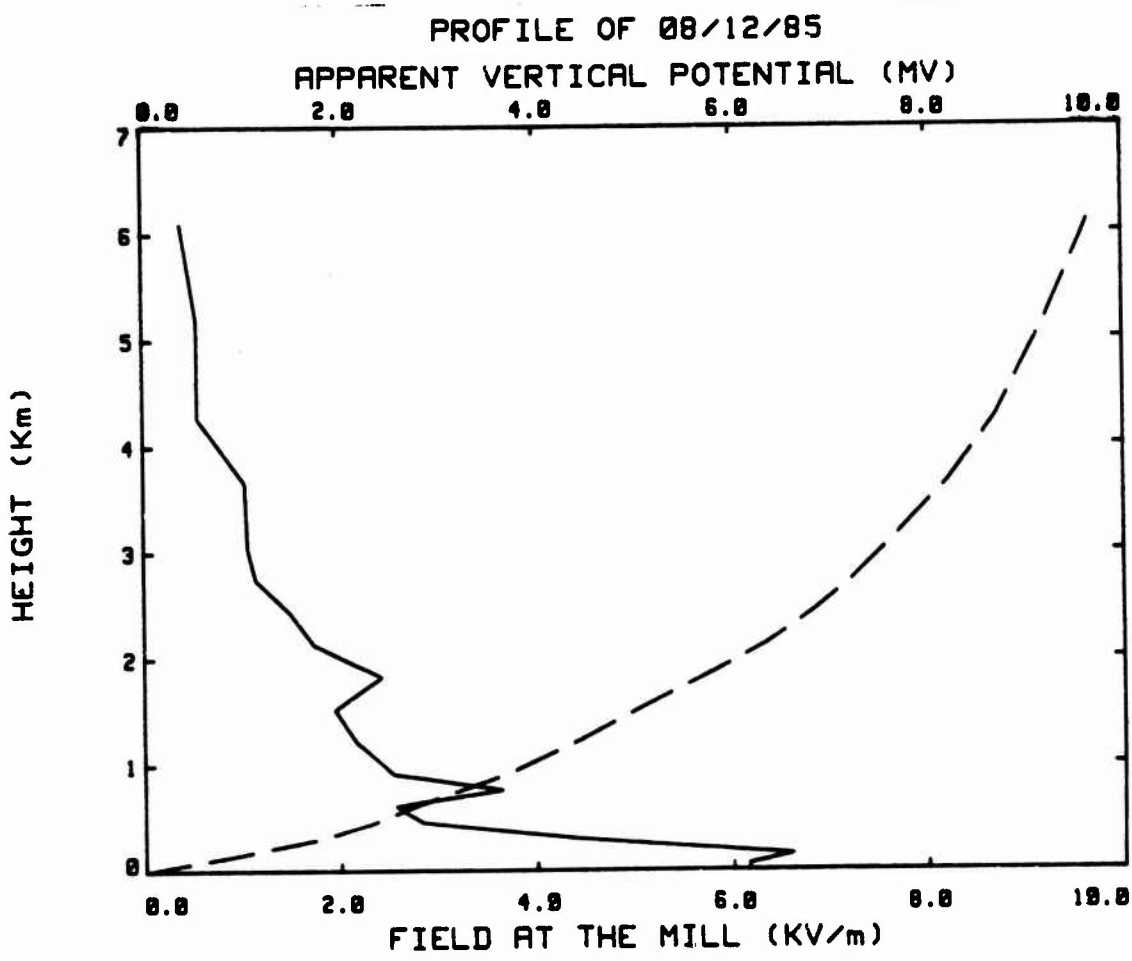

Fig. 9 - Vertical profile of electric field measured aboard the CV-580 aircraft from 200 to 20,000 feet altitudes (61-6100 M)

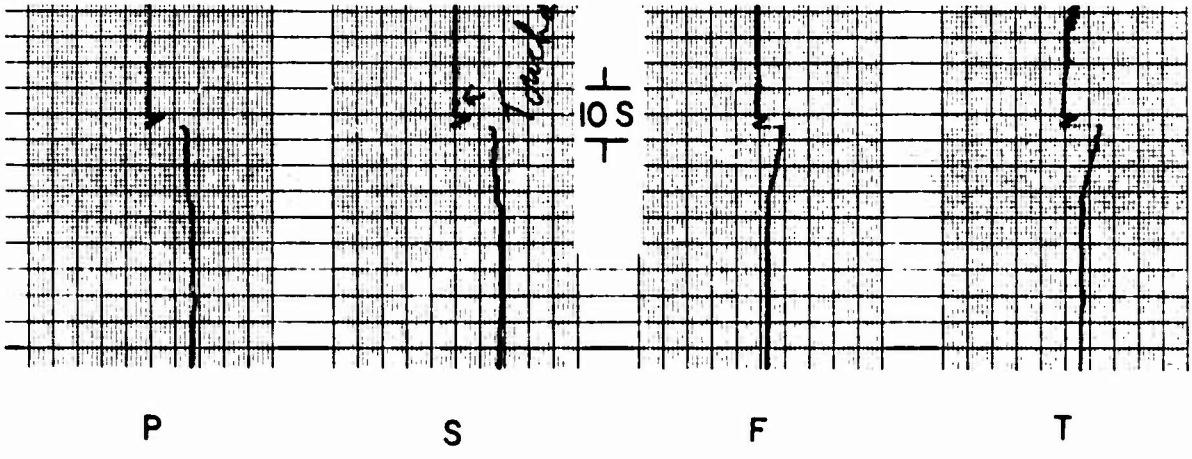

Fig. 10 - Typical data recording obtained during landing showing the effect of the electrostatic image of the aircraft on the measured fields approaching and at touchdown

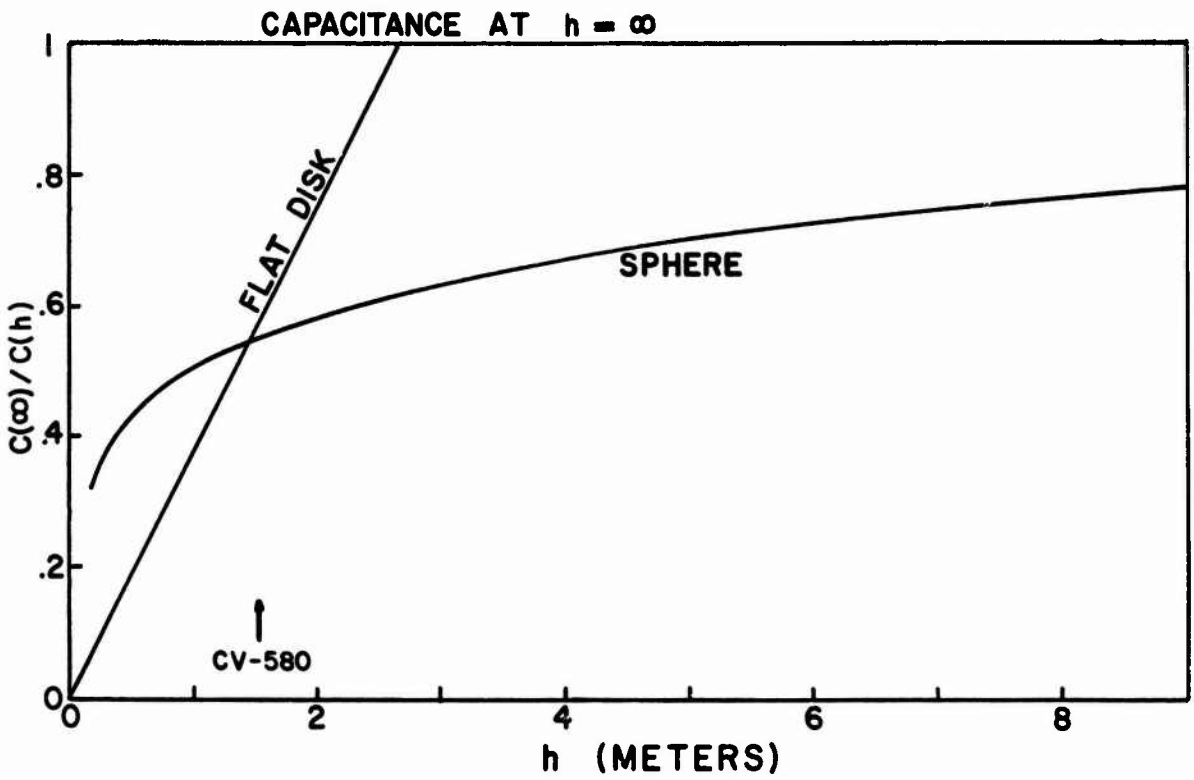

Fig. 11 - Normalized capacitance values for conducting sphere and circular disk as functions of height

LIGHTNING RETURN STROKE CURRENT COMPUTATION

P.R.P. Hoole and J.E. Allen
Department of Engineering Science
Parks Road
Oxford
U.K.

ABSTRACT

The paper briefly reviews the lightning return stroke models currently in use and highlights some weaknesses of these models in relation to basic principles of physics and observed characteristics of the return stroke. The solution of diffusion equation for a distributed line is given. Then a simple distributed LCR model of the return stroke, with all the elements calculated from known data is given. The return stroke currents along the channel are calculated and it's implications to current measurements and applications of the model are discussed.

1. INTRODUCTION

1.1 HISTORICAL BACKGROUND - We may classify the work done on the modelling of lightning return stroke into two broad categories. The first category includes is where some of the parameters determining the parameters determining the height and time variation of the current (e.g. rise time, peak variation of the current (e.g. rise time, peak current rate of decay with height, etc) is specified.[1-8] The first model was due to Bruce and Golde. In its most recent form, attempts have been made to include the finite return to stroke velocity and height variations the latter being determined by measured electric fields at gound. However, to give agreement with fields it was found necessary to postulate two current measurements. These are (i) a peak pulse followed by 2 "corona current"; such double peaks are not observed in subsequent return strokes. In first return strokes they might appear due to time delay in the charge from branches being lowered to ground. (ii) a continuing current of 3100A. Leader and continuing currents are generally of the order of 300A. Sometimes large leader currents (e.g. 3kA) are observed for positive leaders.

In the second category, we consider the modeling work which seeks to determine the characteristics of the return stroke channel, and from that to determine the return stroke currents.[9-11] A lumped LCR circuit model g gives an expression identical to that of the Bruce Golde Model for current. Distributed LCR model in its most complex forms were used by Little[10] and Strawe et al[11]. Although in detail their models appear to differ - neither one of them examined the validity of the transmission line model; and both had problems in obtaining real wavefronts for currents at earth end. Little's model [10] has had a CR elements in the first segment and Strawe et al have used a very large channel resistance. Strawe et al[11] do not give the values of L and Celements used; Little used 2μH/m for inductance. In order to obtain a return stroke velocity less than the velocity of light, large capacitance per unit length were prescribed. The large capacitance values have no physical basis, since they were obtained either with a 15Km plane electrode representing the cloud, or a 100m sphere (cloud) with potential at 15km height arbitarilly set at 15mV. A large capacitance, except at the earth end of the channel, is unreasonable.

Here we report part of the work which tackled two questions in relation to the return stroke modeling (i) Does the transmission line model of the lightning return stroke have a physical basis? The solution of Maxwell's equations was sought for a cylindrical conductor (radius and conductivity specified) suddenly connected to an earthed electrode i.e. the propagation properties of the fourier components of the wave, and in particular the velocity of components in the range of 0 - 100kHz. (ii) to develop a transmission line model which has a reasonable foundation on the cloud - return stroke channel - earth electrode system. It is this second part we shall descrioe below.

1.2 THE PROBLEM - In Fig.1 the lightning return stroke problem to be modelled is shown. The cloud charge centre active during a single leader and return stroke flash is approximately a 500-1000m sphere.[12] The leader channel itself is a highly conducting channel, with a temperature of about 20,000°K which is also the average temperature measured for the return stroke [13.14]. Given the difficulties in making lightning spectroscopic measurements, these values are in good agreement with measurements made on long laboratory sparks. [15-17]. The leader radius is probably of the order of a few millimetres (the visible region in a 15m spark); though the region surrounding the main current carrying region may undergo some excitation and ionization due to random motion of electrons in the channel and emitted photons. No avalanche process takes place. A centimetre or so long, rapidly vanishing wisps which appear at leader edges have been observed - these may sometimes develop in to branches in first strokes.[18]. When the leader makes contact with the ground, a return stroke is initiated, which discharges the leader channel. Sometimes in the first stroke, before the return stroke proper is observed, the current at ground may gradually be seen to increase[19] - since this initial current exists for about 5-10/μs, it must be due to the upward discharge (connecting leader), which is being gradually ionized to become a good conductor like the main leader, so that the connecting leader too will be able to carry the large return stroke current. It is not observed for subsequent strokes, where the connection is made at ground. The radius of the return stroke is in the range of 0.3-2 cm, again in good agreement with the 1-2 cm radius measured for the 15 m spark. It should, however, be pointed out that in the laboratory spark the return stroke only exists for about 10-50ns, a fraction of the current wavefront only is determined by the channel.

2. RETURN STROKE MODEL

2.1 THE CR MODEL - First we illustrate the weakness in solving only for the diffusion equation of a transmission line. The equation is given by

$$\frac{\delta^2 V}{\delta Z^2} - RC\,\frac{\delta V}{\delta t} = 0 \qquad (1)$$

where V is the potential and R, C are per unit resistance and capacitance elements. The solution of (1) is given by the error function[20]

$$V(Z, t) = Vo\left[1 - \operatorname{erf}\left(\frac{(RC)^{\frac{1}{2}}}{\sqrt{4}}\,\frac{Z}{\sqrt{t}}\right)\right] \qquad (2)$$

where Vo is the earth potential impressed on the line at cloud potential, and Z is the distance. It is reasonable to ignore the 1.5MV volt drop (5V(cm) from cloud to leader tip for a 3km, channel. The current is determined from

$$i(Z,t) = \frac{Vo}{R}\sqrt{\frac{CR}{\pi t}}\exp - \left(\frac{\sqrt{CR}\,Z}{4t}\right)^2 \qquad (3)$$

The solution of (3) is given in Fig. 2 for R = 17Ω/m and C = 10pF/m. Note that the mistake made in previous works has been to assume a wavefront, where the current is increasing towards infinity.

2.2 THE LCR MODEL

The capacitance and industance are determined from the idealization indicated in Fig. 3. The capacitance is determined from a charge simulation method, without the cloud electrode. The capacitance of the cloud is set equal to the capacitance of an 'isolated' sphere, given by $C = 4\pi\varepsilon_0 r$, where r is the cloud radius. Inductance is determined for an 'isolated' wire, since the presence of the perfectly conducting earth is to present an image carrying current in the same direction as the source. Energy dissipated in the earth is accounted for, by determining the earth resistance at the point of contact through which all the current flows into the earth. For open ground, assuming a spherical contact point with the radius of the channel, we have the earth resistance, [21], $R_E = \rho/\pi D$, where ρ is the resistivity of the earth and D is the diameter of the channel. When a flask to a grounded object is considered, the resistance of the object as well as it's earth resistance must be accounted for. The channel conductivity, assuming local thermodynamic equilibrium, for a 20,000°k channel is given by Spitzer's, [22], formula as 4242 $\Omega^{-1}m^{-1}$.

The transmission line equations

$$\frac{\delta V}{\delta z} = -Ri - L\frac{\delta i}{\delta t} \qquad (4)$$

$$\frac{\delta i}{\delta z} = -C\frac{\partial V}{\partial t} \qquad (5)$$

are numerically solved by using the finite difference, [23], approximations

$$\left[L + \frac{R\Delta t}{2}\right] V(z, t + \Delta t) = \left[\frac{R\Delta t}{2} - L\right] V(z, t - \Delta t) + \frac{2}{\Delta z^2}\left[L\Delta z^2 - \frac{\Delta t^2}{C}\right] V(z, t) + \frac{\Delta t^2}{C\Delta z^2}[V(z + \Delta z, t) + V(z - \Delta z, t)] \qquad (6)$$

$$In(Z, t) = Io + \sum_{n}^{N} C_n \frac{V(z, t + \Delta t) - V(z, t - \Delta t)}{2\Delta t} \qquad (7)$$

where Io is the leader current.

3. BRIEF DISCUSSION OF RESULTS

In order to illustrate the results, we have given the computation of return stroke currents and voltages for a 3km downward negative discharge and a 1km upward positive discharge, in Fig. 4 and Fig. 5 respectively. The former is the most frequent type of flash observed, and current measurement for the latter has also been reported. The channel radius has been assumed to be 1 cm (Fig. 4) and 4 mm (Fig. 5). The return stroke current waveform at ground is in good agreement with generally observed waveforms. Furthermore photographic measurements show that currents do not significantly decay as the stroke traverses the channel for downward negative strokes. The earth resistance of the upward flash is taken to be 100Ω, the earth resistance for a 2 cm diameter conducted burred 1 m into a $10^{-2}\Omega^{-1}m^{-1}$ conductivity soil. The earth resistance was found to influence the initial rate of rise of currents and time to half peak at ground level (an important limitation of current measurements) though, as would be expected, the current-time characteristics along the channel were mainly determined by the electrical parameters of the channel. The rate of rise of currents near the cloud for an upward flash, is much higher than that for a downward flash. The former type of flash is observed for clouds very close to the earth, and measurement of ground currents have been made [24]. Longer channel lengths and lower channel resistances for an upward flash give rise to oscillatory waveforms, as observed in triggered lightning. For both upward and downward flashes, the peak current rate of rise of current, impulse charge and action integral decrease as the return stroke traverses the channel. The model also permits the simulation of intracloud discharges, as well as flashes where an upward discharge rises to meet the downward leader - the latter may occur in the first stroke and in intracloud flashes. The possibility of a foreign body (e.g. an aircraft) with a low resistance (1 mΩ/m) lying along a small part of the flash (100m) above the ground was also investigated. It was found current rate of rise underwent no significant change for a smooth return stroke waveform (subsequent strokes, as Fig. 4); but if there were any oscillations inherent to the waveform without the external conductor these oscillations were sharpened (higher rate of rise) with the highly conducting material. These sharpened peaks were confined to the external body, and not noticeably reflected on the other portions. This observation might imply a more careful study of the first return stroke to be necessary, as well as seeking a better understanding of channel properties in triggered lightning.

ACKNOWLEDGEMENT

The first author wishes to thank the Culham Lightning Club, U.K. and the ORS Committee of British Universities for financial support.

REFERENCES

1. Bruce, C.E.R., and Golde, R.H., J. IEE, 88: 487 (1941)

2. Denis, A.S., and Pierce, E.T., Radio Sci, 12: 381 (1964)

3. Rao, M., and Bhattacharya, H., J. Geophys Res, 83: 6239 (1966)

4. Uman, M.A. et al, J. Geophys Res, 78: 3523 (1973)

5. Uman, M.A. et al, J. Geophys Res, 78: 3530 (1973)

6. Volland, H., J. Atms Terr Phys., 43: 191 (1981)

7. Master, M.J., et al, J. Geophys Res, 86: 12.127, (1981)

8. Uman, M.A., J. Geophys Res, 90: 6121 (1985)

9. Oetzel, G.N., J. Geophys Res, 73: 1889 (1968)

10. Little, P.F., J. Phys. D., 11: 1893 (1978)

11. Strawe, D.F. et al, Proc. of 7th Int Conf. on Lightning and Static Electricity, C2-9 (1982)

12. Krehbiel, P.R. et al, J. Geophys R., 84: 2432 (1979)

13. Uman, M.A., Lightning, Dover (1984)

14. Orville, R.E., in Golde, R.H. (Ed), Lightning, Academic Press, Vol. 1: 281 (1977)

15. Allibone, T.E., in Golde, R.H. (Ed), Lightning, Vol. 1: 231 (1977)

16. Watters, R.T., in Meek, J.M., and Craggs, J.D. (Eds), Electrical Breakdown of Gases, John Wiley: 385 (1978)

17. Hutzler, B., Riquel, G., and Riu, J.P., Proc. of 10th Int. Conf. on Lightning and Static Electricity: 191 (1985)

18. Allibone, T.E., private communication (1986)

19. Berger, K., in Golde, R.H. (Ed), Lightning, Vol. 1: 119 (1977)

20. Seshadri, S.R., Fundamentals of Transmission Lines, Addison-Wesley (1971)

21. Sraoja, E.K., in Golde, R.H. (Ed), Lightning, Vol. 2: 577 (1977)

22. Spitzer, L., Physics of Fully Ionized Gases, Interscience (1961)

23. Lapidus, L., and Pinder, G.F., Numerical Solution of Partial Differential Equations in Engineering and Science, John Wiley (1982)

24. Garbagnati, E., and Lopiparo, G.B., in 7th Int. Conf. on Lightning and Static Electricity: A.I.I, (1982)

25. Idone, V.P., and Orville, R.E., J. Geophys Res, 89: 7311 (1984)

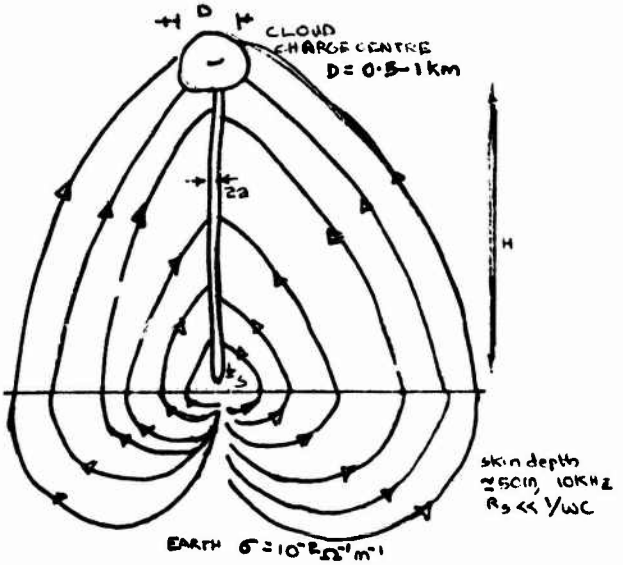

Fig. 1. Electrostatic Fields around Lightning Return Stroke Path (not to scale).

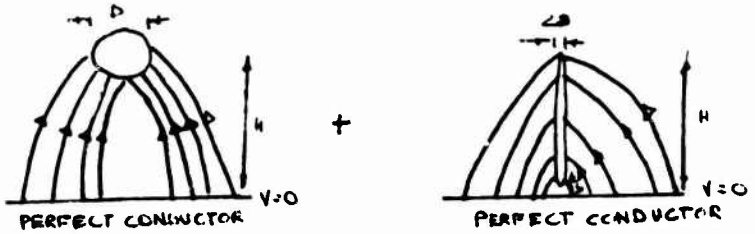

Fig. 3. The idealization made to determine the capacitance and inducta.ce of the system.

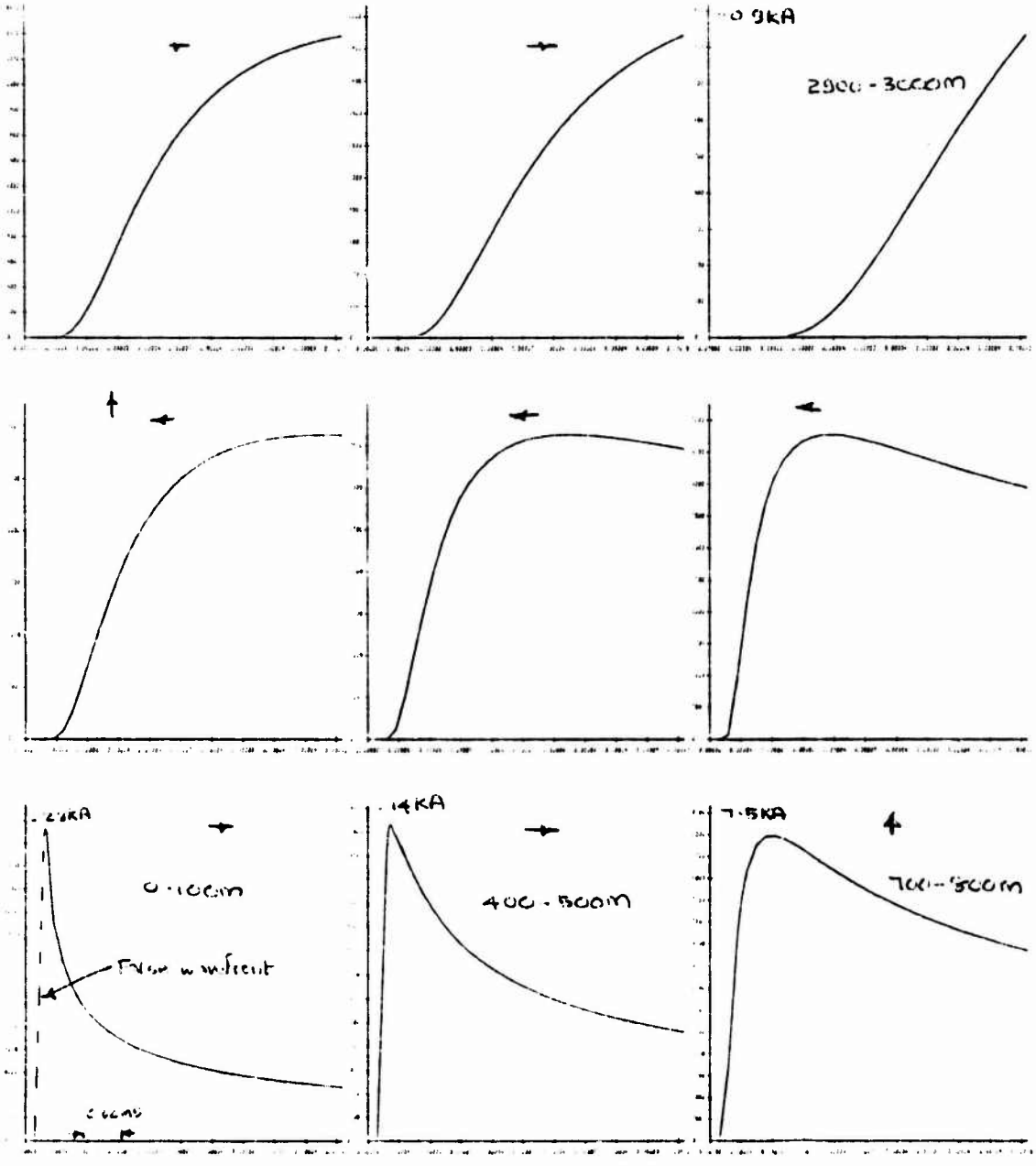

Fig. 2 Currents for a CR Line; illustrating the error of previous models
c = 10pF/m; R = 17Ω/m.

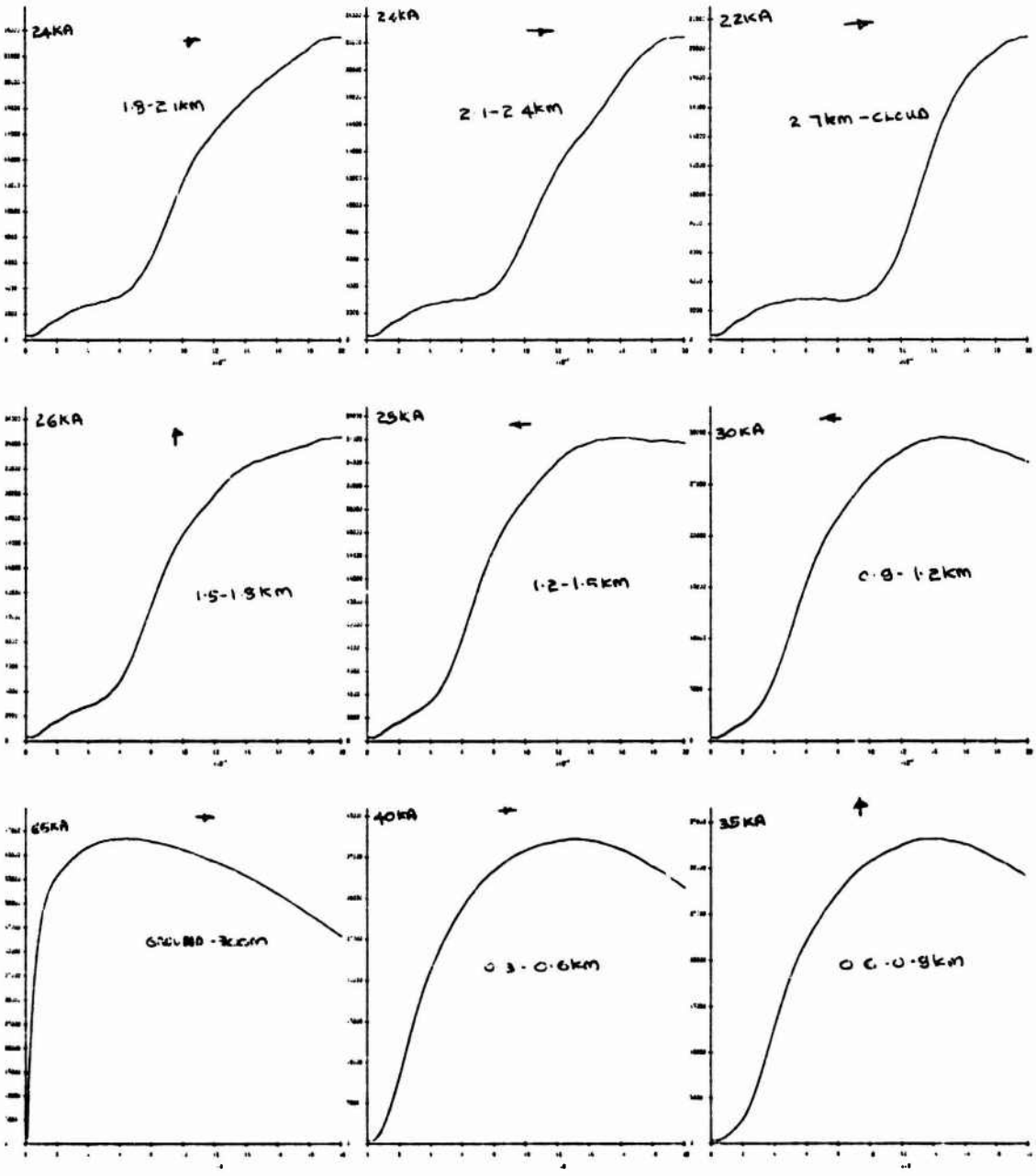

Fig. 4(a) Return Stroke Currents for a downward negative flash
RE = 1500Ω. R channel = 0.8Ω. C_1 = 25pF/m, C_2-C_3 = 4.6pF/M, C Cloud = 0.18μF
L = 3.1μH/m

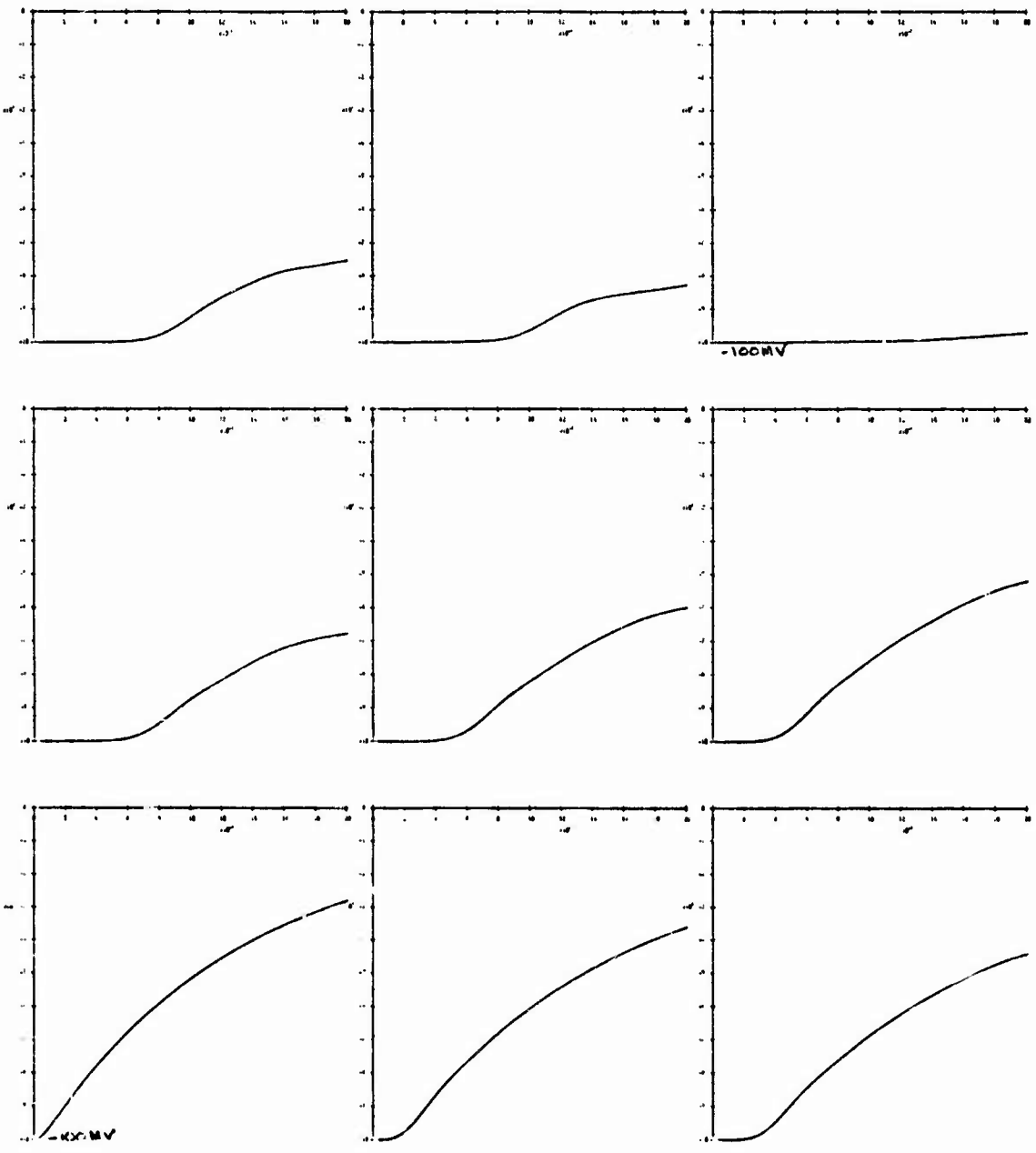

Fig. 4(b). Electric Potentials for currents in 4(a).

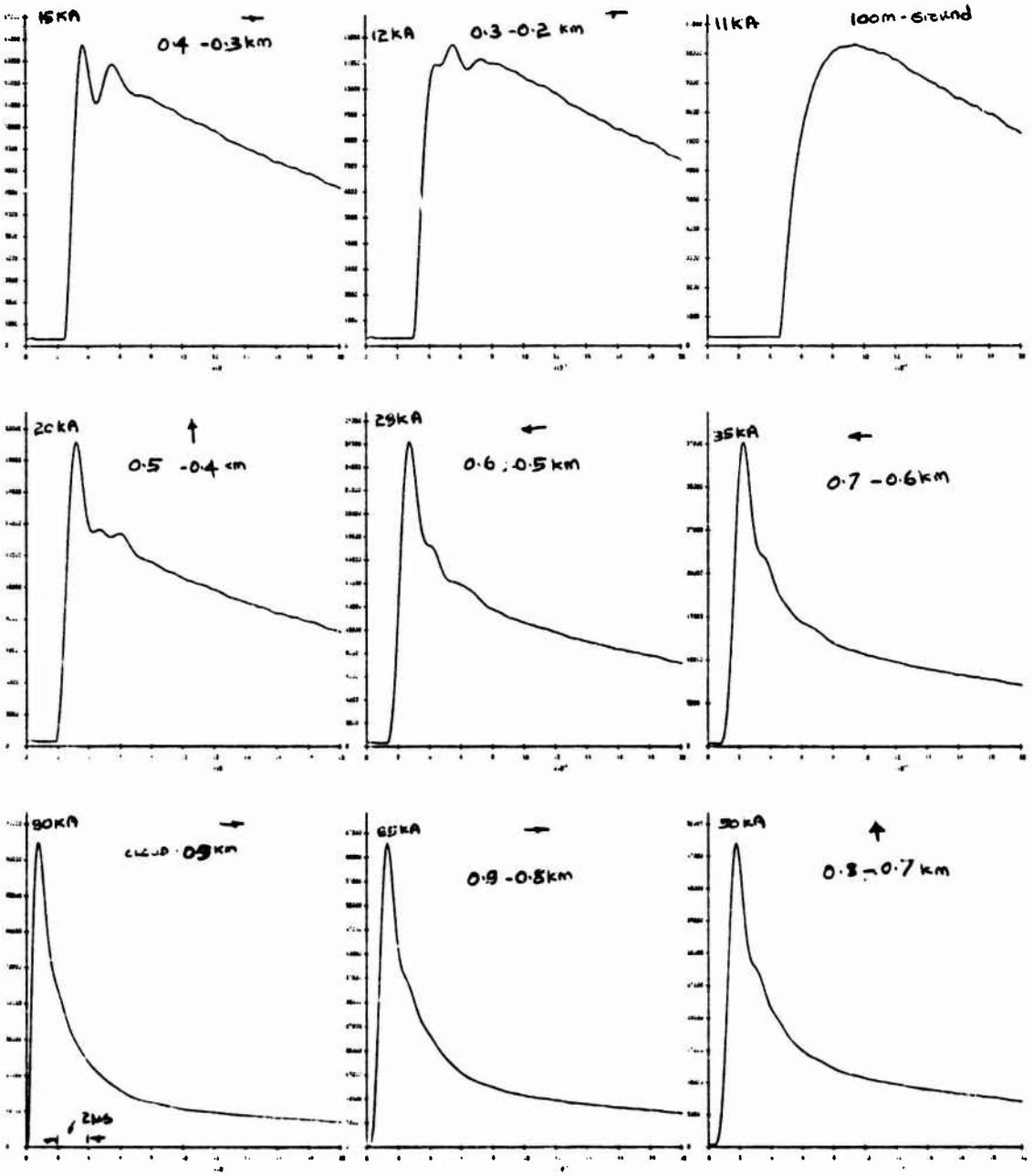

Fig. 5(a) Return Stroke currents for an upward positive discharge.
RE= 100Ω; R Channel = 5Ω; C and L as in 4(a).

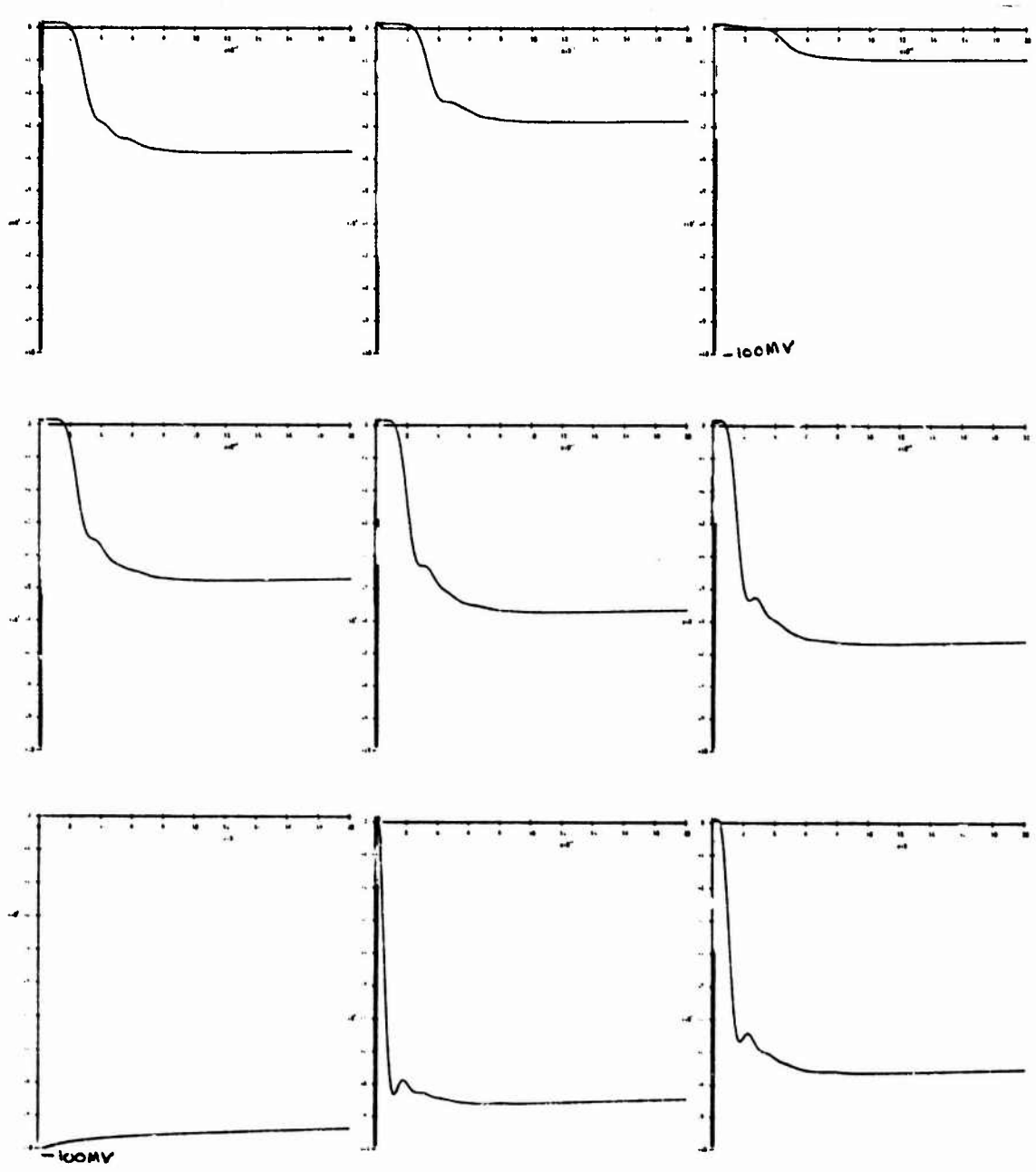

Fig. 5(b). Electric Potentials for currents in 5(a).

LIGHTNING RETURN-STROKE TRANSMISSION LINE MODEL*

Louis Baker
Mission Research Corporation
1720 Randolph Road, S.E.
Albuquerque, New Mexico 87106

ABSTRACT

MRC, in collarboration with the Langmuir Lightning Laboratory at NMIMT and the Air Force Weapons Laboratory, has made simultaneous observation of a return stroke's current, radiated fields, and optical emission. Comparison of the first two of these data has revealed that, near ground level, the return stroke velocity is nearly that of the speed of light, that is, much slower than the average return stroke velocity. The faster velocity is explained according to a model developed by C. Baum as due to a diminished corona near the ground. A fully nonlinear transmission-line model, accounting for channel resistivity and the effects of corona, is presented.

*This work was supported by the Air Force Weapons Laboratory under contract F29601-82-C-0027.
†Air Force Weapons Laboratory, Kirtland Air Force Base, NM.

INTRODUCTION

ANALYTIC MODELS OF LIGHTNING are still rather rudimentary. The velocities of leaders and return strokes, the current waveform, the nature of the stepping phenomena, etc. are not explainable from first principles. It has been suggested (Ref. 1) that the return stroke is the simplest of the lightning phenomena and it would appear to be most profitable to analyze and understand this piece of the lightning puzzle first.

Mission Research Corporation, in collarboration with the Langmuir Lightning Laboratory at the New Mexico Institute of Mining and Technology at Soccoro, New Mexico and the Air Force Weapons Laboratory, Kirtland AFB, New Mexico, has been active in a program to understand and model lightning phenomena. As part of this program, an effort was undertaken to observe a (triggered) return stroke to a tower, simultaneously measuring the current, the radiated electric and magnetic fields, and the optical emissions of a portion of the channel. The optical emission measurements will be discussed in another paper presented at this meeting. Here the analysis of the radiated fields and the current measurements will be discussed. The results must be tentative, as they are based on a single event. Nonetheless, they apparantly give an unprecendented result: the return stroke velocity near the ground is close to the speed of light. Return strokes measured optically have a typical velocity of one-third the velocity of light with one-half the velocity of light being the largest observed. These facts suggest that the return stroke current front decelerates as it rises.

This observation can be explained on the basis of a theory of the lightning channel developed by C. Baum of AFWL, one of our collaborators (1). The velocity of the current wave is determined by the extent of the corona envelope about the conducting lightning channel. Near the ground, the coronal envelope will diminish in intensity die to the ground boundary condition on the electric fields and the smaller time during which charge is introduced by the leader channel. In Reference 1 an analytic model was developed which can, in principle, explain the observations. This model cannot include either a resistive lightning channel or non-uniform channels and still be soluable analytically. For this reason, a numerical model has been developed. That model is described below.

MODEL DESCRIPTION

A segment of the transmission line is shown in Figure 1. The series resistance per unit length R represents the the finite resistance of the channel. The joule heating of the lightning channel results in the observed optical emission of the channel during the passage of the stroke current. This resistance is computed using the channel model (Ref. 13) mentioned above. The model computes the properties of two zones: an inner, conductive plasma core and a surrounding shell which has been shocked into a higher density and temperature than the ambient air. The shock wave defines the boundary between this shell and the ambient. This model differs from the one-zone models (Refs. 9, 14) which assume the shock wave does not separate from the edge of the hot channel. Such models overestimate the channel radius and consequently underestimate the resistance per unit length of the channel. The two-zone model in additions incorporates improved treatments of the air equation of state, radiative losses, and the shock propagation.

The inductance L and capacitance C per unit length of the channel are standard, and require an assumed "return current radius". This corresponds in other models to a choice of wave velocity $v = 1/\sqrt{(LC)}$, or equivalently characteristic impedance $\sqrt{(L/C)}$. For the present model we take this radius as a fixed parameter. Little (Ref. 4) went to some effort to compute effective values for L and C using electrostatic theory, but it is not clear that this resulted in a significantly improved model. An estimate of this radius can be made using antenna theory (Ref. 14). One finds that the effective characteristic impedance, and hence this radius and L and C, is a function of frequency. For a chosen "dominant" frequency, one can choose an appropriate return current radius. This is discussed below. At present, then, following Baum (Ref. 14), we have

$$L = 2 \times 10^{-7} \ln(r_{return}/r_{channel})$$

$$C = 2 \pi \varepsilon / \ln (r_{return}/r_{corona})$$

R = determined by channel radius, temperature model

The corona parameters are C' and G, a capacitance and conductance per unit length. The former measures the ability of the corona to store charge; the latter estimates the conductivity of the weakly ionized coronal volume, and limits the rate at which charge may be drawn out of the corona. These are related simply to the corona's radius; the conductivity of the corona is not predicted by theory at present, and in simulations to date we have ignored this term, setting G to a very small value. The coronal radius is calculated, following Baum (Ref. 10), with the simple approximation that it is equal to that radius at which the radial electric field equals the static breakdown stress of 3 MV/m. This radius is calculated by a Newton-Raphson iteration at each point along the transmission line, given the channel voltage and radius. Thus

$$C' = 2 \pi \varepsilon / \ln (r_{corona}/r_{channel})$$

$$G = 0$$

and r_{corona} is determined from the solution to

$$V/E = r_{corona} \ln (r_{return}/r_{corona})$$

where V is the line voltage and E is the static breakdown field of 3 MV/m. The equations are then

$$\frac{\partial I}{\partial t} = - \frac{RI}{L} - \frac{1}{L} \frac{\partial V}{\partial z}$$

$$\frac{\partial V}{\partial t} = - \frac{1}{C} \frac{\partial I}{\partial z} - \frac{1}{C'} \frac{\partial I}{\partial z}$$

$$\frac{\partial I'}{\partial t} = \frac{\partial I}{\partial t} \frac{GI'}{C'}$$

The boundary conditions are fixed impedances at cloud and ground terminations. The initial conditions are zero current flow everywhere and voltage initialized to an initial value along the line, down to an "initiation point" above the ground (typically, two zones) below which the voltage decreases linearly to zero. This smooth decrease was found to prevent initial transients in the numerical solution. We have used a ground impedance of 100 Ω and a cloud termination of an effectively infinite amount. These may easily be varied, of course, to account for better models of attachment and initiation, to study

the role of surge impedance of towers, etc. on stroke evolution, or to model possible cloud breakdown phenomena.

The finite-difference equations are similar to those of Gardner (Ref. 4), which are similar to those of Richtmyer and Morton (Ref. 15). We have generalized the algorithm to allow fully implicit instead of time-centered implicit calculations, for increased stability. We found that this was desirable if the resistance per unit length R were small or zero.

MODEL RESULTS FOR A TYPICAL INITIAL STATE

A vertical channel 1.5 km high was used. We studied in detail cases with initial radii of 0.001 and 0.01 m (1 mm and 1 cm), but experimented as well with channels of varying radius (0.001 m at ground level increasing linearly to 0.01 m at cloud height, simulating the fact that the older portions of the channel had more time to expand). Twenty-five zones in the vertical, each 60 m, were used. The initial coronal radius was found to be approximately 44 cm for this configuration. Figures 2-8 plot results for the two uniform diameter cases for variables of diagnostic interest, including currents, radiated power ("brightness") and the vertical electric field at 50 km distance. This was calculated in the radiation zone (following Ref. 5, neglecting retardation) and is shown in Figure 3. Note the decrease in signal at early times well before signal reflection at cloud height (~8 μs). This is due to the increase in time scale, which is clearly seen in Figure 2b. The front spreads as it advances, due to the finite resistance. Similar behavior was noted by Strawe (Ref. 9), who did not calculate radiated fields and did not model the corona. It is clear that any tendency of the corona to cause the front to steepen is more than overcome by the finite channel resistance, for the parameters employed. The sharp drop in signal from 7 to 9 μs is due to the wavefront reflection from the top of the channel, resulting in a change of propagation direction and a consequent change of signal sign. The computer plots show a "ringing" of the channel (small amplitude, high frequency "noise"). This may be shown by varying the time step and length increment to be due to the discretization of the transmission line equations. This does not mean that they are completely unphysical, however, since a real lightning channel is not a uniform vertical channel. Its branches would act as "lumped" discrete capacitors loading the main channel, and such ringing (as seen in observations) might have an origin similar in physical basis as the "fuzz" on the computer plots for radiated signal.

Figure 4 shows the radiated signal for a calculation in which $r_{channel}$ = 0.01 m (1 cm) initially. Such a channel has, initially a faster rise and greater peak vertical radiated E field. This quickly decays, however, down to a field typical of the smaller channel. The larger channel diameter case might be more similar to a subsequent return stroke and the smaller diameter channel case to a first return stroke. However, the channel conditions in both cases differ by more than merely the channel radius. The subsequent returns strokes would appear from observations to charge up to a lower voltage before the current wave is launched, since the typical currents are lower. The faster rise typically observed is in accord with the probability that the channel is less resistive, due to larger diameter and possibly higher initial temperature and hence ionization and conductivity. The differences between these two simulations is analagous to observed differences between first and subsequent return strokes. Figures 27-6 and 27-7 of Anderson and Sakshaug (Ref. 16) (based on work of Kroninger (Ref. 17) and Berger (Ref. 18)) show current waveshapes for first and subsequent return strokes. The first return strokes are more like Figure 4, the subsequent strokes more like Figure 6. See also References 19-21 for both current and radiation zone electric field plots.

ANALYSIS AND INTERPRETATION OF B-DOT SIGNALS

RESULTS OF COMPUTER MODELING OF FIELDS FROM THE CURRENT STROKE - The companion paper by Gardner et. al. in this meeting describes the experiment at the Langmuir Lightning Laboratory in full. Briefly, a rocket-triggered lightning strike attaches to a 20-m tower. B-Dot and D-Dot sensors are located approximately 40-m away.

The Lite Mike experiments provided data from B-Dot and D-Dot sensors located at Kiva 1, in addition to the Lite Mike and current sensor data. It was felt that it would be of interest to analyze these data records. While a great deal of data from these sensors have been reported in Lightning Phenomenology Note 3 and Lightning Phenomenology Note 11, a detailed analysis of these data does not seem to have been performed for any cases yet. We hope that the results presented here stimulate the application of sophisticated models to the treasury of data from the Kivas. One novel discovery, that of a higher initial return stroke velocity than previously observed, has been made. It is necessary to confirm this result with additional observed cases. The confirming data may already exist, and merely awaits detailed analysis.

The strike of record 85220 will be analyzed. It appears to be rather typical of strikes. There are two strikes for 85222; these posses anomalously low current amplitudes of about 2000 Amperes, maximum. Furthermore, the B-Dot and D-Dot records have not been made available for analysis.

The measured current of strike 85220 is shown in Figure 9. The polarity is positive vertical current (i.e., the lowering of negative charge or the rise of positive charge), which is the most common form for rocket-triggered lightning. This current was modeled for computational purposes as a double exponential waveform, shown in Figure 9. The fall time is not important as the results are most sensitive to the rise time.

The results of this paper differ somewhat from Price and Pierce (Ref. 2); because of their desire for an analytic solution, they used initial conditions which resulted in the current waveform having an infinite derivative at the leading edge. This is unphysical and neglects the finite impedance at the ground, which would impose an finite L/R time scale on current rise.

Figures 7 and 8 show the radiated power, and therefore give some measure of the optical brightness, of selected points along the channel.

Videotape observations show that the stroke was approximately vertical within the vicinity of the stinger, with an inclination in of approximately 15 degrees to the vertical, off towards the southeast. We will consider a vertical channel, and treat the inclination of the channel through an approximation. The vertical component of the current will be used to compute the vertical electric displacement and the azimuthal magnetic induction at the location of the sensors, and the distance will not be measured from the vertical line but from the displaced channel location, taken to be in the EW plane.

The basic method is that of Uman, McLain, and Krider (Ref. 22), who consider an ideal (lossless) transmission line with the current waveform propagating upward without modification. The ground is assumed to be perfectly conducting, producing ideal image currents in the ground plane. Because of the conducting wire grid in the area of the stinger, this should be an excellent approximation. The ground is not perfectly flat or uniform, with the sensors at Kiva 1 approximately 4 m below Kiva 2. The sensors will be assumed to be 40 m from the channel base. The stinger height is 20 m. To take full account of the physics of stroke initiation, one would have to consider not one wave travelling upward from the ground (and its image), but one wave starting upward from the initiation point, and another starting downward from this point. These waves would have images. In addition, the downward wave would be reflected from the ground, giving rise to an upward wave. To a good approximation, these added complications may be ignored after the transit of the wave back to the initiation point, i.e. after a time 2H/c, where H is somewhat greater than 20 m. This time is roughly 130 nanoseconds. We will make this approximation, which is justified a posteriori by the agreement of the observations and computational results. The wave is assumed to propagate at a velocity V.

The azimuthal magnetic induction B is the sum of two terms, an induction term and a radiation term, the former having an inverse square dependence upon distance from the radiating element, and the latter an inverse dependence upon distance. This results in the radiation term dominating at very large distances. At the very close distances of interest here, the terms are of comparable magnitude. At very early times, the terms are both positive with the radiation term dominating due to the rapidity of the field changes. After 400 ns in the case computed and displayed in Figures 10-13, the induction term is larger than the radiation term. At late times (after 1.7 microseconds for the V = .9 c wave velocity case considered here) the radiation term becomes negative, but it typically remains an order of magnitude smaller than the induction term. The full expression for B is

$$B_\phi(D,t) = \frac{\mu_0}{2\pi}\int_0^H \frac{\sin\theta}{R^2}\, i(z,\ t - R/V)dz + \frac{\mu_0}{2\pi}\int_0^H \frac{\sin\theta}{cR}\,\frac{\partial i(z,\ t - R/V)}{\partial t}\, dz \quad (1)$$

where θ is the angle between the channel and the radius between the radiating element and the observation point on the ground plane. Thus, each term is positive and decreases rapidly as we go up the channel, both because of the factors or R and the factor of $\sin(\theta)$.

The electric field is more complicated, having a static term, an induction term and a radiation term:

$$E_z(D,t) = \frac{1}{2\pi\varepsilon_0}\left[\int_0^H \frac{(2 - 3\sin\theta)}{R^3} \times \int_0^t i(z,\ \tau - R/V)\, d\tau dz + \int_0^H \frac{(2 - 3\sin\theta)}{cR^3}\, i(z,\ t - R/V)dz - \int_0^H \frac{\sin^2\theta}{c^2R}\,\frac{\partial i(z,\ t - R/V)}{\partial t}\, dz\right] \quad (2)$$

The static term is due to the effective dipole moment formed by the moving current pulse and it image, which results in a $1/R^3$ dependence. This term does not vanish at large times due to the finite charge transported by the stroke. All the terms contributing to the electric field and electric displacement have much stronger dependences upon channel height, due either to a factor of $\sin^2\theta$ instead of sin in the radiation term or factors of 2-3 $\sin^2\theta$ in the other terms, and the R^3 dependence of static field term. Note that the static and induction field terms are of indefinite sign. Lower levels of the channel have values of $\sin\theta = D/R$ close to one, giving a negative contribution. Higher portions of the channel have small values of the sine term, giving a positive contribution. The factor (2-3 $\sin^2\theta$) does not vanish with height as the factors of sin in the terms for B, so the induction term might be more significant than the corresponding term in the equation for B. The crossover occurs at a height of 1.414 D, where D is the distance of the observer from the channel base. In our case this height is a mere 60 m or so. It is seen from the downward nature of D and E for upward current that the portions of the channel below this height dominate in their contributions in the measured signal. However, the static term is found to dominate the other terms except at very early times, at which all play a role. Initially, all terms are negative, with the radiation term dominant due to the large time derivatives. Soon the static term dominates, on the same timescale as the induction term in the magnetic induction dominated the radiation term. Both the induction and radiation terms change sign, the former at 1 microsecond and the latter at 1.4 microseconds in the case of Figures 19-22. The static term is about one order of magnitude larger than the induction field which in turn is one order of magnitude larger than the radiation term. Obviously, these relationships will change if the observer is located further from the the channel or if the current pulse differs.

For computational purposes, the radiation terms were integrated by replacing the time derivative of the current with the derivative of current with respect to height. Thus the second integral in the expression for B becomes

$$-\frac{\mu_0 V}{2\pi c}\int \frac{\sin\vartheta\, di}{R} \quad (3)$$

which may be integrated by parts to yield

$$\frac{\mu_0 V}{2\pi c} \frac{D}{(D^2 + z^2)} i + v \int i \frac{d}{dz} \frac{(\sin\theta)}{R} dz \qquad (4)$$

The radiation term in the equation for the electric field is similar except that $\sin^2\theta$ replaces $\sin\theta$. With the substitution $\sin\theta = D/R$ and $R = \sqrt{(D^2 + z^2)}$ we may calculate the derivative in the integral, which is $-2z/(D^2 + z^2)$ for the expression above.

The static field term is calculated by defining a variable q(z) as the time integral of the current at any height. As the observer is stationary, this suffices because the retardation to any point on the channel does not change.

In the transmission-line model the principal free parameter (once the waveform of the current pulse, which is completely free, is specified), is the wave velocity. Good agreement was found for the model used with a wave velocity of V = .9 c, where c is the speed of light. We present the results for this assumed wave velocity as follows: Figure 10 compares observational and computed electric displacement D; Figure 11 compares D-Dot; Figure 12 compares magnetic induction B, and Figure 13 B-Dot. Note that the sensor for D-Dot causes a sign change between the computed and observed results for these quantities.

Figure 14 gives results for computed fields with an assumed wave velocity of c/3. It will be seen that the peaks in the derivative signals are delayed and reduced in magnitude, resulting in poorer agreement with observations.

INTERPRETATION OF EXPERIMENTAL RESULTS - The wave velocity which best matches observations is higher than typically reported for return strokes. Uman (Ref. 23) gives c/3 as a typical values and c/2 as a typical upper limit to reported velocities. The explanation most likely is that near the ground the velocities are higher than average. The wave is traveling in the most recently formed portion of the channel, which is probably still highly conductive and which has not dispersed to any degree. As the wave progresses, it encounters channel segments which have cooled and undergone attachment, recombination and some hydrodynamic dispersal due to turbulence, etc. The corona envelope which would store the charge around the channel is probably of greater diameter as well as more resistive due to attachment. This would account for the reduced wave speed (Refs. 24, 25).

The high wave velocity is also of great interest as it results in a correspondingly larger value of radiated fields for a given current than for low wave velocity. This is of importance in comparing the I of return strokes inferred by different methods (e.g., remote and tower measurements) Reference 35.

In the present work, it has been adequate to assume constant wave speed and wave shape to obtain reasonable agreement with observation. Residual errors might be explained due to the imperfect ground plane (neither flat nor perfectly conducting) and the non-ideal channel geometry (not perfectly vertical). Because, as noted above, the very lowest portions of the channel are dominating the signal, it is quite possible that the wave has moved beyond this region of importance before it has changed significantly in profile or velocity. As this region of significance is roughly the lowest 60 m of the channel, 20 m of which is contributed by the stinger, this should not be surprising.

The details of wave initiation, which would influence the first 10 ns or so of the signal, do not seem to be important in contributing to the observed fields.

EXPERIMENTAL CONCLUSIONS AND RECOMMENDATIONS - Based on the results above, we would conclude the following:

(1) Near field values (B and D) can be adequately explained with simple models.

(2) Wave velocities near the ground appear to approach the speed of light. As this is significantly higher than reported wave velocities in the literature for return strokes; this suggests that the wave slows as it rises. It is quite plausible that the wave changes profile as well as it rises. This can be computed self-consistently (Ref. 25). Such a computaton is not necessary for explaining the fields at a sensor 40 m from the stinger, as only heights of order 60 m or below contribute significantly to the fields here.

We would recommend for future investigations the following:

(1) Analyses similar to that performed here for B-Dot an D-Dot data as contained in Lightning Phenomenology Note 11 for selected strikes. This would give insight into stroke initiation behavior. Such a series of analyses would confirm or refute the high initial wave velocities discovered in this work, and would thereby contribute new facts to the understanding of the lightning return stroke.

(2) More sophisticated analysis using the transmission-line model of Reference 10. This would verify the hypothesis of the slowing of the wave with increasing channel height. Most importantly, it would enable us to build a model in which the wave shape is not arbitrary but determined by the physics of the lightning channel.

(3) Locating other sensors at greater distances from Kiva 2 to obtain information on thewave character at greater heights. This would beuseful only if better information on channel geometrywere available as well. This information might in part be obtained by locating sensors at differentazimuths from the stinger, but probably would require more videotape locations.

CONCLUSIONS AND DIRECTIONS FOR FURTHER THEORETICAL WORK

On the basis of transmission line models, it has generally been assumed that the time dependence of the current along a lightning channel at any point was the same as the time dependence of the vertical electric field in the radiation zone (e.g, Eq. 20 in Ref. 5, which holds until the current pulse reaches the top of the channel). This has lead to the general use of a "double exponential current pulse", i.e. a current of the form $I(t) = i(\exp(-At) - \exp(-Bt))$. This would seem to conflict with direct current measurements by Berger (Ref. 16). The model presented here resolves such problems by demonstrating that a resistive channel accounts for a double exponential radiated signal from a current monotonically increasing at any point in the channel at corresponding (retarded) times. The resistance used was not imposed ad hoc but followed from the channel radius and temperature, which were calculated accounting for hydrodynamic expansion, radiative losses, joule heating, etc. the model discussed here offers, for the first time, the possibility of predicting the form of I(t) instead of imposing it.

There are nonetheless a number of unsatisfying features of the model which suggest directions for future research. As discussed in Reference 11, the model for the corona is crude and its agreement with experiments is questionable. We would argue a more complete, time-dependent model for corona evolution is desirable.

The only ad hoc parameter in the model is the "return current radius" r_{return}. This determines L and C and through them the wave speed and surge impedance of the channel. Antenna theory (Ref. 22) tells us that the impedance is a function of frequency:

$$Z = \sqrt{(L/C)} = 60\ [\ell n(\lambda/2\ \pi\ a) + 0.116 + Ci(bH) - \sin bH/bH] \qquad (5)$$

where H is the channel height, a the channel radius, wavelength $\lambda = c/\nu$ with c the speed of light and ν the frequency, $b = 2\pi/\lambda$ is the wavenumber, and Ci(x) is the Fresnel cosine integral. To a good approximation, $L = 2 \times 10^{-7}\ \ell n(2h/a)$ where h is the smallest of: H, $\lambda/4\pi$, d/2 where d is a coaxial outer return radius which for a lightning stroke may be taken as many tens of kilometers and consequently neglected. For the highest frequencies, which for a 2 km high channel means above 24 kHz or for time scales shorter than 42 μs, r_{return} is effectively $\lambda/4\pi$. This implies that the lightning channel antenna would be dispersive, with the higher frequencies propagating more slowly along the channel, as compared to a conventional transmission line. One could transform the transmission line equations into frequency domain, with I and V functions of frequency rather than time. The broad bandwidth required (from time scales of nanoseconds to milliseconds) would suggest that uniform intervals in frequency space would be prohibitively expensive. However, the use of nonuniform spacing would mean that the fast Fourier transform could not be used. If a transform to time domain is only done once, at the "end" of the problem, this might not be prohibitive. We would have to forgo studying the evolution of the channel hydrodynamically, however, in order to do this.

The wave velocity is (Ref. 1):

$$v = \sqrt{1/L \cdot \frac{d}{dQ}\left(\frac{Q}{C}\right)} \qquad (6)$$

where c is a function of Q due to the dependence of coronal radius on local charge density. This results in $v = c$ for negligible corona and decreased velocity with an initial corona.

The transmission-line equations do not allow a quiescent initial state $I = 0$ for a line with v, Q, and c varying with height. Consequently, the lightning channel within the "striking distance" of the tower ground must be in a transient state, relaxing toward as uniform equilibrium, when contact with the tower first occurs. We have not had the resources to model this complicated situation.

A more satisfying but more complicated solution is to use a fully two-dimensional (cylindrically symmetric) field solver. Such codes have been developed for plasma simulation purposes. Their adoption to the lightning channel therefore appears feasible. Such codes would require significantly more computer resources than the one-dimensional transmission line model. Such an expenditure might be necessary, however, if a significant advance is to be made. We are developing a formulation which allows mutual interaction of all the elements of the channel, and hope to be able to apply it soon.

REFERENCES

1. C.E. . Baum, L. Baker, Return-Stroke Transmission Line Model, Lightning Phenomenology Note, 13, July 1983.
2. G.H. Price and E. T. Pierce, Radio Science, 12, 381 (1977).
3. P.F. Little, J. Phys. D 11, 1893 (1978).
4. R. L. Gardner, Ph.D. thesis, University of Colorado, 1980.
5. M. A. Uman, D. K. McLain, E. P. Krider, Am. J. Phys.,43, 33 (1975).
6. M. A. Uman, Lightning, NY: McGraw-Hill, 1969. 1969.
7. R. H. Golde, in Lightning, Vol 1, ed., R.H. Golde, NY: Academic Press, 1977, p. 335.
8. C. F. Wagner, AIEE 82, pt. 2, 609, 1963.
9. D. E. Strawe, preprint.
10. C. E. Baum, Properties of Lightning-Leader Pulses, Lightning Phenomenology Note 2, 22December 1981.
11. L. V. Bewley, Traveling Waves on Transmission Systems, 2nd ed., NY: Dover, 1963).
12. L. Baker, Lightning Phenomenology Note 12, to appear.
13. S. I. Braginskii, Soviet Physics JETP 34, 1068 (1958).
14. R. D. Richtmyer and R. B. Morton, Difference Methods for Initial Value Problems, second edition, NY: Wiley-Interscience, 1967, pp. 263ff.
15. J. G. Anderson and E. C. Sakshaung, in Standard Handbook for Electrical Engineers, D.G. Fink and H. W. Beaty, ed., NY: McGraw-Hill, 1978, p. 27-8.
16. H. Kroninger, CSIR report ELEK53, 1974, Nat. Elec. Eng. Res. Inst., Pretoria, S.A.
17. K. Berger, J. Franklin Inst., 283, p. 478 (1967).
18. K. Berger, in Lightning, Vol. 1, ed., R. H. Golde, NY: Academic Press, 1977, p. 147ff.
19. M. A. Uman, et al., in Lightning Technolcgy NASA Conference Publication 2128, FAA-RD-80-30, 1980, p. 21.
20. C. D. Weidman and E. P. Krider, in Lightning Technology, NASA Conference Publication2128, FAA-RD-80-30, 1980, p. 29.
21. S. A. Shelkunoff and H. J. Friis, Antennas: Theory and Practice, NY: J. Wiley, 1952.
22. Gardner, R. L., M. H. Frese, J.L. Gilbert, and C. L. Longmire, "A Physical Model of Nuclear Lightning", Phys. Fluids 27 2694 1984.
23. Aleksandrov, G. N., Sov. Phys. Tech. Phys. 2554 (1957).
24. Penney, G. W. and G. T. Hummert, J. Appl. Phys., 41,572 (1970).
25. Kline, L. E. and J. G. Siambis, Phys. Rev. 794,1972.

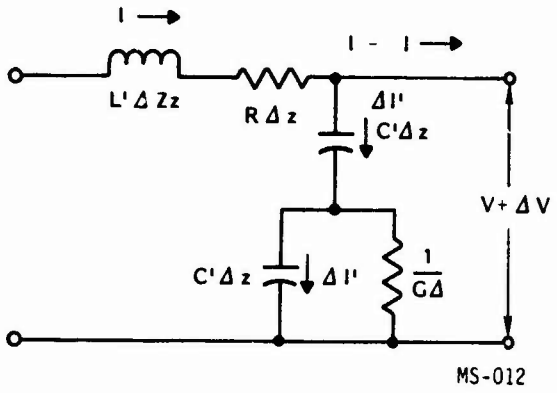

Fig. 1 - An element in the transmission line model for the lightning channel.

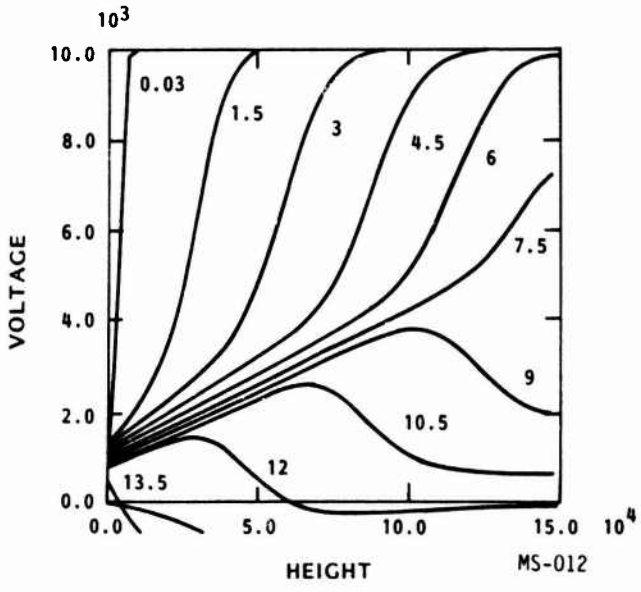

Fig. 2a - Voltage versus position at times shown in microseconds, 0.001 m initial radius.

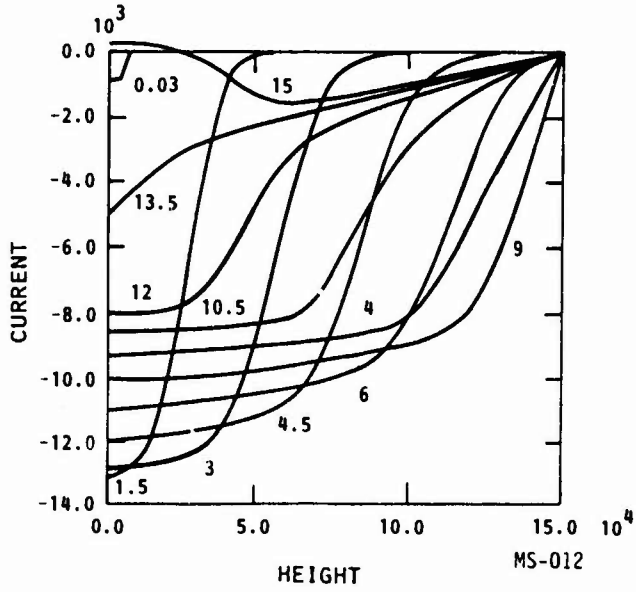

Fig. 2b - Current versus position at times shown in microseconds, 0.001 m initial radius.

Fig. 2 - Results for simulation of return stroke on lightning channel.

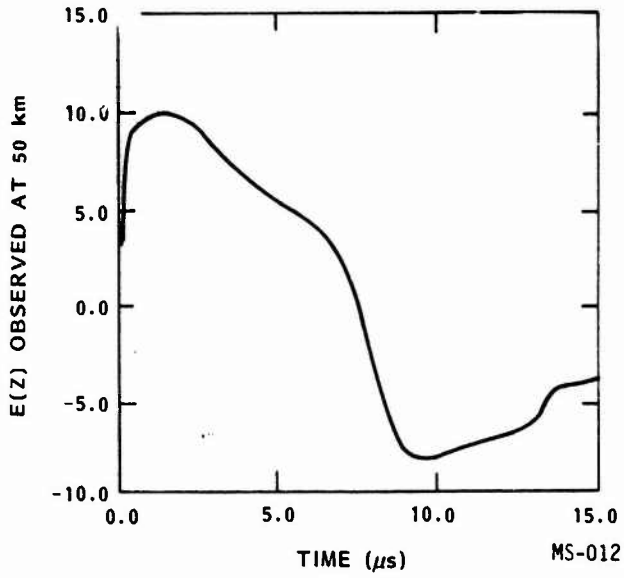

Fig. 3 - Vertical electric field at 50 km distant observation point on the ground plane, computed using the radiation zone approximation, for the case with 0.001 m initial channel radius.

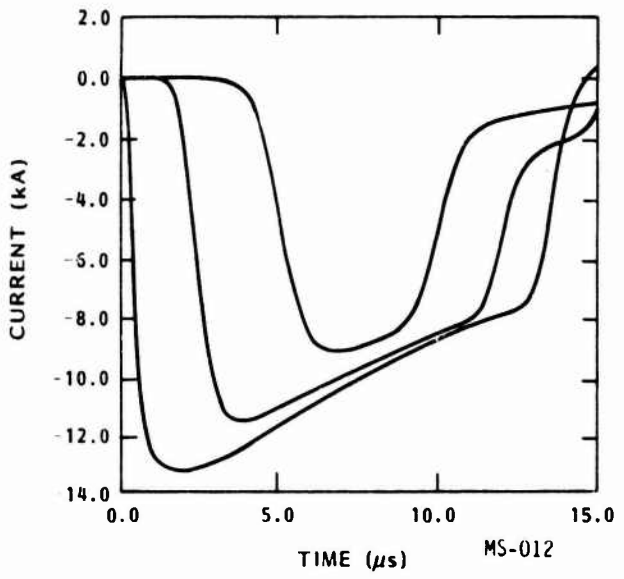

Fig. 4 - Current in the lightning channel for the case with initial channel radius of 0.001 m, at ground level, 1/3, and 2/3 of the total height above the ground.

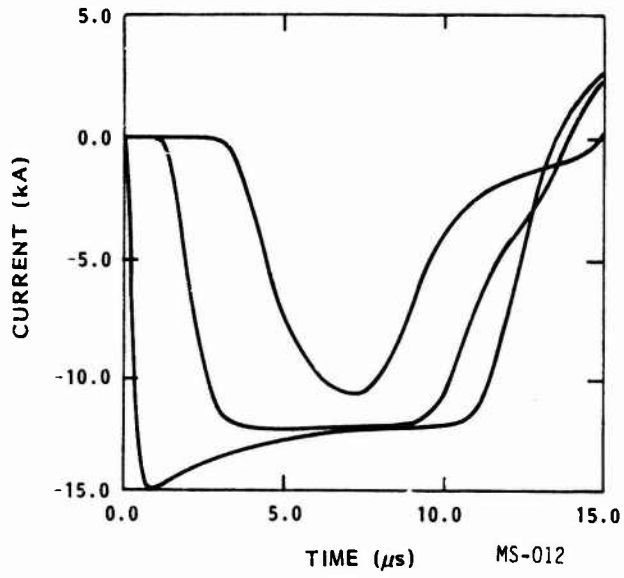

Fig. 5 - Vertical electric field at 50 km distant observation point on the ground plane, computed using the radiation zone approximation, for the case with the channel initially 0.01 m radius.

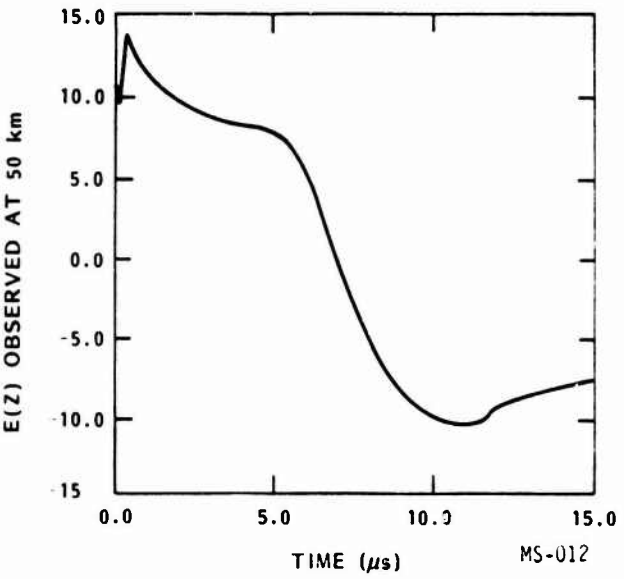

Fig. 6 - Current in the lightning channel for the case with initial channel radius of 0.01 m, at ground level, 1/3, and 2/3 of the total height above the ground.

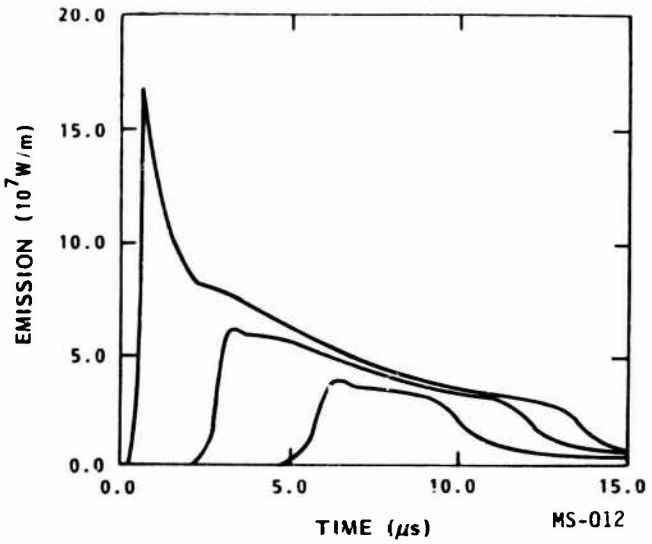

Fig. 7 - Radiant emission (W/m) from the lightning channel for the case with initial channel radius of 0.001 m, at ground level, 1/3, and 2/3 of the total height above the ground.

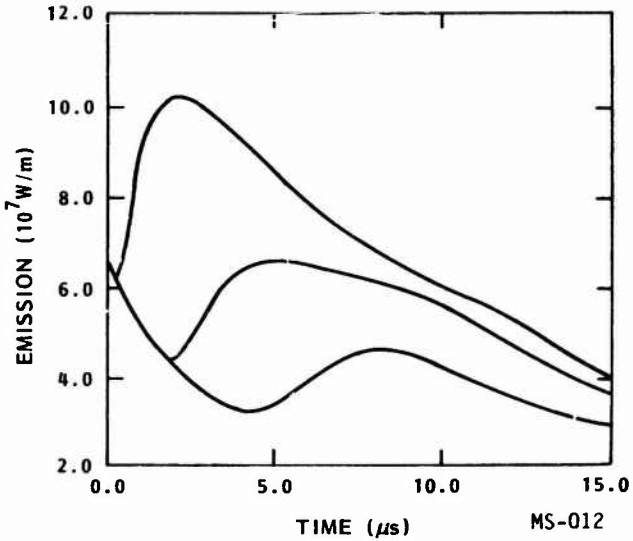

Fig. 8 - Radiant emission (W/m) from the lightning channel for the case with initial channel radius of 0.01 m, at ground level, 1/3, and 2/3 of the total height above the ground.

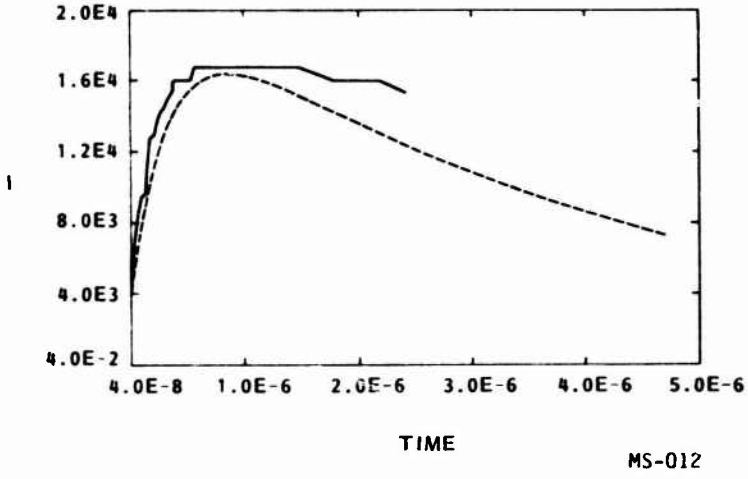

Fig. 9 - Current in channel vs time.

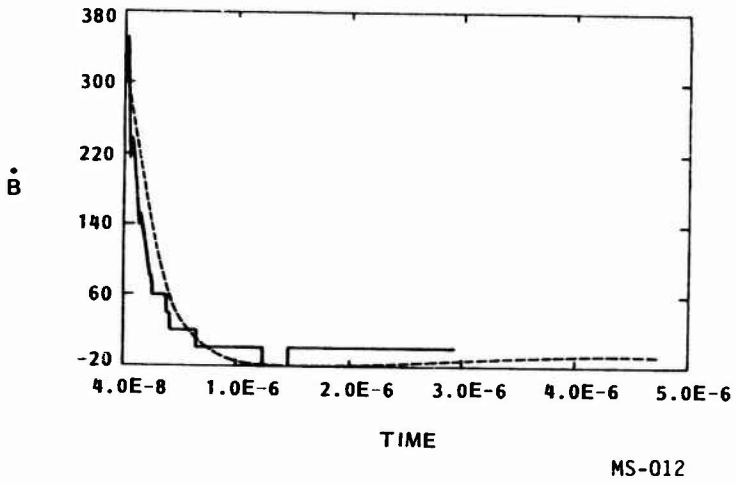

Fig. 10 - Observed (dotted) and computed (solid) electric displacement $\dot{B}$ vs time for wave velocity .9c.

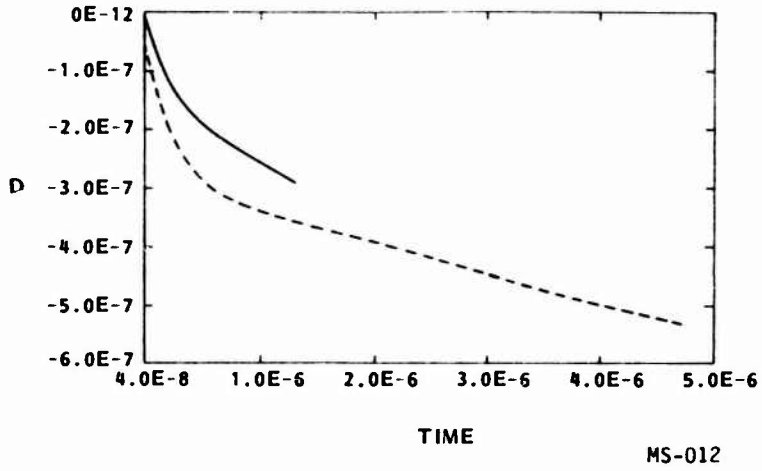

Fig. 11 - Observed and computed derivative of electric displacement, D.

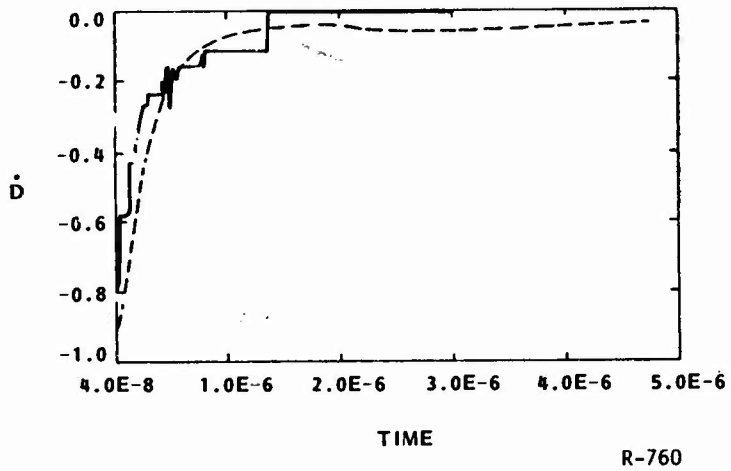

Fig. 12 - Observed and computed magnetic induction $\dot{D}$ vs time for wave velocity .9c.

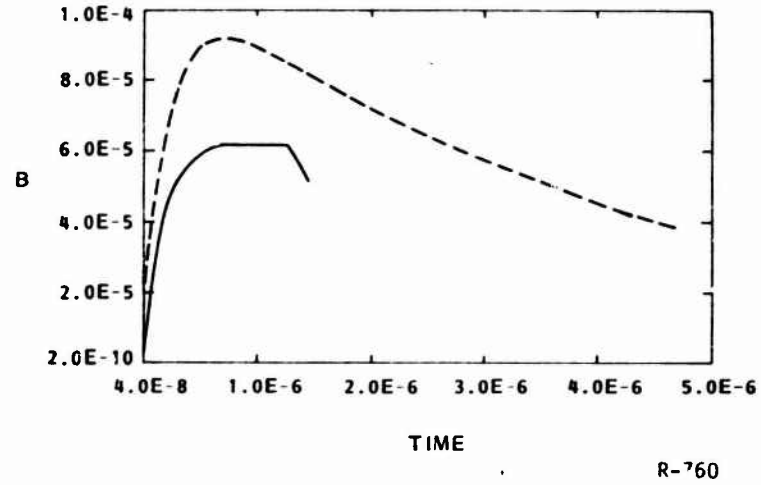

Fig. 13 - Observed and computed derivative of magnetic induction, B.

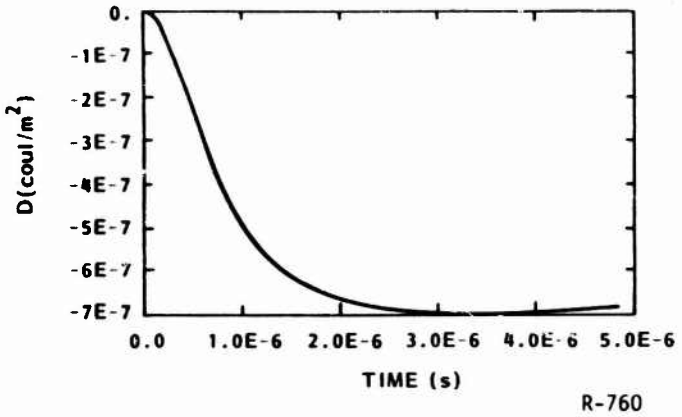

Fig. 14a - Computed results for wave velocity c/3: Electric displacement D.

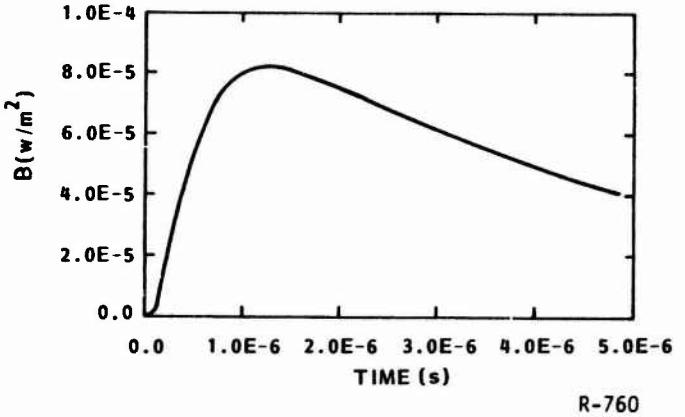

Fig. 14b - Computed results for wave velocity c/3: Magnetic induction B.

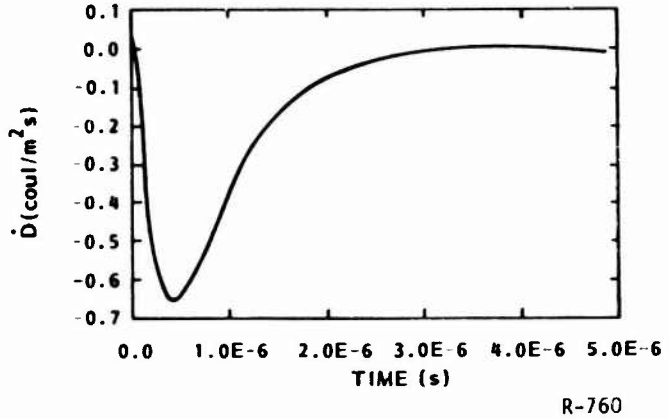

Fig. 14c - Computed results for wave velocity c/3: Derivative of electric displacement, D.

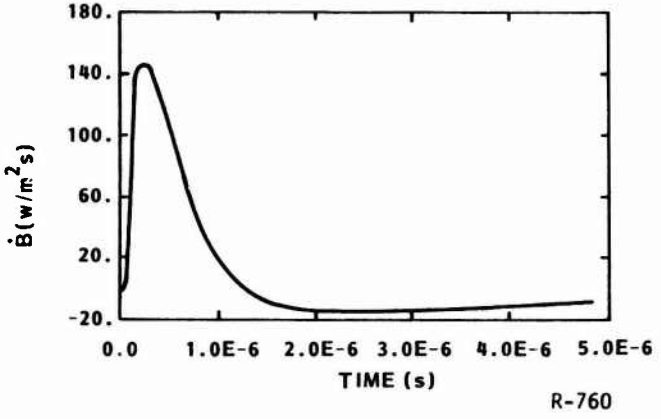

Fig. 14d - Computed results for wave velocity c/3: Derivative of magnetic induction, B.

A SIMPLE RETURN STROKE CURRENT MODEL FOR PREDICTING LIGHTNING-GENERATED ELECTROMAGNETIC FIELDS

T. A. Seliga, W. J. White, and K. A. Ostrsnder
Aviation Safety Systems Project/3M
6530 Singletree Drive
Columbus, Ohio 43229-1119

ABSTRACT

In order to evaluate the system response of lightning detection and location finding instrumentstion, a simplified model of the return stroke is used to predict lightning-generated electromagnetic field waveforms. The wsveforms may then be simulated in the laborstory for testing inatrumentation. The model consists of a vertical line charge which, prior to the return stroke discharge, is generated as a product of the downward-moving stepped leader proceaa. The latter eatablishes an equivalent line charge density between cloud and ground. The return stroke is asaumed to lower all of this line charge to ground via a continuoua current traveling wave, initiated st ground level. The length and intensity of thia wave very with time in accordance with selected parameters of the classical double exponential form of the discharge current. The continuous current condition follows directly from the assumption of conservation of charge along the channel and effectively results in a recharging of the channel after completion of the return stroke discharge. Several properties of the return stroke electromagnetic waveforms, obtained from the model, are given to demonatrate the response to vsrioua current forms given in the literature.

A FIBER-OPTIC ELECTRIC FIELD SENSOR FOR LIGHTNING RESEARCH

B.N. Nelson, C. Menzel, and T.G. DiGiuseppe
Geo-Centers, Incorporated, Boston, Massachusetts

ABSTRACT

A fiber-optic electric field sensor based on the transverse electro-optic effect is described. The sensor is completely dielectric in composition and can monitor both electric field strength and direction. The sensor has a linear sensing range of approximately 1×10^2 to 1×10^7 V/m and an AC measurement bandwidth capability which approaches 1 GHz. In addition, the sensor is immune to the effects of electromagnetic interference. The effect of electro-optic crystal geometry on fiber-optic sensor measurement range and measurement bandwidth is discussed. Sensor test data generated with both DC and AC applied electric fields are presented.*

* This sensor was developed under U.S. Air Force Small Business Innovative Research Contract No. F33615-85-C-3417, Air Force Wright Aeronautical Laboratories (AFWAL/FIESL), Wright-Patterson Air Force Base, Ohio 45433.

INTRODUCTION

THERE EXISTS A NEED to provide electric field sensors which can directly measure both electric field strength and direction for lightning research measurement applications. A sensor for lightning research should have a linear sensing range between 1×10^2 V/m and 3×10^6 V/m and an AC measurement bandwidth capability which approaches 10 MHz. A sensor for this application should not perturb the electric field to be measured, and should have the capability of measuring electric field strength, direction, and AC characteristics. In addition, the sensor output signals should not be compromised by the effects of electromagnetic interference (EMI).

Presently D-sensors are utilized in lightning research measurement applications. These sensors are capacitive in nature and do not measure the electric field directly but, instead, measure the time derivative of the electric field displacement. Hence, the output of these sensors has to be integrated to determine the applied electric field. These sensors are fabricated with metallic components which cause a distortion of the electric field to be measured. These sensors cannot be easily utilized for making electric field directional measurements at a single test location. These sensors require, in many measurement applications, electrical to optical converters to prevent the collected data from being compromised by the effects of EMI.

Fiber-optic and optical electric field and voltage sensors have been designed, which are based on the electro-optic effect with a variety of electro-optic crystals [1,2,3,4,5,6,7,8]. For the design of an electric field sensor for lightning research, $Bi_4(GeO_4)_3$ (BGO) has proven to be an ideal crystal choice based on its optical, electrical, mechanical, and chemical properties [1].

THEORY

The electro-optic effect can be utilized in a fiber-optic sensor to detect electric field strength. Fig. 1 shows a schematic layout of the components and their orientation for a fiber-optic electric field sensor. When an electric field is applied to the crystal in the x direction, the index of refraction increases along that direction, while the index of refraction along the y direction remains constant. A beam of light polarized along the x direction propagates at a slower speed than a beam of light which is polarized along the y direction. Consequently, the x axis is known as the slow axis and the y axis is known as the fast axis. If light is initially polarized at $\pi/4$ with respect to these axes, then a phase shift will occur between the components of light that lie along each of these axes. This phase shift is proportional to the applied electric field strength and the crystal length, and is referred to as electric field induced birefringence.

With the sensor configuration shown in Fig. 1, a change in the electric field induced birefringence causes a change of the optical transmission, which results in a changed light intensity incident on the optical detector. For this configuration, the output intensity for the $\pi/4$ and the $-\pi/4$ analyzer orientations is given by:

$$I_{\pi/4} = I_0 \sin^2 (\Gamma(E) - \pi/4) \quad (1)$$

$$I_{-\pi/4} = I_0 \sin^2 (\Gamma(E) + \pi/4) \quad (2)$$

where

I_0 - input optical intensity

$\Gamma(E)$ = electric field induced birefringence

Consider a BGO crystal cut into a rectangular parallelepiped with edges parallel to the <001>, <110>, and <$\bar{1}$10> crystal directions. Fig. 2 shows the orientation of the fast and slow axes for electric fields applied along the <001> and the <110> crystal directions. These axes are oriented at $\pi/4$ with respect to each other, allowing the use of a single electro-optic crystal to detect electric field strength in two orthogonal directions. The crystal and polarization optics orientation to accomplish this is shown schematically in Fig. 3. By incorporating two electro-optic crystals mounted orthogonally, as shown in Fig. 4, a three axes electric field sensor is created.

The induced birefringence of BGO electro-optic crystal as a function of the applied electric field is given by:

$$(E) = (2\pi n_0^3 r_{41} LE)/\lambda \quad (3)$$

for electric fields applied along <110> and:

$$(E) = (\pi n_0^3 r_{41} LE)/\lambda \quad (4)$$

for electric fields applied along <001>

where:

λ = the wavelength of the optical source

n_0 = crystal index of refraction = 2.07

r_{41} = electro-optic coefficient = 1.03×10^{-12} m/V

L = crystal length (parallel to <$\bar{1}$10>)

E = the applied electric field strength

Equations (3) and (4) show that the electric field induced birefringence, and therefore sensor sensitivity, is dependent on crystal length.

The electro-optic effect is in principle very fast. It can be assumed that the AC measurement bandwidth capability of the sensor is limited by the transit time of light propagating through the crystal. This is given by:

$$t = L\, n_0/c \quad (5)$$

where:

t = time of transit

L = crystal length

n_0 = crystal index of refraction

c = speed of light

Equation (5) shows that the AC measurement bandwidth capability is dependent on crystal length.

EXPERIMENTAL RESULTS

The electric field directional sensitivity exhibited in BGO electro-optic crystal is shown in Figs. 5 and 6. Fig. 5 shows the sensor to be sensitive only to applied electric fields in the <110> crystal direction. In Fig. 6, the sensor is shown to be sensitive only to applied electric fields in the <001> crystal direction. The sensor is made sensitive to either of these two applied electric field directions by orienting the polarization optics at $\pi/4$ with respect to the induced fast and slow axes in the crystal.

Fig. 7 shows the effect of crystal length on the linear sensing range and sensitivity of a fiber-optic electric field sensor. The longer crystals exhibit a larger induced birefringence for a given applied electric field. For lightning research applications, both the 10 mm and 20 mm crystals should afford linear sensing ranges between 1×10^2 V/m and 3×10^6 V/m.

To test the utility of an electro-optic crystal as a sensing element for lightning research, a transformer driven spark gap was utilized. The high voltage pulse generated from this device is shown in Fig. 8. The applied voltage ramp peaks at a voltage of approximately

2.5×10^4 V in approximately 1.2 μs. This ramp is followed by exponentially damped ringing, which has a period of approximately 100 ns. This voltage was applied to parallel plate capacitors with a 1 cm plate spacing, producing a peak applied electric field of 2.5×10^6 V/m. The sensor response for three different crystal lengths is shown in Fig. 9. As expected, the 20-mm crystal exhibited the best signal-to-noise ratio of the three crystals. These data indicate that both the 10-mm or 20-mm crystals would be excellent crystal choices for a fiber-optic electric field sensor for lightning research applications. Crystal lengths of 10 mm or 20 mm are suitable for the development of a completely dielectric three axes electric field sensor system with a sensing head which has a 2-inch cube form factor.

SUMMARY AND CONCLUSIONS

A fiber-optic electric field sensor based on the transverse electro-optic effect in BGO electro-optic crystals is an excellent electric field sensor for lightning research measurement applications. This sensor has a linear sensing range between 1×10^2 V/m and 3×10^6 V/m and an AC measurement bandwidth capability which can approach 1 GHz. This sensor is entirely dielectric in composition, which results in minimal perturbation to the electric field to be measured. The sensor system can be configured such that electric field directional measurements can be made with a sensing head which has a 2-inch cube form factor. The sensor output is also a direct measure of the applied electric field, which eliminates the need for sensor output signal integration. In addition, as an optical sensor, the sensor output is intrinsically immune to the effects of EMI. These properties make a fiber-optic sensor based on the transverse electro-optic effect in BGO crystals superior to other sensors for lightning research measurement applications.

REFERENCES

1.B.N. Nelson, C. Menzel, and T.G. DiGiuseppe, "Non-Intrusive Electromagnetic Field Sensor," Final Report, GEO-CENTERS, INC. GC-TR-85-578, January 1986.

2.K. Shibata, "A Fiber Optic Electric Field Sensor Using the Electro-Optic Effect of $Bi_4Ge_3O_{12}$," Fuji Electric Corporate Research and Development, Ltd., Japan (Presented paper pre-print).

3.K. Kyuma, S. Tai, M. Nunoshita, N. Mikami, and Y. Ida, "Fiber-Optic Current and Voltage Sensors Using a $Bi_{12}GeO_{20}$ Single Crystal," Journal of Lightwave Technology, Vol. LT-1, No. 1, March 1983.

4.S. Ihara, et al, "The Development of BSO/Fiber-Optic Magnetic Field and Voltage Sensors," Sumitomo Electrical Technical Review, Number 23, January 1984, pp. 175-183.

5.Y. Hamasaki, H. Gotolt, M. Katoh, S. Takeuchi, "OPSEF: An Optical Sensor for Measurement of High Electric Field Strength," Electronics Letters, Vol. 16, No. 11, pp. 406-407, 1980.

6.W. Filter, C. Landron, D. Muron, "Photonic Measurement of Microwave Pulses," Presented at SPIE: Fiber Optic and Laser Sensors; Conference 566, August 22, 1985.

7.H. Trinks, G. Matz, H. Shilling, "Electro-Optic System for EMP Measurements," IEEE Trans. Electromag. Compat., Vol. EMC-22, No. 1, pp. 75-77, 1980.

8.G. Massey, J. Johnson, and D. Erickson, "Laser Sensing of Electric and Magnetic Fields for Power Transmission Applications," SPIE Vol. 88 Polarized Light, pp. 91-96, 1976.

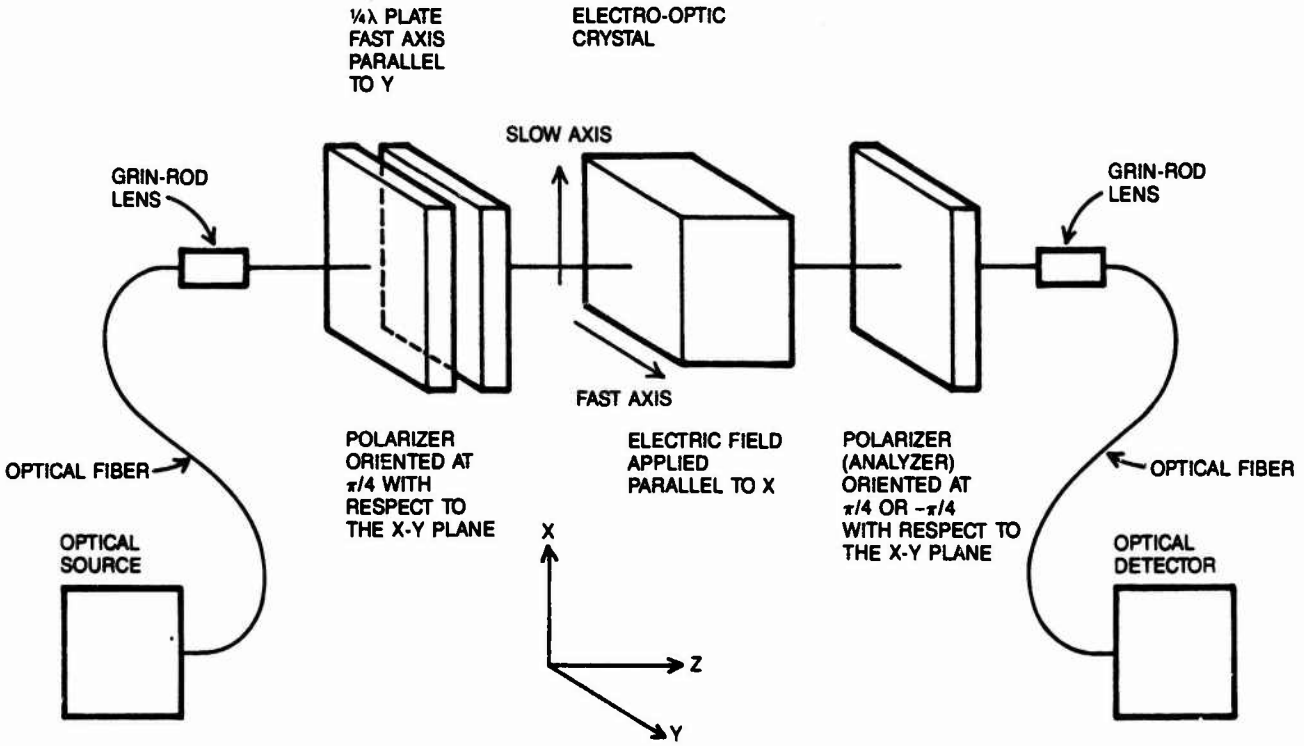

Fig. 1 - Orientation of optical components for a fiber-optic electric field sensor

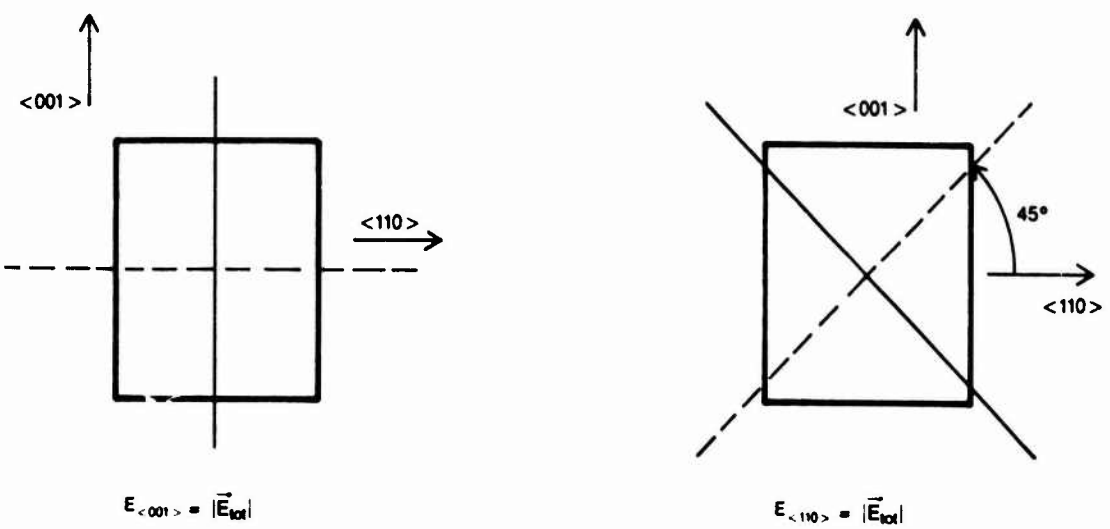

Fig. 2 - Orientation of fast and slow axes in BGO crystal for electric fields applied along the ⟨001⟩ and the ⟨110⟩ crystal directions

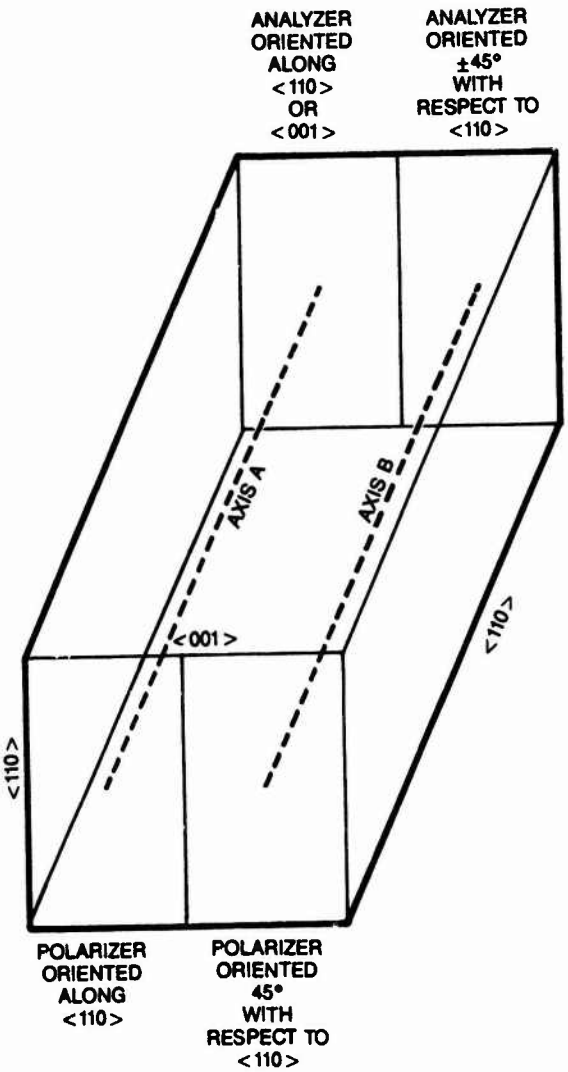

Fig. 3 - Two optical axes in one crystal. By incorporating two optical axes (A and B) and polarizing axes as shown in a single crystal, independent sensors with orthogonal directional sensitivities are realized

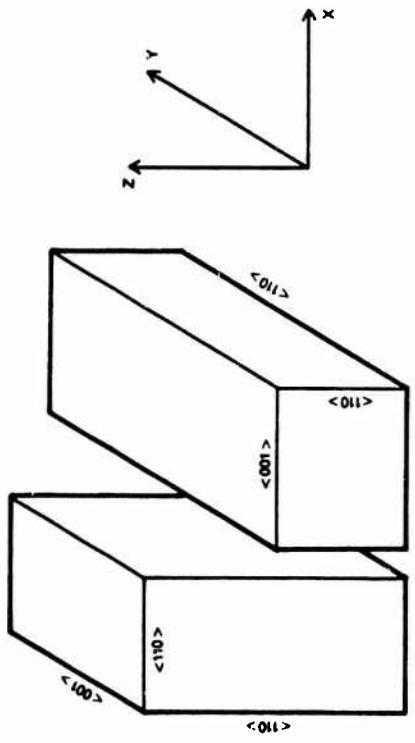

Fig. 4 - Crystal orientations for a three axes electric field sensor utilizing BGO electro-optic crystal (X direction is redundant)

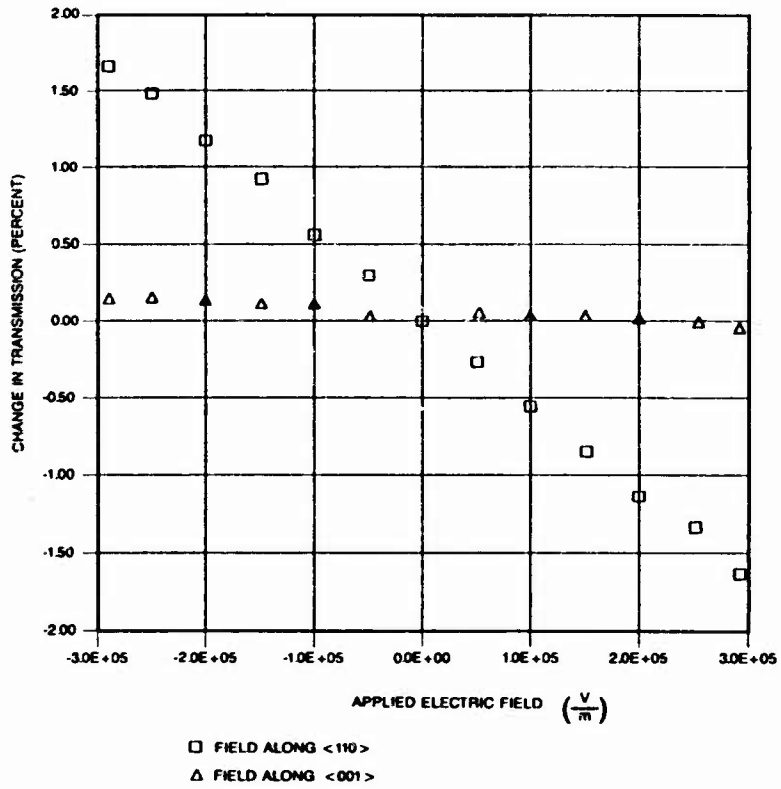

Fig. 5 - Change in transmission versus applied field for 5-mm BGO crystal

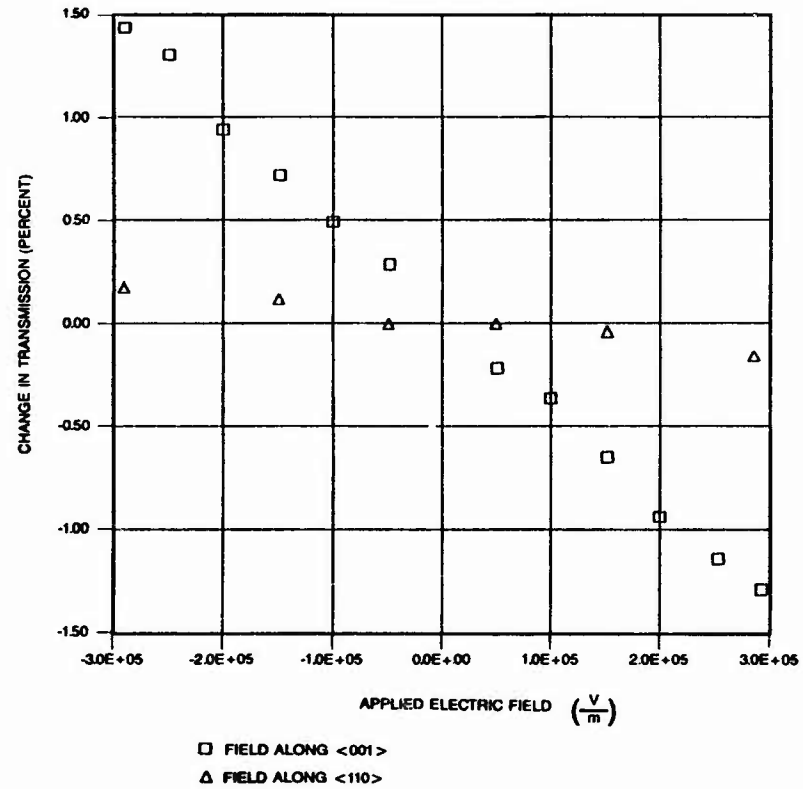

Fig. 6 - Change in transmission versus applied fields for 5-mm BGO crystal

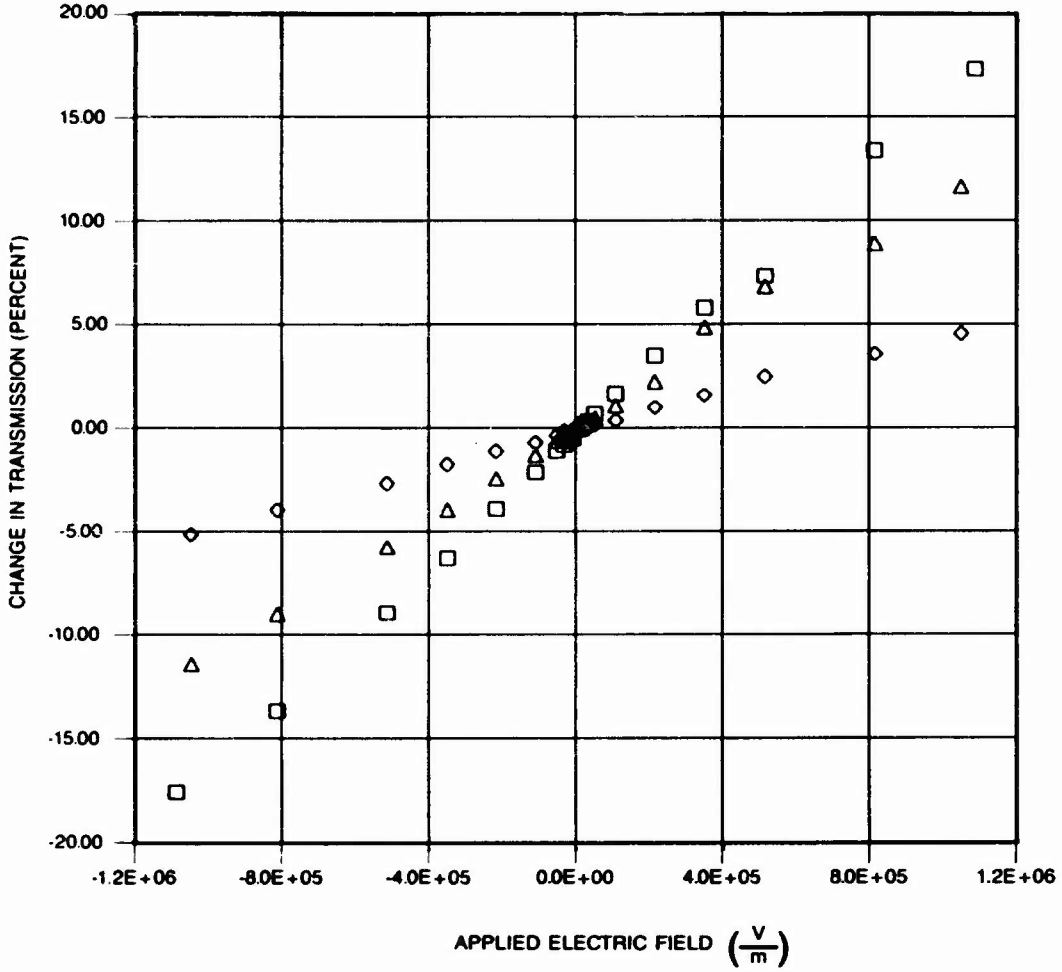

Fig. 7 - Comparison of transmission change for three different crystal lengths in BGO

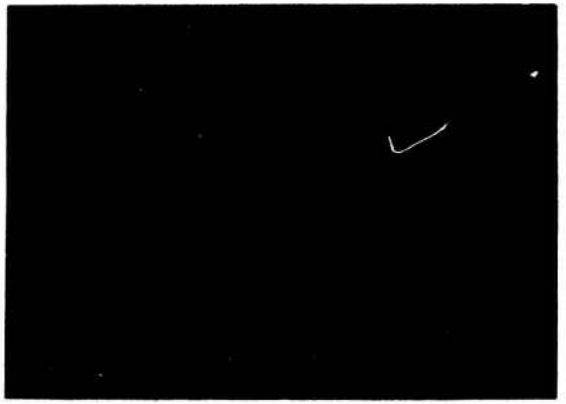

Fig. 8 - Voltage applied to the parallel plates. Vertical scale arbitrary units. Horizontal scale 200 nsec/Div

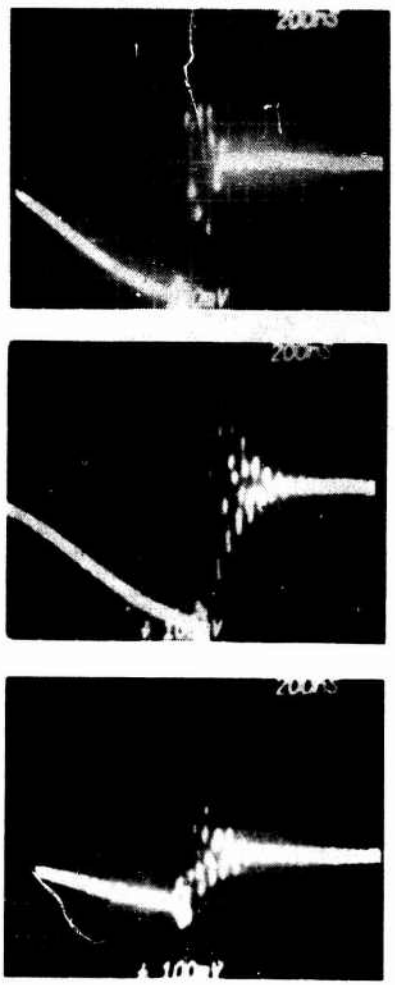

a) 20 mm Crystal —

200 $\frac{\text{mV}}{\text{Div}}$ at 200 $\frac{\text{ns}}{\text{Div}}$

b) 10 mm Crystal —

100 $\frac{\text{mV}}{\text{Div}}$ at 200 $\frac{\text{ns}}{\text{Div}}$

c) 5 mm Crystal —

100 $\frac{\text{mV}}{\text{Div}}$ at 200 $\frac{\text{ns}}{\text{Div}}$

Fig. 9 - A comparison of the response of different length BGO crystals to the same pulse

A LIGHTNING DATA ACQUISITION SYSTEM

B. M. Stevens, Jr. and T. A. Seliga
Aviation Safety Systems Project/3M
6530 Singletree Drive
Columbus, Ohio 43229-1119

ABSTRACT

The design, development, and implementation of a combined airborne data acquisition system and a ground based triangulation system - intended for use in gathering lightning strike data - is presented. The acquired data will be used in the characterization of lightning strokes, correlating to the test aircraft. Airborne data gathered will consist of a vertical electrical field signal, and an x, y, and z axis magnetic field signal (with respect to the aircraft). Each strike waveform will be accompanied by the exact time, and the aircraft position and heading so that correlation to the ground based triangulation data is possible. The acquisition system is relatively unique in that it is comprised largely of readily available, off the shelf sub-systems. A ruggedized IBM PC compatible computer, equipped with a 20 Megabyte ruggedized hard disk, a 60 Megabyte streaming tape drive, and commercially available memory boards (2 Megabytes per board) make up the majority of the system, requiring only the design of the individual analog to digital conversion channels and the high speed acquisition controller. This integration of standard sub-systems results in a considerable time and cost savings in the development of the system.

MODEL OF LIGHTNING FLASHES TRIGGERED FROM THE GROUND

Heinz W. Kasemir
Colorado Scientific Research Corp.
1604 S. County Rd. 15
Berthoud, CO 80513

ABSTRACT

The model is based on the electrostatic lightning theory discussed at previous conferences on lightning and static electricity and on experimental results of a series of triggered flashes at Kennedy Space Center 1984 and 1985.

The purpose of this investigation is to interrelate as many physical parameters of the triggered lightning as possible and to arrive at a consistent model, which can be used to access the danger of lightning discharges triggered inadvertently from launch towers, radiotransmission towers or other high buildings or constructions.

ELECTRON FLUID MODEL SIMULATIONS OF LIGHTNING RETURN STROKES

Z.-I. Kawasaki* and S. Israelsson

Institute of High Voltage Research, Uppsala University
Husbyborg, S-755 90 Uppsala, Sweden

ABSTRACT

Numerical simulations of lightning return strokes are carried out with the electron fluid model to understand both return stroke velocities and the dispersive characteristics of lightning return strokes. The two-step Lax-Wendroff method is applied to the simultaneous non-linear differential equations to simulate one dimensional return strokes. Using a measuring system of luminous components, optical signals emitted from return stroke channels have been observed during the triggered lightning experiments in Japan. It has been found that the mean value of return stroke velocities is almost one third of velocity of light in free space, which seems to be faster than both the drift velocity and the thermal velocity of electrons in the return stroke channels. Therefore, to understand such a high velocity one should consider the ionized potential wave. The simulation results of potential waves show that the tip velocity can progress almost one third of velocity of light. Moreover, the results also show the dispersive characteristics of the potential waves. It is concluded that the electron fluid model is useful to simulate the lightning return strokes.

* On leave from Research Institute of Atmospherics, Nagoya University, Toyokawa, Aichi 442, Japan

INTRODUCTION

IN THE PRESENT PAPER ONE DIMENSIONAL NUMERICAL SIMULATIONS of lightning return strokes are carried out using the electron fluid model. The two-step Lax-Wendroff method is applied to simulate return strokes in one component gas.

The processes of lightning return stroke can be described by a set of fluid equations for electron fluid together with Maxwell's equations for the fields [1]. It is assumed that since the electron fluid motions progress rapidly both the atoms and ions remain static, spatially uniform, and unheated far downstream from the wave-front.

In recent years, there has been a renewal of interest in the return stroke velocity measurements [2, 3, 4, 5, 6 and 7] which can be attributed to the need for not only understanding lightning physics but also a technical sense as well such as protection of facilities from lightning discharge. On the other hand, there are several papers on the characteristics of luminous signals, those are emitted from the lightning return stroke channels [8, 9 and 10]. It is considered that the application of microphysics of breakdown based on Plasma physics should be necessary to understand the above mentioned experimental results. That means, recent observed results of return stroke velocity is almost one third of light velocity in free space, which seems to be much faster than both the drift velocity and the thermal velocity of electrons in the return stroke channels. Moreover, Jordan and Uman reported the dispersive characteristics of luminous signals [8]. It is considered that the electron fluid model is suitable to simulate the lightning return strokes.

Jurenka and Barreto applied the theory of electron waves to discuss the dart leader [11]. They derived the analytical solutions and obtained the theoretically expected velocity. It seems that they obtained the agreement with the previous observed results, and they concluded that the electron fluid theory can be used to predict, for example, the structure of the dart leader, its current, and the variations of the luminosity. Nevertheless, as indicated in the preliminary report by one of the authors [12], electron fluid model is also suitable for the simulation of the lightning return stroke.

In the present paper, the electron fluid equations together with Maxwell's equation are computed numerically and the theoretical return stroke velocity is estimated. The dispersive characteristics is also simulated.

BASIC EQUATIONS

After Albright and Tidman [1], the return stroke can be represented by the following electron fluid equations together with Maxwell's equations.

$$\frac{\partial \vec{E}}{\partial t} = 4\pi e n_e \vec{u} \tag{1}$$

$$\frac{\partial n_i}{\partial t} = S \tag{2}$$

$$\frac{\partial n_e}{\partial t} = + \vec{\nabla} \cdot (n_e \vec{u}) = S \tag{3}$$

$$\frac{\partial}{\partial t}(n_e \vec{u}) + \vec{\nabla} \frac{n_e T}{m} + \vec{\nabla} \cdot (n_e \vec{u}\vec{u}) + \frac{e n_e E}{m} = -\nu n_e \vec{u} \tag{4}$$

$$\frac{\partial}{\partial t}\left(\frac{3}{2} n_e T + \frac{1}{2} m n_e u^2\right) + \vec{\nabla} \cdot \left(\frac{5}{2} n_e T \vec{u} + \frac{1}{2} m n_e u^2 \vec{u}\right) + + e n_e \vec{E} \cdot \vec{u} = -V_i S \tag{5}$$

where n_e and n_i are the electron and ion densities, S is the source term, $\vec{E}$ is the electric field, $\vec{u}$ is the electron drift velocity, ν is the momentum transfer collision frequency, T is the electron temperature, and V_i is the ionization potential of the neutral gas. Though this model is developed for the streamer progression, it is assumed that the return stroke are also well simulated with this model. In other works, considering the situation just before a final jump of a return stroke, the local electric field between the tip of a leader channel and the ground is quite strong and the return stroke is considered to be the development of the potential difference from the ground to the cloud.

As indicated by Albright and Tidman [1], the ionizing potential wave, represented by eqs. (1)-(5), travels so rapidly that ions and neutrals do not have time to be heated before the wave-front has passed on. Since the only energy loss mechanism for electron is ionization, the locally intense electric field is the source of energy for ionization of neutrals and heating electrons.

Eqs. (1)-(5) are the simultaneous nonlinear differential equations and it is impossible to obtain the analytical solutions. Moreover, even if the numerical calculation scheme is applied, it is not so easy to obtain the numerical result due to the numerous machine time and so on. Thus it is concluded that the some assumptions are needed to simplify the equations. Since the electron drift velocity is small compared with its thermal velocity, it is reasonable to neglect the higher order term of the drift velocity, $\vec{u}$. Still more in order to carry out the numerical simulation, it is convenient to scale the equations by the following dimensionless variables following Albright and Tidman faithfully.

$$n = n_e / n_{e_0} \qquad \vec{\varepsilon} = \vec{E} / |\vec{E}_1|$$

$$\tau = \Omega t \qquad \vec{\xi} = \Omega \vec{\alpha} \gamma |\vec{u}_1|$$

where n_{e_0} is the initial downstream electron density, $\vec{E}_1$ is the initial upstream electric field vector, and

$$\vec{u}_1 = - e \vec{E}_1 / m \nu$$

$$\gamma = \left(\frac{5}{2} T_0 + V_i\right) / \left(\frac{3}{2} T_0 + V_i\right)$$

$$\Omega = (e E_1)^2 / 2 m \nu \left(\frac{3}{2} T_0 + V_i\right)$$

It should be noted that the subscript 0 denotes limiting values, downstream, and the subscript 1 upstream limit. Then the following equation are derived.

$$\frac{\partial \vec{\varepsilon}}{\partial \tau} = a_1 n \vec{u} \tag{6}$$

$$\frac{\partial n}{\partial \tau} = a_2 \vec{\nabla} \cdot (n \vec{u}) + S \tag{7}$$

$$\frac{\partial (n\vec{u})}{\partial \tau} = a_3 \vec{\nabla} (nT) + a_4 n \vec{\varepsilon} + a_5 n \vec{u} \tag{8}$$

$$\frac{\partial (nT)}{\partial \tau} = \frac{5}{3} a_2 \vec{\nabla} \cdot (nT\vec{u}) + \frac{2}{3} a_6 n \vec{\varepsilon} \cdot \vec{u} - \frac{2}{3} V_i S \tag{9}$$

$$a_1 = 4\pi e n_{e_0} / |E_1| \Omega \qquad a_2 = -1/\gamma |u_1|$$

$$a_3 = a_2 / m \qquad a_4 = - e |E_1| / m \Omega$$

$$a_5 = -\nu / \Omega \qquad a_6 = m a_4$$

The Eqs. (6)-(9) can be solved as an initial value problem by using the two-stop Lax-Wendroff scheme. Actually, the initial condition can be determined, if the final situation of a lightning stroke is considered very carefully. Nevertheless, another difficulty for carrying out the numerical simulations is remained, that is, what is the reasonable source generation term, S? It is considered that the more reliable measurements related to the change generation mechanism is needed in order to obtain the physically meaningful numerical results.

The assumption of constant temperature can eliminate the charge generation term S and the numerical simulation of the return stroke can be easily carried out. In Figure 1 we show the simulation results, of the potential wave as the return stroke for the initial channel temperature of 20 000°K and 40 000°K and the channels consisted of only nitrogen gas for which the ionization threshold is about 17ev. For the initial condition, the electric field intensity at the tip of the potential wave is assumed to be 5×10^5V/m. We can recognize the dispersive characteristics of potential wave as the return stroke.

We can find that the initial potential difference which corresponds to the left most curve in Figure 1 is propagated with deformations to the direction indicated by the arrow. Moreover the higher the temperature of the return stroke channel, the more deformation of the potential is caused and the higher "the tip velocity" becomes. The theoretical "tip velocities" of these simulations simulations are respectively 1.3×10^8m/sec. and 1.5×10^8m/sec. It should be noted that these theoretical values are very close to the values obtained with measured luminous signals during triggered lightning experiments [12]. It is obvious that the theoretical values depend on initial conditions, such as the electric field intensity and channel temperature etc. Further numerical results for Eqs. (6)-(9) will be presented at the conference.

CONCLUSION

In the present paper, the lightning return stroke was simulated numerically with the electron fluid equations together with Maxwell's equations. The two-step Lax-Wendroff scheme was applied and the theoretical return stroke velocity was estimated. The theoretically expected return stroke velocity was very close to the experimentally observed results. The dispersive characteristics were also simulated. It was concluded that the electron fluid model is useful to simulate the lightning return stroke.

ACKNOWLEDGEMENTS

The authors wish to thank Prof. S. Lundquist for his valuable discussions. The first author's stay in Uppsala during this work was financed by the Swedish Natural Science Research Council. Finally the author thanks M. Björklund for typing of this paper.

REFERENCES

1. N.W. Albright and D.A. Tidman, "Ionizing potential waves and high-voltage breakdown streamers." Phys. Fluids, 18, 86-90. 1972.

2. J.S. Boyle and R.E. Orville, "Return stroke velocity measurements in multistroke lightning flashes." J. Geophys. Res., 81, 4461-4466. 1976.

3. P. Hubert and G. Mouget, "Return stroke velocity measurements in two triggered lightning flashes." J. Geophys. Res., 86, 5253-5261. 1981.

4. V.P. Idone and R.E. Orville, "Lightning return stroke velocities in the Thunderstorm Research International Program (TRIP)." J. Geophys. Res., 87, 4903-4915. 1982.

5. T. Nakano., T. Takeuti., Z.-I. Kawasaki and N. Takagi, "Leader and return stroke velocity measurements in lightning from a tall chimney." J. Meteorology. Soc. Japan, 61, 339-345. 1983.

6. V.P. Idone., R.E. Orville., P. Hubert., L. Barret and A. Eybert-Berard, "Correlated observations of three triggered lightning flashes." J. Geophys. Res., 89, 1385-1394. 1984.

7. Z.-I. Kawasaki., M. Nakano., N. Takagi., T. Takeuti and T. Nakai, "Tip velocity of subsequent return strokes in triggered lightnings." Submitted to J. Geophys. Res., 1986.

8. D.M. Jordan and M.A. Uman, "Variation in light intensity with height and time from subsequent lightning return stroke." J. Geophys. Res., 88, 6555-6562. 1983.

9. Y. Kito., K. Horii., Y. Higashiyama and K. Nakamura, "Optical aspect of winter lightning discharges triggered by the rocket-wire." Technique in Hokuriku District of Japan. J. Geophys. Res., 90, 6147-6157. 1985.

10. V.P. Idone and R.E. Orville, "Correlated peak relative light intensity and peak current in triggered lightning subsequent return strokes." J. Geophys. Res., 90, 6159-6164. 1985.

11. H. Jurenka and E. Barreto, "Electron waves in the electrical breakdown of gases, with application to the dart leader in lightning." J. Geophys. Res., 90- 6219-6224. 1985.

12. Z.-I. Kawasaki., M. Nakano., T. Takeuti and T. Nakai, "Group velocity of lightning return stroke currents." In proceedings 10th International Aerospace and Ground Conference on Lightnings and Static Electricity, Paris, June 10-13 (1985).

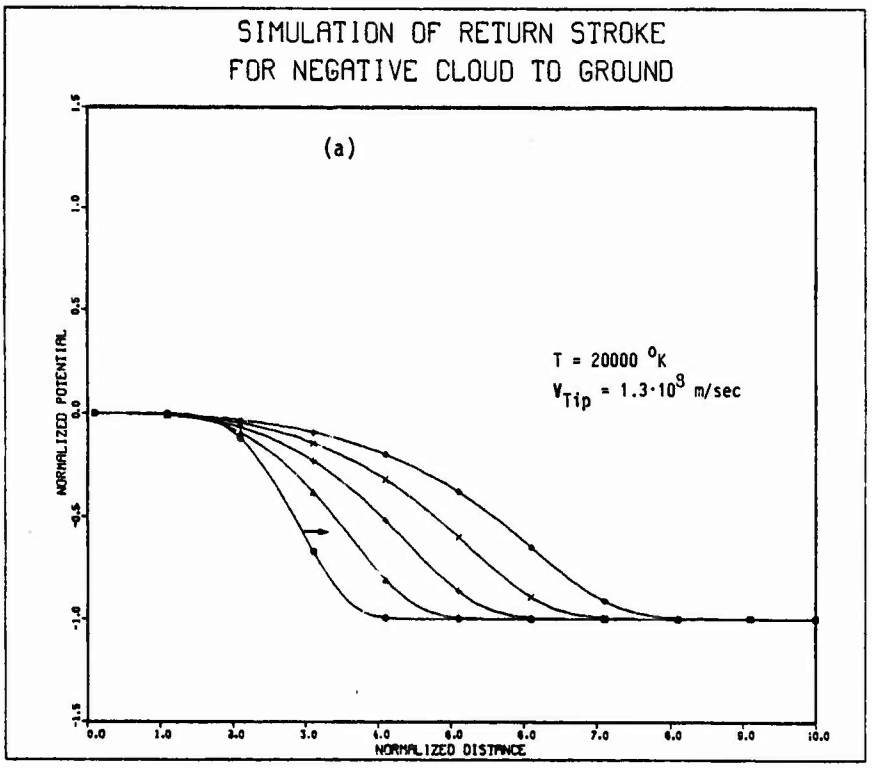

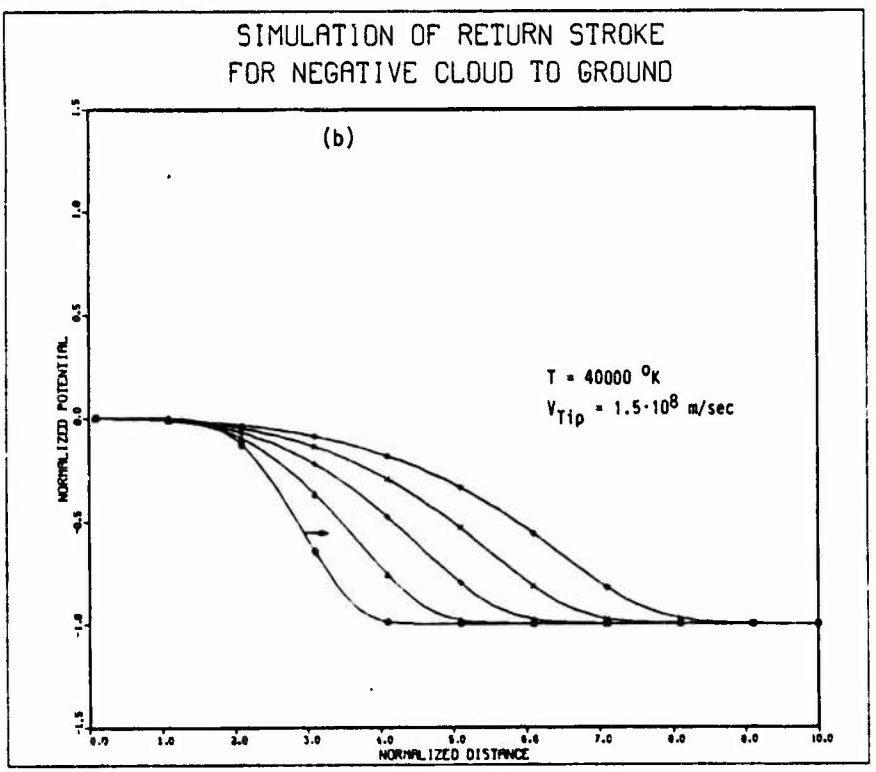

Figure 1. Simulation results of the potential wave as the return stroke. The arrows in the figure indicate the directions to which the potential wave are propagated. The simulation results show the dispersive characteristics of the potential wave. The temperatures of return stroke channel are (a) 20 000°K and (b) 40 000°K, respectively.

CALCULATION OF ELECTROMAGNETIC FIELDS FROM THE LIGHTNING RETURN STROKE USING THE CHARGE SIMULATION METHOD

P.R.P. Hoole
Wolfson College, Oxford OX2 6UD, U.K.

S.R.H. Hoole
Dept. of Electr. and Comp. Eng.
Drexel University
Philadelphia, U.S.A.

ABSTRACT

The authors have previously reported the use of finite element method to calculate the magnetic fields radiated from the leader and return strokes. The finite element method offers a compact, user friendly and highly efficient computer package which may be used for many electrical, mechanical and civil engineering problems. When the user does not possess an interactive, micro-computer system there is a need for a simple (i.e. easily programmable) field calculation procedure using the integral formulation. The integral formulation methods currently used involve intractable mathematics and are limited to straight, vertical conductors. Furthermore, these methods are highly inaccurate for electric field calculations, because the charges deposited along the leader channel are ignored. In this paper the authors propose a simple, semi-analytical method for determining electric and magnetic fields radiated from the transient current surge associated with the return stroke; point and line elements are used to simulate the lightning phenomenon. Electric and magnetic fields are calculated for (1) the transmission line model (2) tortuous lightning channel (3) a straight, vertical lightning channel with a branch. We also report for the first time a comparison between the electromagnetic field radiated from a straight lightning channel and a channel with a complex geometry.

IMPLEMENTATION OF GEMACS FOR LIGHTNING INTERACTIONS ANALYSIS

Dr Edgar L. Coffey
Advanced Electromagnetics
Albuquerque, New Mixico

1Lt James L. Hebert
Air Force Wright Aeronautical Laboratories (AFWAL/FIESL)
Wright-Patterson Air Force Base, Ohio

ABSTRACT

A powerful U.S. Air Force resource "The General Electromagnetic Model for the Analysis of Complex Systems (GEMACS)" has been implemented for the snalysis of lightning's interaction with aircraft. This user-friendly snd well-documented computer code incorporstes the Method of Moments (MOM), and Geometricsl Theory of Diffraction (GTD) and a MOM/GTD hybrid solution technique. This code was selected for the prediction analysis in the U.S. Air Force's Atmospheric Electricity Hazards Protection Advanced Development Progrsm to provide the skin current distributions on sn advanced composite helicopter testbed.

GEMACS contsins geometrical, physics, snd mathematical techniques necessary to model the exterior of a complex airframe at lightning frequencies. The structure is divided into a number of wire mesh or pstch elements (or both). Surface conductivity is added in vis skin effect conductivity or lumped loads. Surfsce currents sre obtained vis the solution of simultaneous equetions or by e banded matrix iterative method. Both near and fer fields may be computed from the surfece currents.

While the present version of GEMACS is limited to exterior problems, a newer version of GEMACS is scheduled for release in eerly 1986. It will include all the cepebility of the present version plus the ability to calculste lightning coupling to cevities due to the penetration of lightning energy through arbitrsrily shsped epertures snd the coupling of those cavity fields onto thin wires within the cevity.

The peper will present predictions of lightning coupling to sircreft using GEMACS. Emphasis will be on ease ot use, including generstion of structure geometry, selection end set-up of physics, and computation of surfsce currents. Exemples will include free-field and direct attechment coupling end perfectly conducting versus finite conducting airframes.

The broad epplicability of GEMACS to e number of electromagnetic problems allows the integration of the enalysis of many EM effects into s unified geometricsl, physics, computationsl, end management plan. Though the emphasis of the peper is on lightning coupling predictiona, the paper will elso endeavor to illustrste how much efficiency end effectiveness cen be geined by using the seme GEMACS lightning model for other EM Predictions as well.

INTRODUCTION

Several recent developments have resulted in an increased intereat in the computer aided electromagnetic (EM) analysis of the electromagnetic interaction of lightning with aircraft. The rapid introduction of advanced compoaite materials and sophisticated low level flight and miasion critical electronic circuits into aeroapace vehiclea has raised concerns that these may increase the vehicle'a inherent suaceptibility/vulnerability to lightning electromagnetically induced damage or upaet. Data from the recent NOAA/AFWAL WC-130 (1,2), NASA F-106 (3), and FAA/AFWAL CV-580 (4) in-flight lightning characterization programs have shown the lightning threat environment to have significant apectral content in the aircraft reaonant regione 2 - 20 MHz (5). The lightning protection requirements levied by the U.S. Air Force are becoming better defined and organized with the introduction of MIL-STD-XXXX, "Lightning Protection of Aerospace Vehicles and Hardware", currently under review by the U.S. Air Force under advisement of the SAE AE4L Committee (6,7). The requirementa for lightning protection and protection from other electromagnetic threata such as NEMP and for electromagnetic compatibility combined with those for lighter aircraft poasessing enhanced capabilitiea presents a formidable task for the electromagnetic analysts and aircraft designers. Balanced protection for all EM threata must be provided with the minimum of additional weight and coats. Theae and other aimilar developments emphaaize the neceasity for accurate computer-aided electromagnetic interaction analytical toola for the protection design of tomorrow'a aeroapace vehicles.

To aimplify the complicated analysis of the aircraft and lightning electromagnetic interaction event, the interaction is often conceptually divided into the aub-problems or processes of external interaction and internal interaction (8,9,10,11). The external interaction analyzes aircraft's interaction with the lightning channel whereas, the internal interaction analyzes the coupling, propagation, and penetration of the energy into the internal aystem circuits. It is well recognized that theoretically these processes are not independent especially when apertures are electrically large with respect to the wavelength of the EM threat (8,9); however, when the mutual coupling between the processea is weak (i.e., the internal components do not greatly affect the external charge and current distributions), the analysis is greatly simplified by decoupling the external and internal interaction processes.

A large number of electromagnetic codes have been developed to assist in the analysis of external interaction of electromagnetic threats with aircraft using this "weak coupling" assumption. Bevensee et. al. presented a thorough review of those which are used to model EMP interaction and coupling (12), and Eriksen, Rudolph, Perala, and Corbin have presented a similarly thorough review of those codes which are applicable to the lightning/aircraft interaction event (13,14).

The Air Force's Atmospheric Electricity Hazards Protection Advanced Development Program (15,16) reviewed many of these codes in their search for an electromagnetic code suitable for aerospace vehicle lightning protection analysis and design. They, like Bevensee et al. (12), found that; although a large number of computer codes exist which are applicable to lightning and EMP interaction and coupling, the problems which the codes could address were too specific: Moreover, certain codes were better suited at solving one particular EM problem and poorly suited to solve any others. Also, most people did not have all of these codes at their disposal nor do they have the facilities or resources to maintain a large number of codes. These factors led to their selection to have the RADC GEMACS code modified and implemented for lightning interaction analysis.

GEMACS is a centrally maintained general purpose EM code applicable to a wide class of EMP problems. This paper discusses the GEMACS code and its modification and implementation for lightning interactions analysis.

GEMACS

The General Electromagnetic Model for the Analysis of Complex Systems (GEMACS) electromagnetic code is discussed in detail in two publications by K.R. Siarkiewicz (17, 18). What follows is a general overview of those aspects of the code which make it particularly attractive for the analysis of the lightning/aircraft electromagnetic interaction.

Resident within the single GEMACS code are three widely used and fairly general physics formulations which: give the code broad applicability to a number of electromagnetic problems; and allow the integration of the analysis of many EM effects into a unified geometrical, physics, computational, and management plan. These physics formulations include: (1) the method of moments (MOM) (low frequency model) which applies to analysis of an aerospace vehicle's interaction with EM phenomena whose wavelength is large compared to the vehicle, or at most a little smaller than the wavelength which corresponds to the vehicle resonant region; (2) the geometrical theory of diffraction (GTD) (high frequency model) which applies to the analysis of aerospace vehicle'a interaction with EM phenomena whose wavelength is small compared to the vehicle; (3) and a hybrid MOM/GTD formulation which allows MOM analysis of small structures (e.g. Antennas, POEs, etc.) located on aerospace vehicles which are electrically large. These formulations have allowed wide application of the GEMACS code to electromagnetic problems dealing with: EMP, EMC, ECM, ECCM, radar cross section, jamming susceptibility, antenna performance, EM radiation and scattering, and most recently to the analysis of the lightning/aircraft interaction. The MOM technique is the one best suited for lightning.

GEMACS is a user friendly, well documented computer code. GEMACS requires that the electromagnetic interaction analyst grid the aircraft into a number of wire mesh or patch elements (or both) for low frequency (MOM) modelling and into a cylinder and plate structure for the high frequency (GTD) model. While this may be formidable task the reader is reminded that: (1) this data may already be available from a CAD/CAM data base, and (2) this same geometrical representation of the aerospace vehicle can be used to solve a number of EM related problems. Surface conductivities are entered either as skin effect conductivity or as lumped loads. The analyst then chooses the physics and mathematical techniques he/she desires to be utilized to solve the problem at hand. Surface currents on the aerospace vehicle are obtained from a MOM physics formulation via the

solution of aimultaneoua equations or by a banded matrix iterative methods. Once the analyst has chosen the type of output he desired (whether skin currenta for external interaction problem or scattered electromagnetic near or far fields), he/she runa the program. From that point on, the phyaics and mathematics are tranaparent to the uaer. These procedurea allow the gridding of the problem by personnel with little or no electromagnetic background and freea the analyst to conaider the more detailed aapects of the electromagnetic problem. For those who desire a more detailed knowledge of the code or those who wiah to apply the code to uaes not already tried and proven, the code is accompanied by readily available detailed documentation. These include a user's manual (19), an engineering manual (20), and a four volume set of code documentation designed to aatisfy the most demanding code mechanic (21).

Other hallmarka of the CEMACS code are: its ability to run on a number of computer systems; its central manegement; and, its ready availability. All coding in GEMACS is in FORTRAN (ANSI Standsrd 1977) and it utilizes no non-ANSI atandard utilities or functions, no overlaying, no graphica packages or other such options which could restrict the transfer of the computer program from one main frame computer to another. The code is currently is uae on aeveral VAX, CYBER, CRAY, IBM and HONEYWELL computera. The Rome Air Development Center (RADC/RBCT) and specifically K.R. Siarkiewicz is the central agency for the diatribution, debugging, and information diaaemination for the GEMACS code. The use of a aingle agency for these purpoaes provides a certain amount of confidence that the latest and beat data regarding GEMACS are available quickly and accurately (18). The FORTRAN aource code for GEMACS is readily available at no coat from K.R. Siarkiewicz at RADC/RBCT who may be contacted at 315-330-2465 (18).

IMPLEMENTATION FOR LIGHTNING INTERACTION ANALYSIS

The Air Force's AEHP ADP had the GEMACS code modified to run on the Aeronautical System Division's CDC 845 computer and implemented for analyzing the electromagnetic interaction of lightning with an advanced all composite helicopter. This modification and implementation and analysis was performed by The BDM Corporation (under ASD/PMRNA contract F33615-83-C-3000). What follows is a summary of the results from this effort as reported in the final BDM Corporation report on this GEMACS modification, implementation, and snalysis (22).

The GEMACS code (Version 3 dated July 1985) was obtained from RADC along with a gridded Blackhawk helicopter model and aeveral test case routines. The code was installed after minor modifications of computer specific routines on the ASD CDC 845 computer. The exact modifications required are detailed in the above mentloned report as well as detailed procedures on how to run the program on the CDC. The code was then used in a preliminary analysis of an all composite, ACAP, helicopter.

Figure 1 presents a graphic representation of the simple wire model of the helicopter which was developed for this analysis. This model is applicable from about 0.5 MHz to 10 MHz snd each segment is less than the required shortest wavelength divided by 10. At low frequencies (below 1 MHz) the entire helicopter is smaller than a wavelength and the resulting current distribution was essentially the static current diatribution. At still lower frequenciea, the radius of each segment, which was chosen to be 1/2 the length, becomes very small in relation to the wavelength resulting in numerical errors. The model presented was valid for the range of 0.5 MHz to 5 MHz, the range for which the preliminary analysis was performed. Composite models of the helicopter were easily formed by loading or changing the conductivity of each segment in the helicopter model. During this effort, the conductivities considered were all metal and all composite (with a conductivities of 100 mhos/m and 1000 mhos/m).

During this effort two lightning channel models were discussed. One was actually implemented while the other was offered as an alternative lightning aource model. The implemented aource was modelled aa a long thin conductor attached to the helicopter as illustrated in Figure 2. The stated reason for the selection of thia aource was that it models the two coupling phenomena: (1) field coupling due to the lightning channel in the atmosphere and (2) current coupling at the attachment/exit point of the helicopter. The length of both the entry and exit channels were approximately 20 times the length of the helicopter. Lightning currents were excited into the far ends of the lightning channel model by delta-gap voltage sources.

An alternative channel model was presented which although not fully tested in this effort would serve as a starting point for adding a current source to GEMACS without modification to the code. In this method, illustrated for the nth aegment in Figure 3, a current source is added to CEMACS by finding equivalent delta-gap voltages for each segment connected to a current driven node (source segmento). These delta-gap voltages are converted to an incident electric field at the center of each source segment. GEMACS then using MOM solves for the current in the segment and the resulting scattered fields based upon its interaction matrix. The Z_{nn} term is for the nth segment, and the Z_{ni} term is a current dependent voltage source in mutual terms. If one node of this segment is driven by a current source, it requires that an incident electric field be determined for that aegment. This is illustrated in Figure 4.

A more general case would be a current source exciting several segments at a node. The current in each segment is found by a current divider based on the admittance of the segments being driven. This is illustrated in Figures 5 and 6. Delta-gap voltage sources and the incident electric field at the center of each term is determined by the segment's interaction matrix term Z_{ij}, the current to be injected J_j, and mutual terms Z_{ij} as

$$-V_i = J_i Z_{ii} l_i + \sum_{j=1} Z_{ij} l_i J_j \qquad \text{(delta-gap)}$$

and

$$E_i = J_j Z_{ij} \qquad \text{(incident field)}$$

Once these delta-gap voltage sources are found for each driven segment, the current diatribution is found on the helicopter by inputting voltage sourcea into the input deck of GEMACS.

An example of the input deck for a long wire run on the helicopter for a metal aircraft and a composite helicopter (with a conductivity of 100 mhos/m and

1000 mhos/m) for 10 frequencies, 0.5 MHz spart, beginning at 0.5 MHz is presented in Figure 7. An example of the results for one run at 2.0 MHz is presented in Figure 8.

The results of the preliminary analysis on the ACAP wire grid helicopter model found that for a main rotor attachment, the current distributiona were more dependent on the aircrsft geometry and resonant frequencies than on the exit point. At frequencies below 2.0 MHz, the distribution was fairly uniform indicating that the aircraft was approaching the static current distribution. In this case, the current distribution could roughly be estimated by lumped circuit analysis of the circuit. At and near the quarter wsvelength resonsnt frequency of the model, 4.5 MHz, the current became much higher than would be expected if only standing waves were present. At 8 and 8.5 MHz, the currents were again somewhat smaller than at reasonance. The conductivity of 100 mhos/m and 1000 mhos/m made little impact on the current distribution. At the frequencies analyzed, this might have been expected because composite materials with these conductivities behave like good conductors above 50 kHz. Basically with all three conductivities, at lower frequencies the current distribution is more uniform than at higher frequencies. As frequency increases, more standing waves form resulting in more currents being distributed along the helicopter. The largest currents form at the front of the helicopter and at the end of the main body.

ON-GOING EFFORTS WITH GEMACS

As with all electromagnetic codes and analysis of the aircraft/lightning interaction, there is a lack of compariaon with the actual natural lightning strike case. A cooperative effort between the AEH Group of AFWAL and the Air Force Institute of Technology has begun in which a GEMACS analysis of the interaction of lightning with a CV-580 aircraft will be compared with actual lightning strikes to that aircraft.

To facilitate an increased user friendliness and speed the application of GEMACS to a variety of EM problems by many organizations, RADC is planning a self tutorial training book which presents examples of how to apply GEMACS to a variety of problems.

The final development is a tremendous increase in GEMACS capabilities by the inclusion of modules which allow the finite difference (FD) analysis of cavities and apertures and a MOM/GTD/FD hybridization to allow the self-consistent analysis of the EM interaction from the source to the aperture, through the aperture, and inside the compartments of aerospace vehicles.

SUMMARY

GEMACS has been shown to be a powerful, user friendly, system independent, well-documented, and readily available general purpose electromagnetic code applicable to solve several of the serious EM problems facing the analyst and designers of aerospace vehicles. At the direction of the AEHP ADP, the code has been modified and implemented to allow the analysis of the aircraft/lightning electromagnetic interaction event. This capability was demonstrated with the preliminary analysis of the ACAP all composite helicopter. GEMACS is a continually evolving code which is being enhsnced to solve other EM problems including the external to internal interaction through apertures.

REFERENCES

1. P.L. Rustan, B.P. Kuhlman and M.J. Reszer, "Airborne Measurements of the Risetimes in Lightning Return Stroke Fields", Proc. of the 8th Internationsl Aerospace and Ground Conference on Lightning and Static Electricity in Ft. Worth, TX, June 21-23, 1933.

2. B.P. Kuhlman snd M.J. Reazer, "Characterization of Fast-Risetime Electromagnetic Field Pulses recorded in Airborne Messurements during Florida Thunderstorms", Proc. of the 9th International Aerospsce snd Ground Conference on Lightning snd Static Electricity held in Orlando, Florida, June 26-28, 1984.

3. F.L. Pitts, "Electromagnetic Measurement of Lightning Strikes to Aircraft", J. Aircraft, Vol. 19, No. 3, March 1982.

4. P.L. Rustan and J. Moresu, "Aircraft Lightning Attachment at Low Altitudes", Proc. of the 10th International Aerospace snd Ground Conference on Lightning and Static Electricity held in Paris, France, June 10-13, 1985.

5. R.A. Perala, T. Rudolph and F. Eriksen, "Electromagnetic Interaction of Lightning with Aircraft", IEEE Trans. on Electromagnetic Compatibility, Vol. EMC-24, No. 2, May 1982.

6. Mil-Std-XXXX, "Lightning Protection of Aerospace Vehicles and Hardware", Currently in draft form under review by the U.S. Air Force, Revised copy dated 10 February 1986.

7. Peraonal Communications with L.C. Walko and R.C. Beavin, members of the SAE AE4 Committee.

8. F.M. Tesche, "Topological Concepts for Internal EMP Interaction", IEEE Trans. on EMC, Vol. EMC-20, No. 1, February 1978.

9. R.A. Perala, T. Rudolph and F. Eriksen, "Electromagnetic Interaction of Lightnig with Aircraft", IEEE Trans. on Electromagnetic Compatibility, Vol. EMC-24, No. 2, May 1982.

10. K.S.H. Lee (Editor), et. al., "EMP Interaction: Principles, Techniques and Reference Data", EMP Interaction Note 2-1, Air Force Weapons Laboratory Technical Report, AFWL-TR-80-402, Kirtland AFB, NM, December 1980.

11. D.T. Auckland, R.F. Wallenberg and J.A. Birken, "Modelling of Direct-Strike Lightning coupling by a Transform Function Technique", Proc. of the 8th International Aerospace and Ground Conference on Lightning and Static Electricity held in Ft. Worth, TX, June 21-23, 1983.

12. R.M. Bevensee, J.N. Brittingham, et. al., "Computer Codes for EMP Interaction and Coupling", IEEE Trans. on EMC, Vol. EMC-20, No. 1, February 1978.

13. F.J. Eriksen, T.H. Rudolph and R.A. Perala, "Atmospheric Electricity Hazards Analytical

Model Development and Application; Vol. III: Electromagnetic Coupling Modelling of the Lightning/Aircraft Interaction Event", Air Force Wright Aeronautical Laboratories Technical Report, AFWAL-TR-81-3084, Vol. III (Performed by Electro Magnetic Applications, Inc.), Wright Patterson AFB, OH 45433.

14. F.J. Eriksen, R.A. Perala, and J.C. Corbin, "State-of-the-Art Methods for Computing the Electromagnetic Interaction of Lightning with Aircraft", NASA Conference Publication 2128, FAA-RD-80-30, Proceedings of Technical Symposium held at NASA Langley Research Center, Hampton, Virginia, April 22-24, 1980.

15. J.R. Lippert, "Vulnerability Assessment of Electricity/Electronic Subsystems and Equipment to Atmospheric Electricity", Proceedings of the 8th International Aerospace and Ground Conference on Lightning and Static Electricity held in Ft. Worth, TX, June 21-23, 1983.

16. R.C. Beavin, J.R. Lippert, and Lt J.E. LaVoie, "Progress of the Atmospheric Electricity Hazards Protection Program", Proceedings of the 9th International Aerospace and Ground Conference on Lightning and Static Electricity held in Orlando, FL, June 26-29, 1984.

17. K.R. Siarkiewicz, "An Introduction to the General Electromagnetic Model for the Analysis of Complex Systems (GEMACS)", RADC-TR-78-181, September 1978, AD 060319.

18. K.R. Siarkiewicz, "GEMACS - An Executive Summary", Conference on Electromagnetic Compatibility, 1985.

19. D.L. Kadlec and E.L. Coffey, "General Electromagnetic Model for the Analysis of Complex Systems (GEMACS) User Manual (version 3), "The BDM Corporation, RADC-TR-83-217, Volume I, September 1983, AD A137461.

20. D.L. Kadlec and E.L. Coffey, "General Electromagnetic Model for the Analysis of Complex Systems (GEMACS), Engineering Manual (Version 3), "The BDM Corporation, RADC-TR-83-217, Volume II, September 1983, AD A137462.

21. D.L. Kadlec and E.L. Coffey, "General Electromagnetic Model for the Analysis of Complex Systems (GEMACS) Computer Code Documentation (Version 3)", The BDM Corporation, RADC-TR-83-217, September 1983, AD A137463, AD A137464, AD A137509, and AD A137510.

22. B.E. Gindelberger, G. Salo, and G.H. Lamb "GEMACS Modification, Implementation, and Analysis for AFWAL/FIEA, Final Report", The BDM Corporation, Air Force Wright Aeronautical Laboratories Technical Report, currently in publication, AFWAL/FIEA, Wright-Patterson AFB, OH 45433.

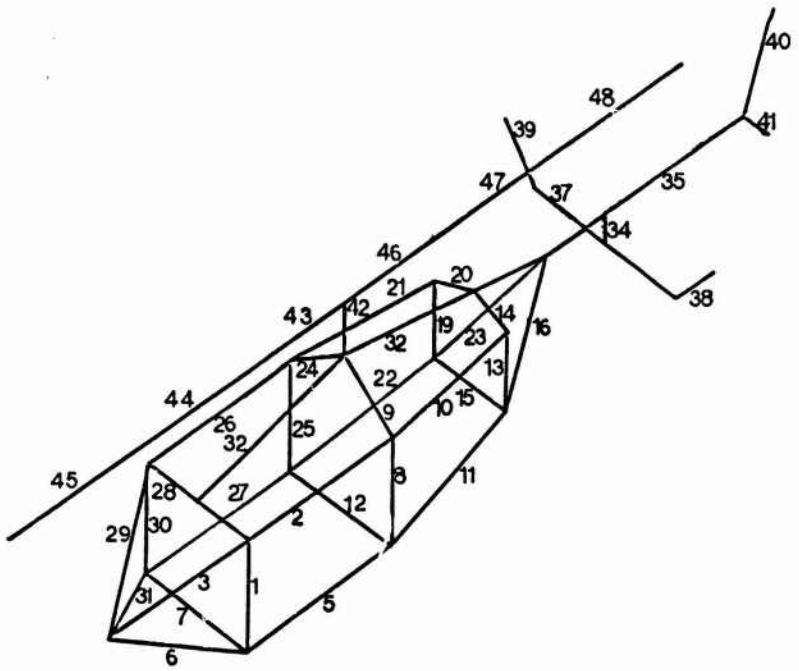

Figure 1. Simple Wire Model of the ACAP Helicopter (Segments Numbered).

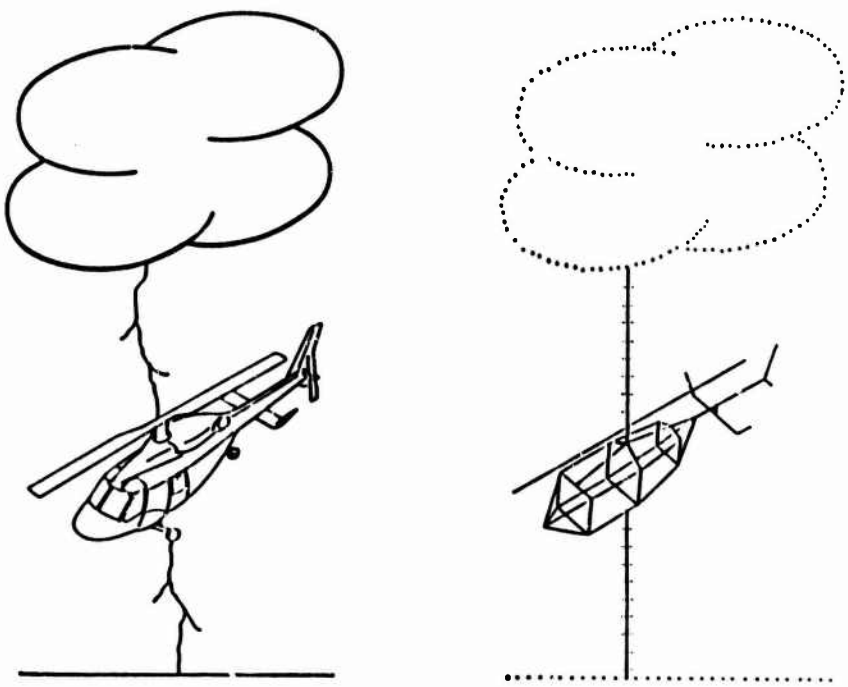

Figure 2. Thin Wire Model of Lightning Channel

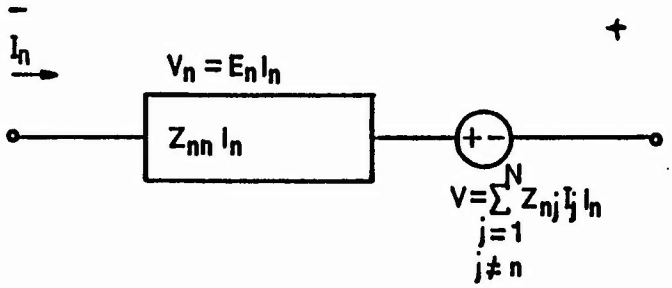

Figure 3. Equivalent Circuit Model of the nth Segment.

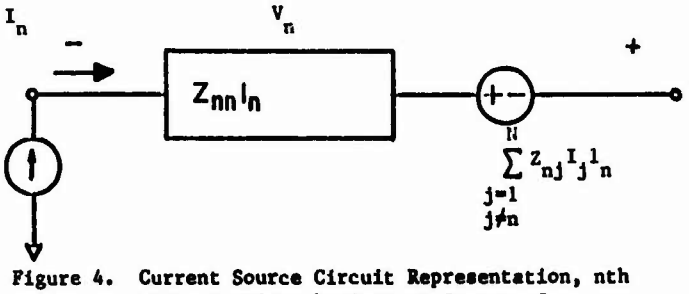

Figure 4. Current Source Circuit Representation, nth Segment Driven by Current Source, J_s.

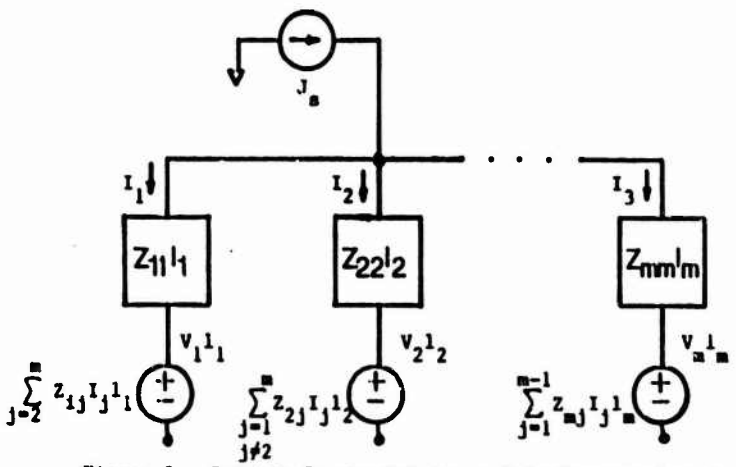

Figure 5. Current Source Driving a Node Connected to m Segments.

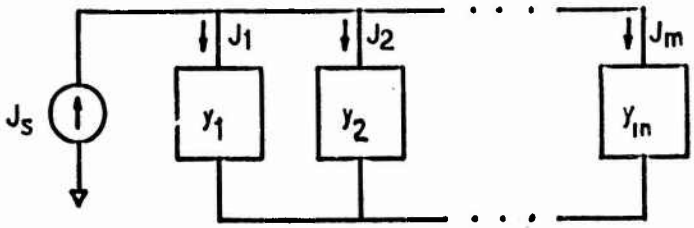

Figure 6. Current Flow Diagram. (Flow determined by input admittance of each segment.)

```
NFIL=23
TIME=1000
FRQ=0.5
SETI MM
GMDT=HELI
LOOP 1,10
VIN=VSRC(HELI),V=1.,0., SEGS=1,248
ZGEN GMDT=HELI,ZMAT=ZHELI
BZH=BAND(ZHELI), BNDW=48
LBZ=LUD(BZH)
LBZ*I=VIN-ZHELI*I, MXIT=5, CNVG=PRE, VALUE=10
PURGE ZHELI,BZH,LBZ
PRINT I
ZLDS=ZL1,GMDT=HELI,COND=100.0,SEGS=1-48
ZGEN GMDT=HELI,ZMAT=ZHELI,ZLDS=ZL1
BZH=BAND(ZHELI), BNDW=48
LBZ=LUD(BZH)
LBZ*I=VIN-ZHELI*I, MXIT=5, CNVG=PRE, VALUE=10
PURGE ZHELI,BZH,LBZ
PRINT I
ZLDS=ZL2,GMDT=HELI,COND=1000.0,SEGS=1-48
ZGEN GMDT=HELI,ZMAT=ZHELI,ZLDS=ZL2
BZH=BAND(ZHELI), BNDW=48
LBZ=LUD(BZH)
LBZ*I=VIN-ZHELI*I, MXIT=5, CNVG=PRE, VALUE=10
PURGE ZHELI,BZH,LBZ,ZHELI
PRINT I
FRQ=FRQ+0.5
LABEL 1
END
```

Figure 7. Example of an Input Deck for the ACAP Preliminary Analysis.

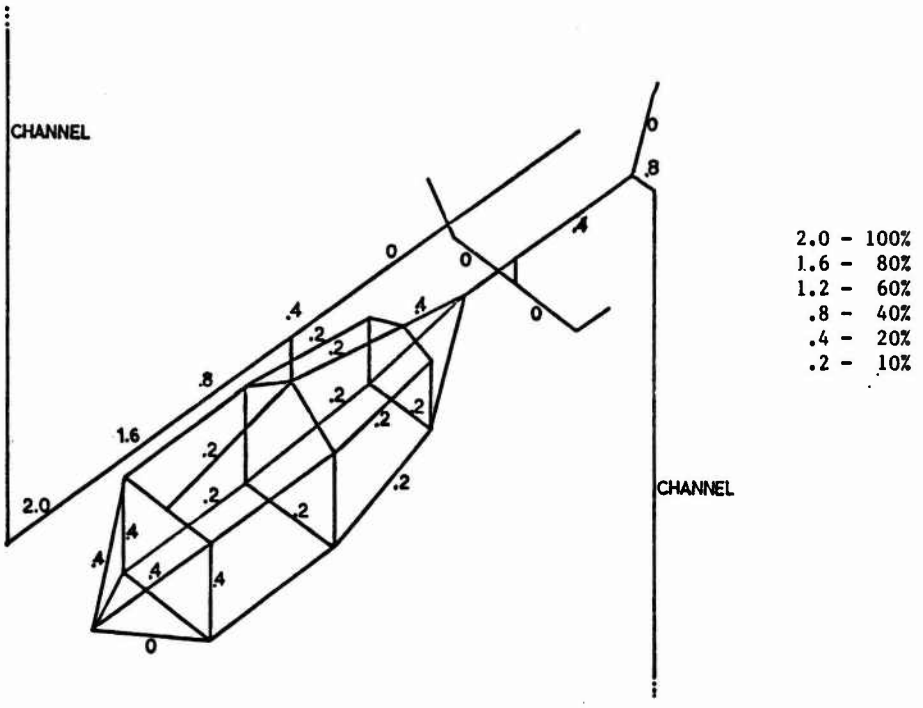

Figure 8. Current Distributions (Source attached at end of rotor blade, exit at tail) for 2 MHz.

LIGHTNING CURRENT REDISTRIBUTION

W. P. Green
Science snd Engineering Associates, Inc.
701 Dexter Ave. N.
Seattle, Washington 98103

ABSTRACT

The distribution of current throughout an aircraft receiving a direct strike is an important factor in lightning protection design. This problem was analyzed by Fisher snd Burrows for metallic structures of constant cross-section. Their approach wss to segment the structure into longitudinal strips, compuce the corresponding self and mutual inductances, and obtsin the current division among the strips by solving the resulting impedance matrix equation relating the currents to the voltage drop along the structure. This is a two-dimensional magnetostatic approximation which yields good results for magnetic fields external to a conducting surface.

With the advent of graphite-epoxy materials in aircraft structures, it became necessary to predict the distribution of currents among electrically-connected conductors having dissimilar conductivities. In addition, since the conductivity of graphite-epoxy is much lower than aluminum, it was also necessary to compute internal magnetic fields. This was done by adding resistive terms to the impedance matrix, corresponding to the sheet resistsnce of the material. The method of dividing the structure into strips and computing the impedsnce matrix will be referred to as the circuit analysis spproach to current distribution. An alternstive approach is to pose the problem as an electromagnetic boundary-value problem and use the method-of-moments to compute current distrbutions. This technique will be referred to as the fields analysis approach.

A computer code, REDIST, has been devised to compute the electromagnetic fields external and internal to a two-dimensional structure composed of electrically-connected thin strips of arbitrary conductivity and thickness. The assumptions fundamental to the analytical approach are:

a. The structure may be locally approximated as two-dimensional.

b. Current flow is directed along the axis of the structure.

c. The cross-section of the structure is electrically small across the frequency range of interest.

The REDIST code has been verified by comparison with a variety of geometries amenable to independent analytical treatment by conformal transforms. Selected results obtained in the course of this verification are presented, along with application to representative aircraft structure consisting in whole or part of graphite-epoxy.

COMPARISON OF ABSORPTION AND RADIATION BOUNDARY CONDITIONS IN A TIME-DOMAIN THREE-DIMENSIONAL FINITE-DIFFERENCE CODE

Captain Clifford F. Williford
1Lt Randy Jost
Air Force Institute of Technology
Wright-Patterson Air Force Base, Ohio

1Lt James L. Hebert
Air Force Wright Aeronautical Laboratories
Wright-Patterson Air Force Base, Ohio

ABSTRACT

A broad class of time-domain three-dimensional finite-difference codes have been developed to investigate EMP interactions with aerospace vehicles. Recently three versions of these codes have been used extensively to provide effective time domain predictions of skin current distributions due to an aerospace vehicle's interaction with nearby and direct lightning strikes. These include T3DFD, G3DXL, and a modified version of the Ryme's T3DFD code. Two common sets of boundary conditions used with these types of codes are absorption and radiation boundary conditions. Basic research was performed on a modified version of the Ryme's T3DFD code to compare the use of these two types of boundary conditions and to validate the use of these types of codes by comparison with actual airborne lighting strike data. The comparison of the radiation and absorption boundary conditions was performed for a nose to tail strike on an F-16 Fighting Falcon with the resulting skin current distributions and electromagnetic fields monitored at ten locations on the aircraft. Predicted electromagnetic fields and skin current distributions are compared with those experienced by a CV-580 lightning research aircraft during an actual wing to wing lighting strike. The results, advantages, and disadvantages of the use each type boundary condition is discussed. The results of the predicted and measured comparison on the CV-580 yield additional validation that these types of codes may be reasonably applied to predict the skin current distributions during an aircraft/lightning interaction.

INTRODUCTION

Several research efforts in the recent past show considerable promise in developing the analytical tools necessary for a theoretical determination or prediction of lightning's electromagnetic interaction with aircraft. One of the most promising developments has been the application and validation of time-domain three dimensional finite-difference codes for the analysis and predictions of lightning's electromagnetic interactions with aircraft.

This development is particularly important because of two general trends. First, the rapid introduction of advanced composite materials and sophisticated low level flight and mission critical electronics into aerospace vehicles has raised concerns that these may increase the vehicle's inherent susceptibility/vulnerability to lightning induced damage or upset. And secondly, weight limitations on future vehicles require that optimized balanced electromagnetic protection be incorporated into these vehicles. The technology needs posed by these developments has been well recognized and advances in aircraft lightning protection analysis have been made in several key areas.

The lightning electromagnetic threat has been better characterized by the recent NOAA/AFWAL WC-130 (1), FAA/AFWAL CV-580 (2), and NASA F-106 (3) lightning characterization programs. While the threat has been better characterized, other research efforts have resulted in considerable advances in the ability to analytically predict the electromagnetic interactions of lightning with aerospace vehicles.

A highlight of this research has been the successful application of time-domain three-dimensional finite difference electromagnetic codes to the EMP/aircraft and lightning/aircraft interactions analysis. F. Pitts, G. Finelli, R. Perala, and T. Rudolph recently completed research which used the Time-domain 3-Dimensional Finite Difference code, T3DFD, to model the interaction of the lightning channel with the F-106 (3). They found that "the reasonable results obtained with the model compared to measured responses yield confidence that the model may be credibly applied to other aircraft types and used in the prediction of internal coupling effects in the design of lightning protection for new aircraft." Another significant research effort by K. Kunz and H. Hudson resulted in the validation of a similar code, the Generalized 3-Dimensional expandable Lawrence Livermore National Laboratory Code, G3DXL3, for predicting internal coupling responses. (4), (5) They found that " in that many internal modes of the test object modes of the test object (a 0.2 m cylinder, 1 m long) were predicted with excellent frequency agreement and typically good amplitude agreement, the time domain finite-difference technique should be considered an experimentally validated tool for interior response predictions of idealized interior coupling geometries when employed with the proper resources and necessary care in specifying the inputs and outputs." Recognizing the promise of this straight forward solution to Maxwell's curl equations and the electromagnetic coupling problem, the Atmospheric Electricity Hazards Group (AFWAL/FIESL) began a cooperative effort with the Air Force Institute of Technology to evaluate this type of code for performing in-house research on lightning/aircraft interactions.

This paper overviews the results of two projects using a modified version of the Ryme's T3DFD code. One project investigated the use of two types of boundary conditions with the code. The second project consisted of a comparison of predicted and measured skin current distributions.

CODE DESCRIPTION

The modified Ryme's version of T3DFD which was employed during this research is a descendant of THREDE developed by Holland (6) which is based on the finite difference methodology developed by Yee (7). The version of the code initially used in this study was one written by M. D. Rymes (8) and modified by Hebert and Sanchez-Castro (9) for the analysis of lightning's interaction with a FAA CV-580 lightning research aircraft. This code was delivered with artificial absorption boundary conditions which are discussed later in this paper. The code was modified by Williford (10) to include radiation boundary conditions similar to those developed by Merewether (11).

Time-domain three-dimensional finite-difference codes predict the electromagnetically induced currents and charges on a modeled vehicle by producing a finite difference approximation to the solution of Maxwell's differential curl equations in a bounded problem space. The problem space utilized in each of the efforts described in this paper was a mesh of dimension 27 x 27 x 27. The vehicle and the lightning channel are modeled into the problem space (ie. by setting the tangential electromagnetic fields to zero in and on all metal aircraft). Models of the F-16 and the CV-580 in carteaian coordinate problem space are depicted in Figures 1 and 2 respectively. Yee recently concluded work which describes how this type algorithm can be expanded to any coordinate system including irregular and non-orthogonal grids (12, 13). The differential form of Maxwell's equations equates time varying fields such as the electric field to the spatial derivatives of the complement field such as the magnetic field. By taking a finite difference of the time derivative the code allows the fields to propagate in time. In order for spatial derivatives to be formed a decentralizing mesh must be incorporated. This is illustrated in Figure 3. This figure shows that the fields are not located at the point in space (i, j, k) which acts as their index. It is this fact which provides quite a challenge and at time confusion to the individual who is modeling the vehicle into the problem space. Hebert goes to great lengths to disspell much of this confusion in Reference 9.

The simplest lightning channel model which can be used in this code is to impose the boundary condition that the magnetic field closest to the channel is given by

$$H = I/2\pi r$$

It should be pointed out that it is not a difficult task to model the lightning channel in terms of non-linear physical processes as the finite difference approximations of differential equstions are readily incorporated into this type of code. The simple source waveforms used for the F-16 and CV-580 efforts are illustrated in Figures 4 and 5 respectively. The F-16 source waveform has a 100 nanosecond risetime with a fall of 20.4 microseconds to the 50% point. The CV-580 source is identical to the actual lightning current measured during an in-flight lightning strike by a boom mounted current shunt located at the aircraft's right wing. This measured waveform is presented in Figure 6.

The computer code solves Maxwell's time dependent curl equations, which in turn solve the boundary

conditions for the object in a "natural way" (14). The code progresses through the problem space in time steps using the algorithm developed by Yee (7). Since an infinite problem space cannot be defined due to computer memory limitations, difficulties arise when the propagating wave reaches the problem space boundary. These boundaries cause reflections unless the fields at these locations are modified to model the ideal analytical situation of free space. Additional algorithms are necessary to handle the fields at these boundaries.

BOUNDARY CONDITIONS

Yee originally started with "hard" lattice truncation (another way of expressing the fields' outer boundary condition) (7). Hard lattice truncation is defined as forcing the outside boundary of the problem space to be a perfect conductor leading the term "tin can" boundary conditions (9). This is accomplished by forcing the tangential electric fields to be zero along the outer boundary.

The two boundary conditions investigated during the F-16 analysis are "soft" lattice truncation methods referred to as absorption boundary conditions and radiation boundary conditions. The absorption boundary condition is accomplished by assign finite conductivities to the cells of the problem space which are near the outer boundaries. As fields propagate through this region they are essentially chipped away or absorbed a small amount at a time. (15) The second set of "soft" boundary conditions investigated with the F-16 analysis was radiation boundary conditions. As developed by Merewether (11), these boundary conditions prevent reflections at the problem space outer boundaries by observing that the fields far from the modeled vehicle behave as:

$$H = K(\theta,\phi)\frac{f(t-r/c)}{r}$$

where K is dependent on the location on the outer boundary, f describes the retarded time behavior of fields propagating at the speed of light, and r is a large distance from the center of the problem space. This relationship allows the parabolic extrapolation of fields near the boundary to the outer boundary. This algorithm simulates free space by setting the fields on the outer boundary as closely as practical to those which would be present were the outer boundaries at infinity.

COMPARISON OF ABSORPTION AND RADIATION BOUNDARY CONDITIONS

Ten sensor locations were selected on the F-16 as illustrated in Figure 7. The F-16 was modelled into two versions of the modified Ryme's code. The code sources and modelling were identical with the exception of the manner in which the problem space boundary conditions were handled. In one version absorption boundary conditions (ABC) were implemented; in the other version radiation boundary (RBC) conditions were used.

Figures 8 through 12 show overlapping plots of the magnetic and electric fields at various sensor locations on the F-16. The general appearance of the time domain responses from each version of the code dramatically illustrates the following:

a) In the majority of the cases the waveforms follow the same general shapes.

b) The absorption boundary conditions introduce resonances which are not present in the radiation boundary condition responses. This is due to considerable reflections at the outer boundary which generate artificial modes between the vehicle and the outer boundaries within the problem space.

c) In each and every case, the RBC curves are smoother and settle to a steady state type response much quicker than the ABC version.

d) The magnitudes of the ABC version are lower but this is partly due to the fact that the source had to propagate through the absorbing outer cells on the way to the object.

In terms of computer resources the difference is also dramatic in that the radiation boundary condition version of the code requires a substantial increase in the memory size and a 25% increase in central processor unit time on the CDC computers used during this effort.

AIRBORNE MEASUREMENTS COMPARED TO CODE PREDICTIONS

The CV-580 lightning research aircraft was gridded into the RBC version of the code. This aircraft has spent the last two summers (1984 and 1985) flying in Florida thunderstorms where it was struck repeatedly by lightning. A lightning strike from 5 September 1984 was selected for the code prediction comparison with lightning because photographic evidence from the on-board VCR cameras indicated that the aircraft was struck on the right wing boom and that at least part of the exit current flowed out the left wing boom (a wing to wing configuration). Initial time domain analysis indicated that at least part of the exit current flowed out the tail of the aircraft.

With the assumptions that the aircraft was struck by a channel from directly overhead on the right wing and that 1/3 of the current exited the aircraft's tail and 2/3 exited the left wing the code's sources were gridded in using a perfectly conducting lightning channel and imposing on the right wing the same current waveform which was measured at the right wing tip boom. This particular strike is discussed in detail in several papers at this conference. In one paper by J. Reaser the spatial and time characteristics of measured current waveforms are discussed (16); in another paper by Hebert, et. al. the skin current distributions are compared to those which resulted during ground lightning simulation tests on this aircraft (17).

The CV-580 occupied the 27 x 27 x 27 grid problem space and was run with time steps of approximately one nanosecond. The interaction was calculated for three microseconds (3000 time steps). Figures 13 and 14 show a comparison of the predicted and measured current distributions on the aircraft. In Figure 13, the measurements correspond to the currents at the left wing skin current sensor near the fuselage and on the bottom. Figure 14 show the currents on the upper forward fuselage. They seem to differ by a scale factor. Figure 15 shows the forward fuselage with a scale factor of 2.7 times the predicted values. No scale factor was applied to Figure 13 and it is readily apparent that these would correspond quite closely were the predicted values multiplied by a factor of 0.8.

For an object as large and as geometrically complex as the CV-580, the measured and the predicted waveforms correspond amazingly well considering that the channel was modelled as a perfect conductor and the airborne data was scaled to produce the airborne measured response. The forward fuselage has more DC

which may have resulted from the asaumption thst 1/3 of the current exited the tail when in reality most probably exited the left wing. These waveforma should add confidence that the time-domain three-dimensional finite-difference codes can provide accurate and reasonable predicted results by which lightning's electromagnetic interaction may be analyzed in order to develop lightning protection.

PROGRESS ON THE MODIFIED T3DFD CODES

The only drswback with these codes is that until recently only small problem spaces and two dimensional problems could be performed on computers smaller than a VAX. The advent of more powerful minicomputers may allow problem spacea as large as 30 x 30 x 30 to be run on smaller less expensive computers. This would relieve some of these type codes' biggeat disadvantage: the cost of running the program in terms of CPU time and money. With mini-computers these techniques should find wide application in the lightning protection area.

SUMMARY

Time domain three dimensional finite difference codes are being applied to a wider spectrum of lightning protection analysis and predictions problems. The code is being validated for an increasing number of applications. This paper has discussed the use of two sets of boundary conditions with theae codes. The radiation boundary conditiona produce a smoother waveform with reaonances which correspond more closely to natural resonancea while the abaorption boundary conditiona produce modes which correspond to length between the aircraft and the outer boundaries of the problem apace. Both boundary conditions produce the same low frequency waveforms or general responae waveform shape. It is more costly to use the radiation boundary conditions although they do produce the most reasonable results. The radiation boundary condition version of the code was uaed to predict lightning' interaction with a CV-580 sircraft producing predicted results which reasonably agreed with those measured during an actual airborne lightning atrike.

REFERENCES

1. B. P. Kuhlmsn and M. J. Reazer, "Characterization of Fast-Risetime Electromagnetic Field Pulses Recorded in Airborne Measurementa During Florida Thunderstorms," Proceedings of the 9th International Aerospace and Ground Conference on Lightning and Static Electricity held in Orlsndo, Florida June 26-28, 1984.

2. P. L. Rustan and J. Moreau, "Aircraft Lightning Attachment at Low Altitudes," Proceedinga of the 10th International Aerospace and Ground Conference on Lightning and Static Electricity held in Paris, France, June 10-13, 1985.

3. F. L. Pitts, C. B. Finelli, R. A. Perala, and T. H. Rudolph, "F-106 Data Summary and Model Results Relative to Threat Criteria and Protection Design Analysis," presented at this conference.

4. K. S. Kunz and H. G. Hudson, "Experimental Validation of Time Domain Three Dimenaional Finite Difference Techniques for Predicting Interion Coupling Responsea," IEEE Tranaactiona on EMC, Vol EMC-28, No 1, February 1986.

5. K. S. Kunz, H. G. Hudson, and J. K. Breakall, "A Shielding Effectiveness Characterization for Highly Resonant Structures Applicable to System Design," IEEE Transactions on EMC, Vol EMC-28, No 1, February 1986.

6. R. Holland, "THREDE: A Free Field EMP Coupling and Scattering Code," IEEE Transactions on Nuclear Science, Vol NS-24, December 1977.

7. K. S. Yee, "Numerical Solution of Initial Boundary Value Problems Involving Maxwell's Equations in Isotropic Media," IEEE Transactions on Antennas and Propsgation, AP-14, May 1966.

8. M. D. Rymea, "T3DFD User'a Manual: Final Technical Report, August 1979 - June 1981," prepared for the Air Force Flight Dynsmica Laboratories (AFWAL/FIESL) WPAFB, Ohio, Contract F33615-79-C-3412, Electro Magnetics Applications, Inc., EMC-81-R-24, Denver, CO, April 1981.

9. J.L. Hebert and C. Sanchez-Caatro, "Implementation of a Three Dimensional Finite Difference Electromagnetic Code for Analysia of Lightning Interaction with a FAA CV-580 Aircraft," AFWAL-TR-86-3008, Air Force Wright Aeronautical Laboratories (AFWAL/FIESL), WPAFB, Ohio, January 1986.

10. C. F. Williford, "Comparison of Absorption and Radiation Boundary Conditiona Using a Time Domain Three Dimensional Finite Difference Electromagnetic Computer Code," Air Force Inatitute of Technology Maater's Thesis, AFIT/GE/ENG/85D-53, WPAFB, Ohio, December 1985.

11. D. E. Merewether, "Transient Currenta Induced on a Metallic Body of Revolution by an Electromagnetic Pulse," IEEE Tranaactions on EMC, Vol EMC-13, May 1971.

12. K. S. Yee, "Numerical Solution to Maxwell's Equations With Non-Orthogonal Grids," SGEMP Note 4, Report No D-DDV-85-0002, Lawrence Livermore National Laboratories, January 1985.

13. K. S. Yee, "Two Ssmple Calculationa Based Upon Irregular Grids To Solve Maxwell'S Equations," SGEMP Note 5, Report No D-DDV-85-0003, Lawrence Livermore National Laboratories, February 1985.

14. Umashankar, Korada, and A. Taflove, "A Novel Method to Analyze Electromagnetic Scattering of Complex Objects," IEEE Transactions on EMC, Vol EMC-24, No 4, November 1982.

15. A. Taflove and M. E. Brodwin, "Numerical Solution of Steady-State Electromagnetic Scattering Problems Using the Time-Dependent Maxwell's Equations," IEEE Transactions on Microwave Theory and Techniques, Vol MTT-23, No 8, Auguat 1975.

16. J. S. Reazer and A. V. Serrano, "Spatial and Temporal Description of Strikes to the FAA CV_580," presented at thia conference.

17. J. L. Hebert, J. G. Schneider, J. S. Reazer, M. Risley, and A. V. Serrano, "Current Levels and Distributiona During Ground Lightning Simulation Tests and In-Flight Lightning Attachment," presented at this conference.

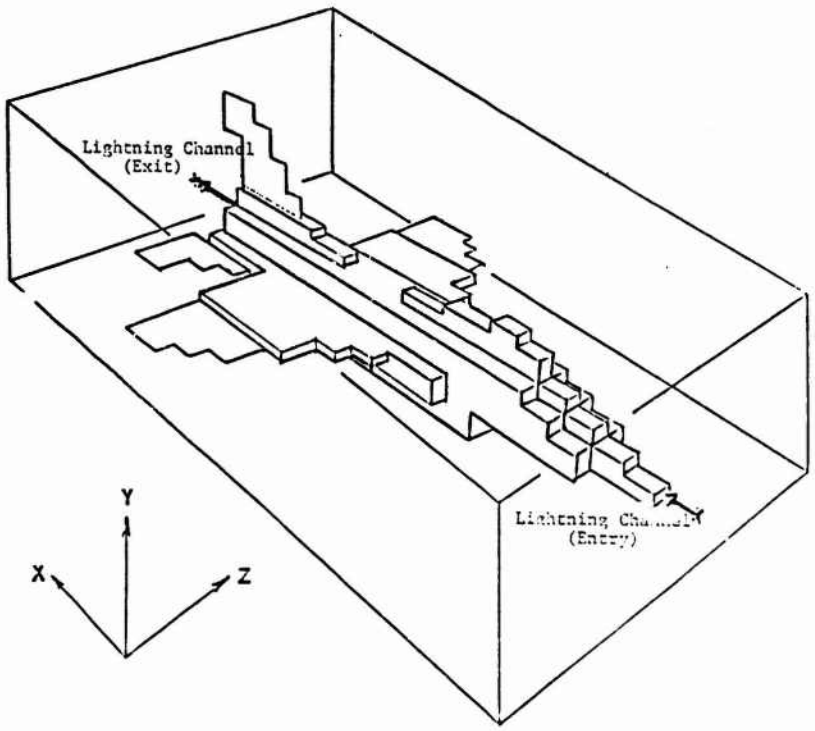

Figure 1. F-16 Aircraft modelled in a Three Dimensional Cartesian Coordinate Problem Space with Sources Illustrated.

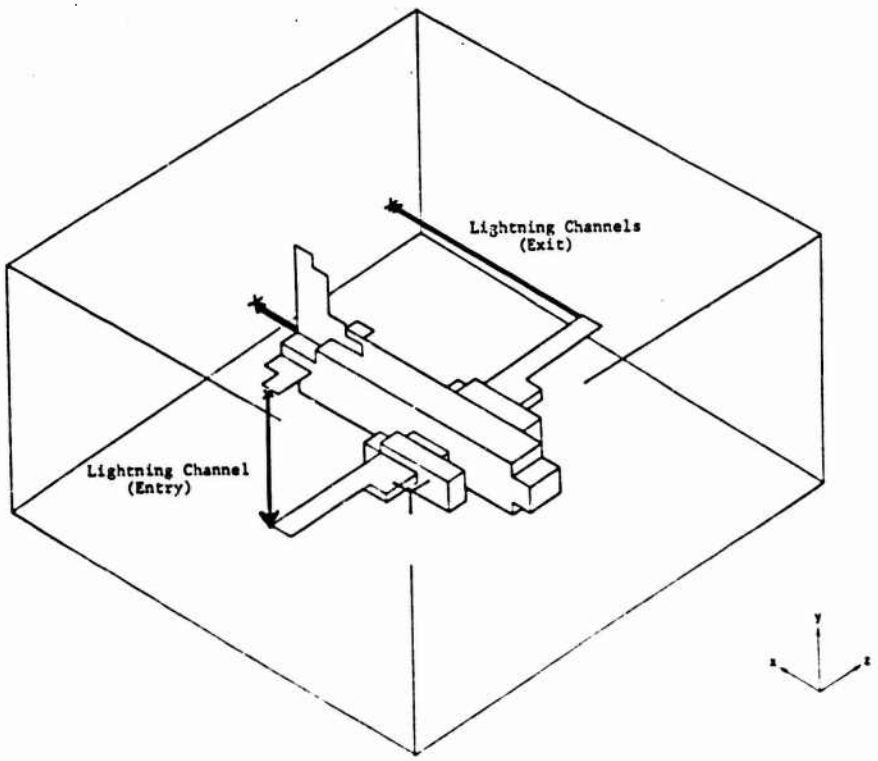

Figure 2 A FAA CV-580 Aircraft modelled in a Three Dimensional Cartesian Problem Space with Sources Illustrated.

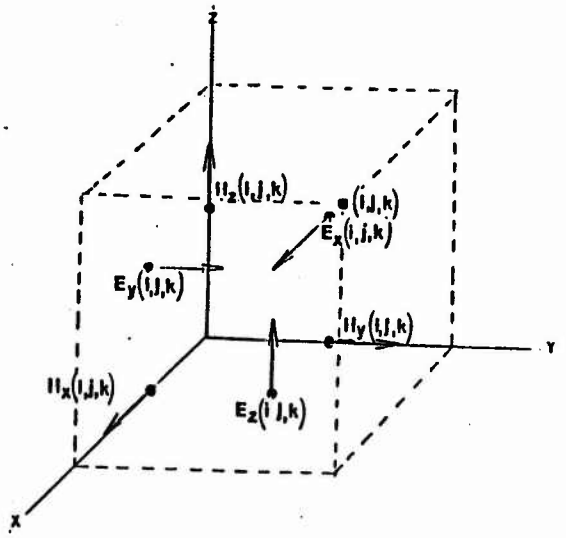

Figure 3. An example of the locations of the fields which are indexed by the point (i,j,k).

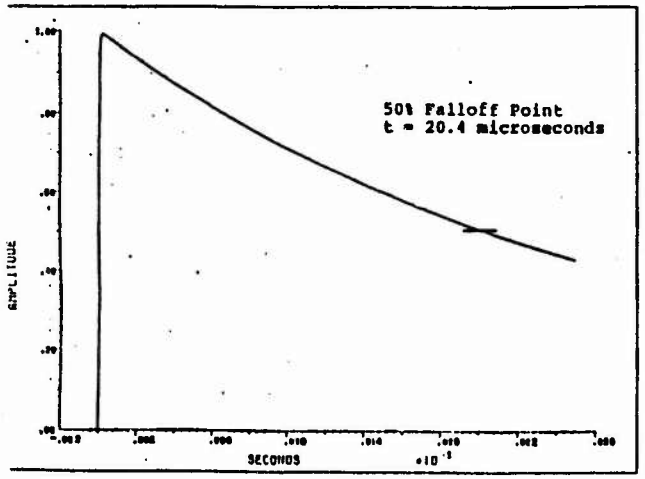

Figure 4. Source Function used for the F-16 Comparison of Boundry Conditions

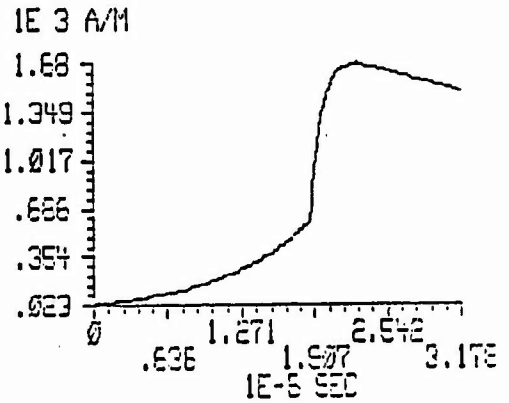

Figure 5. Source Function used for the CV-580 Measured and Prediction Comparison.

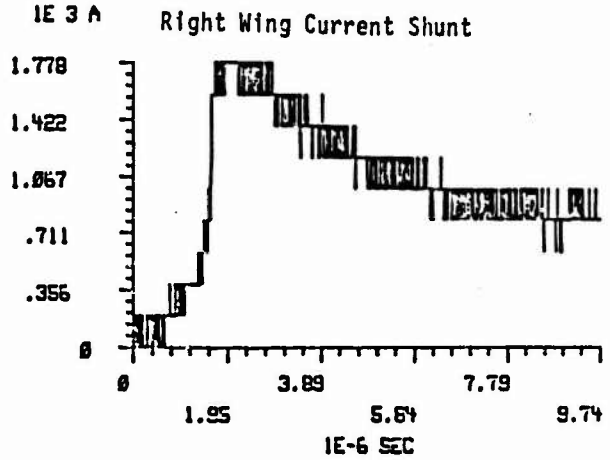

Figure 6. Actual Current Measured on the Right Wing Boom of the CV-580 during a Lightning Strike on 5 September 1984.

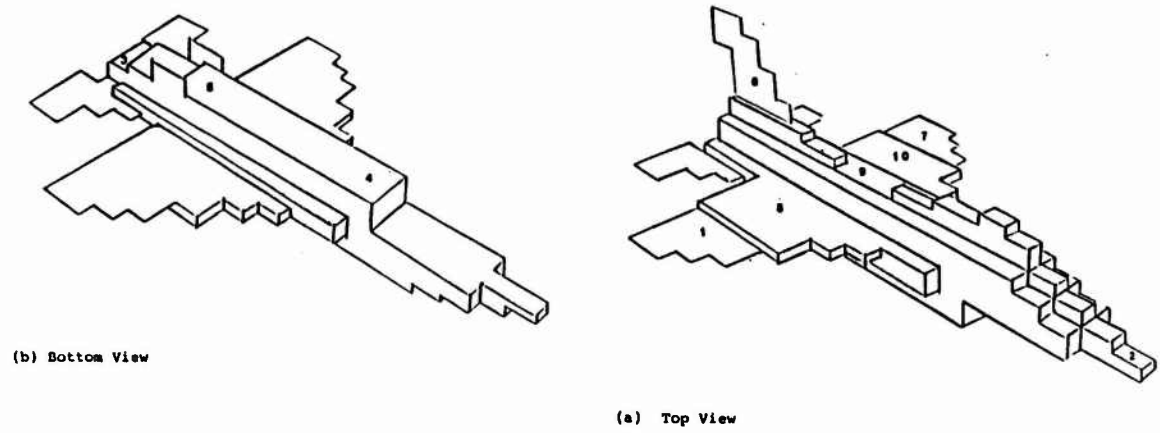

Figure 7. Location of the 10 Test Points on the F-16 where the comparison of the fields were made.

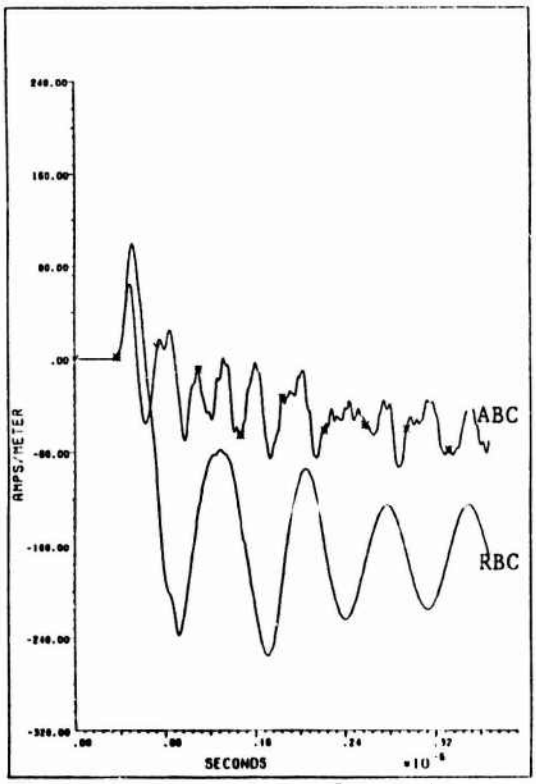

Figure 8. Comparison of H-Fields at Sensor One, Right Wing.

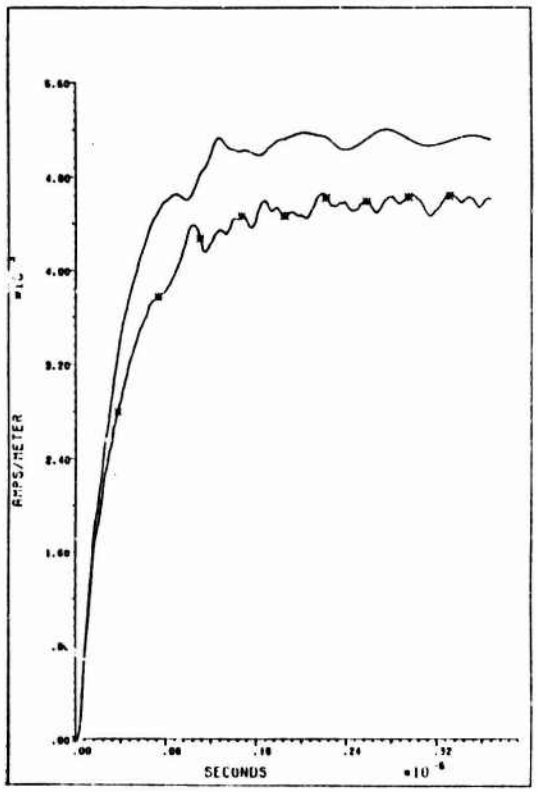

Figure 9. Comparison of H-Fields at Sensor Two, Nose.

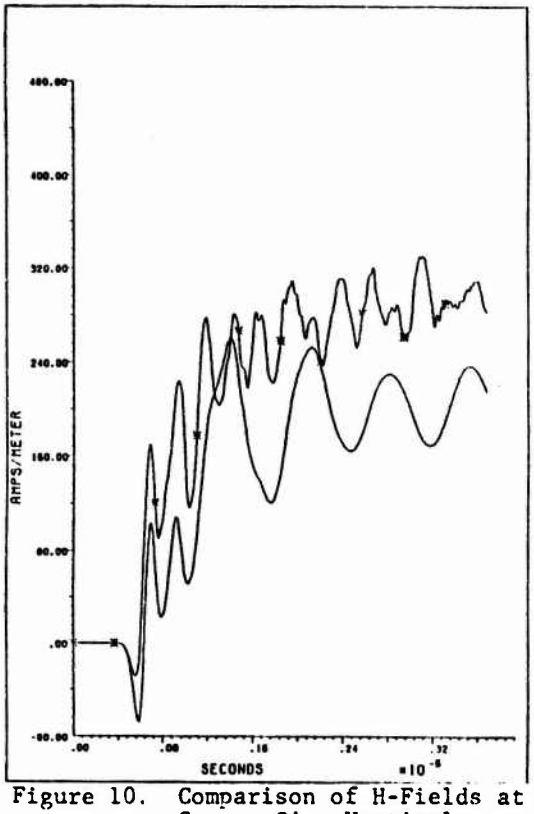

Figure 10. Comparison of H-Fields at Sensor Six, Vertical Stabilizer.

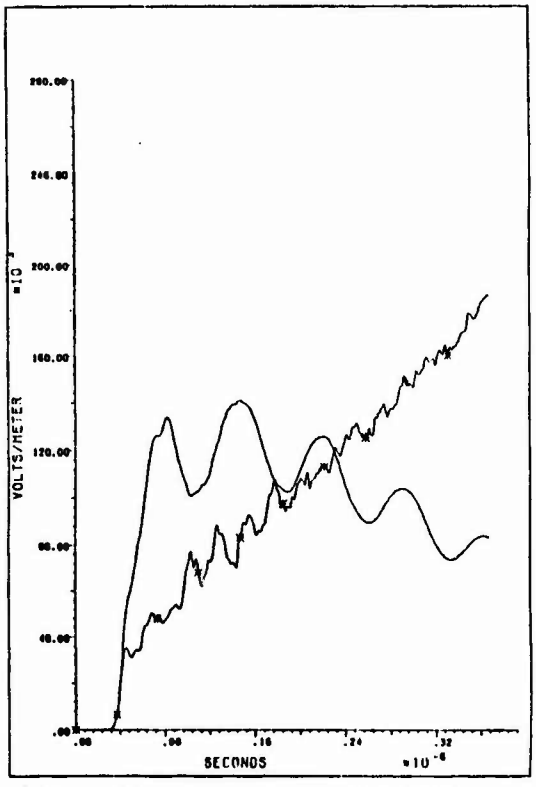

Figure 11. Comparison of E-Fields at Sensor Eight, Right Wing.

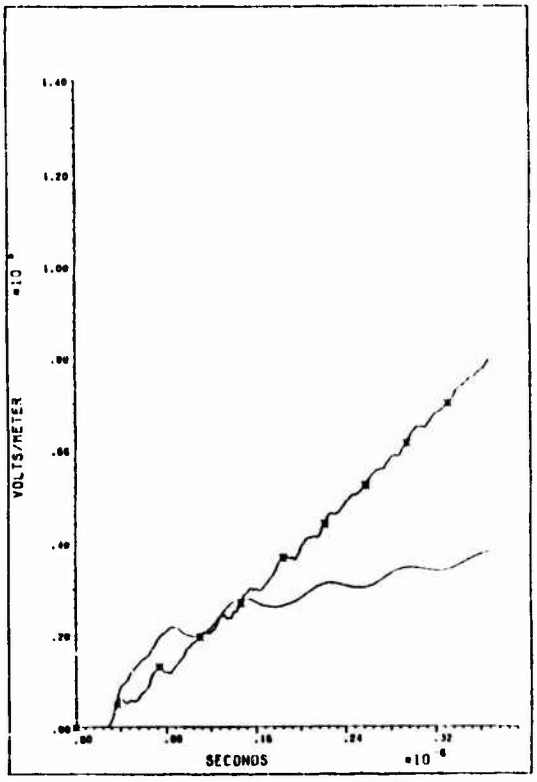

Figure 12. Comparison of E-Fields at Sensor Nine, Middle Top Fuselage.

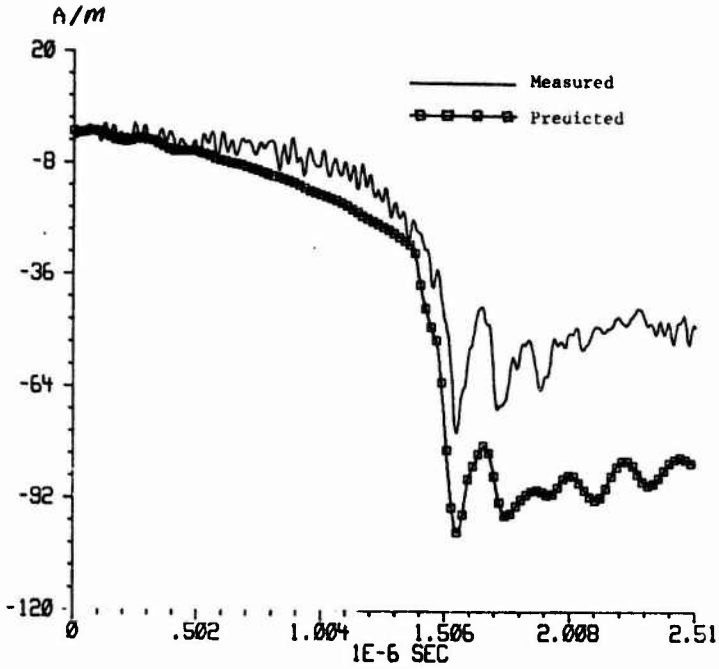

Figure 13. Comparison of Measured and Predicted H-Fields on the Left Wing of the CV-580.

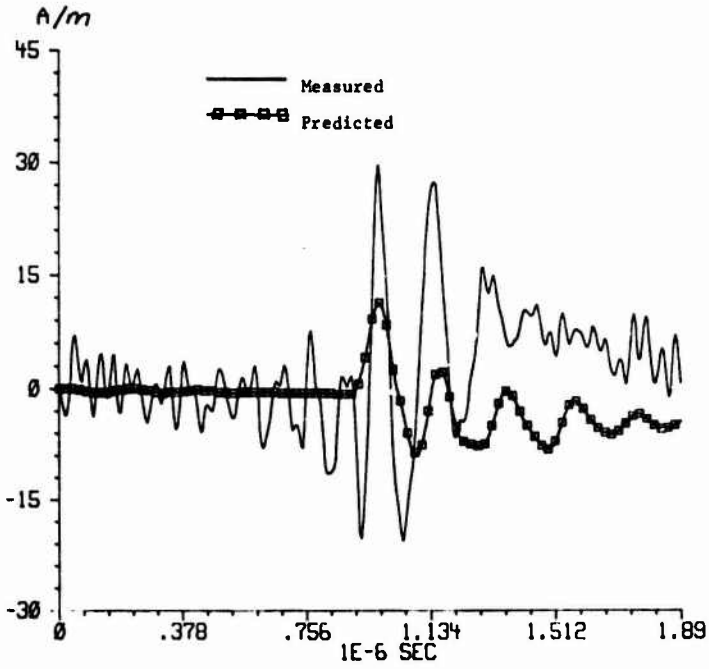

Figure 14. Comparison of H-Fields on the Upper Forward Fuselage of the CV-580 (No Scaling)

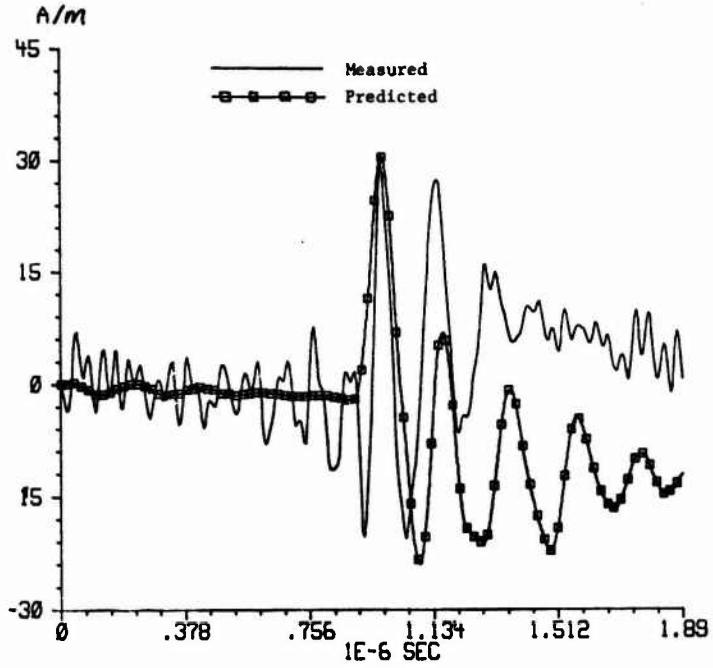

Figure 15. Comparison of H-Fields on the Upper Forward Fuselage of the CV-580 (Scaled X 2.7)

A COMPARISON OF CALCULATED AND MEASURED VALUES OF THE OPTICAL POWER RADIATED BY A LIGHTNING CHANNEL

A. H. Paxton, R. L. Gardner, and Louis Baker
Mission Research Corporation, Albuquerque, New Mexico

William Rison
New Mexico Institute of Mining and Technology, Socorro, New Mexico

C.E. Baum
Air Force Weapons Laboratory, Albuquerque, New Mexico

ABSTRACT

A computer calculation of the time-dependent brightness of a lightning channel is compared to a measured curve. The computer code includes: a one-dimensional finite-difference hydrodynamics algorithm; Joule heating; a tabular equation of state for air; and a multigroup radiative transport treatment. The radiative transport was calculated in the diffusion approximation, and one of the frequency groups corresponded to the 0.41 to 1.24 μ wavelength range, slightly larger than the range of sensitivity of the photodetector. The measured values of the current as a function of time were input to the code and the light radiated by the channel as a function of time was calculated.

The calculated values of the emitted power are compared with the radiance of a lightning channel that was measured at South Baldy Peak near the Langmuir Laboratory of the New Mexico Institute of Mining and Technology. The light output from a short length of a lightning channel was measured at the same time that the current into the ground was recorded.

THE VISIBLE LIGHT EMITTED by a lightning channel is a useful indicator of the detailed physical processes taking place during the discharge, because it is easily detected and its time dependence is not seriously distorted by propagation. Moreover, the lightning stroke can be imaged and the time dependence of the light emitted by any segment of the channel length can be determined. Several authors have recorded the light emitted by lightning strokes into a broad frequency range corresponding approximately to the visible portion of the spectrum[1-4]. The incident light from the entire lengths of the lightning channels was recorded. None of these measurements, however, precisely determined the current and the brightness as functions of time for the same lightning stroke.

A numerical simulation of the optical power radiated by a lightning channel into the spectral range of sensitivity of the detector used in Reference 4 has been performed[5]. The current was specified to have a rise time of 5×10^{-6} sec and a peak value of 20 kA. The optical power was calculated using a one-dimensional hydrodynamics code, in cylindrical coordinates, that included a multigroup radiative transport algorithm. The radiated power was consistent with the measured values of References 1 through 4 but, due to uncertainties of experimental values, a precise comparison was not possible[5].

During the summer of 1985, simultaneous measurements were made of the time dependence of the emitted light and the current corresponding to each of three triggered lightning strokes[6]. One of the strokes (stroke 85220) had a current with a short (1 μs) rise time to its peak value. The lightning, which was triggered by a rocket, struck an aluminum mast that extended 20 m above the ground. A collimator in front of the photodetector limited the field of view to a section of channel about 12 m long, centered 18 m above the top of the mast. The geometry of the light measurement is shown in Figure 1. The time dependence of the emitted light and the current were obtained with a resolution of 10 ns.

The light emission by a lightning channel was calculated numerically using a one-dimensional magnetohydrodynamics code in cylindrical coordinates, CHARTB. CHARTB was developed at the Sandia National Laboratories. It includes a multigroup radiative transport algorithm in the diffusion approximation. The opacity table used in the radiative transport calculation was generated by taking Rosseland means[7] of the data described in Reference 8. CHARTB includes a tabular equation of state for air, and a fully consistent calculation of the current profile in the channel (incorporating magnetic diffusion and advection) is performed. The lightning calculation was begun with a channel with an initial temperature of 1 eV and a 1 mm radius. The time dependence of the current was specified as an input to the calculation, and the optical emission per unit channel length, convolved with the calibration curve of the detector, was calculated. To convolve the spectrum of the emission with the detector response, the radiated light was assumed to have a Planck distribution at the temperature of the radiating cell, within the group that contained the detector response curve. This group covered the 0.41 to 1.24 μ wavelength interval.

The current was specified as a double exponential of the form

$$I = I_0 \left(\exp(-t/t_f) - \exp(-t/t_r)\right) \qquad (1)$$

The rise time was t_r = 0.24 μs; the decay time was t_f = 25 μs; and the value assigned to I_0 was I_0 = 17 kA. The measured current and its functional form used in the calculation are plotted in Figure 2. The current data became very noisy at 14.5 μs, probably because of problems with the power supply for the data recorders. Our assumed functional form fits the data very well for times under 7 μs. Then the measured current becomes constant for times up to 14 μs while the functional form decreases by an additional 3 kA.

The measured and calculated optical emission in the 0.4 to 1.1 micron wavelength range for stroke 85220 are plotted in Figure 3. The light emitted by the 12 m segment of the lightning channel was measured simultaneously by two photodetectors. The data shown in Figure 3 were recorded by only the first photodetector. Values measured by the second detector were similar to those shown in Figure 3 but were about 10% lower. The second detector gave larger values than the first for the brightness of one lightning stroke (not presented here), and the shapes of the curves from both detectors are similar and appear to agree to within about 10% for all three strokes from which data were obtained.

The calculated optical emission curve in Figure 3 has a shape that is similar to the measured curve, but its peak value is a factor of 2.5 too high. The calculated value is still a factor of 2.2 above the measured curve at a time of 7μs. The calculated curve continues to approach the measured curve as the time increases form 7 μs, but the significance is unclear because the assumed current is decreasing with respect to the measured current in this range. The initial channel diameter used in the calculation may have been narrower than the actual initial conducting region. This would have caused the calculated emission to be too high. Another possible explanation is that electrical currents which were not sufficiently large to trigger the date recorders may have heated the channel prior to the main stroke. This would have decreased the gas density in the channel, causing a lower optical emission than would otherwise have occurred.

REFERENCES

1. E.P. Krider, "Some Photoelectric Observations of Lightning", J. Geophys. Res. 71 3095, 1966.

2. O. Mackerras, "Photoelectric Observations of the Light Emitted by Lightning Flashes" J. Atmos. Terr. Phys. 35 521, 1973.

3. B.N. Turman, "Analysis of Lightning Data from the OMSP Satellite, J. Geophys. Res. 83 5019, 1978.

4. C. Guo and E.P. Krider, "The Optical and Radiation Field Signatures Produced by Lightning Return Strokes", J. Geophys. Res. 87 8913, 1982.

5. A.H. Paxton, R.L. Gardner and Louis Baker, "Lightning Return Stroke - a Numerical Simulation of the Optical Radiation," Phys. Fluids, accepted for publication, 1986.

6. W. Rison, "Activities and Data from Kiva 1 and 2 Operations During the Summer of 1985," Technical Report AMRC-R-795, Mission Research Corporation, 1720 Randolph Rd. S.E., Albuquerque, NM, 1986.

7. See, for example, G.C. Pomraning, Radiation Hydrodynamics (Pergamon Press, Oxford, 1973).

8. R.R. Johnston and D.E. Stevenson," Radiative Properties of High Temperature Air, II", Technical Report SAI-056-77-PA, Science Applications, Inc., Palo Alto, CA, NTIS Doc. No. 641577 UCRI-13786, 1977.

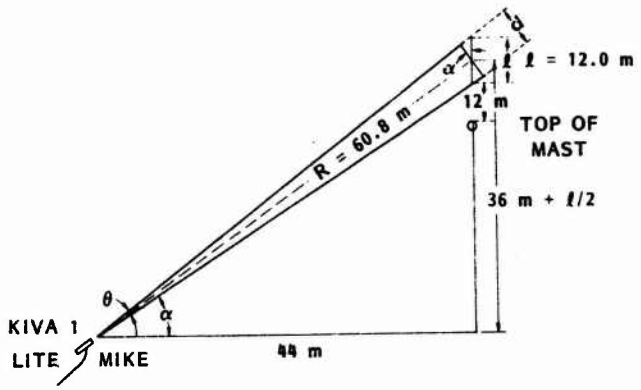

Fig. 1 - Geometry for the measurement of the optical power radiated by a lightning channel.

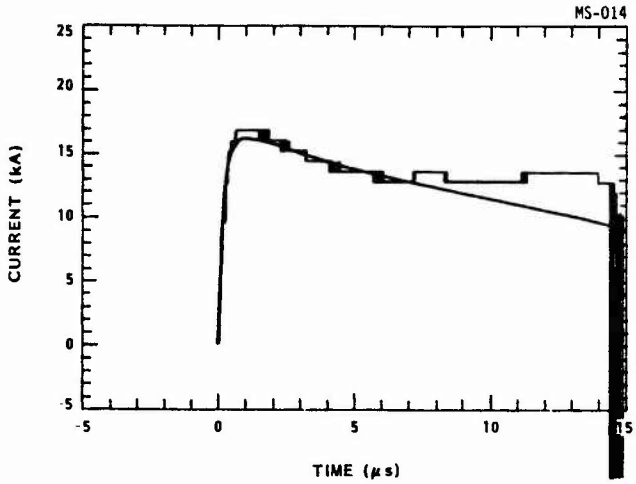

Fig. 2 - Measured current of lightning stroke 85220 and the function that was assumed to be the current in calculating the optical emission. The smooth curve is the assumed current.

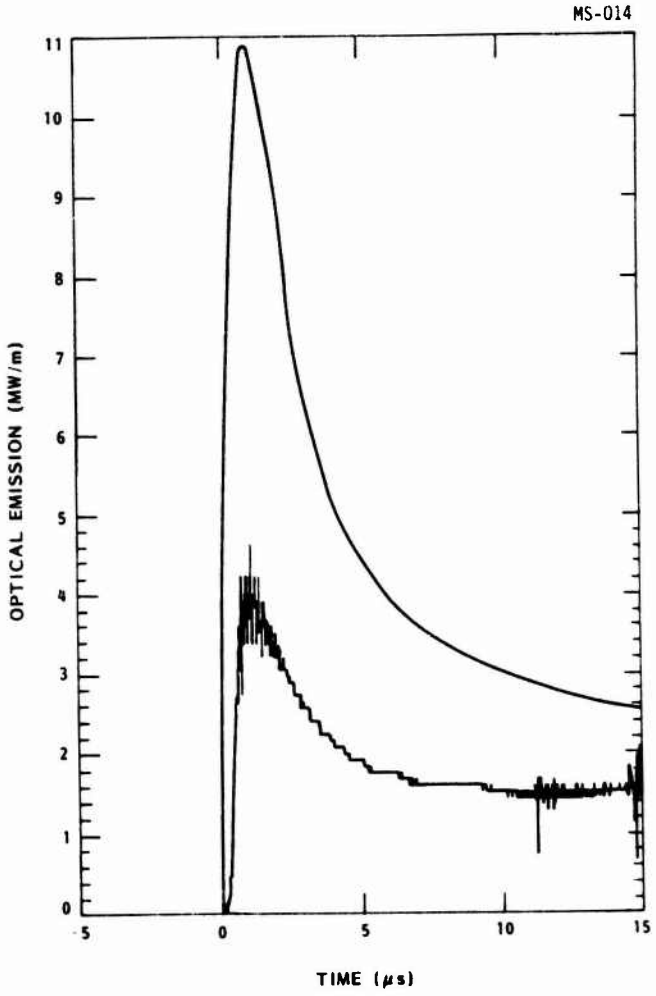

Fig. 3 - Optical power emitted per unit channel length derived from a measurement with an EG&G "Lite Mike" detector (lower curve), and calculated optical power emitted per unit length, convolved with the detector sensitivity (upper curve).

SPECTRUM ANALYSES OF POSITIVE GROUND STROKES DURING WINTER IN JAPAN

Z.-I. Kawasaki* and S. Israelsson

Institute of High Voltage Research, Uppsala University
Husbyborg, S-755 90 Uppsala, Sweden
T. Takeuti and M. Nakano
Research Institute of Atmospheric, Nagoya University
Toyokawa, Aichi 442, Japan

ABSTRACT

Spectra of electric field changes due to the positive ground first strokes during the winter period in Japan are estimated in order to understand positive lightning in more detail. The spectra show the two striking characteristics; a peak in the neighbourhood of 16 kHz and an anomalous slope in the frequency range from 0.8 to 10 kHz. The former is related to the bipolar oscillation and the latter to the height of the vertical lightning channel. Moreover, it can be also related to the bipolar oscillations.

* On leave from Research Institute of Atmospherics, Nagoya University, Toyokawa, Aichi 442, Japan

INTRODUCTION

SPECTRUM ANALYSES OF ELECTRIC FIELD CHANGES due to lightning return strokes have been discussed by several investigators [1, 2, 3 and 4]*. In addition, many papers treat the effect of propagation distance on the spectra [2, 4 and 5]. The effect of the tortuosity on the return stroke channels [6] and the theory of the frequency spectra of lightning currents [7, 8 and 9] have also been studied. Moreover, Preta et al. [4] recently presented spectra of the electric field changes measured with a wide band system from 1 kHz to 1.5 MHz, during the Thunderstorm Research International Program (TRIP) and the experimental characterization of the frequency spectra of both the first and the subsequent stroke electric fields over a distance range from 1 to 200 km was discussed. All these papers treated the electric field changes due to the negative ground strokes during summer.

The positive ground stroke during winter was discovered by one of the authors during the anomalous winter thunderstorms of the Hokuriku Coast in Japan [10 and 11]. Now the research on the positive ground strokes has become one of the major topics in the field of lightning research [12, 13 and 14]. However, the spectra of the electric field changes due to the positive ground strokes are not presented. Concerning the positive cloud to ground strokes, some interesting characteristics have been found such as the bipolar oscillating phenomena of electric field changes [15 and 16] and the relative long durations of continuous currents [10 and 11].

It follows that it is interesting to compare the spectra of positive ground strokes during winter thunderstorms with the spectra of negative ones during summer in order to understand positive lightnings in more detail. The following procedures are adopted in this paper:

Initially, the observed data are classified into three groups corresponding to the propagation distances and then, the spectra of these data are estimated using the maximum entropy method (MEM) [17]. The effect of both the bipolar oscillations and the propagation distances are discussed quantitatively. The spectra of the field changes due to the normal summer ground strokes are also obtained and both results are compared. Finally, an interpretation with some numerical results calculated by the Lin-Uman-Standler's model [18] are presented.

EXPERIMENT AND DATA ANALYSIS

The electric field changes were recorded during the four winters from 1979 through 1982 at different locations in the Hokuriku area in Japan as shown in Figure 1. The measuring system has already been described in detail [10 and 16]. In order to make the cause and effect between source and observed data be clear, the analysed data in the present paper are restricted to the following conditions.

- to be a first cloud to ground stroke
- to be a natural lightning
- to know the distance to the striking point

From the several data, 17 first cloud to ground strokes can be selected and they are recorded on magnetic tape with the measurement system which frequency range is from 160 Hz to 1 MHz [16].

Some typical examples of the 17 electric field changes are shown in Figure 2. The distances from the striking point to the observation site for these examples are respectively, 3, 8 and 20 km from the top to the bottom. Concerning these examples, the abrupt changes followed by relative slow changes can be recognized and some of these abrupt changes are bipolar oscillations as is the case of Takagi and Takeuti [16]. These wave forms resemble the current shapes of Lin-Uman-Standler's model [18 and 19] and it is assumed that their model is useful to understand the observed data. It should be noted that the other 14 electric field changes are almost the same. If the attentions are paid on the part of relative slow changes, Lin et al. named this part the ramp part [20], on finds that the 17 strokes can be classified into three groups, viz. (1) close lightnings (in the range 0 to 5 km); (2) intermediate lightnings (in the range 5 to 10 km); (3) far lightnings (in the range 10 to 30 km) although according to the ordinary classification, all of them should belong to the close lightning groups [21]. The result of the classification of these data is summarized in the legend for Figure 2.

In the present paper, wave forms are digitized every 2.4 μs with a 12 bits signal analyser [SMR2100 IWATSU] and processed with the computer [ACOS Model 650 NEC]. It is considered that a duration of a electric field change due to a return stroke corresponds to a pericd from the beginning to the abrupt change through the peak of the ramp part. The Maximum Entropy Method (MEM) is applied to 2^9 sampling points and the spectra are determined.

The record length must, therefore, be extended to become 1028.8 μs following the same procedure as that of Serhan et al. [2]. The MEM technique provides an extrapolation of the time domain data to longer times and the frequency domain data in lower frequencies. The analyses presented here are valid at least in the frequency range from 0.8 to 200 kHz. It should be noted that these results have been compared with spectra determined by using the standard Fast Fourier Transform (FFT) on simultaneous records with the window von Han and it was concluded that the both results do not differ from each other.

RESULTS

In Figure 3, typical examples of the spectra of the first positive ground strokes during the winter are shown. In this figure, according to the special classifications of the present paper (a), (b) and (c) are for the close lightnings, the intermediate lightnings and the far lightnings, respectively. In order to examine the procedure of the present paper, the spectra of the first negative ground strokes during summer, those are observed at Ohtu as shown in Figure 1, are estimated and shown in Figure 4. It should be noted that all of them are normalized to the spectral intensity at 0.8 kHz. It is considered that the relative spectral intensity has a physical meaning in the distance range discussed in this paper, since the absolute spectra depends on the amplitudes of the return stroke currents strongly and it is not so easy to know the exact amplitudes of them. If one compares the spectra of positive strokes with those of the negative strokes, one can easily find that the former have some maximum values in the neighbourhood of 16 kHz, and in the slopes of the former in the frequency range 0.8 to 10 kHz. The spectra vary remarkably in the frequency range below 10 kHz (hereafter the term VLF region is used), depending on the propagation distances. Nevertheless, the spectra of the negative strokes have similar trends as those of previous presented results [2 and 4]. It should be noted that the procedure of this paper is reliable. The discussions are therefore restricted to the above mentioned anomalous characteristics of the positive ground strokes.

THE FREQUENCY COMPONENTS OF THE BIPOLAR OSCILLATIONS — The bipolar oscillating electric field changes

---

* Numbers in brackets designate References at end of paper.

are often observed in the positive lightnings during winter [15]. Takagi and Takeuti [16] have tried to explain these phenomena using the reflection of a the return stroke current. Though it seems to be difficult to understand the physical meaning of the reflection current in the natural return stroke channel, it is expected that the spectra have peak values at the frequency corresponding to those of the bipolar oscillating. It can be considered the maxima in the neighbourhood of 16 kHz are due to bipolar oscillations. Nine electric field changes of the 17 have the characteristics of bipolar oscillations and the average of the fundamental frequency component estimated with spectral intensities is 16.4 kHz and its standard deviation is 2.2 kHz. Moreover, such kind of maxima including higher order components of frequency exist in the frequency range between 14 kHz to 30 kHz. It can be assumed that these frequencies are related to the velocity of the return stroke and the height of the vertical channel. It should be noted that one cannot recognize such maxima of the spectra of the negative strokes during summer as shown in Figure 4.

THE EFFECT OF THE PROPAGATION DISTANCE - Except the maxima due to the bipolar oscillations, the spectra of positive strokes have a normal tendency of falling of in the frequency range over 10 kHz. These are coincident with the results of Preta et al. [4] and the spectra of the negative strokes during summer have also the same characteristics. The feature of the spectra of the positive strokes in VLF region is however quite different from that of the negative strokes. One can hardly recognize the effect of the propagation distance in the spectra of negative strokes. Concerning the spectra of the positive strokes, the slopes in the VLF region tend to become less steep proportionally to the propagation distances. This is quite opposite in characteristic to the normal sense. With the same measurement system and the same process of analysis, one cannot find such a characteristic in the spectra of negative strokes. The higher frequency components of electric fields should be attenuated more than the lower components due to the conductivity of the ground which means that normally the slopes should become steep proportionally to the propagation distances. It is considered that the characteristic mentioned above must be an intrinsic characteristic of the positive strokes during winter. Figure 5 shows the spectral ratios of 8 kHz against 0.8 kHz in order to indicate the effect of the propagation distances. It can be found that the variation of the slope for the positive strokes spectra is 16 dB per 10 km with the least square error method.

DISCUSSION

Up to now, many numeri al models for the return stroke current have been proposed and the Lin-Uman-Standler's model seems to be the most suitable among all of them the reason being that their model can explain many observed results without contradictions. In this section, the Lin-Uman-Standler's current model is applied to obtain some interpretations of the characteristics of the positive ground strokes. Concerning parameters, which are included in this model, we faithfully follow Master et. al. [19]. In the Lin-Uman-Standler's model, the lightning current is composed of a breakdown pulse current, a corona current and a uniform current [18]. Starting with the discussion of the anomalous spectra in the VLF region, if one compares the observed electric field changes shown in Figure 2 with the current shape of the Lin-Uman-Standler's model, one can easily come to the conclusion that the abrupt changes of the electric field are mainly due to the breakdown pulse, whether they are bipolar oscillating or not. Moreover, the relative slow change which follows the abrupt change, so-called the ramp part, is assumed to be mainly caused by the uniform current as indicated by Lin et al. [18] and the uniform current, I_u, is given by the following equation:

$$I_u = -2\pi\varepsilon_0 \frac{V(H^2+D^2)^3}{H} \frac{dE(Dt)}{dt} \qquad (1)$$

where ε_0 is the permittivity of the free space and E, H and D are the vertical electric field to the ground, the height of vertical channel and the distance to the striking point, respectively.

As both the rise time and the velocity of the breakdown pulse are very fast, it can be assumed that the main component of the abrupt change must be the radiation component and that the first peak value must be decreased inversely proportional to the distance. Actually, the numerical results for every 5 km, given in Table 1 and calculated with the Lin-Uman-Standler's model, show that they are almost inversely proportional to the distance. It should be noted that these values are normalized to the amplitude at 5 km and that absolute values hardly depend on the height of vertical channel, H.

On the other hand, it is obvious that the slope of the ramp part depends on both the height of the vertical channel and the propagation distance. In Table 1 the numerical results of slopes of the ramp part calculated with Equation (1) are shown for every 5 km, where the height of vertical channel is treated as a parameter. They are also normalized to the value at 5 km. Table 1 shows that shorter the height of the vertical channel is, the more the distance affects the slope the ramp part. The spectra in the VLF region, are determined by the relative relation between the peak amplitude of the first abrupt change and the slope of the ramp part. It can, therefore, be assumed that the difference of the characteristic of spectra in the VLF region between the positive strokes during winter and the negative strokes during summer must be caused by the difference of the effective height of the vertical channel. Indeed, if one checks the ratios of the peak value of the abrupt change versus the slope of the ramp part, one can recognize that the case of the channel height of 2.5 km can explain the anomalous spectra of the positive strokes during winter. That is, the ratios at 5 km and 15 km are respectively 1.0 and 0.13 and these values are coincident with the "16 dB per 10 km". Unfortunately, the observations which are discussed in this paper, were carried out with a single station method, and therefore the height of charge center cannot be estimated. Nevertheless, one can find almost the same analyses results given by Brook et al. [11] (for example storm M and Q). 2.5 km is not improbable for the height of the vertical channel. On the other hand one can find that some of the strokes in their paper have higher charge center than 2.5 km (for example storm F and H). Even in such a case, and if the return stroke channel has some branches, there is some possibility that the effective channel may become rather short. In any case the further observation will be needed before definite conclusions can be presented.

In the following, the discussion on the bipolar oscillations is presented. Takagi and Takeuti [16] have already presented the paper in order to explain these phenomena with the current reflection model at the cloud base. However, the physical meaning of the current reflection is not clear for the lightning return stroke. As indicated above, there is some possibility that the height of the vertical channel of the positive strokes during winter is not so high.

Moreover, Takeuti et al. [10] have indicated. Figure 8 of their paper, that some of the flashes during winter have horizontal branches at rather low altitude. Weidman and Krider [22] have indicated unipolar oscillations due to branches. There is a possibility that both the shortness of height of the vertical channel and the horizontal branch can cause the bipolar oscillations.

In Figure 6, the ratio of the peak amplitude of vertical electric fields radiated by a horizontal dipole to those radiated by a vertical dipole versus propagation distance are shown. Those are computed theoretically using Norton's formulas [23] and the Fourier Transform [24]. The altitudes of the dipole are 1 and 3 km. One can find that if the altitude of the dipole is low, the horizontal dipole does not contribute to the vertical electric fields so much. In other words, as is the case of the winter thunderstorm in Japan, one can neglect the horizontal branch of the return stroke channel, when one discusses the vertical electric fields. That means that if the effective channel height is low, only the vertical component of the electric current can be contribute to the vertical electric field. The direction of the horizontal branch has no meaning and only the distance to the striking point must be considered. The observation results show that the critical distance of the bipolar oscillations is 10 km and, if the calculation is carried out for this distance and the channel height 2.5 km the numerical results show the 20 kHz bipolar oscillation. The physical meaning of this result is that so-called radiation zone become rather closer to the striking point, due to the shortness of the height of vertical channel. It should be noted that if the calculation is executed for more than the height of 5 km of the vertical channel, only the unipolar oscillation, have obtained. Concerning this case the static field is large enough and it never becomes bipolar oscillations.

CONCLUSIONS

In this paper spectra of electric field changes due to the positive first ground strokes were estimated with the maximum entropy method and the following conclusions were obtained.

- The average fundamental component of bipolar oscillations, which are often observed during positive ground strokes, is 16 kHz.
- Frequency spectra fall of roughly as 1/f for frequency between 10 kHz through 100 kHz. This shows the same tendency as of previous results and there is no contradiction.
- Anomalous frequency spectra for the frequency range from 0.8 to 10 kHz of positive strokes is recognized and this may be caused by the effective shorter height of vertical channel. That means that some of the effective height of vertical channel of positive strokes during winter may be shorter than that in summer. Moreover, it could be related to the bipolar oscillations.

REFERENCES

1. A.S. Dennis, and E.T. Pierce, "The return stroke of the lightning flash to earth as a source of VLF atmospherics." Radio Science, 68D, 777-794, 1964,

2. G.I. Serhan, M.A. Uman, D.G. Childers, and Y.T. Lin, "The RF spectra of first and subsequent return strokes in the 1 to 200 km range." Radio Science, 15, 1089-1094, 1980.

3. C.D. Weidman, E.P. Krider, and M.A. Uman, "Lightning amplitude spectra in the interval 100 kHz to 20 MHz." Geophys. Res. Lett., 8, 931-934, 1981.

4. J. Preta Jr, M.A. Uman and D.G. Childers, "Comments on 'The rf spectra of first and subsequent lightning return strokes in the 1 to 200 km range' by Serhan et al. Radio Science, 20, 143-145, 1985.

5. D.L. Croom, "The frequency spectra and attenuation of atmospherics in the range 1-15 kc/s." J. Atmos. Terr. Phys., 26, 1015-1046, 1064.

6. D.M. Levine, and R. Menegini, "Simulation of radiation from lightning return strokes: The effects of tortuosity." Radio Science, 13, 801-809, 1978.

7. J.A. Leise, and W.L. Taylor, "A transmission line model with a general velocities for lightning." J. Geophys. Res., 82, 391-396, 1977.

8. H. Volland, "Wave form and spectral distribution of the electromagnetic field of lightning currents." J. Atmos. Terr. Phys., 43, 1027-1041, 1981.

9. M.A. Uman, M.J. Master, and E.P. Krider, "A comparison of lightning electromagnetic fields pulse in the frequency range 10^4 to 10^7 Hz." IEEE Trans. Electromagn. Compat., EMC-24, 410-416, 1982.

10. T. Takeuti, M. Nakano, M. Brook, D.J. Raymond, and P. Krehbeil, "The anomalous winter thunderstorms of the Hokuriku Coast." J. Geophys. Res., 83, 2385-2394, 1978.

11. M. Brook, P. Krehbiel, and T. Takeuti, "The electrical structure of the Hokuriku winter thunderstorms." J. Geophys. Res., 87, 1207-1215, 1983.

12. W.D. Rust, D.R. MacGorman, and R.T. Arnold, "Positive cloud-to-ground lightning flashes in severe storms." Geophys. Res. Lett., 8, 791-794, 1981.

13. V. Cooray, and S. Lundquist, "On the characteristics of some radiation fields from lightning and their possible origin in positive ground flashes." J. Geophys. Res., 87, 11203-11214, 1982.

14. W. Beasley, "Positive cloud-to-ground lightning observations." J. Geophys. Res., 90, 6131-6138, 1985.

15. T. Takeuti, S. Israelsson, S. Lundquist, E. Åström, and M. Nakano, "Fine structures of field changes due to positive ground flashes." Paper presented at the 6th Int. Conference on Atmospherics Electricity, Manchester, July 28 to August 1, 1980.

16. N. Takagi, and T. Takeuti, "Oscillating bipolar electric field changes due to close lightning return strokes." Radio Science, 18, 391-398, 1983.

17. D.G. Childers, ed, "Modern Spectrum Analysis." IEEE Press, New York, 1978.

18. Y.T. Lin, M.A. Uman, and R.B. Standler, "Lightning return stroke models." J. Geophys. Res., 85, C3, 1571-1583, 1980.

19. M.J. Master, M.A. Uman, Y.T. Lin, and R.B. Standler, "Calculations of lightning return stroke electric and magnetic fields above ground." J. Geophys. Res., 86, 12127-12132, 1981.

20. Y.T. Lin, M.A. Uman, J.A. Tiller, R.D. Brantley, E.P. Krider, and C.D. Weidman, "Characterization of lightning return stroke electric and magnetic fields from simultaneous two-station measurements." J. Geophys. Res., 84, 6307-6314, 1979.

21. J.A. Tiller, M.A. Uman, Y.T. Lin, R.D. Brantley, and E.P. Krider, "Electric field statistics for close lightning return strokes near Gainsville, Florida." J. Geophys. Res., 81, 4430-4434, 1976.

22. C.D. Weidman, and E.P. Krider, "The fine structure of lightning return strokes wave forms." J. Geophys. Res., 83, 6239-6247, 1978.

23. K.A. Norton, "The propagation of radio waves over the surface of the earth and in the upper atmosphere." Proc. IRE, 25, 1203-1236, 1937.

24. Z-I. Kawasaki, and S. Israelsson, "Calculations of lightning return stroke electric fields above ground with finite conductivity." Submitted to J. Geophys. Res., 1986.

Table 1. Theoretically estimated values of the initial peak amplitudes of the electric field charges and the gradients of the ramp part. Those are normalized to the value at 5 km. If the height of the vertical channel is enough high the relative gradient of the ramp part does not charge so rapidly in the range of 30 km.

distance	normalized peak value of abrupt change	gradient of ramp part the height of vertical channel 7.5 km	5.0 km	2.5 km
5 km	1.00	1.00	1.00	1.00
10 km	0.62	0.37(0.60)	0.25(0.40)	0.16(0.26)
15 km	0.38	0.16(0.42)	0.09(0.24)	0.05(0.13)
20 km	0.25	0.08(0.32)	0.04(0.16)	0.01(0.04)

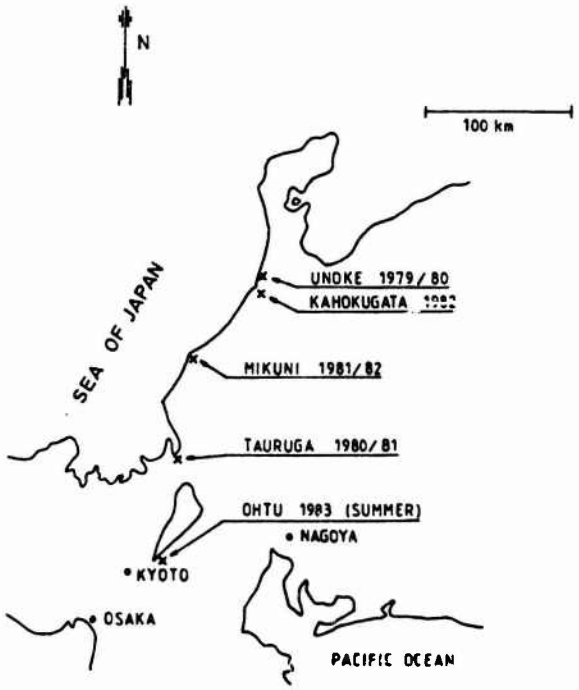

Figure 1. The observation sites from 1979 to 1983.

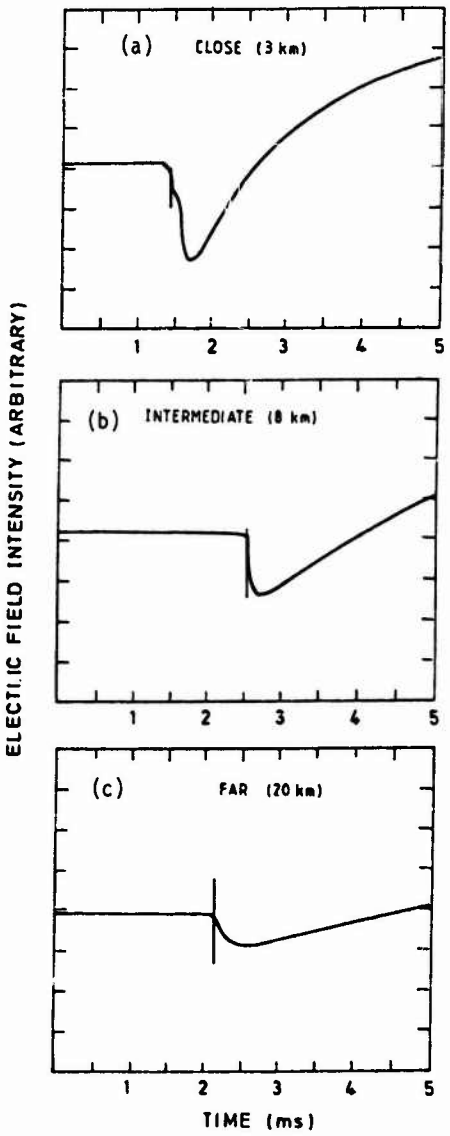

Figure 2. Typical wave forms of the electric field changes due to the first cloud to ground strokes. The distances are, from the top to the bottom, 3, 8 and 20 km, respectively. Observed 17 strokes are classified into three groups, (a) close lightning 6 strokes, (b) intermediate lightning 3 strokes, and (c) far lightning 8 strokes.

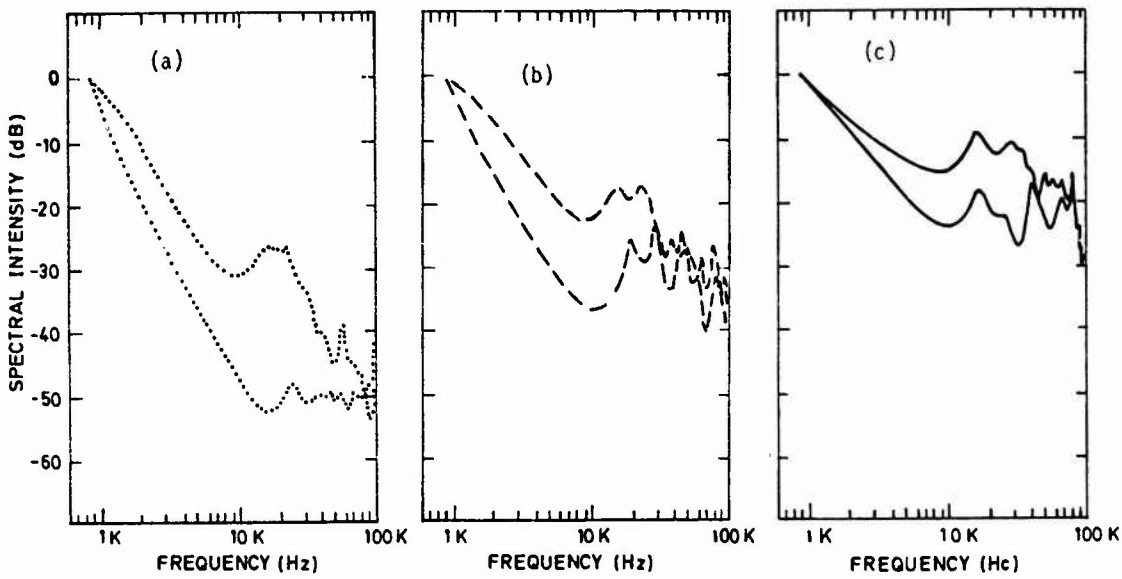

Figure 3. Frequency spectra of electric field changes due to the first positive ground strokes during winter thunderstorms. According to the classification of the present paper, (a), (b) and (c) are for the close lightnings, the intermediate lightnings and the far lightnings, respectively.

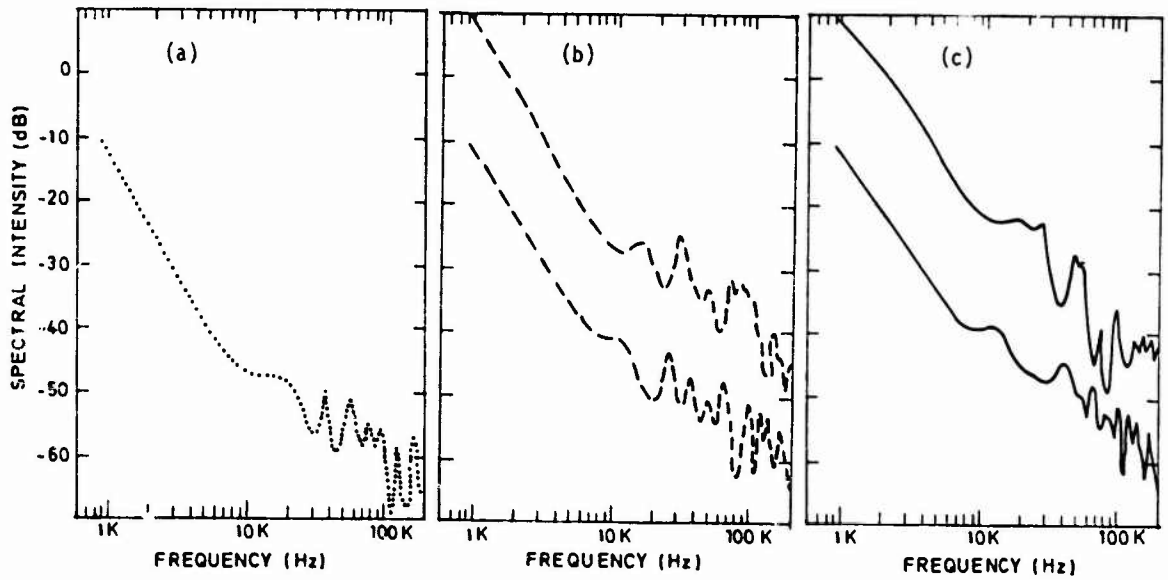

Figure 4. Frequency spectra of electric field changes due to the first negative ground strokes during summer thunderstorms. See caption of Figure 3.

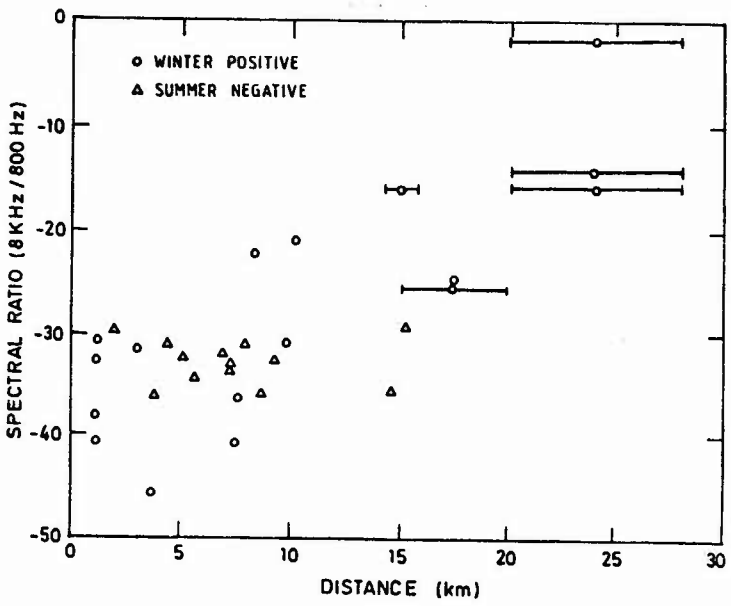

Figure 5. Spectral ratios of 8 kHz against 0.8 kHz versus the propagation distance. This shows the anomalous propagation effect of the positive strokes during winter thunderstorm in the frequency range from 0.8 to 8 kHz. ● denotes the ratios of positive lightnings, Δ those of negative lightnings during summer. Error bars indicate the ambiguity of the distance.

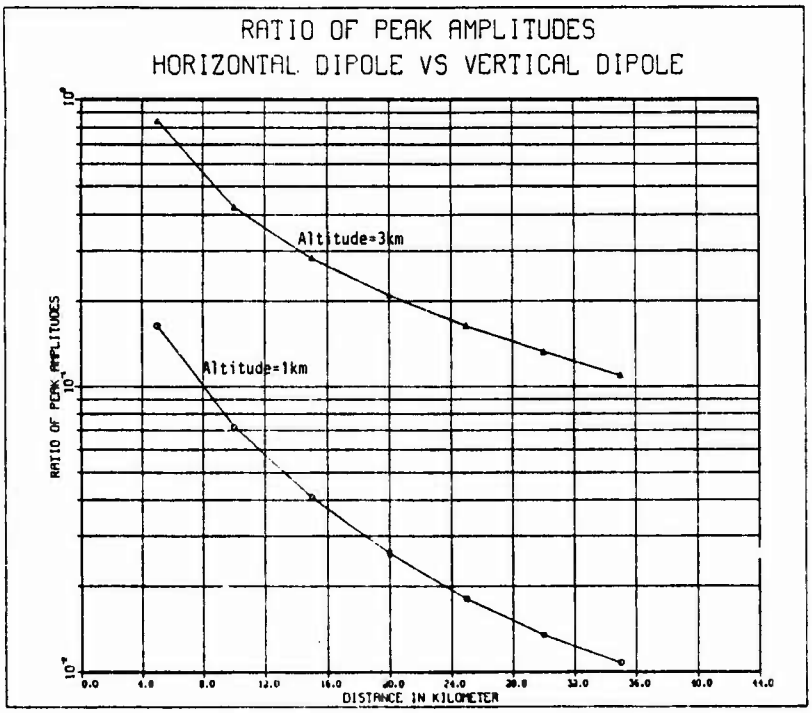

Figure 6. The ratio of the peak amplitude of vertical electric fields radiated by a horizontal dipole to those radiated by a vertical dipole.

ELECTROSTATIC FIELD MEASUREMENTS IN A FOAM FILLED C-130 FUEL TANK DURING FUEL SLOSHING

Adam R. Bigelow, Capt, USAF
M. Patricia Hebert, Capt, USAF
Pagop Jibilian, 2Lt, USAF
Air Force Wright Aeronautical Laboratories
Wright-Patterson AFB, OH 45433

Jean S. Reazer
Technology/Scientific Services, Inc.
Dayton, Ohio 45431

ABSTRACT

An electric field sensor integration package has been improved for measuring the electric field inside a fuel tank during fuel sloshing. Five flush plate dipole sensors were mounted to a U.S. Air Force C-130 external fuel tank to determine the electrostatic charging characteristics of the explosion suppressant foam contained in the tank during sloshing. The outputs of the sensors were integrated electronically using a modernized version of the Bright, et al integration package (Ref 1). The external fuel tank was secured to a hydraulically activated platform designed specifically for this test effort. The platform was capable of tilting up to 30° of pitch at rates up to 30°/second. The tank was tested with two separste foam configurations: the operational configuration of non-conductive foam and a second configuration which contained an experimental conductive foam. Electric fields as high as 136 kilovolts/meter were recorded during slosh tests with the nonconductive foam at a 600 gallon fuel level (total capacity 1350 gallons). No measurable fields were recorded with the conductive foam installed in the tank. Two electrostatic discharges and ignitions occurred during testing of the nonconductive foam while no discharges or ignitions occurred during testing of the conductive foam.

INTRODUCTION

U.S. Air Force C-130 aircraft have been experiencing fires in explosion suppressant foam filled fuel tanks since the introduction of nonconductive polyether blue foam in 1977. The foam provides explosion protection to the fuel tank in the event of an ignition in the ullage due to either a ballistic penetration or an electrical discharge such as lightning. When an ignition occurs, the foam suppresses the expansion of the flame front, thereby keeping the amount of overpressure in the fuel tank within a range the tank can withstand. The problem with the foam is that it is nonconductive in nature and can therefore build up a static charge as fuel sloshes through it. When the charge level is sufficient and the proper conditions exist, an electrostatic discharge can occur. If the electrostatic discharge is in the form of a spark discharge and occurs in the ullage of the fuel tank, the fuel vapors may ignite. Obviously, this is a very undesirable situation.

Fuel slosh tests were performed to determine the electrostatic charging characteristics of fuel and explosion suppressant foam in external fuel tanks of C-130 aircraft. A number of parameters were varied throughout the experiment including the fuel level inside the tank, the type of foam in the tank, how fast the fuel was sloshed (pitch rate), and how far the tank was tipped (pitch angle). A Lockheed designed external fuel tank was used throughout the tests. Two different types of foam kits were used in the fuel tank, an operational foam kit containing both type IV blue and type II yellow foam and an experimental kit made of a conductive safety foam, CSF-204. This foam is the coarse pore blue foam with a coating to improve its conductivity. It is dyed beige to distinguish it from the blue foam. It has been suggested that the beige foam (because of its higher conductivity) should replace the blue/yellow foam in order to relieve the electrostatic charging/discharging problem. This paper discusses the difference in the measured charge build up as a result of using the two different foam kits. Although the fuel level was varied during testing (fuel level was either 300, 600, or 900 gallons), only the 600 gallons test results are presented. The effects of pitch rate and pitch angle are not discussed either.

SET UP

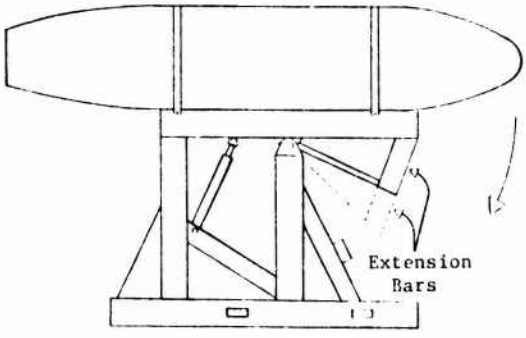

Figure 1. C-130 External Fuel Tank On Slosh Platform

Tank and Slosh Platform

Figure 1 shows the tank and support fixture setup used through out the experiment. A Lockheed external fuel tank was securely mounted to the slosh platform, which was designed to produce pitch rates up to 30° per second(s) through pitch angles of 30°. Two hydraulic cylinders pushed the rear of the platform upwards as it pivoted about a central axle. As the front end of the platform traveled downward, it contacted a deceleration switch which stopped the motion of the platform. The cylinders could then be actuated to return the platform to the horizontal position. A calibrated deflection potentiometer was attached to the platform to record the angular displacement of the test rig. When the output of the deflection pot was plotted as a function of time, the pitch rate could also be determined.

The pitch angle was varied by replacing the extension bars (see Figure 1). With a longer set of extension bars, the distance to the deceleration switch was decreased, thus limiting the range of motion of the platform. A shorter set of extension bars allowed for more motion. The pitch rate was changed by adjusting the hydraulic pressure.

The tank itself was 25 ft long and 45 inches in diameter. Internal bulkheads divided it into nose, center, and tail sections (see Figure 2). For the series of tests in the operational configuration, the nose and tail sections contained blue foam while the center section contained yellow. For the conductive foam test, all three sections contained beige foam. Total capacity of the external fuel tank was 1350 gallons.

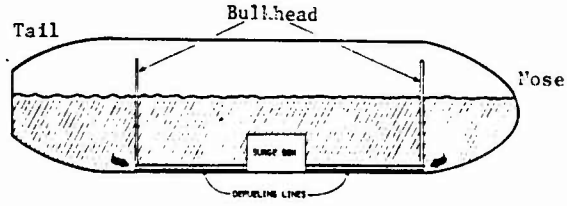

Figure 2. Lockheed External Fuel Tank, Surge Box, and Defueling Lines

Instrumentation

1. Electric Field Meters

Electric field meters with no moving parts were constructed by AFWAL/FIESL using a design developed by Bright, et al at the University of Southampton (Ref 1). A plate mounted flush with the inner surface of the tank is maintained at ground potential by a circuit which detects the plate potential and supplies the charge needed to keep it near ground. The charge flows through a capacitor whose output voltage is monitored to measure the total charge supplied.

Using Gauss's Law, the electric field, E, on the front of the sensor inside the tank is related to the charge, Q, induced on the sensor by

$$Q = A\epsilon_0\epsilon_v E \qquad (1)$$

Where A is the area of the probe, ϵ_o is the permittivity of free space and ϵ_v is the dielectric constant of the vapor. The voltage, V_o, across the capacitor, C, is given by:

$$V_o = Q/C \quad (2)$$

and the field, therefore, is:

$$E = \frac{V_o C}{A\epsilon_o \epsilon_v} \text{ V/meter} \quad (3)$$

This type of field meter was selected over the rotating vane type because it was rugged, small in size, and, most important, had no moving parts which might produce a spark and possible fuel ignition.

Five of these sensors were installed in the tank. One was installed at the aft end of the tank in an orientation that would detect horizontal fields. The other four were installed so as to detect vertical fields, with one in the front section, two in the center section and one in the aft section. Figure 3 shows where the sensors were positioned on the Lockheed tank. Dielectric caps were placed on four of the five sensors (all but sensor D) to prevent fuel from splashing on them. The outputs from the electric field meters were recorded on a six channel TXP 2065 Linseis strip chart recorder running at 50 centimeters/minute (1.2 seconds/centimeter). The frequency response of this system is from DC to 3 Hz.

2. Thermocouples

Six chromel/alumel type K thermocouples, manufactured by Omega Engineering Inc., with a temperature range of -50° to 1250°C were installed in the tank. One was positioned in the lowest part of each of the three sections to record fuel temperatures and one was positioned near the top of each section to record ullage temperatures. All of the thermocouples were bonded to the tank by attaching a grounding wire to prevent any possibility of a static discharge. The thermocouple gauge outputs were fed into an LED display.

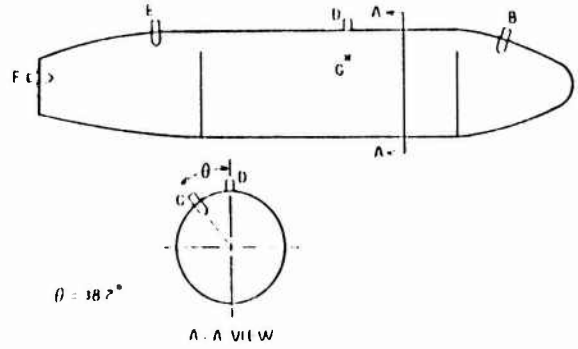

Figure 3. Placement of Electric Field Sensors

3. Radio Receivers

Three AM radio receivers tuned to a frequency of 540 kilohertz (kHz) were installed in the tank in fuel-proof containers, one in each section. A fourth radio was mounted outside of the tank to provide a reference showing baseline noise due to hydraulic system switching, etc. Outputs from the radios were recorded on FM channels of a Bell and Howell 3700E recorder.

4. Deflection Potentiometer

A deflection potentiometer manufactured by Celesco Inc. was used to measure the pitch rate and angle. It has a resolution of 0.001 inch and frequency response of up to 60 hertz. The output was recorded on the Linseis strip chart recorder simultaneously with the electric field data to provide time correlation between pitch, pitch rate, and the measured electric field.

Fuel

The fuel used throughout the experiment was JP-4 without antistatic additives (ASA). This fuel was chosen because of its extremely low conductivity (10 conductivity units (CU)), and its high volatility (flash pt = -13°F). Many of the C-130 foam fires have occurred when the aircraft fuel tanks contain a mixture of JP-4 with ASA and JP-5 or Jet A-1 without ASA. If the mixture contains largely JP-5 or Jet A-1, then the mixture has essentially the same electrostatic properties as JP-4 without ASA. This is why no ASA was used with the JP-4. The fuel was chilled so that its temperature during testing was between 20° and 40°F. This temperature range provided optimum potential for ignition (Ref 2,3).

Safety

Because of the inherent danger of working with aviation fuel and the possibility of an ignition, the tests were performed inside an explosion proof facility - Range 3 of the AFWAL Aircraft Survivability Research Facility. During sloshing, test personnel were located in a separate blockhouse which housed the slosh platform control equipment and data acquisition equipment. Grounding straps were attached to the fuel tank and refueling nozzle during fueling and defueling in order to prevent any electrical discharges.

TEST METHOD

A test matrix was developed to allow determination of the effects of five variables: type of tank, type of foam, quantity of fuel, pitch angle and pitch frequency. (This report covers only the results for the Lockheed Tank.) The Lockheed tank with the blue/yellow foam combination was installed on the slosh test fixture for the first series of tests. Baseline noise measurements from the electric field meters and AM radios were determined by recording their outputs as the empty tank was tipped several times. Three hundred gallons of chilled JP-4 fuel were then metered into the tank and preliminary tip tests were conducted to ensure the correct pitch frequency and angle. After completion of fueling and preliminary tip testing, the tank was left undisturbed for ten minutes to allow time for fuel relaxation. The standardized test sequence was as follows:

1) Record pre-test thermocouple readings.
2) Adjust electric field meters.
3) Tip the tank two and one half times, allow tank to remain down for 30 seconds, then return tank to level attitude.
4) Record post-test thermocouple readings.
5) Verify recording of electric field meter, flowmeter, and radio outputs.
6) Verify pitch rate and angle from deflection potentiometer output.

This aequence was repeated three times at ten minute intervals for each fuel level (300, 600, and 900 gallons). Temperatures in the fuel and ullage were monitored closely to ensure that fuel temperatures stayed within range. When necessary, fuel was removed, chilled, and returned to the tank to keep temperatures nominally between 20° and 40°F.

Pitch angles of 10°, 20° and 30° were used. Pitch frequencies were 10°/s and 20°/s for the 10° pitch angles and 10°/s, 20°/s and 30°/s for the 20° and 30° pitch angles.

After completion of the blue/yellow foam combination test series, the blue/yellow foam was replaced by the beige foam. The same test sequence was followed during beige foam testing. Pitch angles and frequencies used were 10° at 10°/s and 20°/s and 30° at 10°/s, 20°/s and 30°/s. The measurements at the 20° pitch angle were eliminated due to time constraints. Also, the over-the-wing filler neck and the fuel cage surrounding the SPR valve were removed before this series of tests to allow for direct fuel impingement on the beige foam.

RESULTS

General

The results presented in this section are for data acquired from testing a C-130 External Fuel Tank manufactured by Lockheed. The electric field data is presented to compare the results of testing the blue/yellow foam configuration (nonconductive) versus the beige foam configuration (conductive). Data on one of the electrostatic discharges which produced an ignition is also presented. All results reported in this section are for fuel levels of 600 gallons.

Electric Field Data

The outputs from two electric field sensors are used to demonstrate the difference in the charge build-up between the nonconductive and conductive foam kits. One sensor, C in Figure 3, measured the vertical component of the electric field in the center section, while sensor F measured the horizontal component of the electric field in the tail section of the tank.

Figure 4 shows the vertical electric field measured in the center section. The top trace is from the nonconductive blue/yellow foam test and the middle trace is repreaentative of the conductive beige foam tests. The bottom trace is the output from the deflection potentiometer. All traces are from tests performed at a 600 gallon fuel level, 30° pitch angle, and a 10°/s pitch rate. The deflection pot shows the tank tipping downward to an angle of 30°, returning to the horizontal position, tipping downward, returning to horizontal, then tipping once more. It also provides time correlation between the measured electric field and the angular displacement of the tank.

A comparison of the two electric field traces in Figure 4 reveals the charging characteristics of the two different foam configurations. For this particular test, the nonconductive foam kit produced an initial peak electric field of 6.8 KV/m, measured when the tank had tipped to its full deflection. The conductive foam kit produced no measurable electric field.

Figure 5 shows the horizontal electric field measured in the tail section for the same tests as shown in Figure 4. The top trace is the horizontal electric field for the nonconductive foam configuration, the middle trace is the horizontal electric field for the conductive foam configuration, and the bottom trace is the deflection pot output. The nonconductive foam kit produced an initial peak electric field of 136 KV/m. The conductive foam kit produced no measurable electric fields as indicated hy the middle trace in Figure 5.

The two conductive foam traces reveal that no electric fields were measurable. Similar results were found for all sensors regardless of the pitch angle, pitch rate, or fuel level.

Diacharge and Ignition

The following is presented to compare electric field data from a normal test with data from a test during which an electrostatic discharge produced an ignition. Figure 6 compares two vertical electric fields measured in the center section of the fuel tank. The top trace shows the usual type of output from this sensor and is the same trace shown in Figure 4(top). The parameters during this test were a pitch angle of 30°, a pitch rate of 10°/s, a fuel level of 600 gallons, and nonconductive foam. The middle trace in Figure 6, which shows an electrostatic discharge, is a recording of the vertical electric field during the test subsequent to the one shown in the top trace. The pitch angle, pitch rate, and fuel level remained the same. The bottom trace is the output from the deflection potentiometer.

An electrostatic dischsrge manifests itself by a sudden collapse of the electric field. This can be seen in the middle trace in Figure 6 just past the 19 second mark. The tank had gone through two complete slosh cycles and had just begun its third tip when the discharge occurred. Four of the five electric field sensors mounted on the tank detected the discharge.

The horizontal electric field sensor in the tail section of the tank did not register a sudden collapse of the electric field. Figure 7 shows the horizontal fields measured in the tail section that correspond to the vertical fields in Figure 6. The top trsce in Figure 7 shows the horizontal field for a normal test, the middle trace shows the horizontal field for a test which produced an electrostatic dischsrge, and the bottom trace is output from the deflection pot. As can be seen from Figure 7, the trace for the test with a dischsrge is essentially identical to the trace for a test without a discharge.

There are two possible reasons why the horizontal electric field sensor in the tail section did not detect the discharge. A bulkhead separated the tail and center sections and may have shielded the horizontal field sensor from the discharge. It is also possible that the discharge occurred in the vertical plane or direction. Since the horizontal electric field sensor can only detect fields in the horizontal plane, it would not detect a discharge in the vertical plane.

CONCLUSIONS AND RECOMMENDATIONS

Both conductive and nonconductive explosion suppression foam kits were tested for electrostatic charging characteristics during fuel sloshing in a C-130 Lockheed external fuel tank. It was found that the conductive foam kit (CSF-204) produced no measurable electric fields and no static discharges. The nonconductive foam kit (Type II yellow and Type IV blue) produced electric fields as high as 136 KV/m as well as two electrostatic discharges and fuel vapor ignitions. The CSF-204 beige foam decreased the charge build-up by over two orders of magnitude. The conductive foam, because of its enhanced electrical conductivity properties, is far superior to the nonconductive blue/yellow foam for minimizing fuel tank electrostatic discharges and resultant ignitions. If the CSF-204 beige foam meets all of the basic requirements for conductive foam (i.e. lifetime, water solubility, corrosion, etc.), then based on its electrostatic qualities, it would be a favorable candidate to replace nonconductive explosion suppression foam.

REFERENCES

1. Bright, A.W., Bloodworth, G.G., Smith, J.G., and Yuratich, M.A., "The Development of Electric Field Meters for Use in Automatic Systems for Control of Electrostatic Charge in Fuel Tanks", Lightning and Static Electricity Conference, Culham Laboratory, England, 14-17 April 1975.

2. Smith, Maxwell, Aviation Fuels, G.T. Foulis & Co Ltd, Cambridge, England, 1970, pp 170-190.

3. Handbook of Aviation Fuel Properties, Coordinating Research Council, Society of Automotive Engineers, Inc., May 1984, pp 64-80.

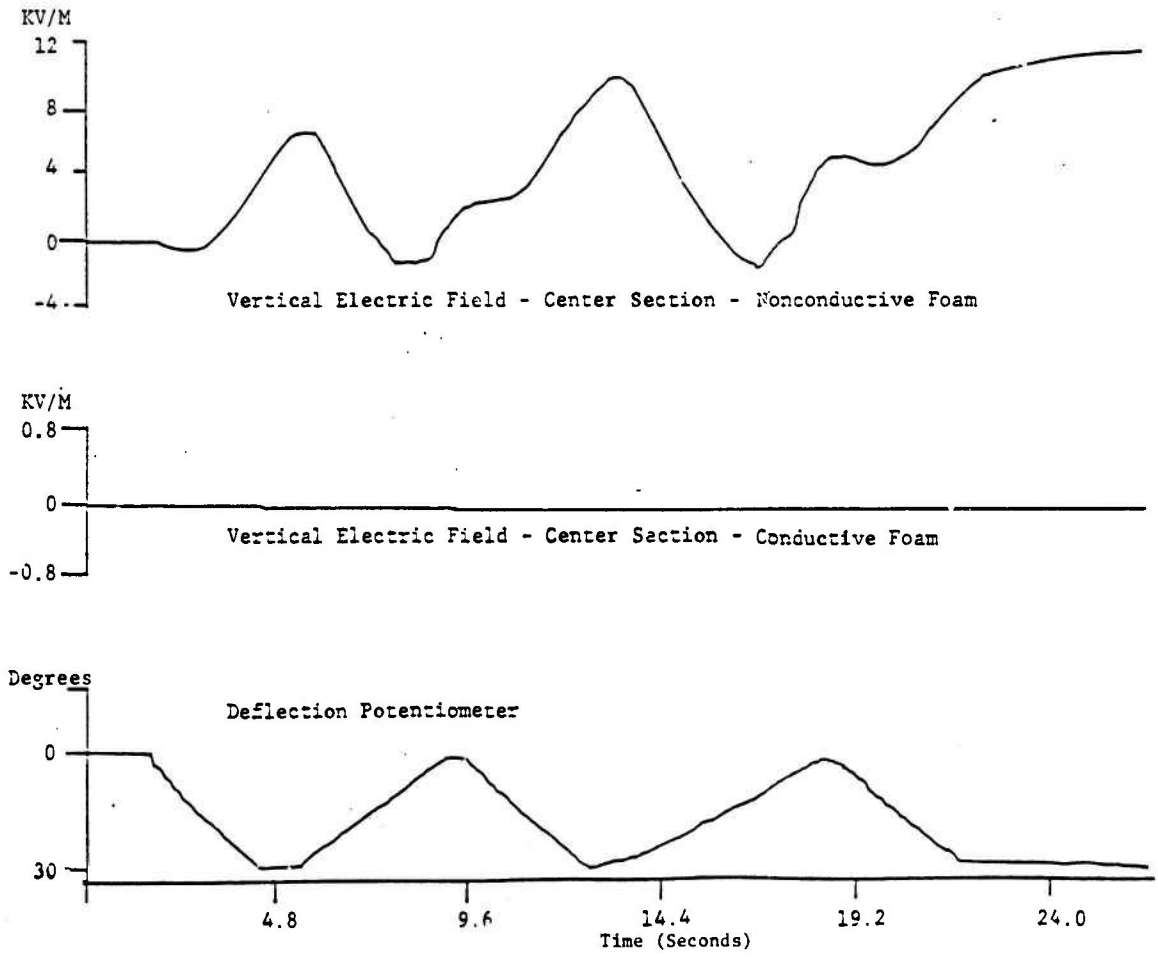

Figure 4. Vertical Electric Field, Nonconductive vs. Conductive Foam

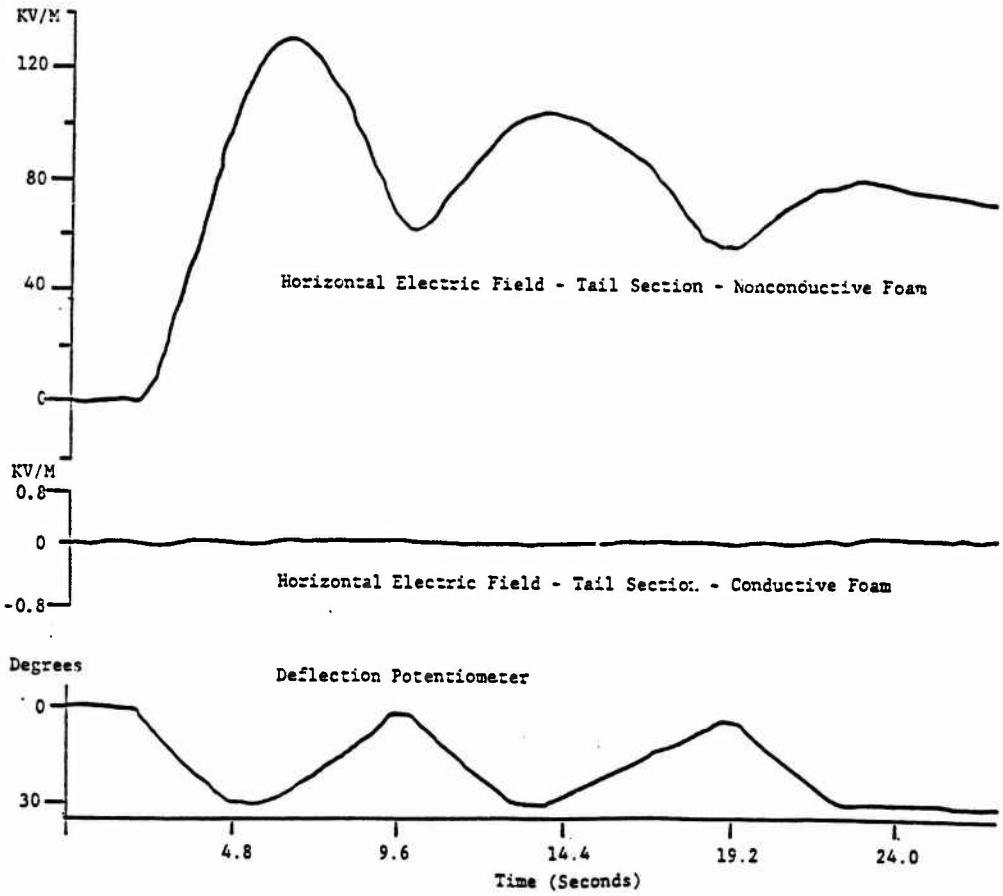

Figure 5. Horizontal Electric Field, Nonconductive vs. Conductive Foam

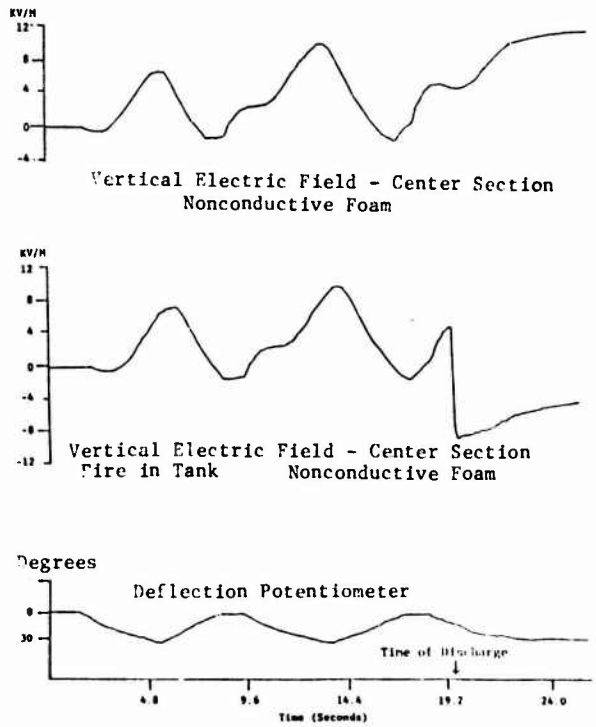

Figure 6. Electrostatic Discharge, Nonconductive Foam

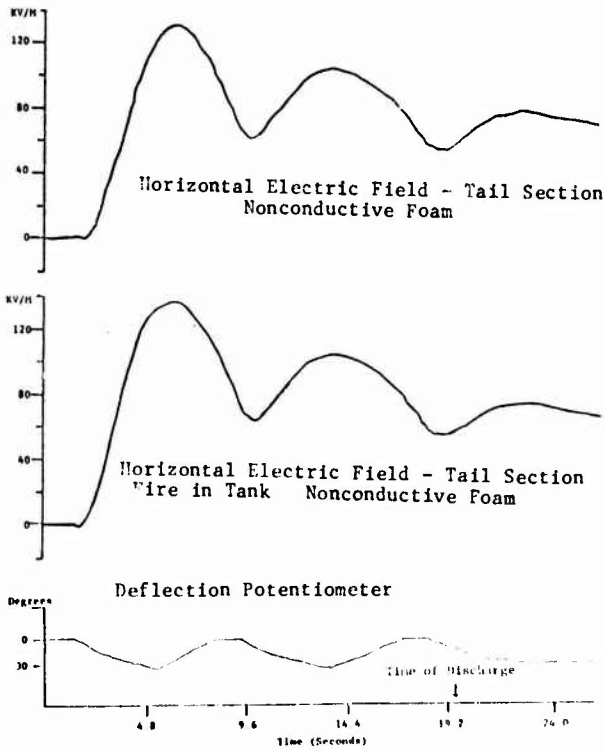

Figure 7. Electrostatic Discharge, Nonconductive Foam

MINIMUM IGNITION LEVELS OF AIRCRAFT FUEL CONSITUENTS TO LIGHTNING RELATED IGNITION SOURCES

K. E. Crouch
Lightning Technologies, Inc.

ABSTRACT

Lightning strike related hazards to aircraft fuel systems have been responsible for many of the catastrophic aircraft incidents to date. To develop meaningful methods of evaluating fuel system protection designs, an understanding of the basic ignition process is required. Three basic ignition sources were investigated to establish conditions leading to the minimum ignition of mixtures of fuel vapors and air.

A 200 microjoule spark was found to have an ignition probability of 0.01 to 0.1%. Sparks of 600 to 700 microjoules represent a 50% ignition probability. Hot spots of $1cm^2$ required temperatures of greater than 800^0C to ignite. Corona, glow discharge, was found incapable of ignition until the discharge transitioned into an arc.

INTRODUCTION

THE NEED FOR TEST PROCEDURES to evaluate the lightning protection design of aircraft fuel systems has long been recognized. The Naval Air Development Center (NADC), with the support of the Air Force Wright Aeronautical Laboratories (AFWAL/FIESL), contracted Lightning Technologies, Inc. and Lightning Transients Research Institute to develop, document and verify such a set of test procedures. The objective of the effort is specification which can be used to verify the performance of a fuel system lightning protection design. It will include both engineering design and qualification test procedures and will establish a means for determining if a protection design provides a margin of safety against lightning related fuel vapor ignition hazards in conventional, advanced composite or any new technolgoy design.

The first phase of the effort was a review of the present state of the art and established practice. In that effort, a plan for developing the required techniques and detection criteria was established. Lightning Technologies, Inc. reviewed and investigated fuel/air test techniques while Lightning and Transient Research Institute concentrated on optical techniques

The second phase of the effort, investigated and quantified minimum ignition source levels. That effort, which is reported here, was carried out by Lightning Technologies, Inc.

The 200 microjoule spark ignition threshold established by Lewis and Von Elbe (Ref. 1) during their work for the Bureau of Mines in the 1950's has long been applied as the criteria for evaluating the results of simulated lightning tests on aircraft fuel systems. This criteria has been interpreted in MIL-STD-1757 (Ref. 2) and FAA AC20-53 (Ref. 3) to be the absence of visible light on an ASA 3000 speed film exposed through an F4.7 lens or, in cases where the detection of light is not practical, the non-ignition of a 1.2 stoichimetric mixture of air and propane. The fact that these two criteria, photography and fuel mixture ignition, are not equivalent has been widely recognized, but better alternatives have not been available.

A study of Lewis and Von Elbe's work revealed that they were attempting to determine the lowest spark energy level which would ignite a fuel air mixture and did not address the problem of establishing an ignition source criteria. A review of the literature (Ref. 4) reveals that no studies have been carried out which would establish and/or document a criteria which can be used to evaluate the results of simulated lightning tests of aircraft fuel system designs.

Formulation of a criteria which can be used to evaluate lightning test results requires an understanding of the potential ignition sources and the ignition process. Four sources have been identified; sparks, the electrical breakdown of a gaseous fuel/air mixture between two electrodes; corona, the continuous electrical discharge from an electrode into a gaseous fuel/air mixture, hot spot, the evaluation of a small material surface in contact with a fuel/air mixture to a relatively high temperature; and arcs, the injection of hot or burning particles and plasma into a gaseous fuel/air mixture.

Each of these potential ignition sources, operating in different ways and over different time frames, transfer heat from the source to the fuel air mixture. At some critical time-temperature point, the heat transferred to the fuel and oxygen molecules promotes a self-sustaining reaction which quickly spreads throughout the volume of concern as a flame front. This rapid combustion creates an over-pressure condition or explosion.

The amount of heat or energy deposited into the mixture by a short duration source, a spark or an arc, is more easily determined than energy from a long duration source, hot spot or corona. For the short duration source, the energy needed for ignition will all be deposited at once while for the other sources, heat loss will occur during the process. For the longer duration process, the rate of energy added must reach a level such that the difference between energy input and energy loss will achieve a temperature where the reaction becomes self-sustaining. These modes of energy injection suggest that the ignition source duration will affect the ignition behavior. The importance of this observation lies in predicting the role of statistics in the description of the source behavior. Transient processes normally have wider statistical variations in their behavior than do steady state processes.

Experiments were designed and conducted to quantify and gain an understanding of mechanisms involved in the ignition sources. This paper describes these experiments and the results.

TEST PROCEDURES

Tests were conducted by introducing the ignition source at various levels into a test chamber containing a specific fuel/air mixture. The test chamber, shown in Figure 1, was loaded using partial pressure techniques. The chamber was evacuated to levels below 0.3 mmHg and refilled with appropriate pressures of oxygen, nitrogen and fuel. Liquid fuels, pentane and JP-4, were vaporized by boiling at low pressures. Pressure measurements were made using a mercury manometer. The chamber was fabricated by welding steel flanges on a 12 inch diameter steam pipe. Observation and electrical connections into the chamber were made through a one inch thick polycarbonate plate on one end. A blow out vent was installed on the other end of the chamber. Originally it was intended that the explosion would be contained but the high temperatures associated with a confined burn would have destroyed the plastic components in the chamber. All tests were vented as shown in Figure 2.

Safety considerations were foremost in the design and operation of the test system. Venting the explosions introduces a flame and precuations were taken to insure that no flammable materials were exposed. All tubing to the chamber also contained explosive mixtures, including those leading to the mercury manometer. Valves and flame arresters were installed on all lines to prevent flames in the tubing. In addition to all other measures, the operator worked behind a 1 inch thick sheet of polycarbonate as shown in Figure 3, to protect him from any flying objects.

MINIMUM ENERGY SPARK IGNITION TESTING

A simple spark gap, shown in Figure 4 was used for the experiments. Aluminum electrodes, 3.2 mm dia, and spaced 2 mm apart were used. The assumption was made, following the work of Lewis and Von Elbe, that all capacitive stored energy would be dissipated in the spark. Energy levels were changed by varying the system capacitance. Short heavy leads were used to connect the capacitors to the gap. Isolation resistors of 50×10^9 ohms were used to isolate the gap and capacitors from the charging power supply and to control the voltage rate-of-rise at the gap. The gap voltage was monitored with an electrostatic volt meter. Two 5×10^9 ohm resistors were used to isolate the electrostatic meter from the gap.

In air, the 2mm gap had a breakdown of 7950 volts $\pm$ 2%. However, when it was operated in the fuel/air mixtures, the breakdown levels varied considerably. The breakdown level ranged between 8 and 11kV and indicated a tendency to condition with repeated breakdowns. To eliminate any conditioning effects, the electrodes were polished and cleaned after every test. Only ignitions occurring during the first spark were counted and all mixtures were ignited by raising the charge voltage and allowing the gap to spark at higher voltages. The data point was not used if the mixture could not be ignited.

The variation in gap sparking level complicated the analysis of the data since over the 8 to 11 kV range, the energy at a given capacitance value almost doubles. The resulting data represented a continuum of points of energies. A computer program was used to sort and calculate the probability of ignitions over specific energy ranges. Table 1 shows a typical summary of energy versus ignition probability. Figure 5 shows a typical plot of ignition energy versus probability of ignition. Due to the random energy levels obtained during testing, the number of data points in each of the energy levels varied greatly and wasn't known until the analysis was completed. Consequently, all data points to be plotted do not have equal weight. To account for the possible variance in data points obtained from small data bases, the point was plotted as a line representing a change of plus or minus one ignition.

A total of 21 plots were made. In some cases, the data plots gave no indication of any trend, see Figure 6, so the line was plotted through the center of the data using an average slope determined from other plots.

From these plots, a tabulation of ignition probability versus energy was determined, as shown in Table 2. From this plot several conclusions can be drawn. First, 200 µJ ignitions are quite rare, between 1 in 1000 and 1 in 10,000, Pentane indicates a slightly lower ignition energy than propane but it should be noted that three times as many propane data points were taken, so the pentane data has a much lower confidence factor. This is illustrated by the fact that the 1.4 pentane data is not consistant with the 1.3 and 1.5 levels. At this point it can not be determined which is correct and therefore the true ignition level is probably an average of these numbers.

Second, increased oxygen (and fuel) concentrations radically reduce the ignition level, about 5:1. Since the ignition levels of JP-4 are even higher than those of propane and pentane, it may be that 200 µJ is too low a number to be practical and levels of 500 µJ (1 to 10%) should be considered.

If the 200 µJ criteria is retained, oxygen enriched mixtures must be used in fuel air testing.

MINIMUM HOT SPOT IGNITION TESTS

Hot spot testing was patterned after experiments conducted by Demetri & White (Ref. 5) who reported temperatures approaching 1000°C were required to ignite fuel air mixtures. Figure 7 is a photograph of the hot spot test fixture. Figure 8 is a schematic diagram of the electrical circuit. Two strips of 304 stainless steel, 1 cm wide and 7.6×10^{-2}mm thick, were mounted in the fixture, giving a thickness of 0.152 mm. The length of the foils exposed to the atmosphere was 1.6 cm. Approximately 3 mm of foil on either side of the fixture was cooled by the presence of the clamps.

The pulse circuit and dc power supply heated the foil quickly to predetermined temperature and held it. The circuit was shut off by the operator at the end of about one second. The foil temperature was monitored using a GE L14C1 NPN Planner Silicon phototransistor. The monitoring circuit, shown in Figure 9 was positioned 8.5 cm from the foil. Its output was calibrated by comparing its output to the reading of a type S Platinum vs Platinum 10% Rhodium thermocouple. The thermocouple, 0.76 mm diameter, was sandwiched between the two foils and insulated electrically with mica. The calibration process was very critical and had to be performed in a confined area as air currents caused by the hot foil could cause significant errors. Keeping the thermocouple in contact with the foil also presented problems since the foil expands and moves as it heats. The phototransistor was found to be very accurate and responsive over the 700 to 1000°C range.

Since the stainless steel surface texture and color change from its original state when heated, the foil emmissitivity changes affecting the radiation. New foils had to be conditioned by heating to 950 $\pm$ 5°C for one minute prior to using them. After conditioning, very little variation in calibration between foils was noted.

At high temperatures, 1000°C, the foils are very fragile and tend to break quite easily. The fixture was designed to give slight spring tension to hold the foil straight as it expanded. However, too much tension would tear the foil when it was hot. Anytime a foil tears or breaks while carrying current, sparking results which will immediately ignite the chamber. If the foil broke during a test, no data was taken because it had to be assumed that sparking had occurred.

Sincethere is no reason to presume that the hot foil would affect the chamber atmosphere, consecutive tests were conducted with the same mixture until ignition occurred. The fan was left running for the entire test duration.

Tests were conducted at 100°C intervals, starting at 700°C and increasing to ignition or 1100°C (the system upper limit). If a mixture did not ignite at 1100°C it was spark ignited to verify its flammability. Three tries at each temperature level

were applied.

The phototransistor output was recorded on a Tektronix 7633 storage oscilloscope. Typical test recordings are shown in Figure 10.

Table 3 presents a summary of the hot spot ignition test results. All ignitions occurred at the 900°C test level. No ignitions occurred at the 800°C level. The ignition was not sensitive to stoichiometric mixture or oxygen content. Tests outside or near the flammability limits were not conducted. The insensitivity to oxygen content or stoichiometric level reflects the steady-state aspect of the ignition process and any time-statical relationships present are undetectable.

Present hot spot detection techniques are based on the AIT (auto ignition temperature) of JP-4 and JP-5 which are 245°C and 238°C respectively. Hot spot temperature of 235°C (455°F) or higher are generally considered ignition hazards. The present data and that generated by Demetri & White indicate that temperatures of up to 800°C should be safe which is three times that presently used.

It is interesting to note that propane, pentane and JP-4 all ignite at the same temperatue even though their AIT's are quite different. Propane has an AIT of 495 to 505°C while pentane is reported to be between 285 and 290°C.

Figure 11 shows oscillograms of several typical ignitions. In most tests, the ignition occurs on the temperature rise and no delay is observed. Some of the few delays observed are shown in the figure, and even these delays were only about 300ms. Figure 12 shows photographs of the hot spot at several of the test levels used. At 500°C, the light emitted can just barely be detected in a darkened room but at 700 and 900°C, the hot spot can easily be detected in a well lighted room. Light detected by a camera does not appear to be a likely method of detecting hot spot ignition sources.

CORONA IGNITION TESTS

Corona is defined as a continuous, glow discharge breakdown of air. It is characterized by a low level current (microamperes), bluish luminosity and is usually associated with a sharp point.

The test fixture used is shown in Figure 13. The electrical circuit schematic is shown in Figure 14. Views of the test fixture in the chamber are shown in Figure 15.

Tests were conducted using two electrodes, a needle point (approximately 0.13 mm radius) and a blunt point (approximately 3.2 mm). The gap between the electrode and the ground plane was 2.0 cm. Both electrode positive and negative with respect to the plate were tested. The voltage was raised to a predetermined current level, typically 100μA, held for one minute. The current would then be raised to the next level, 110μA, and held for another one minute, This procedure was continued until ignition occurred.

The negative corona currents were supplied to the fixture through a 3 megohm resistor by a Hipotronics 100 series hipot tester. The current was measured on the panel meter. The meter was checked using a precision (1%) resistor and a digitial voltmeter.

Positive polarity currents were supplied from a Plastics Capacitors 50 kV dc power pack and a variac. The currents were monitored on the precision resistor and the digital voltmeter.

Aircraft changing mechanisms, i.e. ice and dust particles, almost always leave the aircraft with an excess negative charge. Consequently, the only time positive corona will exist is during a lightning flash, either attaching to the aircraft or charge centers in the near vicinity. During a flash attachment, a negative leader approaching the vehicle or a positive leader forming from the vehicle, positive corona can exist, but the duration will be short. Positive corona induced by nearby charge centers in clouds can exist for much longer times.

Since negative corona is the most prevalent and positive dc corona may not exist, most testing has concentrated on negative corona. In the interest of completeness, both were conducted during this program.

During the testing positive ignitions occurred at levels of 100 and 120μA. Negative ignitions occurred between 250 and 340μA. During the positive tests, it was obvious that the fixture was sparking over since at levels below 100μA, streamers were forming as shown in Figure 16. With fuel absent, the fixture sparked at the same levels indicating that the ignitions were resulting from sparks.

Negative ignitions were due to the same phenomina, but it was not nearly as obvious. With fuel removed, negative levels of 400 to 500μA would not cause fixture spark over and no evidence streamering could be seen. Initially, it was believed that the ignitions were corona induced. However, with rich fuel/air mixtures, non-flammable, in the chamber, fixture sparkovers occurred at the same range of current levels. Increasing the gap length increased the voltage level required to attain a given current level but fixture sparkover still occurred at the same corona current level for both positive and negative polarity.

Both positive and negative corona sources are visible to the eye and the camera at levels significantly below the ignition level.

The levels required for ignition are also well above the threshold for interference with HF radio equipment on the aircraft.

Glow discharges-Saint Elmo's Fire- cannot transfer sufficient heat to the fuel/air mixture to initiate an ignition. This agrees with Barreto (Ref. 6) who found that corona could not ignite a fuel/air mixture. The discharge must transition from the glow mode to the arc mode before ignition can take place. This happens at 100 to 120μA electrode positive, and 250 to 350μA electrode negative.

Examples of negative corona are shown in Figures 17 and 18. As can be seen in the Figures, the corona is visible to the eye and the camera at levels well below the onset of streamering and arc formation.

CONCLUSIONS

A 200 microjoule ignition appears to occur between 0.01% and 0.1% of the time. This may imply that a 200μJ criteria is too severe. A 0.01% ignition level coupled with 200kA strike (0.2%) and a favorable mixture (0.1%) will lead to a risk of 10^{-8} to 10^{-9}.

If the 200μJ criteria is retained, it must be detected by oxygen enriched fuel air mixtures.

Hot spot temperatures in excess of 800°C appear to be required to ignite flammable fuel/air mixtures. Light emitted by the hot spot prior to reading the ignition level makes photography a poor candidate for detecting hot spot ignition hazards.

The present temperature limits 235°C (455°F) based on AIT (SIT) data appear to be very low and must be reconsidered.

Corona glow discharges, cannot ignite fuel/air mixtures unless they can transition into an arc (heavy streamer) mode. It appears unlikely that metallic components contained within a dielectric fuel tank will be able to streamer.

REFERENCES

1. Von Elbe, G., Lewis, B., et al., "Ignition of Explosive Gas Mixtures by Electric Sparks", Third Symposium on Combustion & Flame & Explosion Phenomena, Baltimore: Williams & Wilkins Co., 1949.

2. MIL-STD-1757 "Lightning Qualification Test Techniques for Aerospace Vehicles and Hardware", dated 17 June 1980.

3. FAA Advisory Circular AC20-53 "Protection of Airplane Fuel Systems Against Fuel Vapor Ignition Due to Lightning", dated 12 April 1985.

4. Crouch, K.E. and Robb, J.D., "Aircraft Fuel System Lightning Protection Design and Qualification Test Procedures Development", NADC Report No. NADC-85090-20, dated February 1985.

5. Demetri, Elia P., White Bruce, F., "Development of a Model for Hot-Surface Ignition of Combustible Liquids", Advanced Mechanical Technology, Inc. Newton, MA for Air Force Wright Aeronautical Laboratories, WPAFB, OH Contract No. F33615-83-C-2380, dated May 1984.

6. E. Barreto, S.I. Reynolds, and H. Jurenka, "Ignition of Hydrocarbons and the Thermalization of Electrical Discharges. Journal of Applied Physics Vol. 45 No. 8, August 1974, pp. 3317-3327.

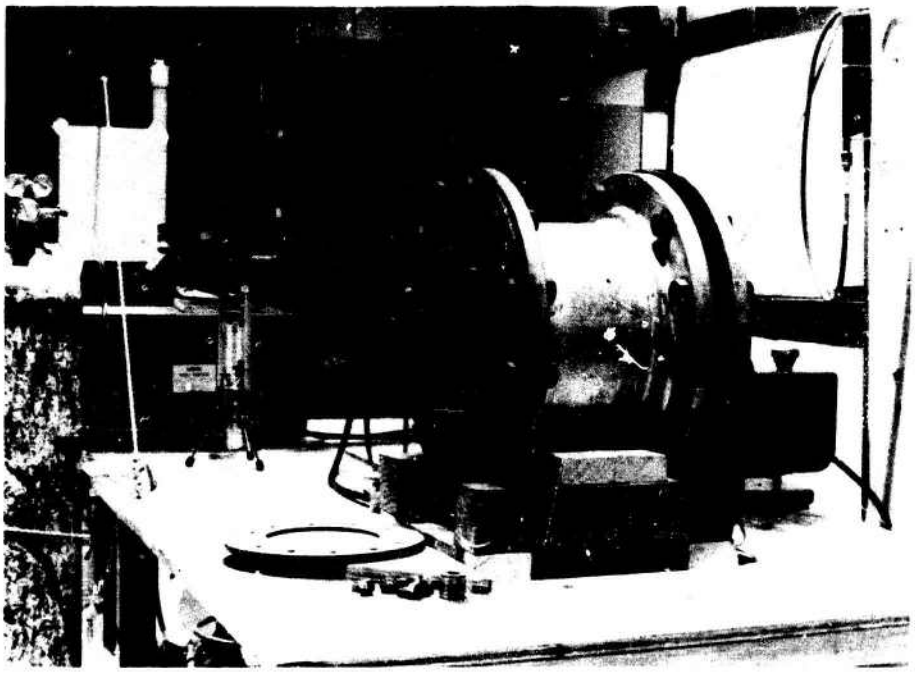

Fig. 1 - Explosion test chamber used for ignition tests

Fig. 2 - Test chamber venting an ignition during spark tests

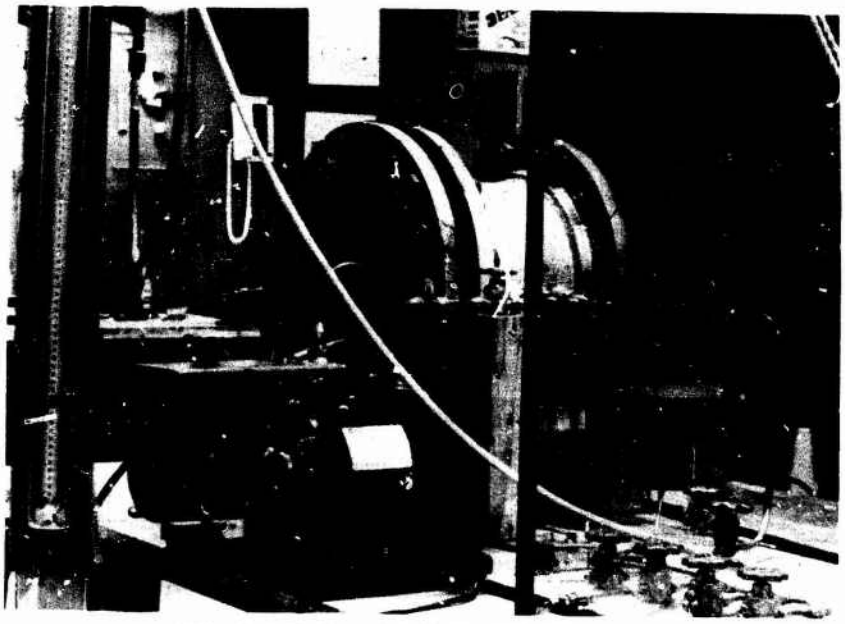

Fig. 3 - Minimum ignition test area

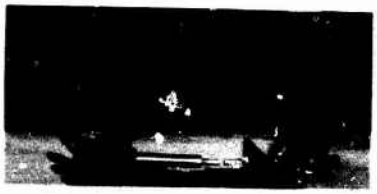

Fig. 4 - Spark ignition test fixture

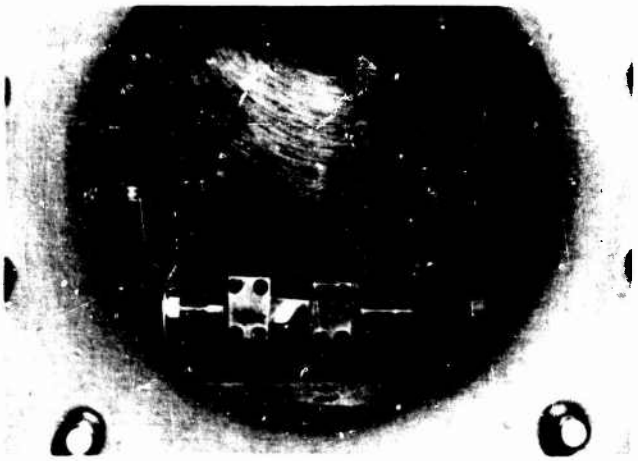

Fig. 7 - Hot spot test fixture installed in the chamber

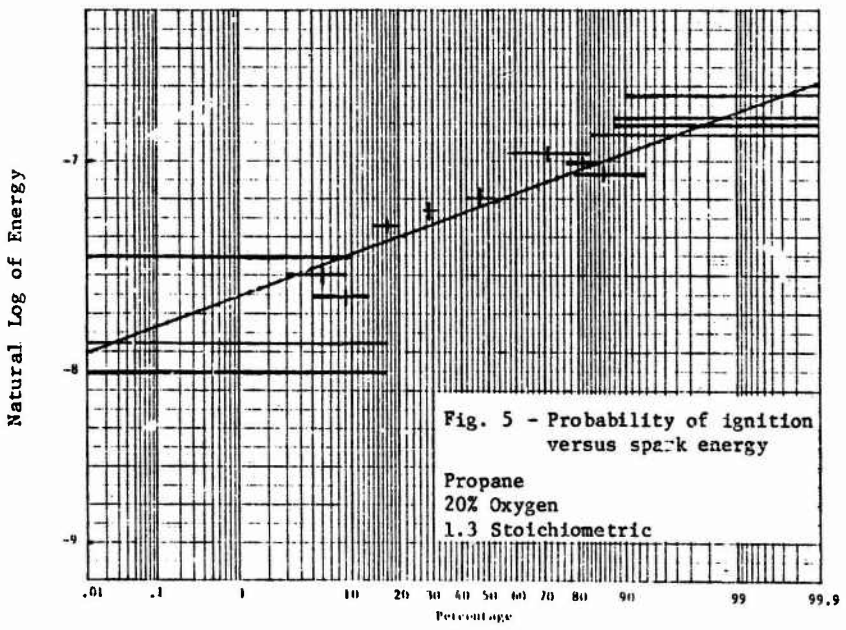
Natural Log of Energy
-7
-8
-9
.01
.1
1
10
20
30
40
50
60
70
80
90
99
99.9
Percentage
Fig. 5 - Probability of ignition versus spark energy
Propane
20% Oxygen
1.3 Stoichiometric

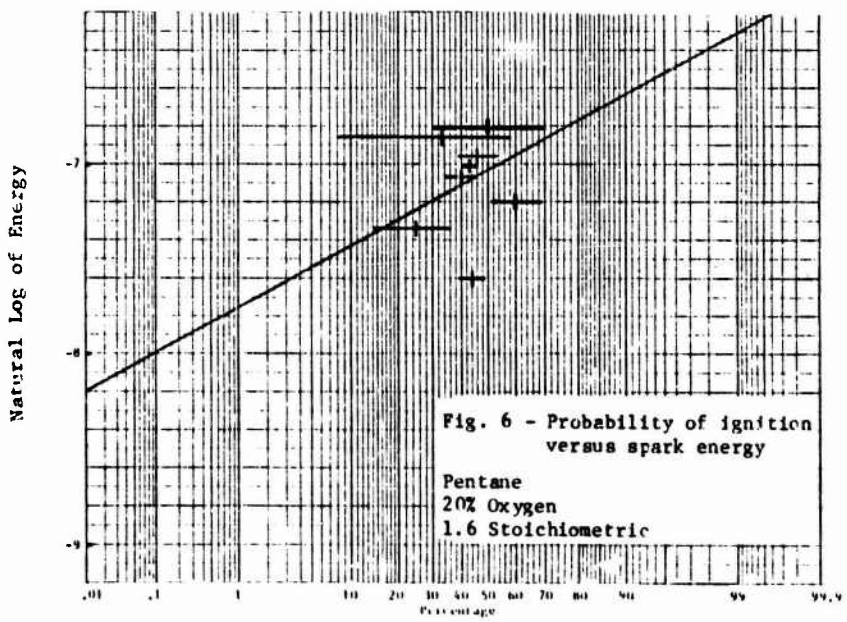
Natural Log of Energy
-7
-8
-9
Percentage
Fig. 6 - Probability of ignition versus spark energy
Pentane
20% Oxygen
1.6 Stoichiometric

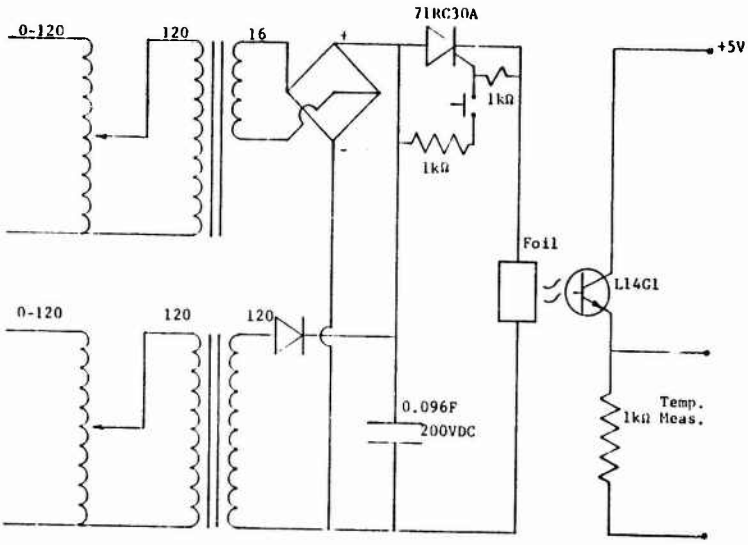

Fig. 8 - Hot spot test circuit schematic

Note: Stainless steel foils not installed

Fig. 9 - Hot spot fixture and temperature monitoring circuit

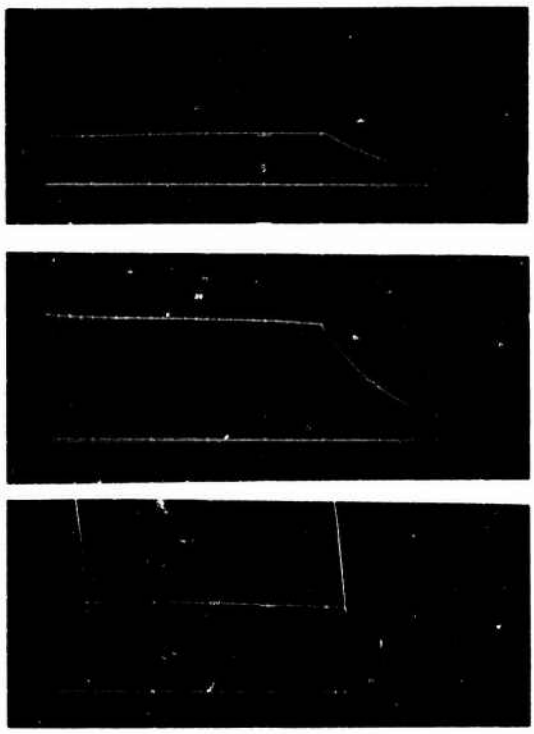

700°C
0.1V/div
0.2s/div

800°C
0.2V/div
0.2s/div

900°C
1V/div
0.2s/div

Fig. 10 - Typical hot spot temperature oscillograms

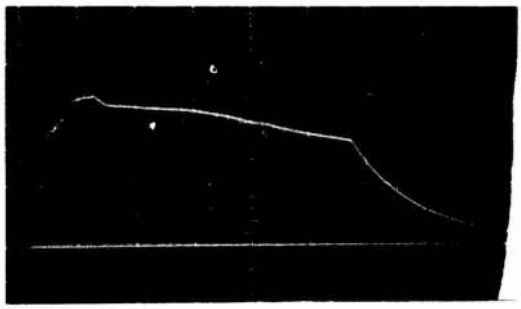

JP-4
2.5%
20% Oxygen
900°C Ignition
1V/div
0.2s/div

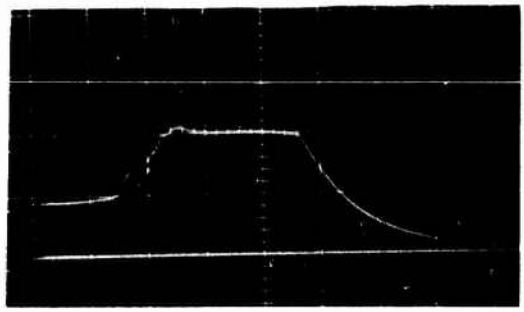

JP-4
2.5%
20% Oxygen
900°C Ignition
1V/div
0.2s/div

JP-4
2.5%
20% Oxygen
900°C Ignition
1.0V/div
0.2s/div

Fig. 11 - Typical hot spot test level ignitions

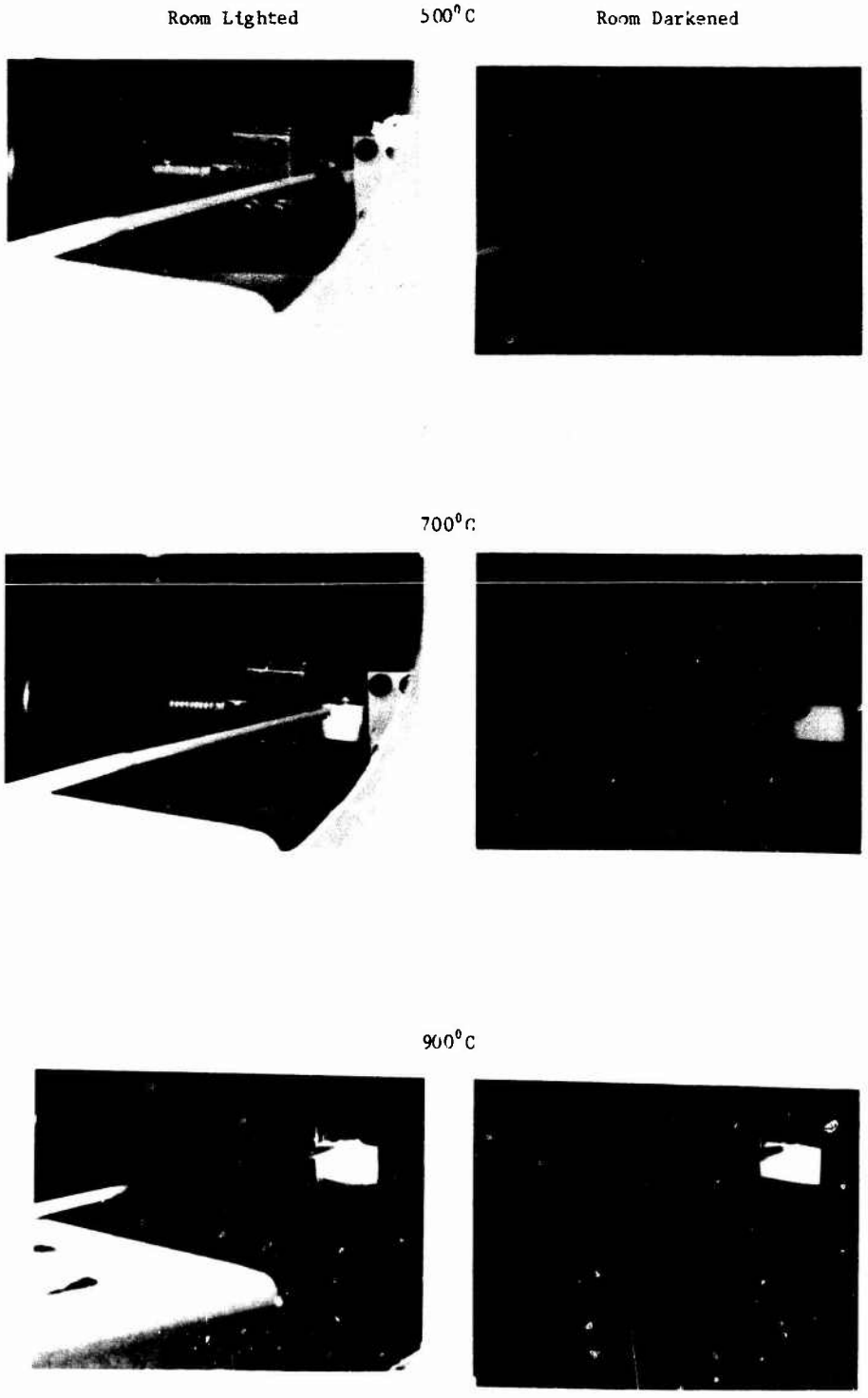

Fig. 12 - Photographs of typical hot spot test levels
(No fuel present for photographs)

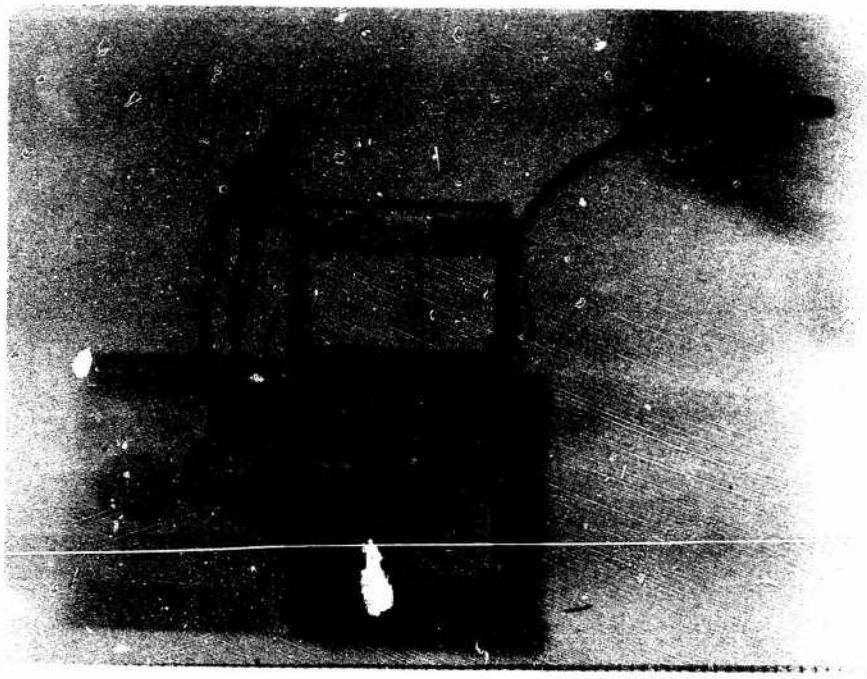

Fig. 13 - Corona test fixture

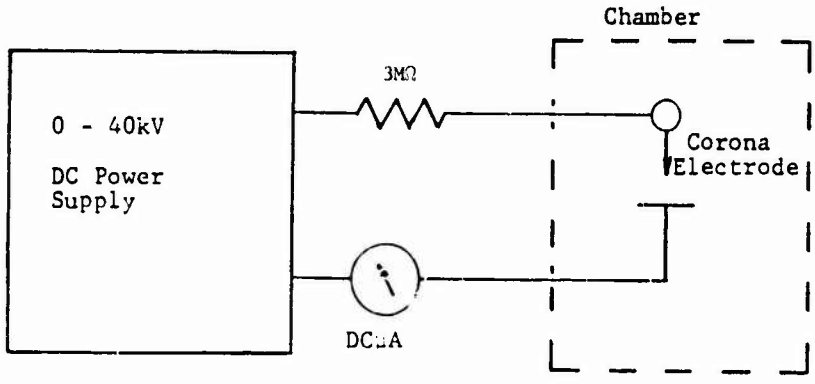

Fig. 14 - Corona test circuit schematic diagram

Sharp Electrode

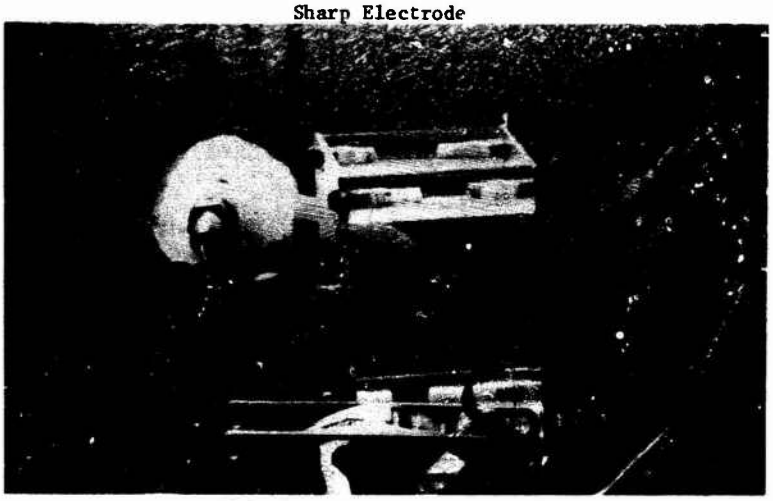

Blunt Electrode

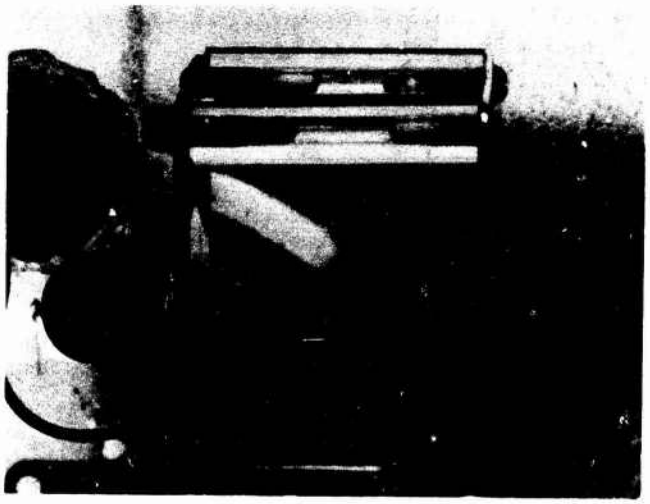

Fig. 15 - Corona test configuration

Fig. 16 - Positive corona, nonignition level showing streamer formation

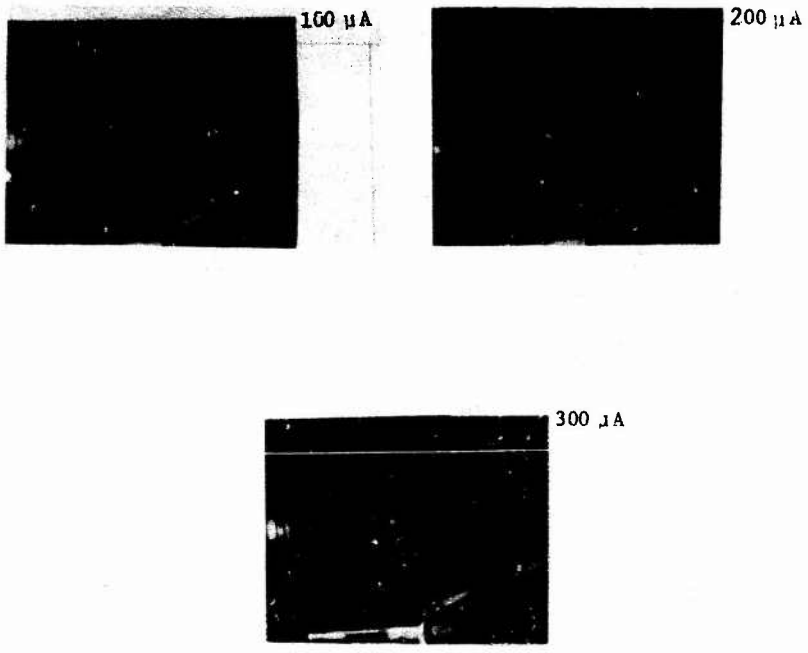

Fig. 17 - Typical corona test levels
- Pointed electrodes
Negative polarity

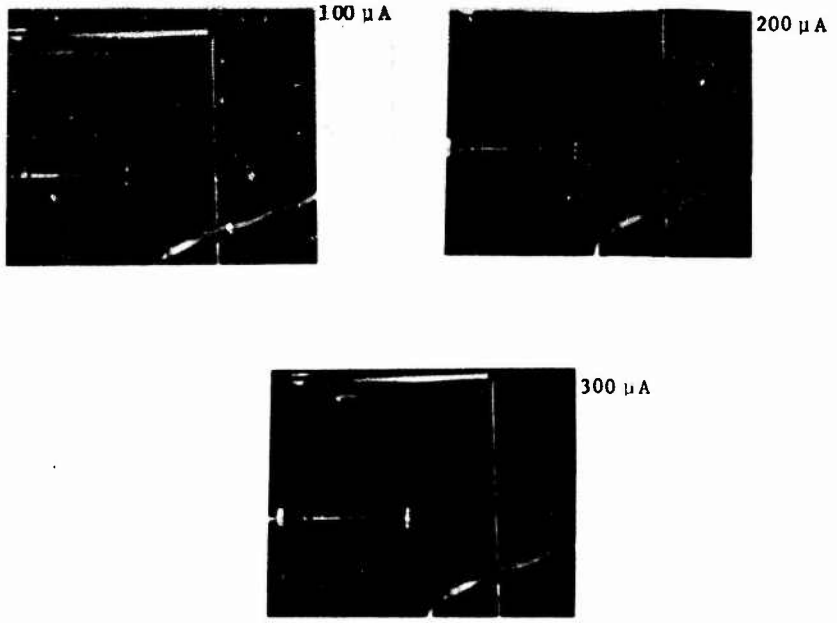

Fig. 18 - Typical corona test levels
- Blunt electrode
Negative polarity

Table 1 - Summary of Spark Energy Ignition Data

Energy Interval (Joules$\times 10^{-6}$)	Plotted at (Joules$\times 10^{-6}$)	ln(J)	Ignitions (%)	No. Tests	Range
		Propane 1.0 Stoic., 20% Oxygen			
600-700	650	-7.34	0	13	7
700-800	750	-7.20	0	7	13
800-900	850	-7.07	18	17	6
900-1000	950	-6.96	18	11	8
1000-1100	1050	-6.86	59	17	6
1100-1200	1150	-6.77	100	7	13
1200-1300	1250	-6.68	100	5	17
1300-1400	1350	-6.61	100	18	5
1400-1500	1450	-6.54	94	18	5
1500-1600	1550	-6.47	100	11	8
500-700	600	-7.42	0	7	13
700-900	800	-7.13	12	24	4
900-1100	1000	-6.91	43	28	3
1100-1300	1200	-6.73	100	12	8
1300-1500	1400	-6.57	97	36	3
1500-1700	1600	-6.44	100	12	8
		Propane 1.1 Stoic., 20% Oxygen			
600-700	650	-7.34	0	6	14
700-800	750	-7.20	14	28	3
800-900	850	-7.07	38	34	3
900-1000	950	-6.96	87	30	3
1000-1100	1050	-6.86	83	18	5
1100-1200	1150	-6.77	100	2	33

Table 2 - Summary of Spark Ignition Probabilities

Fuel Mixture	0.01% uJ	0.1% uJ	1% uJ	10% uJ	50% uJ
		Propane - 20% Oxygen			
1.0	520	585	675	810	1020
1.1	515	565	625	725	865
1.2	440	485	550	645	710
1.3	335	385	450	560	730
1.4	440	515	625	810	1110
		Pentane - 20% Oxygen			
1.3	185	230	295	420	645
1.4	320	370	430	530	690
1.5	170	210	270	390	610
1.6	275	335	425	595	885
		Propane - 30% Oxygen			
1.0	70	80	100	130	185
1.1	45	55	70	100	155
1.2	40	50	70	100	160
1.3	50	60	80	110	165
1.4	65	85	105	150	230
		Pentane - 30% Oxygen			
1.3	50	60	70	95	130
1.4	35	55	70	100	145
1.5	45	55	70	100	150
1.6	75	85	100	125	165
		JP-4 - 20% Oxygen			
2.5%	895	1000	1140	1360	1700
3.0%	630	705	805	965	1210
3.5%	715	725	910	1090	1360

Table 3 - Summary of Hot Spot Ignition Data

Stoichiometric Mixture	Temperature °C									
	1	2	3	4	5	6	7	8	9	10
				20% Oxygen - Propane Fuel						
1.1	900	900	900	900	900	900	900	900	900	900
1.2	900	900	900	900	900	900	900	900	900	900
1.3	900	900	900	900	900	900	900	900	900	900
				30% Oxygen - Propane Fuel						
1.1	900	900	900	900	900	900	900	900	900	900
1.2	900	900	900	900	900	900	900	900	900	900
1.3	900	900	900	900	900	900	900	900	900	900
				20% Oxygen - Pentane Fuel						
1.3	900	900	900	900	900	900	900	900	900	900
1.4	900	900	900	900	900	900	900	900	900	900
1.5	900	900	900	900	900	900	900	900	900	900
				30% Oxygen - Pentane Fuel						
1.3	900	900	900	900	900	900	900	900	900	900
1.4	900	900	900	900	900	900	900	900	900	900
1.5	900	900	900	900	900	900	900	900	900	900
				20% Oxygen - JP-4						
2.5%	900	900	900	900	900	900	900	900	900	900
3.0%	900	900	900	900	900	900	900	900	900	900
3.5%	900	900	900	900	900	900	900	900	900	900

IMPROVED ELECTROSTATIC DISCHARGE WICKS FOR AIRCRAFT

R. V. Anderson and J. C. Bailey
Naval Research Laboratory
Washington, D. C. 20375

ABSTRACT

The history of static discharge wicks used for the control of precipitation static is briefly reviewed. The need for reduction in aircraft potential in order to measure the small fair weather electric fields which must be used to calibrate the effects of aircraft geometry is presented. Preliminary tests of the use of fine metallic wires as auxilliary dischargers are presented as a prelude to a systematic evaluation conducted in 1985. Results of the 1985 tests are presented in which dependencies of aircraft potential were observed for number of wicks, length, and diameter. Theoretical studies of corona discharge are reviewed, and their applicability to the aircraft discharge problem is discussed. It is concluded that a significant reduction in aircraft potential can be obtained by applying metallic wicks either in addition to the standard existing dischargers or in their place. No information is available on whether the metal wires have any effect on radio noise. It is concluded that further study of this phenomenon might be valuable.

BACKGROUND

ELECTROSTATIC DISCHARGE WICKS were developed as part of the Precipitation Static Project in the late 1940's as a means to reduce the deleterious effects of the large aircraft potentials encountered in precipitation on communications [1],[2]*. Before long, their use became mandatory. In a companion paper [3], the large aircraft charges associated with turbine engines is mentioned as a problem in electric field meter calibration. This phenomenon was first discovered in 1956 in connection with tests of an experimental instrumentation system aboard a Navy jet fighter [4]. The fighter was placed on insulating chocks, variable high voltage was applied to the aircraft, and instrument tests were conducted at normal engine power settings. It was found that even in the absence of any applied voltage, radio communication between observers aboard the aircraft and those on the ground was difficult to impossible with the engines in operation. In order to continue the test schedule, a quick fix remedy was required. This was achieved by taping lengths of fine copper wire to the trailing edges of the wings to serve as corona points with a low (voltage) threshold. Upon completion of the test sequence, there was no further investigation of this observed phenomenon.

In 1984, the FAA CV-580 research aircraft was instrumented for lightning strike research. The NRL static electric field measurement system was a part of this effort to record lightning characteristics, and a calibration of the effect of aircraft geometry was required. The high self-charge values encountered defeated initial attempts at calibration; so the 1956 experience was recalled as a possible approach to a solution of this problem. During the summer of 1984, two 0.003" diameter stainless steel wires were attached to each wing on a flight from Patrick AFB to Cape Canaveral AFS for refueling. It was observed that the charge on the aircraft was reduced by a factor between two and three with this simple addition to the standard wick system. Subsequently, in the autumn of that year, there was an opportunity for calibration flights at the FAA Technical Center. Since a reduction significantly greater than one third was required, and since only one brief opportunity would be available for the attempt, the principle of overkill was adopted. A total of some 400 wicks of the same stainless wire each about 20 cm long were attached to the trailing edges of ailerons, flaps, and horizontal stabilizer with pressure sensitive tape. The aircraft charge was reduced sufficiently so that fair weather fields could be measured, but no quantitative data was obtained.

* Numbers in brackets refer to References at end of paper.

EXPERIMENT

The 1985 lightning campaign provided an opportunity to investigate the discharge wick phenomenon in more detail. A systematic variation in wick parameters was determined in which the number, length, location, and diameter of the wicks would be tested for their influence on aircraft charge. The wicks were still composed of stainless steel wire which was chosen for its strength, durability, and electrical conductivity. The only location used was the trailing edge of the ailerons, and attachment was made with 2 inch wide fabric based pressure sensitive tape. The wick location is shown schematically in Fig. 1, and a photograph of a typical wick configuration as seen in flight is shown in Fig. 2.

An attempt was made to test some wick configuration on every flight whether it was a lightning encounter flight or merely a refueling mission. Both takeoffs and landings provided useful data since a zero value for aircraft potential was obtained with wheel contact with the ground. Data from the four electric field meters was recorded continuously on a six channel strip chart recorder and also on a multi-channel FM analog tape recorder. Potential differences between the in-flight condition and zero (on the ground) were derived and, the effect of the electric image was eliminated (see [3] for an analysis of image effects). It was impossible to obtain data on some flights because of bad weather or instrument malfunctions, but good recordings were made on most of the flights. The calibration of the field meter system relates measured fields at the meter sensors to the voltage on the aircraft with respect to its surroundings. This calibration used flight data, ground measurements, and model calculations to relate observable field values to the aircraft potential. Calibration details are provided in [3]; so they are not repeated here.

RESULTS

It was possible to obtain at least 28 observations of aircraft potential during 1985. Wick lengths between 10 inches (25 cm) and 24 inches (61 cm) were tested, diameters from 0.003" (0.076 mm) to 0.020" (0.51 mm) were used, and the number of wicks varied from none to 28 per wing. The first of the parameters to be tested was number of wicks. On three successive flights in June, 1985, the number per wing was 0, 2, and 4 with all of the same length (10"). The aircraft potential with no wicks added was 118 KV; while the potentials with 2 and 4 wicks were 65 KV

and 27 KV, respectively. Immediately after these tests, the effect of length was evaluated by comparing the measurements with no added wicks and two 10" wicks with two wicks per wing of a 24" length. This last configuration produced an aircraft potential of 27 KV also. Apparently the effects of number and length are quite comparable for such small numbers.

Later in the summer, a similar test was made of the effect of wick diameter. A configuration of ten wicks per wing of length 10" was implemented successively with three wick diameters: 0.003", 0.010", and 0.020". The aircraft potentials observed with these three configurations are shown in Fig. 3. It is seen that the decrease in potential is an inverse function of wire diameter. The data is probably too sketchy to allow any further conclusion to be drawn.

Several other analyses were attempted on this body of data a few of which are worthy of note. Fig. 4 shows the aircraft potential as a function of the number of wicks per wing without consideration of the length or diameter of the wicks. A better display is seen in Fig. 5 in which the potential is plotted versus number of wicks at a constant length of 10" and D=.003. The effect of increasing number, while still obvious, is not as strong as seen with two and four wicks of the same length. An attempt to include all of the meaningful parameters in one presentation is shown in Fig. 6 where the aircraft potential is plotted as a function of the ratio NL/D where N is the number (per wing), L is the wick length, and D the wick diameter. A definite relationship is seen to exist which suggests the possibility that an empirical equation might be viable for use in wick system design.

THEORY

There have been numerous laboratory and theoretical analyses of the behavior of a corona point. In particular, Ette [5] presents both measurements and a model in which he considers the effect of the space charge cloud around the point on the effectiveness additional points. He rather convincingly concludes that it is possible for the addition of points to add to the discharge current or even for the discharge current to be diminished by the added points. Chapman [6] builds on the analysis of Ette by defining an effective charge sphere whose radius determines the point spacing at which added discharge points add to the total discharge current. His radius is proportional to the length of the corona probe and to the electric field, and it is inversely proportional to the wind velocity over the points. Note that since all of the data in this study was taken on takeoffs and landings, the appropriate speed is very nearly the aircraft's stall speed.

CONCLUSIONS

It is seen that it is readily possible to reduce an aircraft's potential by a factor of ten. Reduction by a significantly greater factor might be significantly more difficult because of the apparently asymptotic nature of the results. Extant theoretical studies have been shown to be consistent with the observed results. No attempt was made to assess whether there were any effects on radio noise by the use of metallic wicks although satisfactory communications were maintained during storm penetrations with the steel wicks in place. It is concluded that fine metal discharge wicks can significantly reduce the potential of turbine engine aircraft and that the pnenomenon, while qualitatively understood, is not perfectly known and might be a profitable area for further study.

REFERENCES

1. R. Gunn, W.C. Hall, and G. Kinzer, "The Precipitation-Static Interference Problem and Methods for Its Investigation", Proc IRE and Waves and Electrons,34,April 1946.

2. W.C. Hall, "Apparatus for Preventing Radio Interference", U.S. Patent 2,466, 311, April 1949.

3. R.V. Anderson and J.C. Bailey, "Experimental Calibration od an Aircraft Vector Electric Field Meter System", International Aerospace and Ground Conference on Lightning and Static Electricity, June 1986 (This volume).

4. R.E. Bourdeau and J.L. Donley, personal communication, 1956.

5. A.I.I. Ette, "Laboratory studies of point-discharge from multiple points in irregular configuration", J. Atm.& Terr.Phys., 28,1966.

6. S. Chapman, "The Magnitude of Corona Point Discharge Current", J. Atm. Sci., 34, Nov. 1977.

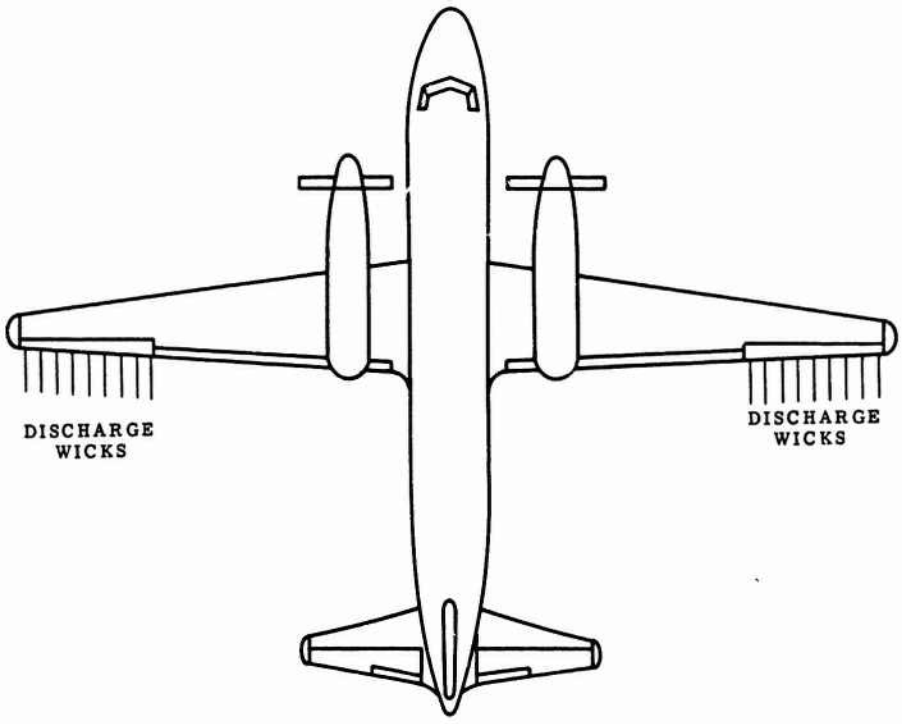

Fig. 1 - Aircraft outline, showing location of discharge wicks

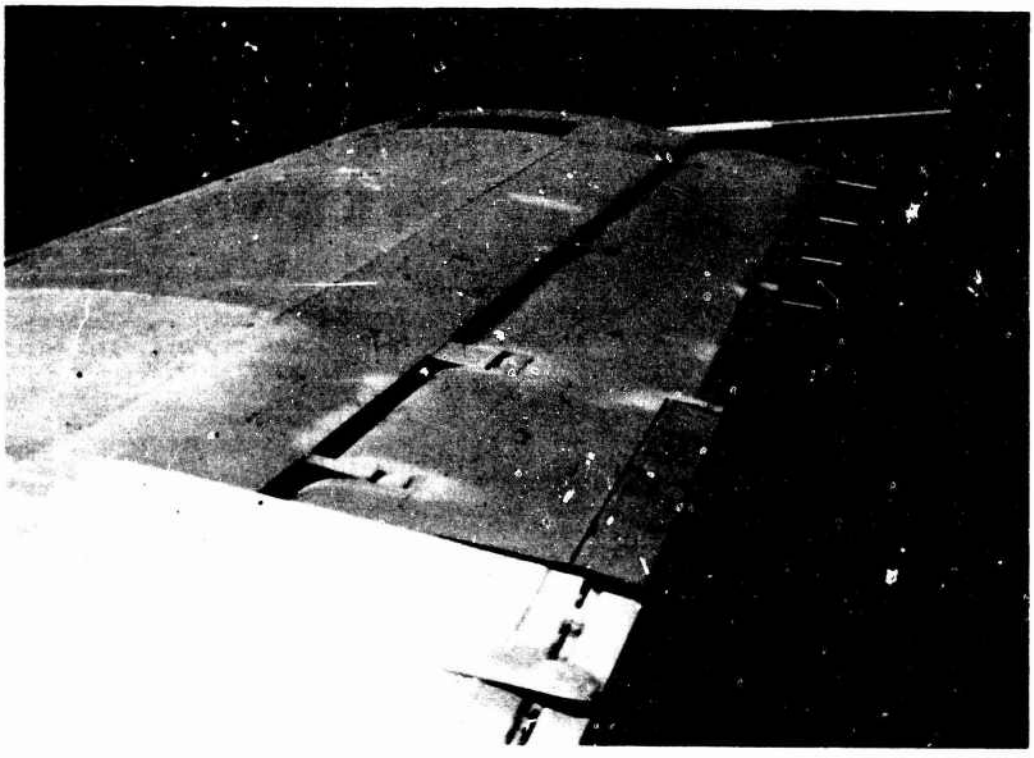

Fig. 2 - Photograph of aircraft in flight showing wicks on trailing edge of aileron

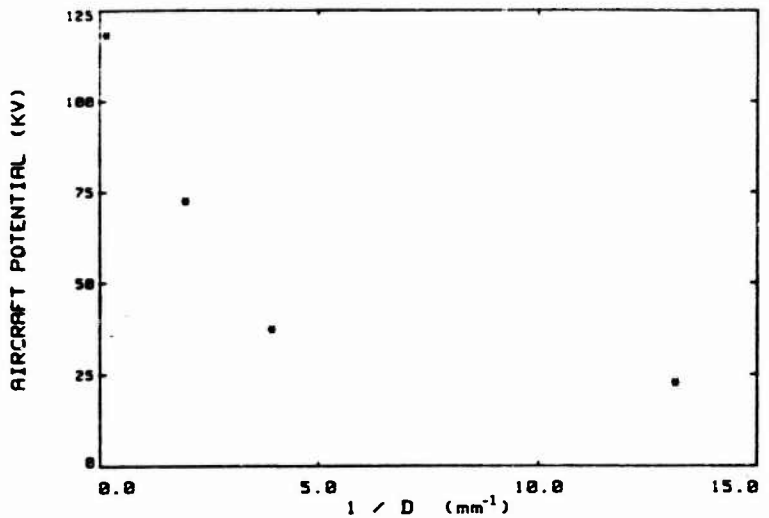

Fig. 3 - Aircraft potential for various wick diameters

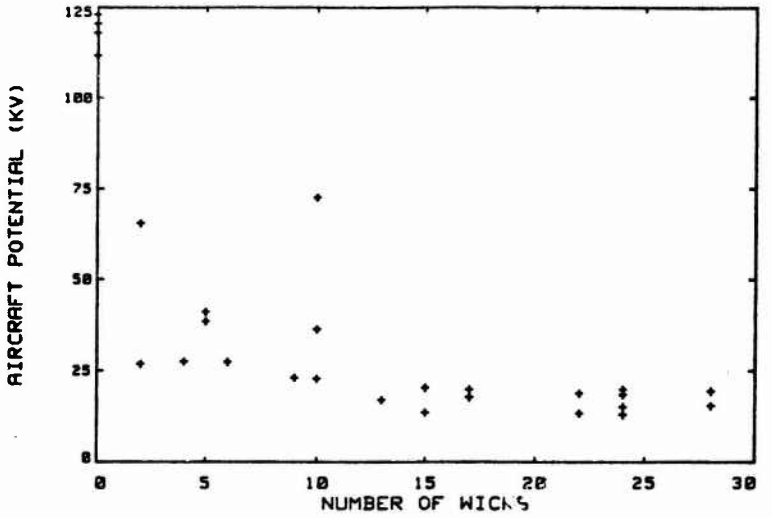

Fig. 4 - Aircraft potential as function of number of wicks

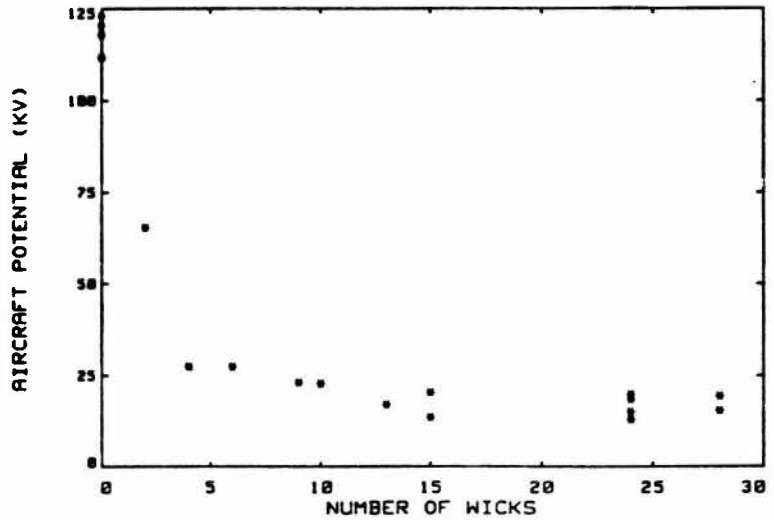

Fig. 5 - Potential as a function of number of wicks of constant length (10") and diameter (0.003")

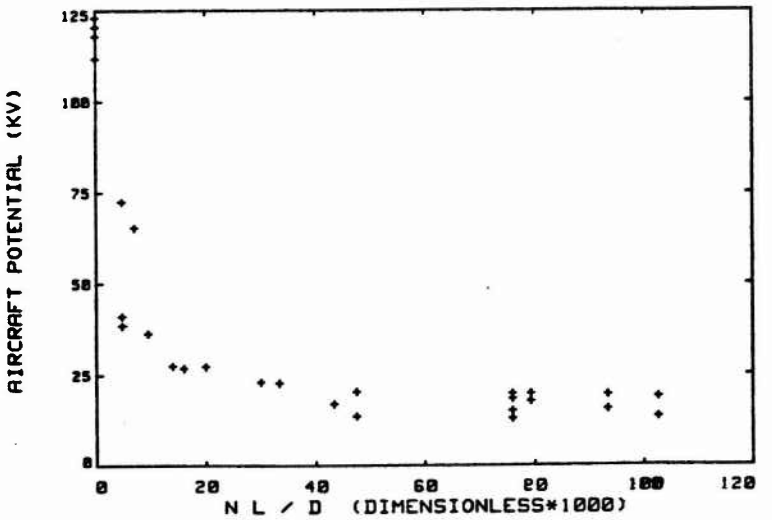

Fig. 6 - Aircraft potential as function of ratio NL/D

SPATIAL AND TEMPORAL CHARACTERIZATION OF THE VHF-UHF LIGHTNING RADIATION (*)

A. Bondiou, I. Taudiere, and P. Richard
Office National d'Etudes et de Recherches Aerospatiales
BP 72, 92322 Chatillon Cedex, France

ABSTRACT

Wide band measurements show up that the VHF-UHF emission associated with natural lightning is mainly impulsive; these pulses of very fast rise time (five nanoseconds) being either isolated or repeated at a rate of several tens of pulses per microsecond.

A physical analysis of this radiation, based upon different laboratory studies of the breakdown mechanisms in air, showed that it can be associated with a transient arc phenomenon involved in the streamer leader transition.

The validation of the models describing this breakdown mechanisms and associated electromagnetic radiation implies a precise knowledge of some fundamental parameters such as the absolute levels of VHF-UHF radiation, the location of emissive sources and their propagation velocity, the shape and repetition frequency of pulses, the polarization of electromagnetic signal.

For this purpose, ONERA operated, during the "Landes Fronts 84" campaign, several instruments:

- a three dimensional location system, which consists in a 300 MHz, one microsecond resolution, interferometric imaging system;

- a spectrum analyser system working at 60 and 300 MHz with dual bandwidth, giving informations on the submicrosecond structure of the signal (temporal coherence) during the whole flash duration;

- a polarization analyser working at 300 MHz with dual bandwidth measurements on each of the three polarizations of analysis.

Results are correlated with E-field measurements and radar measurements, and provide elements for breakdown mechanisms and discharge propagation analysis.

(*) This work was supported by DRET (Direction des Recherches, Etudes et Techniques).

SOME REMARKS ON LIGHTNING CHARACTERISTICS NEAR THE GROUND.

Y. Nagai
Sagami Institute of Technology, Fujisawa 251, Japan
and
Y. Edano, T. Miyazaki, S. Kokubu, Y. Nishida and S. Kawamata
Faculty of Engineering, Utsunomiya University, Utsunomiya 321, Japan

ABSTRACT

Charscteristics of the negstive downward stroke near the ground are discussed based on the photographic observations of lightnings and lightning conditions designated from the field survey of the striking points. The results show that the lightning is strongly influenced by a gust of wind near the ground and that the striking points of the subsequent stroke have been observed to shift from the previous one in a multiple stroke flash.

A LIGHTNING STROKE has been said to strike usually a highest point above the ground, e.g., the highest structure in a town, the highest tree in a forest and so forth. This is true in case of lightnings started with an upward stroke, but it is not true in case of those with a downward stroke, because one can find some struck points by lightnings on a side structure or ground work of he steel high tower. We also experience the elec ric power stop due to the shielding failure of the overhead grounded wire.

Hitherto, the authors have tried to take photographs of many lightning flashes in order to locate the struck points of them and to investigate how the lightning is influenced from the surface condition above ground or the structures on the ground. In this paper, we would like to describe all of the results mentioned above.

OBSERVATION SITE AND APPARATUS

Observations have been performed mainly in Tochigi Prefecture, which locates about 100 km north of Tokyo and is one of the most frequent thunderstorm area in Japan. Tochigi is surrounded by mountain areas of ASHIO, NIKKO and NASU in western to northern, while it opens to plain areas in southern and eastern parts. Most of the lightning activities start in north-western mountain areas and the active thunderstorm crosses over the Tochigi Prefecture to cease in plain area. Therefore, we have advantages to observe thunderstorm from their occurrence to disappearance.

In order to investigate the lightning characteristics near the ground, two stations, Utsunomiya and Nikko, are selected, because the geographical features at each station is quite different from each other, i.e., the former locates in the center of the plain area and the latter is on the boundary.

Utsunomiya station—Apparatus used in the present observation includes some still cameras and two moving-film cameras. Each of the moving-film camera is an improved version of oscillographic camera with 35 mm film which makes record continuously for sufficiently long time. The recording speed is changeable with 5, 10, 20, 50, 100 and 200 mm/sec. Errors involved in the speed of film are less than 2 %, including the power source variations. Most of the speed employed is of 20 mm/sec. A still camera is mounted on a common metal base with the moving-film one for viewing the same field.

We also used a 9.375 GHz Plane Position Indication (PPI) weather radar system which could locate the thunderstorm area in Tochigi Prefectrue.

Nikko station—This station locates about 30 km north-west from Utsunomiya, and is in the course of thunderstorm called "NIKKO-RAI", the thunderstorm grown in Nikko mountain area. As is described above, the station locates on the boundary between plain and mountain areas and, therefore, has the variety of the ground-surface configuration. Hence, it is convenient to investigate how the lightning is influenced from the configuration of the ground. In this station, we used mainly a VTR-camera to take photograph of lightning discharges.

In both stations, the distance to a lightning was estimated by measuring the thunder delay time and by using the triangulation method.

RESULTS AND DISCUSSIONS

Based upon the lightning observations on Mount San Salvatore, Berger [1]* classified the lightning stroke into four kinds: (1) negative downward stroke, (2) positive downward stroke, (3) positive upward stroke and (4) negative upward stroke. On the other hand, in our observations only the first type of lightnings have been observed, i.e., almost all of the lightning flashes have the downward branching with negative charges. Therefore, we restrict our discussions to the negative downward stroke only, hereafter.

The downward stroke initiates from the cloud base and progresses toward the ground with stepping processes. Its behaviour may depend on the characteristics of the leader head and, also, on the distribution of the electric field in front of it. The leader stroke may travel down nearly uniformly in the initial stage and, approaching the ground, it is influenced from the field distribution which is deformed from the grounded objects such as strucutres, trees and, in some cases, the geographical features, and in the final stage the leader determines the striking point of itself. Hence, it is important to estimate how high the grounded objects affect on the field distortion.

INFLUENCE OF THE GROUNDED OBJECTS—Generally, it is very difficult to solve analytically the distribution of the electric field using the Laplace or Poisson equation after taking account the boundary conditions. However, if we restrict ourselves to two-dimensional case, we can use the comformal mapping mehtod to calculate the distribution of the electric field.

In Fig. 1 is shown the electric field distributions obtained from the simulation on the building with a lightning rod. This figure shows that the field distribution far from the object becomes uniform and parallel to the terrain and that the height which affects on the field distortion is within several times of that of object.

On the other hand, there exist many positive and negative ions in the atmosphere including many electrons. As a result, it is suspected that the charged particles make the sheath region around the grounded objects to decrease the electric field in the atmosphere by the shielding effect. The region in which shielding effect extends can be estimated by calculating the Debye shielding distance which is defined as

$$D = (\varepsilon_0 \, k \, T \, / \, n_0 \, e^2)^{1/2}, \qquad (1)$$

where e is the electron charge, n_0 is the density, T is the temperature, ε_0 is the dielectric constant, and k is the Boltzmann constant [2]. Under the assumption that the atmosphere is composed of electrons and singly ionized nitrogen ions, the Debye shielding distance D is estimated as the order of 10 - 100 m with $n_0 \sim 10^7$ m^{-3}, and kT $\sim$ 0.1 eV. It is interesting to note that these values coincident nearly with the values of striking distances defined by Golde [3]. From the above results, it becomea clear that the downward stroke is not affected from the grounded objects until it reaches the height which is several times as high as the grounded

* Numbers in brackets designate References at end of psper.

objects.

These results may be applied to the case of horizontal displacement from a vertical structure or from a steep mountain side. The typical example of this case is shown in Fig. 2, which shows that a lightning strikes the tree on the flatland not in the mountainous district.

CHANNEL SPLITTING AND DISPLACING OF STRUCK POINTS—It is important and interesting phenomena of the splitting of the discharge channel and the displacing of the struck points of lightning for realizing the protection against the lightning. According to photographs taken by a still camera, there are some cases where a lightning channel splits into two or more channels and each of them seems to strike the ground simultaneously. However, by comparing the photographs taken by the still camera with that by the moving-film one it becomes clear that these phenomena can be classified into two categories: (1) single stroke flash splits into two or more channels on its travelling down to the ground and each tip of the forked channels reaches simultaneously to the ground, and (2) in the multiple-stroke flash the time interval between adjacent strokes is relatively long (e.g., 7 to 100 msec according to Kitagawa et al [4]). For convenience, we call the former as "simultaneous-bi-stroke flash" and the latter as "multi-strike-point flash" [5].

Simultaneous-bi-stroke flash—A typical example of the simultaneous-bi-stroke flash is shown in Fig. 3. In this picture, two discharge channels, A and B, are shown. By comparing the photograph taken by the still camera with that by the moving-film camera, it is seen that each channel is composed of a single stroke flash, channel A is formed 74.5 msec ahead of channel B, and channel A is the simultaneous-bi-stroke flash. The distance from the observation site to the striking point of the lightning is estimated as 12.6 km from the thunder delay time, and the height of the channel splitting point is estimated as 206 m from terrain.

An another example of this type is shown in Fig. 4, which shows a single stroke flash and, hence, simultaneous-bi-stroke flash. The distance to the striking point and the height of the splitting point of the channel are estimated as 7.8 km and 41 m, respectively.

From two examples, it should be noted that the height of the splitting point of the discharge channel is relatively low.

Multi-strike-point flash—A typical example of the multi-strike-point flash is shown in Fig. 5. The distance to the lightning is estimated as 13 km and the height which seems to be the channel splitting point in the still photograph is estimated as 450 m, as determined from the still photograph and the triangulation method. The photograph taken by the moving-film camera shows that the time interval between the first and subsequent stroke is estimated as 87.4 msec, which should be compared with that obtained by Kitagawa et al [4]. Schonland et al [6] and Kitsgawa et al [4] indicate that this phenomenon is caused by the decrease of the conductivity in the discharge channel because of long time interval between adjacent strokes. However, we should stress here that it is caused by the gust or wind shear just above the ground.

If the wind blows uniformly over a relatively wide space, the ribbon type lightning can be seen. On the other hand, when the leader followed by the subsequent stroke travels down along the path built by the previous stroke and meets the gust of wind, the leader tip of the subsequent stroke ia blown off from the previously formed channel. As a result, the struck points of the subsequent strokes could be displaced along the direction of the wind.

An example of the damage of the distribution lines caused by this phenomenon is shown in Fig. 6, in which five power lines under the grounded wire were melted down by the power current. Here, the lightning flashes caused the breakdown of the power line insulation during the multiple stroke flash. In this figure, we can see that the power lines are struck from the side, not from the top of the structure. It seems to be caused by the shift of the discharge channel from a wind shear.

The relation of the accumulated frequency versus the height of the channel splitting is shown in Fig. 7, including the simultaneous-bi-stroke and the multi-strike-point flashes. The height which corresponds to the 50 % value is about 300 m. It is interesting to note that the most of simultaneous-bi-stroke flashes occur below this value, while the most ot multi-strike-point flashes set in above that value except one point.

CONCLUSION

From the above discussions, it is concluded that (1) the presence of a simultaneous-bi-stroke flash is confirmed, and also that (2) the lightning is strongly influenced by the gust or wind shear above the ground, i.e., the discharge channel of lightning shifts by a wind and the struck points of the subsequent strokes displace along with the direction of the wind in a multiple-stroke flash.

ACKNOWLEDGEMENTS

The authors would like to express their thanks to the Tokyo Electric Power Co. Inc. and those who extended us their kind assistance.

REFERENCES

1. Berger K., "Novel observations on lightning discharges: Results of research on Mount San Salvatore", J. Franklin Inst., 283 (1967) 478-525.

2. Chen F.F., "Introduction to Plasma Physics", (Plenum Press, 1974).

3. Golde R.H.,"The lightning conductor", in Lightning (ed. by R.H. Golde, Academic Press 1977), pp.545-576.

4. Kitagawa N., M. Brook and E.J. Workman, "Continuing current in cloud-to-ground lightning discharges", J. Geophys. Res., 67 (1962) 637-647.

5. Edano Y., Y. Nagai and S. Kawamata, "Observations of simultaneous-bi-stroke flashes", Research Letters on Atmospheric Electricity, 2 (1982) 49-52 [in Japanese].

6. Schonland B.F.J., D.J. Malan and H. Collens, "Progressive lightning VI", Proc. Roy. Soc. of London, A-168 (1938) 455-469.

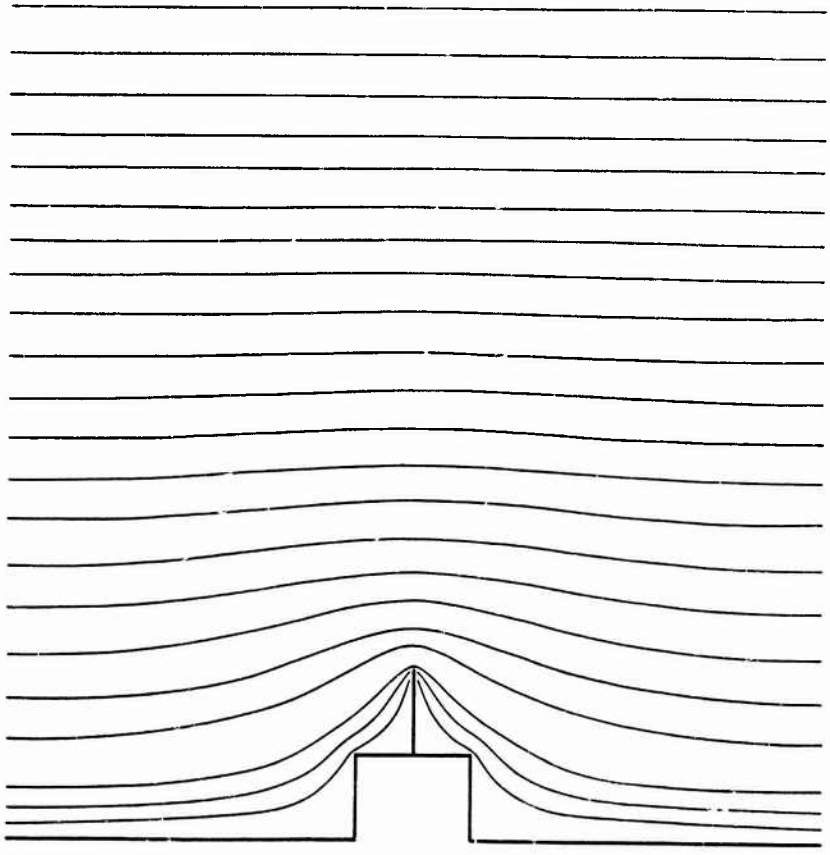

Fig. 1—Electric field (equi-potential) distribution near the building with a lightning rod.

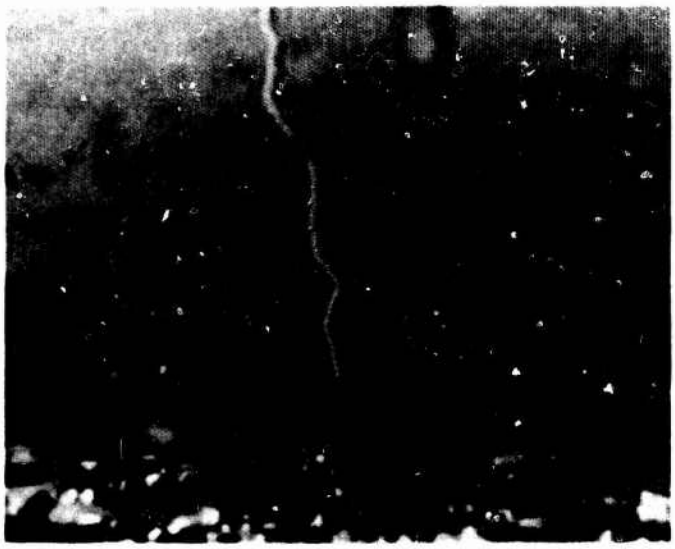

Fig. 2—Downward flash which is not affected from the grounded objects.

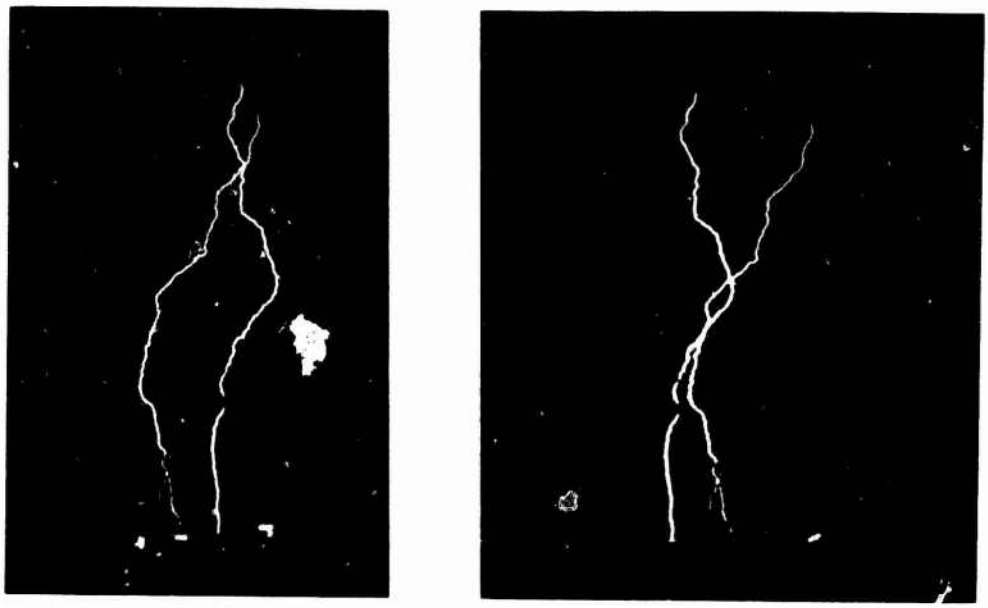

Fig. 3—Simultaneous-bi-stroke flash. (a) Photograph on still film. (b) Photograph on moving-film.

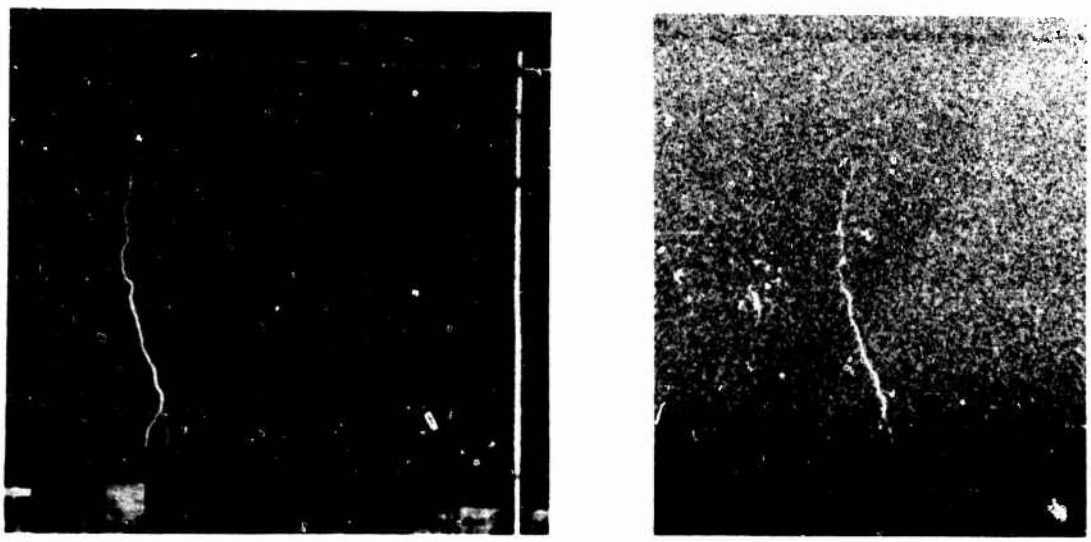

Fig. 4—Simultaneous-bi-stroke flash. (a) Photograph on still film. (b) Photograph on moving-film.

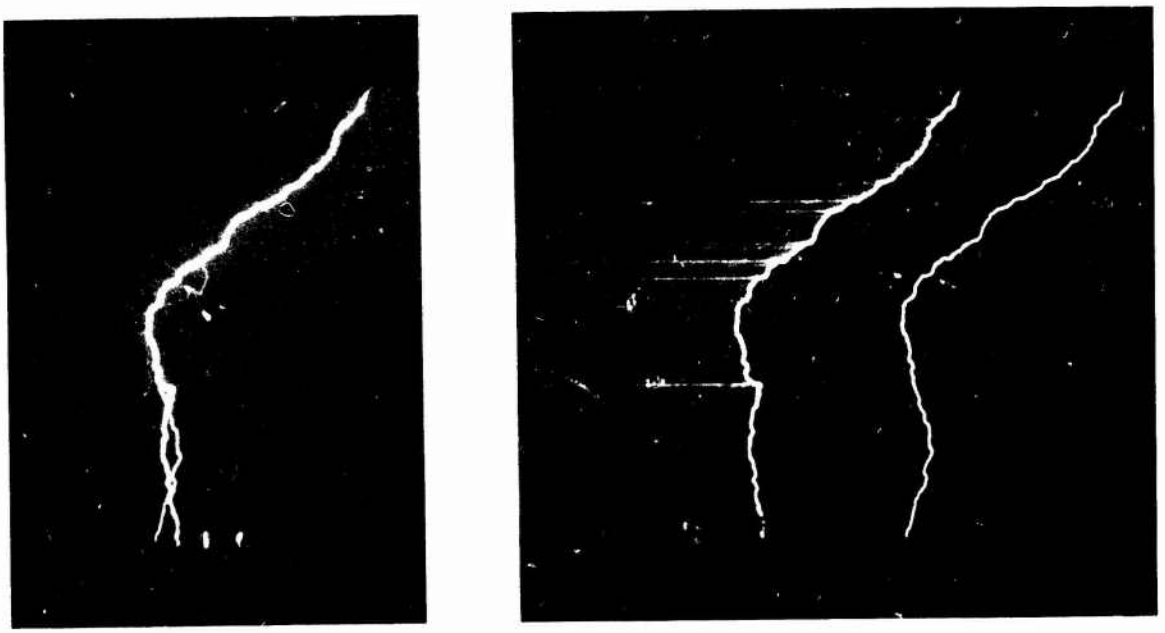

(a) (b)

Fig. 5—Multi-strike-point flash. (a) Photograph on still film. (b) Photograph on moving-film.

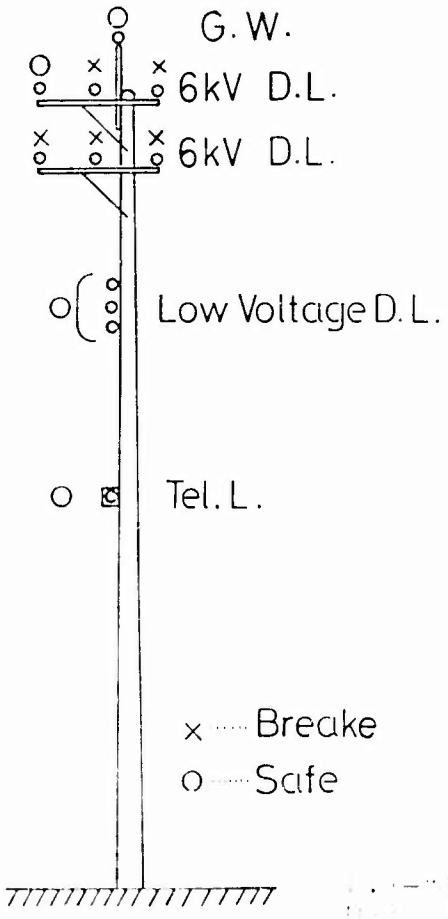

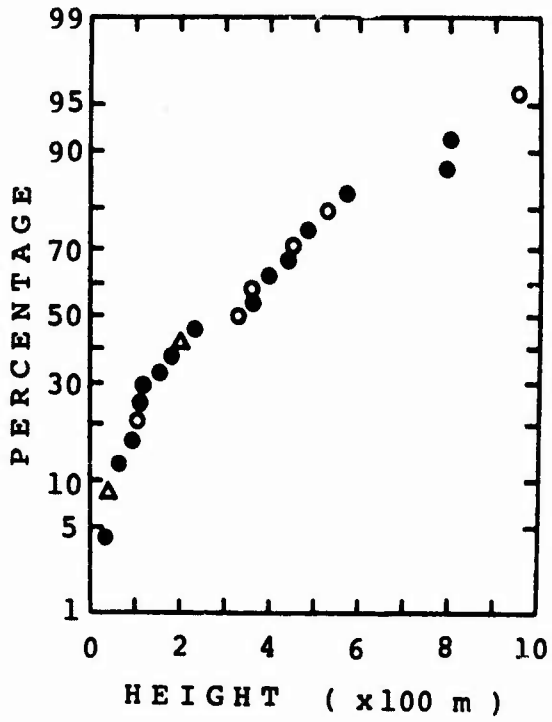

Fig. 7—Relation of cumulative frequency versus height of channel splitting point.
Δ : simultaneous-bi-stroke flash
o : multi-strike-point flash
• : unconfirmed flash

INTRACLOUD DISCHARGES STUDIED FROM THE SIMULTANEOUS MEASUREMENTS OF ELECTROSTATIC FIELD CHANGES, THUNDER AND RADIATION FIELDS FROM OVERHEAD TROPICAL THUNDERSTORMS

P. Pradeep Kumar and J. Rai
Department of Physics, University of Roorkee,
Roorkee - 247667, India

ABSTRACT

Simultaneous measurements of electrostatic field change, thunder and radiation fields were carried out for overhead tropical thunderstorms at Roorkee during the summer of 1984. The records were analysed in detail to study the finer aspects of intracloud discharges . The observation strongly suggests the initiation of the intracloud discharge in a stepwise manner followed by recoil streamers. The above observations therefore support the potential gradient wave mechanism of intracloud discharges.

INTRODUCTION

The mechanism of intracloud discharges is still of question of dispute due to the lack of observational evidence. Although extensive measurements of electric field changes due to intracloud discharges have been done by many workers from different parts of the world, their interpretation varied most probably because of the observations being made in different latitudes. As more than 90% of the intracloud discharges occuring over Roorkee are intracloud discharges measurements of electrostatic field changes, thunder and radiation fields were carried out to examine the mechanism of intracloud discharges.

EXPERIMENTAL SET UP

For measuring the electrostatic field changes a plate antenna was employed as a sensor the output of which was recorded on a chart recorder. For obtaining the distance to the discharge and the channel length thunder was also recorded simultaneously on a tape recorder. The radiation fields were received by a ELF-VLF receiver and the signals were stored on a tape recorder. Later these signals were fed to the oscilloscope and were photographed by a high speed camera. The complete experimental set up has been described in detail by Pradeep and Rai [1].

OBSERVATIONS

The observations revealed that the observed field changes can be classified into four different catogaries as shown in Fig.1. Within the field reversal distance about 40% were of type I, 20% were of type II both giving negative field changes 18% were of type III, 10% were of type IV producing positive field change and the rest 12% were complex in nature. So it can be concluded that in most of the case for near distances the electrostatic field change during intracloud discharge was negative.

The radiation field records of intracloud discharges showed that in general an intracloud flash can be divided into three portions (i) initial (ii) active and (iii) final. It was observed that not all the flashes produced all the three portions, but if the interflash time interval was large all the three portions were normally present.

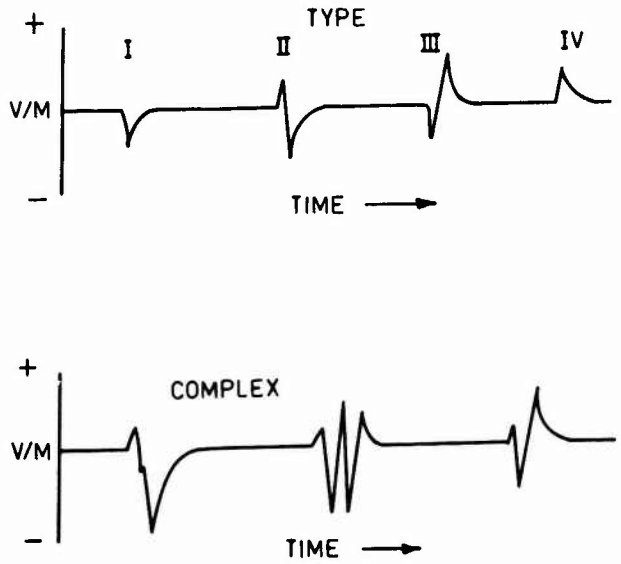

Fig.1 - Types of observed electrostatic field changes

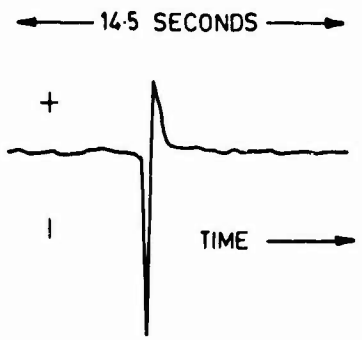

Fig.2 - Electrostatic and radiation fields of an intracloud discharge. Total duration of flash 400 millisecond. Field change is positive.

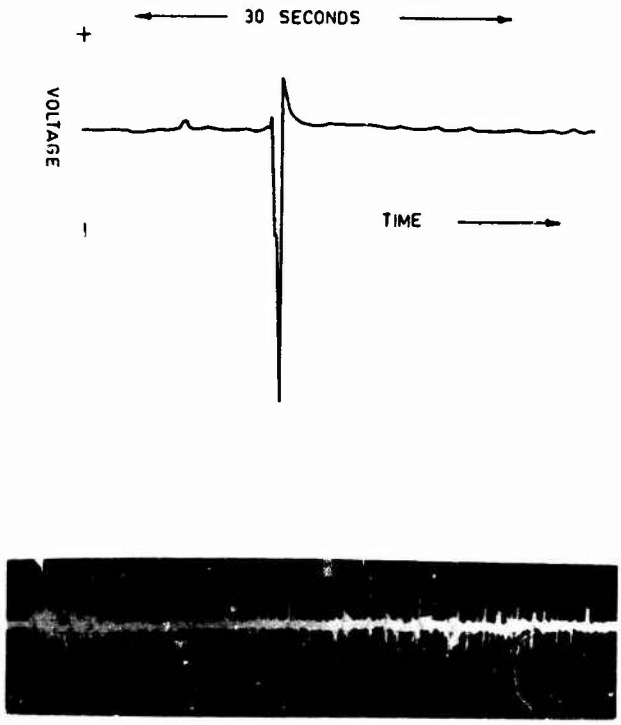

Fig.3 - Electrostatic and radiation fields of an intracloud discharge. Total duration of flash 700 millisecond. Field change is complex.

The initial portion is characterised by rapid pulsations of the order of microseconds and lasting for a duration of 100 to 200 millisecond. The active stage comprised of large amplitude bursts, bipolar in nature with the pulse interval of the order of millisecond. The final stage comprises of small amplitude bursts spaced at intervals ranging from 10 to 60 milliseconds. The quiescent times observed between the initial and active stage ranged from 10 to 120 milliseconds, and that from active to final ranged from 10 to 80 milliseconds. The electrostatic and radiation fields of two typical intracloud discharge are shown in Figures 2 and 3.

DISCUSSION

Theoretically it has been shown [2,3] that in an intracloud discharge the raising of negative charge from the lower N-region gives a positive field change on the ground and the lowering of positive charge from the upper P-region gives a negative field within field reversal distance. Our records show that about 60% of the field change within the field reversal distance was negative, so in light of the theoretical calculations [2,3] it can be suggested that an intracloud discharge is initiated by the raising of negative charge from the bottom of the cloud followed by the lowering of positive charge from the top of the cloud. The initial portion of the radiation field strongly suggests that the raising of negative charge from the bottom of the cloud is in a stepwise manner. The active portion confirms the existence of recoil streamers (K-changes) bringing positive charge downwords in the pre ionized channel. The final portion suggests the posibility of the existence of dart like streamers which quenches the remaining charge. It is therefore suggested that the mechanism of intracloud discharge is very much similar in nature to that of cloud to ground discharges. The mechanism of intracloud discharges can therefore be explained in terms of the potential gradient wave proposed by Loeb [4] and Winn [5].

MECHANISM

a) Pilot leader

1. Electron avalance from the lower positive pocket charge p centre to N centre - possibility of corona discharge.
2. Electrons that are accelerated disperse sideways - ions are created, +ve ions move to the N centre while -ve ions to the P centre.

b) Stepping

1. Asymmetry of charges at the ionized and unionized boundary creates potential gradient wave which propagation upwards.

2. Sequence of potential gradient wave propagate forgeing their way to the P centre in stepwise manner.

c) Recoil Streamer

1. Initial discharge reaches P region - there is an increase in potential as a result ambient air breaks down.

2. Downward propagating wave starts forgeing its way in the preionized channel without stepping (K-change).

3. Sequence of events takes place and the flash vanishes.

REFERENCES

1. Pradeep Kumar P., Rai J., 'Design and fabrication of electric field sensors for the measurement of lightning parameters'. Indian Journal of Radio and Space Phys., 14, 68-72, 1985.

2. Ogawa T., Brook M., 'The mechanism of intracloud lightning discharge'.J.Geophys. Res., 69, 5141-5150, 1964.

3. Khastagir S.R., Saha S.K., 'On intracloud discharges and their accompanying electric field changes'. J. Atmos. Phys., 34, 115-126, 1972.

4. Loeb L.B., 'Ionizing waves of potential gradient'. Science, 148, 1471, 1965.

5. Winn W.P., 'A laboratory analog of the dart leader and return stroke of lightning, J. Geophys. Res., 70, 5265, 1965.

Author Index

Allen, J. E. 34
Alliot, J. C. 18, 27
Anderson, R. V. 33, 49

Bailey, J. C. 33, 49
Baker, L. 35
Baldwin, R. E. 2
Barrett, L. 21, 22
Baum, C. E. 35, 45
Beavin, R. 24
Bicknell, J. A. 28
Bigelow, A. R. 47
Bondiou, A. 50
Brown, P. W. 4, 20
Burket, H. D. 17, 20

Chen, Y. G. 7
Christopoulos, C. 14
Coffey, E. L. 42
Crouch, K. E. 48

Diguiseppe, T. G. 37
Dunkley, V. P. 13

Edano, Y. 51
Evans, R. H. 13
Eybert-Berard, A. 21, 22

Finelli, G. B. 5
Fisher, B. D. 4, 20

Galicki, E. 7
Garabedian, R. 27
Gardner, R. L. 35, 45
Geren, F. 43
Gobin, V. 27

Hamelin, J. 21, 26
Hanson, A. W. 11
Hardwick, C. J. 13
Hardy, J. S. P. 13
Harrison, J. L. 7
Hebert, J. L. 8, 19, 42, 44
Hebert, M. P. 24, 47
Hobb , P. A. 13
Hoole, P. R. P. 34, 41
Hoole, S. R. H. 41
Hutzler, B. 27

Israelsson, S. 40, 46

Jibilian, H. 47
Jones, C. C. R.2, 3, 11
Jost, R. 44

Kasemir, H. W. 39
Kawamata, S. 51
Kawasaki, Z. 40, 46
Kershaw, D. 3
Kokubu, S. 51
Krantz, L. A. 30
Kumar, P. P. 52

Labaune, G. 27
Laroche, P. 22
Leteinturier, C. 21, 26

MacDiarmid, I. P. 3
Mallik, A. 14
Mazur, V. 31
Menzel, C. 37
Miyazaki, T. 51
Moreau, J. P. 18, 27

Nagai, Y. 51
Nakano, M. 46
Nelson, B. N. 37
Nicot, L. 26
Nishida, Y. 51

Odam, G. A. M. 11
Olson, B. 3
Ostrander, K. A. 36

Paxton, A. H. 45
Perala, R. A. 5, 31
Pitts, F. L. 5
Plumer, J. A. 4

Rai, J. 52
Reazer, J. 8, 15, 16, 47
Reid, G. W. 2
Richard, P. 50
Richardson, W. 7
Richmond, R. D. 16, 23
Ricquel, G. 27
Risley, M. D. 8
Rison, W. 45
Rudolph, T. H. 5, 31
Ruhnke, L. 31
Rustan, P. L. 1

Schneider, J. G. 8, 19
Seliga, T. A. 36, 38
Serrano, A. V. 8, 15
Shelton, R. W. 28
Simpson, M. M. 25
Stevens, B. M. 38

Takeuti, T. 46
Taudiere, I. 50
ter Haseborg, J. L. 29
Terry, J. S. 20
Thomson, J. M. 14
Trost, T. F. 6

Vaughn, R. L. 12

Walen, D. B. 9
Weidman, C. 26
White, W. J. 36
Williford, C. 44
Wolf, F. 29
Wunschel, A. J. 20

Zaepfel, K. P. 32
Ziegler, W. 10

U.S.Government Printing Office: 1986 — 748-061/60548